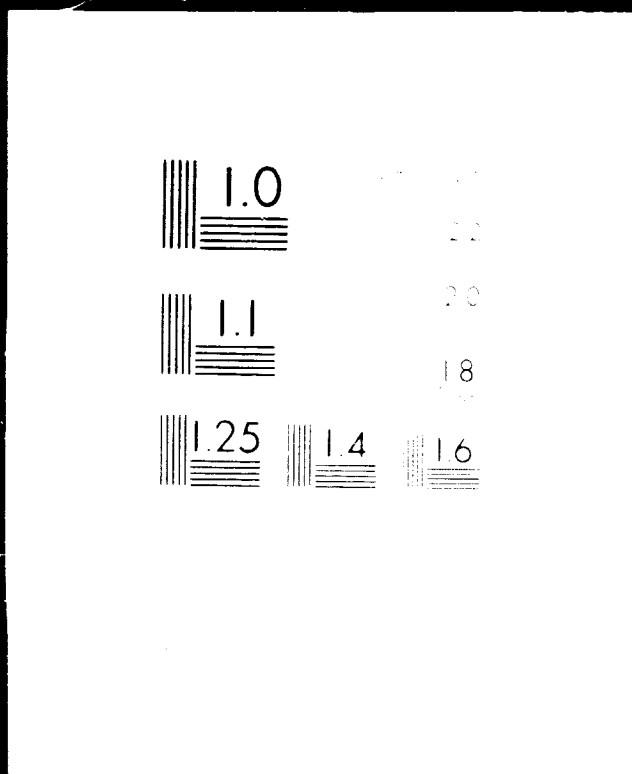


# 1 OF 5

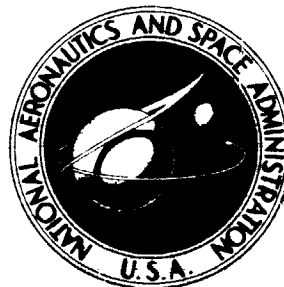
## N78

## 18134

## UNCLAS



**NASA TECHNICAL  
MEMORANDUM**



**NASA TM X-3377**

**NASA TM X-3377**

Publicly Released

**THIRD CONFERENCE ON FIBROUS COMPOSITES  
IN FLIGHT VEHICLE DESIGN**

**Part II**

*Held at  
Williamsburg, Virginia  
November 4-6, 1975*



1. Report No. NASA TM X-3377	2. Government Accession No.	3. Recipient's Catalog No.	
4. Title and Subtitle THIRD CONFERENCE ON FIBROUS COMPOSITES IN FLIGHT VEHICLE DESIGN - PART II		5. Report Date April 1976	
		6. Performing Organization Code	
7. Author(s)		8. Performing Organization Report No. L-10640	
		10. Work Unit No. 505-02-41	
9. Performing Organization Name and Address NASA Langley Research Center Hampton, Va. 23665		11. Contract or Grant No.	
		13. Type of Report and Period Covered Technical Memorandum	
12. Sponsoring Agency Name and Address National Aeronautics and Space Administration and U.S. Air Force		14. Sponsoring Agency Code	
		15. Supplementary Notes Held at Williamsburg, Va., November 4-6, 1975.	
16. Abstract <p>The National Aeronautics and Space Administration and the United States Air Force sponsored a 3-day conference November 4-6, 1975, to focus national attention on the use of fibrous composite materials in the design of flight vehicle structures and the important impact the use of such materials will have on future vehicle systems.</p> <p>Significant milestones have been achieved in composite structures design, test, and flight operations for a wide spectrum of aircraft, space vehicle, and civil sector applications. The continuing growth of the data base for material properties, design procedures, environmental exposure effects, manufacturing procedures, and flight service reliability has increased the level of acceptability and confidence necessary for widespread, routine composite applications. By including composites as baseline design materials, significant payoffs can be expected in terms of reduced structural weight fractions, longer structural life, reduced fuel consumption, reduced structural complexity, and reduced manufacturing cost.</p> <p>Technical papers are presented which describe work performed by the Government and Industry. The topics covered include recent flight test work on composite components, unique design concepts and hardware, specialized applications, operational experience, certification and design criteria, and significant contributions to the design technology base.</p>			
17. Key Words (Suggested by Author(s)) Composites Materials Structural design Reliability		18. Distribution Statement  Subject Category 24	
19. Security Classif. (of this report) Unclassified	20. Security Classif. (of this paper) Unclassified	21. No. of Pages 410	22. Price \$10.50

CONTENTS PRECEDING PAGE BLANK NOT FILMED

Part I\*

KEYNOTE ADDRESS . . . . .	1
George G. Deutsch	

SESSION IA - CURRENT COMPONENT DESIGN EFFORTS

Chairman: Frank D. Cherry  
Air Force Flight Dynamics Laboratory

FLIGHT SERVICE PROGRAM FOR AN ADVANCED COMPOSITE FIN FOR A WIDE-BODY COMMERCIAL JET . . . . .	9
Robert L. Vaughn and Arthur M. James	
THE REALIZATION OF COST AND WEIGHT SAVINGS BY THE APPLICATION OF ADVANCED COMPOSITES TO THE B-1 VERTICAL STABILIZER . . . . .	33
D. E. Parker, W. L. O'Brien, and W. R. Johnston	
DESIGN, FABRICATION AND TEST OF THE B-1 COMPOSITE HORIZONTAL STABILIZER . . . . .	51
Walter Ludwig, Herman Erbacher, and Joseph Visconti	
DEVELOPMENT OF AN ADVANCED COMPOSITE RUDDER FOR FLIGHT SERVICE ON THE DC-10 . . . . .	71
George M. Lehman	
DEVELOPMENT OF CONCEPTUAL HARDWARE FOR THE LIGHTWEIGHT FIGHTER . . . . .	93
R. Roberts	
SIMPLIFIED LOW COST ADVANCED COMPOSITE FUSELAGE STRUCTURE FOR FIGHTER AIRCRAFT . . . . .	95
Lee Bernhardt	

SESSION IB - CURRENT COMPONENT DESIGN EFFORTS

Chairman: R. S. Berrisford  
Army Air Mobility R&D Laboratory

SHUTTLE ORBITER - GRAPHITE/EPOXY PAYLOAD BAY DOORS . . . . .	115
D. Garcia and C. E. Halstead	

\*Sessions I and II are presented under separate cover.



SESSION II - OPERATIONS ENVIRONMENT EXPERIENCE

Chairman: Eldon E. Mathauser  
NASA Langley Research Center

TIME-TEMPERATURE-STRESS CAPABILITIES OF COMPOSITE MATERIALS FOR ADVANCED SUPERSONIC TECHNOLOGY APPLICATIONS . . . . .	383
J. Haskins and J. Kerr	
MOISTURE - AN ASSESSMENT OF ITS IMPACT ON DESIGN OF RESIN BASED ADVANCED COMPOSITES . . . . .	405
Charles D. Shirrell, John C. Halpin, and Charles E. Browning	
FLIGHT SERVICE EVALUATION OF KEVLAR-49/EPOXY COMPOSITE PANELS IN WIDE-BODIED COMMERCIAL TRANSPORT AIRCRAFT . . . . .	427
Robert H. Stone and H. Benson Dexter	
PROGRESS REPORT OF THE NASA GRAPHITE SPOILER FLIGHT SERVICE PROGRAM . . . . .	441
Robert L. Stoecklin and Richard A. Pride	
ENVIRONMENTAL EXPOSURES OF ADVANCED COMPOSITES FOR AIRCRAFT APPLICATIONS . . . . .	455
Richard A. Pride and Marvin B. Dow	
THE AIR FORCE IN-SERVICE ADVANCED COMPOSITE EVALUATION PROGRAM . . . . .	471
T. Bennett	
ADVANCED COMPOSITE FAN BLADE FLIGHT EVALUATION PROGRAM . . . . .	473
Matthew H. Chopin	

Part II

SESSION III - DESIGN CRITERIA AND RELIABILITY

Chairman: Philip A. Parmley  
Air Force Flight Dynamics Laboratory

APPLICATION OF THE AIR FORCE'S NEW STRUCTURAL REQUIREMENTS TO COMPOSITES . . . . .	491
Gary K. Waggoner	
CERTIFICATION REQUIREMENTS FOR CIVIL COMPOSITE COMMERCIAL AIRFRAME STRUCTURES . . . . .	501
James E. Dougherty, Jr.	
FAIL-SAFE DESIGN AND RELIABILITY IN COMPOSITE COMMERCIAL AIRCRAFT STRUCTURE . . . . .	513
Dale S. Warren	
FAIL-SAFE DESIGN AND RELIABILITY IN COMPOSITE COMMERCIAL AIRCRAFT STRUCTURE . . . . .	523
Robert E. Watson	
LIFE ASSURANCE TECHNOLOGY . . . . .	533
J. Halpin and M. Waddoups	
STATISTICAL DESIGN CRITERIA . . . . .	535
B. Walter Rosen	
DESIGN, FABRICATION, AND FLIGHT SERVICE EVALUATION OF COMPOSITE- REINFORCED C-130 CENTER WING . . . . .	547
W. E. Harvill and H. Benson Dexter	

SESSION IVA - DESIGN TECHNOLOGY BASE

Chairman: Michael F. Card  
NASA Langley Research Center

BOLTED JOINT STATIC STRENGTH MODEL FOR COMPOSITE MATERIALS . . . . .	563
James R. Eisenmann	
DESIGN OF THE B-1 COMPOSITE HORIZONTAL STABILIZER ROOT JOINT . . . . .	603
B. Whitman, P. Shyprykevich, and J. Whiteside	
CURRENT LANGLEY RESEARCH CENTER STUDIES ON BUCKLING AND LOW-VELOCITY IMPACT OF COMPOSITE PANELS . . . . .	633
Martin M. Mikulas, Jr., Harold G. Bush, and Marvin D. Rhodes	

ADVANCED COMPOSITE TORQUE BOX OPTIMIZATION . . . . .	665	D10
Donald Y. Konishi, George Hayase, and Jonas Surdenas		
AN AEROELASTIC TAILORING STUDY OF A HIGH ASPECT RATIO WING . . . . .	687	D11
Kenneth E. Griffin		
ADVANCED DESIGN COMPOSITE AIRCRAFT . . . . .	711	D12
R. N. Hadcock		
A HYBRID COMPOSITE FUSELAGE DESIGN WITH INTEGRAL CRACK ARRESTERS . . . . .	737	D13
S. L. Huang and T. E. Hess		

SESSION IVB - DESIGN TECHNOLOGY BASE

Chairman: Edward J. McQuillen  
Naval Air Development Center

BATTLE DAMAGE TOLERANT WING STRUCTURAL DEVELOPMENT . . . . .	759	D14
Ken deBooy		
LIFE ASSURANCE OF COMPOSITE STRUCTURES . . . . .	779	D15
R. V. Wolff and D. J. Wilkins		
ON PROCESS ZONE INTERACTIONS IN THE WEAROUT PROCESS . . . . .	803	<del>D16</del> omit
M. Waddoups, J. Halpin, and G. Lemon		
FATIGUE OF NOTCHED COMPOSITES . . . . .	805	D16
P. V. McLaughlin, Jr., S. V. Kulkarni, S. N. Huang, and B. Walter Rosen		
FRACTURE BEHAVIOR OF NOTCHED COMPOSITE LAMINATES . . . . .	829	D17
James M. Whitney and Ran Y. Kim		
SUPER-HYBRID COMPOSITES - AN EMERGING STRUCTURAL MATERIAL . . . . .	851	D18
C. C. Chamis, R. F. Lark, and T. L. Sullivan		
ADVANCED COMPOSITES IN BURD II . . . . .	879	D19
Edward Crawley and John Wendell		



APPLICATION OF THE AIR FORCE'S NEW  
STRUCTURAL REQUIREMENTS TO COMPOSITES

By

Gary K. Waggoner  
Aeronautical Systems Division

SUMMARY

The new requirements, contained within the Air Force's approach to achieving structural safety and durability in military aircraft, are reviewed. The approach to be taken, when qualifying and certifying structures made from composites, is described. While structures made from composites can be qualified and certified to these requirements, it appears that the limited state of the technology today in predicting life and residual strength under combined service loading and environmental effects will result in increased test requirements over that normally anticipated in qualifying and certifying metal components. This points up the need for significant advances in the understanding of life limiting factors in composites coupled with the development and validation of analytic tools to predict behavior under real life conditions.

INTRODUCTION

Within the last five years, significant changes have occurred in the Air Force philosophy toward achieving structural safety and durability in military aircraft. The necessity for these changes became evident when a number of Air Force systems began experiencing unsatisfactory service histories in terms of both safety of flight problems and unacceptably high maintenance costs. These problems were an indication that the requirements which were used to insure structural integrity throughout the life of the system were not completely adequate. Therefore, a complete revamping of the requirements was begun to eliminate those requirements that did not work, to minimize arbitrary requirements, and to develop new requirements which addressed the specific causes of the problems. Reference 1 presents an excellent summary and discussion of the rationale behind the revisions that took place.

Basically, the new requirements are geared to the development of a structure that is capable of accommodating flaws induced either in manufacture or in service (damage tolerant), in addition to having an economic life in excess of the design usage life (durable). In addition, a force management program has been defined in order to maintain

structural integrity by tracking actual service usage and determining individual aircraft inspection and maintenance times, based on that usage.

#### MIL-STD-1530A REQUIREMENTS

The basic elements of the revised requirements are presented in a document entitled Aircraft Structural Integrity Program, MIL-STD-1530A. This standard identifies five tasks to be accomplished during the development and use of an airframe. These tasks are as follows:

**TASK I - DESIGN INFORMATION** - defines those actions involved in bringing the appropriate criteria and planning to bear on an airframe design so that the specific operational requirements will be met. This task begins as early as possible in the conceptual phase and is finalized in subsequent phases of the airplane life cycle.

**TASK II - DESIGN ANALYSIS AND DEVELOPMENT TESTS** - encompasses the work necessary to determine the environments in which the airframe must operate (load, temperature, chemical, abrasive, vibratory and acoustic environment) and to perform preliminary analyses and tests based on these environments to design and size the airframe to meet the required strength, damage tolerance, and durability requirements.

**TASK III - FULL SCALE TESTS** - assists in determining the adequacy of the structure in meeting the basic design requirements through a series of ground and flight tests. These tests include static, durability, damage tolerance, ground and flight operations, sonic durability and flight vibration and flutter.

**TASK IV - FORCE MANAGEMENT DATA PACKAGE** - describes the minimum required elements of a data package which the contractor shall provide so that the Air Force can maintain structural integrity of the force during actual service usage. Basic elements of this package include the final updated analyses, development of inspection and repair criteria, an initial and an updated force maintenance plan, and a plan for individual and force tracking procedures geared toward providing actual service usage data.

**TASK V - FORCE MANAGEMENT** - describes those actions that must be conducted by the Air Force during force operations to ensure the damage tolerance and durability of each airplane. The objective is to determine adjusted times at which the force structural maintenance actions must be performed on individual aircraft and each critical area thereof. This task is primarily the responsibility of the Air Force and will be performed by the appropriate commands utilizing the data package supplied by the contractor in Task IV with the minimum amount of contractor assistance.

As stated previously, each of these tasks are pointed toward developing and maintaining a structure which exhibits an adequate level of damage tolerance and durability. Within the program just described, the general procedure to be taken in arriving at a damage tolerant and durable design is described below.

#### DAMAGE TOLERANCE

The specific requirements and procedures for achieving damage tolerance are defined in MIL-A-83444 and MIL-A-8867B and are based on the design concept selected (slow crack growth or fail safe) and upon the level of inspectability of the structure (6 categories ranging from in-flight evident to noninspectable.) Then, for any given design concept and level of inspectability, it is assumed that specified defects (flaws) exist within the structure as it comes off the assembly line. These assumed defects are based on those types and sizes that have been found to escape detection by good NDI methods commonly employed by airframe manufacturers. The defects are then grown by analytic techniques and actual tests to demonstrate that the structure, at any time within a specified service usage interval, will possess an adequate residual strength capability.

Throughout this process, a controlling document called a damage tolerance control plan is to be developed and maintained to identify all of the tasks to be accomplished in meeting the damage tolerance requirements. It includes the development of a fracture critical parts list, the inspection, process control and quality control procedures necessary to verify the initial defect type and size assumptions and identification of all analysis and testing that is to be performed within the program.

#### DURABILITY

The specific requirements for durability are contained in MIL-A-8866B and MIL-A-8867B. They require that a disciplined procedure for durability design be instituted to minimize the possibility of incorporating adverse residual stresses, local design details, materials and processes, etc, that could lead to early maintenance problems or uneconomic service experience. In addition, analyses are to be conducted which account for factors affecting the time for production variables (defects) to reach repair sizes such as: initial quality and variations, environment, load sequence and environmental interactions, and material property variations. If various protection systems are used in the design they must be shown to provide acceptable endurance for one design lifetime under the chemical/thermal environment which the structure will see in service. Finally, design development tests are required to verify the analytical predictions.

These, then, are the basic requirements and methods by which the Air Force develops airframe components which will exhibit adequate damage tolerance and durability.

#### APPLICATION OF REQUIREMENTS TO COMPOSITES

APPROACH. In addressing the application of these requirements to composites it is determined that the basic requirements contained within MIL-STD-1530A must be maintained. It must also be stated that the procedures which must be employed in qualifying, certifying, and managing components made from composite materials to these requirements are in a state of development at the present time. Therefore, the discussion that follows describes the procedures which are determined necessary based on the level of the technology (data base, analytical capability, and service experience) at this point in time. It appears that the static design capability within the industry is quite well in hand although this capability can vary significantly from one company to another. However, it is felt that in the area of life and residual strength prediction capability a technology deficiency exists. This deficiency will impact the qualification, certification, and force management portions of the overall program.

LIFE AND RESIDUAL STRENGTH PREDICTION CAPABILITY. A data base presently exists on a number of individual factors which affect the strength and stiffness behavior of the material. We have, for example, information on the creep behavior of the material, both wet and dry, as well as the wet and dry static strength behavior of the material with temperature. We also have fatigue information on wet and dry laminates. However, the majority of the data that is available is basically tension-tension fatigue with very little information available for either fully reversed cycling or compression-compression fatigue with a wet (pre-soaked) material. Moreover, we do not have a sufficient data base on the fatigue behavior of the material under real time flight-by-flight load/environmental service conditions, nor do we have a validated analysis capability to take the bits and pieces of data we do have from individual effects and combine them in some sort of an analytic prediction method. In addition, a number of questions have been raised within recent months concerning moisture distribution effects, possible dimensional changes due to moisture absorption, and the effects of revised service usage, about which limited data exists today and which therefore cannot be easily dismissed. With the current state of the technology it appears that in order to predict life or residual strength, an empirical method must be employed; that is, tests must be conducted during the design development program which applies those conditions which are deemed to either affect life/residual strength or which pose a question for which we have no data.

RESULTS OF LIMITED AIR FORCE SERVICE EXPERIENCE PROGRAMS. Within the past six months the Air Force has been evaluating a number of service experience programs utilizing composite parts that were placed in

service some 3-5 years ago. While the success that the individual articles experienced in service is varied (in some cases, quite good and in other cases, not so good), the conclusion that can be drawn at the present time from this limited evaluation is that the qualification and certification procedures utilized within the individual development programs did not identify the life limiting factors that some of these structures would eventually see. In addition, force management procedures such as tracking actual usage and providing adequate levels of inspection and/or maintenance actions were not adequate to identify emerging problems. It therefore appears that some revisions to the approaches that have been used in the past are warranted.

I would like to briefly highlight what some of those procedures that appear to need revision are. In the qualification portion of the program emphasis has been placed upon achieving sufficient static strength and residual strength after fatigue testing to account for such things as manufacturing and processing variables and for the effects of load, environment, time, etc. Also, the factors that were shown to effect strength degradation such as moisture and temperature were not adequately simulated during the design development and verification tests. Finally, the moisture levels that were applied to the structure did not account for those moisture levels that the structure might see during its service life. In terms of certification, a standard NDI procedure was employed. However, the effects of the manufacturing and processing variables which were identified were not determined under real service conditions and therefore the validity of the results of those tests are not known. In the force management area no tracking was required to determine actual aircraft or force environmental usage. Generally, only visual inspections were called for at the depot levels, if even that was required. Moreover, the inspection intervals were not based on possible damage growth rates with environment since those rates were not determined within the certification program, nor was information available on what the actual service environment was. In looking at these procedures it appears that a number of things should be done differently in order to properly address the damage tolerance and durability questions which must be answered in moving toward satisfying the requirements. The approach that will be described has been developed by comparing MIL-STD-1530A requirements with the current state of the technology and determining appropriate procedures which are necessary to meet these requirements.

#### CURRENT APPROACH TO QUALIFICATION, CERTIFICATION, AND FORCE MANAGEMENT.

It appears that the following should be accomplished: (a) A more extensive design development and test program which will account for service environmental effects on design details and production variables; (b) Possibly a more extensive full scale durability test program; (c) An individual article certification procedure which will account for the variables which may be introduced into production articles and which will determine the effects of these variables on stiffness and

strength degradation with actual service usage; (d) A force management program that will adequately track critical factors which have been determined to affect structural life and which will define inspection and maintenance requirements based on the known production variables and damage growth rates under the actual service usage conditions.

I will discuss each of these areas of revision in more detail.

QUALIFICATION PROGRAM - DESIGN DEVELOPMENT. During the design development program a design analytic spectrum should be developed based on the specified usage which accounts for such factors as load, time, and environment. Coupon and element tests should then be conducted to define which parameters of the analytic spectrum affect structural life and residual strength. The results of these tests are to be used in determining a final test spectrum which will be applied throughout the remainder of the program. Using this test spectrum, subcomponent and component tests should be conducted to determine the strength and stiffness degradation behavior of all critical structural details and production variables. Specifically, we are looking at the development of these strength behavior trajectories for design details which are determined by the contractor to be critical, such as joints (both mechanically fastened and bonded), areas of minimum margin, and possible matrix sensitive areas such as those areas subjected to compression, shear, bearing, and out-of-plane loads. In addition, the effects of production variables resulting from incoming materials, processing, manufacturing, and assembly operations which have been determined to exist in production hardware based on program, quality control, and NDI procedures employed shall be determined utilizing this final test spectrum.

QUALIFICATION PROGRAM - FULL SCALE DURABILITY TESTING. In the area of full scale durability testing there are two main overall objectives which need to be met. These are: (1) the identification of "hot spots", or areas of unexpectedly high stresses within the complete structure; and (2) the demonstration that the economic life of the airframe is greater than the required life. The test article(s) to be used for this program may be the complete aircraft airframe, or it may be separate components of that airframe. In either case, an early full scale development or RDT&E article is to be tested. The test spectra to be imposed shall be a flight-by-flight spectrum coupled with the degree of service load/environmental simulation which has been determined to be necessary from the design development program. That is, the full service conditions must be applied if significant questions still exist after the design development program to warrant their inclusion in the test (inadequate completeness in number or types of tests or test conditions; confusing results; undesirable effects; etc.)

However, in this type of testing the desire always exists to minimize the overall test costs by truncating as many parameters as

possible without affecting the ability to reach the objective. In order to determine the allowable level of truncation the rationale of Figure 1 must be applied. In order to truncate a given parameter, the effect of that parameter on the structure must be fully defined in terms of its either having no effect, or that the effect can be predicted and accounted for in the results obtained. It is only when these conditions are met that a parameter can be truncated.

The test duration is to include a minimum of two lifetimes unless the economic life is reached prior to that point in time. If the economic life is not reached within the first two lifetimes, an option is to be provided for the Air Force to conduct additional lifetimes of testing, if desired.

The schedule requirements for this test provide for the completion of one lifetime prior to production decision and two lifetimes prior to the delivery of the first production aircraft.

At the completion of the fatigue testing it is a requirement that functional checks be performed on the article to indicate any change in its operational capability. After completion of these checks it is felt that more information may be gained by conducting additional tests other than the residual strength test which currently is common practice. Consideration should therefore be given to conducting such tests as service damage and repair tests, damage tolerance tests, and fail safe tests. At the completion of all testing a detailed inspection is to be conducted on all design details to identify damage not found during normal test inspections.

INDIVIDUAL ARTICLE CERTIFICATION. The objective of this program is to assure that variables (in materials, processing, manufacturing, and assembly) which could result in structural failure or loss of functional capability prior to the required design life will not be introduced into service. Therefore, regardless of the method of certification chosen, the allowable acceptance limits on production variables must be defined and their effect on life and residual strength with actual service usage established. This requires that strength degradation trajectories be developed for each failure mode which is present within the structure. Again, with the current state of the technology, this must be established primarily by test. The actual variables which must be tested are based on the level and type of NDI which the program is utilizing and which may escape detection. Based on the results of those tests the contractor has a number of options (See Figure 2) by which he may certify a structure. If the strength degradation trajectories show that adequate residual strength exists after the required usage interval, the method used to establish the initial variation level is adequate for the full service usage interval. If, however, the inspection used to establish the initial level allows variables to exist in the structure which will provide inadequate residual strength for the full

lifetime, the certification concept will require either in-service NDI or an in-service proof test in order to adequately maintain structural integrity.

FORCE MANAGEMENT. The objective of this program is to maintain the overall force structural integrity by determining the actual aircraft usage and by taking appropriate maintenance actions at the required times. There are two portions to this overall program. The first is the establishment of overall force maintenance estimates based on actual service usage. The information is used for force maintenance planning purposes in terms of scheduling and budgetary requirements. This portion of the program requires that the contractor develop a plan which will provide for the tracking of parameters that are determined to significantly affect structural life. This information is then to be utilized in developing a "baseline operational spectra" which in turn is used to develop revised maintenance times and actions (revised maintenance times from those specified at the conclusion of the development program which were based on the design usage spectra.) The updated force structural maintenance plan specifies the when, where, and how for actual force inspection and modification requirements. As in previous portions of the overall program our capability to analytically predict life and residual strength capability forces us into a test mode to determine revised maintenance times.

The second part of the force management program is the individual aircraft tracking program which results in individual aircraft inspection and maintenance times. It is this portion of the overall program that actually maintains the structural integrity of each aircraft in the force. It is analogous to the overall force maintenance plan with the exception that each airplane usage is now tracked and appropriate maintenance actions for each individual aircraft are developed. It is in this area that we foresee a relatively large impact due to the lack of a validated analysis capability. In the normal determination of revised inspection and maintenance times we now have each airplane in the fleet flying to a different spectrum and we must determine individual aircraft actions based on each different flight usage. Since running tests for each aircraft usage is impractical, we will be required to conduct tests based on the most severe and least severe usage, and then interpolate between the two for every other aircraft in order to plan for the required actions.

#### CONCLUSIONS

The foregoing has discussed those procedures and actions that are determined to be necessary in qualifying, certifying, and managing airframe structures made from composite materials. It is our belief that the composite structures today can be adequately designed, developed, and managed in order to allow them to be put in the Air Force inventory today. However, a rather cumbersome test requirement



appears necessary on any development program at this point in time due to the limited data base and life prediction analysis capability that exists today.

At the present time, there are a number of laboratory programs addressing numerous areas of deficiencies and the data base in these areas is expanding very rapidly. There is still, however, a great need for research and development programs to address the many questions which exist in the areas of: life limiting factors in composites; manufacturing, and processing procedures to minimize variables; NDI procedures for bonded structures; development and verification of life and residual strength analysis methods; and the development of environmental test procedures.

The goal in addressing and answering these questions is to improve the data base, analytic capability, and our understanding to the point that improved procedures to meet qualification, certification, and force management requirements may be developed in the very near future.

The answers to these questions will not come easily, or by themselves, but will only become available through a dedicated, coordinated effort on the part of industry and the government.

#### REFERENCES

1. "New Air Force Requirements for Structural Safety, Durability and Life Management", by M. D. Coffin and C. F. Tiffany - AIAA Paper 75-781.

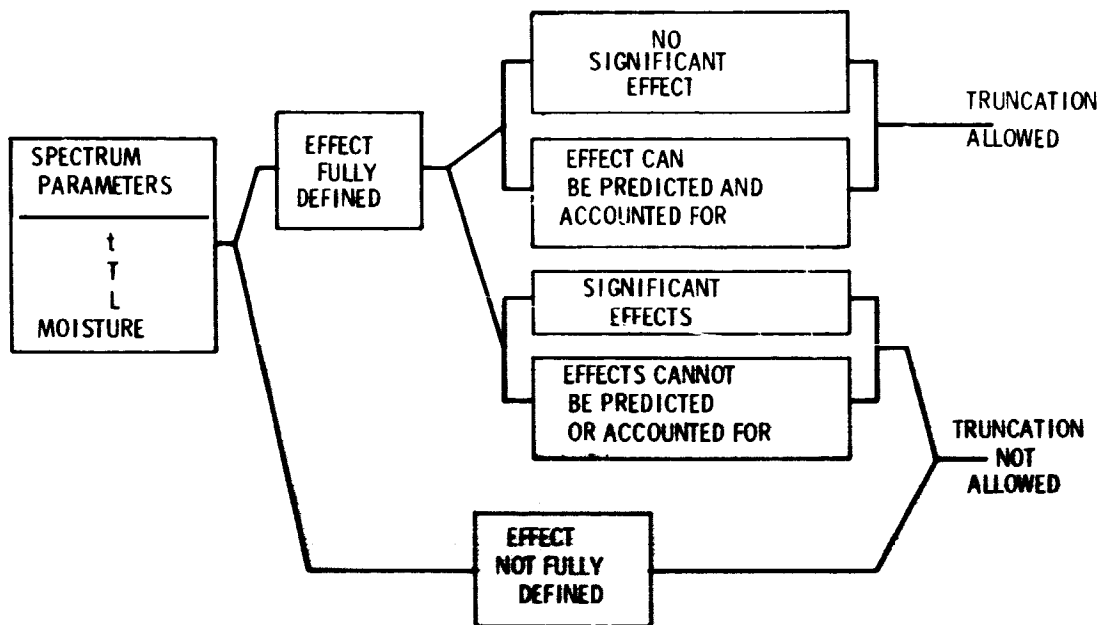


Figure 1.- Full scale durability test determination of allowable truncation level.

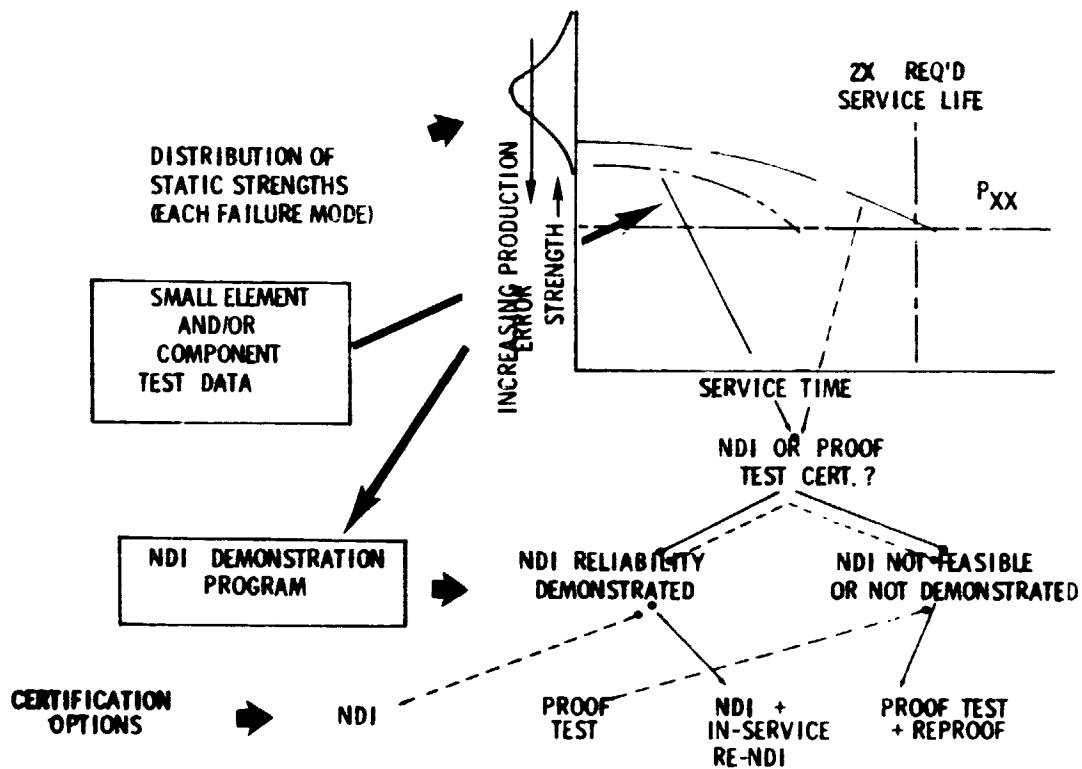


Figure 2.- Certification options.

# CERTIFICATION REQUIREMENTS FOR CIVIL COMPOSITE

## COMMERCIAL AIRFRAME STRUCTURES

By James E. Dougherty, Jr.

Federal Aviation Administration

### SUMMARY

This paper discusses the regulatory implications associated with the use of fibrous composite materials in civil aircraft primary structures. It briefly reviews the applicable requirements. It highlights some of the major problems confronting the FAA when such materials are used extensively throughout primary structures. The paper summarizes the current thinking of the FAA in regard to how best such arrangements could be accepted for use in civil aircraft. It recognizes that further inputs from the aviation industry are needed to assure uniform development and application of such requirements.

### INTRODUCTION

As you know, the FAA has certificated advanced composite secondary structure for use in commercial service in recent years. Although the service history has been relatively short, the experience to date with these structures has been good.

With the award of the advanced composite vertical fin contract by NASA Langley Research Center and the anticipated application to a complete wing and to a pressurized fuselage, the aviation community is on the threshold of a new technology application - advanced composites in aircraft primary structure. Advantages such as strength to weight ratios, cost and fuel savings warrant careful assessment by all in order to make certain that this new technology can assure a structural integrity equal to or better than the level provided by current structures fabricated from state-of-the art and non-metallic materials.

There is a need to utilize aircraft to accumulate large numbers of hours of normal service to produce a broad base of data and experience to increase producer's and user's confidence in advanced composite structures. In this process it is essential to assure that any new materials, such as advanced composites, will not introduce features hazardous to the operational safety of the aircraft involved - whether commercial or military.

Herein are discussed current FAA thoughts on the certification basis of advanced composite primary structure in commercial aircraft. They are predicated on use of the current effective issue of FAR 25\* to the maximum extent

\* Federal Aviation Regulations, Part 25, "Airworthiness Standards - Transport Category Airplanes."

practicable. When deemed necessary these standards are adapted to cope with unique problems of design, fabrication and operation.

Where necessary, special conditions may be required. Several are proposed in the Appendix of this paper. The guidelines discussed herein, in conjunction with FAR 25, are therefore proposed as the certification basis for advanced composite primary structure employed in transport aircraft. The special emphasis on "proposed" and "tentative" is deliberate on our part as it is necessary to explore further with the industry on the exact terminology to set forth.

As part of the overall aircraft safety record, there has been a constant increase in the reliability of safety of aircraft structures. Composite primary structure would, therefore, be expected to meet a level of safety at least equivalent to its metallic counterparts at the time of certification.

### MATERIAL AND FABRICATION DEVELOPMENT

The objective in developing materials, processes and joining methods for primary advanced composite structure is to concentrate on those formulations which will result in an efficient structure that provides adequate strength, reliability, and service life. The selection of materials and processes, including joining for tension-loaded primary structure, is dominantly controlled by weight, cost, and service life considerations. A primary factor in the final selection should be the results of the design concept/material/weight/cost tradeoff studies performed as an initial part of the fracture and fatigue control program. Problem areas peculiar to advanced composites should be addressed early in the design development phase of the program, resolved by analytical methods, and verified by coupon and subcomponent testing.

Before testing and analyses are done the material composition and material processing are to be defined to the degree needed to provide a basis for producing a reproducible and reliable structure. Process specifications are especially critical for composite materials.

Absorption and saturation levels of water vapor in the composite matrix and/or adhesives must be determined. Absorption and saturation studies should conservatively reflect service lifetime and usage conditions. The effect of water absorption to the anticipated saturation level, upon design allowable stiffness, strength, and fatigue/residual strength changes and the engineering properties at elevated temperatures need particular attention. Emphasis should be also directed to the potential impact of moisture and temperature on mechanical and/or adhesive joint allowables, both in static and cyclic loading modes.

Subcomponent tests conducted should employ the primary load transfer region (mechanical and/or adhesive). The specimens should be tested statically in a humid environment and to an environmental/fatigue history. The performance of the subcomponent static and fatigue tests should provide initial information on the expected failure locations and/or modes. An analytical methodology supported by extensive testing is needed to assess the occurrence and/or growth

of bonding defects, cracks and other damage in composite structure in the environmental and cyclic stress environments to which that portion of the component is expected to be subjected in service. Once the damage growth rates and acceptance limits are determined, the inspection, repair, or replacement time can be estimated. It will be essential to develop reliable non-destructive testing methods. Experimental studies are needed on the impact of quasi-real time/environmental fatigue history versus the traditional accelerated fatigue history. Studies should emphasize coupon size test specimens of typical joining modes, mechanical and/or adhesive. This evaluation should include examination of residual static strength changes and, where possible, fatigue life. Tests should be repeated to establish characteristics on a statistically sound basis.

The maximum allowable defects (voids, etc.) permitted by process specifications should be established by test and analysis in order to show adequacy for the fatigue/fail-safe/residual strength requirements. Production components should receive 100% inspection to assure that process specification limits are adhered to.

#### PROOF OF STRUCTURE-GENERAL

Analysis and specimen, subcomponent, and full-scale tests are the normal methods for proof of structure. All of these methods are typically used in a major program but in the case of advanced composites, all may be required to provide adequate substantiation. Analysis provides a practical method to evaluate the many loading conditions and failure conditions not tested and to determine the conditions to be tested. Analysis also provides assurance (where test verification is not practical) that all parts will have adequate strength. Specimen testing provides the opportunity to evaluate many variables including the variation between specimens.

However, due to the complexities and uncertainties involved, full-scale and subcomponent static and fatigue tests of the primary structure are needed. Subcomponent testing provides a practical method of evaluating environmental effects, the variation of strength between specimens, the location of the more obvious failure modes, and the growth of partial failures. The full-scale testing assures that all critical structure is tested and that test loading and environment is realistic. There is some indication that variation of strength between individual structure may be greater in composites than conventional structure. Strength scatter should be established by component testing. Ultimate static tests and the scatter factors used in conjunction with fatigue testing should take into account strength scatter effects.

#### PROOF OF STRUCTURE-STATIC

Ultimate load static test - original and residual strength determination -

Experience with regard to several complete aircraft test programs indicates that major components on some aircraft have experienced major test failures under loads less than design ultimate. For advanced composite primary structure,

the methods of (1) establishing material allowables, (2) analysis of different types of construction, and (3) assessing effects of environment, will be somewhat comparable to past practice. However, reliance on these procedures to substantiate structures, either by analysis only or by analysis and limit load tests, is questionable since new materials, new fabrication means, new configurations, and new environmental effects will make dependence on current methods less reliable. Therefore, a comprehensive static test program to ultimate strength is considered essential.

Tests of laboratory specimens and service articles have indicated that water (or water mixed with fuel) absorption in the matrix reduces static strength and that repeated loads usually reduce but may under some conditions increase static strength. Consequently, it is believed that ultimate full-scale static tests should be performed after fatigue testing in a humid environment unless the effects of water absorption can be predicted reliably with subcomponent tests. This suggests sufficient subcomponent static tests should be performed on both static and fatigued articles in humid/dry environments to determine humidity effects, the variation of strength between specimens, and to assure that static testing after fatigue test is conservative.

#### Proof load test requirements -

Current nondestructive inspection techniques are inadequate for detecting weak bonded joints. Also in initial production, there is a significant chance of a void or other defect existing and a possibility of not detecting it in production inspection. Therefore, proof testing is considered necessary where bonding is used in primary structure or where ample static margins are not provided for ultimate loads with the maximum defect permitted by inspection. In such cases each full-scale production article should be proof tested to limit load under the critical design condition during initial production run or whenever drastic changes are made in production methods. The proof load should be adjusted to cover the expected environmental degradation over a service lifetime and any increase in material or component strength scatter over that of conventional structures. The proof test will ensure that the structure will not enter service without sufficient strength to withstand the maximum load expected in service.

#### PROOF OF STRUCTURE - FATIGUE

The present fatigue requirements, FAR 25.571, provide for either a fail safe or safe life approach in establishing the fatigue strength of the flight structure. Current jet transport fleets have been designed using the fail safe approach for the flight structure. This design concept, in conjunction with inspection procedures, has proven effective. The safe life approach primarily considers only the classical fatigue failure concept. It does not directly account for damage or structural deterioration due to other causes or circumstances. Furthermore, it is extremely difficult to assure that fatigue cracking of the structure will not occur in service or to predict where it will occur. It is therefore contemplated that the fail-safe concept would continue to be used in advanced composite design.

The desired objective is to assure that the primary structure is capable of supporting the expected environmental/repeated loads and design limit loads in a humid environment after an obvious partial failure. It is believed that the environmental effect on the composite matrix and/or adhesive is of sufficient magnitude to justify including it in the repeated loads test.

The present fatigue requirements, FAR 25.571, do not specifically provide that the structure must support environmental/repeated loads after obvious partial failure. The structure is, in fact, exposed to environmental/repeated loads after each partial failure until failure is detected. Therefore, it is believed that the structure should be capable of supporting such repeated loads until the partial failure can be detected in lieu of assuming that residual static strength requirements will provide the needed strength. Also, it is believed the structure should remain capable of supporting limit loads in a humid environment after partial failure since they are the maximum loads expected in service and may be imposed, especially if the inspection period is long, or if the partial failure occurs in severe turbulence. Further, this larger fail-safe load may be needed with advance composites because it is more difficult to predict the extent of fail-safe damage and the strength of the partially failed structure. While the proposed guidelines do not include a dynamic magnification factor on fail-safe loads, they would require that the design limit be supported under realistic partial failure conditions. Thus the fail-safe evaluation would involve a determination of probable failure areas by fatigue tests on subcomponent and full-scale articles. The residual fatigue and static strength would then be demonstrated with obvious partial failures in the probable failure areas and in other critical areas. The residual fatigue strength would have to be sufficient to provide assurance that the partial failure would be discovered with the inspection program. An obvious partial failure would usually consist of complete failure of one element but may involve partial failure of an element, or complete failure of several elements depending on the nature and location of the failure and the type of inspection contemplated but, in any case, it should be obvious during the planned inspection.

It is expected that new failure modes associated with advanced composites will require special inspection method. The planned inspection method should, therefore, assure detection with a high degree of confidence.

A full-scale fatigue test is needed and must be performed to unearth all failures that would occur in a fleet with the predicted variability of fatigue strength and loading spectrum under the expected environment such as described in AFML-TR-74-174 "Joint Aircraft Loading Structure Response Statistics of Time to Service Crack Initiation." In this regard, the period of the full-scale fatigue test should be at least two lifetimes predicated on civil operational spectra. Higher factors but not to exceed four lifetimes may prove necessary as the test program evolves. The fatigue test should include application of a conservative loading spectrum in a humid environment, simulating actual flight vehicle usage in a realistic flight-by-flight sequence of loading. For each failure location it must be shown by full-scale or subcomponent testing that the structure with an obvious partial failure will support the expected repeated loads and design limit load until detected by the planned inspection program.

Residual strength determination should be made on the full-scale fatigue test article, under a humid environment. The residual strength so determined should be equal to or greater than the critical ultimate static load adjusted for material scatter, component static strength scatter, and any environmental degradation determined in the material and subcomponent tests which is not included in the full-scale fatigue tests. The regulations state that the structure shall be able to sustain ultimate static load throughout a service lifetime. This residual strength, then, is the strength level that the article must be able to sustain with deterioration present without endangering safety of flight or degrading performance of the article for a specified minimum period of unrepaired service usage. This includes loss of strength, loss of stiffness, excessive permanent deformation, or loss of control.

A minimum of ten coupon specimens should be trimmed off the full-scale fatigue test article in the predicted failure location during fabrication. These specimens should be statically tested to determine where in the static structural distribution (determined from prior coupon and subcomponent tests) the fatigue test article is situated. The material scatter can then be determined as being the difference between the fatigue test article static strength and the material "B" allowable providing the specimen is part of a redundant structure in which the failure of the element would result in the load being safely distributed to other load-carrying members.

#### SPECIAL REQUIREMENTS

As part of the function of the structure, crashworthiness aspects should be considered. Assessment of composite capability to contribute to safety under crash conditions is needed, including consideration of energy absorption and fire characteristics.

Boron and graphite filament organic matrix composites are susceptible to lightning damage and do not dissipate P-static electrical charges nor provide electromagnetic shielding. Test evidence should demonstrate that advanced composite-faced honeycomb or laminated structures have been provided with lightning strike protection for levels of intensity expected in service. Galvanic and other interactions between the basic structural material and materials added to cope with electrical charges should be part of the long-range reliability assessments.

The environmental spectrum for this installation must consider random occurrences such as hail and foreign object impacts as well as the long-term effects of factors such as aging, humidity, erosion, ultraviolet radiation, thermal and chemical deteriorations. This should take into account the effects of glycol, hydraulic fluid, fuel, and other generally used agents.

To insure successful application of advanced composite structure, it is essential that a quality assurance program be established to provide a consistently sound structure. Quality control inspection requirements are numerous. Incoming raw materials must be inspected for conformance to material



specifications; in-process quality control must be established for conformance to processing specifications in the fabrication of the composite material; and, as a final check, some combination of destructive/nondestructive and proof testing of the finished material must be scheduled. Further tests are then required to inspect structures fabricated from composite materials. Sufficient testing of raw material must be performed to establish material uniformity from batch-to-batch and within specific individual batches.

#### CONCLUDING REMARKS

Advanced composite material development has progressed considerably; however, there are several problem areas which must be addressed and resolved. Related aspects to consider in finalizing this basis include the following:

1. Structural reliability is equal to or better than conventional designs in use today.
2. Extensive evaluations of the material properties is needed to statistically establish minimum design allowables covering a wide range of properties.
3. For large structural components, special emphasis must be directed to:
  - a. Humidity effects
  - b. Fuel wetting
  - c. Adverse chemical composition effects
  - d. Lightning protection
  - e. Elevated temperature effects
  - f. Hail and ablation
  - g. Reproducibility of fabrication processes and quality controls
  - h. Static tests to ultimate
  - i. Fatigue evaluations under fail-safe and life concepts
  - j. Inspectability of structure
  - k. Detail design of load transfer areas and fittings.
4. Extensive service experience is needed. The means whereby this is attained must be identified.
5. Development of reliable non-destructive testing methods is essential.

It is realized meetings of this type go a long way towards clarifying some of these issues, but well before major components such as the tail, wing, or pressurized fuselage are put into commercial service a fuller understanding of this new technology is needed. It is contemplated therefore, that the exact certification basis will be an evolutionary program over the next decade, with need for periodic meetings between the FAA and key aviation specialists to further define the certification basis.

#### ACKNOWLEDGEMENT

The author wishes to acknowledge, with thanks, the assistance given by Messrs. Joseph Soderquist, Fred Doering, and Arnold Anderjaska in the preparation of these proposed standards.

## APPENDIX A

### Tentative Special Conditions

#### 1. Add New FAR 25.307(e)

For advanced composite primary structure, a program of ultimate tests performed in a humid atmosphere, which validates the original and residual strength for the major design loading conditions, is required. Supplemental tests are required to the extent and level necessary to validate the methods of analysis used for conditions and areas not tested. Where a program of subcomponent static tests in a humid atmosphere on new and environmentally fatigued structure demonstrates that it is more critical to perform the ultimate static test on the fatigued article, the full scale ultimate load static test on the new structure may be waived.

#### 2. Add New FAR 25.307(f)

For advanced composite primary structure, a production proof inspection plan shall be established. The magnitude of the proof load employed shall be that of the critical design limit load condition adjusted to reflect material and component scatter, and the expected environmental repeated load degradation over a service lifetime.

3. For transport aircraft utilizing advanced composites in primary structure, the following applies in lieu of FAR 25.571 and FAR 25.573:

##### a. Fatigue and Fail-safe Characteristics:

The strength and design of the primary structure must be adequate to insure that the catastrophic failure in the service environment under the expected repeated loads is extremely improbable. Primary structure consists of that portion of the structure, failure of which could be catastrophic.

##### b. Fatigue Evaluation Procedure:

It must be shown by analysis, environmental repeated load tests, and static load tests (performed in a humid environment) that the primary structure, in conjunction with the inspection program, meets the provisions of paragraph a. The probable failure locations must be determined by fatigue tests in subcomponent articles. The loading and environmental spectra used in these tests must be representative of critical types of operations. The effects of maneuvers, ground-air-ground cycles, gusts, landing and taxiing pressure and temperature cycles, moisture absorption, weathering, aging, fluid exposure (skydrol, anti-icing), sump water and other pertinent environmental effects must be included in spectra, if significant. The expected static strength dispersion of the composited structural components shall be determined from these tests. All primary structure must be evaluated to show compliance with paragraph a in accordance with (1) and (2).

(1) It must be shown that adequate residual strength is provided to assure that any obvious partial failure will be detected before a hazardous condition develops. This involves showing that the structure remains capable of supporting the expected repeated loading, temperature and environmental spectrum, and critical design limit loads in a humid environment without catastrophic results during the period after any obvious fatigue failure or partial failure has progressed to obvious proportions and prior to detection by inspection.

(2) The durability of the structure shall be verified by a full-scale fatigue test, in a humid environment, the period of which shall be at least two lifetimes and for as much as four lifetimes unless shown to be inappropriate by the results of the overall test program. Fuel or a fluid of similar chemical constituency shall be included in the test if applicable. The structure shall be able to withstand the repeated loads of variable magnitude of a typical loading spectrum expected in service. In the substantiation of the pressure cabin by fatigue tests, the cabin, or representative parts of it, must be cycle - pressure tested, using the normal operating pressure plus the effects of external aerodynamic pressure combined with the flight loads. The effects of flight loads may be represented by an increased cabin pressure or may be omitted if they are shown to have no significant effect upon fatigue. Upon completion of the fatigue test, a residual strength determination shall be made by conducting a static test employing the critical static design condition, on the full scale fatigue test article, repaired for obvious defects. The residual strength test shall be performed in a humid environment to failure or to achievement of the residual strength goal. The residual strength goal is defined as the ultimate static design load adjusted upward for material scatter, component static strength scatter, and any environmental degradation determined in the material and subcomponent tests which is not included in the full scale fatigue test.

(3) It must be shown by tests, by analysis, and supporting tests, or by the service history of airplanes of similar structural design and sonic excitation environment, that:

(i) Sonic fatigue cracks are not probable in any part of the flight structure subject to sonic excitation; or

(ii) Catastrophic failure caused by sonic fatigue cracks is not probable, assuming that the loads prescribed in paragraph (1) of this section are applied to all areas affected by those cracks.

(4) The following apply as ultimate loading conditions:

(i) For a pressurized cabin, the normal operating pressures combined with the expected external aerodynamic pressures must be applied simultaneously with the flight loading conditions specified in paragraph (1) of this section; and

(ii) The combined pressures set forth in subparagraph (i) of this paragraph multiplied by a factor of 1.33 must be applied to the pressurized cabin without any other load.

4. For transport aircraft utilizing advanced composites in primary structure, the following addition is made to FAR 25.581:

a For advanced composites primary structure compliance with paragraph (a) of this section must be shown by analysis and tests that

(1) An acceptable means of diverting the resulting electrical current has been incorporated, so as not to endanger the airplane.

5. For transport aircraft utilizing advanced composites in design of control surfaces, the following addition is made to FAR 25.651:

a Ultimate load tests of the advanced composite control surfaces are required. These tests must include the horn or the fitting to which the control system is attached.

#### HIGHLIGHTS OF APPLICABLE REGULATIONS

1. FAR 21.16 Special Conditions
2. FAR 25.301 Loads including Flight Loads Survey
3. FAR 25.307 Proof of Structure
4. FAR 25.571 Fatigue
5. FAR 25.581 Lightning Protection
6. FAR 25.603 Materials
7. FAR 25.605 Fabrication Methods
8. FAR 25.613 Material Strength Properties and Design Values
9. FAR 25.615 Design Properties
10. FAR 25.629 Flutter
11. General Design Criteria of FAR 25 Subpart D on Protection of Structure 25.609, Accessibility provisions (25.611), Special factors 25.619 (fitting), Bird Strike Damage, 25.631.
12. Fuel tank provisions.

# FAIL-SAFE DESIGN AND RELIABILITY IN COMPOSITE COMMERCIAL AIRCRAFT STRUCTURE

by  
Dale S. Warren

Douglas Aircraft Company  
McDonnell Douglas Corporation

## ABSTRACT

A brief review of principal fail-safe and reliability considerations for incorporation of fibrous composites in commercial aircraft structure is presented. The considerations include basic philosophy and current practices in fail-safe design of metal airframes, and relevant trends in the behavior of fibrous composites. Emphasis is on maintaining the present high level of safety of primary structure of commercial aircraft.

## INTRODUCTION

Advanced composite materials offer a major structural weight reduction, and the economic and sociological significance of this saving is compounded by the energy shortage. A potential saving of 25 percent of structural weight in commercial jet transports may be expected. The resulting impact on direct operating cost (DOC) is 8 to 12 percent (for fuel at 65 cents per gallon), and perhaps even more important is a potential saving of a billion gallons of jet fuel in the U.S. annually.

At this time, it appears that only the following three significant problems stand in the way of realizing the benefits of extensive use of advanced composites in commercial aircraft structure:

1. The technology is just emerging to the level that cost-competitive applications of advanced composites are feasible. However, as utilization increases, the unit costs will decrease and projections indicate that this problem will disappear.
2. Many material problems unique to advanced composites have been solved, at least in principle. The list includes void control, machining, special test equipment, special analysis methods, alleviation of local stress concentrations, lightning strike, and self-pressurizing tooling. Presently the "last" basic materials problem is degradation due to moisture absorption. The industry is strongly focused on the moisture problem, and a practical understanding should be available soon.
3. The "last" general problem is evolution of a means to assure an acceptable level of reliability. The requirement is a level of reliability as good as current airframes, as viewed by all concerned, primarily the manufacturers, operators, financing agencies, and passengers. The following paragraphs summarize the current approach and results and describe some of the steps required to match the record of today's commercial jet transport fleet.

~~PRECEDING PAGE BLANK NOT FILMED~~

## RELIABILITY OF COMMERCIAL JET FLEET

Structural failures are a minor factor in the accident record presented in Figure 1. As recorded in the World Airline Accident Summary found in the report of the Civil Aviation Authority (CAA of the United Kingdom), only three accidents due to structural causes occurred during 20 years of jet passenger service. Two of these three are the well-known Comet accidents over the Mediterranean Sea and were the result of a previously unencountered phenomenon essentially unique to the high cruising altitude of jet aircraft. The third is listed by CAA as an "accident which resulted in substantial damage"; however, the accident actually is testimony of success in fail-safe design. An undetected fatigue crack grew to critical length, fast fracture and crack arrest occurred, and the aircraft landed safely without serious injury to passengers or crew.

CAUSE	NO. OF FAILURES
FATIGUE	3
GUST OVERLOAD	5
FIRE	5
TOTAL	<u>5</u> 13

FIGURE 1. AIRFRAME FAILURES (1954-1973) COMMERCIAL JETS - PASSENGER SERVICE (CAA)

Many factors are important to the excellent record of safety of the commercial jet fleet as indicated in Figure 2. Design, manufacturing, and inservice phases are equally important in that failure in any phase can defeat the best efforts of other phases. The single most significant factor is probably a set of design criteria compatible with the factors of all three phases.

### CURRENT DESIGN CRITERIA AND PROCEDURES

The design criteria used in commercial transport development are frequently misunderstood. The misunderstanding probably stems from the legal option to prove certificability by either fail-safe or safe-life analyses. As shown in Figure 3, the actual design criteria used today are three times redundant. For example, at significant expense as expressed by the increase in man-hours expended for tests listed in Figure 4, the DC-10 development program included the following measures:

1. Working stress levels and design details were established by development tests to provide a crack-free life of 20 years (and an economic life of 40 years). These features were verified by a full-scale fatigue test under flight-by-flight spectrum loading.

**DESIGN \***

- EXTENSIVE TEST DATA — MATERIALS, JOINTS, ASSEMBLIES
- SOPHISTICATED, PROVEN METHODS
- "FORGIVING" MATERIAL (ALUMINUM)
- LARGE TRAINED WORK FORCE

**MANUFACTURING \***

- EXTENSIVE MATERIAL/COMPONENT SUPPLY SYSTEM
- LARGE TRAINED WORK FORCE
- ELABORATE AUTOMATIC EQUIPMENT
- EFFECTIVE QUALITY CONTROL

**IN-SERVICE \***

- STANDARD INSPECTION/REPAIR PROCEDURES
- LARGE TRAINED WORK FORCE
- \* COMPATIBLE DESIGN CRITERIA

FIGURE 2. FUNDAMENTAL STRUCTURAL RELIABILITY FACTORS

1. CRACK-FREE FOR ONE LIFETIME
2. DETECTABLE CRACKS
3. SLOW CRACK GROWTH
4. FAIL-SAFE

FIGURE 3. CURRENT COMMERCIAL AIRCRAFT CRITERIA (REDUNDANT STRUCTURE AND REDUNDANT CRITERIA)



	<u>DC-8</u>	<u>DC-9</u>	<u>DC-10</u>
<b>MATERIAL PROPERTIES</b>	20	---	34
<b>DEVELOPMENT TESTS</b>	670	74	429
<b>COMPONENT TESTS</b>	250	118	196
<b>FULL-SCALE TESTS</b>	460	262	1866

**FIGURE 4. DOUGLAS COMMERCIAL JET STRUCTURAL TEST PROGRAMS (APPROXIMATE COST IN THOUSANDS OF MAN-HOURS)**

2. Extensive development testing was conducted to establish tapers, scallops, and fastener patterns in multilayer built-up joints so that the critical sections are in outside elements of the joints, thereby providing excellent inspectability. In addition, the cracks that developed during the full-scale fatigue test were monitored and cataloged to provide guidance for inservice inspections.
3. Based on tests of coupons, panels, and sophisticated components, materials and stress levels were selected to ensure crack growth rates that are slow relative to standard intervals for inspection of commercial passenger aircraft. Predicted rates were verified by monitoring crack growth during the full-scale fatigue test.
4. Materials, stress levels, reinforcement schemes, and fastener methods were selected on the basis of extensive development testing to assure fail-safe strength. The fail-safe performance of the final design was verified by realistic testing of sophisticated subcomponents representing the final design.

#### UNIQUE FEATURES OF COMPOSITE MATERIALS

Most material changes which have occurred within the recent history of aviation have been evolutionary as the aircraft industry progressed from one aluminum alloy to another. These material changes were readily accommodated within the existing criteria and procedures, and, in general, changes in criteria did not result from material changes. Advanced composite materials present a radical departure from the material systems of the past, and it is important to consider the new characteristics of the systems in order that they may be properly accommodated. The principal characteristics requiring technology advances are lack of service experience and brittle stress-strain characteristics.

The lack of service experience results in a general lack of specific knowledge concerning the susceptibility to damage from the service environment and repair procedures for damaged components.

Figure 5 is a comparison of stress-strain data for two representative composite patterns with 7075-T6 aluminum. The curves show the complete lack of ductility in high-strength graphite epoxy. This

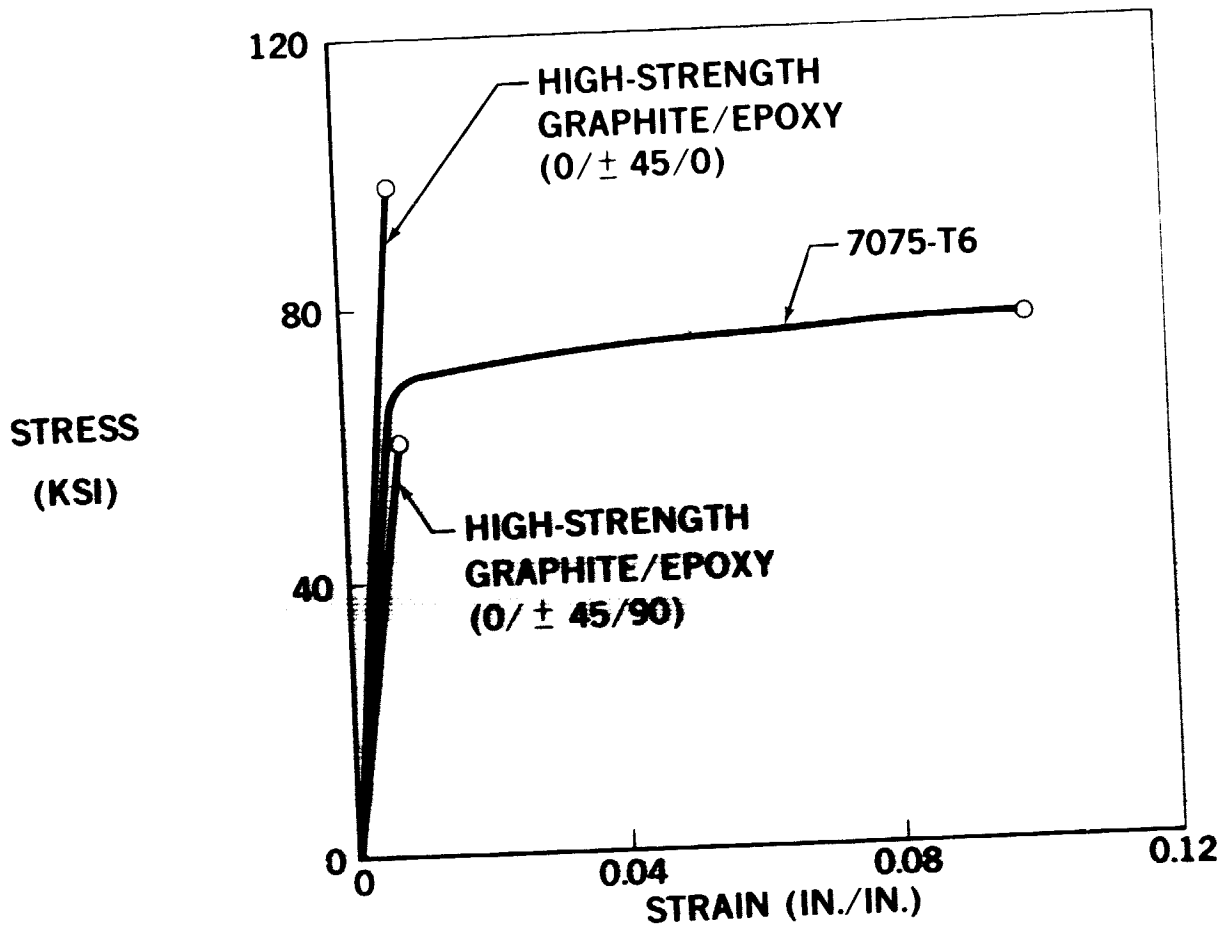


**FIGURE 5. TYPICAL STRESS-STRAIN DATA FOR ALUMINUM AND COMPOSITES**

characteristic implies the need for a far greater amount of detail in analyses required for design using composites. Current design of multifastener joints in aluminum takes advantage of nearly complete plasticity at ultimate load. In contrast, effects of plasticity are essentially nonexistent in multifastener joints using composites. Figure 6 shows a test theory correlation of the load distribution at failure in the bolts of a multifastener joint. Bolt loads were determined experimentally from strain gage data, and the load in the end bolt agrees within 7 percent of the value predicted by a linear elastic analysis. As part of the process of developing a composite design, bolt patterns, bolt size, and laminate tapering must all be very carefully established by detail design analysis for every major joint.

Figure 7 is an indication of the extreme range of options available in the selection of a laminate pattern for one advanced composite system (Thornel 300/5208). In a particular design, the structural engineer will have the choice of patterns for a particular material system and, in addition, may select blends of numerous available material systems. A high level of technical skill is required of the designer on these projects.

### **MODIFICATIONS TO CRITERIA AND PROCEDURES**

The unique characteristics of composite materials lead to the conclusion that more extensive modifications in criteria are necessary than was the case for material changes of the recent past. The lack of service experience causes major difficulties in establishing criteria that will result in composite

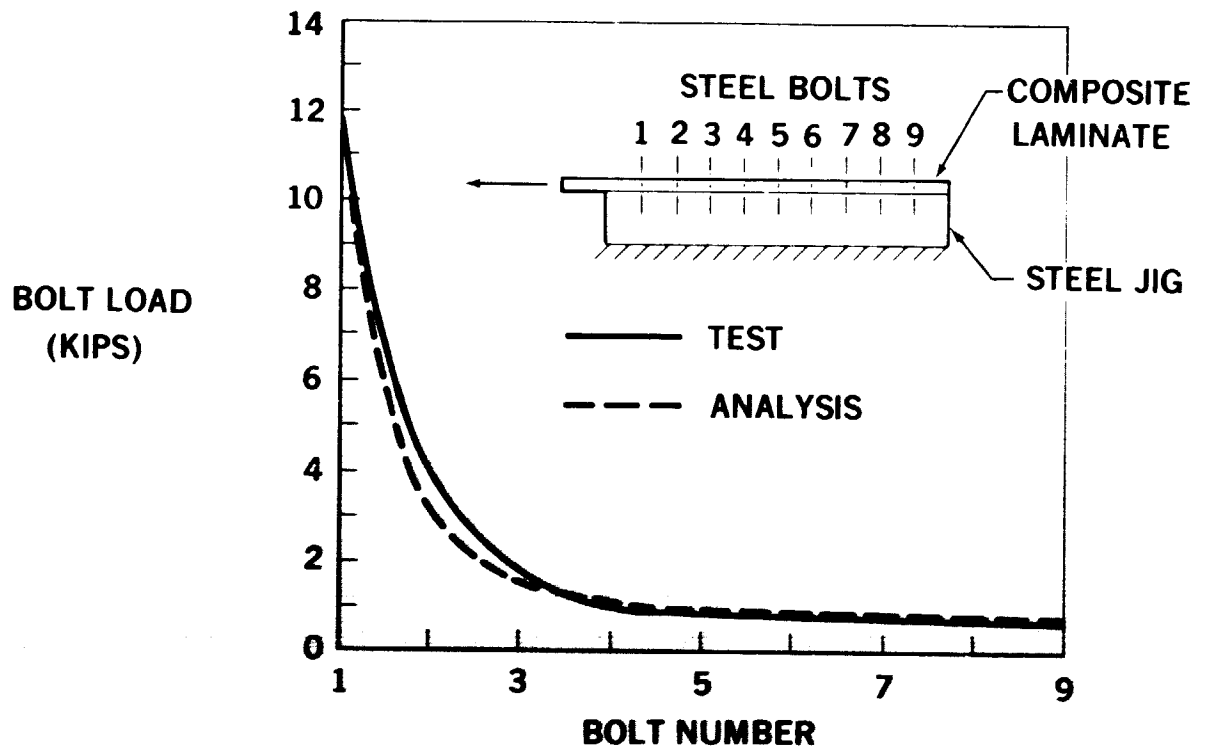


FIGURE 6. TEST-THEORY CORRELATION - BOLTED-JOINT LOAD DISTRIBUTION AT FAILURE

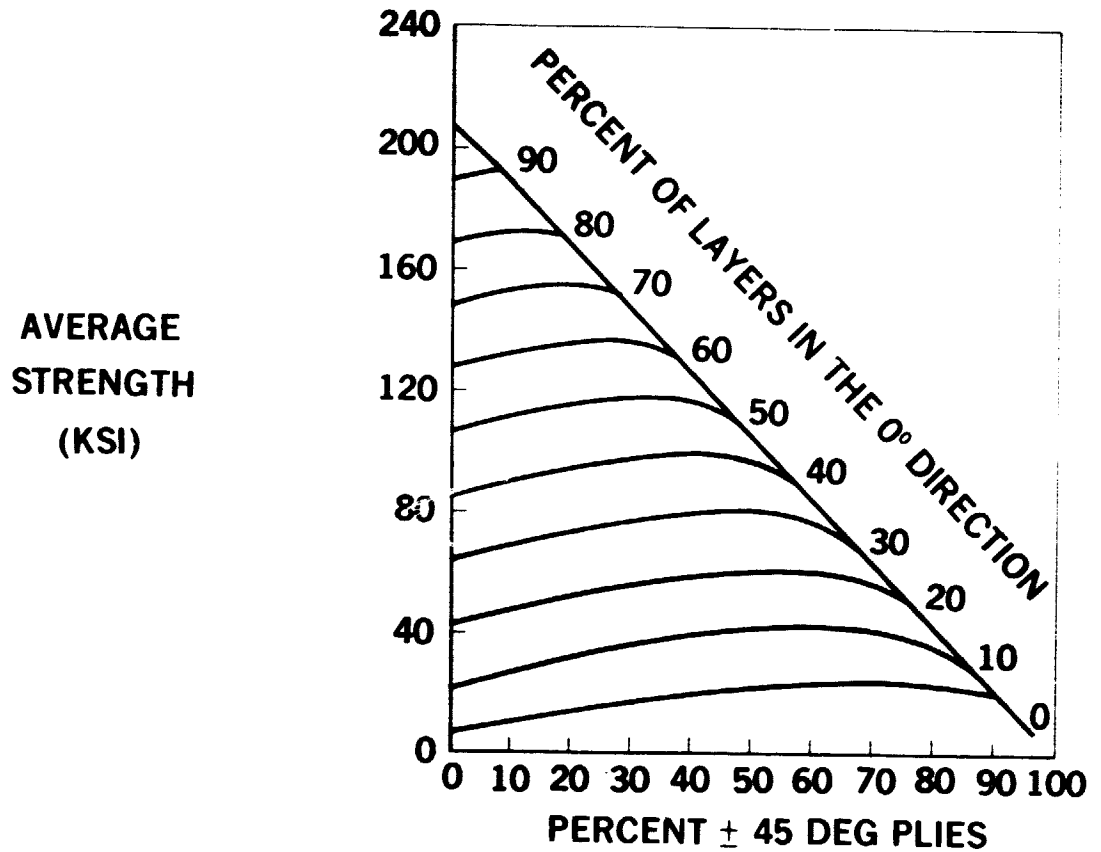
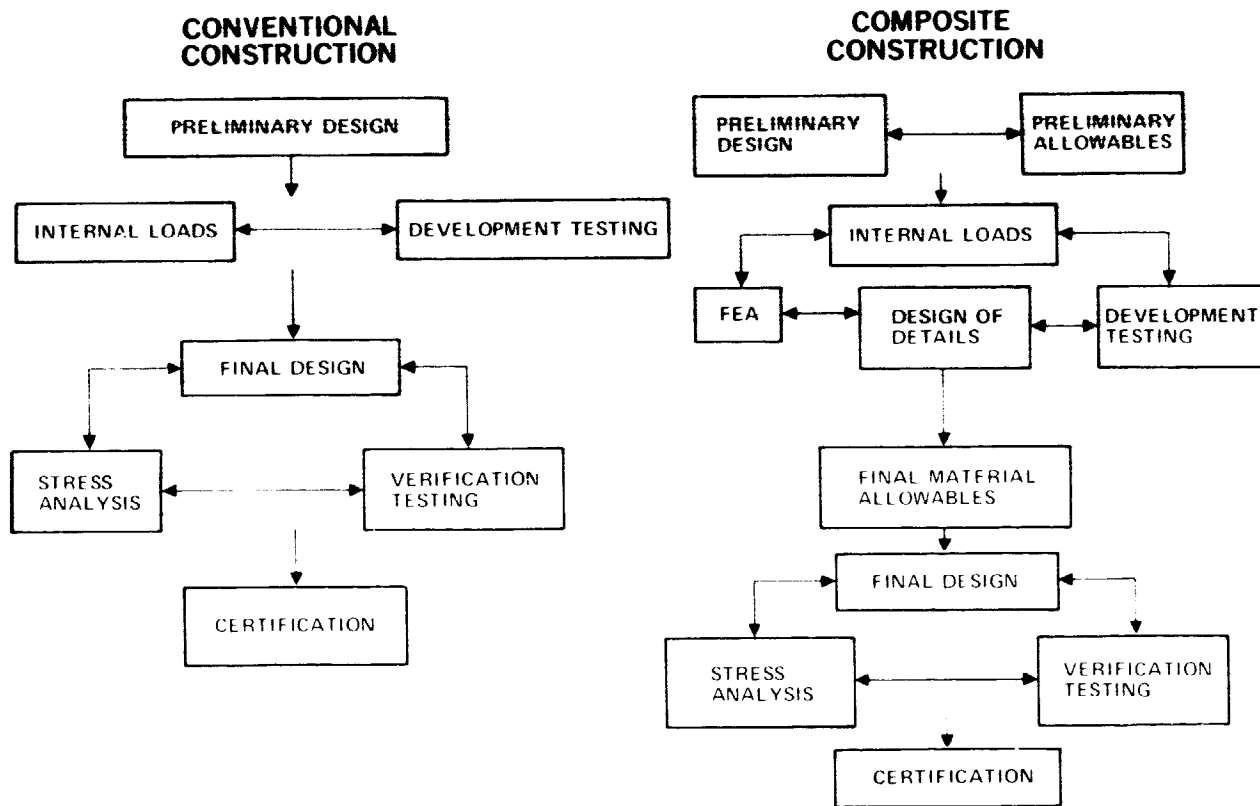


FIGURE 7. 5208/T300 LAMINATE STRENGTH/STIFFNESS CARPET PLOTS

structure with the reliability of existing structures. In the interim, the existing criteria must be used with conservatism, backed by extensive testing and thorough inservice inspection.

In addition to potential changes in criteria, basic differences can be expected in the basic design/verification procedures designated in Figure 8. First, the material allowables activity is significantly different for metal structures. A greater number of basic material properties are required and they must be generated from specimen tests. The specimen configurations are generally different and the data must be generated by each company since processing differences have fundamental impact on properties.



**FIGURE 8. DESIGN/VERIFICATION PROCEDURES**

The structural analysis activities are changed considerably. The nonductile and nonisotropic nature of the materials results not only in requirements for new and modified methods but also for higher quality analysis with more accurate results. In major fittings and splice areas shown in Figure 9, considerably more refined analyses are necessary in order to determine detailed stresses and bolt load distributions. Overall, it is anticipated that the structural analysis activities will increase from 35 to 75 percent. Figure 10.

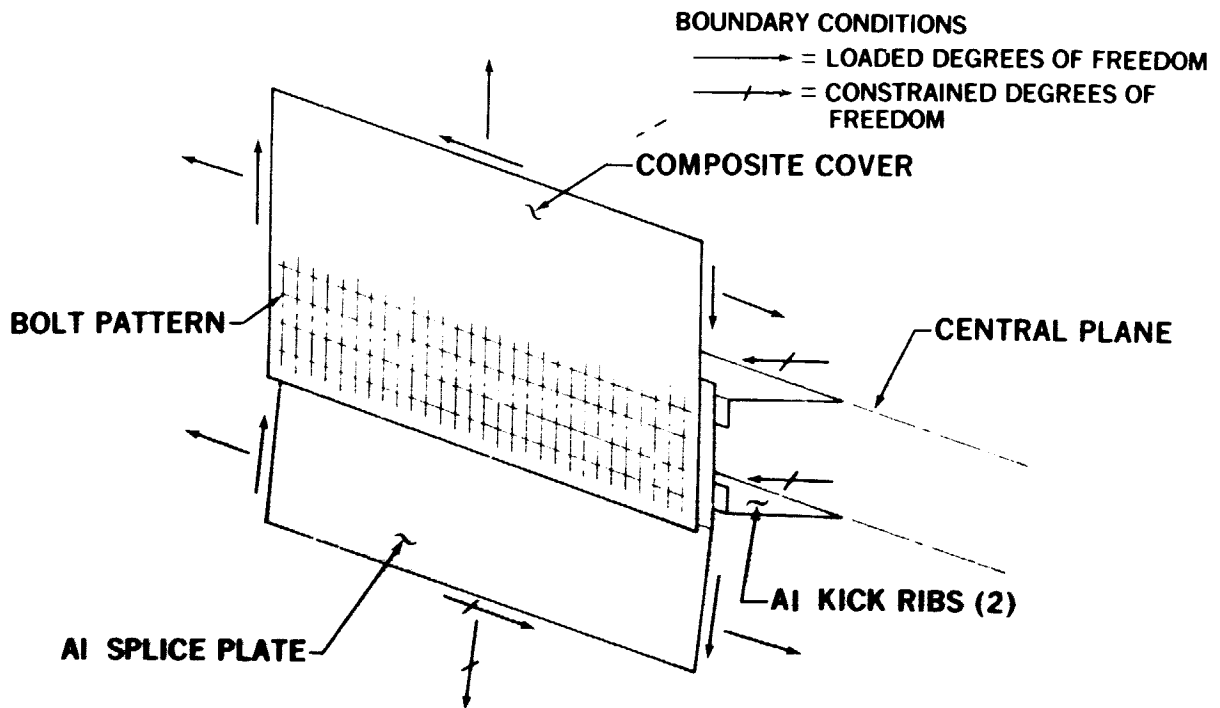


FIGURE 9. ALUMINUM TO COMPOSITE MULTI-FASTENER JOINT

	<u>METAL COMPONENT</u>	<u>COMPOSITE COMPONENT</u>
EXTERNAL LOADS	0.05	0.05
INTERNAL LOADS	0.2	0.25 — 0.30
FEA OF DETAILS	0.05	0.2 — 0.3
STRESS ANALYSIS	0.5	0.6 — 0.8
FLUTTER AND VIBRATION ANALYSIS	0.2	0.25 — 0.3
	<u>1.00</u>	<u>1.35 — 1.75</u>

FIGURE 10. ANALYSIS ACTIVITY COMPARISON FOR A MAJOR COMPONENT

	<u>CONVENTIONAL AIRCRAFT</u>	<u>COMPOSITE AIRCRAFT</u>
MATERIAL PROPERTIES	0.01	0.10 — 0.15
DEVELOPMENT TESTS	0.17	0.50 — 0.75
COMPONENT TESTS	0.08	0.25 — 0.40
FULL-SCALE TESTS	0.74	1.00 — 1.50
	<hr/> <b>1.00</b>	<hr/> <b>1.85 — 2.80</b>

FIGURE 11. COMPOSITE AIRCRAFT STRUCTURAL TEST PROGRAM

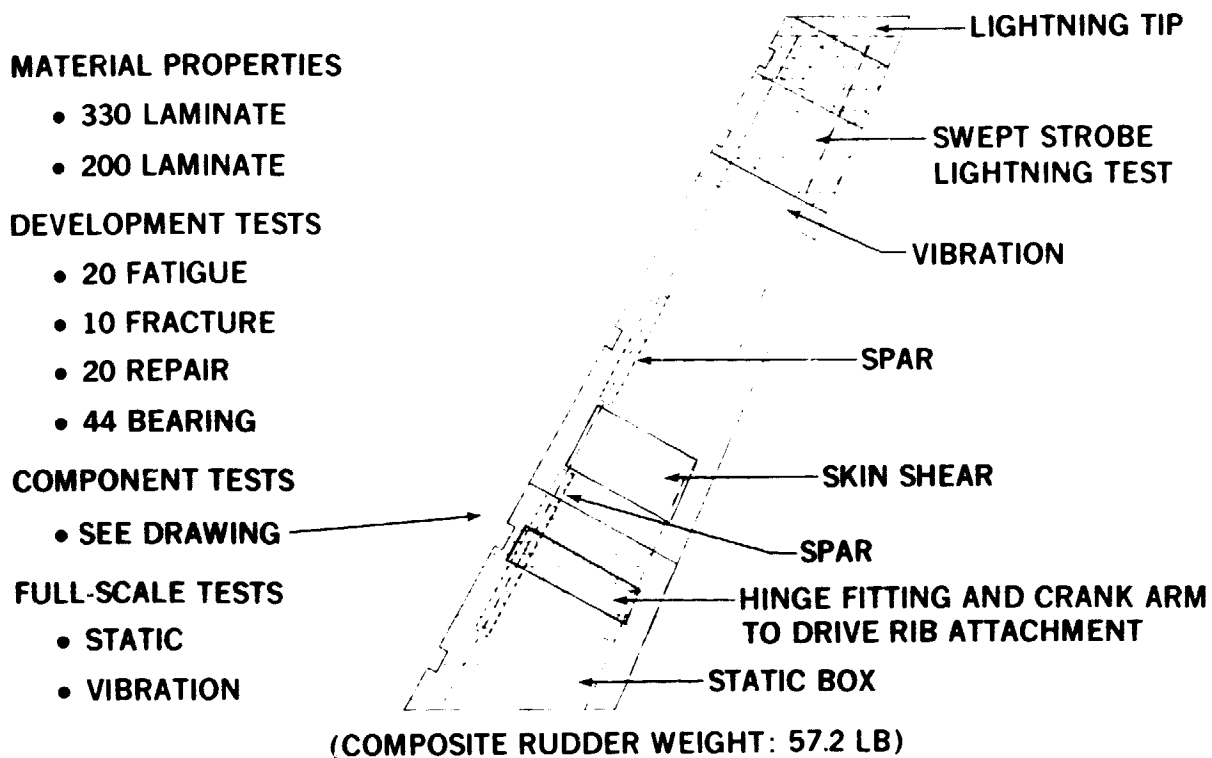


FIGURE 12. DC-10 COMPOSITE RUDDER TESTS

The testing activities indicated in Figure 11 are increased over those required for metal structures not only because of the differences in the materials but also due to the lack of service experience. The lack of service experience requires better simulation of the service environment for both static and fatigue tests to enable the structures to be qualified for a 20-year life. Early components require more extensive development testing than will be needed after the basic forms of construction are established and significant service experience is available. The extensive development test program specified in Figure 12 for the DC-10 graphite rudder program will be considerably less extensive on future components using similar construction.

### CONCLUSIONS

Current commercial airframes have a high degree of reliability, and advanced composite structure must meet or beat this record to be acceptable for general use in primary structure. As an interim approach, advanced composites may be used by conservative application of existing criteria supported by extensive testing and special inservice inspection procedures. **Effective general use requires significantly more service experience and criteria specialized for composites. With these advances and a competitive cost status, advanced composites will be used extensively in commercial jet aircraft.**

## FAIL-SAFE DESIGN AND RELIABILITY IN COMPOSITE

### COMMERCIAL AIRCRAFT STRUCTURE

By Robert E. Watson

Boeing Commercial Airplane Company

#### INTRODUCTION

Dale Warren of McDonnell Douglas and I were asked to present industry views on fail-safe design and reliability using composites in primary structures of commercial aircraft.

I would like to present my views by first reviewing relevant commercial aircraft criteria, the design philosophy we expect to follow, and then discuss some concerns and actions, such as the development testing, which must be accomplished before we can realistically expect to commit significant primary commercial aircraft structure using advanced composites.

#### DESIGN CRITERIA AND APPROACH

In commercial aircraft design we have two fundamental structural criteria - safety and durability. Obviously the first, safety, is of utmost importance. Safety in aircraft structure has been acquired through the efforts of many people thinking, developing, testing, and adjusting existing criteria where required from service experience, to insure structural safety. Engineers from both the military and civil sectors have contributed to the perfection of this criteria.

In commercial aircraft design criteria we also have the option of designing to either "fail safe" or "safe life" criteria. All present day U.S. commercial aircraft are designed to the fail safe concept as defined in Figure 1. To date I am not aware of any instance where this criterion has failed us.

The second fundamental criteria which I believe all U.S. commercial manufacturers use is one I will call durability. Commercial aircraft are designed for a useful life on the order of twenty years and therefore many thousands of flight cycles. Just as in all good products bought today some form of warranty and service life policy is demanded of the manufacturers and we provide these. Therefore, we must design as best we can to insure a minimum of in-service surprises and thereby maintain the economic risk to an acceptable level throughout the life objective. Significant testing is associated with assuring meeting our objectives.



For any new structural concept I see no reason to alter our basic philosophy of design which has proven to be successful with the present forms of construction. As noted in Figure 2, we have built up over many years a design and analysis discipline in metal structures that has been verified by long term service operations. As we change over to composite structures we must follow these fundamental design philosophies but the work in composites to date has shown that full scale development programs are required to establish the detail design-analysis disciplines and service verification is essential for a production commitment in commercial aircraft.

An example of this design/analysis discipline concern that must be understood is shown in Figure 3. To provide structural safety in these new structures we must design for damage containment. We all recognize the basic brittle nature of advanced composites so we must develop designs which recognize this characteristic and still provide the over-all damage tolerance and fail safety at least equivalent to what we have today in metal structures.

Specifically, the FAA certification requirements we believe adequately provide for potential damage to the structure whether they be accidental service damage, inadvertent manufacturing defects, or service induced fatigue or partial environmental damage of the structure as shown in Figure 4.

In metal structures we have used a combination of slow crack growth materials and multiload path methods to obtain the necessary safety. We can see some new ways to go using these brittle fiber forms of construction, such as material tailorability, and we must perfect and demonstrate this capability.

An example of this material tailorability to provide damage containment is shown in Figure 5. By a combination of "soft" strips incorporated in the structure we can alter the stress intensity thereby reducing the crack growth rate and permitting larger crack lengths to exist and still maintain fail safe strengths. This then would permit us to use the same sort of inspection controls used today in providing obvious partial failure inspection detection to prevent exceeding fail safe limits.

Probably one of the most important known "unknowns" of a technical nature in the use of advanced composites is this problem of durability. Let's look at some of these concerns as shown in Figure 6.

In metals we can, for example, analyze for fatigue failure locations. In advanced composites we have some new failure characteristics in the failure mode problem. Further, we have seen some evidence of environmental degradation which may be greater, and is less understood as compared to metals. And, of course, we must satisfy our concern about the combination of these. These concerns are shown graphically in the lower portion of the figure. If not resolved they could be "show stoppers" for the use of composites in primary commercial aircraft structures.

Figure 7 outlines some specific considerations when we tackle this problem of durability. In the past economic considerations have provided the necessary design controls and this will continue for this new structure. And,

of course, we must continue to provide the service life policies and design life goals of the past metal structures.

As in all designs we must establish and follow some criteria. With advanced composites we must examine the existing criteria and alter it where required based on the new structural material behavior and characteristics envisioned. One of these is certainly an expansion or altering of the environmental criteria. What about water degradation? How much soaking should we use in the laboratory to simulate a realistic long life service environment? are some of the criteria considerations.

Other concerns directly associated with the analysis and design discipline are the specifics of detail design of aircraft parts utilizing the full advantages of the characteristics of composites, not just substitution for metals. Although a number of structures have been designed and some are in service, this discipline of detail design is in its infancy and we are not yet ready for the commercial aircraft design without unacceptable private company risks.

A lot of attention has been given to the fiber and its mechanical characteristics, but the role of the matrix in this structure is vital and therefore must be equally understood. We have used accelerated test methods in the past for metal structures and they have become standard. No standards have been established yet for accelerated environmental testing of composites.

Designs using composites show a high payoff potential from several standpoints. Not only do they show the possibility of the largest weight payoff in aircraft structures since we changed from spruce and fabric to aluminum structures, but they show promise of other potential benefits as shown in Figure 8. Due to the anticipated high cost of these fabricated structures we must make every effort to simplify the designs as shown in the figure. Not only could these simplified design ideas reduce fabrication costs, many also reduce the severity of the durability problem where past experience with metal structures has shown a critical problem to be the intersection of structural members. In composites we see the potential to have a significant reduction in intersecting parts.

Through material tailoring we can also see the potential of reducing stress concentrations around necessary cutouts and mechanical fastener installation by shunting the load around the mechanical joint where required. As we know the advanced composites today, they also have the potential of being easier to environmentally protect against corrosion characteristics of the metal structures. However, as mentioned before, we must ensure against unacceptable environmental degradation of the matrix in the composite structure.

We have mentioned material tailorability in the use of composites. Figure 9 shows graphically what can be done by altering the  $E$  of the structure in the vicinity of a cutout to reduce the effective  $K_T$  and thereby control the detail stresses within acceptable limits.

Although it is impossible at this time to outline specifically all of the number and types of tests required to reach an acceptable risk production commitment for commercial aircraft structures, Figure 10 scopes the problem as we see it. The length of time to accomplish all of this is of course dependent upon many factors, some of which are outside the control of the technical community, such as funding. Experience has shown us that if we fail to understand the structure by overlooking some of the activities shown on the chart, we can get ourselves into serious trouble. The example of the 7079 aluminum alloy forging is but one example of where we have failed in the past. We cannot afford to make this kind of mistake in the gross primary structure of commercial aircraft.

### SUMMARY AND RECOMMENDATIONS

In summary, Figure 11, we believe that today's existing fundamental criteria and design economics considerations are adequate to provide safety and durability guidance. We believe we recognize the material properties of concern and must pursue these to insure no "fatal flaws". As we develop more and more structures our design capability will be validated. Concurrently we are accumulating service experience at an increasing rate. In commercial applications the service experience on secondary structures has been good to date and that encourages us to proceed with primary structural design development.

It is recommended that we expand primary structural development as presently proposed by both the Air Force and NASA focusing on the items shown in Figure 12. We are certainly not completely in the dark on composite structures. We have used them in the form of fiberglass parts for years with generally good success. However, for primary structures using the high strength and generally more brittle fibers, we have a lot of ground to cover. With today's environment on product liability alone, the commercial aircraft manufacturer must understand the risks and be able to justify to not only our own company officials but to the customers and the certifying agency that we understand what we are doing and how the structure will perform throughout its expected life. The Boeing Commercial Airplane Company is prepared to step up to this challenge and has high confidence that the proposed activities are the major steps leading to the commitment of advanced composite structures in a future commercial transport.

<b>SAFETY</b>	<b>FAIL SAFETY</b>	<b>NO CATASTROPHIC FAILURE AFTER FAILURE OR OBVIOUS PARTIAL FAILURE OF A STRUCTURAL ELEMENT</b>
<b>DURABILITY</b>	<b>FATIGUE/ENVIRONMENTAL LIFE</b>	<b>SERVICE LIFE POLICY FOR SPECIFIED SERVICE LIFE</b>

Figure 1.- Design criteria.

**STRENGTH-DURABILITY-FAIL SAFETY**

<b>METAL STRUCTURE</b>	<b>DESIGN/ANALYSIS DISCIPLINES VERIFIED BY SUCCESSFUL LONG- TERM SERVICE OPERATIONS</b>
<b>COMPOSITE STRUCTURE</b>	<b>FOLLOW DESIGN PHILOSOPHIES PROVEN SUCCESSFUL FOR METAL STRUCTURES</b>  <b>CONDUCT DEVELOPMENT PROGRAMS AND OBTAIN SERVICE EXPERIENCE NECESSARY TO PROVIDE COMPOSITE DESIGN/ANALYSIS TECHNOLOGY</b>

Figure 2.- Design philosophy.

- MAJOR CONCERN—DAMAGE CONTAINMENT
- DESIGN APPROACH MUST RECOGNIZE BRITTLE NATURE OF MATERIAL

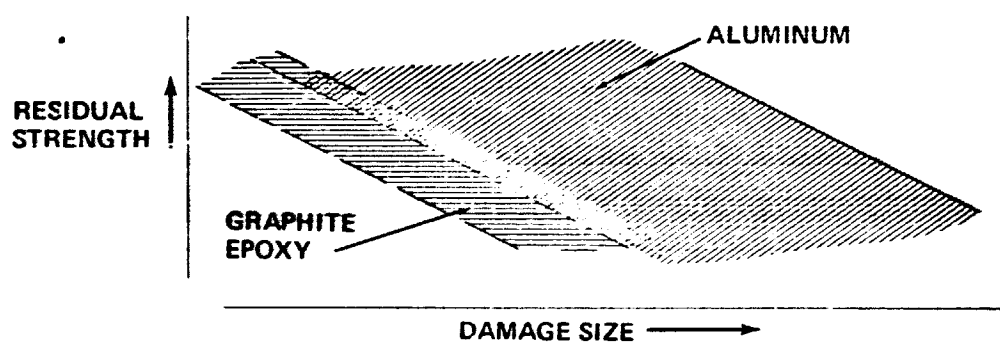


Figure 3.- Safety.

- CRITERIA
  - CURRENT CERTIFICATION REQUIREMENTS ADEQUATELY PROVIDE FOR POTENTIAL DAMAGE
- POTENTIAL DAMAGE SOURCES
  - ACCIDENTAL SERVICE DAMAGE
  - MANUFACTURING DEFECTS
  - FATIGUE DAMAGE
- DESIGN APPROACH—FAIL-SAFE DESIGN
  - MULTILOAD PATH
  - MATERIAL TAILORABILITY

Figure 4.- Safety considerations.

- MATERIAL TAILORABILITY PERMITS UNIQUE DAMAGE CONTAINMENT DESIGN

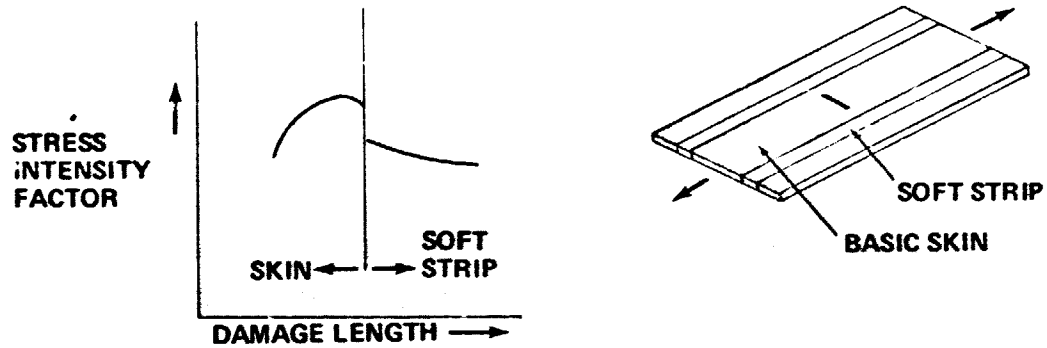


Figure 5.- Safety - composite design.

- MAJOR CONCERNS:

- MULTIPLE FATIGUE FAILURE MODES
- ENVIRONMENTAL DEGRADATION
- COMBINED EFFECTS

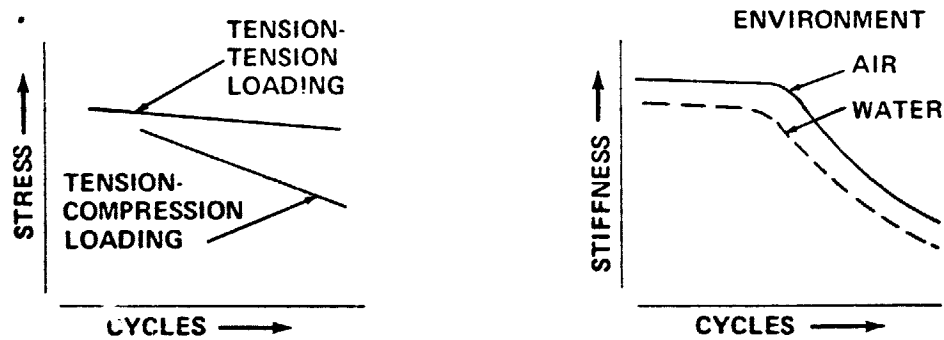


Figure 6.- Durability.

- **ECONOMIC CONSIDERATIONS PROVIDE ADEQUATE DESIGN CONTROL**
- **DESIGN POLICY**
  - **SERVICE LIFE POLICY**
  - **DESIGN GOAL: 20 YEARS**
- **DESIGN APPROACH**
  - **ENVIRONMENTAL CRITERIA NEEDED**
  - **ESTABLISH ANALYSIS AND DESIGN DISCIPLINE:**
    - **DETAIL DESIGN**
    - **MATRIX ROLE**
    - **ACCELERATED TEST METHOD STANDARD**

Figure 7.- Durability considerations.

- **COMPOSITES ENABLE DESIGN SIMPLIFICATION**
  - **REDUCED PART COUNT**
  - **REDUCED PART INTERSECTION**
  - **REDUCED JOINTS**
  - **ADAPTABLE TO BONDED JOINTS**
- **MATERIAL TAILORABILITY**
  - **REDUCED STRESS CONCENTRATION AT:**
    - **CUTOUTS**
    - **MECHANICAL FASTENER INSTALLATIONS**
- **POTENTIALLY EASIER TO ENVIRONMENTALLY PROTECT (NO CORROSION)**

Figure 8.- Durability - composite design.

MATERIAL TAILORABILITY PERMITS UNIQUE DURABILITY DESIGN

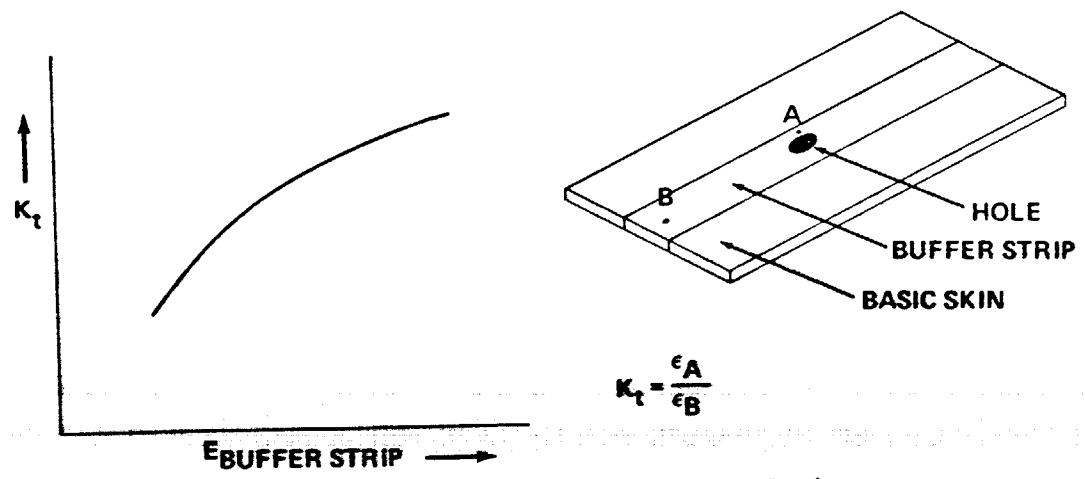


Figure 9.- Durability - composite design.

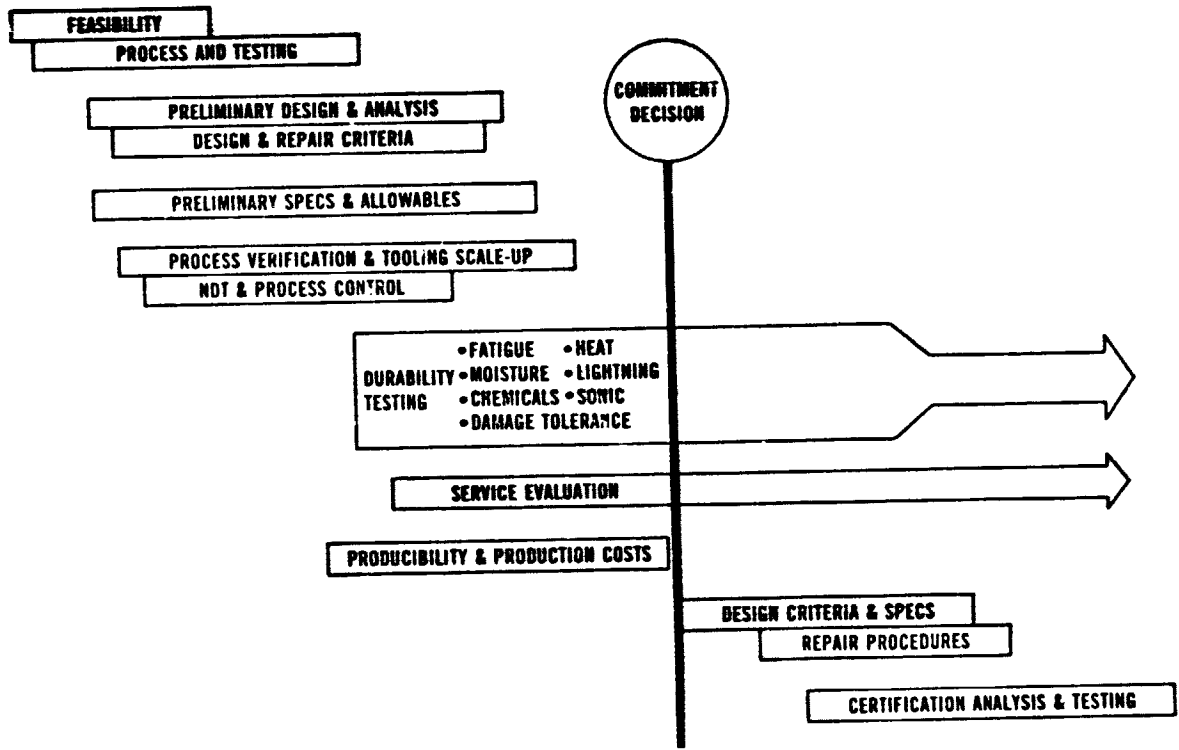


Figure 10.- Composite development plan.



- EXISTING CRITERIA AND DESIGN ECONOMICS CONSIDERATION ADEQUATE TO PROVIDE DESIGN SAFETY AND DURABILITY
- MATERIAL PROPERTIES OF CONCERN RECOGNIZED
- DESIGN POTENTIAL BEING VALIDATED
- SERVICE DATA ACCUMULATING
- SERVICE DATA (HISTORY) GOOD TO DATE

Figure 11.- Summary.

- PROCEED WITH EXPANDED PRIMARY STRUCTURE DEVELOPMENT PROGRAMS TO ALLOW:
  - FOCUSING ON DEVELOPMENT OF REAL DESIGN/ ANALYSIS DISCIPLINE NEEDS
  - EXPOSURE OF ADDITIONAL ECONOMIC INFORMATION NEEDS
  - EXPANDED SERVICE EXPERIENCE ACCUMULATION

Figure 12.- Recommendation.

omit

LIFE ASSURANCE TECHNOLOGY

By J. Halpin  
Air Force Flight Dynamics Laboratory

and M. Waddoups  
General Dynamics

Paper not available for publication

## STATISTICAL DESIGN CRITERIA

By B. Walter Rosen

Materials Sciences Corporation

### INTRODUCTION

The critical design condition for aircraft structures may be the repeated application of a spectrum of loads, none of which, when applied separately, would produce static failure of the structure. Failure, under such conditions, may be viewed as the culmination of a process of gradual weakening of the structure. For this concept, the critical design parameter is time to failure, rather than structural strength; and design reliability is secured by life assurance rather than safety factor. When this approach is applied to composite structures, the multiplicity of potential failure modes associated with composites increases the complexity and decreases the confidence level of the design process.

This lecture, which is a background statement for the panel discussion which follows, addresses some of the basic concepts associated with the prediction of lifetime for composite structures. The objective is to expose the underlying philosophy, rather than the detailed, specific, experimental and analytical methods and material models. This includes treatment of the philosophy inherent in the wearout design methodology. The aim is to highlight some of the problems associated with incorporating the problems unique to composite materials into the life assurance design criteria.

### DESIGN APPROACHES

A design methodology may be built upon factors of safety, both for static load and for fatigue lifetime. For composites, the simple approach of using large factors of safety on static loads may well have the effect of assuring long lifetimes for the kinds of composite structures that we're presently designing. This approach can be used with statistically defined material allowables, to enable us to design the flight hardware needed to obtain practical service experience. However, the safety factor approach will encounter problems when there are local strain levels which are high enough to cause local material damage. These damage zones may experience significant growth during the lifetime of the structure. With our present limited understanding of composite damage growth, lifetime predictions are unreliable. The problems associated with lifetime predictions include not only the fact that we are dealing with a structure which has statistical

load histories and a significant degree of material variability, but also that this material variability influences the fatigue deterioration of material properties in a different manner than it influences material static strength.

Thus, it becomes imperative that for lifetime prediction, we deal with probability of static failure and its consequences. Figure 1 presents a simple schematic superposition of a load exceedance curve and a material allowable probability density function. This is intended to convey the capability of predicting probability of failure when both of these statistical quantities are defined. The probability of failure being simply the probability that the stress(s) which results from a given load exceedance is greater than the allowable strength  $\sigma$ . The complicating factor which becomes of exaggerated importance in composite materials is that the probability distribution function for allowable material strength  $g(\sigma)$ , varies with time, and in addition, it can be affected by environment so that our  $g(\sigma)$  function becomes in actuality  $g(\sigma, t)$ .

This effect is illustrated in Figure 2. This representation of time dependent strength shows the initial static strength distribution function at time zero and the changes in this function with lifetime. The changes result from the effects of repeated loads and environmental exposure. One can observe that at any particular point in time there will be a strength distribution function defined as residual strength, which will differ from the initial static strength distribution function. This deterioration of residual strength with time may eventually bring the material strength down within the applied load envelope thus causing what we commonly describe as a fatigue failure. Fatigue, in this terminology, is the reduction of the residual strength capability down to the applied stress levels.

It is important to emphasize here that residual property characterization need not necessarily be limited to strength. In situations where stiffness critical design occurs it may well be a deterioration of material stiffness; it may be a change in material damping characteristics; it may be a change in the susceptibility of the material to any of the various aspects of its environment that becomes the critical design factor.

The prediction of failure at any point in time can be accomplished if the residual strength distribution functions are known. Thus we define  $p(t)$  as the probability density function for failure of one member of the set. It follows, from the concept illustrated in Figure 1, that the failure probability is the intersection of the probability of experiencing a stress and the probability of a stress causing failure. Thus:

$$p(t) = \int_0^{\infty} f(S) \left\{ \int_0^{\sigma(S)} g[\sigma(S), t] d\sigma \right\} ds$$

and the cumulative distribution function is:

$$P(t) = \int_0^t p(\tau) d\tau$$

From this, the reliability,  $R(T)$ , is defined by:

$$R(t) = 1 - P(t)$$

Hence, reliability is a function of time.

If we define  $R_n(t)$  as the probability of zero failures of  $n$  units, at time,  $t$ , we find:

$$R_n(t) = [R(t)]^n$$

Hence, if  $P_n(t)$  is the probability of at least one failure of the set:

$$P_n(t) = 1 - R_n(t)$$

From this it follows that the probability distribution function for time to first failure:

$$p_n(t) = \frac{d}{dt} \{ 1 - [R(t)]^n \}$$

This indicates that in our statistical design criterion, the key variable is time to failure. We can translate the failure probability or the reliability of a structural element into a distribution function for time to first failure in a group of structures coming from that population. Given this distribution function, then we can do such things as determine the expected time to first failure, or any other measure which we desire to impose upon the lifetime variable. The expected time to first failure,  $\bar{t}_n$ , is defined by

$$\bar{t}_n = \int_0^{\infty} t p_n(t) dt$$

This translation of static strength variability to lifetime prediction is the essence of what has come to be called "wearout".

## WEAROUT

Wearout is a mathematical and physical residual strength model in which we quantify the concept that a load which does not produce failure in a single application can produce failure after multiple applications. The physical consequence of that fact is that there is an inherent deterioration of material properties; and in the case of composites, this is a measurable deterioration. The philosophy is that failure is caused by initially existing flaws; that these flaws extend in a known manner; that this increased flaw or damage size causes decreased material strength. Thus, the elements of this wearout model are first, a definition of the initial defect geometry. This includes defect geometry which exists by virtue of design (such as holes, attachments, etc.) and defect geometry which exists as a consequence of the imperfections of the manufacturing process. We must also know the material properties initially. Secondly, we must be able to define changes in both geometry and material properties as a function of load and environment. Third, in order to define failure at any point in time, we must have a relationship between the strength and any possible instantaneous characterization of geometry and properties. These are the basic elements that one must deal with and these are the elements that have been dealt with very successfully in metal design, through the methodology of fracture mechanics.

This methodology is illustrated schematically in Figure 3. The first sketch, upper left, suggests the fact that the initial static strength must be defined in a statistical sense. For metals, if we apply the concepts of fracture mechanics, there is a one to one correspondence between the size of the initial

defect,  $a$ , and the material strength,  $\sigma$ , given by: 
$$\sigma = \frac{k_c}{\sqrt{\pi a}}$$

Here,  $k_c$ , the critical fracture toughness is the material constant which makes this translation from flaw size to strength. The initial defect population changes when subjected to the total environment (which may include factors other than loading) and what happens is that we have a new statistical distribution of defects at any later time. The change in defect size is described

for metals by a crack growth rule law: 
$$\frac{da}{dt} = ca^n \quad n \geq 1.$$

This new statistical defect distribution can be retranslated back into a new strength distribution function using the fracture toughness relation. This leads to the residual strength characterization as a function of time,  $g(\sigma, t)$ . This is precisely the input that is necessary for the design criteria for lifetime prediction.

## COMPOSITES

The critical question here is how can this methodology be applied to composites. The principal problem is that there are multiple failure modes so that initial defects do not necessarily propagate in a self-similar way. This is suggested in Figure 4. A composite laminate is composed of layers of material which are highly anisotropic in their strength characteristics. Thus, there are possibilities for defects to grow perpendicular or parallel at least to any of the different fiber directions in the composite. One may find that the same defect may propagate in different modes depending upon the load history and the environmental effects. Thus, unlike the fact that for metals where the most important damage growth mechanism is a self similar propagation of an initial defect; i.e. the case of flawed composites, we have to deal with this multiplicity of failure modes.

Initially, we deal with fibers which are broken and with defects in the matrix. This initial flaw geometry could change by propagation in the form of adjacent fiber breaks, a growth that is similar to a metal defect. The initial damage could change due to matrix damage resulting in a crack parallel to the fibers. This may be dependent upon load history and environment (e.g. moisture). Furthermore, there are damage mechanisms which will result from the interaction between layers which may cause local delamination. Thus, even for fiber dominated laminates, the changes in the matrix stress-strain characteristics can influence the nature of the propagation and hence the design lifetime.

The importance of matrix effects is suggested in Figure 5, by the fact that even in simple notched laminate tests of boron-epoxy laminates, there is a change in failure mode as one changes from static to fatigue loads. Thus, if we consider these two laminates  $0_2/\pm 45$  and  $\pm 45$  with a sharp central slit notch, static loading results in a colinear propagation to two-part failure of the specimen. Similar specimens subjected to fatigue loading experience failure mechanisms in which the plane of failure is parallel to a fiber direction. This change in failure mechanism can have some serious consequences in what happens to our flaw distribution function.

One example of the problems associated with lifetime prediction for composites is presented in Figure 6. The curve,  $t = 0$ , is a probability distribution function for the initial defect sizes. Two alternate damage growth paths are suggested on the right with the growth of the damage in either a colinear or self-similar

fashion or in a mode which reflects some additional local failure mechanism in the material. The existence or nonexistence of either of those modes of failure can change the character of the distribution function for the flaws. For a self-similar propagation,  $db = 0$ , we see the classical effect of the largest cracks growing fastest; the mean size of the flaw growing; and the dispersion in the flaw growing because the rate of growth is proportional to some power of the initial size. In the case of damage growth in the presence of secondary failure mechanisms,  $db = 0$ , there is something of a local blunting of some of the stress irregularities and this can serve to narrow the dispersion associated with the flaw distribution. Thus, although we get an increase in the mean flaw size, there will be a decrease in dispersion.

The primary consequence of these multiple failure modes upon lifetime is that we may lose the ability to make the desired translation from static strength to lifetime. Figure 7 is a simple schematic representation of this problem. The initial static strength distribution function has been broken down into two separate distribution functions which add together to give the measured strength function. If these two failure mechanisms are of the two types shown in Figure 6, it is entirely conceivable that the change in dispersion of one failure mode can result in a situation where lifetime prediction will be governed by a mechanism of failure that differs from the one that governs the initial static strength distribution. Thus, the critical life-limiting defects may not be identified by initial proof testing. One cannot rule out the need to make additional nondestructive inspections, or perhaps even additional proof testing, after a portion of the lifetime environment has been experienced by the structure.

## CONCLUSIONS

In summary, these comments are intended to support the view that there is a rational approach to lifetime assurance for structures. The development of this approach for composite structures is incomplete at this time. These shortcomings are compensated for in contemporary aircraft structural design by the use of conservative design approaches for static loads. This includes the use of low static allowables and fail safe design configurations. As we gain service experience with the current composite structures, and as we advance our understanding of the failure process, we will be able to design for higher reliability, and better performance with longer life.

Current mathematical models for lifetime prediction for composites are inadequate, although perhaps of transitory value. The existing wearout methodology is a desirable framework for



life assurance. However, when applied to composites, it must be modified because the initial static strength distribution does not define the initial flaw distribution in a unique fashion. This difficulty is a result of the existence of many different failure modes. In composites, defects grow at different rates and in different directions depending upon initial crack geometry and load history and environmental effects upon matrix properties. As a result of these characteristics of composites, static proof tests may not guarantee safe crack growth life.

If we want to use the safelife design philosophy, we are going to have to move forward with developing an understanding of these failure mechanisms. We must also keep in mind that residual properties other than strength may become important at some later time in the service life. What this means is, that we are going to have to recognize that we are living with design criteria and qualification procedures which are inevitably going to change over a period of time as our knowledge increases. At the present time our shortcomings in the understanding of the growth of damage within a composite should be compensated for by the use of overly conservative design procedures.



$$P_{\text{FAILURE}} = P(S \geq \sigma)$$

Figure 1.- Probability of static failure.

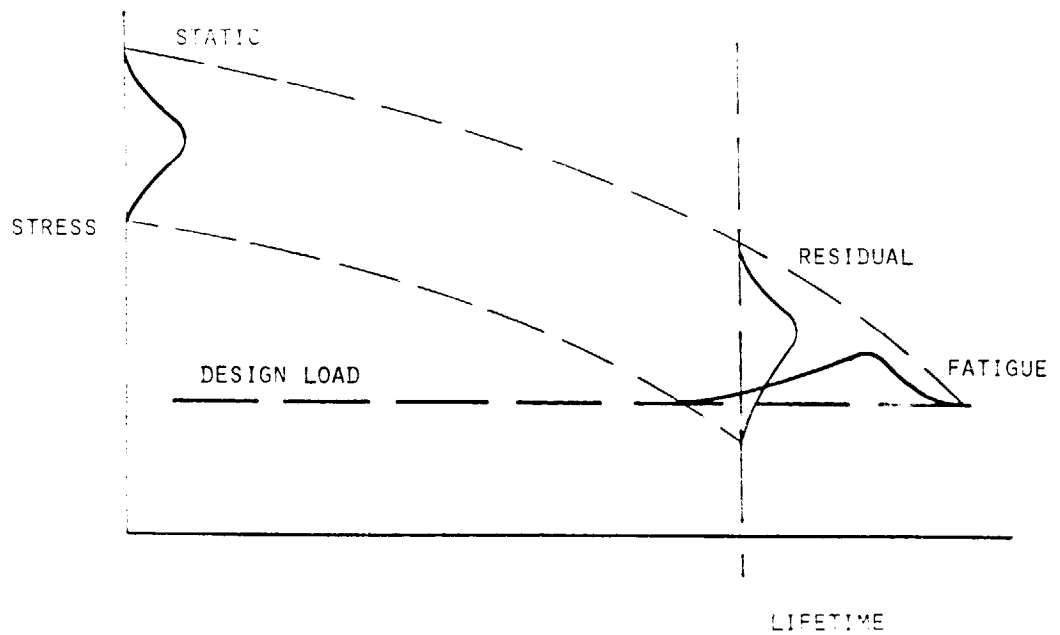
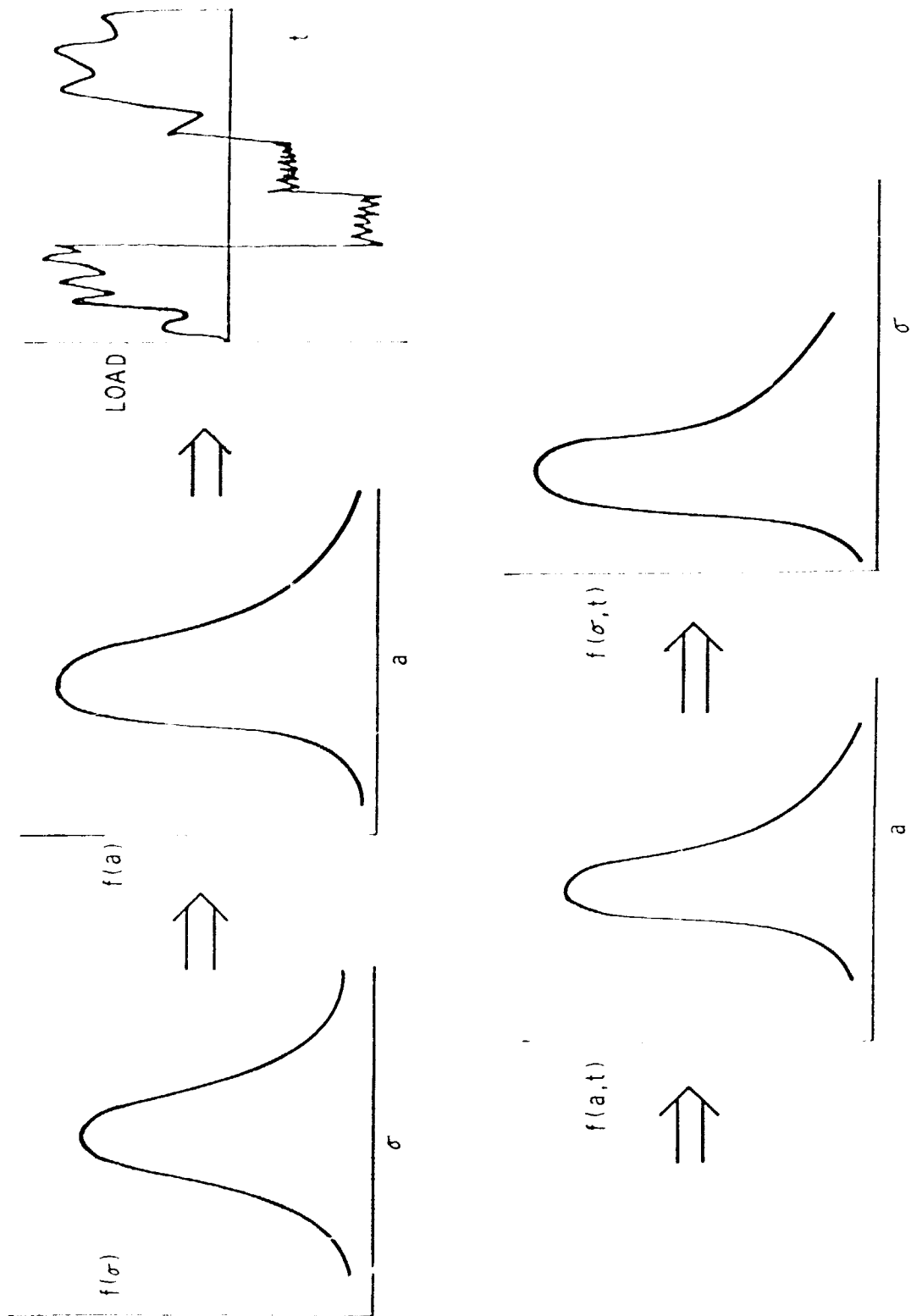


Figure 2.- Time dependent strength.



TRANSLATION FROM STATIC DOMAIN TO FATIGUE DOMAIN

Figure 5.- Metal wearout.

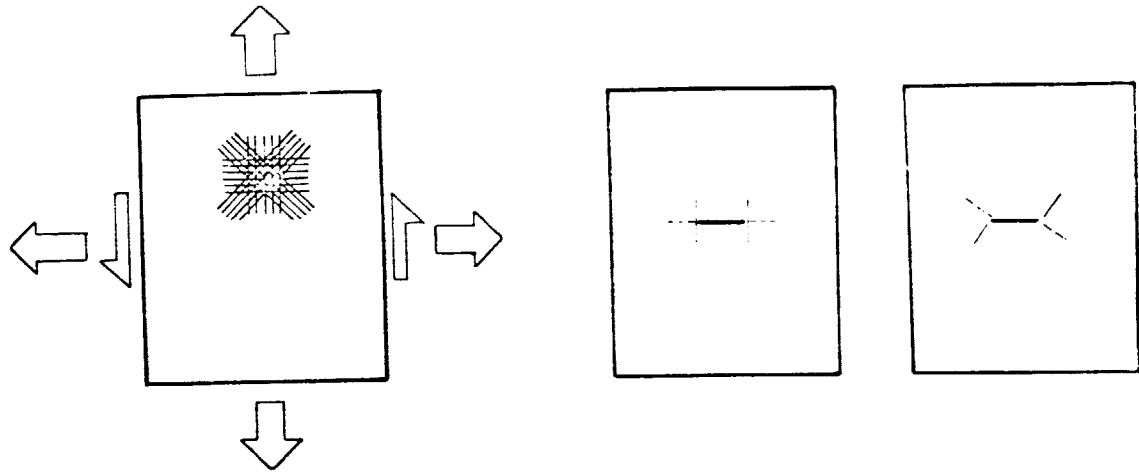


Figure 4.- Damage growth.

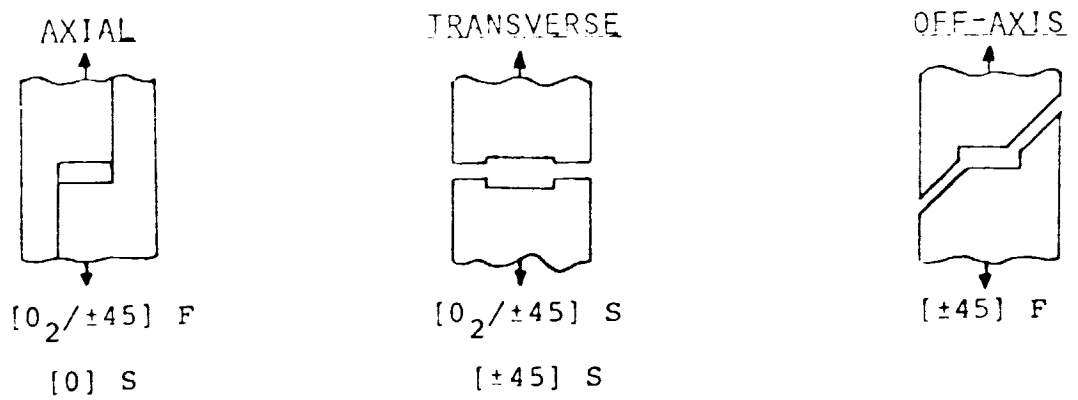


Figure 5.- Observed static and fatigue failure modes in tension.

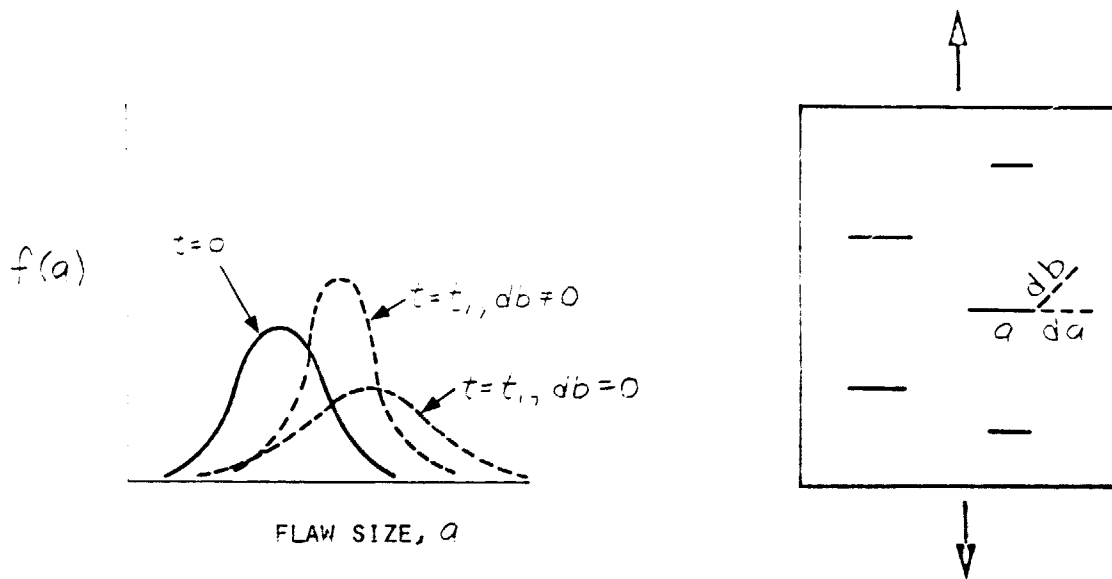


Figure 6.- Changes in flaw distribution function.

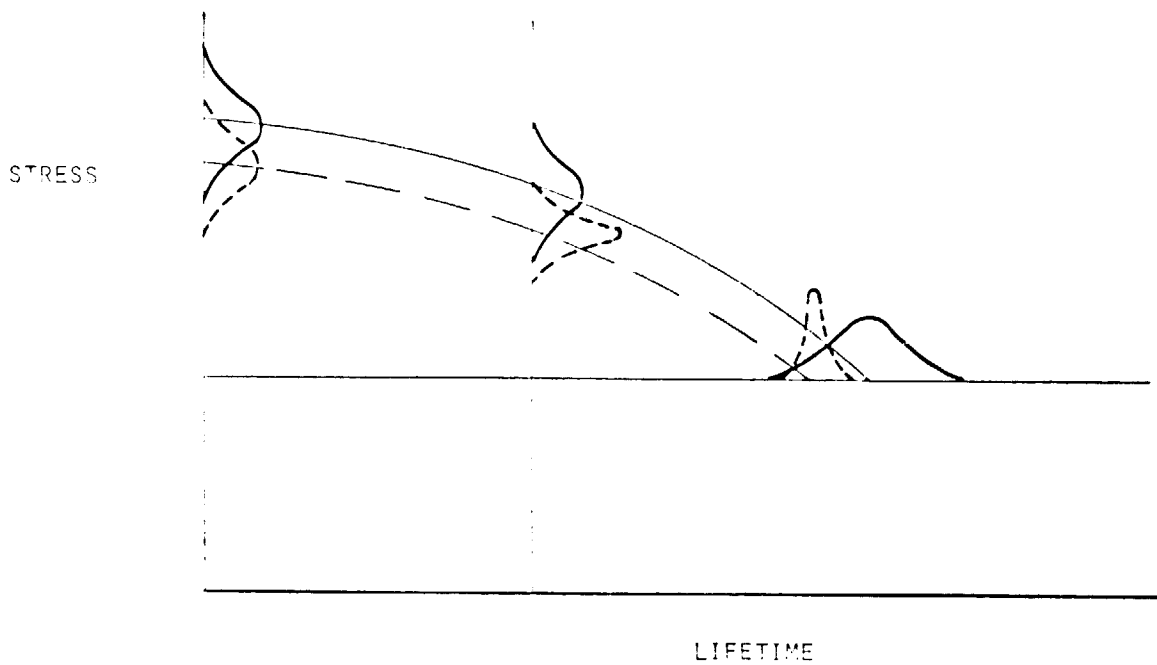


Figure 7.- Translation from static strength to lifetime.

# DESIGN, FABRICATION, AND FLIGHT SERVICE EVALUATION OF COMPOSITE-REINFORCED C-130 CENTER WING

By W. E. Harvill, Lockheed-Georgia Company,  
and H. Benson Dexter, NASA-LaRC

## SUMMARY

The efficiency and longevity of selective reinforcement of metallic structures with boron-epoxy laminates is now being demonstrated by flight evaluation of two C-130 composite-reinforced center wing boxes. The first year's flight evaluation of these structures, which are being used by the U. S. Air Force in regular operational service, has been completed and is summarized. Ground tests in support of the service utilization are reviewed, including static, fatigue, and ground vibration test results. Basic structural design/fabrication problems and solutions are discussed, including the achievement of minimum residual thermal stresses after bonding and the NDI techniques employed. Results of periodic service inspections are discussed, and tentative reliability projections for the composite-reinforced structure are defined.

The information reported was generated by Lockheed-Georgia and NASA-LaRC personnel during conduct of Contract NAS1-11100, "Program for Establishing Longtime Flight Service Performance of Composite Materials in the Center Wing Structure of C-130 Aircraft."

## INTRODUCTION

Application studies and development tests (References 1 and 2), conducted for NASA by Lockheed, showed that boron-epoxy composite laminates bonded to the skin panels and spanwise stiffeners of the C-130 aircraft center wing box significantly improved the overall fatigue endurance of the structure, at a lower weight than that possible if metal reinforcements were used to achieve the same endurance levels. These advantages are being demonstrated by designing, fabricating, and testing three boron-epoxy reinforced C-130H center wing boxes, in a five-phase program extending over 6 1/2 years. Fabrication was completed in late 1974; ground tests will be complete in early 1976; and flight service evaluations will continue into 1978.

The C-130 center wing box size and location are illustrated in Figure 1. The structural box is 11.2 m (440 in.) in length, 2.03 m (80 in.) in chord, and, in the all-metal configurations, weighs approximately 2243 kg (4944 lb.). The structural configuration of the center wing box consists of upper and lower surfaces that are reinforced with hat-shaped spanwise stringers, the forward and aft wing beams, and truss-type ribs. The configuration of the C-130H all-metal wing box, illustrated in Figure 2, is applicable to all of the C-130 and L-100 series aircraft.

The same structural arrangement was used for the composite-reinforced center wing box as for the all-metal box. The structural criterion for design of the composite-reinforced wing box was to provide sufficient metallic structure to support limit design loads. Reinforcement by adhesive bonding unidirectional boron-epoxy laminates to the wing surface panels and stringers provided additional strength for ultimate design loads (1.5 x limit load), and for required fatigue strength and stiffness. Composite reinforcements were used in the wing surface panels only; spars, ribs, and major joints were retained in the basic metal configuration.

The final composite reinforcement concept, shown in Figure 3, satisfied all structural requirements. The boron-epoxy laminates were made from AVCO 5505 Rigidite<sup>®</sup>, and were bonded to the metal adherends with AF 127-3 epoxy adhesive. Fasteners at the ends of laminates were provided to prevent initiation of peeling. Where fasteners were used, additional bearing strength was provided by titanium shims interleaved in the laminates.

Although weight saving was not a major program goal, and was actually subordinated to accomplishment of flight service program goals, it was, nevertheless, an important factor. Actual weighings of the completed wing boxes showed savings of 222 kg (488 lb.) for the test article and 205 kg (450 lb.) for the flight articles. This represents an average saving of 15 percent in the surfaces where a metal removed/composite added ratio of 2.5 was achieved. Based on total wing box weight, a saving of better than nine percent was attained.

Fabrication involved laying-up and curing boron-epoxy laminate reinforcements on an autoclave tool followed by adhesive bonding the cured boron-epoxy laminates to the spanwise stringers and wing surface panels. The laminate and metal adherends were bonded together on a massive steel tool, designed specifically to overcome the warpage problems inherent in elevated temperature bonding of materials with different thermal expansion properties.

This special tool restrained the aluminum alloy, reducing its expansion during the curing operations. The reinforcing laminate was allowed to expand without restraint, to compensate for the slight tool expansion encountered due to some tool temperature changes. The resulting parts were essentially straight, indicating

achievement of a practically stress-free bondline at room temperature. This achievement eliminated assembly problems which might have been incurred if the bonded parts had not been straight. A schematic of the special restraint tool is shown in Figure 4.

Assembly of the composite-reinforced components into the center wing box was accomplished without difficulty by C-130 production personnel, using normal production fixtures and techniques. In the first stage of this process, shown in Figure 5, the hat-section stiffeners were joined to the surface panels and to the production joint fittings to form a complete upper or lower surface. In subsequent operations ribs, spars, and trailing edges were installed to complete the box. Design and fabrication details are fully reported in References 3 and 4.

Three C-130 center wing boxes were fabricated; two were installed on operational aircraft, and one was used for extensive ground-testing. The C-130 aircraft on which the composite-reinforced center wing boxes are installed have successfully completed a full year of operational service. Ground tests and flight evaluations are discussed hereafter.

## TECHNICAL DISCUSSION

### Ground Vibration Tests

Vibration tests were conducted on the first aircraft with the composite-reinforced center wing to verify analytical predictions that the existing aircraft flutter speeds had not been adversely affected by the modification. Accelerometers were attached to selected locations on the aircraft structure to measure amplitude vectors at each important resonant frequency. The overall vibration test set up is shown in Figure 6. For one set of measurements, the shakers were attached to the wing rear beam at each wing tip, and for the second set, the shakers were located at the aft end of each external fuel tank.

The vibration test was conducted by making constant force frequency sweeps from 0.5 Hz to 50 Hz, symmetrically and asymmetrically, with the shakers located at the wing tip rear beams first, and then relocated to the aft end of the external fuel tanks. Plots of output acceleration versus frequency were made to identify the resonant frequencies. Also, a modal survey was made at each important resonant frequency using a roving accelerometer to make recordings at pre-selected locations on the structure. The resonant frequencies recorded during the vibration test were compared with results from a similar test on an aircraft with an all-metal center wing. It was concluded from the comparative results that the vibration characteristics of the two aircraft are essentially identical.



## Static Proof Load Tests

The composite-reinforced wing test article was proof-loaded for the most critical of the design upbending and downbending conditions. The critical upbending condition was a symmetrical flight maneuver representative of a positive 2.5 g load factor. The critical downbending condition results from taxiing the aircraft with capacity wing fuel at maximum gross weight. Prior to applying four lifetimes of fatigue loading to the wing test article, critical upbending and downbending loads were applied to it. Upon successful completion of four simulated lifetimes of fatigue loading, the wing test article was successfully loaded to the critical upbending condition. Figure 7 shows the wing test article installed in the test fixture prior to conducting the first proof load test.

The test article was instrumented with a mixture of axial, shear and rosette electrical resistance strain gages. A total of 337 gage elements were used. All rosette and shear gage installations included "back-up" gages for cancellation of bending strains. Loads were applied to the wing test article by hydraulic actuators in the test fixture that were electro-hydraulic servo-controlled and hydraulic servo-controlled with hydraulic power supplied by a pump system rated for continuous duty at an output pressure of 3000 psi. A calibrated dual-bridge load transducer was located in series with each actuator in each load control channel. One bridge of the transducer supplied feedback to the load control system, and the other was used for load monitoring and recording.

Measured strains, taken during limit load tests before and after the four-lifetime fatigue endurance demonstration, showed a very close comparison. Thus, at loads up to the maximum upbending design load expected in service, there has been no apparent degradation in structural integrity. The comparison of "before" and "after" strains in Figure 8 illustrates the excellent agreement achieved.

## Fatigue Tests

Four simulated lifetimes of fatigue loading were successfully applied to the wing article upon completion of the first upbending proof load test and the downbending proof load test. Spectrum loads were applied that were identical to those used for full-scale testing of the Model C-130 all-metal wing structure. Strain surveys and ultrasonic inspections were conducted at the beginning of the fatigue test and after completing each lifetime. Pulse-echo techniques were the primary ultrasonic method used for this and subsequent ultrasonic inspections. In addition, local ultrasonic inspections were conducted after each load pass in areas of suspected disbonds detected after the proof load tests. No disbond propagation was found in four lifetimes of fatigue testing.

The applied fatigue loads spectrum simulated four lifetimes representing 40,000 flight hours and 28,868 aircraft landings. Each simulated lifetime consisted of 10 passes, and forty passes were completed during the fatigue test: a total of 1,028,900 load cycles. Each load pass consisted of incremental blocks of load cycles for gust, taxi, and ground-air-ground conditions. During the fatigue test, each strain survey was made applying the maximum upbending local condition (gust) and maximum downbending load condition (taxi) from the fatigue spectrum and recording the strains. Strains were recorded at each load increment for comparison with initial strain measurements. Four channels were used for continuous strain monitoring on a strip recorder. Strains on all channels were recorded once in each load pass for one selected load condition as a check on test specimen behavior.

During the course of the four simulated lifetimes, only minor damage was detected in the wing test article until the last load pass in the fourth lifetime was nearly completed. At that time, two cracks were found in the front beam web of the test article where it was attached to the lower front beam cap. Both cracks were outside the composite-reinforced areas of test article. They were not judged to be detrimental in completing the fatigue test, and the test was completed without repairing them. The only other minor damage that occurred during the fatigue test involved a few broken fastener collars and heads. Fasteners having broken collars or heads were replaced at the end of the load pass in which they were detected.

Local ultrasonic inspections of the suspected adhesive bondline defects detected after the proof load tests did not show any propagation during the four simulated lifetimes of fatigue loading. Ultrasonic inspections performed on the accessible composite-to-metal bondlines after each of the four lifetimes did not reveal any defects.

#### Crack Growth Test

Successful completion of the required fatigue tests, with no apparent damage to the composite-reinforced surface panels, allowed an extension of the original test to develop crack growth data. After a satisfactory limit upbending load test, the crack growth tests were initiated. The crack growth test was a cyclic load test on the artificially damaged wing test article. The cyclic loads were identical to fatigue loads applied during the four lifetimes endurance demonstration. Artificial damage was inflicted in the wing test article at twelve selected locations in the upper and lower wing surface skin panels and in the composite-to-metal bondlines common to the wing surface skin panels. The types of damage in the wing test article are described below, and locations are illustrated in Figure 9.

- a. Saw cut in the wing surface plank at the outer fastener hole in the composite reinforcement run-out area. Fastener was reinstalled in the hole after saw cut. (See Figure 10.)

- b. Saw cut in the wing surface plank at the outer fastener hole in composite reinforcement run-out area. All fasteners were removed from the composite-reinforced run-out area, and the boron-epoxy laminate was disbanded from the end of the laminate to the most-inboard fastener location.
- c. A saw cut was induced through the lower wing surface skin panel in the aft edge of the access door cut-out that extended 0.25 cm (0.10 inch) into the access door fillet. (See Figure 11.)
- d. Adhesive bondline was disbanded on the inboard side of the access door cut-out from the composite reinforcement termination to the first fastener. All fasteners were removed from the composite reinforcement run-out area.
- e. Adhesive bondline was disbanded on the inboard side of the access door cut-out from the composite reinforcement termination to the first fastener. Fasteners were not removed from the composite reinforcement run-out area.
- f. A saw cut was induced through the lower wing surface skin panel between two stringers in the chordwise direction. The length of the saw cut extended across the uninterrupted distance between flanges. (See Figure 12.)

The artificially induced disbonds were ultrasonically inspected to establish a "baseline" of disbanded areas prior to initiating fatigue cycling. During the crack growth test, visual and ultrasonic inspections are being performed on the wing test article exterior surfaces after each load pass. During cycling, the saw cuts are being monitored to determine when they have reached critical proportions. When a saw cut has propagated to its calculated critical length, the cyclic loading will be suspended and a residual strength test will be conducted on the wing test article. If, at the end of the sixth load pass, none of the cracks have reached critical proportions, crack lengths will be extended to assure that at least one crack will reach its calculated critical length by the end of the tenth load pass. Cycling into the tenth load pass will be continued until one crack reaches the critical crack length or the tenth pass is completed. The damaged wing test article will be tested to failure or 130 percent limit design load, whichever occurs first, applying the critical up-bending load condition.

## Flight Service Evaluation

Upon completion of the flight acceptance tests on the two C-130 aircraft, AF73-01592 and AF73-01594, on which the composite-reinforced center wing boxes were installed, they were delivered to the Air Force and flown to the Little Rock Air Force Base, Jacksonville, Arkansas. Both aircraft are currently being used in basic and proficiency training, including cargo airlift missions. This is the regular assignment for the operational command, which includes rotation of aircraft to other widely dispersed bases. The aircraft have been in operational service for one year. During that period, as shown in Figure 13, the first composite-reinforced center wing box to enter operational service has been inspected three times, and the second composite-reinforced center wing box has been inspected twice. No disbonds or other irregularities were detected that exceeded the specification limits. The specification limits for adhesive bond quality are:

1. The maximum allowable area of any individual disbond is 0.5 square inch.
2. Disbonded areas shall not exceed 5 percent of the total bonded area of each detail part.
3. The distance between two adjacent disbonds shall not be less than four times the largest dimension of the largest disbond.
4. No detectable disbonded areas shall be within 0.125 inch of any bondline edge.

The service evaluation has proceeded uneventfully thus far, and (based on ground test results) no difficulties are anticipated. After successful completion of the initial three-year service evaluation, it would be desirable to continue monitoring the operational experience for an extended period to verify the longevity of composite-reinforced primary structures.

Tentative estimates of structural reliability, based on an assessment of the adhesive bondline and the probability of disbonds, indicate that, in production, 99 out of every 100 structures would be delivered without unbonded areas. Since no disbond propagation was found in four lifetimes of fatigue testing, it can be concluded that this would not significantly degrade structural integrity, and that the quality of the composite-reinforced structure will assure satisfactory achievement of program goals.

## CONCLUDING REMARKS

Progress to date on the C-130 composite-reinforced center wing has shown this concept to be an efficient method for design and fabrication of primary aircraft structures. Using the conservative approach of designing the center wing metallic structural components to support design limit load, and adding composite reinforcements for satisfaction of other structural requirements, the resulting design weighed significantly less than the all-metal center wing. In the first year of operational service, no problems have developed with either of the two composite-reinforced center wing boxes. During this trouble-free operational period, no special considerations have been accorded to the two aircraft having the composite-reinforced center wings, and they have been used in routine operational service typical of other C-130 aircraft.

Ground tests, including proof load, fatigue, and ground vibration, have been successfully accomplished satisfying or surpassing all structural requirements. The successful completion of the four simulated lifetimes of fatigue loading on the composite-reinforced center wing test article allowed development of crack propagation data using the composite-reinforced center wing test article for further tests.

## REFERENCES

1. Petit, P. H., "An Application Study of Advanced Composite Materials to the C-130 Center Wing Box," NASA CR66979, Lockheed-Georgia Company, June 1970.
2. Harvill, W. E., et al., "Program for Establishing Long-Time Flight Service Performance of Composite Materials in the Center Wing Structure of C-130 Aircraft: Phase I - Advanced Development," NASA CR-112126, Lockheed-Georgia Company, November 1972.
3. Harvill, W. E., et al., "Program for Establishing Long-Time Flight Service Performance of Composite Materials in the Center Wing Structure of C-130 Aircraft: Phase II - Detailed Design," NASA CR-112272, Lockheed-Georgia Company, April 1973.
4. Harvill, W. E., and Kays, A. O., "Program for Establishing Long-Time Flight Service Performance of Composite Materials in the Center Wing Structure of C-130 Aircraft: Phase III - Fabrication," NASA CR-132495, Lockheed-Georgia Company, September 1974.

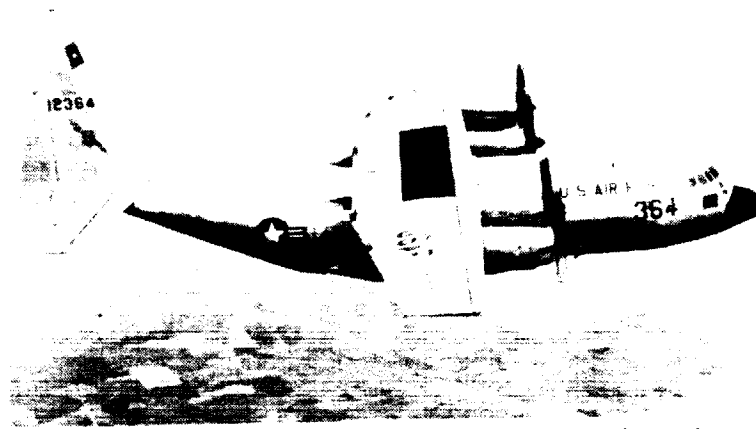


Figure 1. C-130 Center Wing Box Location

1. UPPER SURFACE PANELS
2. UPPER SURFACE STRINGERS
3. UPPER SURFACE RAINBOW FITTING
4. LOWER SURFACE PANELS
5. LOWER SURFACE STRINGERS
6. LOWER SURFACE RAINBOW FITTING
7. FRONT BEAM
8. REAR BEAM

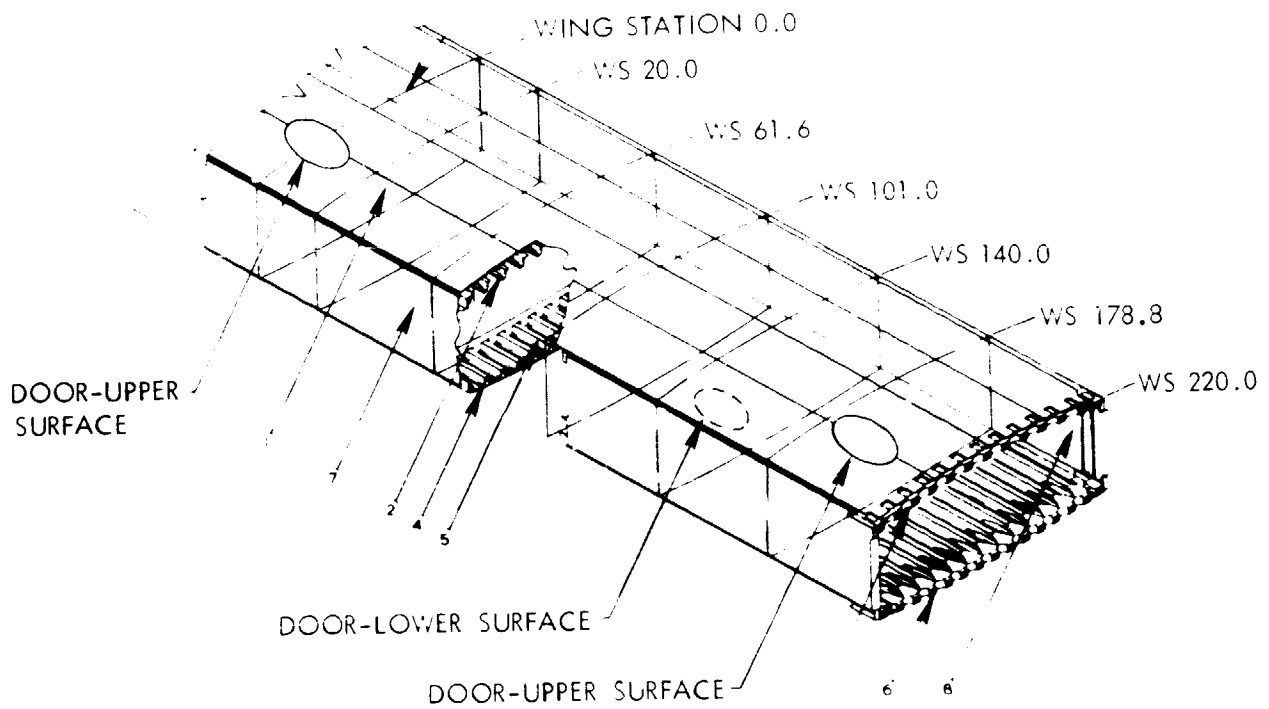


Figure 2. Model C-130H Aircraft Center Wing Box

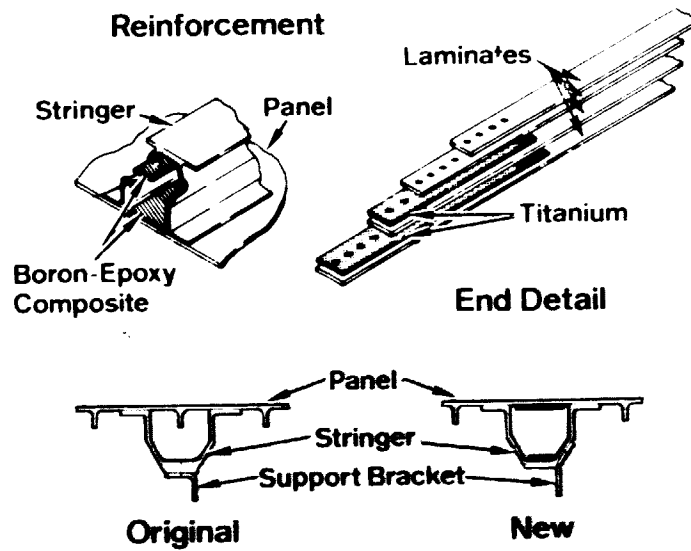


Figure 3. Composite Reinforcement Concept

### Restraining Device Concept

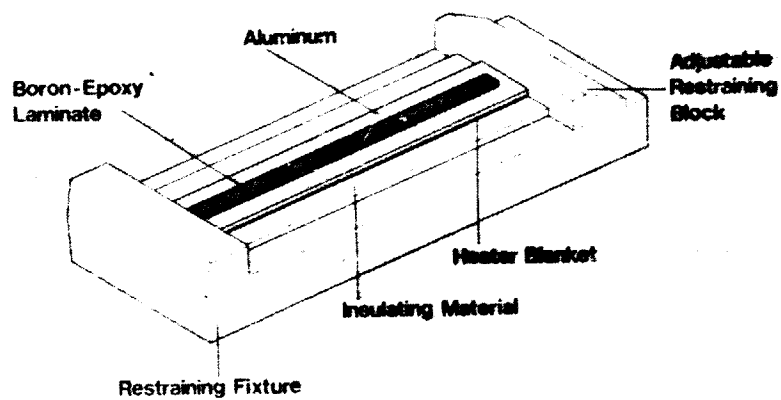


Figure 4. Adhesive Bonding Restraint Tool

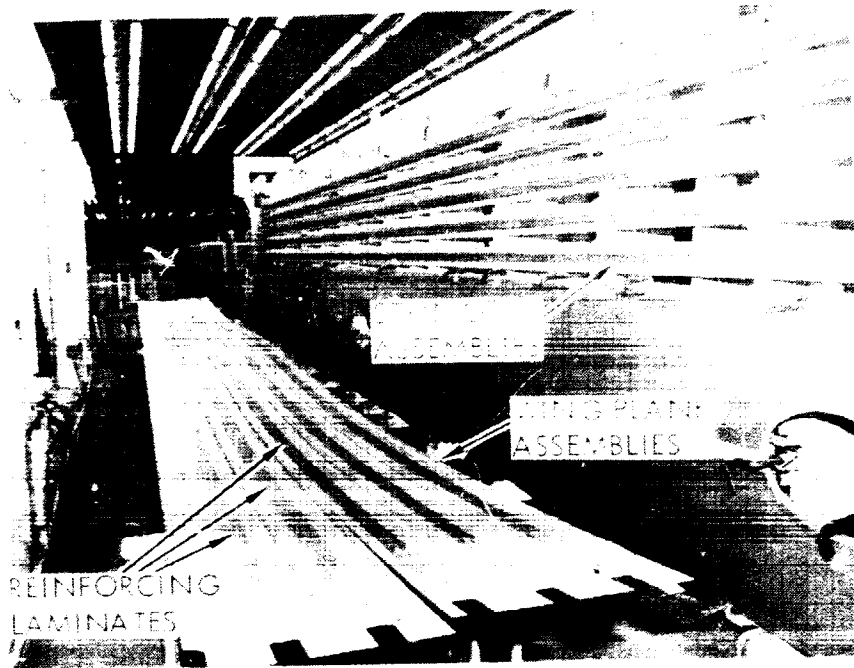


Figure 5. Upper Wing Surface in First Assembly Stage

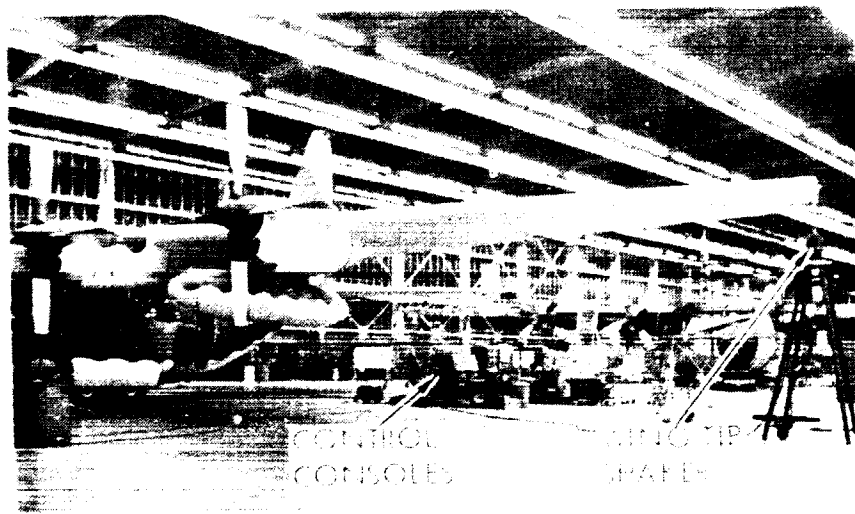


Figure 6. Ground Vibration Test - A C 73-01592

ORIGINAL PAGE IS  
OF POOR QUALITY.





Figure 7. Center Wing Box in Test Fixture

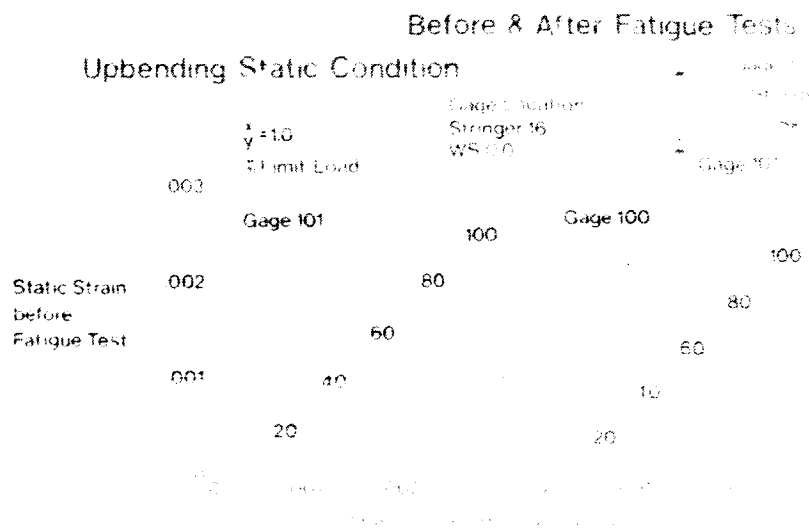


Figure 8. Typical Comparison of Strains Before and After Four - Lifetime Fatigue Test

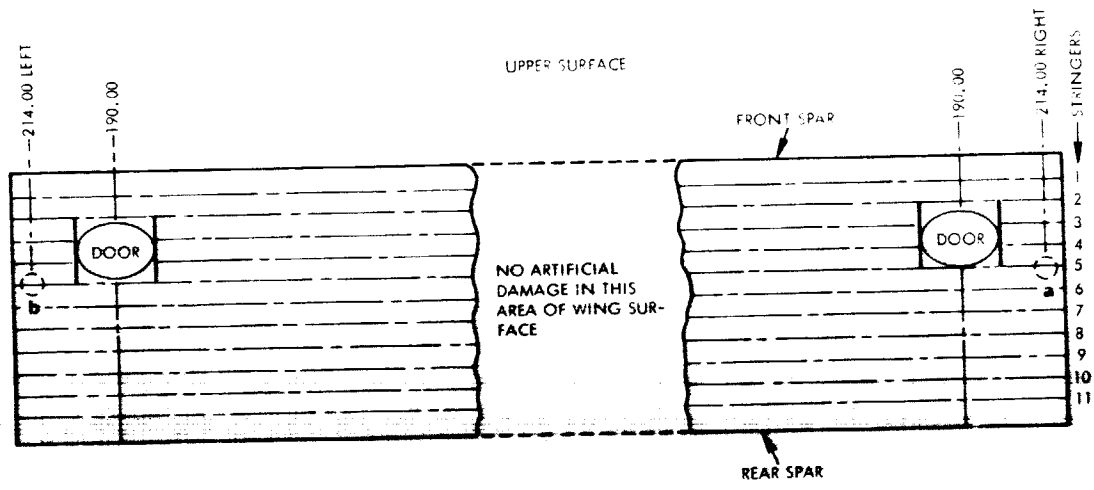
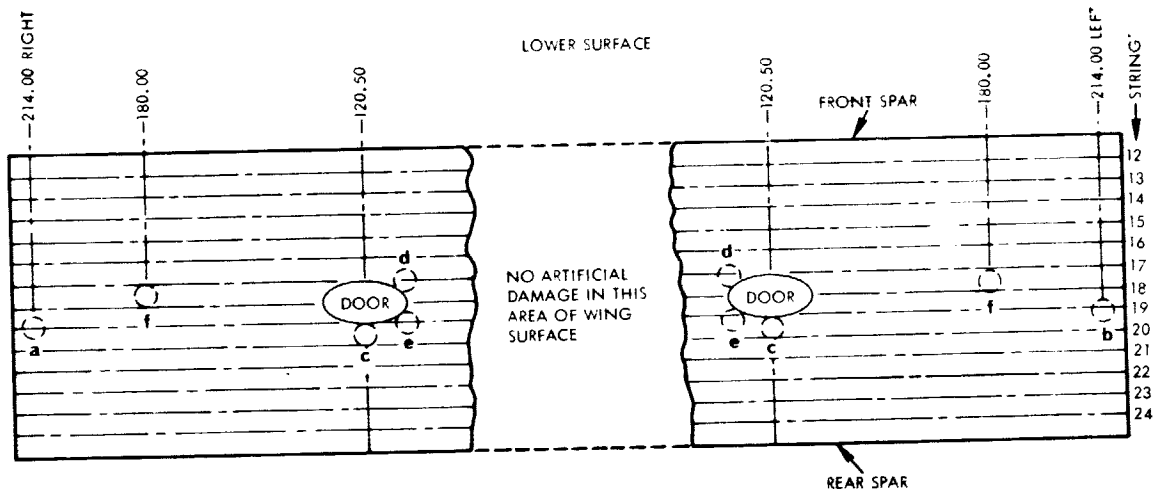


Figure 9a. Location of Artificially-Induced Damage on Center Wing Box Surface



○ DAMAGED AREAS AS DEFINED IN TEXT

Figure 9b. Location of Artificially-Induced Damage on Center Wing Box Surface

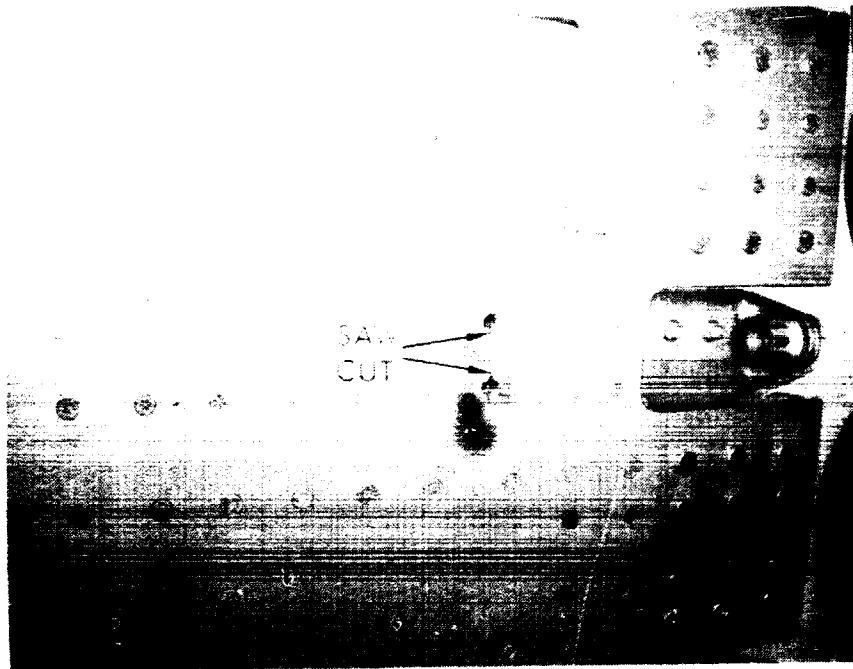


Figure 10. Saw Cut in Surface Panel - Wing Station 214 at Fastener Hole

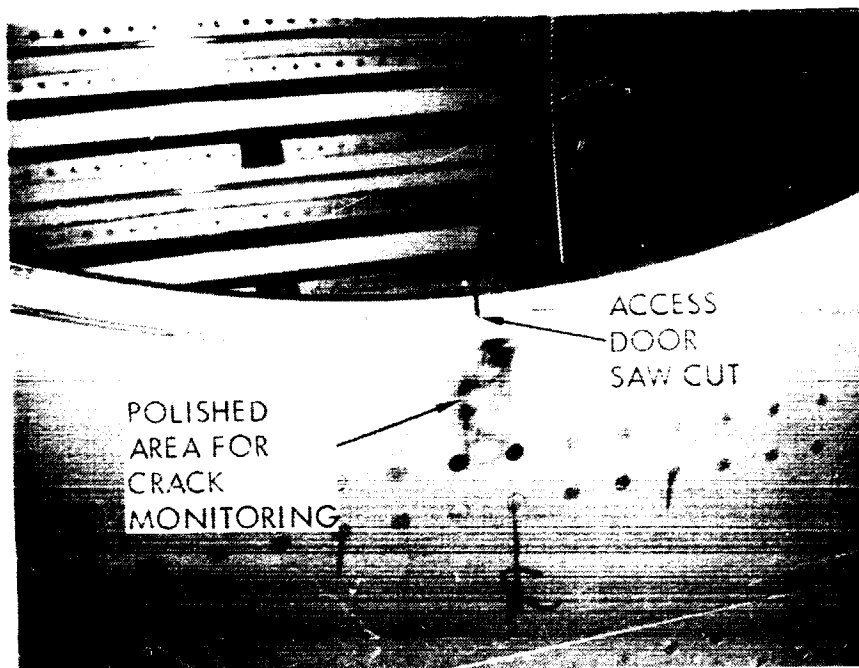


Figure 11. Saw Cut at Aft Access Door Flange - Lower Surface at W. S. 120

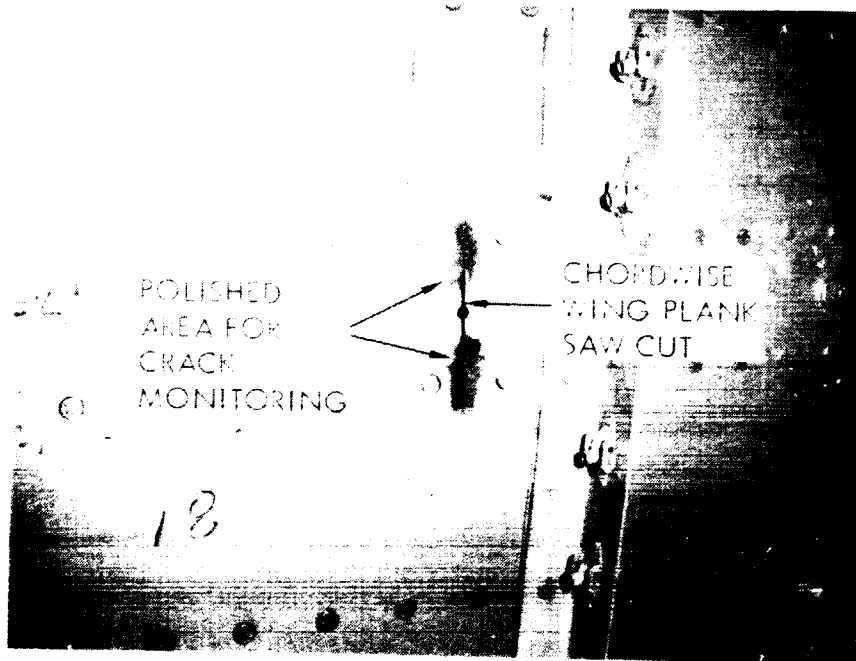


Figure 12. Saw Cut Between Stringers - Lower Surface at W. S. 180

A/C Serial Number	Inspection Schedule												
	1975				1976				1977				
	1	2	3	4	1	2	3	4	1	2	3	4	
AF73-01592	▼	▼	▼	▼	▼	▼	▼	▼					(PDM)
AF73-01594	▼	▼	▼	▼	▼	▼	▼	▼					(PDM)

Figure 13. Service Evaluation of Composite Reinforced C-130 Center Wings

BOLTED JOINT STATIC STRENGTH MODEL  
FOR  
COMPOSITE MATERIALS

James R. Eisenmann  
General Dynamics Fort Worth Division

ABSTRACT

A method is presented for predicting the static strength of bolted joints in advanced composite materials. This strength model predicts failure load and failure location accounting for the effects of geometry, absolute fastener diameter, laminate orientation, and stress state. The approach is based on the now accepted observation that failure of advanced composite materials is modelled more closely by stress intensity than by absolute stress magnitude. Results of a series of forty-eight static tests indicate excellent correlation of measured failing load and observed failure location with strength model predictions.

SCOPE

The technique proposed in Reference 1 for modelling the strength of notched composite laminates has been expanded into a form suitable for the analysis of a bolted joint element. The approach consists of comparing values of laminate fracture toughness measured by test with values of the Mode I stress

intensity derived analytically at selected points on the boundary of the fastener hole.

This technique can be applied to the analysis of complex joints on an element-by-element basis as shown in Figure 1. Each of these elements is subject to a general set of uniform membrane stresses and to a bolt load acting in some arbitrary direction with respect to the primary laminate axes as shown in Figure 2. Examination of many failed joint test specimens led to the selection of the eight locations shown on the hole boundary which will be included in this analysis. Failures were observed to initiate at or very near one or more of these eight points as through cracks propagating radially for a short distance before losing the distinct features of a through crack. Values of laminate strength and fracture toughness at these locations can be measured using tensile coupons and edge-notched beams fabricated such that they represent laminate properties in the direction tangent to the hole boundary as shown in Figure 3. Because of material symmetry, tests representative of points 1, 2, and 3 are usually sufficient. A good discussion of fracture toughness test techniques, data reduction schemes, and extension of the edge-notched beam data to other laminates can be found in References 2 and 3.

As discussed in Reference 1, once the laminate strength and fracture toughness have been determined the characteristic

dimension,  $a^i$ , can be calculated for each of the eight selected locations.

$$a^i = \frac{1}{\pi} \left( \frac{K_Q^i}{\sigma_{ult}^i} \right)^2 \quad (1)$$

For the purpose of estimating the stress intensity at each of the eight locations on the hole boundary, the dimension  $a^i$  will be taken as the length of a through crack extending radially outward from the hole boundary. The Mode I stress intensity is then calculated at each of the eight locations for each of the five basic unit load conditions as indicated by the example for location 2 as shown in Figure 4.

Using linear superposition, the expression for the stress intensity at location  $i$  can be written for the general load case

$$K_I^i = K_{I_{tx}}^i \sigma_{tx} + K_{I_{ty}}^i \sigma_{ty} + K_{I_{xy}}^i \sigma_{xy} + K_{I_{bx}}^i \sigma_{bx} + K_{I_{by}}^i \sigma_{by} \quad (2)$$

For any set of applied stresses the stress intensity at point  $i$  can be calculated and compared to the corresponding value of fracture toughness. The failure criterion is

$$K_I = K_Q^i \quad (3)$$

An alternate form of Equation (2) which has proven useful is obtained by expressing the stress intensity resulting from a unit applied stress as

$$K_I = \sqrt{\pi a} f\left(\frac{a}{r}\right). \quad (4)$$

Substituting Equation (4) into Equation (2) gives

$$\begin{aligned} \sigma^i &= \frac{K_I^i}{\sqrt{\pi a^i}} = f\left(\frac{a^i}{r}\right)_{tx} \sigma_{tx} + f\left(\frac{a^i}{r}\right)_{ty} \sigma_{ty} \\ &+ f\left(\frac{a^i}{r}\right)_{xy} \sigma_{xy} + f\left(\frac{a^i}{r}\right)_{bx} \sigma_{bx} + f\left(\frac{a^i}{r}\right)_{by} \sigma_{by} \end{aligned} \quad (5)$$

In this form the function  $f\left(\frac{a}{r}\right)$  appears as an "effective stress concentration factor" giving rise to an "effective tangential stress" at the hole boundary,  $\sigma^i$ . The failure criterion for this form of the equation is

$$\sigma^i = \sigma^i_{ult} \quad (6)$$

In practice it is often more convenient to calculate values of stress intensity, or of  $f\left(\frac{a}{r}\right)$ , for an infinitely large plate and apply finite width correction factors to account for the finite boundaries of the rectangular joint element. Equation (5) is then rewritten as:

$$\begin{aligned} \sigma^i &= \lambda^i_{tx} f\left(\frac{a^i}{r}\right)_{tx} \sigma_{tx} + \lambda^i_{ty} f\left(\frac{a^i}{r}\right)_{ty} \sigma_{ty} \\ &+ \lambda^i_{xy} f\left(\frac{a^i}{r}\right)_{xy} \sigma_{xy} + \lambda^i_{bx} f\left(\frac{a^i}{r}\right)_{bx} \sigma_{bx} \\ &+ \lambda^i_{by} f\left(\frac{a^i}{r}\right)_{by} \sigma_{by}. \end{aligned} \quad (7)$$



A test program has been conducted to assess the usefulness of the bolted joint strength model as developed here. Correlation between the strength model and the test data will be discussed in the next section.

#### CONCLUSIONS AND SIGNIFICANCE

A series of forty-eight graphite-epoxy coupons were tested to static failure at room temperature. The test fixture had provisions for apportioning the load between axial tension acting throughout the coupon and local bearing load introduced in double shear by a 0.375 inch diameter untorqued fastener at the center of the coupon. In fabricating the test coupons, the  $[0_2/\pm 45]_c$  laminate was oriented at an angle with respect to the applied axial tension and bearing loads. In this way it was possible to simulate biaxial tension, shear, and biaxial bearing stresses acting on an element in the vicinity of the fastener as shown in Figure 5. The test series included laminates oriented at  $0^\circ$ ,  $22.5^\circ$ ,  $45^\circ$ , and  $67.5^\circ$  with respect to the applied load axis. Bearing loads equal to 0, 30, 50, and 100 percent of the total load were applied to the coupons. Three coupons were tested at each combination of bearing load and laminate orientation. The test results are summarized in Table I and plotted in Figures 6 through 9. For this test series the critical failure locations were 1, 2, 3, 7, and 8. The applied stress

required to cause failure at each of these locations as predicted by Equation (7) is plotted as a solid line. The lowermost boundary of this family of curves represents the failure envelope for the coupon describing both the applied stress at failure and the location of the failure on the hole boundary. The data for the laminate oriented at  $0^\circ$  are shown again in Figure 10 to demonstrate the interaction between tension stress and bearing stress more clearly. As shown in Figure 11, the measured failing stresses agree very well with the strength model predictions for all four load ratios. Likewise, the predicted failure locations are included within the set of observed failure locations tabulated in Table I.

The strength estimation technique developed here is only a first step toward a thorough understanding of composite mechanical joints. It does, however, provide for the first time a single approach which relates the effects of geometry, applied stress state, and laminate mechanical properties to the strength of a composite bolted joint.

#### SUPPLEMENTARY INFORMATION

Stress intensities for each load case shown in Figure 4 were obtained numerically for several values of crack length using the boundary integral equation solution technique (References 4 and 5). The expressions in Table II were then

obtained by curve-fitting the numerical results and are applicable to infinite isotropic elements. In order to correct these isotropic results for use with orthotropic elements, the elastic stress concentration factors for holes without edge cracks are used to form an orthotropic correction factor for each load case and crack location. The elastic stress concentration factors for open holes (Reference 6) and holes loaded in bearing (Reference 4) are given in Table III in terms of the engineering constants for the orthotropic laminate. These values are used in Table IV to form the orthotropic correction factors as follows:

$$f\left(\frac{a^i}{r}\right) = \left\{ B1 \left[ 1 - \left(\frac{a^i}{r}\right) B2 \right] \left[ \hat{f}\left(\frac{a^i}{r}\right) - B3 \right] + B3 \right\} B4 \quad (8)$$

The effect of the correction factor defined by the expression in braces in Equation (8) is to insure the two conditions:

$$f\left(\frac{a^i}{r}\right)_{\alpha} = 1.13 Kt_{\alpha}^i \text{ for } \frac{a^i}{r} = 0.0,$$

and

$$f\left(\frac{a^i}{r}\right)_{\alpha} = \hat{f}\left(\frac{a^i}{r}\right)_{\alpha} \text{ for } \frac{a^i}{r} \geq \left(\frac{a^i}{r}\right)_c$$

where  $\left(\frac{a^i}{r}\right)_c$  is the denominator of the expression for B2 in Table IV. The correction factor should only be applied for

$$0 \leq \frac{a^i}{r} \leq \left(\frac{a^i}{r}\right)_c.$$

The values of  $f\left(\frac{a}{r}\right)_\alpha^i$  obtained in this manner are inexact in that the boundary conditions at the hole which were assumed for the analysis are not those which actually exist in the application. Analysis for the tension and shear load cases assumes no applied stresses or specified displacements on the hole boundary when in fact the presence of the fastener in the hole alters both the deformation and state of stress nearby. Similarly the analysis of the two bearing load cases was based on the assumption of a cosine distribution of radial stress to represent the bearing load. Here the presence of the fastener affects the displacement of the hole boundary and the shape of the applied bearing load distribution. Discrepancies between analytical predictions and test results for the individual load cases were noted, and the empirical constants  $B_4$  in Table IV were included to correct for effects beyond the capability of the current analysis. It is recommended that the values of these constants be updated whenever test data for the individual load cases is available.

Tables V and VI provide typical values of radial crack length and unnotched laminate strength, respectively. These two tables are applicable to Narmco 5208/T300 laminates of the  $[0_i/(\pm 45)_j]$  family for room temperature, dry conditions where  $10 \leq PCTO \leq 50$ .

Tables VII through XIX provide values of finite width correction factors,  $\lambda_{\alpha}^i$ , for the  $[0_i/(\pm 45)_j]$  family of orthotropic laminates. The correction factors were obtained in the same manner as those discussed in Reference 4. Although the engineering constants for boron-epoxy were used in generating these correction factors, they will be approximately correct for other material systems if interpolation within the tables is based on the value of  $Kt_{\alpha}^i$  for the material system of interest.

#### REFERENCES

1. M. E. Waddoups, J. R. Eisenmann, B. E. Kaminski, "Macroscopic Fracture Mechanics of Advanced Composite Materials," J. Composite Materials, Vol. 5 (1971), p. 446.
2. T. A. Cruse, "Tensile Strength of Notched Composites," J. Composite Materials, Vol. 7 (1973), p. 218.
3. H. J. Konish, T. A. Cruse, "The Determination of Fracture Strength in Orthotropic Graphite/Epoxy Laminates," Presented at ASTM Composites Reliability Conference, Las Vegas, Nevada, April 15/16, 1974.
4. J. P. Waszczak, T. A. Cruse, "A Synthesis Procedure for Mechanically Fastened Joints in Advanced Composite Materials," AFML-TR-73-145, Volume II, September 1973.
5. T. A. Cruse, J. R. Osias, "Exploratory Investigations of Fracture Mechanics of Composite Materials," AFML-TR-74-111, June 1974.
6. S. G. Lekhnitskii, Anisotropic Plates, translated by S.W. Tsai and T. Cheron, Gordon and Breach (1968).

## SYMBOLS

$r$	Hole radius
$a^i$	Value of crack length used to calculate stress intensity at location $i$
$\sigma_{ult}^i$	Unnotched laminate ultimate strength in tangential direction at location $i$
$K_Q^i$	Laminate fracture toughness corresponding to radial crack propagation at location $i$
$Kt_\alpha^i$	Elastic tangential stress concentration factor at location $i$ for applied load condition $\alpha$
$K_{I\alpha}^i$	Mode I stress intensity at location $i$ for applied load condition $\alpha$
$f\left(\frac{a^i}{r}\right)_\alpha$	Effective orthotropic stress concentration factor at location $i$ for applied load condition $\alpha$
$\hat{f}\left(\frac{a^i}{r}\right)_\alpha$	Effective isotropic stress concentration factor at location $i$ for applied load condition $\alpha$
$\lambda_\alpha^i$	Finite width correction factor at location $i$ for applied load condition $\alpha$
$\sigma_\alpha$	Applied stress for load condition
$\alpha$	Subscript denoting applied load condition as follows: = tx tension in x-direction = ty tension in y-direction = xy shear = bx bearing in x-direction = by bearing in y-direction
$E_x, E_y, G_{xy}, \nu_{xy}$	Engineering constants for orthotropic laminate

$E_{\theta}$  Laminate modulus in tangential direction at locations  
2, 4, 6, 8;

$$E_{\theta} = 4 \left( \frac{1-2\nu_{xy}}{E_x} + \frac{1}{E_y} + \frac{1}{G_{xy}} \right)^{-1}$$

PCT0, PCT45 Percentages of 0-degree and  $\pm 45$ -degree plies in  
orthotropic laminate

Table I TEST DATA SUMMARY

$\theta$	Fraction of Total Load Carried in Bearing	Average Gross Failing Stress	Failure Locations
0°	0.0	50060	i = 3,7
	0.3	34960	i = 3,7
	0.5	31440	i = 3,7
	1.0	18070	i = 1,2,3,7,8
22.5°	0.0	37440	i = 3,7,8
	0.3	29530	i = 8
	0.5	25530	i = 1,3,8
	1.0	16510	i = 1,2,3,8
45°	0.0	31280	i = 8
	0.3	22750	i = 1,8
	0.5	20050	i = 1
	1.0	11540	i = 1,2,3
67.5°	0.0	21880	i = 1
	0.3	17240	i = 1
	0.5	16220	i = 1,2
	1.0	13800	i = 1



Table II EFFECTIVE ISOTROPIC STRESS  
CONCENTRATION FACTORS

$\alpha$	$i$	$\hat{f}\left(\frac{a^i}{r}\right)$
tx ty	1,5 3,7	$-0.16 + 0.095 \left(\frac{a^i}{r}\right) + 0.97 \exp \left[ -4.169 \left(\frac{a^i}{r}\right) \right]$ minimum value: 0.0
tx ty	2,4,6,8 2,4,6,8	$0.73 - 0.14 \left(\frac{a^i}{r}\right) + 0.40 \exp \left[ -3.689 \left(\frac{a^i}{r}\right) \right]$ minimum value: 0.5
tx ty	3,7 1,5	$\left\{ 0.2949 + 0.7051 \left(\frac{a^i}{r}\right) / \left[ 1 + \left(\frac{a^i}{r}\right)^{1.2} \right]^{.8333} \right\}^{-1}$ minimum value: 1.0
xy	2,4,6,8	$1.682 \left[ \left\{ 0.2949 + 0.7051 \left(\frac{a^i}{r}\right) / \left[ 1 + \left(\frac{a^i}{r}\right)^{1.2} \right]^{.8333} \right\}^{-1} - 1.0 \right] + 0.5$ minimum value: 0.5
bx by	1 3	$0.452 - 0.085 \left(\frac{a^i}{r}\right)^{\frac{1}{2}} - 0.171 \left(\frac{a^i}{r}\right)^{1/3}$ minimum value: 0.0
bx by	2,8 2,4	$0.406 - 0.116 \left(\frac{a^i}{r}\right) + 0.447 \exp \left[ -4.344 \left(\frac{a^i}{r}\right) \right]$ minimum value: 0.0
bx by	3,7 1,5	$0.370 - 0.070 \left(\frac{a^i}{r}\right) + 0.545 \exp \left[ -4.914 \left(\frac{a^i}{r}\right) \right]$ minimum value: 0.0
xy bx by	1,3,5,7 4,5,6 6,7,8	0.0

Table III ELASTIC TANGENTIAL STRESS  
CONCENTRATION FACTORS

$\sigma$	$i$	$Kt_{\alpha}^i$
$\tau_x$	1,5	$-\sqrt{E_y/E_x}$
$\tau_y$	3,7	$-\sqrt{E_x/E_y}$
$\tau_x$	2,4,6,8	$\frac{Ee}{2E_x} (Kt_{tx}^3 + Kt_{ty}^3)$
$\tau_y$	2,4,6,8	$\frac{Ee}{2E_x} (2 - Kt_{tx}^3 + Kt_{ty}^3) (Kt_{ty}^3)$
$\tau_x$	3,7	$1 + \sqrt{2 \left[ \sqrt{\frac{E_x}{E_y}} - \nu_{xy} \right]} + \frac{E_x}{G_{xy}}$
$\tau_y$	1,5	$1 + \sqrt{2 \left[ \sqrt{\frac{E_y}{E_x}} - \nu_{yx} \right]} + \frac{E_y}{G_{xy}}$
$\tau_{xy}$	2,6	$\frac{Ee}{2E_x} (Kt_{tx}^3 - Kt_{ty}^3) (Kt_{tx}^3 - 1)$
$\tau_{xy}$	4,8	$-Kt_{xy}^2$
$b_x$	1	$1.671 Kt_{tx}^1 + 1.280$
$b_y$	3	$-0.036(Kt_{tx}^3)^2 + 0.418Kt_{tx}^3 - 1.205$
$b_x$	2,8	$1.023Kt_{tx}^2 - 0.050$
$b_y$	2,4	$0.576 Kt_{tx}^2 + 0.754$
$b_x$	3,7	$0.403 Kt_{tx}^3 - 0.403$
$b_y$	1,5	$0.401Kt_{ty}^1 - 0.399$
$\tau_{xy}$ $b_x$ $b_y$	1,3,5,7 4,5,6 6,7,8	0.0

Table IV ORTHOTROPIC CORRECTION FACTORS

$\alpha$	i	B1	B2	B3	B4
tx	1,5	$-Kt_{tx}^1$	$(1.0-1.0/B1)/0.5$	0.0	0.9
ty	3,7	$-Kt_{ty}^3$			0.8
tx	2,4,6,8	$(1.13Kt_{tx}^2 - 0.5)/0.63$	$(1.0-1.0/B1)/0.30$	0.5	0.9
ty	2,4,6,8	$(1.13Kt_{ty}^2 - 0.5)/0.63$			
tx	3,7	$(1.13Kt_{tx}^3 - 1.0)/2.39$	$(1.0-1.0/B1)/0.25$ $(1.0-1.0/B1)/0.30$	1.0	0.9
ty	1,5	$(1.13Kt_{ty}^1 - 1.0)/2.39$			0.8
xy	2,6	$(1.13Kt_{xy}^2 - 0.5)/4.02$	$(1.0-1.0/B1)/0.30$ $(1.0-1.0/B1)/0.30$	0.5	0.7
xy	4,8	$(1.13Kt_{xy}^2 - 0.5)/4.02$			
bx	1	$Kt_{bx}^1/0.40$	$(1.0-1.0/B1)/0.30$	0.0	1.0
by	3	$Kt_{by}^3/0.40$			
bx	2,8	$Kt_{bx}^2/0.52$	$(1.0-1.0/B1)/0.70$	0.0	1.0
by	2,4	$Kt_{by}^2/0.52$			1.2
bx	3,7	$Kt_{bx}^3/0.81$	$(1.0-1.0/B1)/0.50$	0.0	1.0
by	1,5	$Kt_{by}^1/0.81$			
xy	1,3,5,7	No Correction Required			
bx	4,5,6				
by	6,7,8				

Table V RADIAL CRACK LENGTH

i	$a^i$ (inches)
1,5	$0.210 - 0.00178(\text{PCTO})$
2,4,6,8	$0.0658 - 0.00081(\text{PCT45}) + 0.381 \times 10^{-5}(\text{PCT45})^2$
3,7	$0.184 - 8.66 \times 10^{-3}(\text{PCTO}) + 2.04 \times 10^{-4}(\text{PCTO})^2 - 1.77 \times 10^{-6}(\text{PCTO})^3$

Table VI UNNOTCHED LAMINATE STRENGTH

i		$\sigma_{ult}^i$ (psi)
1,5	Tension Comp.	$20100 + 697(\text{PCTO}) - 12.82 (\text{PCTO})^2$ $0.0132 E_y$
2,4,6,8	Tension Comp.	$0.0047 E_e + 526 (\text{PCT45})$ $0.0132 E_e$
3,7	Tension Comp.	$0.00976 E_x$ $0.0132 E_x$

Table VII  $\lambda_{tx}^i$   $i=1,5$

E/D	W/D	$Kt_{tx}^i$ $i=1,5$						
		-.30	-.38	-.46	-.55	-.66	-.80	-1.00
2.00	2.00	2.60	1.95	1.74	1.62	1.52	1.43	1.28
2.00	2.50	2.40	1.79	1.63	1.53	1.45	1.38	1.26
2.00	3.33	2.17	1.60	1.46	1.38	1.33	1.30	1.23
2.00	5.00	1.97	1.45	1.30	1.24	1.18	1.14	1.11
2.00	10.00	1.87	1.39	1.24	1.16	1.11	1.06	.98
2.50	2.00	2.10	1.63	1.52	1.45	1.41	1.35	1.25
2.50	2.50	1.97	1.55	1.43	1.38	1.33	1.28	1.19
2.50	3.33	1.80	1.42	1.35	1.31	1.26	1.24	1.18
2.50	5.00	1.63	1.29	1.22	1.18	1.15	1.14	1.12
2.50	10.00	1.53	1.24	1.15	1.09	1.06	1.03	.99
3.33	2.00	1.73	1.47	1.41	1.38	1.36	1.33	1.24
3.33	2.50	1.60	1.37	1.30	1.27	1.26	1.23	1.12
3.33	3.33	1.50	1.29	1.24	1.20	1.18	1.16	1.13
3.33	5.00	1.37	1.18	1.15	1.13	1.12	1.11	1.11
3.33	10.00	1.30	1.11	1.07	1.05	1.03	1.01	.97
5.00	2.00	1.53	1.39	1.37	1.36	1.35	1.31	1.20
5.00	2.50	1.37	1.26	1.24	1.24	1.23	1.21	1.11
5.00	3.33	1.27	1.16	1.15	1.15	1.14	1.13	1.11
5.00	5.00	1.20	1.11	1.09	1.07	1.08	1.06	1.06
5.00	10.00	1.13	1.05	1.04	1.02	1.02	1.01	.99
%0°		100	83.4	66.7	50	33.3	16.6	0
%+45°		0	16.6	33.3	50	66.7	83.4	100

Table VIII  $\lambda_{tx}^i$   $i=2,4,6,8$

E/D	W/D	$Kt_{tx}^i$ $i=2,4,6,8$						
		.17	.25	.35	.49	.71	1.14	2.61
2.00	2.00	1.65	1.04	.89	.84	.86	.91	1.11
2.00	2.50	1.88	1.32	1.14	1.06	1.06	1.09	1.27
2.00	3.33	2.12	1.48	1.29	1.18	1.15	1.17	1.29
2.00	5.00	2.18	1.60	1.37	1.27	1.21	1.19	1.28
2.00	10.00	2.24	1.64	1.40	1.29	1.23	1.18	1.25
2.50	2.00	1.18	.84	.77	.78	.82	.89	1.13
2.50	2.50	1.41	1.08	.97	.98	.99	1.05	1.23
2.50	3.33	1.59	1.20	1.11	1.08	1.08	1.11	1.23
2.50	5.00	1.71	1.32	1.20	1.14	1.13	1.13	1.21
2.50	10.00	1.76	1.36	1.23	1.16	1.14	1.13	1.21
3.33	2.00	.88	.72	.71	.76	.82	.89	1.07
3.33	2.50	1.12	.92	.91	.94	.97	1.04	1.26
3.33	3.33	1.24	1.04	1.03	1.02	1.04	1.08	1.21
3.33	5.00	1.35	1.12	1.09	1.06	1.07	1.10	1.16
3.33	10.00	1.41	1.16	1.11	1.10	1.08	1.10	1.20
5.00	2.00	.71	.68	.71	.76	.82	.91	1.13
5.00	2.50	.88	.88	.91	.94	.99	1.05	1.26
5.00	3.33	1.00	1.00	1.00	1.02	1.04	1.09	1.25
5.00	5.00	1.12	1.04	1.03	1.04	1.06	1.08	1.15
5.00	10.00	1.18	1.08	1.06	1.06	1.06	1.08	1.16
%0°		100	83.4	66.7	50	33.3	16.6	0
%+45°		0	16.6	33.3	50	66.7	83.4	100

Table IX  $\lambda_{tx}^i$   $i = 3, 7$

		$Kt_{tx}^i$ $i = 3, 7$						
E/D	W/D	8.24	5.27	4.17	3.47	2.91	2.39	1.77
2.00	2.00	1.45	1.38	1.39	1.42	1.47	1.56	1.85
2.00	2.50	1.39	1.30	1.28	1.28	1.30	1.34	1.49
2.00	3.33	1.36	1.24	1.22	1.20	1.21	1.22	1.27
2.00	5.00	1.33	1.21	1.17	1.15	1.14	1.14	1.16
2.00	10.00	1.31	1.19	1.14	1.12	1.09	1.07	1.05
2.50	2.00	1.37	1.33	1.35	1.39	1.46	1.56	1.83
2.50	2.50	1.31	1.24	1.23	1.24	1.27	1.32	1.46
2.50	3.33	1.28	1.19	1.17	1.16	1.17	1.19	1.24
2.50	5.00	1.26	1.16	1.13	1.12	1.12	1.12	1.14
2.50	10.00	1.24	1.14	1.10	1.08	1.07	1.05	1.05
3.33	2.00	1.31	1.30	1.34	1.39	1.45	1.56	1.86
3.33	2.50	1.24	1.20	1.20	1.23	1.26	1.32	1.48
3.33	3.33	1.20	1.14	1.13	1.14	1.15	1.17	1.24
3.33	5.00	1.19	1.11	1.09	1.09	1.09	1.10	1.12
3.33	10.00	1.18	1.10	1.07	1.06	1.05	1.04	1.04
5.00	2.00	1.27	1.30	1.34	1.39	1.46	1.56	1.85
5.00	2.50	1.18	1.18	1.20	1.22	1.26	1.32	1.49
5.00	3.33	1.14	1.11	1.11	1.12	1.14	1.17	1.25
5.00	5.00	1.12	1.07	1.06	1.07	1.07	1.08	1.11
5.00	10.00	1.11	1.06	1.05	1.04	1.04	1.03	1.03
%0°		100	83.4	66.7	50	33.3	16.6	0
%+45°		0	16.6	33.3	50	66.7	83.4	100

Table X  $\lambda_{bx}^i \quad i = 1$

		$Kt_{bx}^i \quad i = 1$						
E/D	W/D	1.28	.78	.57	.39	.18	-.13	-.67
2.00	2.00	.91	.89	.86	.80	.56	1.54	1.00
2.00	2.50	.86	.84	.79	.72	.39	1.69	1.04
2.00	3.33	.83	.84	.79	.69	.33	1.92	1.12
2.00	5.00	.82	.86	.84	.80	.56	1.54	1.09
2.00	10.00	.83	.89	.91	.92	.89	.92	.93
2.50	2.00	1.00	.98	.95	.90	.67	1.46	1.00
2.50	2.50	.95	.92	.90	.85	.61	1.54	1.04
2.50	3.33	.91	.90	.86	.80	.50	1.62	1.07
2.50	5.00	.88	.90	.88	.82	.56	1.62	1.12
2.50	10.00	.89	.94	.95	.95	.89	1.08	1.00
3.33	2.00	1.07	1.04	.98	.90	.67	1.54	1.03
3.33	2.50	1.02	1.00	.97	.90	.67	1.54	1.06
3.33	3.33	.97	.96	.95	.90	.72	1.46	1.07
3.33	5.00	.95	.95	.93	.87	.67	1.46	1.09
3.33	10.00	.94	.96	.97	.95	.83	1.15	1.04
5.00	2.00	1.11	1.05	1.00	.92	.67	1.54	1.06
5.00	2.50	1.06	1.03	.98	.90	.67	1.46	1.03
5.00	3.33	1.02	1.00	.98	.92	.72	1.46	1.07
5.00	5.00	.99	.99	.98	.95	.78	1.31	1.07
5.00	10.00	.97	.99	.98	.95	.83	1.23	1.06
%0°		100	83.4	66.7	50	33.3	16.6	0
%±45°		0	16.6	33.3	50	66.7	83.4	100



Table XI

$$\lambda_{bx}^i \quad i = 2,8$$

$$Kt_{bx}^i \quad i = 2,8$$

E/D	W/D	-.28	.04	.24	.44	.70	1.16	2.60
2.00	2.00	.00	5.75	1.67	1.34	1.24	1.21	1.31
2.00	2.50	.07	5.75	1.71	1.36	1.27	1.25	1.37
2.00	3.33	.11	5.75	1.71	1.41	1.30	1.27	1.34
2.00	5.00	.11	6.00	1.83	1.45	1.34	1.30	1.36
2.00	10.00	.11	6.50	1.92	1.55	1.41	1.35	1.40
2.50	2.00	.21	4.75	1.54	1.29	1.23	1.21	1.33
2.50	2.50	.32	4.50	1.54	1.29	1.24	1.23	1.34
2.50	3.33	.39	4.25	1.50	1.29	1.23	1.22	1.30
2.50	5.00	.43	4.25	1.54	1.32	1.24	1.22	1.27
2.50	10.00	.43	4.50	1.63	1.36	1.28	1.26	1.30
3.33	2.00	.36	4.25	1.54	1.30	1.23	1.20	1.27
3.33	2.50	.50	3.75	1.46	1.27	1.23	1.23	1.35
3.33	3.33	.57	3.25	1.38	1.25	1.20	1.21	1.28
3.33	5.00	.64	3.00	1.33	1.20	1.17	1.17	1.22
3.33	10.00	.64	3.25	1.38	1.23	1.18	1.18	1.22
5.00	2.00	.47	4.25	1.54	1.30	1.23	1.20	1.27
5.00	2.50	.61	3.50	1.46	1.27	1.23	1.23	1.35
5.00	3.33	.72	3.00	1.38	1.23	1.20	1.20	1.27
5.00	5.00	.79	2.50	1.29	1.18	1.16	1.15	1.21
5.00	10.00	.82	2.25	1.25	1.13	1.13	1.12	1.15
%0°	100	83.4	66.7	50	33.3	16.6	0	
%+45°	0	16.6	33.3	50	66.7	83.4	100	

Table XII  $\lambda_{bx}^i$   $i = 3,7$

		$Kt_{bx}^i$ $i = 3,7$						
E/D	W/D	2.92	1.72	1.28	.99	.77	.56	.31
2.00	2.00	2.44	2.34	2.44	2.66	2.96	3.56	5.75
2.00	2.50	2.32	2.11	2.11	2.20	2.34	2.68	3.90
2.00	3.33	2.26	1.99	1.93	1.95	2.00	2.16	2.81
2.00	5.00	2.24	1.89	1.80	1.78	1.78	1.86	2.22
2.00	10.00	2.18	1.83	1.70	1.65	1.61	1.61	1.77
2.50	2.00	2.26	2.23	2.38	2.62	2.94	3.56	5.61
2.50	2.50	2.10	1.96	1.99	2.11	2.28	2.64	3.88
2.50	3.33	2.04	1.81	1.77	1.82	1.88	2.05	2.71
2.50	5.00	2.00	1.72	1.65	1.65	1.66	1.73	2.06
2.50	10.00	1.96	1.66	1.55	1.52	1.49	1.50	1.68
3.33	2.00	2.11	2.18	2.35	2.61	2.94	3.54	5.71
3.33	2.50	1.92	1.87	1.94	2.09	2.27	2.62	3.87
3.33	3.33	1.82	1.67	1.66	1.74	1.82	2.02	2.68
3.33	5.00	1.76	1.56	1.51	1.53	1.54	1.63	1.94
3.33	10.00	1.74	1.49	1.42	1.40	1.39	1.41	1.55
5.00	2.00	2.02	2.17	2.35	2.61	2.94	3.54	5.61
5.00	2.50	1.79	1.83	1.93	2.08	2.27	2.62	3.91
5.00	3.33	1.63	1.59	1.63	1.72	1.82	2.02	2.68
5.00	5.00	1.54	1.42	1.42	1.45	1.49	1.57	1.90
5.00	10.00	1.51	1.34	1.30	1.29	1.28	1.30	1.42
%0°		100	83.4	66.7	50	33.3	16.6	0
%+45°		0	16.6	33.3	50	66.7	83.4	100

# 2 OF 5

N78

18134

UNCLAS

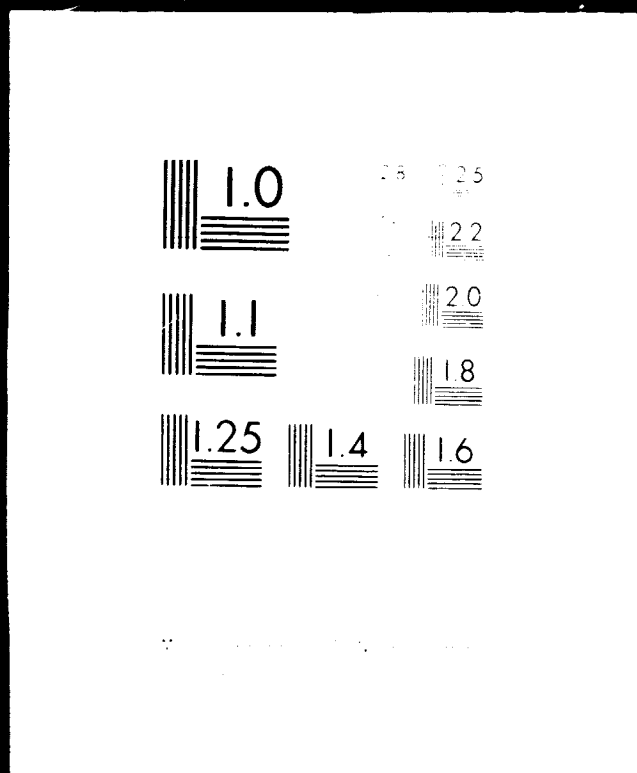


Table XIII  $\lambda_{ty}^i$   $i = 1,5$

E/D	W/D	$Kt_{ty}^i$ $i = 1,5$				
		2.453	2.358	2.260	2.111	1.770
2.0	2.0	1.187	1.194	1.202	1.213	1.235
2.0	4.0	1.125	1.138	1.154	1.180	1.215
2.0	6.0	1.109	1.114	1.121	1.135	1.184
2.0	10.0	1.108	1.113	1.119	1.129	1.180
3.0	2.0	1.143	1.154	1.168	1.185	1.210
3.0	4.0	1.077	1.086	1.093	1.099	1.123
3.0	6.0	1.060	1.066	1.074	1.086	1.099
3.0	10.0	1.049	1.052	1.054	1.057	1.084
4.0	2.0	1.143	1.151	1.159	1.166	1.180
4.0	4.0	1.061	1.066	1.070	1.072	1.078
4.0	6.0	1.047	1.054	1.060	1.065	1.064
4.0	10.0	1.045	1.050	1.055	1.060	1.050
%0°		66.7	50.0	33.3	16.6	0
%+45°		33.3	50.0	66.7	83.4	100

e-2

Table XIV  $\lambda_{ty}^i$   $i = 2,4,6,8$

E/D	W/D	$Kt_{ty}^i$ $i = 2,4,6,8$				
		1.659	1.768	1.880	2.059	2.610
2.0	2.0	1.407	1.440	1.491	1.578	1.750
2.0	4.0	1.074	1.091	1.113	1.149	1.284
2.0	6.0	1.046	1.061	1.076	1.098	1.196
2.0	10.0	1.045	1.062	1.081	1.114	1.200
3.0	2.0	1.399	1.427	1.476	1.565	1.730
3.0	4.0	1.082	1.093	1.109	1.140	1.269
3.0	6.0	1.049	1.054	1.064	1.082	1.185
3.0	10.0	1.039	1.048	1.057	1.071	1.153
4.0	2.0	1.395	1.423	1.472	1.560	1.730
4.0	4.0	1.078	1.085	1.096	1.113	1.257
4.0	6.0	1.044	1.051	1.061	1.081	1.196
4.0	10.0	1.035	1.045	1.055	1.070	1.157
%0°		66.7	50.0	33.3	16.6	0
%+45°		33.3	50.0	66.7	83.4	100

Table XV  $\lambda_{ty}^i \quad i = 3,7$

		$Kt_{ty}^i \quad i = 3,7$				
E/D	W/D	-2.176	-1.817	-1.517	-1.251	-1.000
2.0	2.0	1.518	1.413	1.323	1.217	1.125
2.0	4.0	1.298	1.286	1.274	1.252	1.170
2.0	6.0	1.189	1.171	1.161	1.153	1.130
2.0	10.0	1.147	1.123	1.105	1.087	1.085
3.0	2.0	1.401	1.360	1.317	1.242	1.100
3.0	4.0	1.169	1.150	1.126	1.093	1.067
3.0	6.0	1.120	1.111	1.116	1.116	1.068
3.0	10.0	1.040	1.037	1.039	1.043	1.037
4.0	2.0	1.424	1.390	1.343	1.251	1.125
4.0	4.0	1.101	1.089	1.077	1.060	1.013
4.0	6.0	1.071	1.077	1.077	1.065	1.011
4.0	10.0	1.030	1.030	1.030	1.030	1.008
%0°		66.7	50.0	33.3	16.6	0
%±45°		33.3	50.0	66.7	83.4	100

Table XVI  $\lambda_{by}^i$   $i = 1,5$

E/D	W/D	$Kt_{by}^i$ $i = 1,5$				
		1.341	1.294	1.260	1.212	.310
2.0	2.0	2.288	2.360	2.477	2.708	3.150
2.0	4.0	1.801	1.846	1.910	2.031	2.520
2.0	6.0	1.751	1.785	1.831	1.922	2.340
2.0	10.0	1.748	1.782	1.826	1.911	2.295
3.0	2.0	2.172	2.254	2.386	2.611	3.000
3.0	4.0	1.591	1.621	1.667	1.753	2.073
3.0	6.0	1.475	1.495	1.524	1.580	1.854
3.0	10.0	1.450	1.466	1.488	1.531	1.743
4.0	2.0	2.147	2.214	2.314	2.484	2.770
4.0	4.0	1.540	1.565	1.613	1.712	1.885
4.0	6.0	1.389	1.405	1.430	1.478	1.692
4.0	10.0	1.329	1.339	1.353	1.380	1.542
%0°		66.7	50.0	33.3	16.6	0
%+45°		33.3	50.0	66.7	83.4	100

Table XVII  $\lambda_{by}^i$   $i = 2,4$

E/D	W/D	$Kt_{by}^i$ $i = 2,4$				
		.992	1.148	1.340	1.693	2.600
2.0	2.0	1.929	1.884	1.864	1.850	1.850
2.0	4.0	1.302	1.287	1.277	1.276	1.350
2.0	6.0	1.260	1.246	1.234	1.223	1.262
2.0	10.0	1.258	1.246	1.234	1.223	1.240
3.0	2.0	1.926	1.881	1.866	1.865	1.850
3.0	4.0	1.275	1.262	1.257	1.260	1.374
3.0	6.0	1.198	1.188	1.181	1.178	1.240
3.0	10.0	1.183	1.175	1.168	1.162	1.190
4.0	2.0	1.927	1.884	1.870	1.870	1.850
4.0	4.0	1.265	1.252	1.246	1.248	1.390
4.0	6.0	1.175	1.167	1.164	1.165	1.244
4.0	10.0	1.145	1.139	1.135	1.132	1.165
%0°		66.7	50.0	33.3	16.6	0
%±45°		33.3	50.0	66.7	83.4	100



Table XVIII  $\lambda_{by}^i$   $i = 3$

E/D	W/D	$Kt_{by}^i$ $i = 3$				
		.016	-.174	-.311	-.450	-.670
2.0	2.0	5.0	4.343	2.002	1.167	1.000
2.0	4.0	4.0	2.776	1.786	1.394	1.093
2.0	6.0	3.0	2.067	1.468	1.234	1.077
2.0	10.0	3.0	1.993	1.438	1.223	1.064
3.0	2.0	5.0	4.255	2.182	1.356	1.000
3.0	4.0	3.0	2.485	1.607	1.276	1.031
3.0	6.0	3.0	1.871	1.410	1.224	1.070
3.0	10.0	3.0	1.559	1.267	1.148	1.062
4.0	2.0	6.0	4.654	2.346	1.407	1.000
4.0	4.0	3.0	2.276	1.535	1.264	.968
4.0	6.0	3.0	1.834	1.382	1.203	1.041
4.0	10.0	3.0	1.399	1.204	1.121	1.059
%0°		66.7	50.0	33.3	16.6	0
%+45°		33.3	50.0	66.7	83.4	100

Table XIX  $\lambda_{xy}^i$   $i = 2, 4, 6, 8$

E/D	W/D	$Kt_{xy}^i$ $i = 2, 6$				
		3.518	3.858	4.316	5.074	7.211
2.00	2.00	1.133	1.139	1.151	1.175	1.269
2.00	2.50	1.098	1.098	1.101	1.115	1.188
2.00	3.33	1.080	1.074	1.070	1.071	1.117
2.00	5.00	1.074	1.069	1.063	1.060	1.085
2.00	10.00	1.072	1.063	1.058	1.057	1.070
2.50	2.00	1.127	1.136	1.148	1.170	1.266
2.50	2.50	1.089	1.093	1.099	1.113	1.178
2.50	3.33	1.064	1.062	1.062	1.068	1.114
2.50	5.00	1.054	1.050	1.045	1.041	1.062
2.50	10.00	1.052	1.048	1.044	1.040	1.057
3.33	2.00	1.122	1.130	1.140	1.162	1.273
3.33	2.50	1.085	1.090	1.097	1.109	1.176
3.33	3.33	1.056	1.058	1.060	1.067	1.109
3.33	5.00	1.039	1.037	1.034	1.034	1.059
3.33	10.00	1.037	1.034	1.030	1.026	1.038
5.00	2.00	1.117	1.119	1.119	1.115	1.100
5.00	2.50	1.082	1.085	1.088	1.096	1.135
5.00	3.33	1.054	1.057	1.058	1.064	1.118
5.00	5.00	1.033	1.034	1.033	1.034	1.057
5.00	10.00	1.025	1.023	1.019	1.015	1.022
%0°		66.7	50.0	33.3	16.6	0
%+45°		33.3	50.0	66.7	83.4	100

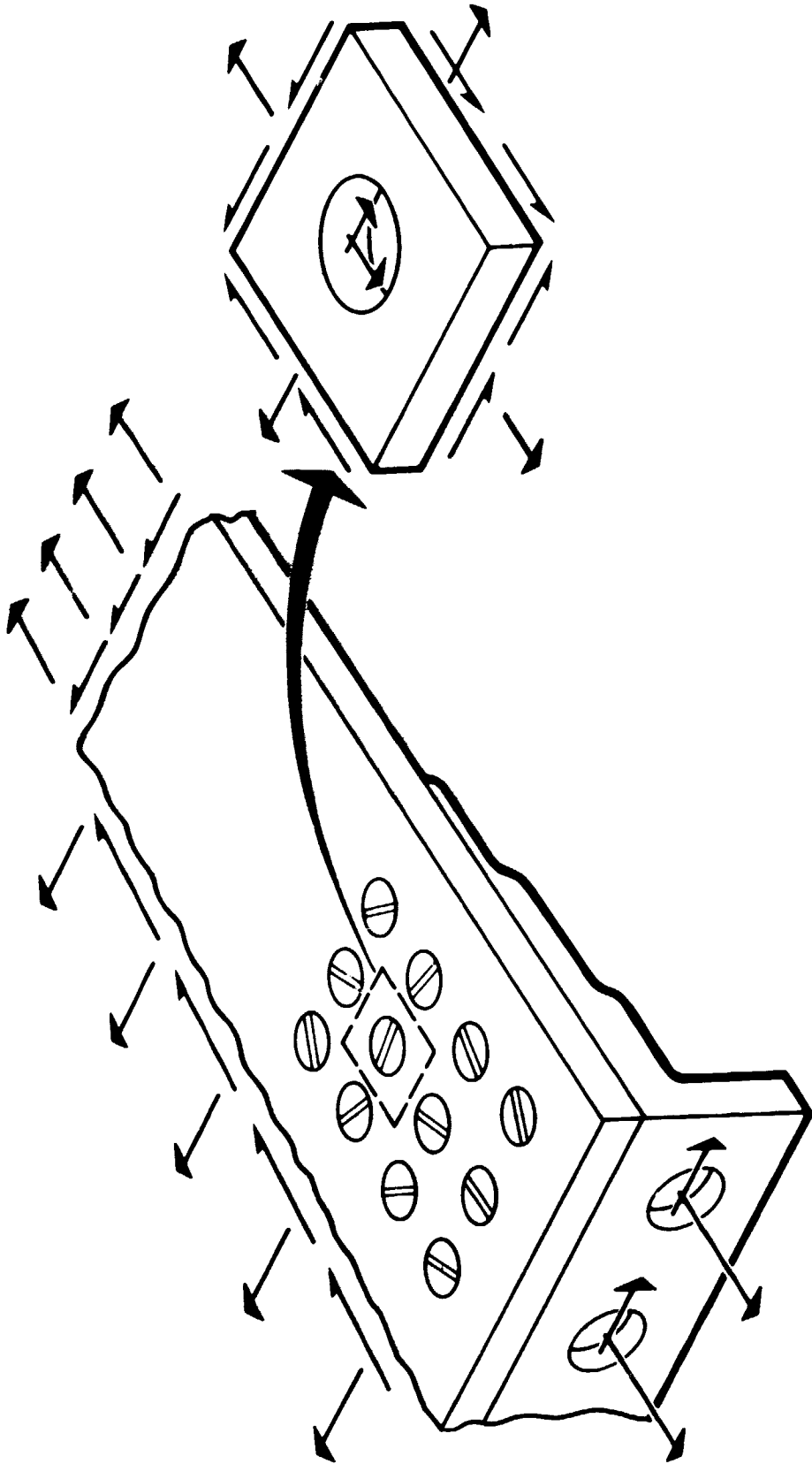


Figure 1 Complex Joints Are Analyzed Element by Element

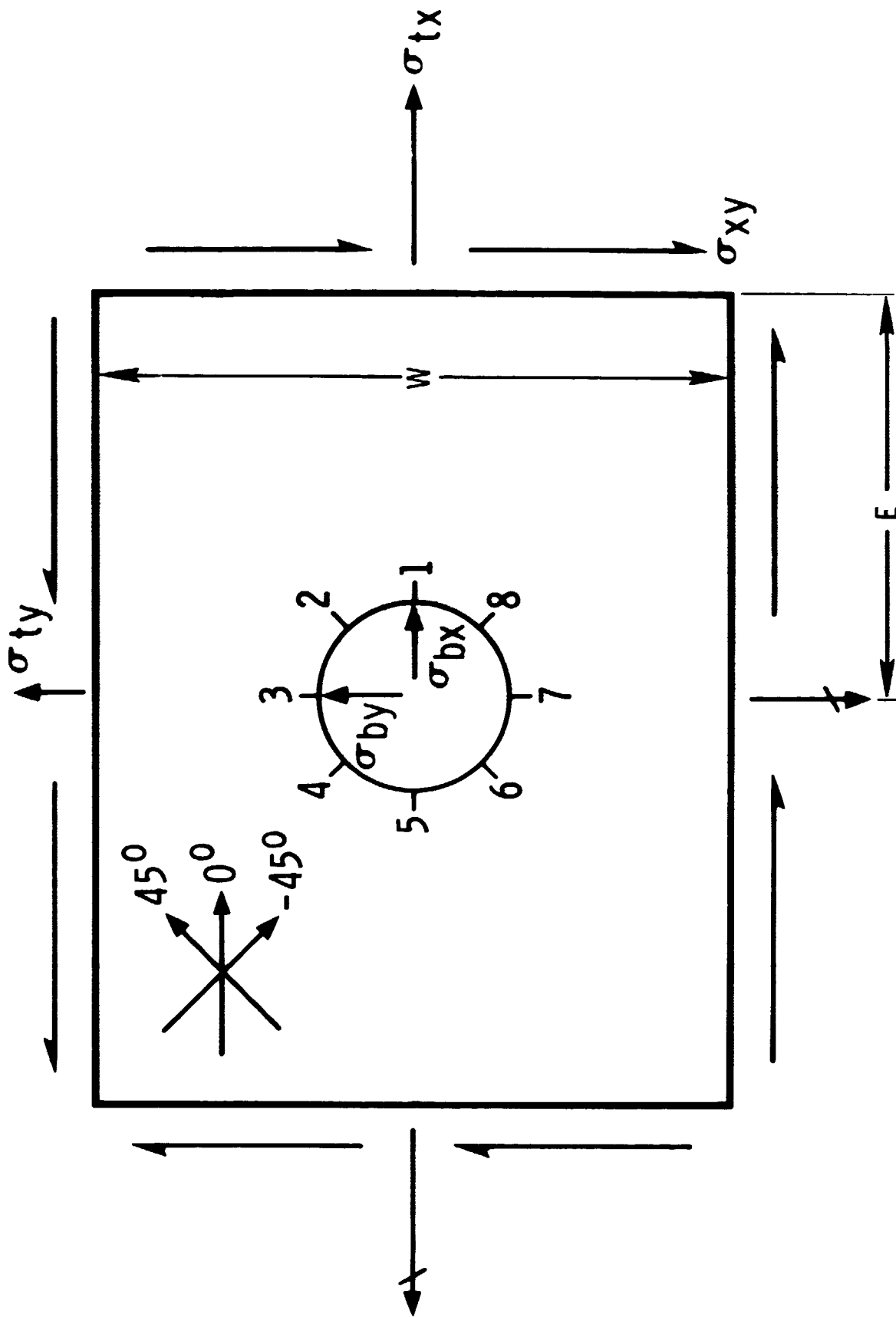
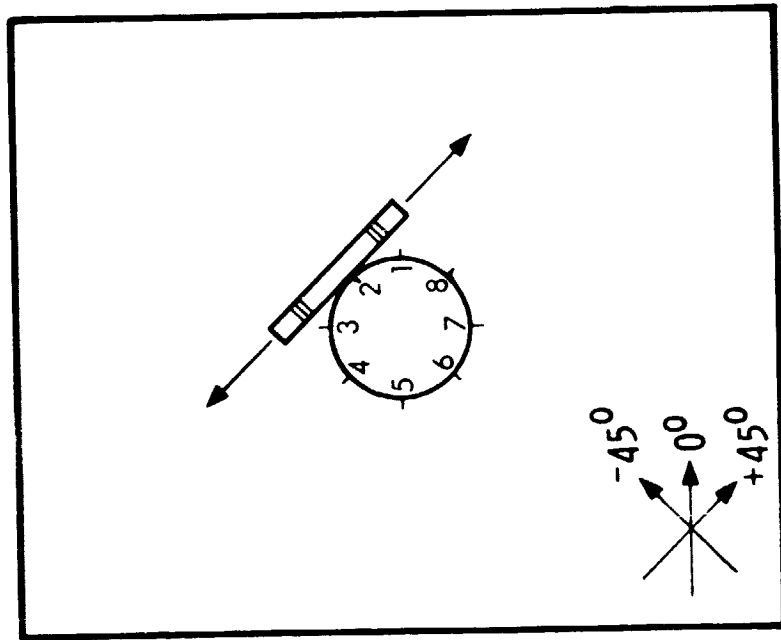
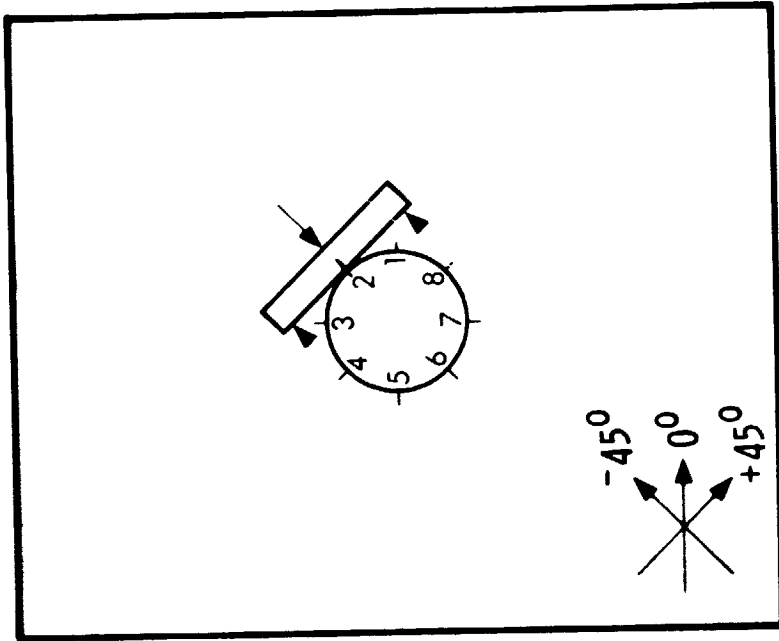


Figure 2 Joint Element Freebody



Ultimate Strength,  $\sigma_{\infty}^i$   
 $i = 1, 2, 3, 4, 5, 6, 7, 8$



Fracture Toughness,  $KQ^i$   
 $i = 1, 2, 3, 4, 5, 6, 7, 8$

Strength & Fracture Toughness are Related by  $\sigma_{\infty}^i \sqrt{\pi a^i} = KQ^i$

Figure 3 Laminate Strength and Fracture Toughness Characteristic of Selected Points on the Hole Boundary are Obtained by Test

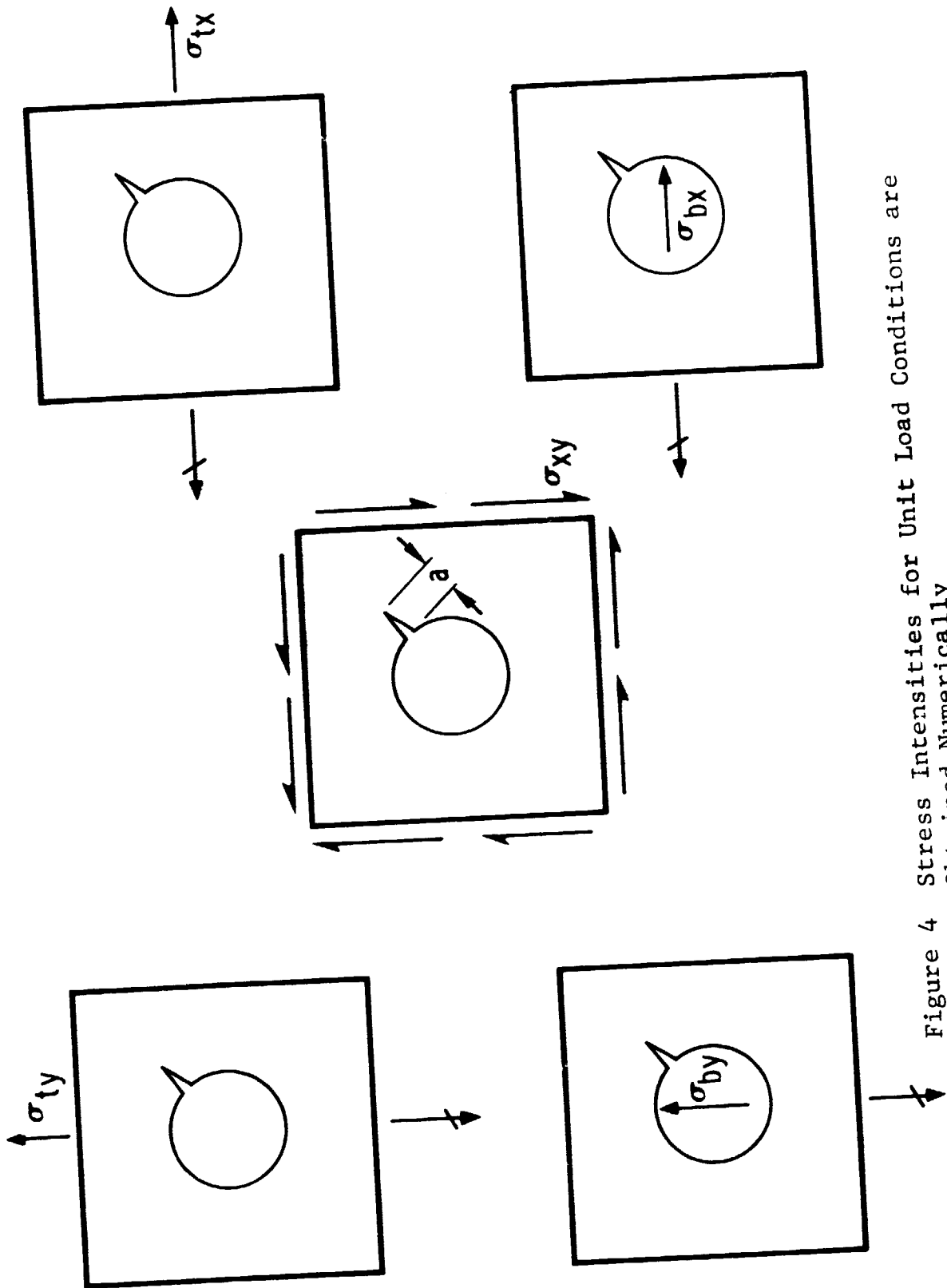
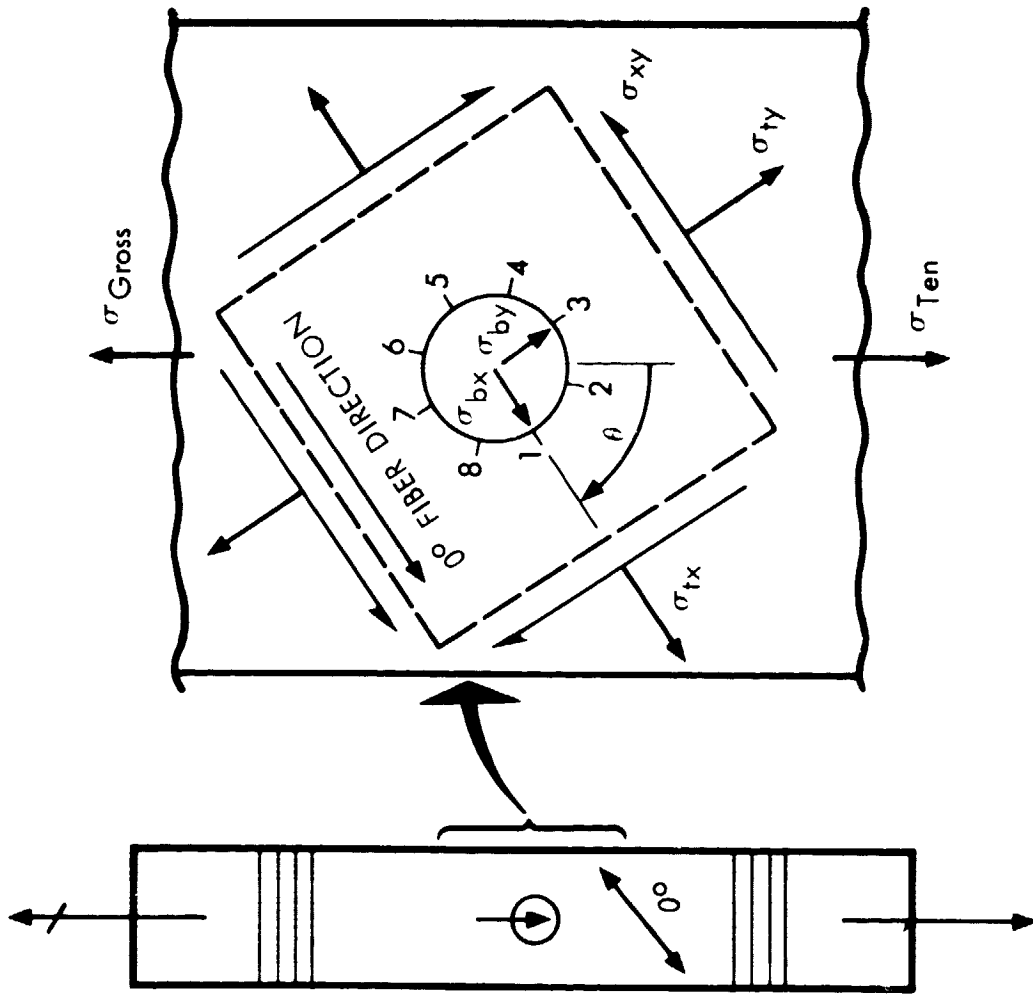


Figure 4 Stress Intensities for Unit Load Conditions are Obtained Numerically



LET  $\alpha$  = FRACTION OF TOTAL LOAD CARRIED IN TENSION:

$$\sigma_{tx} = .5\sigma_{Gross} (1 + \cos 2\theta)\alpha$$

$$\sigma_{ty} = .5\sigma_{Gross} (1 - \cos 2\theta)\alpha$$

$$\sigma_{xy} = .5\sigma_{Gross} (\sin 2\theta)\alpha$$

$$\sigma_{bx} = 6\sigma_{Gross} \cos\theta(1 - \alpha)$$

$$\sigma_{by} = 6\sigma_{Gross} \sin\theta(1 - \alpha)$$

Figure 5 Axial/Bearing Coupons Provide Biaxial Joint Element Test Data by Inclining Material Axis to Load Direction

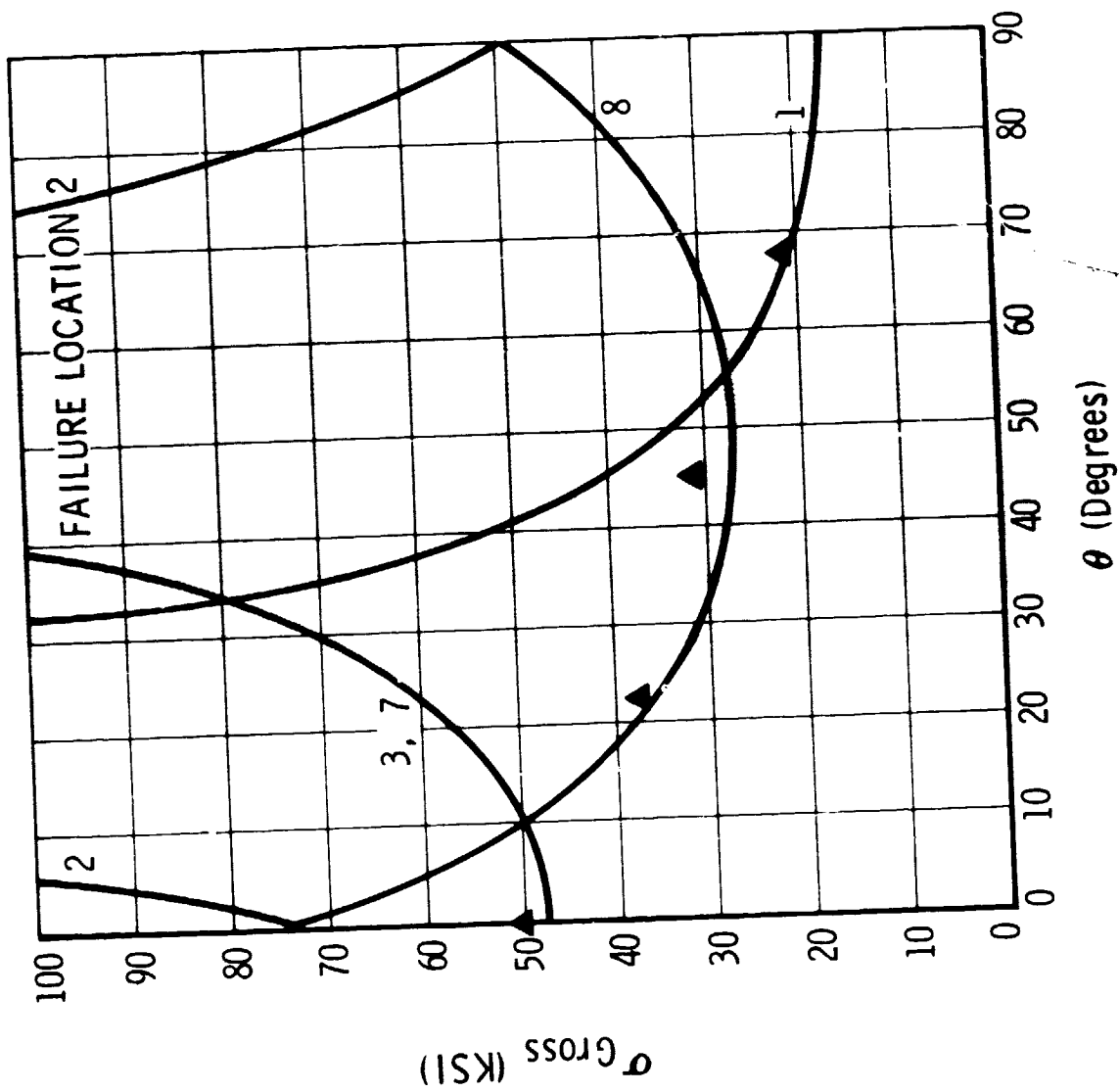


Figure 6 Correlation of Test Data and Strength Model for 100 Percent Tension Load Case



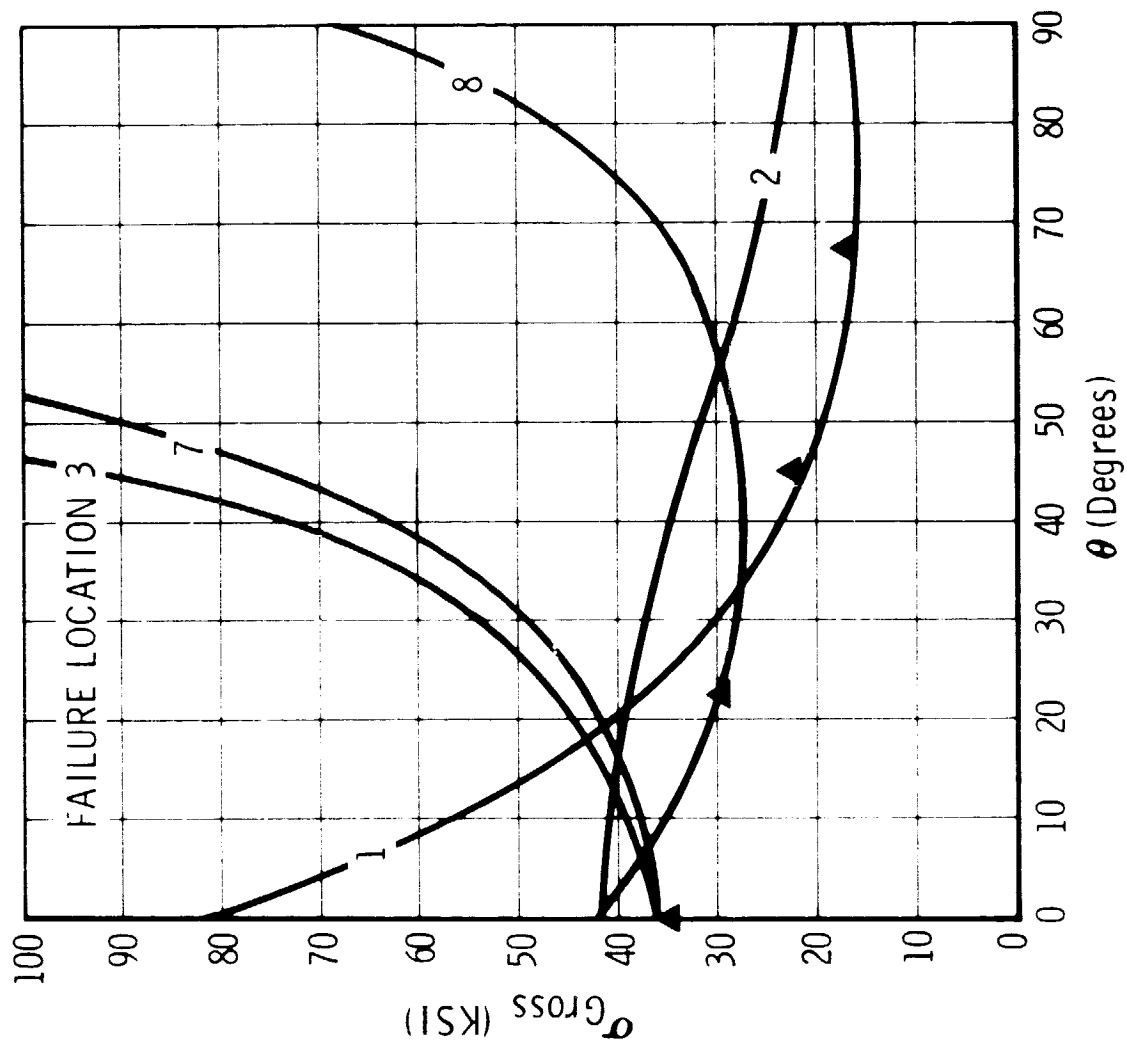


Figure 7 Correlation of Test Data and Strength Model for 70 Percent Tension Load Case

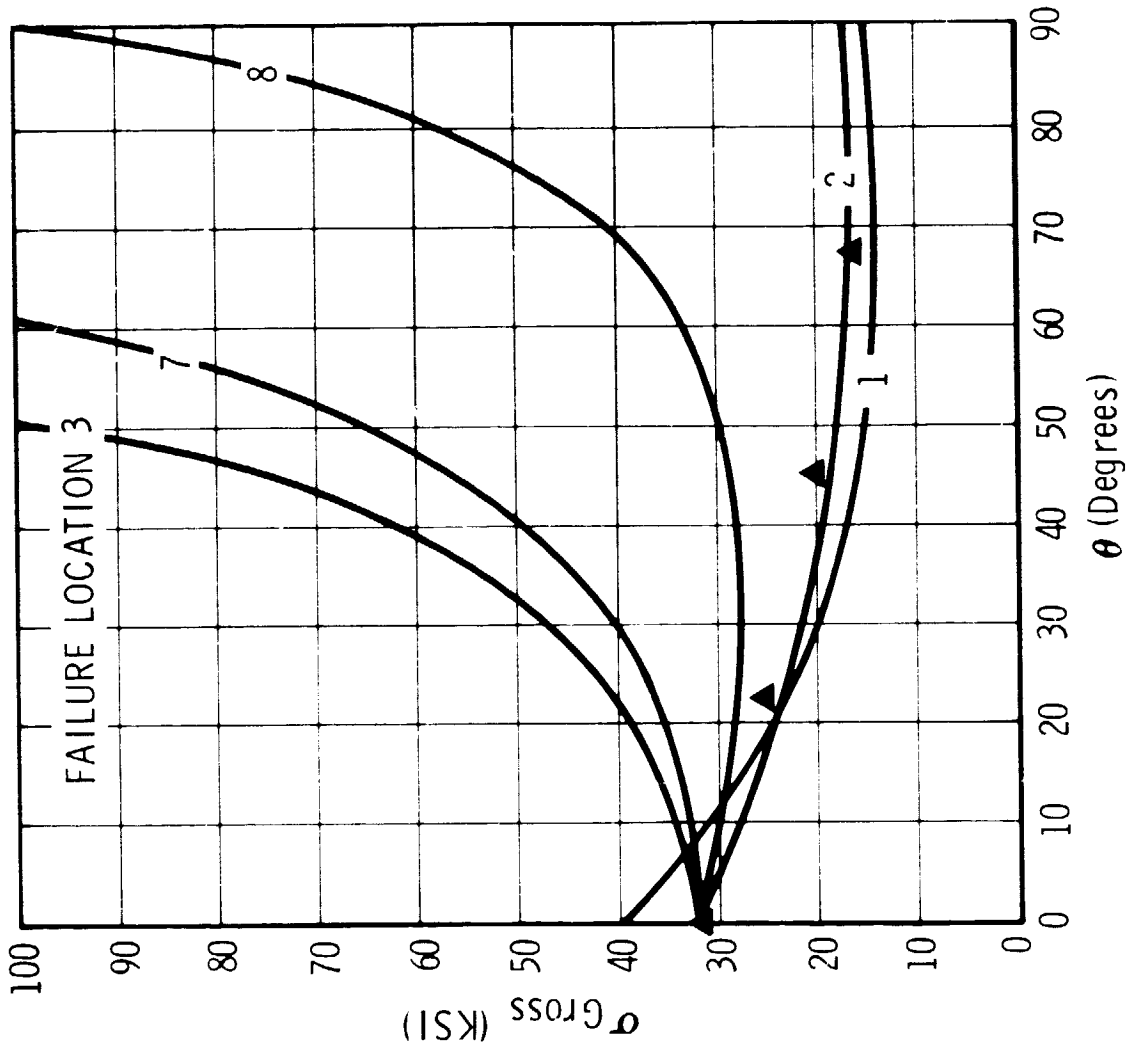


Figure 8 Correlation of Test Data and Strength Model  
for 50 Percent Tension Load Case

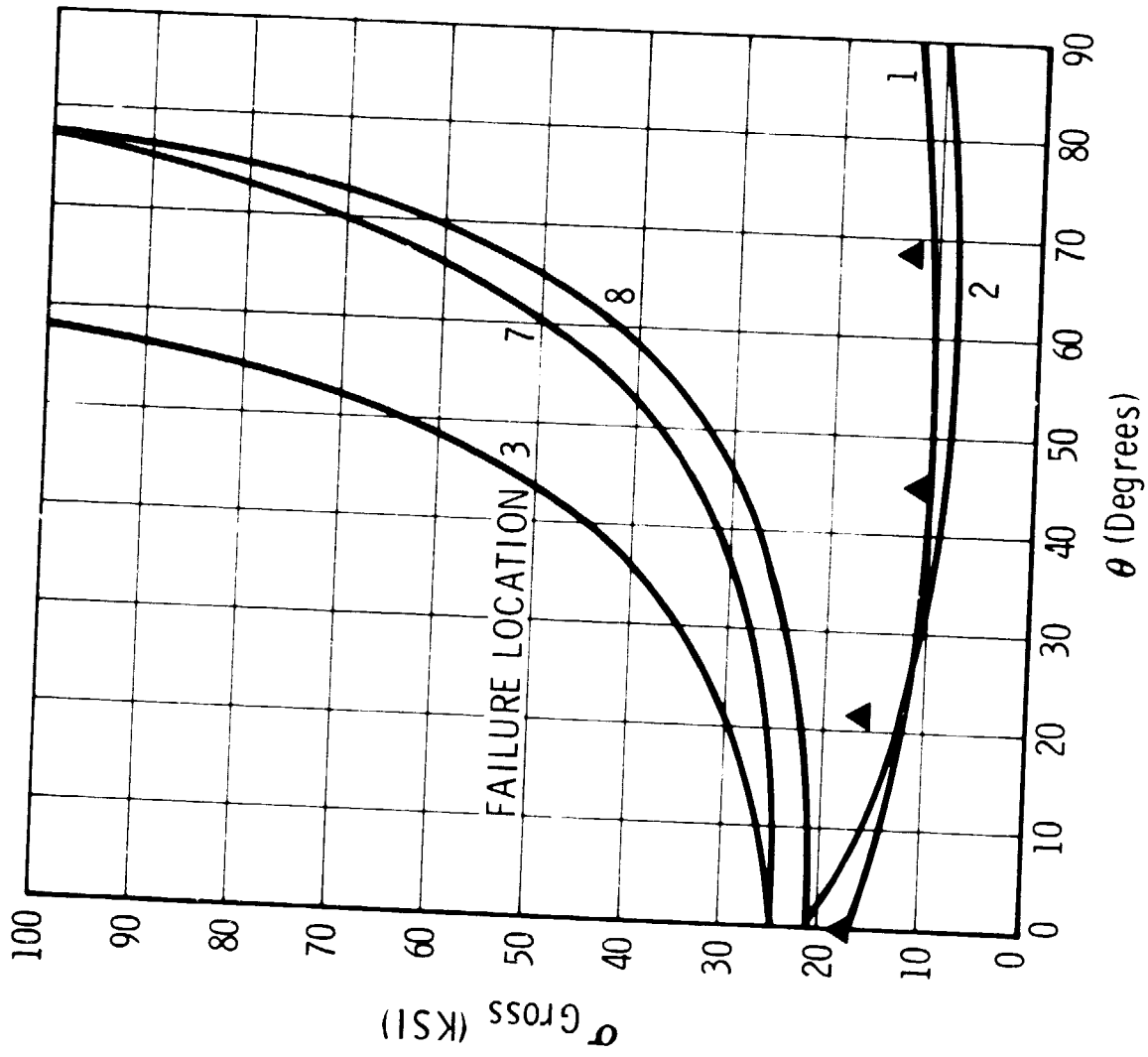


Figure 9 Correlation of Test Data and Strength Model for 100 Percent Bearing Load Case

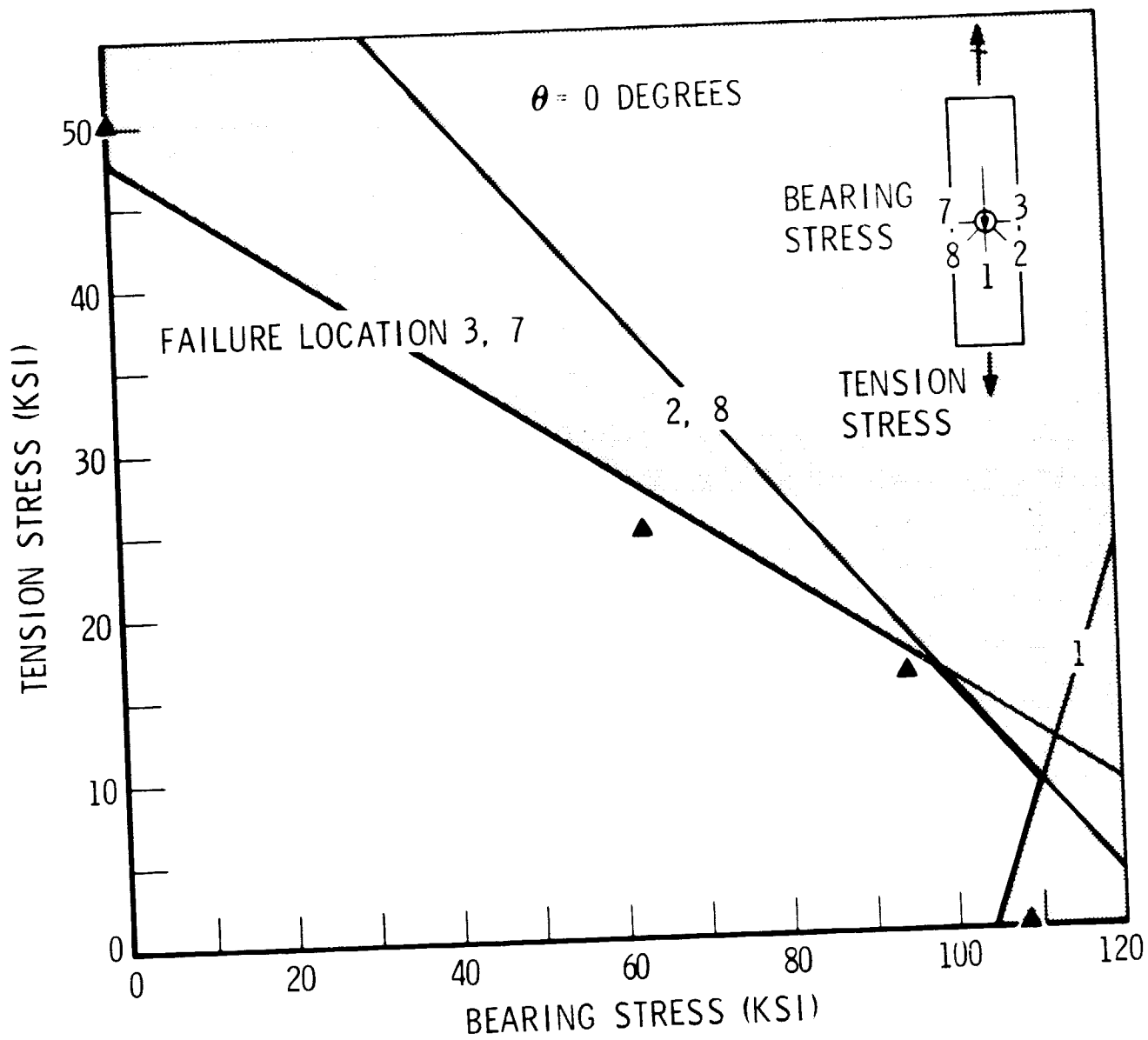


Figure 10 Strength Model Predicts Shape of Bearing/Tension Interaction Curve

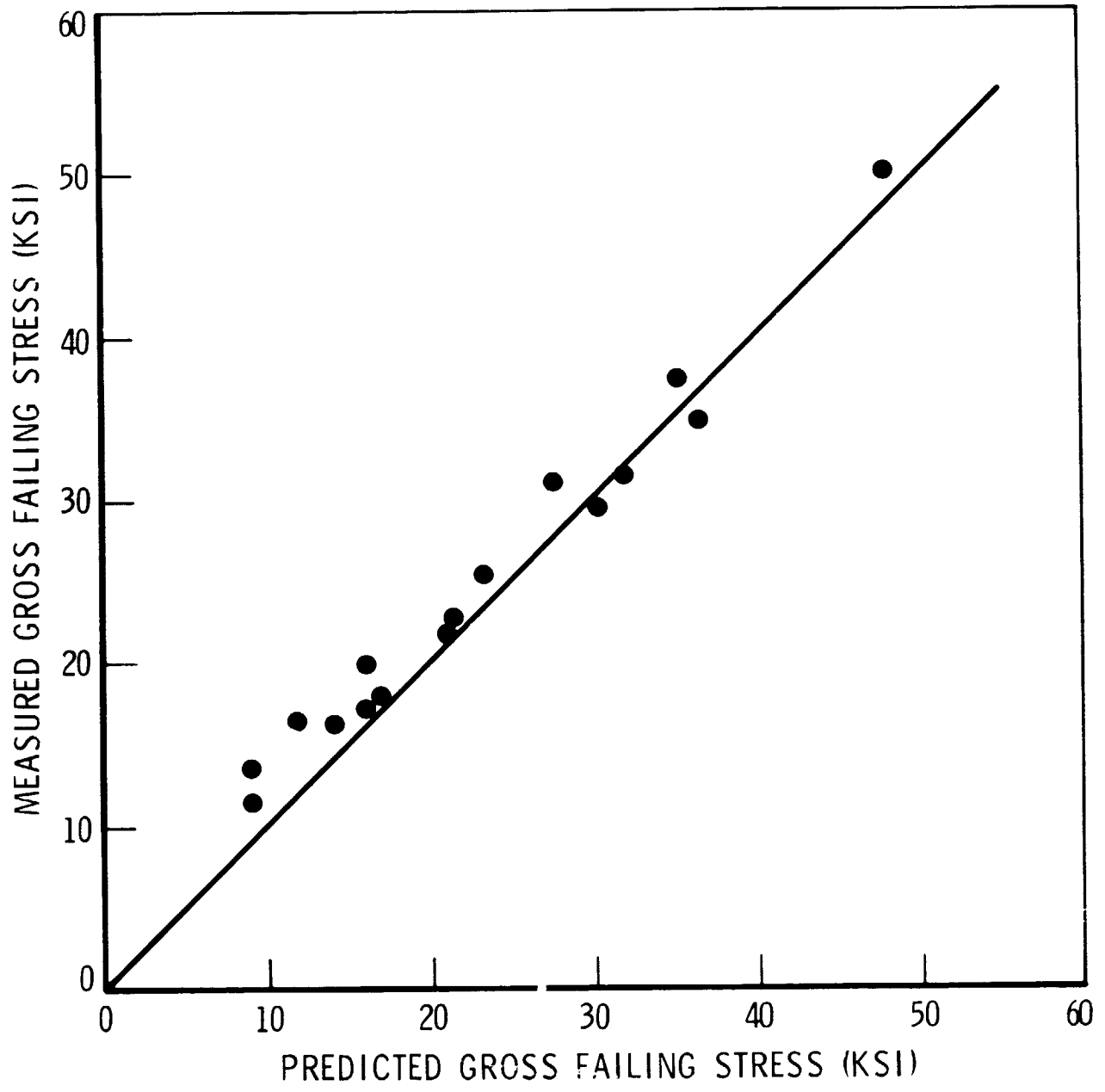


Figure 11 Strength Model Accurately Predicts Bearing/Tension Interaction for Biaxial Loading

DESIGN OF THE B-1 COMPOSITE  
HORIZONTAL STABILIZER ROOT JOINT

B. Whitman, P. Shyprykevich, and J. Whiteside  
Grumman Aerospace Corporation

SUMMARY

This paper describes the problems encountered and solutions developed for the design of the attachment of the stabilizer covers to the root fitting. A combined analysis and test approach was used and the problems and lessons learned are discussed. The results of over 200 joint tests are reported.

INTRODUCTION

The B-1 composite horizontal stabilizer is being developed, reference 1, to provide cost and weight advantages over a metal design. Bonded splices are effectively eliminated from the structure by considerations of cost and a desire to utilize the durability qualities of fiber-dominated advanced composite laminates. The composite cover is bolted directly to the substructure in a manner similar to that employed in the metal stabilizer.

The root area splice where cover loads are transferred to the titanium bearing support fitting presents an especially challenging design problem. The composite cover forms air passage contour; hence bolts are countersunk into the laminate and loads are transferred by single shear. The composite design uses the same titanium forgings for the bearing support fitting as does the metal stabilizer design because any alternative is economically unattractive. The thickness of the composite cover over the fitting is bounded by the geometry available in the forgings and by the air passage surface. Under these constraints, adequate joint strength cannot be realized from a graphite-epoxy laminate. A boron-graphite-epoxy hybrid laminate with the boron layers oriented in the primary (spanwise) cover load direction provides satisfactory strength margins.

This paper describes the approach used to design the root joint of the horizontal stabilizer and the data base generated to provide design strengths for the hybrid boron-graphite-epoxy laminate under combined stress with single-shear pin load reaction at an arbitrary angle.

### SYMBOLS

D	bolt diameter
E	Young's modulus of elasticity
f	stress
F	allowable stress
N	membrane load intensity, force/width
P	bolt load
t	thickness
w	width
a	joint flexibility, $\delta/P$
$\delta$	displacement of bolt centerline at inner plate midplane relative to outer plate midplane
$\theta$	angle between load axis and laminate reference axis

#### Subscripts:

b	bolt
B	boron-epoxy
br	bearing condition
G	graphite-epoxy
oh	open hole or unloaded bolt condition
net	net area condition

## DESIGN ANALYSIS OF THE ROOT JOINT

### Splice Configuration

The planform arrangement of the stabilizer covers and bearing support fitting is illustrated in figure 1. The splice design must transmit 500,000 lb ultimate in-plane cover load to the bearing support fitting through a pattern of 130 bolts to the titanium bearing support fitting. Figure 2 presents a scale view of the root area bolt pattern. The geometry of this splice configuration is typical of current aerospace practice. The use of advanced composite material for the stabilizer covers, however, requires the design analyst to approach his task in a different fashion than would typically be the case for metal designs.

Geometric stress raisers such as notches and, in particular, loaded bolt holes reduce the static strength of filament dominated composites. This notch penalty is analogous to the behavior of a brittle metal with a crack at the stress raiser. Under fatigue, however, composites do not tend to develop and grow through-the-thickness cracks as metals do. Paradoxically, notched composites under fatigue appear to grow stronger. The softening strip concept can reduce the static notch penalty and provide a means to reduce drilling time in hybrid boron-graphite epoxy. But the softening strip concept is impractical for the complex bolt pattern required to accommodate the bearing support fitting of the horizontal stabilizer.

The durability of advanced composite materials structures may exceed that of aircraft metals. The essential problem in design is to achieve a structure that is dominated by the properties of the graphite or boron fibers rather than by the organic matrix materials which may degrade under fatigue and environmental exposure. Matrix dominated failures are found in bonded joints, compressive local instability modes, sandwich face wrinkling and laminates which cannot be classified as filament dominated laminates because of their fiber orientations and/or their loading, e.g., local thickness-direction shear and normal loads. Matrix dominated failures are characterized by high scatter and sensitivity to fatigue and environment. A laminate may be regarded as a filament dominated laminate if the fiber orientations are such that primary loads are reacted by fibers and the resulting layer shear and transverse stresses are inconsequential. Transverse crazing of a layer is regarded as inconsequential if there are fibers oriented transverse to the layer in question.



## Fastener Flexibility

The strength of a composite laminate loaded in tension and bolt bearing depends upon the amount of load reacted through bolt bearing. Data will be presented which shows that increasing the portion of load reacted through bolt bearing reduces the total strength in a linear fashion. Further, the distribution of internal loads within the complex redundant structure comprising the root joint depends upon the stiffnesses both of the plate members and the fasteners connecting them. It is necessary to determine the effect of bolt load on the load carrying capacity of a given laminate and the effect of bolt flexibility on the accuracy of bolt loads derived from a finite element analysis of the joint area.

Examination of the five-bolt splice element illustrated in figure 3 shows that the relatively flexible character of the bolts and the relatively stiff character of the splice plates dominates the bolt load distribution. The results of analyses are included in figure 3. In each analysis, the splice is treated as a redundant structure comprised of axially loaded bars interconnected by shear loaded bolts. The bar flexibilities are taken as  $(\text{length}) \div (\text{area} \times \text{elastic modulus})$ . Single shear bolt joint flexibilities are estimated using a semi-empirical formula developed by Richard N. Hadcock (unpublished research, 1961):

$$\alpha = \frac{\delta}{P} = \frac{(t_1 + t_2)^2}{E_b D^3} + 3.72 \left( \frac{1}{t_1 E_1} + \frac{1}{t_2 E_2} \right) \quad (1)$$

The results summarized in figure 3 indicate that it is necessary to obtain reasonable estimates of individual bolt flexibilities. Further, the bolts in this splice are so flexible compared to the plates that doubling the bolt flexibilities has a rather small effect upon the final bolt loads. This does not imply that bolt flexibilities can be varied indiscriminantly.

A composite-metal bolt load-displacement curve typical of that which is found in the stabilizer root joint is illustrated in figure 4. Equation (1) tends to overestimate the flexibility of this configuration by about 40 percent. It is emphasized that any such estimate of bolt flexibility must be assessed carefully both with respect to its applicability and to the sensitivity of the design to the bolt loads being estimated.

## Design Approach

The state of combined in-plane loads,  $N_x$ ,  $N_y$ ,  $N_{xy}$ , and the bolt load reactions,  $P_x$ ,  $P_y$  must be established for each bolt in the joint before detailed strength analysis can proceed. These internal loads are obtained from a structural model using a finite element analysis, reference 2. A relatively fine grid of membrane stress elements is constructed representing the orthotropic composite cover and the isotropic bearing support fitting structure. At each bolt location, coincident nodes are assigned to the cover and fitting and are connected by a spring element representing the stiffness of the bolt. In practice, every single bolt cannot always be represented by a node pair, particularly in tightly spaced areas, and after the inevitable small adjustments to the structure are made. Judgement and hand analyses are sometimes required to assign equivalent lumped stiffnesses to the appropriate members. Similar judgement is obviously required to interpret the results of the analysis.

The structure was analyzed by the finite element method using bolt stiffnesses obtained from equation (1). Test results indicated that equation (1) overestimates bolt flexibility (underestimates bolt stiffness). To assess the impact of increased bolt stiffness, the analysis was repeated twice with the bolt stiffnesses increased by 30 percent and then 60 percent. Figure 5 illustrates the effects upon the bolt loads produced by multiplying the stiffness of equation (1) by a factor,  $K_p$ . A 60 percent overall increase in bolt stiffnesses raises the leading bolt loads about 10 percent. Following the determination of internal loads in the root joint, a point-by-point strength analysis was performed at each bolt location using design strength data obtained from the joint test program.

The entire root joint design analysis effort, including design strength test data generation, took place in about six months. The authors recognize and wish to emphasize that all the analysis methods employed, including strength margins, could be incorporated into a data processing and post-processing scheme with considerable savings of engineering effort. The data and methods were not available in time to automate the splice analysis for the stabilizer root joint.

## DESIGN STRENGTH DATA

### Test Program

A test program strongly oriented to the horizontal stabilizer design was performed to provide allowable stress data for boron-graphite-epoxy hybrid laminates ( $0^\circ\text{B}/\pm 45^\circ\text{G}/90^\circ\text{G}$ ) under combined stress with bolt load reaction at an arbitrary angle. The scope of the test program is given in table 1. A total of 237 specimens were tested. Off-axis specimens were used to determine failure under tension-tension-shear stress field, while biaxial specimens were used for the tension-compression loadings. The specimens were configured as straight-sided tension type specimens with fiberglass end grippers for load introduction. The specimens were made 24 in. long to lessen the end effects in the off-axis tests. All specimens had a 5/16 or 3/8 in. diameter hole with standard  $100^\circ$  countersink. The widths of the coupons were made 1.875 or 2.25 in. so as to maintain a constant width to diameter ratio,  $W/D = 6$ .

The test fixture used for these tests is shown in figure 6. It contains two intermediate hydraulic jacks to allow controlled partial load reaction through a single shear fastener. Provisions were made to allow adjustment of the jacks to align the specimen in the fixture. Bending across the thickness and width was monitored by strain gages. For loaded hole tests additional restraining blocks were used to minimize bending across the joint. Strain gage readings were used to check the stiffness properties of the laminate.

### Test Results

Test results are presented in terms of the principal variables. All test results are tabulated in the Appendix. The effect of bolt load on net tension strength is shown in figures 7 and 8. Net tension failure stress is reduced in the presence of bolt load from the open hole value; the reduction being nearly linear with increase in the ratio of bolt load to total load. Specimens loaded at  $22.5^\circ$  and  $45^\circ$  to the laminate axis (tension-tension-shear loading in the laminate axis) show least degradation. Overall laminate load-strain response was observed to be essentially linear to failure. The behavior shown in figure 4 however, is typical of the joint load-displacement curve at high bolt loads. It is possible to produce yielding of the bolt and local crushing of the laminate without catastrophic laminate tensile rupture.

Temperature effect on tension strength, figures 9 and 10, is seen to be small. The strength of boron-epoxy critical laminates increases at  $-67^{\circ}\text{F}$  and deteriorates at  $300^{\circ}\text{F}$ . The reverse seems to be true for hybrids where failure is traced to graphite-epoxy layers.

### Design Allowables

Test results shown in figures 7 through 10 were used to establish design allowables. These results are obtained from two laminates,  $48_{\text{B}}-12_{\text{G}}-36_{\text{G}}$  and  $32_{\text{B}}-16_{\text{G}}-48_{\text{G}}$ , which comprise two thirds of the test data. Test results from five other laminates were used to verify and extend the strength data base.

Open hole data for  $48_{\text{B}}-12_{\text{G}}-36_{\text{G}}$  and  $32_{\text{B}}-16_{\text{G}}-48_{\text{G}}$  laminates were used to relate breaking load to far-field layer stresses calculated from lamination theory. Layer longitudinal stresses for the  $0^{\circ}$ ,  $90^{\circ}$ ,  $\pm 45^{\circ}$  plies were determined using test results for the two laminates loaded in the  $0^{\circ}$ ,  $22.5^{\circ}$ ,  $45^{\circ}$ , and  $90^{\circ}$  directions. The average of far-field gross layer longitudinal stress values derived from test was then reduced by a factor of 0.8 to determine the following design allowables:

$$\begin{aligned} F_{0^{\circ}} &= 80 \text{ ksi (Boron)} \\ F_{90^{\circ}} &= 45 \text{ ksi (Graphite)} \\ F_{45^{\circ}} &= 45 \text{ ksi (Graphite)} \end{aligned} \quad (2)$$

The next step is to incorporate the effect of bolt loading into the combined stress allowables. Figures 7 and 8 indicate that the degradation of strength due to bolt load is a function of laminate orientation and loading direction. Specimen loaded at  $22.5^{\circ}$  and  $45^{\circ}$  show the least degradation. In order to maintain a simple, conservative approach, it was decided to penalize the  $\pm 45^{\circ}$  layers (critical in the  $22.5^{\circ}$  and  $45^{\circ}$  load direction tests) by an amount corresponding to the maximum bolt load and to assign the components of the bolt load to the  $0^{\circ}$  and  $90^{\circ}$  layers. That is, although the entire bolt load is assumed to be reacted by the  $0^{\circ}$  and  $90^{\circ}$  layers, the  $\pm 45^{\circ}$  layers are limited to a stress level corresponding to that seen when maximum bolt loads are applied in the tests. Accordingly, the  $\pm 45^{\circ}$  (Graphite) allowable layer longitudinal gross stress is reduced from 45 ksi to 41 ksi. For the  $0^{\circ}$  and  $90^{\circ}$  layer, the steepest slope seen in figures 7 and 8 was applied to obtain

$$(F)_{\text{net}} = (F_{\text{oh}})_{\text{net}} - 0.208 f_{\text{br}} \quad (3)$$

where  $f_{br}$  is the nominal bearing stress,  $P/Dt$ . (Here  $P$  is the component of bolt load in the  $0^\circ$  or  $90^\circ$  direction and the net stress is a function of the laminate and the load direction.) As a matter of design philosophy biaxial contributions to uniaxial strength are ignored while reductions of strength are taken into account.

Variation of width to diameter ratio is accounted for by maintaining a constant net section allowable stress for  $W/D$  ratios less than six. Hole size effect is accounted for by correlating the open hole test data at diameters of  $5/16$  and  $3/8$  inch with the analysis method of Whitney and Nuismer, reference 3. The hole size correction factors are given in table 2.

Tests on five-bolt splice elements similar to figure 3 indicate that tension is more critical than compression at temperatures from  $57$  to  $300^\circ F$ , even after four lines of spectrum fatigue. A test program is underway to verify the root joint design under humid environment conditions simulating a twenty-year aircraft life with runway storage.

#### Comparison With Test Data

The test results are plotted against predicted values in figures 11 through 13. Since the predictions are based on the  $48_B-12_G-36_G$  and  $32_B-16_G-48_G$  laminates, good correlation is to be expected for those cases. The plots show very good agreement for the other laminates as well. More scatter is evident for the  $90^\circ$  layer failures. This may be due to the low percentage of  $90^\circ$  plies in those cases. Statistical analysis of the specimens breaking in the  $\pm 45^\circ$  layers produced a 'B-basis' factor higher than the 0.8 value used here for design.

#### CONCLUSIONS

The strength of thick hybrid boron-graphite-epoxy laminates connected to metal in single shear bolted joints depends upon the bolt bearing load transferred at each bolt. The internal bolt load distribution is a function of the plate stiffnesses and the interconnecting bolt stiffnesses, hence reasonable estimates of joint flexibility are important in design analysis. Equation (1) provided a reasonable estimate in this application but measurement of joint stiffness is still deemed necessary and should be undertaken as soon as preliminary sizing of a new design permits.

The integration of the design analysis procedures directly into the finite element analysis would significantly reduce the effort required in the preparation of input data and interpretation of results.

Bolt bearing reaction interacts with laminate notched tension strength in a linear fashion. Reduced lamina far-field allowables provide a simple load and design analysis approach which was verified for combined loading by off-axis and biaxial testing. Yielding of the bolt and local laminate crushing (bearing failure) can occur without catastrophic laminate tension rupture although laminate load-strain response is essentially linear to failure. Tensile strength was found to be relatively insensitive to temperature.

#### ACKNOWLEDGMENTS

The work described here is part of the Advanced Development of Conceptual Hardware - Horizontal Stabilizer program, contract F33615-73-C-5173, initiated by the Air Force Materials Laboratory and now sponsored by the Air Force Flight Dynamics Laboratory. Mr. R. Rapson was the Air Force project engineer during the course of this work. Mr. R. Stanton is now the Air Force project engineer.

The authors wish to acknowledge the contributions of R. Hadcock, L. Murrin, and R. Sadler of Grumman Corporation.

APPENDIX A  
Tabulation of Test Results

Individual test results are given below. All thicknesses are based on a nominal layer thickness of 0.00525 inches and loads are given in customary units ( $K = 1000 \text{ lbs}$ ). All failures occurred in net tension.

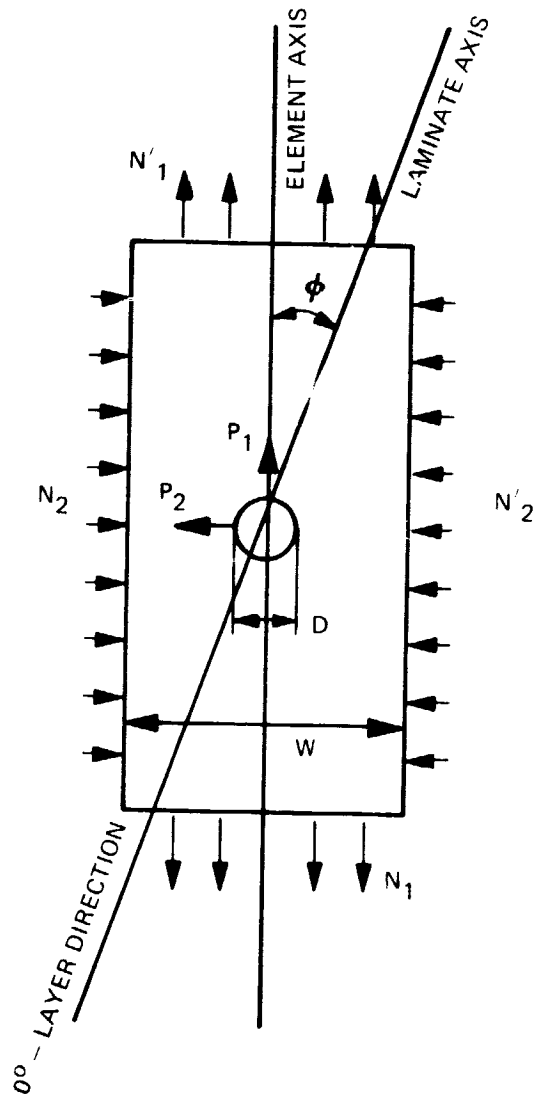


Table A-1 Joint Test Results

LAMINATE 0/90/45	Ø (DEG)	TEMP (°F)	t (in.)	W (IN)	D (IN)	N <sub>1</sub> (K/IN)	N <sub>2</sub> (K/IN)	P <sub>1</sub> (K)	P <sub>2</sub> (K)
48 B - 12 G - 36 G	0	RM	0.504	1.85	0.312	28.84	0	0	0
				1.88		28.64		0	
				1.82		28.79		0	
				1.875		29.48		0	
				1.873		24.56		4.17	
				1.875		25.44		4.79	
				1.876		23.99		5.98	
				1.871		26.44		6.64	
				1.875		27.28		0	
				1.875		27.43		0	
				1.875		27.08		0	
				1.875		23.95		4.08	
				1.880		25.03		4.28	
				1.875		24.43		4.15	
				1.875		26.99		7.00	
				1.875		22.37		5.85	
				1.875		25.12		6.99	
				2.253	0.375	26.94		0	
				2.255		27.67		0	
				2.259		25.55		5.15	
			2.252		23.07		4.72		
			2.25		20.87		8.07		
			2.25		22.69		8.76		
		-67	1.78	0.312	32.24		0		
			1.868		29.87		0		
			1.87		30.86		0		
			1.87		25.90		6.97		
			1.88		26.77		4.58		
			1.88		27.13		4.67		
		300	1.87		28.13		0		
			1.79		29.69		0		
			1.87		30.80		0		
			1.87		25.91		4.39		
			1.875		25.93		4.43		
			1.80		27.92		6.00		
			1.87		25.86		7.00		

ORIGINAL PAGE IS  
OF POOR QUALITY



Table A-1 Joint Test Results

LAMINATE 0/90/±45	θ (DEG)	TEMP (°F)	t (in.)	W (IN)	D (IN)	N <sub>1</sub> (K/IN)	N <sub>2</sub> (K/IN)	P <sub>1</sub> (K)	P <sub>2</sub> (K)
48 <sub>B</sub> - 12 <sub>G</sub> - 36 <sub>G</sub>	0	300	0.504	1.875	0.312	30.61	0	0	0
				1.875		28.90		0	
				1.88		27.70		4.74	
				1.88		27.29		4.65	
				1.875		27.17		4.64	
				1.88		25.21		6.99	
				1.875		25.88		7.00	
	22.5	RM		1.82		15.44		0	
				1.82		15.11		0	
				1.82		14.84		0	
				1.889		13.83		2.37	
				1.882		13.12		2.24	
				1.880		11.70		2.00	
				1.88		11.97		4.47	
				1.88		11.27		4.23	
				1.885		11.90		4.49	
				1.88		17.11		0	
				1.875		15.16		0	
				1.875		16.54		0	
				1.875		16.54		2.89	
			1.882		14.52		2.46		
			1.875		15.84		1.66		
			1.875		14.93		5.58		
			1.875		16.59		6.99		
			1.875		16.44		7.02		
	45		1.879		10.38		0		
			1.879		9.739		0		
			1.881		10.23		0		
			1.881		10.19		1.75		
			1.877		9.185		1.57		
			1.882		9.52		1.61		
			1.878		9.047		3.39		
			1.881		9.064		3.40		
	90		1.872		9.631		3.59		
			1.81		8.591		0		
	90		1.87		8.181		0		

Table A-1 Joint Test Results

LAMINATE 0/90/±45	θ (DEG)	TEMP (°F)	t (in.)	W (IN)	D (IN)	N <sub>1</sub> (K/IN)	N <sub>2</sub> (K/IN)	P <sub>1</sub> (K)	P <sub>2</sub> (K)
48 <sub>B</sub> · 12 <sub>G</sub> · 36 <sub>G</sub>	90	RM	0.504	1.887	0.312	7.022	0	1.20	0
				1.883		7.998		1.36	
				1.88		6.410		1.10	
				1.88		6.537		2.44	
				1.88		6.027		2.24	
				1.883		6.399		2.42	
				1.885		4.987		4.61	
				1.88		4.787		4.49	
				1.85		7.432		0	
				1.89		3.857		3.65	
48 <sub>B</sub> · 12 <sub>G</sub> · 32 <sub>G</sub>		300		1.89		9.466		3.48	
		300	0.483	1.78		10.19		0	
	0	RM		3.00		25.80	0.82	4.24	4.90
	0	-67		3.00		25.90	0.82	4.27	4.92
	5	-67		3.00		27.20	0.75	3.93	4.47
	7	RM		3.00		26.10	0	6.63	0
	7	-67		3.02		26.30	0	6.55	0
	10	RM		2.99		26.10	0.11	6.17	0.65
	10	-67		3.01		22.30	0.11	6.57	0.69
		RM		1.875		24.90	0	0	0
44 <sub>B</sub> · 12 <sub>G</sub> · 32 <sub>G</sub>			0.462	1.880		26.56		0	
				1.875		24.57		5.82	
				1.875	0.375	20.28		9.98	
				1.875	0.375	20.41		0.00	
				1.875	0.375	20.16		9.98	
				1.875	0.312	24.96		4.25	
				1.88	0.312	24.13		6.97	
				1.875	0.312	8.827		0	
				1.865	0.312	7.083		5.00	
				1.865	0.312	7.389		5.00	
				1.875	0.375	8.112		0	
				1.875	0.375	6.352		7.00	
				1.880	0.375	7.261		7.00	
				1.855	0.375	5.639		7.01	
				1.870	0.312	5.610		5.50	
				1.8800	0.312	10.61		1.82	

Table A-1 Joint Test Results

LAMINATE 0/90/± 45	θ (DEG)	TEMP (°F)	t (in.)	W (IN)	D (IN)	N <sub>1</sub> (K/IN)	N <sub>2</sub> (K/IN)	P <sub>1</sub> (K)	P <sub>2</sub> (K)
44 B · 12 G · 32 G	0	RM	0.462	3.00	0.375	22.55	5.00	1.00	0
	90					22.07	3.00	1.00	
32 B · 16 G · 48 G	90					9.40	5.00	1.50	
	90					8.56	5.00	1.25	
	0		0.504	1.80	0.312	6.57	5.00	7.50	
				1.856		21.14	0	0	
				1.82		20.74	0	0	
				1.875		21.04	0	0	
				1.87		21.11	0	0	
				1.872		19.86		3.36	
				1.870		18.98		3.33	
				1.87		18.90		3.20	
				1.87		18.43		8.63	
				1.88		17.59		7.70	
				1.875		17.95		6.71	
				1.875		21.70		0	
				1.89		22.04		0	
				1.88		22.04		0	
				1.875		21.26		3.65	
				1.865		21.28		3.63	
				1.875		20.92		3.57	
				1.865		21.08		6.97	
				1.860		21.14		6.99	
				2.256		20.31		7.00	
			2.256		20.08		0		
			2.260		20.08		0		
			2.253		17.51		3.39		
			2.26		17.57		3.61		
			2.26		16.83		7.58		
		67		2.26	17.32		6.99		
			1.87		0.312	21.52		0	
			1.877			21.68		0	
			1.878			20.57		0	
			1.88			19.25		3.31	
			1.88			18.79		3.17	
			1.88			17.96		5.76	

Table A-1 Joint Test Results

LAMINATE 0/90±45	Ø (DEG)	TEMP (°F)	t (in.)	W (IN)	D (IN)	N <sub>1</sub> (K/IN)	N <sub>2</sub> (K/IN)	P <sub>1</sub> (K)	P <sub>2</sub> (K)
32 <sub>B</sub> · 16 <sub>G</sub> · 48 <sub>G</sub>	0	-67	0.504	1.88	0.312	18.52	0	5.95	0
		300		1.78		20.65		0	
				1.82		20.44		0	
				1.80		20.72		0	
				1.88		19.12		3.30	
				1.885		19.33		3.32	
				1.88		18.44		5.78	
				1.865		18.56		5.93	
				1.860		22.07		0	
				1.880		22.16		0	
				1.868		20.23		3.42	
				1.870		20.75		3.50	
				1.875		21.51		7.00	
				1.870		21.78		6.98	
				1.875		22.58		0	
	22.5	RM		1.890		16.19		0	
				1.886		13.31		0	
				1.889		13.45		0	
				1.894		13.19		2.26	
				1.885		14.62		2.55	
				1.90		15.19		2.62	
				1.885		13.94		5.25	
				1.890		14.46		5.44	
				1.890		13.56		5.12	
				1.875		14.84		0	
				1.875		13.40		0	
				1.885		14.56		0	
				1.875		14.30		2.45	
				1.875		15.12		2.53	
				1.880		13.67		5.13	
				1.880		14.65		6.51	
				1.875		14.41		7.06	
				1.875		13.29		7.02	
	45.0			1.882		11.53		0	
				1.881		12.01		0	
				1.878		12.30		0	

ORIGINAL PAGE IS  
OF POOR QUALITY



MINI L PAGES  
FOR QUALITY

Table A-1 Joint Test Results

LAMINATE 0/90±45	θ (DEG)	TEMP (°F)	t (in.)	W (IN)	D (IN)	N <sub>1</sub> (K/IN)	N <sub>2</sub> (K/IN)	P <sub>1</sub> (K)	P <sub>2</sub> (K)
6 <sub>B</sub> -2 <sub>G</sub> -16 <sub>G</sub>	90	-67	0.126	1.125	0.188	3.35	0	0	0
	→	-67	→	1.125	→	3.33	→	→	→
8 <sub>B</sub> -28 <sub>G</sub> -32 <sub>G</sub>	0	300	0.357	1.125	0.50	3.38	→	→	→
	→	300	→	1.125	→	7.60	→	→	→
→	17	RM	→	3.00	→	6.48	→	→	→
	→	-67	→	3.00	→	7.94	→	→	→
→	300	300	→	3.00	0.312	7.25	3.80	5.80	3.21
	→	RM	→	3.00	0.375	6.62	2.89	5.70	3.16
→	17	-67	→	3.00	0.312	11.23	0.87	4.22	5.20
	→	RM	→	2.99	0.375	10.28	0.89	4.34	5.36
→	67	-67	→	2.97	0.312	13.50	0.68	3.92	4.06
	→	RM	→	3.01	0.312	11.91	0.68	3.97	4.11
→	75	-67	→	3.00	0.375	10.37	0	0	0
	→	RM	→	1.868	→	11.05	0	0	0
→	70	300	→	1.878	→	9.75	0	0	0
	→	RM	→	1.873	→	8.75	0	0	0
→	72.5	-67	→	1.858	→	7.29	0.19	7.08	1.12
	→	-67	→	1.867	→	10.20	0.18	7.00	1.10
→	71	300	→	1.861	→	9.20	0.18	6.79	1.075
	→	300	→	1.873	→	9.87	0.19	7.33	1.16
→	72	300	→	1.875	→				
	→	300	→		→				

## REFERENCES

1. W. Ludwig, H. Erbacher, and J. Visconti, "Design, Fabrication, and Test of a Composite Horizontal Stabilizer," Third Conference on Fibrous Composites in Flight Vehicle Design, November 4-6, 1975, Williamsburg, Virginia.
2. G. Wennagel, P. Mason, and J. Rosenbaum, "Ideas, Integrated Design and Analysis System," Paper No. 680728, Soc. Auto. Engrs. Aeronautical and Space Engineering and Manufacturing Meeting, Los Angeles, Oct. 7-11, 1968.
3. J. Whitney and R. Nuismer, "Stress Fracture Criteria for Laminated Composites Containing Stress Concentration," Journal of Composite Materials, Volume 8, 1974, pg 253-265.

Table 1 Number and Type of Tests

TEMPERATURE	-67°F			RM			300°F			TOTAL
	LONG. OR TRANSV. TENSION	OFF AXIS TENSION	BI AXIAL (TEN- COMPR.)	LONG. OR TRANSV. TENSION	OFF AXIS	BI AXIAL	LONG. OR TRANSV. TENSION	OFF AXIS	BI AXIAL	
48 <sub>B</sub> · 12 <sub>G</sub> · 36 <sub>G</sub>	8	-	-	33	27		16			84
44 <sub>B</sub> · 12 <sub>G</sub> · 32 <sub>G</sub>	3	-	-	12		5	2	-	-	22
32 <sub>B</sub> · 16 <sub>G</sub> · 48 <sub>G</sub>	7	-	-	32	27	-	15	-	-	81
8 <sub>B</sub> · 4 <sub>G</sub> · 12 <sub>G</sub>	-	-	-	12	-	-	-	-	-	12
6 <sub>B</sub> · 2 <sub>G</sub> · 16 <sub>G</sub>	3	-	-	6	-	-	5	-	-	14
48 <sub>B</sub> · 12 <sub>G</sub> · 32 <sub>G</sub>	-	3	1	-	2	1	-	-		7
8 <sub>B</sub> · 28 <sub>G</sub> · 32 <sub>G</sub>	1	5	1	1	4	1	1	3	-	17
TOTAL	22	8	2	96	60	7	39	3		237

Table 2 Hole Size Corrections

D IN.	1/8	3/16	1/4	5/16	3/8	7/16	1/2
k <sub>D</sub>	1.26	1.15	1.07	1.0	0.95	0.90	0.87



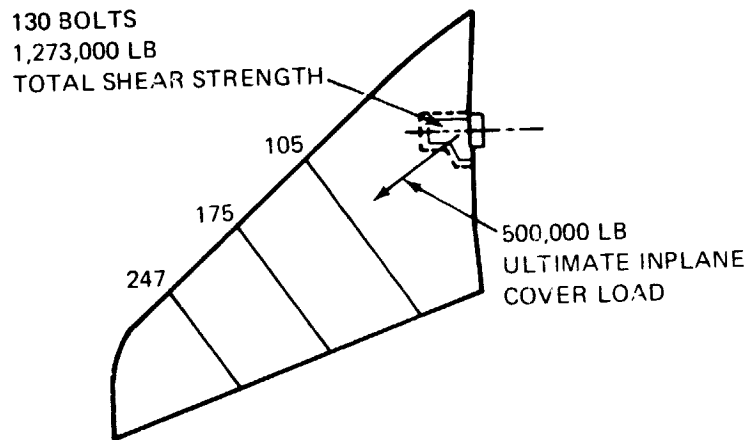


Figure 1 Planform of the Horizontal Stabilizer Showing the Location of the Bearing Support Fitting

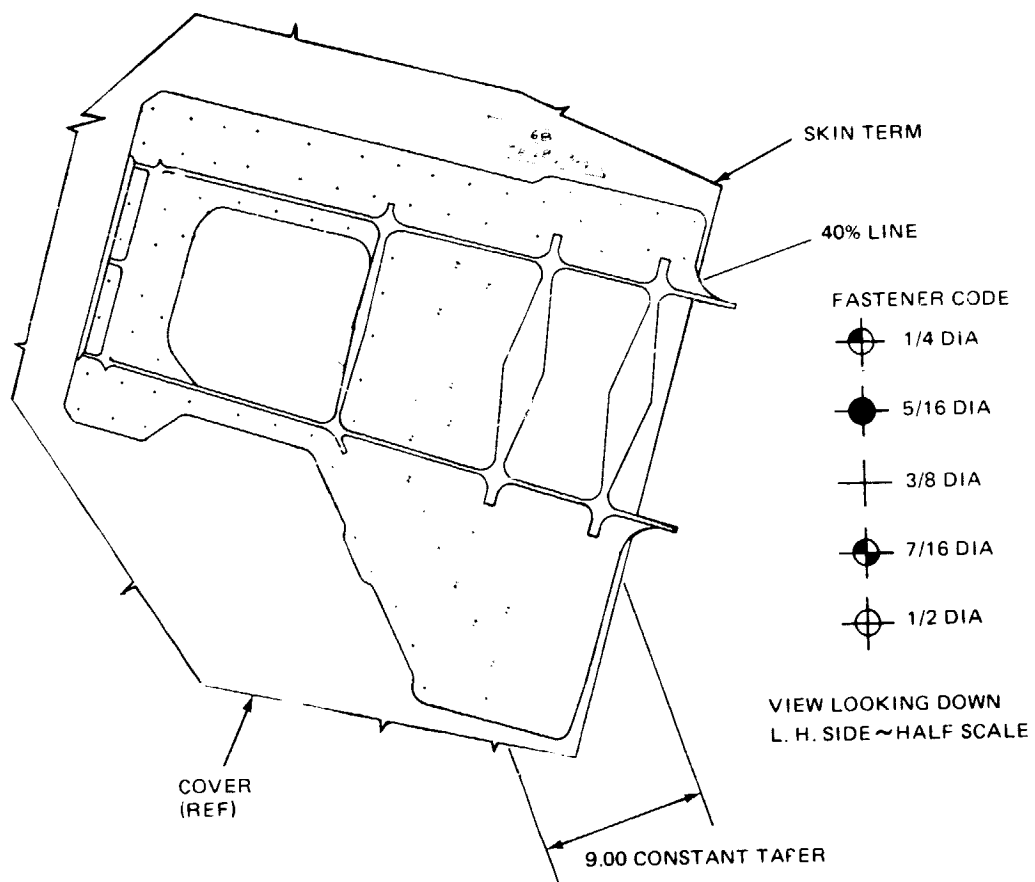
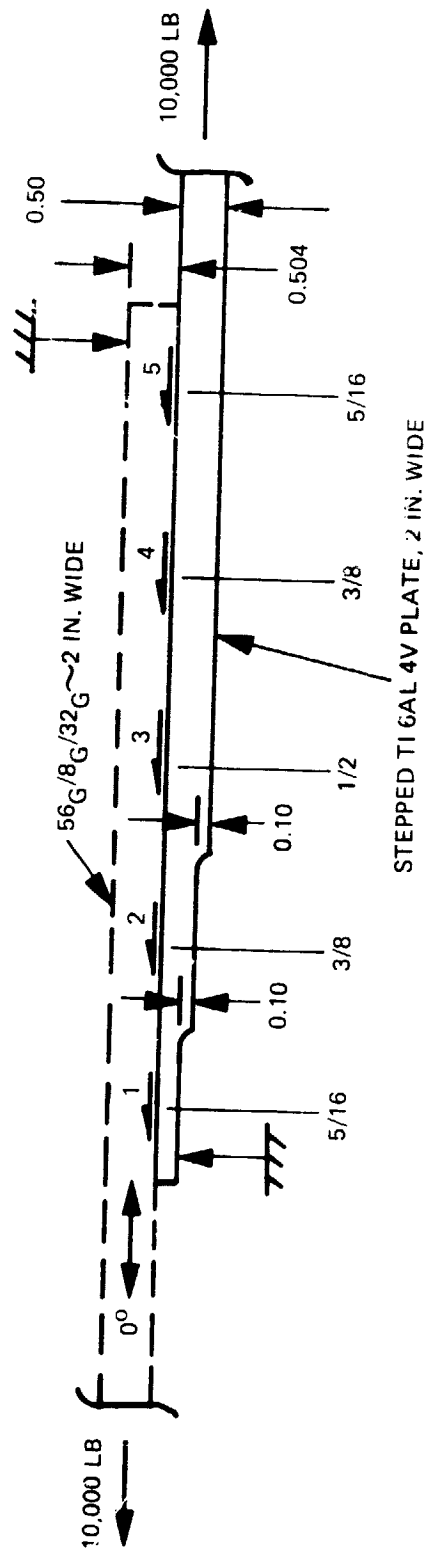


Figure 2 Root Area Bolt Pattern

(BOLTS ARE COUNTERSUNK IN THE COMPOSITE)



	P1	P2	P3	P4	P5
1 BASELINE: FLEXIBLE BARS & BOLTS	1983	2032	2298	1903	1784
2 SAME AS 1 EXCEPT BOLT $\alpha$ X 2	1826	2047	2453	1974	1700
3 SAME AS 1 EXCEPT RIGID BARS	1635	2055	2630	2062	1618
4 SAME AS 1 EXCEPT RIGID BOLTS	4423	903	373	4	4297

Figure 3 Importance of Estimating Bolt Flexibility in Joint Analysis

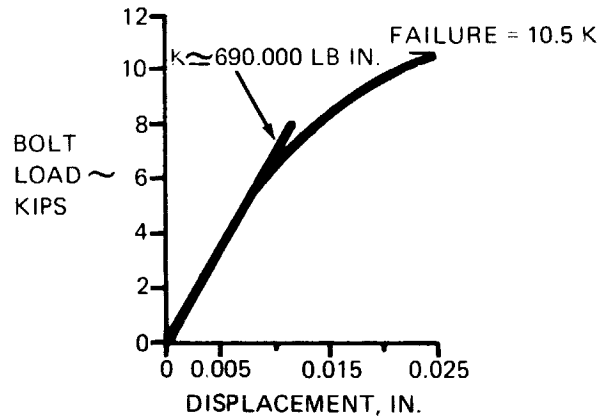
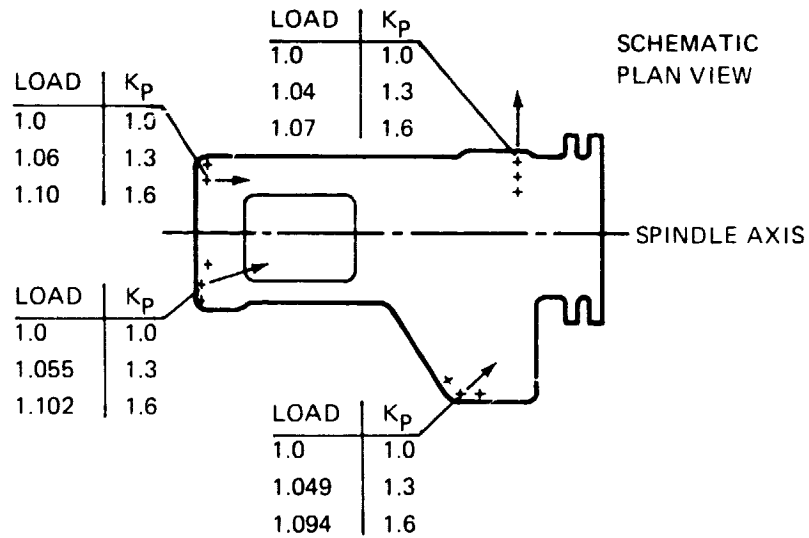


Figure 4 Typical Room Temperature Test Load-Displacement Curve for a 3/8- inch diameter Titanium Bolt Connecting 44<sub>B</sub>/12<sub>G</sub>/32<sub>G</sub> to 1/4 inch Titanium



(NOTE: K<sub>p</sub> IS BOLT PATTERN STIFFNESS FACTOR)

Figure 5 Effect of Bolt Stiffness Variation on Analytical Bolt Loads



Figure 6 Tension-bearing Test Rig

ORIGINAL PAGE IS  
OF POOR QUALITY

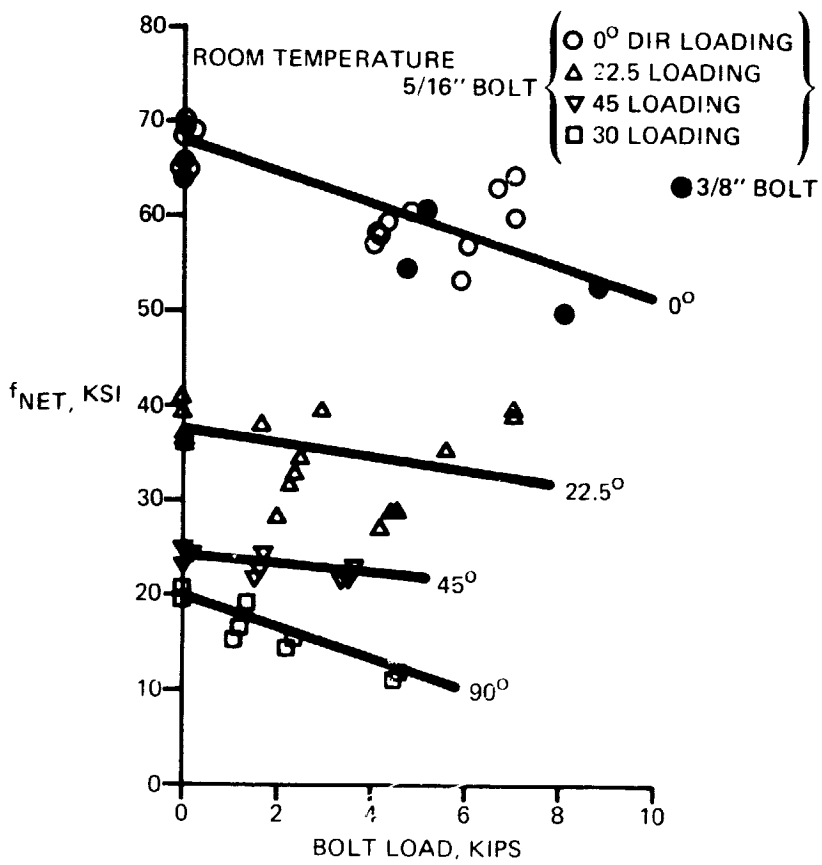


Figure 7 Effect of Bolt Load on Net Tension Stress for 48<sub>B</sub>-12<sub>G</sub>-36<sub>G</sub> Laminate

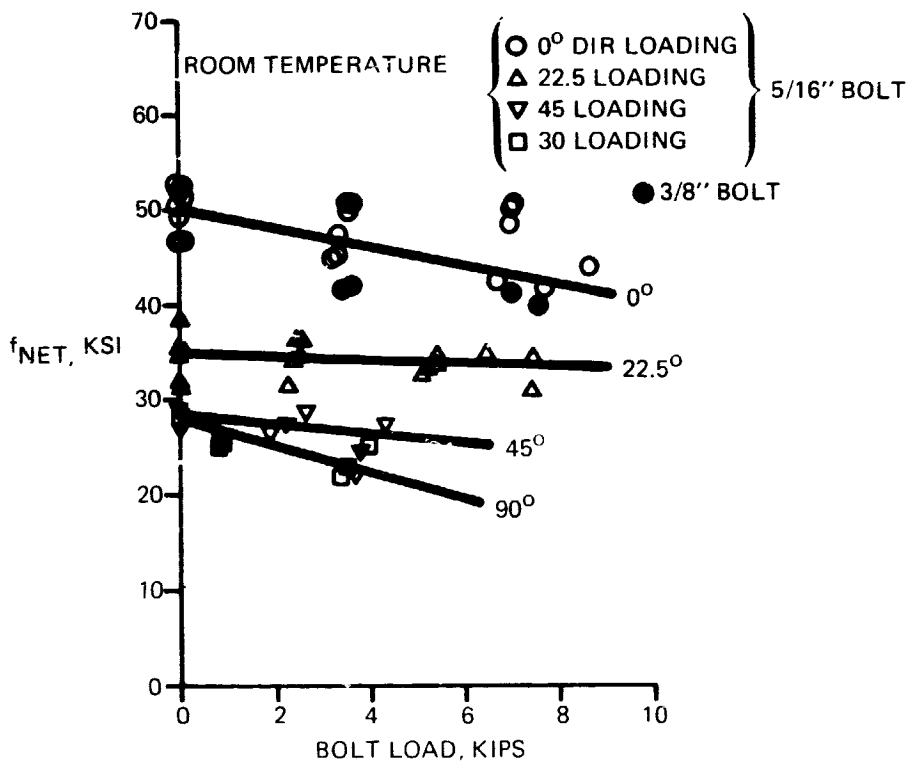


Figure 8 Effect of Bolt Load on Net Tension Stress for  $32_B-16_G-48_G$  Laminate

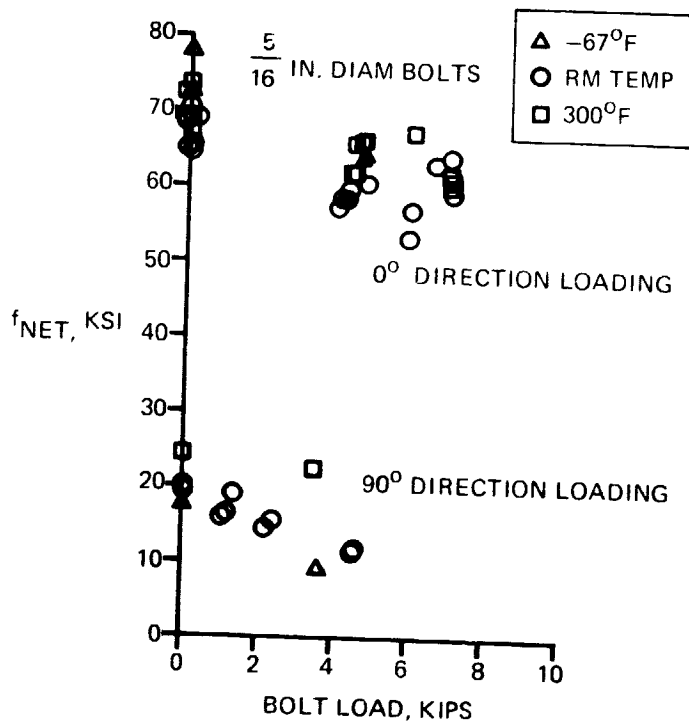


Figure 9 Effect of Temperature on Net Tension Stress for  $48_B-12_G-36_G$  Laminate

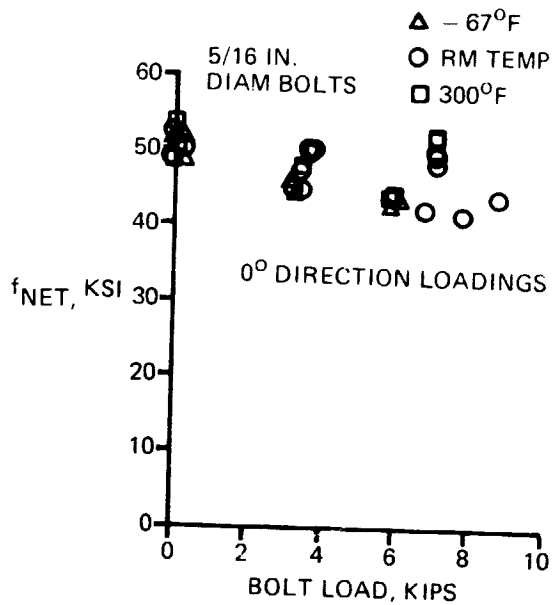


Figure 10 Effect of Temperature on Net Tension Stress for  $32_B-16_G-48_G$  Laminate

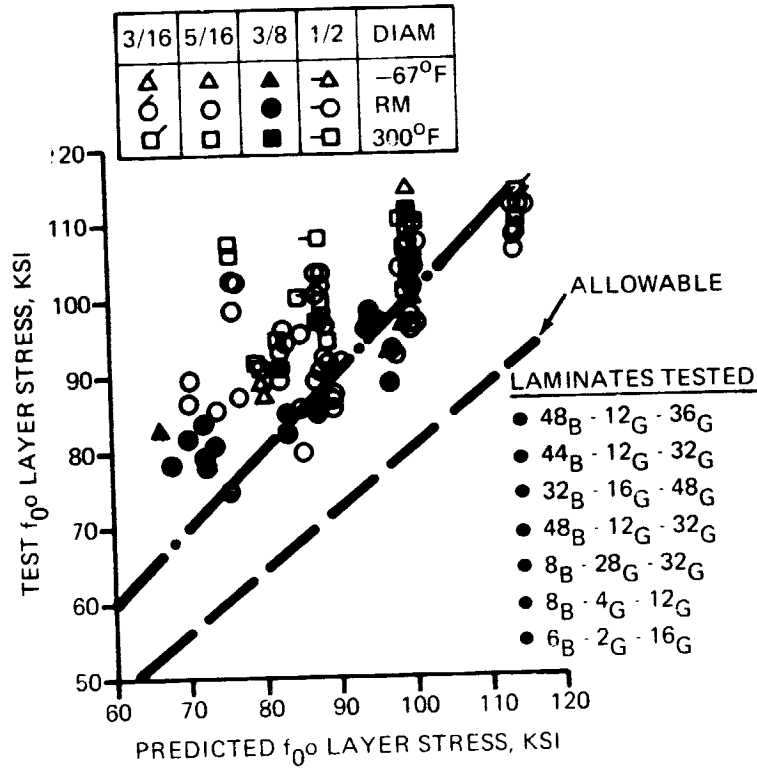


Figure 11 Comparison of Test and Predicted  $0^0$  Layer Longitudinal Strength for Hybrid Laminates with Loaded and Unloaded Holes



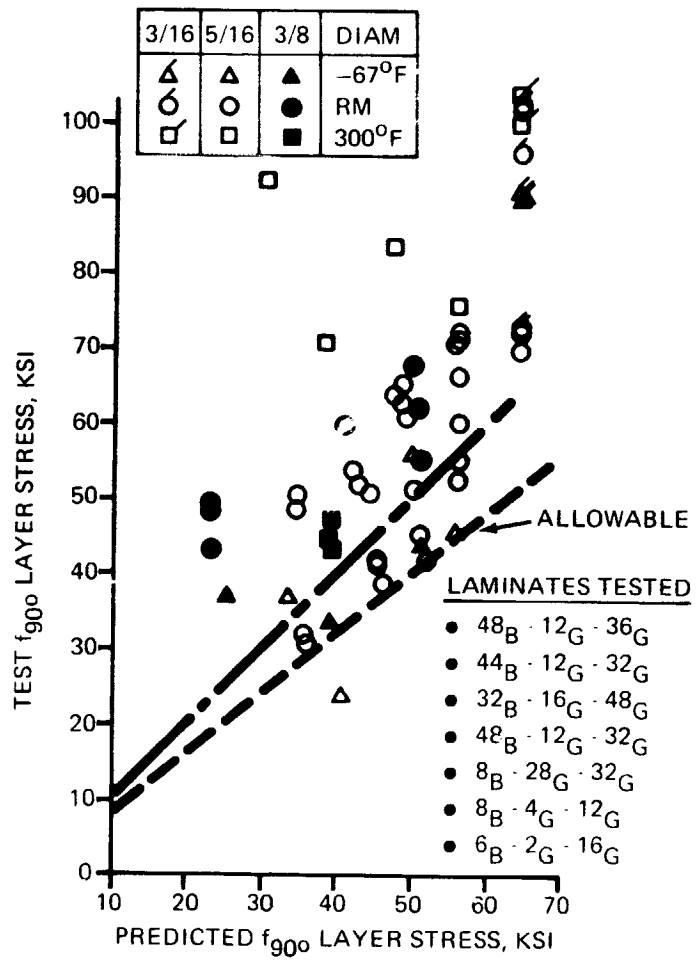


Figure 12 Comparison of Test and Predicted 90° Layer Longitudinal Strength for Hybrid Laminates with Loaded and Unloaded Holes

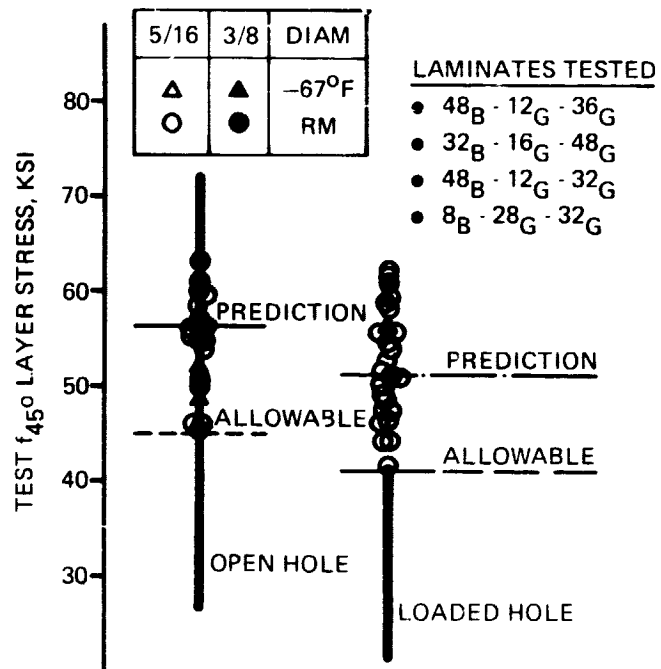


Figure 13 Comparison of Test and Predicted  $45^\circ$  Layer Longitudinal Strength for Hybrid Laminates with Loaded and Unloaded Holes

CURRENT LANGLEY RESEARCH CENTER STUDIES ON BUCKLING  
AND LOW-VELOCITY IMPACT OF COMPOSITE PANELS

By Martin M. Mikulas, Jr., Harold G. Bush,  
and Marvin E. Rhodes  
NASA Langley Research Center

SUMMARY

This paper reviews results from ongoing programs at the NASA Langley Research Center which have as their objective the establishment of a weight and strength data base for efficient graphite/epoxy structural components. Efficiency studies are presented which were obtained from a newly developed synthesis code for designing structural panels subjected to combined loads. Results from an experimental evaluation of two 91- by 119-cm (36- by 47-in.) graphite/epoxy sandwich shear webs are presented, as well as recent test results on 152-cm-long (60-in-long) hat-stiffened graphite/epoxy compression panels. Also reviewed are new results from an experimental program being conducted to study the low-velocity impact behavior of graphite/epoxy structures. Some design implications of this research are discussed in the context of redesigning commercial-aircraft aluminum wings with graphite/epoxy material.

INTRODUCTION

A comprehensive program is being pursued at the NASA Langley Research Center (LaRC) to advance the technology for designing and for building advanced composite structures comparable to the technology which presently exists for aluminum structures. Although there have been significant advances in composite mechanics and design methods over the past 10 years, further efforts are necessary to fully exploit the potential advantages offered by advanced composite materials. For example, in addition to offering weight advantages and tailorable structural properties when compared with aluminum, composite materials with their radically different fabrication processes also offer the potential for reducing manufacturing costs. It should be expected then that the development of advanced composite structures will be an evolutionary development with many iterations between manufacturing and structural design.

In an effort to obtain the needed interaction between design, analysis, and manufacturing activities, a program is being conducted at the Langley Research Center to establish an experimentally verified weight-strength data base for various generic structural components. Establishing this data base not only provides experience with composite hardware but provides a much needed standard against which the relative merits of various structural concepts can be compared. The critical experience that is obtained only from the actual

PRECEDING PAGE BLANK NOT FILMED

design of flight hardware is provided through interaction with industry and with composite-structures flight programs at the Langley Research Center.

In the present paper a review is given of graphite/epoxy composite structural design technology studies in progress at LaRC. Specific items discussed include: development of new analyses and design procedures, establishment of a weight-strength data base for compression panels, establishment of a weight-strength data base for shear webs, and a study of the impact behavior of composite laminates. Also presented is a discussion of some design implications associated with composite materials, with specific attention given to the design of substitution wings for medium-size commercial aircraft.

#### SYMBOLS

Measurements and calculations were made in the U.S. Customary Units. They are presented herein in the International System of Units (SI) with the equivalent values given parenthetically in the U.S. Customary Units.

A	panel surface area
B	panel width
b	shear web depth
L	panel simple support length
$L_e$	effective experimental panel length
$N_x$	compressive load per unit width
$N_{xy}$	shear load per unit width
P	total applied load
$P_u$	ultimate applied load
$t_1$	thickness of skin under hat cap
$t_2$	thickness of vertical webs
W	panel weight
$\gamma$	shear angle
$\theta$	filament orientation
$\sigma_a$	allowable stress

## PANEL ANALYSIS AND DESIGN PROCEDURES

In this section a review is given of the analysis and design procedures which are currently being used or are under development at LaRC for composite panels under combined loads. Current research is focused primarily on stiffened composite panels; however, many of the methods discussed are equally applicable to sandwich panels.

### Panel Stability Analysis Methods

Due to the large number of variations in laminate geometry, filament orientation, and material properties associated with composite structures, computer codes with rather general stiffness and geometry capability are necessary for analyzing their stability. The needed codes are being obtained both by converting existing codes to deal effectively with anisotropic properties and by developing new ones. A list of nine computer codes presently being used and their associated features are listed in table I. Also listed in the table are the references (refs. 1 to 9) in which each code is discussed.

The first four codes listed, BUCLASP 2, VIPASA, BOSOR 4, and SRA, are rapid one-dimensional codes and are used primarily to study the complex buckle modal behavior commonly associated with stiffened composite panels tailored for high structural efficiency. An example of the BUCLASP 2 code being used to study a hat-stiffened panel which exhibited modal interaction is presented in reference 10. The fifth code, BUCLAP 2, is used to study the stability of curved unstiffened anisotropic panels which exhibited bending-extension coupling. The next four codes listed, BOP, NASTRAN, SPAR, and STAGS, are used to study composite panels where the assumption of a single trigonometric shape (as in the one-dimensional code) for the buckle mode is not adequate because of boundary conditions or variations in stiffness, loading, or temperature. The STAGS computer code can also efficiently handle geometrically nonlinear problems. The STAGS code was used in reference 11 to solve the nonlinear problem of shear web buckling with an initial imperfection.

### Panel Design Procedures

The two panel optimization programs (POP) presently being used at LaRC are given in figure 1. In both programs, mathematical programming techniques are used as the basic optimizing tool for arriving at minimum weight designs. These programs provide the weight of a panel required to carry a given set of combined loads and also provide a complete description of all skin thicknesses and stiffener element lengths. In addition, design constraints such as shown in figure 1 may be specified. In the first procedure (POP-I) the assumption is made that the panel buckling behavior for the local modes and wide column Euler modes can be represented independently by simple closed-form solutions, such as was done in reference 12 for metal panels. Typically, 1000 to 2000 iterations and about 25 seconds of computer time are required to obtain a single design. A more complete discussion of this procedure is presented in reference 13 and

some applications of it are presented in reference 10. Although panel designs obtained using this procedure (POP-I) must be checked with a complete stability analysis such as BUCLASP 2 or VIPASA, the POP-I procedure has been found to be a very useful tool for performing parametric studies or even generating final designs for well-understood stiffener concepts.

In the second procedure (POP-II), an exact eigenvalue buckling solution technique (BUCLASP 2 or VIPASA) is utilized to properly account for element connections and complex buckle modes. In POP-II, complete buckling solutions are not obtained for each iteration; instead, approximate analyses are made and are updated periodically with the exact analysis. This procedure requires about 100 to 300 seconds of computer time to obtain a single design. A discussion of the optimization technique used in the POP-II code is presented in reference 14. This design procedure (POP-II) implicitly uses an exact stability analysis; therefore, it is used for studying open section stiffeners that are highly susceptible to large load reductions due to rolling of the stiffener. Research is also underway using this procedure (POP-II) to design panels with mode shapes controlled in such a fashion as to minimize the effects of initial imperfections.

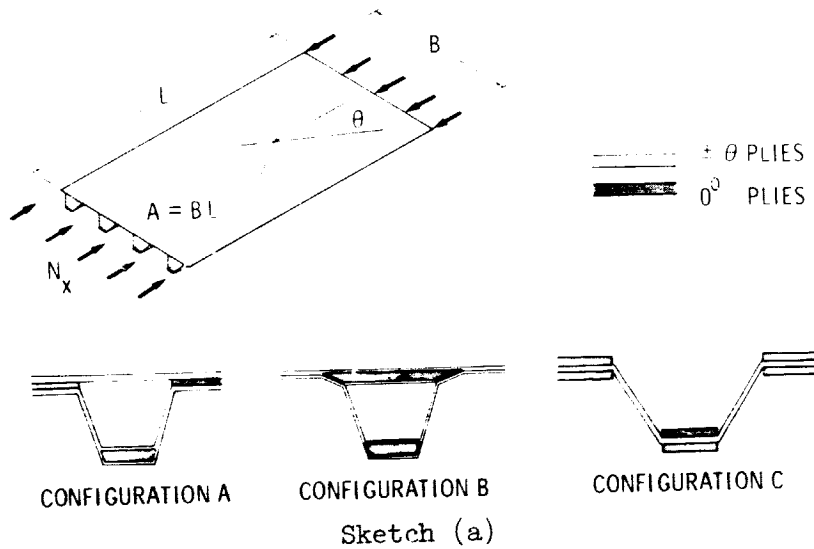
Sample results for the weight-strength performance of hat-stiffened graphite/epoxy panels under combined loads are presented in figure 2. These results were obtained using the POP-I panel design code. On this chart the weight index  $W/AL$  is plotted as a function of the loading index  $N_x/L$  for several ratios of applied shear to applied compression  $N_{xy}/N_x$ . For low values of the loading index, the panels are mainly stability critical; whereas, for high values the panel weights are controlled by strength considerations, as indicated by the steeper slopes on the curves above  $N_x/L = 1000$ . For all the results shown in figure 2,  $\theta$  was constrained to be  $45^\circ$ .

## COMPRESSION PANEL STUDIES

Recent test activities on composite panels at the Langley Research Center have been focused on establishing a weight-strength data base for highly efficient hat-stiffened and open-corrugated graphite/epoxy panels designed for compression load only. The simple load condition was chosen to facilitate the understanding of failure mechanisms and to provide a standard for ready comparison of various stiffening concepts. The validity of various design procedures and analyses is being tested by comparisons with experimental results on the compression load designed panels, and efforts are underway to expand the testing program to combined loads.

### Panel Designs

The three panel cross-sectional configurations presently being considered are shown in sketch (a). The shaded and unshaded areas distinguish between the orientations of the plies and their distribution. Configuration A was shown in



reference 10 to be a structurally efficient arrangement for carrying axial compression loads with the ply orientation angle  $\theta$  being  $\pm 45^\circ$ . The essential features of this design are (1) that  $0^\circ$  (high axial stiffness) plies are located in the hat cap and skin to provide maximum column bending stiffness and (2) that the vertical webs are composed of all  $\pm\theta$  (low axial stiffness) plies to minimize the amount of axial load carried by the webs, thus permitting thin, lightweight webs. Also, the  $\pm\theta$  plies in the vertical webs provide the shearing stiffness needed to minimize column transverse shearing deformations. Configuration B, also shown to be efficient in reference 10, had  $0^\circ$  plies concentrated in the skin under the hat. Configuration C is a symmetrical open corrugation which is applicable where smooth skins are not required.

In wing panels the compressive load levels are typically between 3500 to 5300 kN/m (2000 to 30 000 lb/in.) with a rib spacing of about 76 cm (30 in.). In space vehicles, compressive load levels are generally much lower - typically, 88 to 525 kN/m (500 to 3000 lb/in.). The three load levels chosen for this study as being representative of these loading conditions were 158, 525, and 1580 kN/m (900, 3000, and 9000 lb/in.). The panels were designed using the POP-I design code discussed previously. Selected panel designs were fabricated and tested. For each design, specimens 41 cm (16 in.) long were used to evaluate local buckling and ultimate strength, and specimens 152 cm (60 in.) long were used to evaluate Euler and interactive buckling modes.

### Panel Tests and Results

To date, panels have been designed and tested at load levels of 158, 525, and 1580 kN/m (900, 3000, and 9000 lb/in.). The 158 kN/m panel was an open corrugation while the 525 and 1580 kN/m panels were of hat-stiffened design. Comparisons of test results with BUCLASP 2 results are reported in reference 10 for twenty-three 41-cm (16-in.) specimens and for six 152-cm (60-in.) specimens.

Typical failures of the 525 and 1580 kN/m (41-cm-long) panels are shown in figure 3. It can be seen that failure of the 525 kN/m panel has accompanied a

delamination of the skin from the stiffeners while the 1580 kN/m panel failed in an explosive fashion with one of the stiffeners totally separating from the skin. The nature of the failures are apparently closely related to the level of strain at failure. The strain at failure for the 525 kN/m panel was about 0.005 whereas the strain at failure for the 1580 kN/m panel was 0.0076, which is very close to the ultimate strain of the graphite/epoxy panel in compression (0.0086). The 525 kN/m panels had relatively low strain levels at initial buckling (0.0036 for the panel just discussed) and typically exhibited some post buckling strength. The 1580 kN/m panel had relatively high strains at initial buckling and exhibited very little, if any, post buckling behavior.

Panels 152 cm long (twice the simple support design length) were used to evaluate the wide column behavior of the various designs, as discussed in reference 15. A photograph of a panel being tested in a compression test machine is shown in figure 4. The strains in these panels were recorded with 80 strain gages, and out-of-plane displacements were recorded with 15 electrical displacement transducers. The strains were used to determine the location of zero curvature in the panels to establish the effective simple support panel length, as was done in reference 15. Further details of the panel tests are presented in reference 10.

#### Panel Weight-Strength Performance

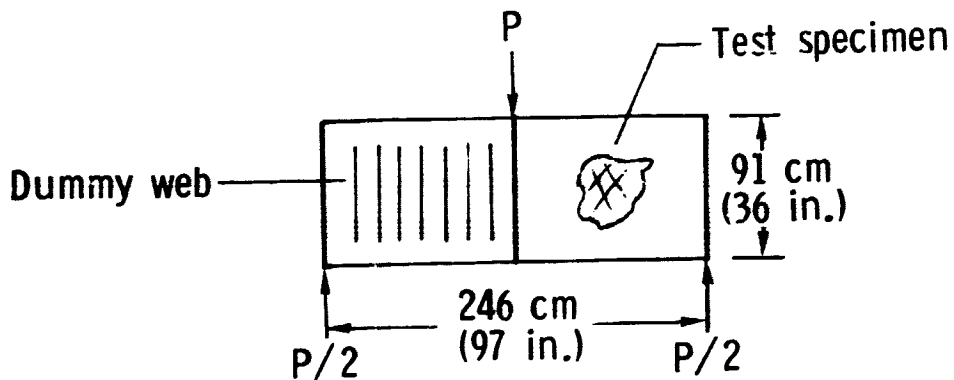
The weight-strength performances of the panels tested are presented on the structural efficiency chart in figure 5. For comparison, data points from over 2000 NACA aluminum panels of three different cross sections are shown. The dashed line is the theoretical minimum weight for hat-stiffened panels predicted by the present design procedure, and the solid lines are for comparably designed hat-stiffened and corrugated graphite/epoxy panels. The cusps in the graphite/epoxy curves are due to balanced laminate considerations which require that the  $\pm 45^\circ$  layers be used in incremental sets of four plies. The comparably determined theoretical curves show a 50-percent weight savings for graphite/epoxy panels when compared with aluminum panels. It can be seen that none of the graphite/epoxy panels achieved the theoretical efficiencies defined by the solid lines; this is due to reductions in predicted load, as well as increases in predicted panel weight. The reductions in load are due primarily to imperfections (both local and overall), and the increases in weight are due to practical manufacturing processes and tolerances which were not considered in the design procedure. However, even with these losses in performance the graphite/epoxy panels tested were still 35 to 42 percent lighter in weight than the theoretical minimum weight for comparable aluminum panels.

It should be pointed out that the closer a panel is designed to the theoretical minimum weight curve the more sensitive it is to imperfections. In most practical structures, panels are designed for multiple load conditions as well as other constraints such as stiffness or fatigue. A discussion of such practical constraints is given in a subsequent section on design implications.



## SHEAR WEB STUDIES

An analytical and experimental program to investigate the shear strength of graphite/epoxy structures is also being conducted. In this section the material and structural evaluation of two large graphite/epoxy sandwich shear webs will be reviewed (ref. 16). One sandwich web was designed to exhibit strength failure of the facings, and the other web was designed to exhibit general instability failure. Each shear web was tested as one-half of a deep beam which was supported and loaded as indicated in sketch (b).



Sketch (b)

### Laminate Tests

The laminate selected for the sandwich facings was  $\pm 45^\circ$  graphite/epoxy (T300/5208). The elastic shear modulus and allowable shear strength of this laminate was determined from material tests conducted using the biaxially loaded picture-frame shear test shown in figure 6. This test method subjects a sandwich specimen to a uniform shear deformation. Details of the specimen design may be found in reference 16. Using this method, the average membrane shear modulus of the  $\pm 45^\circ$  laminate was found to be 41 GPa ( $5.99 \times 10^4$  psi) and the "B" value shear strength was found to be 400 MPa (58 000 psi).

### Structural Specimen Design

The two shear webs were each 91 by 119 cm (36 by 47 in.), which was the same size as the titanium-clad boron/epoxy web of reference 17. The faces of both webs were molded with an integral doubler area for bolting around the periphery which was of pseudoisotropic (0/ $\pm 45$ /90) construction. The strength critical web was designed to exhibit strength failure of the facings (assuming uniform shear flow) at the same shear loading of 1340 kN/m (7638 lb/in.) as the web of reference 17 to provide a direct comparison of structural efficiencies of the two webs; it was constructed with 1.68-mm (0.066-in.) faces (12 plies)

and 1.52-cm (0.60-in.) aluminum-honeycomb core. The stability critical web was designed to exhibit general instability failure at a shear loading of 875 kN/m (5000 lb/in.). The purpose of this web was to identify problem areas for sandwich shear webs which are stability critical and to assess the adequacy of current analytical tools for predicting shear buckling; this web was constructed with 1.40-mm (0.055-in.) faces (10 plies) and 0.95-cm (0.375-in.) aluminum-honeycomb core. An initial NASTRAN (ref. 7) model of the test web and frame was assembled and was used to design the stability critical web core thickness. Further design features of these two shear webs may be found in reference 16.

#### Shear Web Test Method

Both sandwich shear webs were tested in the same manner as the web of reference 17. The test frame, complete with a sandwich web, is shown in figure 7 installed in a compression test machine.

Tension rods provided lateral restraint to the deep beam during test but offered no restraint to inplane deformations of the test web. While the deep-beam test method subjects the web to the desired shear loading, it also subjects the web to small bending deformations. Consequently, both shear webs were instrumented to survey the beam bending strains as well as the overall shear field.

#### Test Results

The strength critical shear web failed at 1055 kN/m (6028 lb/in.) average shear load, which is approximately 79 percent of the design value. The failed shear web is shown in figure 8 where the tension and compression cracks are identified. These cracks are consistent with a material failure in shear. It is believed that failure initially occurred near the crossing of the tension and compression cracks since preliminary analysis and experiment indicate that this is an area of increased stress. The theoretical and experimental load-strain responses in shear are shown in figure 9. Curve I, on the figure, is the theoretical response based on average shear flow over the full depth of the web and indicates that the ultimate facing strain (0.00972) would be reached at the design load of 2.45 MN (550 kips). Shear flow calculations (i.e.,  $VQ/I$  type) which more correctly account for material distribution, including the test frame, indicate that the ultimate strain would be reached at approximately a 5-percent lower load. The measured strains for a given load were significantly higher than elementary flows predicted. Curve II is the average shear strain response determined from gages located over the central portion of the web. When this curve is extrapolated to the ultimate strain level, approximately a 10-percent reduction in maximum load is indicated. However, curve III shows the greatest experimental shear strain on the entire web. This response, which was determined from gages located near the suspected failure point, indicates that a localized area was strained very near the material limit at the failure load. In order to analyze such a web, something beyond elementary theory is required to predict the peak shear stresses which can deviate from the average. In a metal structure, yielding would occur and would allow a uniform stress condition to be approached; but this is not the case for composite materials.

The stability critical web failed at 600 kN/m (3000 lb/in.) average shear load, which is approximately 60 percent of the anticipated buckling load as predicted by linear NASTRAN analysis. The moire fringe photograph of the stability critical web, presented in figure 10, shows the primary pattern to be one large skewed buckle. The buckle is a result of initial out-of-plane displacements that grew from the onset of loading.

The theoretical and experimental load-strain responses in shear of the stability critical web are shown in figure 11. The design load, indicated by a dashed line, was determined from NASTRAN stability analyses by varying core thickness to obtain a web design which was stability critical at an average shear load of 875 kN/m (5000 lb/in.) or 1.6 MN (360 kips) total load. Curve I is the theoretical load-strain response, based on average shear flow over the full web depth and indicates that the buckling load would be reached at an average shear strain of approximately 0.0076. This strain level is approximately 22 percent less than the facing ultimate strain of 0.00972, which is also shown on the figure, indicating an adequate margin to preclude facing strength failure. Curve II is the average load-strain response determined from gages located over the central region of the web. This curve indicates that the resultant average shear stiffness of the web and test frame combination was less than expected, similar to the strength critical web behavior. Curve III shows the greatest shear strain response on the entire web. Back-to-back strain gages at this location reversed at approximately 1 MN (220 kips), thereby indicating the presence of high local bending deformations. Since the web failed at a maximum strain level of approximately 0.00708 (curve III), it appears that membrane strength failure of the facings did not precipitate web collapse. Rather, it is believed that collapse occurred as the result of localized effects such as core, or interlaminar failure after buckling.

#### Weight-Strength Performance

The weight-strength characteristics of various shear web constructions are shown in figure 12, where test section weight per unit area per unit depth ( $W/Ab$ ) is plotted as a function of the shear flow per unit depth ( $N_{xy}/b$ ). The shaded area of figure 12 bounds the region over which aluminum data (summarized in ref. 12) were generated by the NACA. The solid curves are theoretical predictions (ref. 18) which show the limiting behavior for various structural concepts. The experimental stability critical performance of the Ti-clad B/E test web 3 of reference 17 is also shown in the figure. The dashed line is a theoretical prediction of strength critical Gr/E sandwich behavior for the web tested. The stability critical web is an off-optimum design; therefore, its design point does not lie on the strength critical curve. The web experimental results of both the strength critical and the stability critical webs were plotted using average shear loads and full web depth. The strength critical web is shown to weigh approximately one-third as much as the most efficient aluminum structure at that load index and approximately 46 percent as much as the Ti-clad B/E web. Although the design was off-optimum and influenced by initial curvature, the stability critical shear web weighed approximately one-half as much as an aluminum structure which would carry the same load.

In spite of the lower-than-anticipated failure loads, the graphite/epoxy sandwich shear webs have outstanding weight-strength characteristics. The webs achieved average shear stresses of 275 to 350 MPa (40 to 50 ksi), and were found to be 50 to 67 percent lighter than the most efficient aluminum structures known, as indicated by the shaded area of figure 12.

#### LOW-VELOCITY IMPACT

An experimental investigation has been conducted to study local failure modes and impact initiated failures in high-strength graphite/epoxy sandwich structures. This program has been underway for some months and previous results are reported in references 19 and 20.

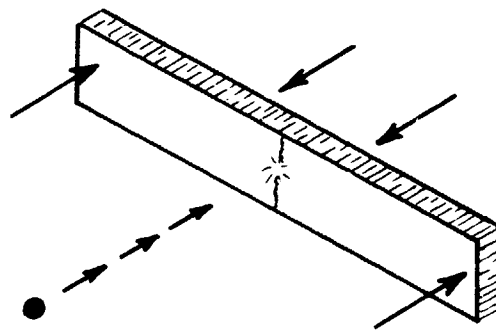
#### Tests

The tests have been conducted on sandwich panel specimens typical of those proposed for use in aircraft secondary structures. Projectiles and energy levels were selected to simulate rock-type impacts. Rock damage is of interest because commercial aircraft are occasionally damaged by rocks and runway debris that is kicked up by reverse thrusters during landing.

Projectiles used in this investigation were 1.27-cm (0.5-in.) diameter solid aluminum spheres. Aluminum was chosen as the projectile material because it has about the same density as common rock materials. All projectile impacts were at normal incidence in the velocity range of 15 to 61 m/s (50 to 200 ft/sec).

#### Specimens

In order to evaluate the effect of impact on the load-carrying capacity of graphite/epoxy composites, sandwich-beam test specimens were used. The specimens were 56 cm (22 in.) long by 8 cm (3 in.) wide and had a composite laminate on one face and a steel plate on the opposite face. The specimens were loaded in four-point beam bending (see sketch (c)) which imposed a uniform stress field



Sketch (c)

on an 8- by 8-cm (3- by 3-in.) test area in the center of the specimen. The 4-ply  $(0,90)_S$  laminates and 8-ply  $(90,\pm 45,0)_S$  laminates fabricated from high strength graphite/epoxy were tested. The 4-ply laminates were supported on  $48 \text{ kg/m}^3$  ( $3 \text{ lb/ft}^3$ ) Nomex honeycomb and the 8-ply laminates were supported on  $130 \text{ kg/m}^3$  ( $8.1 \text{ lb/ft}^3$ ) aluminum honeycomb.

#### Load Frame

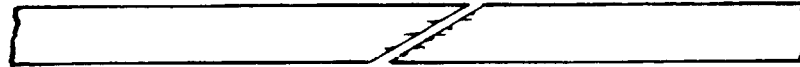
Static loads were applied to the specimens using the loading frame shown in figure 13. A typical test specimen is shown under compression load in the frame. The frame was also used for tensile testing with the load for both cases applied through a screw in the rear of the frame. A load cell was incorporated into the frame to determine the stress in the composite face sheet panel. Specimens were placed in the loading frame and impacted under combinations of load and projectile velocity to determine the combination necessary to initiate catastrophic failure of the specimen.

#### Results

Test results for tensile stressed  $(0,90)_S$  graphite/epoxy laminates supported on  $48 \text{ kg/m}^3$  ( $3 \text{ lb/ft}^3$ ) Nomex honeycomb core are shown in figure 14. The ordinate is the load in the specimen prior to impact (P) divided by the measured average ultimate load ( $P_u$ ) of several virgin specimens, and the abscissa is the kinetic energy of the impacting projectile. The solid symbols represent test specimens in which catastrophic failure occurred upon projectile impact, and the open symbols represent specimens which may have incurred local damage but did not fail catastrophically. The curve labeled "failure threshold" is faired between those specimens which failed upon impact and those which did not. The failure threshold indicates that a sharply defined region of safe loading may exist for graphite/epoxy composite laminates. A similar behavior was noted in reference 21 although thicker laminates and different layups were evaluated for ballistic damage. The range of impact evaluated in the present investigation included energies well below the value required to initiate visible damage to energies that precipitated significant local surface damage. The lowest projectile kinetic energy at which surface fiber breakage can be detected visually is called the visible damage threshold and is noted in figure 14. The data indicate that impacts at energy levels well below the visible damage threshold can initiate catastrophic failure in loaded composite structures.

Some typical impact damage in graphite/epoxy sandwich structures is shown in figure 15. Damage is of a local nature and at penetration is about the same diameter as the projectile. The susceptibility of some graphite/epoxy to foreign object damage has been examined in references 19 and 22. The conclusions from these references are that the chief contributing factors to damage susceptibility appear to be the low longitudinal strain to failure of graphite/epoxy and the local crippling of the honeycomb beneath the point of impact.

The failure threshold for two laminate configurations in both tension and compression is shown in figure 16. All curves are based on experimental data such as that for the  $(0,90)_S$  tension test shown previously in figure 14. All failure threshold curves indicate similar trends and have strength reductions of 55 to 65 percent at the higher energy levels. The low impact resistance of compression stressed laminates was not anticipated because similar phenomena are not common in most structural type materials. Close examination of the failure surface indicates that the impact precipitates a transverse shear type of failure in the laminate, as shown in sketch (d).



Sketch (d)

The increase in impact resistance at the lower energy levels (0.1 to 0.2 J (1 to 2 in-lb)) demonstrated by the  $(90,\pm 45,0)_S$  laminate may be due more to the honeycomb substrate than to the number of plies or the layup configuration. The higher density aluminum core used in the 8-ply specimens has higher crippling properties and provides better local support in the region of impact than does the lower density Nomex core used on the 4-ply specimens.

Photographs which show typical impact initiated failures in tensile loaded test laminates are shown in figure 17. The  $(0,90)_S$  laminate (fig. 17(a)) is seen to fail with a well-defined crack while the failure in the  $(90,\pm 45,0)_S$  laminate is accompanied by a considerable amount of tearing and delamination.

#### Effect of Impact on Commercial Aircraft Design

An alternate way of looking at the data in order to better understand the implications on design is shown in figure 18 where the failure threshold curves based on strains for the test laminates are shown. In figure 18, the calculated stiffness for the given laminate was used to convert the load to strain. Also shown on the plot are the limit load and ultimate load strain levels which are representative of values found in commercial aircraft wing panels (see next section on design implications). Although impact causes considerable reductions in strength, as shown in figure 16, the severity of these reductions is best evaluated by the strain comparisons of figure 18. It should be pointed out that the ultimate and limit load strain levels indicated are for heavily loaded wing panels and that most other components on commercial aircraft would operate at much lower strain levels. Only a limited number of laminates have thus far been tested, and additional work in this area is necessary.

#### DESIGN IMPLICATIONS

In this section the design implications of constraints other than material strength or buckling are discussed. Attention is focused on the compression wing panels of contemporary medium-size commercial aircraft and specifically on

their redesign considering graphite/epoxy as the structural material. A few simple fundamental concepts are developed which provide a basis for understanding the design of composite substitution wings and lend insight, as well, into the design of advanced wing structures.

### Wing Panel Weight and Stiffness Comparisons

In a previous section, a comparison was made between the weight-strength characteristics of aluminum panels and graphite/epoxy panels designed for a compression load only (see fig. 5). In this section, compression panel data from contemporary commercial aircraft are included in the comparison. In figure 19 the theoretical minimum weight curves for hat-stiffened panels from figure 5 are shown. For simplicity the cusps on the graphite/epoxy curve of figure 5 are not included; this exclusion is equivalent to removing the constraint of incremental  $\pm 45^\circ$  ply thicknesses. Also shown in figure 19 are data for typical medium-size commercial aircraft aluminum wing panels. The lower values of the loading index  $N_x/L$  represent the lightly loaded outboard portion of the wing while the higher values of the loading index correspond to that portion of the wing near the fuselage interface. It can be seen that the commercial wing panel data are considerably higher than the theoretical minimum weight for aluminum in the low loading index range. These data approach the theoretical minimum weight in the high loading index range as the strength limit of the aluminum is approached. The main reasons for exceeding the theoretical minimum weight for the aluminum panels seem to be (1) added constraints for wing bending and torsional stiffnesses, (2) fatigue considerations, and (3) system or manufacturing constraints such as a requirement for constant stiffener spacing. In figure 20 the extensional and shear stiffnesses of both the commercial wing panels and graphite/epoxy panels are compared to assess the implications of using strength optimized panels in substitute wings. It can be seen on this logarithmic plot that the stiffnesses of the compression-load-designed graphite/epoxy panels are on the order of one-half to one-third of the stiffnesses of the aluminum wing panels. It should be noted that the stiffnesses of minimum weight aluminum panels designed for a compression load only would be very close to those shown for graphite/epoxy. Since the panel extensional and shearing stiffnesses translate directly into wing bending and torsional stiffnesses, it can be seen that a compression-load-designed minimum weight wing would be considerably more flexible than existing commercial aircraft wings.

A practical option for designing a substitution composite wing for an existing aircraft is to match bending and torsional stiffnesses of the wings. Such an option would minimize the effort required to requalify the aircraft aeroelastically and would minimize induced loads which are transmitted into the secondary structure of the leading and trailing edge. In figure 21 the results are shown for graphite/epoxy compression panels where their extensional and shearing stiffnesses are constrained to be the same as the values given for the commercial aircraft aluminum panels in figure 20. In addition, the practical constraint of a minimum 13-cm (5-in.) stiffener spacing, typical of the aluminum wing panels, was imposed. (The same data that were presented in fig. 19 are also presented in fig. 21 for comparison purposes.) It can be seen from figure 21 that the stiffness constraints result in a significant weight penalty

for the graphite/epoxy panels. In fact, the weight of the panels is doubled in the low loading index range. However, it is significant that even with the severe stiffness constraints, graphite/epoxy panels weigh only 50 percent as much as commercial aircraft compression panels.

During the design study, it was also observed that none of the stiffener elements were local buckling critical when the stiffness constraints were imposed on the hat-stiffened panels and that the constant 13-cm (5-in.) stiffener spacing could be obtained with no further weight increase. This suggests that simpler stiffeners could be used where stiffness is a severe design constraint and that manufacturing and cost considerations could well dictate the stiffener cross-sectional design. Subsequent studies indicated that simple blade stiffeners, such as those investigated in reference 23, would meet the buckling and stiffness requirements of the substitution composite wing, previously discussed, with no further weight penalty.

### Wing Strain Levels

In the substitution wing panel study presented in the previous section, the stiffnesses of the composite wing were constrained to be the same as the stiffnesses of the original aluminum wing. Matching stiffnesses (bending and torsional) at each station along the wing also result in the operational strain levels along the wing being the same. The compressive strain levels along the wing span are shown in figure 22 for medium-size commercial aircraft. (These strains correspond to the stiffness data shown in fig. 20.) Also shown for reference are the corresponding stresses in the aluminum wing. It can be seen that the maximum ultimate strain levels in the wing are between 0.005 and 0.006 at the wing root and drop to very low levels of about 0.0015 near the wing tip. Even with matched stiffness constraints, it is recalled that the graphite/epoxy wing panels are one-half of the weight of aluminum panels. Thus it is shown that graphite/epoxy can reduce the weight of existing commercial aircraft compression panels by about 50 percent without working the material past strain levels of 0.006.

A stress-strain curve is shown in figure 23 in which three different laminates of graphite/epoxy are compared with two common aluminum alloys. Although some composite laminates such as  $(\pm 45^\circ)_s$  shown in figure 23 have very large strains to failure ( $\approx 0.04$ ), laminates which have filaments in the direction of the major load (filament controlled laminates) have failure strains close to the failure strain ( $\approx 0.01$ ) of a  $0^\circ$  laminate. The  $(\pm 45^\circ, 0_4)_s$  laminate is shown as being representative of the laminates used in winglike panels. Also shown in figure 23 is a band which represents the maximum strain levels at ultimate load for present commercial aircraft. Failure data for damaged structures such as that presented in figure 18 for impact suggest that a maximum allowable working strain level for composite materials must be established and that the allowable strain level will be close to that which exists in present commercial aircraft. It seems reasonable that some conservative strain design criteria should be established for initial primary structural designs for applications to commercial aircraft. This allowable level of strain could gradually be increased with the introduction of design improvements such as softening strips and with



an accumulation of design and flight experience on composite components in much the same fashion as the accumulation of design and flight experience with commercial aircraft has permitted the introduction of better aluminum alloys over the years.

Also shown in figure 23 are the maximum strain levels in the DC-10 rudder and the L-1011 fin, both of which are being redesigned with composites as part of the LaRC flight service program. The rudder and the fin both are stiffness designed, and this is reflected in their low operational strain levels. If other advanced composite flight components were added to this chart, a much clearer picture of the level-of-loading experience being obtained on the various flight programs would result.

#### CONCLUDING REMARKS

One of the main goals of LaRC efforts on composite design technology has been to establish standards against which the performance of structural components can be measured. In this paper, structural efficiency charts are presented for compression panels and shear webs which permit a ready comparison of various structural concepts. These charts show that stiffened panels made of graphite/epoxy offer a 50-percent weight savings when compared with comparably designed aluminum panels. The redesign of aluminum compression panels for commercial aircraft wings using graphite/epoxy material is studied. The results showed that structural stiffness is a controlling design condition which overrides material strength and buckling requirements. Maximum strain levels at ultimate load were found to be less than 0.006 when the stiffnesses of the redesigned graphite/epoxy wing were constrained to be the same as the original aluminum wing. The relatively low operation strain levels suggest that simple wing panels can be used and that manufacturing and cost considerations could well dictate panel cross-sectional design. The substitution graphite/epoxy panels were about 50 percent lighter than the original aluminum panels even with the severe stiffness constraint. The maximum strain levels for three commercial aircraft structural components are compared, and it is suggested that such maximum strain levels be used to identify the level-of-loading experience being obtained on various flight service programs.

A review is given of the stability analyses and design procedures used to conduct and support the structural efficiency studies. Also presented are sample results of an experimental program being conducted to determine the impact behavior of graphite/epoxy laminates. Results of the impact studies are presented on both a failure strength and failure strain basis. The evaluation of the impact behavior of laminates on the basis of failure strain permits a direct comparison to be made with the maximum strain levels expected in various structural components. In fact, it seems that the use of maximum expected strain levels should provide a convenient guide for all structural integrity evaluations.

#### REFERENCES

1. Viswanathan, A. V.; and Tamekuni, M.: Elastic Buckling Analysis for Composite Stiffened Panels and Other Structures Subjected to Biaxial Inplane Loads. NASA CR-2218, 1973.
2. Wittrick, W. H.; and Williams, F. W.: Buckling and Vibration of Anisotropic or Isotropic Plate Assemblies Under Combined Loadings. Int. J. Mech. Sci., vol. 16, no. 4, Apr. 1974, pp. 209-259.
3. Bushnell, David: Stress, Stability, and Vibration of Complex Branched Shells of Revolution: Analysis and User's Manual for BOSØR4. NASA CR-2116, 1972.
4. Cohen, Gerald A.: Computer Analysis of Ring-Stiffened Shells of Revolution. NASA CR-2085, 1973.
5. Viswanathan, A. V.; Tamekuni, M.; and Baker, L. L.: Elastic Stability of Laminated, Flat and Curved, Long Rectangular Plates Subjected to Combined Inplane Loads. NASA CR-2330, 1973.
6. Housner, Jerrold M.; and Stein, Manuel: Numerical Analysis and Parametric Studies of the Buckling of Composite Orthotropic Compression and Shear Panels. NASA TN D-7996, 1975.
7. MacNeal, Richard H., ed.: The NASTRAN Theoretical Manual (Level 15). NASA SP-221(01), 1972.
8. Whetstone, W. D.: SPAR Reference Manual. NASA CR-120504, 1974.
9. Almroth, B. O.; Brogan, F. A.; Meller, E.; Zele, F.; and Petersen, H. T.: Collapse Analysis for Shells of General Shape. Volume II - User's Manual for the STAGS-A Computer Code. AFFDL-TR-71-8, U.S. Air Force, Mar. 1973. (Available from DDC as AD 762 543.)
10. Williams, Jerry G.; and Mikulas, Martin M., Jr.: Analytical and Experimental Study of Structurally Efficient Composite Hat-Stiffened Panels Loaded in Axial Compression. AIAA Paper No. 75-754, May 1975.
11. Stein, Manuel; and Starnes, James H., Jr.: Numerical Analysis of Stiffened Shear Webs in the Postbuckling Range. Numerical Solution of Nonlinear Structural Problems, R. F. Hartung, ed., ASME AMD-Vol.6, American Soc. Mech. Eng., c.1973, pp. 211-223.
12. Shanley, F. R.: Weight-Strength Analysis of Aircraft Structures. Second ed., Dover Publ., Inc., c.1960.
13. Agarwal, Banarsi; and Davis, Randall C.: Minimum-Weight Designs for Hat-Stiffened Composite Panels Under Uniaxial Compression. NASA TN D-7779, 1974.

14. Schmit, Lucien A., Jr.; and Muira, Hirokazu: Approximation Concepts for Efficient Structural Synthesis. NASA CR-2552, 1976.
15. Schuette, Evan H.; and Roy, J. Albert: The Determination of Effective Column Length From Strain Measurements. NACA WR L-198, 1944. (Formerly NACA ARR L4F24.)
16. Bush, Harold G.: Experimental Evaluation of Two 36" x 47" Graphite/Epoxy Sandwich Shear Webs. NASA TM X-72767, 1975.
17. Laakso, J. H.; and Straayer, J. W.: Evaluation of a Metal Shear Web Selectively Reinforced With Filamentary Composites for Space Shuttle Application. NASA CR-2409, 1974.
18. Gerard, George; and Becker, Herbert: Handbook of Structural Stability. Part VII - Strength of Thin-Wing Construction. NASA TN D-162, 1959.
19. Rhodes, Marvin D.: Low Velocity Impact on Composite Sandwich Structures. Proceedings of the Second Conference on Fibrous Composites in Flight Vehicle Design, AFFDL-TR-74-103, U.S. Air Force, Sept. 1974, pp. 275-298.
20. Rhodes, Marvin D.: Impact Fracture of Composite Sandwich Structures. AIAA Paper 75-748, May 1975.
21. Olster, E. F.; and Roy, P. A.: Tolerance of Advanced Composites to Ballistic Damage. Composite Materials: Testing and Design (Third Conference), ASTM Spec. Tech. Publ. 546, 1974, pp. 583-603.
22. Slepetz, John M.; Oplinger, Donald W.; Parker, Burton S.; and Tremblay, Robert T.: Impact Damage Tolerance of Graphite/Epoxy Sandwich Panels. AMMRC TR 74-20, U.S. Army, Sept. 1974.
23. Spier, E. E.: Crippling/Column Buckling Analysis and Test of Graphite/Epoxy-Stiffened Panels. AIAA Paper 75-753, May 1975.

TABLE I.- COMPUTER CODES FOR THE BUCKLING OF COMPOSITE PANELS

PROGRAM	SOLUTION PROCEDURE	ONE OR TWO DIMENSIONAL	COMPRESSION OR SHEAR*	BRANCHES AND MULTIPLE ELEMENTS	FLAT OR CURVED ELEMENTS	ANISOTROPIC OR ORTHOTROPIC	BENDING-EXTENSION COUPLING	REFERENCE
BUCLASP2**	EXACT	1	C	✓	C	0	✓	1
VIPASA	EXACT	1	C,S	✓	F	A	-	2
BOSOR4**	FINITE DIFF. SHELL OF REV.	1	C	✓	C	0	✓	3
SRA	NUM. INTEG. SHELL OF REV.	1	C,S	✓	C	0	✓	4
BUCLAP2**	EXACT	1	C,S	-	C	A	✓	5
BOP	TRIG. FINITE DIFF.	2	C,S	-	F	0	-	6
NASTRAN**	FINITE ELEMENT	2	C,S	✓	F	A	-	7
SPAR	FINITE ELEMENT	2	C,S	✓	F	A	-	8
STAGS**	FINITE DIFF.	2	C,S	✓	C	A	✓	9

\* FOR 1-D PROGRAMS. SHEAR LOADING OR ANISOTROPIC PROPERTIES IMPLIES AN INFINITELY LONG PANEL

\*\* AVAILABLE THROUGH COSMIC-COMPUTER SOFTWARE MANAGEMENT AND INFORMATION CENTER,  
UNIVERSITY OF GEORGIA, ATHENS, GEORGIA

SYNTHESIS PROCEDURES

- POP- I — SIMPLE CLOSED FORM BUCKLING SOLUTIONS USED TO REPRESENT PANEL BUCKLING BEHAVIOR
- POP- I — TYPICAL DESIGN TIME - 25 seconds
- POP- II — EXACT EIGENVALUE SOLUTION TECHNIQUE USED TO DETERMINE PANEL BUCKLING BEHAVIOR
- POP- II — TYPICAL DESIGN TIME - 100 TO 300 seconds

CROSS SECTIONS CONSIDERED



LOADINGS AND CONSTRAINTS FOR BOTH POP- I AND POP- II

- COMPRESSION AND SHEAR LOADINGS
- MATERIAL STRENGTH CONSTRAINTS
- AXIAL AND SHEAR STIFFNESS CONSTRAINTS
- MINIMUM GAGE CONSTRAINTS
- STIFFENER SPACING CONSTRAINTS

Figure 1.- Features of panel optimization design procedures (PDP) used at LaRC.

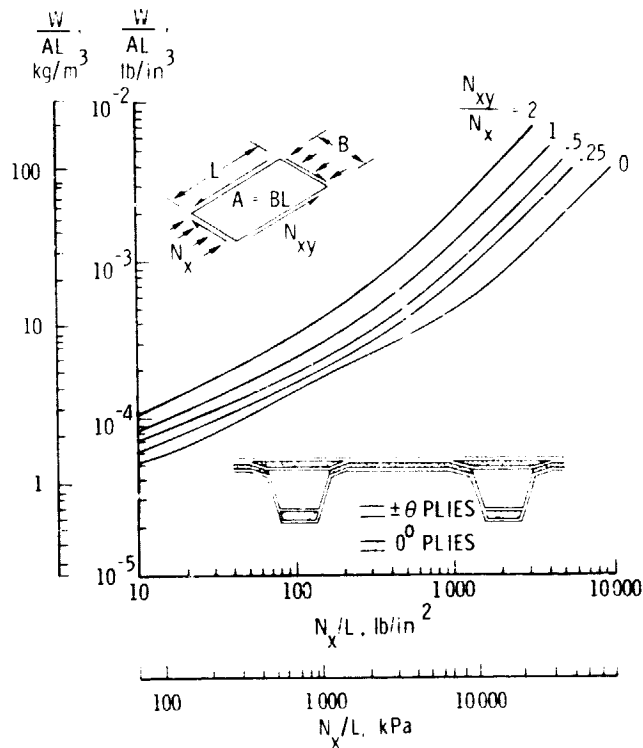


Figure 2.- Weight-strength chart for graphite/epoxy panels under combined loads.

REPRODUCIBILITY OF THIS ORIGINAL PAGE IS POOR

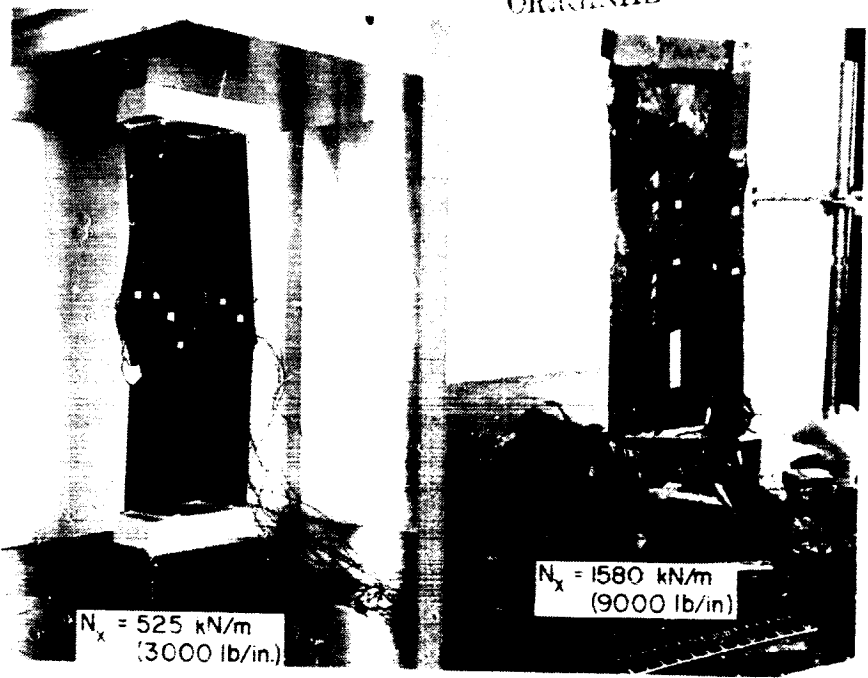


Figure 3.- Typical failures observed on 41-cm (16-in.) local buckling specimens.

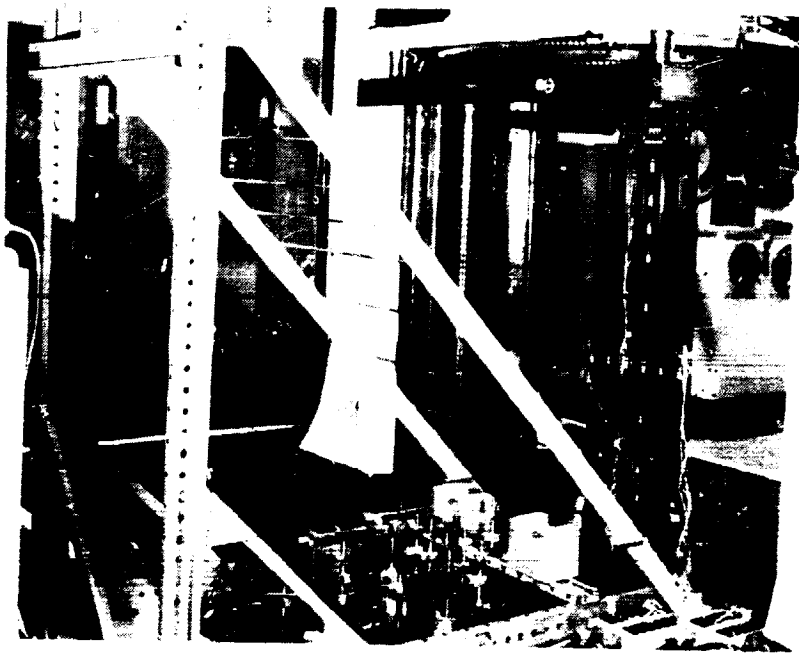


Figure 4.- Graphite or xy pencil 3.0 cm long in compression test machine.

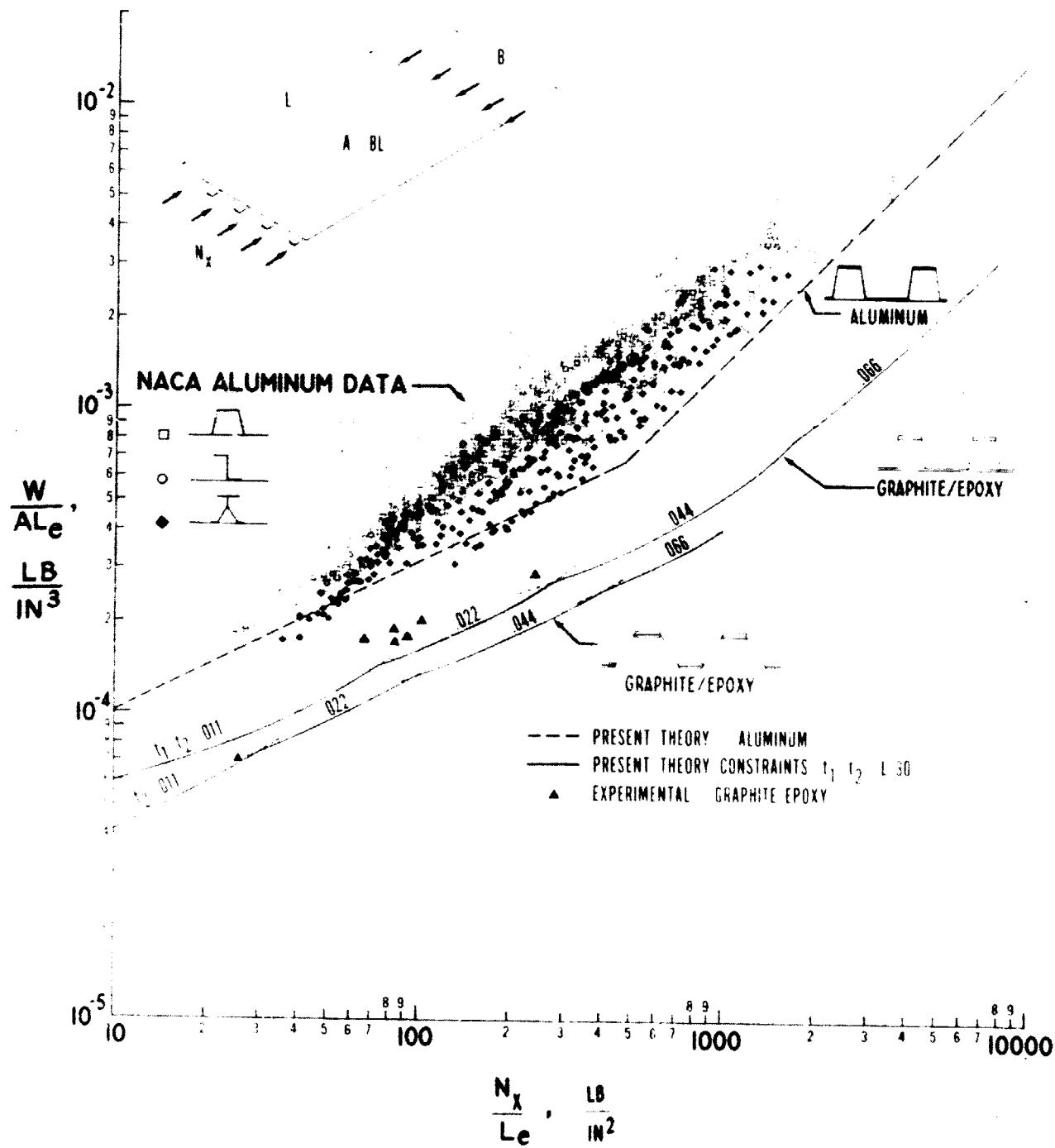


Figure 5.- Structural efficiency comparison of graphite/epoxy and aluminum compression panels. (1 lb./in<sup>3</sup> = 27.680 kg m<sup>-3</sup>, 1 lb./in<sup>2</sup> = 6.89 kPa.)

ORIGINAL PAGE IS  
OF POOR QUALITY

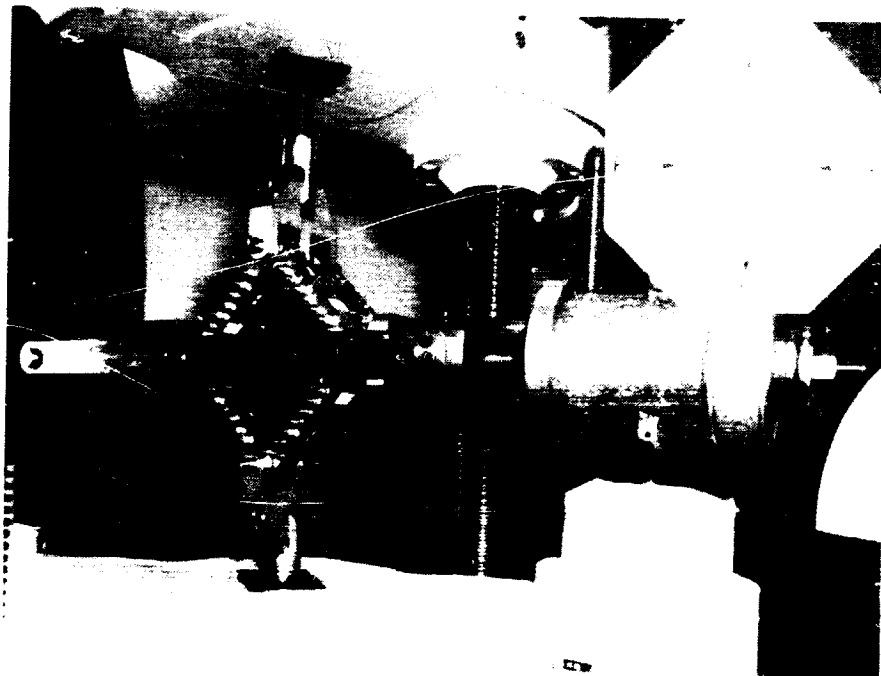


Figure 6.- Biaxially loaded picture-frame testing fixture.

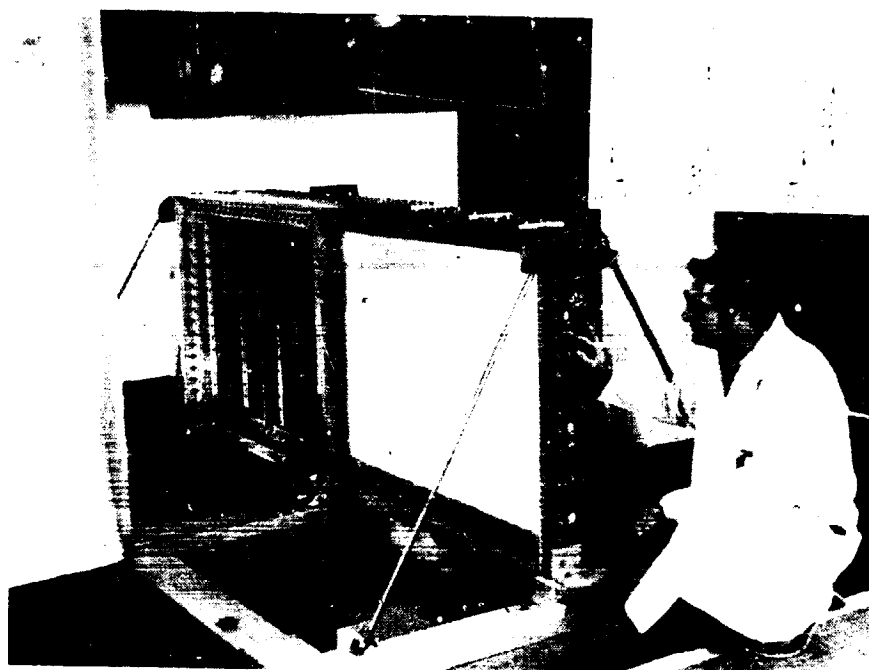


Figure 7.- Biaxially loaded picture-frame testing fixture.



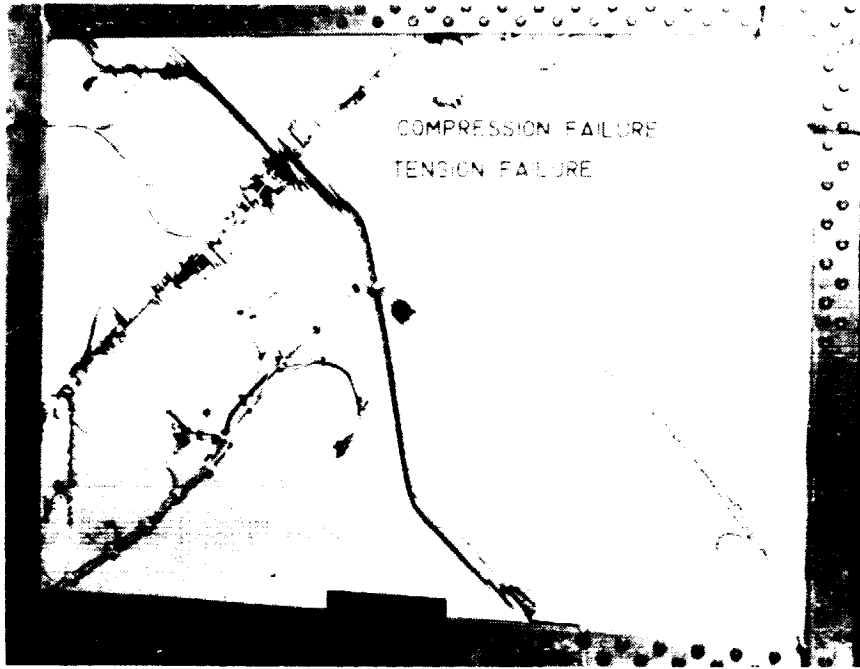


Figure 3.- Failure observed in a graphite-epoxy specimen under shear which was materially stronger in tension.

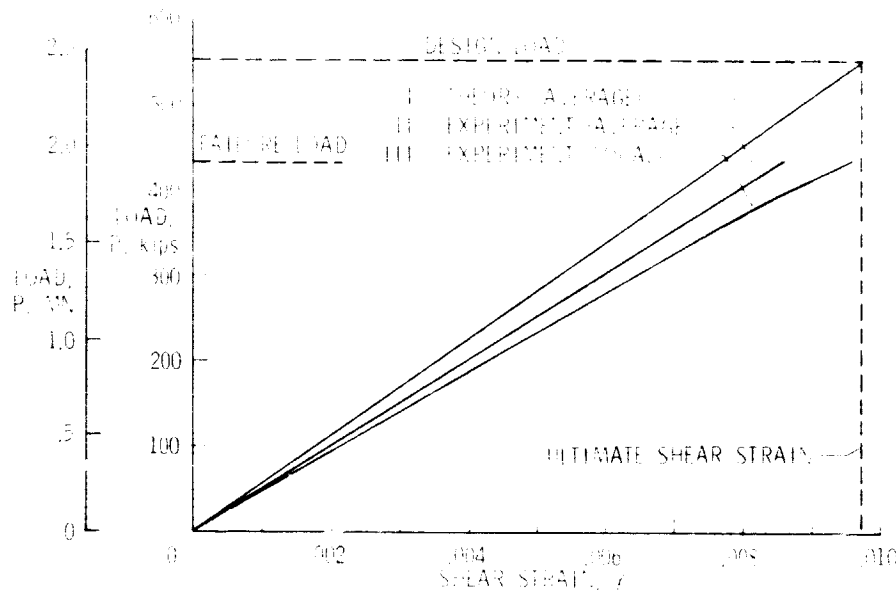


Figure 4.- Graphical method of determining ultimate shear strength.

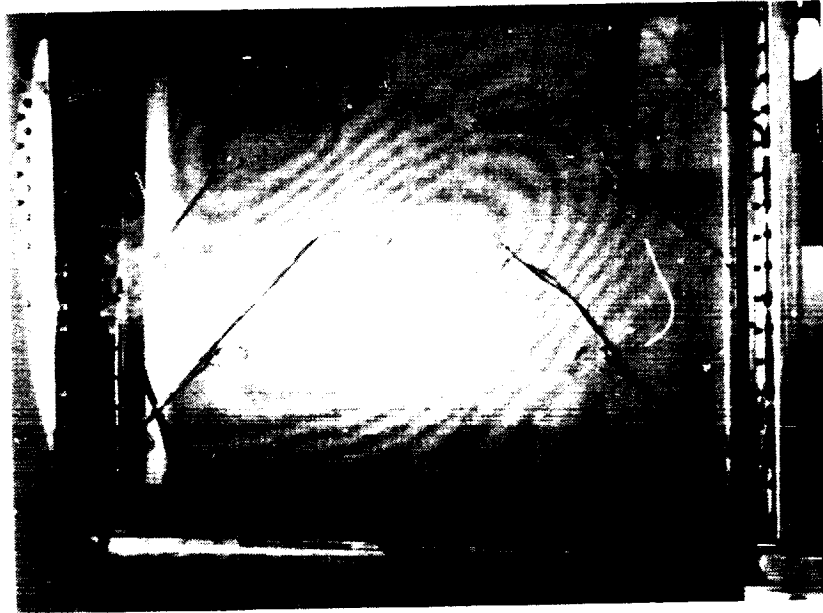


Figure 10.- Buckling pattern observed in a graphite/epoxy sandwich shear web which was stability critical (P = 1.1 MN or 25 kips).

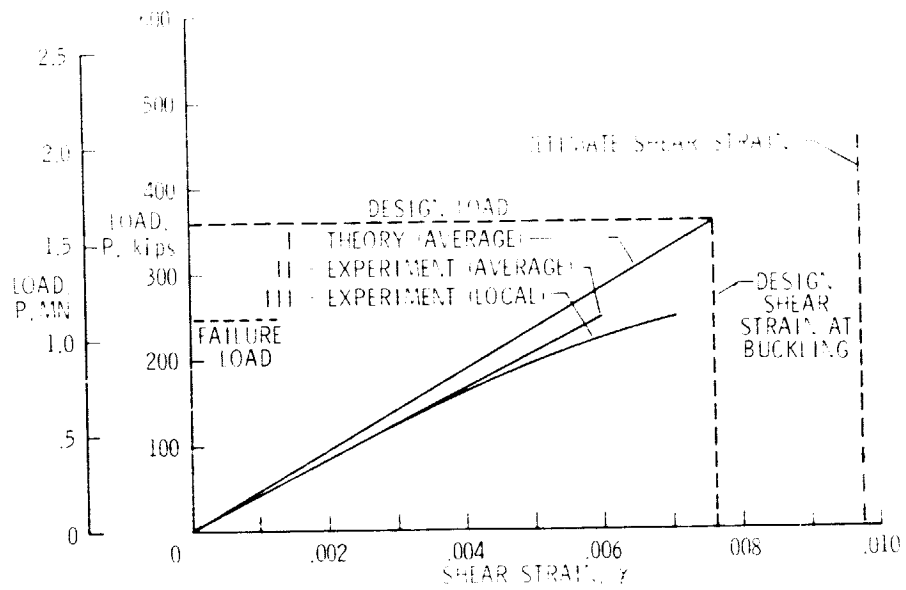


Figure 11.- Stability critical shear web I in-strain response.

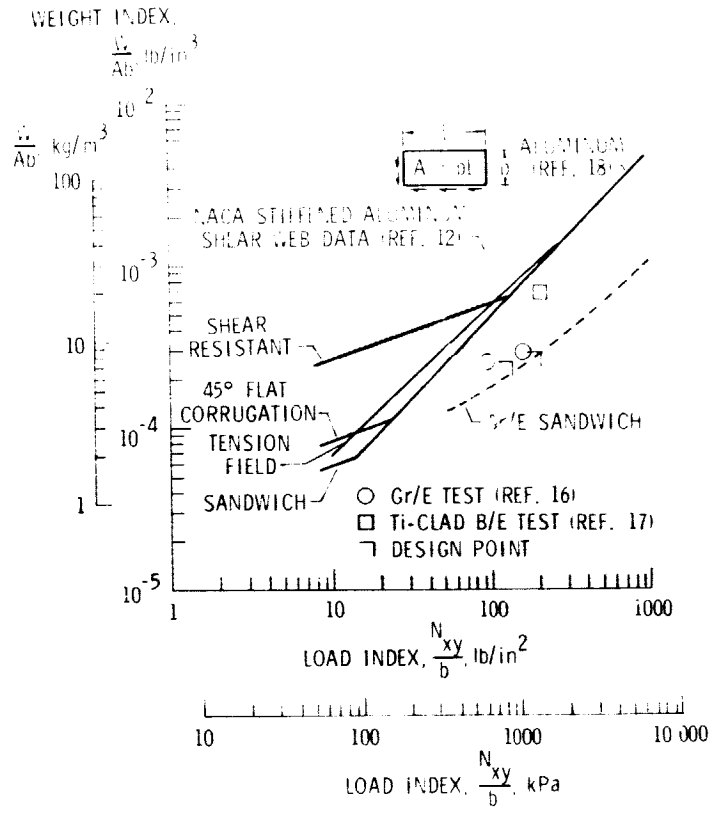


Figure 12.- Structural efficiency comparison of graphite/epoxy and aluminum shear webs.

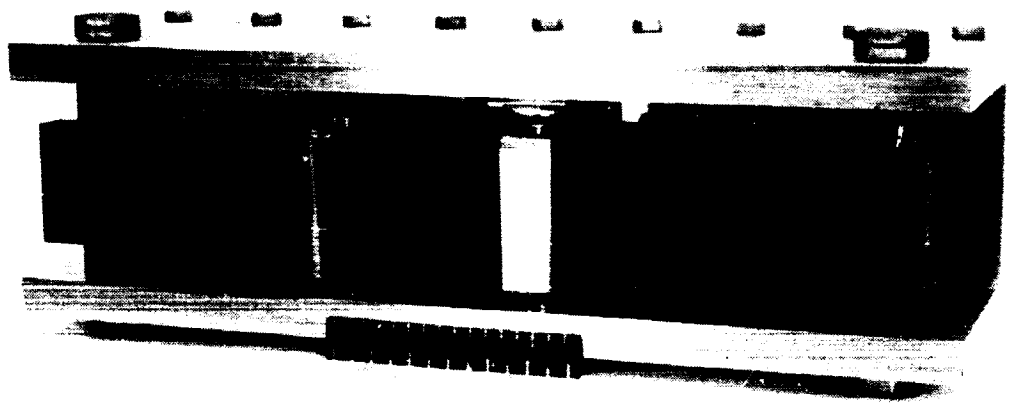


Figure 13.- Four-point loading frame for sandwich-beam impact specimens.

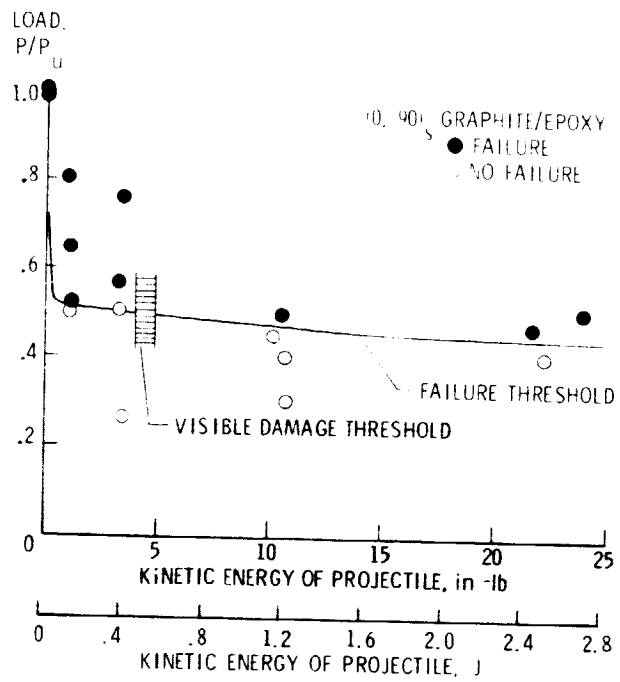


Figure 14.- Impact initiated failure in tensile stressed graphite/epoxy sandwich beams.

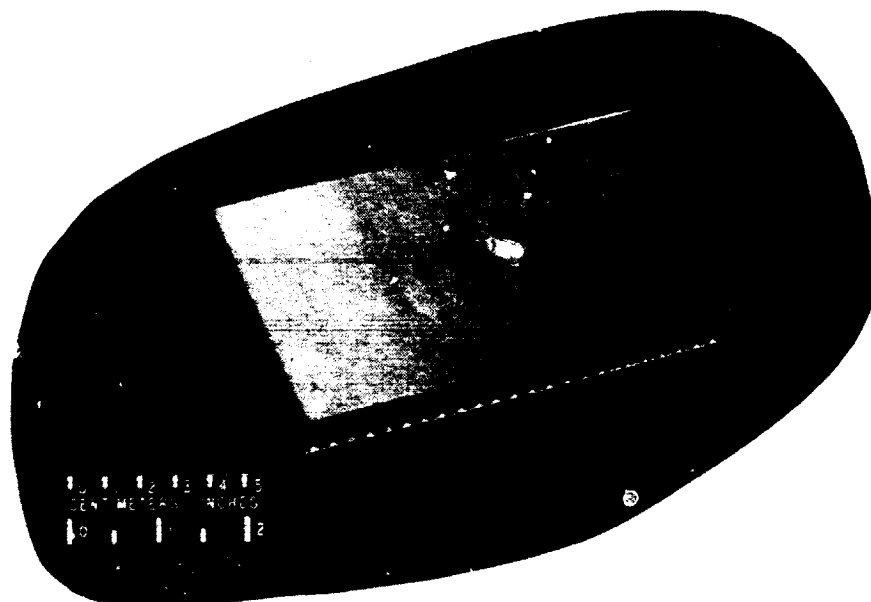


Figure 15.- Local damage in a crossplied 4-ply laminate.

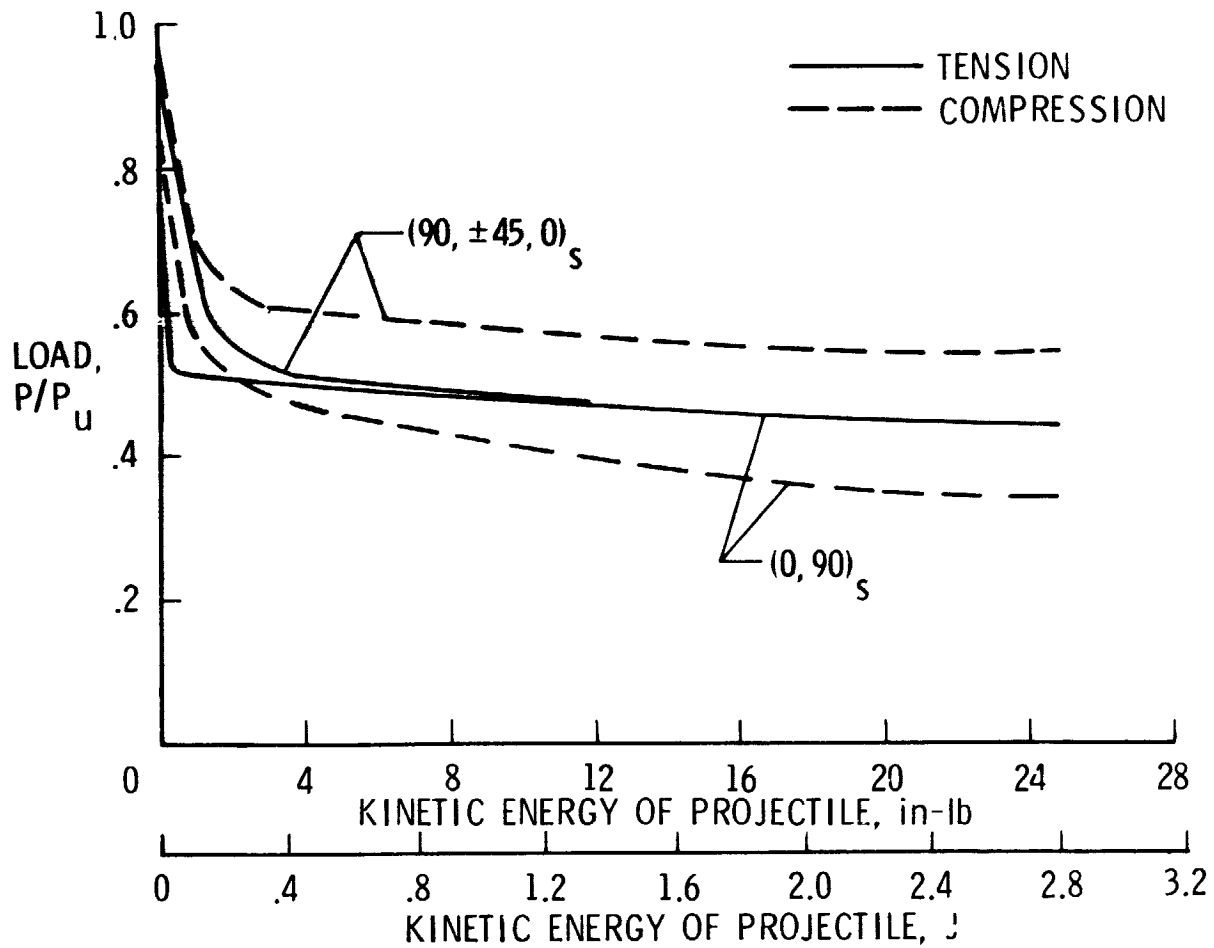
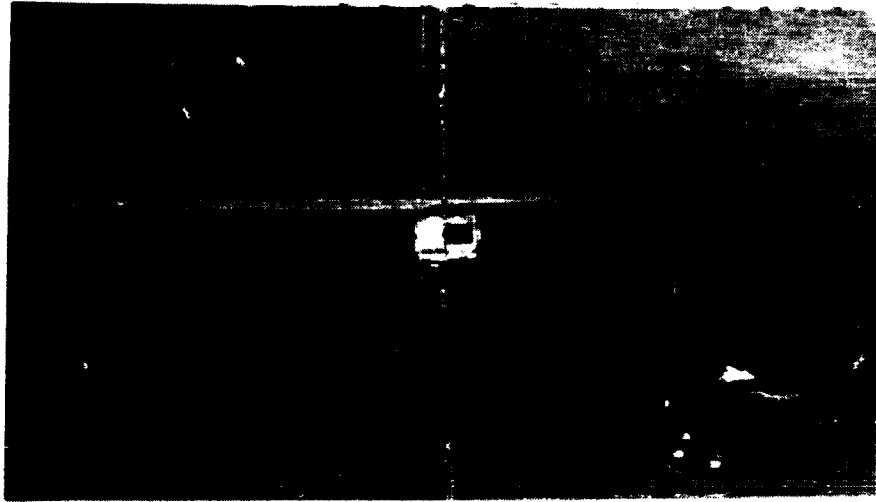
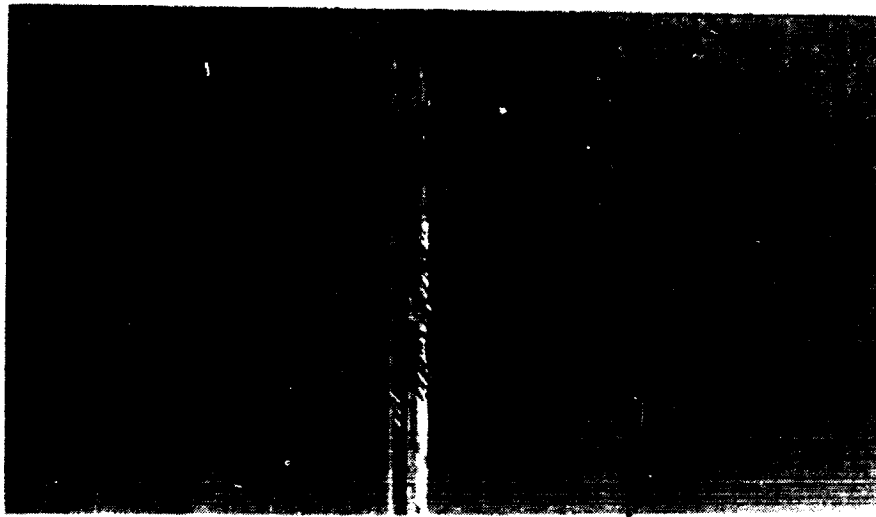


Figure 16.- Failure threshold curves for graphite/epoxy sandwich test laminates.



(a) 10,000 lb.



(b) 10,000 lb.

ORIGINAL PAGE IS  
OF POOR QUALITY

Figure 11.- Typical impact induced failure.

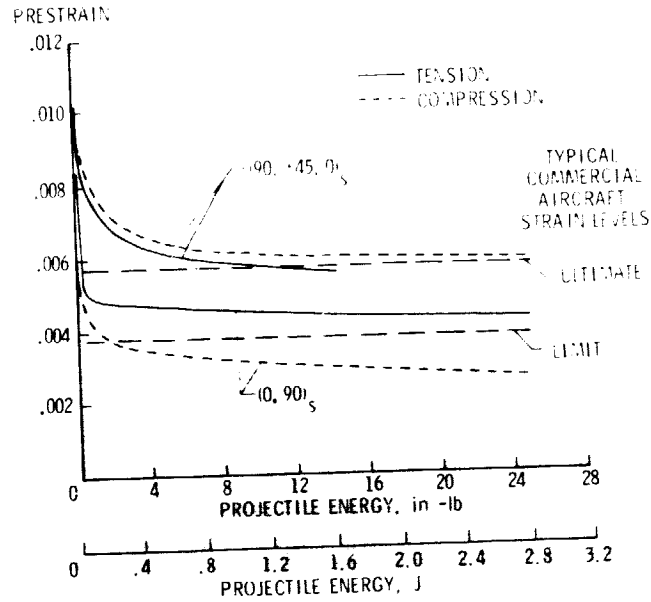


Figure 18.- Failure strains in prestressed graphite/epoxy laminates subjected to impact.

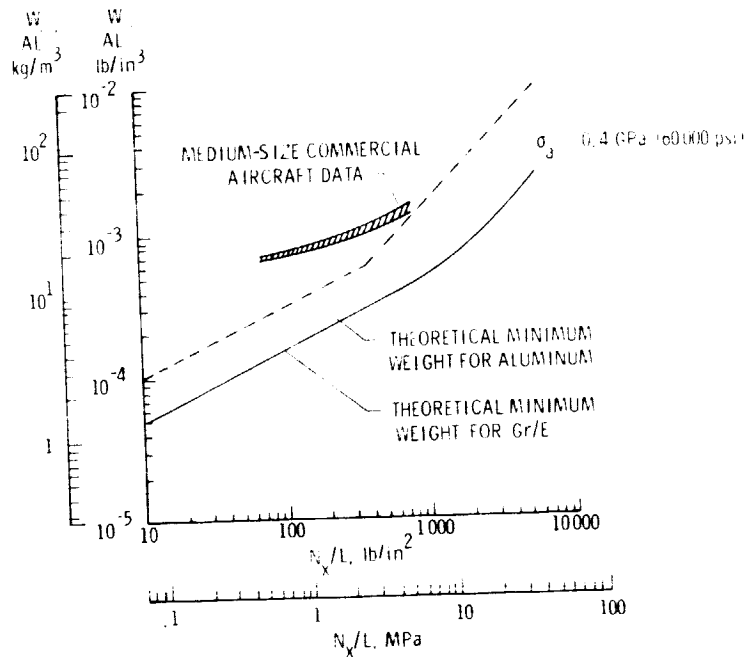


Figure 19.- Weight-strength characteristics of medium-size commercial aircraft aluminum wing panels, strength-optimized aluminum panels, and strength-optimized graphite/epoxy (Gr/E) panels.

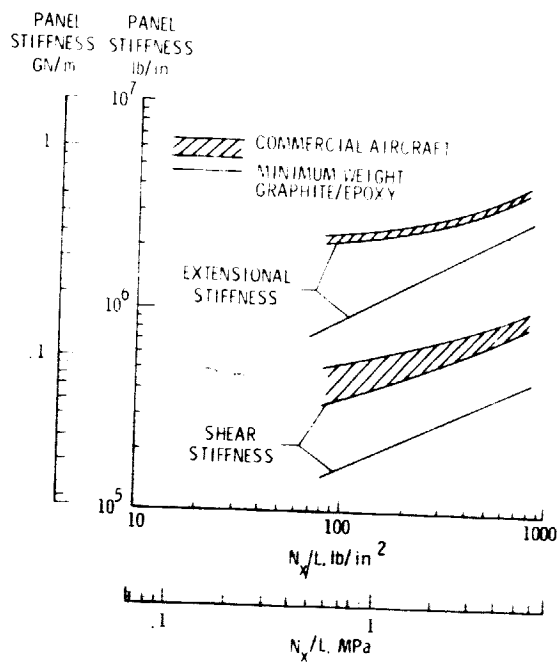


Figure 20.- Extensional and shear stiffness characteristics of commercial aircraft aluminum wing panels and strength-optimized graphite/epoxy panels.

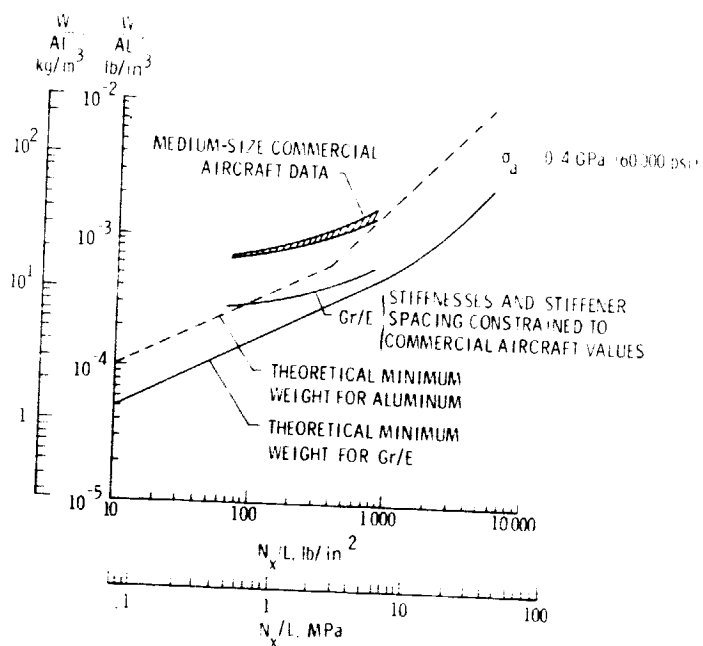


Figure 21.- Effects of extensional and shear stiffness constraints on the weight of graphite/epoxy panels.



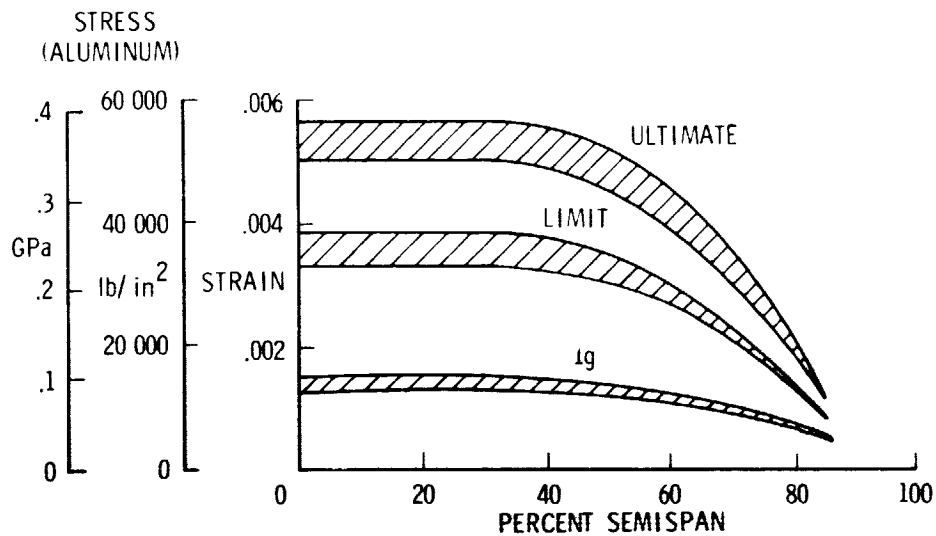


Figure 22.- Compressive strains and stresses in typical medium-size commercial aircraft wings.

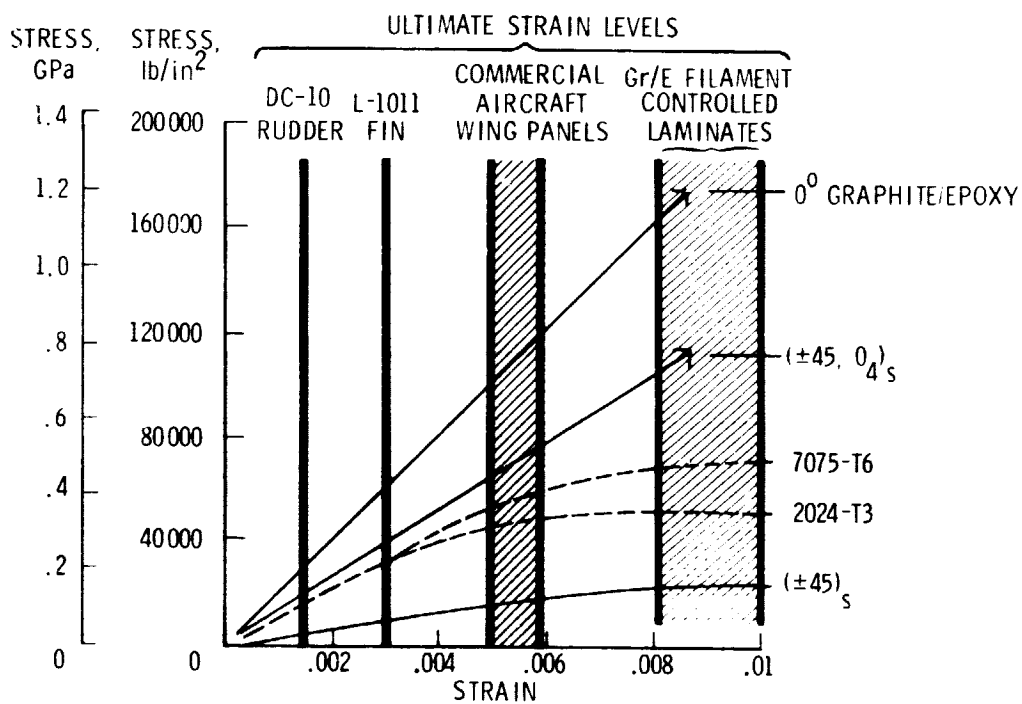


Figure 23.- Typical compressive stress-strain curves for aluminum and graphite/epoxy materials with the maximum strain levels at ultimate load shown for several structures.

ADVANCED COMPOSITE TORQUE  
BOX OPTIMIZATION

Donald Y. Konishi, George Hayase, Jonas Surdenas  
Rockwell International Corporation

ABSTRACT

The Advanced Composite Torque Box Optimization Program (ACTBOP) is a structural optimization program capable of rapidly evaluating the weight/cost merits of torque boxes constructed with advanced composite materials. It was developed as a part of the wing and empennage module of the Structural Weight Estimation Program (SWEEP).

The torque box model in ACTBOP consists of a box composed of upper and lower covers, front and rear spars, root and tip ribs, and internal support spars and ribs as required. Box shear, moment, and torsional degrees of freedom are considered in the optimization.

Three types of construction can be analyzed: multispar with conventional or honeycomb sandwich covers, multirib with skin/stringer covers, and full depth honeycomb sandwich. The substructure, spars/ribs, can be circular corrugation or honeycomb sandwich panels.

INTRODUCTION

ACTBOP is a computer program written to ease the task of preliminary advanced design composite wing box. It is capable of rapidly sizing and evaluating the relative weight merits of various structural wing boxes composed of advanced composite materials. Approximately one day is required for input data setup. The usual run times on an IBM 370 computer are approximately one minute. The algorithm has also been incorporated into Rockwell Los Angeles Aircraft Division's Structural Weight Estimation Program (SWEEP) (ASD/XR-74-10) developed under Air Force contract F33615-71-C-1922.

The ACTBOP advanced composite analysis is designed to determine structural requirements of torque boxes with all cover and supporting structures fabricated from laminated layers of filamentary fibers. The prediction procedure determines the necessary number and orientation of fiber layers to provide the

PRECEDING PAGE BLANK NOT FILMED

strength, stability, and stiffness characteristics required for each element of the box. Assumptions are made to adapt detail analysis procedures to the quick-response, preliminary nature of the synthesis procedures. Equations used to evaluate the behavior of laminated webs under load are based on existing detail filamentary analysis equations. Where possible, similarity to the metallic structure analysis is maintained; structural idealization assumptions and scope of the synthesis/weight analysis procedures are similar.

## WING DEFINITION

### General Behavior of Composite Laminates

All advanced composite laminates considered in ACTBOP are assumed to consist only of laminae with  $0^\circ$ ,  $\pm 45^\circ$ , or  $90^\circ$  orientations. The relative ply directions for each structural wing box element are defined in Figure 1. Plies oriented at 0 degree (longitudinal) are strongest in the axial direction, while the  $\pm 45$ -degree plies are best at resisting shear. 90-degree plies are added to keep the laminate balanced. Although the order in which these laminae are laid up has a bearing on the properties of the laminate, a particular layup sequence is not implied in the sizing results; i.e., computations are based on an equivalent number of plies in a homogeneous (as opposed to layered) laminate. The laminate layups must, however, be balanced (the number of  $+45^\circ$  and  $-45^\circ$  plies must be equal) and symmetric about its middle surface. The laminate configurations used in ACTBOP are then

$$\left[ 0^{\circ}_l / \pm 45^{\circ}_m / 90^{\circ}_n \right]_s$$

where  $l$  = number of 0-degree plies,  $m$  = number of  $\pm 45$ -degree sets, and  $n$  = number of 90-degree plies in half of the laminate.

The stress-strain relationships used in ACTBOP are derived from classical lamination theory. Only a summary of these is presented here. Further information is available in the "Advanced Composite Design Guide; Volume III."

An orthotropic composite material is characterized by its elastic constants  $E_L$ ,  $E_T$ ,  $G_{LT}$ , and  $\nu_{LT}$ , and the allowable stresses  $F_0^{tu}$ ,  $F_0^{cu}$ , and  $F_{45}^{su}$ . Further, the physical constants  $\rho$  and  $t_L$  are necessary. The stress-strain relationship for a symmetric balanced composite laminate is expressed by

$$\begin{bmatrix} N_x \\ N_y \\ N_{xy} \end{bmatrix} = \begin{bmatrix} A_{11} & A_{12} & 0 \\ A_{12} & A_{22} & 0 \\ 0 & 0 & A_{66} \end{bmatrix} \begin{bmatrix} \epsilon_x \\ \epsilon_y \\ \epsilon_{xy} \end{bmatrix}$$

where  $A$  is the extensional stiffness matrix of the laminate and is defined by

$$A_{ij} = \sum_{k=1}^{NL} t_k Q_{ij}^{(k)} \quad i, j = 1, 2, 6.$$

NL is the number of plies in the laminate,  $t$  is the thickness of each lamina and  $Q$  is the matrix of elastic constants for each corresponding ply.

For the  $[0_t / \pm 45_m^o / 90_n^o]_s$  laminate family the A-matrix can be simplified by noting that

$$Q_{11}^0 = \frac{E_L}{(1 - \nu_{LT}\nu_{TL})} = Q_{22}^{90}$$

$$Q_{22}^0 = \frac{E_T}{(1 - \nu_{LT}\nu_{TL})} = Q_{11}^{90}$$

$$Q_{12}^0 = \nu_{LT} Q_{22}^0 = \nu_{TL} Q_{11}^0 = Q_{12}^{90}$$

$$Q_{66}^0 = G_{LT} = Q_{66}^{90}$$

$$Q_{11}^{45} = Q_{22}^{45} = 0.25 [Q_{11}^0 + Q_{22}^0 + 2(Q_{12}^0 + 2G_{LT}^0)]$$

$$Q_{12}^{45} = 0.25 (Q_{11}^0 + Q_{22}^0 - 4G_{LT}^0 + 2Q_{12}^0)$$

$$Q_{66}^{45} = 0.25 (Q_{11}^0 + Q_{22}^0 - 2Q_{12}^0)$$

At times, it is necessary to calculate the gross elastic properties of a laminate,  $E_x$  and  $G_{xy}$ . The equations used are

$$E_x = \frac{2t_L}{t} \left[ \frac{(l Q_{11}^0 + 2m Q_{11}^{45} + n Q_{11}^{90}) - \frac{[(l+n) Q_{12}^0 + 2m Q_{12}^{45}]^2}{[l Q_{11}^{90} + 2m Q_{11}^{45} + n Q_{11}^0]}}{2} \right]^2$$

and

$$G_{xy} = \frac{2t_L}{t} \left[ \frac{m}{2} (Q_{11}^0 + Q_{11}^{90} - 2Q_{12}^0) + (l+n) G_{LT} \right]$$

where  $t$  is the laminate thickness.

All engineering materials are subject to changes in properties at elevated temperatures. To account for these changes, all necessary material constants are computed in ACTBOP as a function of the design temperature for each set of design loads. Straight-line interpolation of the properties between predetermined control temperature points is used.

#### Wing Box Geometry

The wing box is modeled in ACTBOP as a long slender beam composed of covers and supporting spars and ribs. This wing is divided into 10 discrete spanwise segments by 11 stations (Figure 2). Geometry is defined at each station prescribing the axis of analysis location and physical section dimensions - width, average box depth, and depths of front and rear spars (Figure 3).

Torque-box construction types that can be analyzed by ACTBOP include:

1. Multispar plate cover designs
2. Multirib stringer-stiffened cover designs
3. Full-depth honeycomb sandwich designs

Spar and rib support structures are idealized as sheet web plus cap systems; the webs for these structures can be designed as either corrugated webs or honeycomb panels. Spars may be either advanced composite circular corrugated spars or honeycomb sandwich spars. The circular corrugation is assumed to have a  $60^\circ$  corrugation angle and a prescribed corrugation radius. The skin may be either flat advanced composite panels or honeycomb sandwich panels. In all cases, honeycomb sandwich members are designed with the input core properties. Each face sheet is assumed to have the same configuration and to be half the thickness of a flat advanced composite panel.

The cover and support structures are assumed to be mechanically fastened at cover-to-spar/rib joints to provide an integrated torque-box structure. Face sheets for full-depth honeycomb sandwich boxes are considered to be bonded to the supporting core material. Cover laminae are assumed to be rearranged locally along attachment lines to include filler material, replacing relocated 0-degree lamina, for attachment hole drilling. Lightning protection material (aluminum flame spray) is applied to all exterior surfaces and sealer films to all interior surfaces.

For the multirib type of wing box construction, different stringer concepts can be specified for the upper and lower covers. However, the spacings or number of elements in each cover will remain the same. Stringer areas consist of only 0-degree longitudinal plies. The permissible types of stiffeners are shown in Figure 4.

## STRUCTURAL ELEMENT SIZING

### Assumptions

At each of the 11 structural analysis stations, torque-box material requirements are synthesized for the five major elements - upper cover; lower cover; front spar; rear spar; and intermediate spars, ribs, or honeycomb core. The covers and spar caps are sized to withstand the spanwise bending moment,  $M$ . Spar webs are designed to resist the vertical shear load,  $V$ . The torsional moment,  $T$ , is resolved into shear loads resisted by the upper and lower covers and the front and rear spar webs.

In general, the synthesis procedures are similar to that used for metallic designs. The following summarizes the major differences:

1. Only longitudinal fibers (0-degree plies) resist axial loads, and cross ply fibers ( $\pm 45$ -degree plies) resist shear loads.

2. All plies contribute to laminate panel stability.
3. Skin material requirements are analyzed for axial loads and panel stability requirements due to combined effects of inplane axial and shear loads.
4. Skin and spar webs are designed to resist torque shear loads. Intermediate spar webs are assumed to react part of the vertical shear loads.
5. Laminates are synthesized with integer number of laminae. For honeycomb panels, laminate plies are assumed to be equally divided between the inner and outer face sheets.
6. Addition of  $\pm 45$ -degree plies only are made to increase stiffness levels of panels with inadequate stability stress allowables.
7. Addition of  $\pm 45$ -degree plies only are made to torque-box webs to increase section stiffness to levels required to satisfy torsional stiffness requirements.
8. Additional plies oriented at  $90^\circ$  are added to carry any transverse inplane loads. These are chosen as a percentage of  $0^\circ$  and  $\pm 45^\circ$  plies.

#### Design Loads and Constraints

Section design loads in ACTBOP are defined in terms of shear ( $V$ ), bending moment ( $M$ ) and torque ( $T$ ) at each of the 11 wing analysis stations for up to 20 different loading conditions (Figure 5). Corresponding structural design temperatures are also specified. Section torsional stiffness required to prevent flutter can be prescribed.

Design constraints dictated by manufacturing requirements can also be input into ACTBOP. Among these are maximum and minimum number of spars or maximum and minimum spar/rib spacing and the minimum value for  $0^\circ$  and  $\pm 45^\circ$  plies in any laminate. To account for unrealistic sizings of the front and rear spars, a factor is provided for the value of the shear load on these spars.

Bending loads are resolved into axial load intensities,  $N_x$ , for cover design. In addition, shear loads,  $N_{xy}$ , are computed for skin and spar designs. The skin loads are computed using the following equations.

$$N_{x,u} = \frac{M}{H(W + C_4 N_{SPAR})}$$

where  $C_4$  is the equivalent width of skin in the spar caps

$$N_{x,L} = -N_{x,u}$$

$$N_{xy,uL} = \frac{T}{2HW}$$

where H and W are the depth and width of the wing box.

For the front spar (FS), intermediate spar (IS) and rear spar (RS):

$$N_{xy,IS} = \frac{V}{H \cdot N_{SPAR}}$$

$$N_{xy,FS} = C_1 \left( \frac{V}{H \cdot N_{SPAR}} + \frac{T}{2HW} \right)$$

$$N_{xy,RS} = C_2 \left( \frac{V}{H \cdot N_{SPAR}} - \frac{T}{2HW} \right)$$

where  $C_1$  and  $C_2$  are front and rear spar load magnification factors. The term  $T/2HW$  is included only if it increases the magnitude of  $N_{xy}$ . These shear loads are used to determine the initial number of m-ply sets in each spar web.  $t$  - plies are based on spar crushing loads determined from cover stiffness, load intensities, and local geometry parameters.

$$P_{cr} = \frac{2 N_x^2 b}{t_{sk} E_{sk} D'}$$

Where b is the spar spacing and D' the web depth.

The rib crushing loads due to wing bending are determined in a like manner.



$$P_{cr} = \frac{2N_x^2 L_{Rib}}{\left[ t_{sk} E_{sk} + \bar{t}_{Str} \cdot Q_{11}^0 \right] \cdot D'_{ave}}$$

Where

$L_{Rib}$  = Rib spacing

$\bar{t}_{Str}$  = Equivalent stringer thickness

$D'_{ave}$  = Average rib web depth

### Strength

For a composite laminate subject to  $N_x$  and  $N_{xy}$  loads, ACTBOP uses the following design equations:

$$l \geq \frac{N_x}{2t_L F_{tu}^0} ; N_x \text{ is tensile}$$

$$l \geq \frac{N_x}{2t_L F_{cu}^0} ; N_x \text{ is compressive}$$

$$m \geq \frac{N_{xy}}{4t_L F_{su}^{45}}$$

$$n \geq c(l + 2m)$$

Where  $c$  is a prescribed fraction. All load cases are considered and the load case which requires the largest number of plies is chosen.

## Stability

In general, four types of structural members need to be checked for stability under axial and shear in-plane loads. They are:

1. Advanced composite plate skins
2. Advanced composite sine wave spar or rib webs
3. Honeycomb panel covers with advanced composite face sheets
4. Honeycomb panel webs with advanced composite face sheets

Wing box covers are assumed to buckle in an infinite aspect ratio plate mode, while the spars/ribs behave as wide columns. The governing stability equations for these structural elements are summarized in Figure 6.

## Stringer Columns

The integral stiffeners used in multirib designs are sized first for strength requirements, then for local stability of flanges and webs, and finally for column stability requirements. Local stability requirements are as follows:

For outstanding flanges:

$$(b/t) \leq \left[ \frac{G_{LT}}{f_c} \right]^{1/2}$$

For webs:

$$(b/t) \leq \left\{ \left[ \frac{\pi^2}{6f_c} \right] \left[ (Q_{11}^0 \ Q_{22}^0)^{1/2} + Q_{12}^0 + 2G_{LT} \right] \right\}^{1/2}$$

The stringer load is determined from the strain compatibility relationship between the skin and stringer elements. The skin element of the column section is made up of  $l$ ,  $m$ , and  $n$  plies whereas the stringer element consists only of  $l$  plies. The distribution of cover load between the elements is computed for any instance where ply makeup of the skin or stringer is changed.  $l$ -ply fiber stresses for both skins and stringers are checked for compressive and tensile

strength requirements. Since the elastic properties of the skin is dependent on m-ply sets, skin stability is always checked to insure proper proportions of skin plies. In the programmed logic, stringer area is varied until both the skin and stringer are within ultimate strength allowables and the skin is stable for combined compression and shear loading.

The allowable (b/t) for flange and webs, along with physical constraints on minimum and maximum dimensions and minimum number of stringer l-ply, are used to proportion the total developed l-ply length implied in the  $A_{str}$  value into a stringer section. This results in stringer geometry dimensions for  $b_f$ ,  $b_w$ , and  $t_{str}$ , satisfying requirements for (P/A), (b/t), and  $t_{min}$  gage. With these dimensions, the sectional inertia properties of the stringer can be computed and final determination made for the allowable column length,  $L_{rib}$ , of the skin/stringer column.

The required rib spacing is determined from wide column behavior of the stiffened skins.

$$L_{Rib} = \left[ \frac{C \pi^2 D_{col}}{N_x} \right]^{1/2}$$

Where

C = Column fixity factor

$D_{col}$  = Stiffened skin bending stiffness  
per unit wing box width

#### Element Sizing Procedure

Initially, integer number of l-ply and m-ply sets are computed for each cover from the  $N_x$  and  $N_{xy}$  values. All loading conditions are processed to determine the minimum number of plies. The cover skin panels are then checked for panel stability under application of the compression and shear loads for each design condition:

$$R = R_x + R_{xy}^2 < 1$$

where

$$R_x = \frac{N_x}{N_{xcr}}$$
$$R_{xy} = \frac{N_{xy}}{N_{xycr}}$$

If R is greater than 1, the panel is unstable. m-ply sets are thus added to the panel until it becomes stable for all design conditions. The number of n-ply is always computed after addition of m-ply sets.

The stability of each spar web under the combined effects of applied shear and crushing loads are checked. If required, m-ply sets are added to stabilize the structure. Intermediate rib webs are designed for strength and stability requirements due to crushing loads only. The ribs are checked for rigidity as supports for the cover stringer column under compression loads. The available rib inertia,  $I_{rib}$ , includes effects of 1-inch-wide upper and lower caps. The required web stiffness is expressed in terms of EI required for the web. If the available rib EI is insufficient m-ply sets are added to the web.

#### Full Depth Honeycomb Sandwich

Full-depth honeycomb sandwich face sheets are sized initially for strength requirements. The skin-core combination is then checked for core wrinkling and crushing.

Core wrinkling:

$$F_{cw} = 0.43 \left[ E'_c \quad G'_c \quad E_f \right]^{1/3}$$

where  $E'_c$  and  $G'_c$  refer to the core and  $E_f$  to the face sheet

Core crushing:

$$P'_c \geq P_{cr}$$

$$P'_c = 2.31 \left( \frac{\rho'_c}{\rho_c} \right)^{1.464} \frac{F_{cy}}{D_{ave} 0.16}$$

$$P_{cr} = \frac{2N_x^2}{t_{sk} E_{11} D_{ave}}$$

where

$P_{cr}$  = Crushing load on core

$P'_c$  = Core allowable crushing load

ACTBOP's synthesis logic includes three options for determining design requirements of full-depth honeycomb sandwich torque boxes. These include:

1. Sizing skin requirements so that the sandwich structure will be stable for specified core type and densities
2. Sizing skin laminates to strength requirements and determining required core densities to satisfy stability requirements
3. Sizing for optimum skin/core combinations to satisfy strength and stability requirements.

In cases 1 and 3, skin stiffness increases are made by additions of m-ply sets only. When core densities are varied during optimization, the input core density is treated as the minimum.  $E'_c$  and  $G'_c$  values are obtained by

$$E'_c = 2.13 \left( \frac{\rho'_c}{\rho_c} \right)^{1.415} E_c$$

$$G'_c = 2.43 \left( \frac{\rho'_c}{\rho_c} \right)^{1.54} G_c \quad ; \quad \left( \frac{\rho'_c}{\rho_c} \right) < 0.0338$$

$$G'_c = 0.40 \left( \frac{\rho'_c}{\rho_c} \right) G_c \quad ; \quad \left( \frac{\rho'_c}{\rho_c} \right) \geq 0.0338$$

In the foregoing equations,  $\rho_c$ ,  $F_{cy}$ ,  $E_c$  and  $G_c$  refer to the core material and  $\rho'_c$ ,  $G'_c$  and  $E'_c$ , refer to the core.

### Stiffness Requirements

Torque-box stiffness at each station is estimated based on procedures similar to those used in the metallic analysis. For output evaluation of stiffnesses, a reference design temperature is specified so that computed EI and GJ at all stations are compatible. There additional stiffness computations are made as required. These are made at analysis temperatures specified for flutter design and at the design points for flexible loads and flutter optimization analysis. In all cases, EI's and GJ's are computed for the final lamina sets resulting, first, from strength and stability sizings and, second, from the results of the flutter stiffness analysis. The section stiffness is derived as the sum of the stiffness contribution of each element.

The value of GJ for the wing box section is calculated from:

$$GJ = \frac{4A^2}{\sum \frac{s}{tG}}$$

Where s is the length of a particular element, t is its thickness and G is its shear modulus. A is the area of the wing box.

The value of EI is calculated from

$$EI = \sum_i E(A_y^2 + I_0) \quad i = \text{skins, stringers}$$

For strength-designed sections that must be resized to meet flutter stiffness requirements, integer number of m-ply sets are added to the four elements contributing to the section torsional stiffness; upper and lower skin covers and front and rear spars. The m-ply sets are added to the thinnest element first until its thickness is equal to the next thinnest element or the required stiffness level is met. Additional plies are added in an ordered manner so that, in the extreme case, the four elements will consist of ply sets producing equal thickness webs.

## WEIGHT ANALYSIS

Results of the structural analyses are transformed into predicted weights at each of the 11 analysis stations representing the final assembly structure for the wing box. Structural weight per unit span length and panel weights are computed during each optimization loop; the total predicted weight is used to select the optimal design. Panel weights for each of the five torque box elements plus miscellaneous structural provisions for manufacturing and fabrication are computed, summed and printed for output evaluation. The weight analysis provides the detail information required to compute vehicle mass distribution data. Detail structural and weight data are also available for support of torque box manufacturing cost studies.

## TORQUE BOX OPTIMIZATION

### Multispar

A single-level optimization search procedure is used for the synthesis of multispar torque boxes. The total torque-box weight is optimized with respect to the number of cover support elements - intermediate spar webs. The search loop is designed to select the spar spacing that will produce the minimum torque-box weight. Search parameter value checks are made so that it is between minimum and maximum values. These limit values, which can be controlled by the user, insure that resulting sizings will reflect practical producible designs.

Design values for intermediate spar spacings or number of elements at each station is specified during each analysis pass, determining the unique cover plate dimensions between supports,  $b_s$ . Cover and web loads are computed based on this value. Each element is then sized to strength and stability requirements. Plate width for cover stability evaluation is based on the spar spacing,  $b_s$ . Local depths, adjusted for cover plates and cap thickness allowances are used for the height dimension in the web stability analysis.

The total torque-box is initially sized for strength and stability under the imposed design loads. Total weight computed at each station consists of the five major elements, upper cover, lower cover, intermediate spar caps and webs, front spar caps and web, and the rear spar caps and web. Miscellaneous items include the mechanical attachment provisions at cover-spar joints, spar web protective finish, and honeycomb core and bond weights for honeycomb panel spar designs. Torsional stiffness computations are made and flutter stiffness checks and resizings made as required after the optimum design is selected.

## Multirib

The multirib optimization procedure requires two major search levels. The first level consists of optimization of a number of stringer elements in the compression cover, similar to the number of spar element search in multispar analysis. The second level consists of determination of the best combination of  $l$ -plies in the skin panels that will result in minimum cover and support weight at each analysis station. The rationale for the programmed logic is that, for each assumed number of  $l$ -plies in the skin, there is one skin  $m$ -ply plus stringer area set that will satisfy all conditions of strength and stability for the skin, stringer and skin/stringer column resulting in a minimum total volume required for cover and supporting ribs. The compatibility equations for all the conditions do not allow for direct solutions; therefore, a numerical search procedure is programmed.

The computations for stringer area are all made for a given skin  $l$ -ply value. Stringer area is sized first for ultimate stress conditions. The search requires the determination of that stringer area that will result in maximum applied tension or compression stress on the skin or stringer element that is equal to or below the allowable ultimate stresses. For each assumed stringer area, skin  $m$ - and  $n$ -ply requirements as well as the skin and stringer loads  $P_{sk}$  and  $P_{str}$  are determined. The numerical search procedure is used here since the load distribution and stability equations are implicitly related. The loads  $P_{sk}$  and  $P_{str}$  plus the number and widths of  $l$ -plies in the stringer allow for computations of the applied stress levels. These values are checked to determine acceptable stringer areas.

It is then determined if the stringer section can be proportioned into acceptable geometries to conform to the type of stringer specified for the cover and the crippling requirement dictated by the minimum  $(b/t)$ . Acceptable sections are optimized to develop maximum stringer area moment of inertia by maximizing stringer heights.

## OUTPUT

Summary results of the optimization are printed in tabular format (Figure 7) showing the pertinent design information for the five basic structural elements of the torque box. Output content is dependent upon the construction type analyzed. Data output includes structural gages and laminate ply layup information; critical design loads, stresses and loading identification; section stiffnesses in terms of  $EI$  and  $GJ$ ; and torque box weights in terms of spanwise weight per inch and weights for each of the 10 panels.



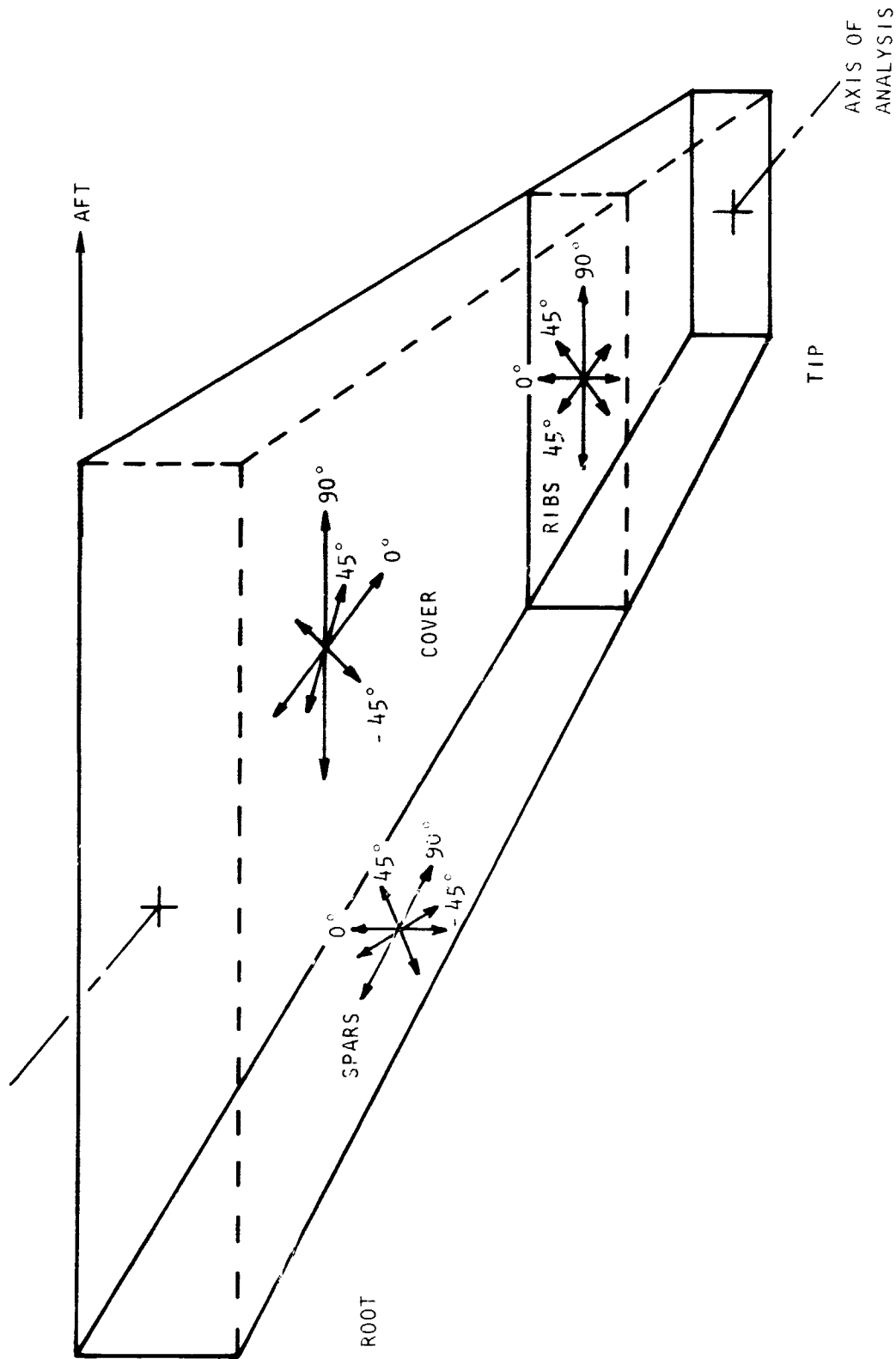


Figure 1. - Lamina orientations for ACTBOP structural elements.

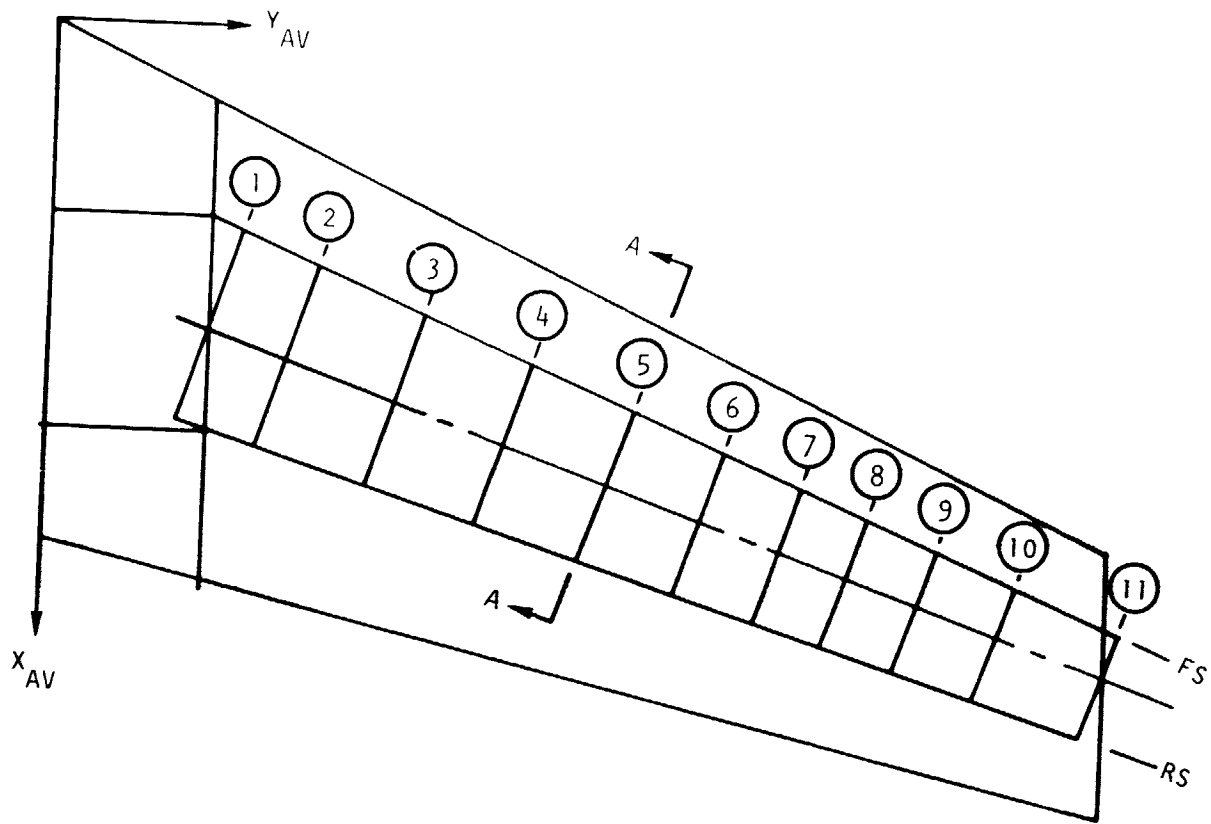


Figure 2.- ACTBOP torque box model.

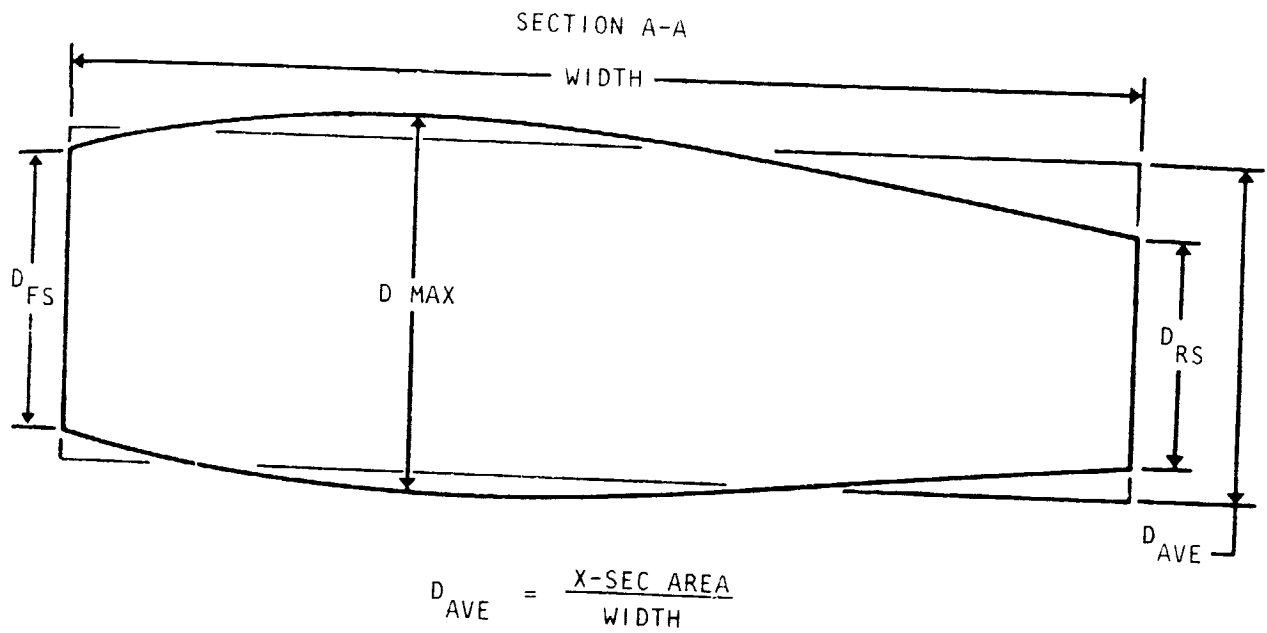
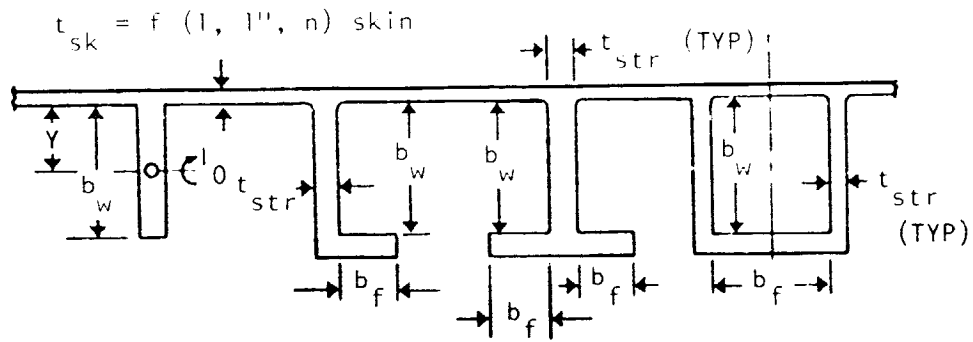


Figure 5.- Idealized cross-section.

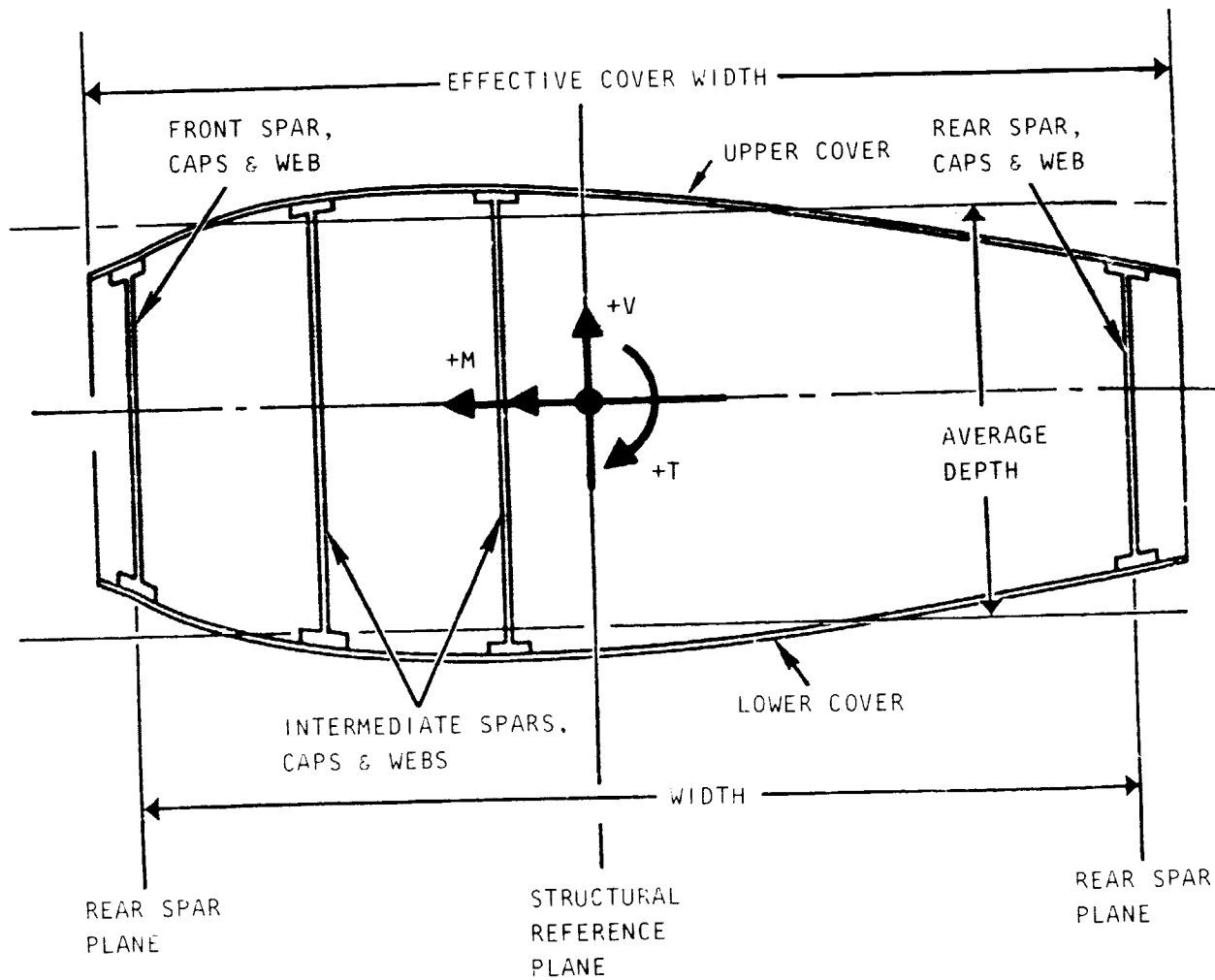


TYPE:	I	Z	T	HAT
CODE:	(1)	(2)	(3)	(4)
$N_h$	1	1	1	2
$N_f$	0	1	2	1
$N_c$	0	1	1	2

GENERAL EQUATION FOR AREA,  $A_{str} = t_{str} [N_h b_w + N_f b_f + N_c t_{str}]$

$$t_{str} = t_{Lstr}$$

Figure 4.- Permissible stringer types for ACTBOP multirib torque box covers.



NOTE RIGHT-HAND RULE FOR LOADS.

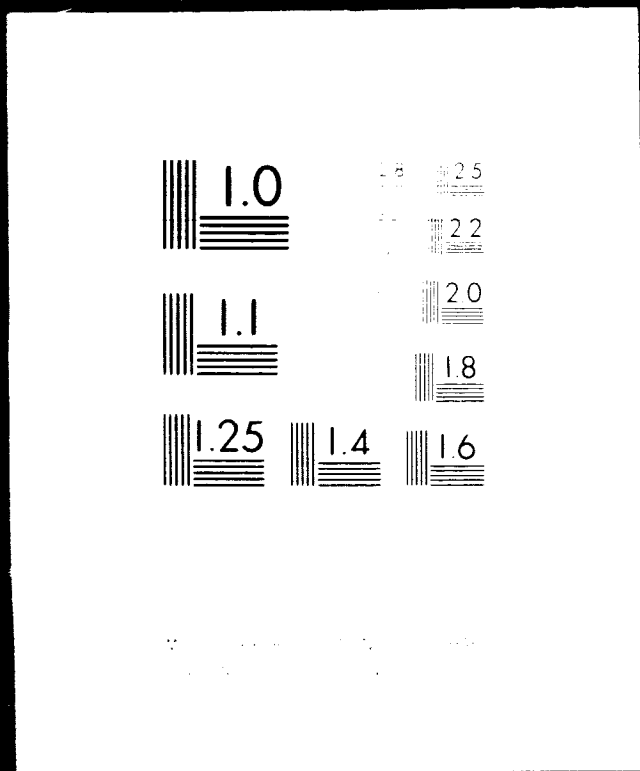
Figure 5. Torque box cross section loads.

# 30F5

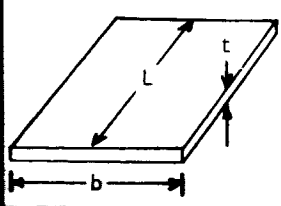
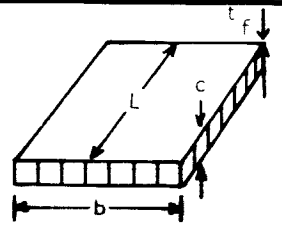
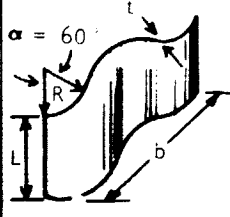
N78

18134

UNCLAS



REPRODUCIBILITY OF THE ORIGINAL PAGE IS POOR

	LAMINATED PLATE	HONEYCOMB SANDWICH PANEL <sup>4</sup>	CIRCULAR CORRUGATED WEB
			
<b>BENDING STIFFNESSES</b>	$D_{ij} = \frac{A_{ij} t^2}{12}$ $i, j = 1, 2, 6$	$D_{ij} = A_{ij} \frac{(c + t_f)^2}{12}$ $i, j = 1, 2, 6$	$D_{11} = 0.157R^2 A_{11}$ $D_{12} = \frac{A_{12}}{1.21} \frac{t^2}{12}$ $D_{22} = \frac{A_{22}}{1.21} \frac{t^2}{12}$
$K_C$	$2(1 + \frac{1}{\theta})$	$\frac{C_1 B_1 + 2B_2 + \frac{1}{C_1 B_1} + AZ(1 + \frac{1}{C_1})}{1 + \frac{Z}{C_1} [C_1 B_1 + B_3 (1 + C_1) + \frac{1}{B_1} + AZ]}$ $K_C$ , MINIMIZED WITH RESPECT TO $C_1$	$2(1 + \frac{1}{\theta})$
$K_V$	1	$\frac{1 - B_3 Z}{1 - B_3 Z - 4B_1 Z}$	1
$K_{CO}$	1	$\frac{1}{1 + Z/B_1}$	1
<b>PANEL COMPRESS. STABILITY</b>	$N_{X_{CR}} = K_C \frac{\pi^2}{b^2} (D_{11} D_{22})^{1/2} \quad \frac{b}{L} \rightarrow 0$		
<b>PANEL SHEAR STABILITY</b> $\frac{b}{L} \rightarrow 0$	$\theta \leq 1 \quad N_{XY_{CR}} = \frac{4K_V}{b^2} [D_{22} (D_{12} + 2D_{66})]^{1/2} (0.938\theta^2 + 0.532\theta + 11.7)$ $\theta > 1 \quad N_{XY_{CR}} = \frac{4K_V}{b^2} [D_{11} D_{22}^3]^{1/4} [8.125 + \frac{5.05}{\theta}]$		
<b>WIDE COLUMN COMPRESSION STABILITY</b>	$N_{X_{CR}} = K_{CO} \frac{\pi^2}{L^2} D_{11}$		

$$\theta = (D_{11} D_{22})^{1/2} / (D_{12} + 2D_{66}) \quad Z = \pi^2 [D_{11} D_{22}]^{1/2} / [b^2 G_c (c + t_f)]$$

$$B_3 = D_{66} / (D_{11} D_{22})^{1/2} \quad B_1 = (D_{22} / D_{11})^{1/2} \quad B_2 = 2B_3 + \nu_{xy} B_1$$

$$A = 1 - 2B_2 + B_3 \left\{ B_1 (C_1 + 2\nu_{xy}) + 2B_1 + \frac{1}{C_1 B_1} \right\} \quad C_1 = (L/nb)^2 \quad n = 1, 2, 3, \dots$$

Figure 6.- Summary of ACTBOP stability equations.

0-3 684

DESIGN SUMMARY DATA--MX=KIPS/IN, STRESS=KSI--		SECTION LOAD AND THICKNESS DATA--STRENGTH DESIGN--		T-U		T-L		TC/U		TM/IS		R/SP		N/SP		TM/FS		TM/RS	
SECT	MX/UC	MY/UC	MZ/UC	MX/S	MY/S	MZ/S	Q/RS	TSK/U	TSK/L	T-U	T-L	TC/U	TM/IS	R/SP	N/SP	TM/FS	TM/RS		
1	7.68	-7.98	-0.69	0.11	0.82	2.80	3.89	0.350	0.250	0.356	0.256	0.0	0.060	11.44	4.0	0.100	0.120		
2	6.89	-7.14	-0.86	0.11	0.84	2.75	4.19	0.320	0.230	0.326	0.236	0.0	0.060	10.53	4.0	0.100	0.120		
3	6.16	-6.36	-0.91	0.11	0.81	2.60	4.19	0.290	0.210	0.296	0.216	0.0	0.060	9.82	4.0	0.080	0.120		
4	5.36	-5.52	-0.86	0.11	0.74	2.41	3.93	0.260	0.200	0.266	0.206	0.0	0.060	9.12	4.0	0.080	0.120		
5	4.62	-4.75	-0.81	0.11	0.68	2.24	3.71	0.240	0.180	0.246	0.186	0.0	0.060	8.48	4.0	0.080	0.120		
6	3.78	-3.86	-0.75	0.11	0.61	2.01	3.40	0.210	0.150	0.215	0.155	0.0	0.040	7.78	4.0	0.080	0.100		
7	2.93	-2.93	-0.68	0.11	0.53	1.75	3.04	0.180	0.130	0.185	0.135	0.0	0.040	7.07	4.0	0.060	0.100		
8	2.09	-2.09	-0.58	0.10	0.43	1.43	2.54	0.150	0.110	0.155	0.115	0.0	0.040	6.37	4.0	0.060	0.080		
9	1.37	-1.37	-0.48	0.10	0.33	1.12	2.08	0.130	0.100	0.135	0.105	0.0	0.040	5.73	4.0	0.060	0.080		
10	0.68	-0.68	-0.35	0.10	0.23	0.71	1.45	0.100	0.080	0.104	0.084	0.0	0.040	5.03	4.0	0.040	0.060		
11	0.20	-0.20	-0.20	0.10	0.10	0.30	0.62	0.060	0.060	0.063	0.063	0.0	0.040	4.33	4.0	0.040	0.040		
*APPLIED STRESS LEVELS AND CRITICAL LOAD CONDITION ID#*																			
SECT	FS/UC	FS/UC	CLCU	CLSU	FT/LC	FS/LC	CLCL	CLSL	FS/IS	CLSI	FS/FS	CLSF	FS/RS	CLSR	FS/RS	CLSR	FS/RS	CLSR	FS/RS
1	21.94	-1.97	2.0	21.0	-31.92	-2.76	1.0	21.0	13.62	21.0	28.05	21.0	32.38	1.0	32.38	1.0	32.38	1.0	32.38
2	21.54	-2.59	2.0	21.0	-31.04	-3.74	1.0	21.0	13.93	21.0	27.47	21.0	34.92	1.0	34.92	1.0	34.92	1.0	34.92
3	21.24	-3.13	2.0	21.0	-30.30	-4.33	1.0	21.0	13.44	21.0	32.56	1.0	34.88	1.0	34.88	1.0	34.88	1.0	34.88
4	20.61	-3.30	2.0	21.0	-27.59	-4.29	1.0	21.0	12.39	21.0	30.12	1.0	32.77	1.0	32.77	1.0	32.77	1.0	32.77
5	19.27	-3.38	2.0	21.0	-26.37	-4.50	1.0	21.0	17.11	1.0	27.96	1.0	30.92	1.0	30.92	1.0	30.92	1.0	30.92
6	18.00	-3.56	2.0	21.0	-25.75	-4.98	1.0	22.0	15.25	1.0	25.07	1.0	34.03	1.0	34.03	1.0	34.03	1.0	34.03
7	16.29	-3.78	2.0	22.0	-22.55	-5.21	2.0	22.0	13.19	1.0	29.13	1.0	31.71	2.0	31.71	2.0	31.71	2.0	31.71
8	13.91	-3.90	2.0	22.0	-18.97	-5.31	2.0	22.0	10.76	1.0	23.79	1.0	26.01	2.0	26.01	2.0	26.01	2.0	26.01
9	10.34	-3.72	2.0	22.0	-13.70	-4.83	2.0	22.0	8.31	2.0	18.65	1.0	24.15	2.0	24.15	2.0	24.15	2.0	24.15
10	6.60	-3.52	2.0	22.0	-8.50	-4.40	2.0	22.0	5.64	2.0	17.81	2.0	24.15	2.0	24.15	2.0	24.15	2.0	24.15
11	3.27	-3.34	2.0	22.0	-3.27	-3.34	2.0	22.0	2.59	2.0	7.47	2.0	15.60	2.0	15.60	2.0	15.60	2.0	15.60

ORIGINAL PAGE IS  
OF FOUR QUALITY

Figure 7.- Typical ACTBOP output.

AN AEROELASTIC TAILORING STUDY  
OF A HIGH ASPECT RATIO WING

By Lt Kenneth E. Griffin

Air Force Flight Dynamics Laboratory

SUMMARY

A study is made of various aeroelastic tailoring objectives and the impact of design freedom on those objectives for a composite wing. A modified version of the General Dynamics/AFFDL TSO wing optimization program including control effectiveness and wing inertial loading effects was used to study a high aspect ratio sweepable wing. Several composite wing designs are compared with various tailoring objectives of minimum weight, load relief, control effectiveness, and flutter. Designs are compared on the basis of weight, angle of attack requirements for similar trimmed load factors, trim angle, flutter speed, control effectiveness, configuration flexible lift to rigid lift ratio, divergence dynamic pressure and wing pivot load levels.

INTRODUCTION

Aeroelastic tailoring is a lifting surface design concept in which the coupling that exists between the airloads that act on an aircraft lifting surface and the elastic characteristics of the wing structural box that must react these airloads is exploited for maximum benefit. This coupling occurs because the airloads on a wing are sensitive to the elastic deformations of the wing while the elastic deformations of the wing are a function of the airloads. Aeroelastic tailoring, first and foremost, is used to eliminate unwanted aeroelastic phenomenon such as flutter, divergence, control reversal, and violation of strength criteria for the design at any of the required design points of the flight envelope. If there is sufficient latitude to manipulate the design, the static airloads can be better tuned to give improved performance at various design points of the flight envelope. As these tailored designs are developed the designer must always be sensitive to the weight changes that may occur due to aeroelastic tailoring and the potential manufacturing difficulties that might be incurred with a highly tailored design approach. It is this effect on manufacturing that requires more information, and this study attempts to generate some trend information in this area.

In this study a high aspect ratio wing is selected to investigate four aeroelastic tailoring objectives. Eight levels of structural box design freedom in fiber orientation and ply distribution are used to evaluate the impact of these levels of freedom on the capability to accomplish the tailoring objectives.



---

From the resulting tailored designs some insight is obtained on tradeoffs that must be made in future wing designs between aeroelastic effectiveness and design simplicity when these present conflicting requirements. Some of the results obtained thus far from the study are presented here. This study is an ongoing one that will continue to explore areas mentioned here with variations in the ways in which each of the objectives are pursued to determine sensitivities to analysis types and modeling methods used for these analyses.

#### PRACTICAL CONSIDERATIONS FOR AEROELASTIC TAILORING

The level of tailored aeroelastic response of many tailored designs using advanced composite materials can be limited by restrictions in the freedom the designer has to specify fiber orientations and the ply distributions, and the amount of freedom a designer has can be very dependent on the required mission for that aircraft. If, for example, the concept of softening strips is used in the wing box covers to allow fastener penetration of the tension cover or for crack arrestment, certain restrictions could be imposed on the fiber orientations and distributions. The primary load carrying fiber orientation would probably prescribe the direction of the softening strip. For fastening the covers to conventional substructure, the strips would be required to be parallel to the spar direction. This type of requirement then "defines" the primary load carrying fiber orientation even before aeroelastic tailoring can begin. As more information becomes available, minimum requirements in softening strips for cross ply angles and thickness imbalance may put further restrictions on tailoring design freedom. How close to a  $\pm 45^\circ$  ply angle array must the cross plies be; or, at any point in the softening strips, how close to an exact balance in number of cross plies does the "soft" region have to be? What is the efficiency trade between the above concepts, off angle vs. unbalanced thickness? What is the weight trade and/or performance trade for these concepts? Another requirement will be manufacturing simplicity. Certain minimum ratios between number of cross plies and/or primary plies may be required for prevention of warpage or for thermal match to a substructure of a different type of material. To minimize scrapage or maximize automated layup efficiency certain restrictions may be made on the degree of tailoring in the composite covers for the structural box either in fiber angles or the amount of sculpturing in ply distributions. It is these restrictions on orientation angle and requirement of cross ply thickness balance that defined the design freedom cases addressed in this study. It should be emphasized that the trends in these areas may be very sensitive to wing geometry and relative requirements for flutter and control effectiveness, and the results for this wing may not translate to configurations of greatly different geometry or performance.

#### CONFIGURATION DESCRIPTION

The wing geometry used in this study is shown in Figure 1. The wing is of the variable sweep type with the pivot and structural box as shown. The configuration chosen for this evaluation is at a wing sweep angle of  $26^\circ$  and a

gross weight condition of 72,750 pounds. The flight condition for consideration here is sea level at a Mach number of .88. The wing fuel tanks are empty and the static design condition is a symmetric pullup with a load factor of 7.33 g's.

A variable geometry wing was chosen to simplify the comparisons in wing root moment reactions. With a typical cantilever wing various load paths would be defined to transmit wing loads into the fuselage at the wing root/fuselage intersection, depending on whether a load relieving, maximum flutter speed, or minimum weight design was chosen. In the example used here, all loads feed through the pivot pin, regardless of the aeroelastic objective emphasized. The low value of sweep of the wing was chosen to keep the wing aspect ratio high. The high load factor used was consistent with that required of similar aircraft thus making the wing box depth, gross weight, and load factor of proper relative proportions. The control surface used in this study does not appear on many vehicles of this type, but rather these vehicles use spoilers coupled with the empennage for roll control. The control surface (an aileron) was used in this simulation to examine whether aeroelastic tailoring could make it usable for a reasonable weight because this type of high aspect ratio configuration classically suffers from loss of control effectiveness with conventional trailing edge devices. Thus, this should be considered a limiting case and feasibility study only. For some aeroelastic tailoring objectives, the control surface was not considered. Flutter calculations were made only for the subsonic case and a flutter speed requirement of 1242 km./hr. was used. Studies also were made to meet an 1853 km./hr. requirement using mass balancing along with stiffness changes and are included here for comparisons. A minimum value of .20 was chosen as the control effectiveness requirement for those studies in which this parameter was included. The control effectiveness parameter is defined under the computer program description. For simplicity of discussions, the distributions of numbers of plies over the box planform will be referred to as ply distributions of a particular orientation. This does not refer to a variance in the standard prepreg ply thickness. In all cases high strength graphite epoxy material values were used in the structural simulation. In all references to ply angles, 0° is defined as that parallel to the middle spar in the structural wing box which is approximately the mid-chord sweep of the wing. The angle sense of + or - was chosen to be negative for all angles of higher sweep than the middle spar and positive for angles less than that.

#### COMPUTER PROGRAM DESCRIPTION

To develop the various designs used in this study a computer program was used that was developed specifically to produce preliminary designs with optimized aeroelastic qualities. The program, Wing Aeroelastic Synthesis Procedure, TSO, was originally developed for AFFDL by General Dynamics, Fort Worth, Reference 1. This version of TSO was modified by the author to include, either as a constraint or as a merit value, the flexible/rigid roll ratio, or roll effectiveness, of a trailing edge control surface on the wing. This modification was intended to make the optimization process sensitive to losses of effectiveness of a trailing edge control surface due to the elastic characteristics of the structural box, as well as other effects such as flutter,

---

divergence, flexible lift curve slope, flexible lift to rigid lift ratio, structural weight, and lamina strain capacity. As formulated each of these items were treated simultaneously in an optimization procedure based on math programming methods. A Fiacco-McCormick penalty function, Reference 2, was used with a Fletcher-Powell one dimensional minimization technique, Reference 3. Aeroelastically corrected airloads were obtained using a program based on the Woodward-Carmichael approach, Reference 4. Unsteady subsonic aerodynamics were obtained from a modified Doublet-Lattice procedure, Reference 5. The idealization for structural simulation with TSO can be seen in Figure 2 with the static aerodynamic simulation in Figure 3 and unsteady aerodynamic simulation in Figure 4. The structural parameters available to be optimized with TSO were the ply distributions and the fiber orientations of up to three layers of material in the cover skins of the structural box. Also up to ten nonstructural balance masses could be used for flutter speed improvement. A complete description of TSO can be found in Reference 1.

Control effectiveness computations were made using only the effects of the elastic structural wing box and were steady state calculations only. The control surface itself was rigid for this simulation. It was given a deflection angle and an effectiveness ratio was then obtained based on the ratio of the rolling moment obtained from the flexible wing divided by that from a hypothetical rigid wing.

#### GENERAL DESIGN OBJECTIVES AND CASE DESCRIPTIONS

Several objectives of aeroelastic tailoring were pursued in this study. First, a low structural weight objective was pursued. This is a requirement to remove as much structural weight as possible and find a balance between the conflicting requirements of structural strength for minimum lamina strain and structural stiffness for control effectiveness and preventing flutter or divergence. For this type of wing important parameters can be the moment and shear carried at the pivot during high g maneuvers. For this reason a second objective, which decreases the flexible lift to rigid lift ratio (referred to henceforth as F/R ratio) while striving for a minimum of structural weight, was pursued to provide more washout of high g airloads. This objective can result in a wing design providing an overall shift inboard of the resultant air loads and a decrease of the moment and shear requirements at the wing root. This objective was examined with and without a control effectiveness requirement. A third objective pursued was that of an increase in the roll effectiveness of a wing aileron. While a minimum of .20 was the required value for the other designs on which it was imposed as a constraint, the control effectiveness for this objective was specified at .45 while developing a design at a minimum of weight. The fourth objective addressed was that of minimum weight with an increase in flutter speed. In conjunction with this objective, flutter mass balancing variables were activated. An added tool available to the designer when dealing with flutter is the use of small, non-structural masses located on the wing which affects the inertia contribution to the aeroelastic coupling involved in flutter instabilities. These were included to observe any potential they may offer in tailoring a wing that only needs mass increases for

flutter improvement. The required flutter speed for this fourth objective was increased to 1853 km./hr.

In order to develop trends of impact from non-aeroelastic tailoring restrictions on aeroelastic tailoring efforts such as those discussed in the Introduction, each objective was examined with eight design cases. These design cases allow different parameters to be manipulated as design variables in order to achieve the aeroelastic objectives. These cases are summarized in Table 1. Progressing from Case 1 through Case 8, the gradual increase in design freedom should be noted. Case 1 prescribes a  $0^\circ/\pm 45^\circ$  orientation family with the further requirement that cross ply ( $\pm 45^\circ$ ) distributions be the same everywhere in the box covers. Thus even though the number of plies in either the  $+45^\circ$  or  $-45^\circ$  direction varies continuously in the wing box covers, they are always in exact balance with each other. This could correspond to a severe limitation on aeroelastic tailoring of a high aspect ratio wing. Case 2 relaxes one of the requirements of Case 1 in that the cross ply distributions are not required to be the same anywhere in the covers. Case 3 allows the cross ply orientations to deviate from the increment of  $45^\circ$  to some other angle  $\beta$ , thus providing a  $0^\circ/\pm\beta^\circ$  family. In case 3, however, the distributions for the cross plies are required to be the same. The balance requirement for the cross plies is relaxed in Case 4. Case 5 removes all angle requirements on the cross plies, having only the  $0^\circ$  orientation as a fixed value and allowing the cross ply thicknesses to be independent. Case 6 develops a new fiber orientation family by allowing the original  $0^\circ$  orientation to be a variable, with the cross ply angles required to be linked in  $\pm 45^\circ$  increments giving a family of  $0/\theta+45^\circ/\theta-45^\circ$ . In Case 6 the cross ply distributions are required to be the same. In Case 7 the linkage of the cross ply distributions of Case 6 is removed. Finally, in Case 8 all ply orientations and their distributions are independent variables. This last case should give an indication of the maximum amount of tailoring available in the covers with the TSO procedure. In all designs at least part of the objective includes a requirement to reduce weight to a minimum. However, as will be discussed later, for objectives other than minimum weight only, certain aeroelastic parameters are given more importance in the optimization process than weight in order to emphasize the desired objective. This will force the design process to sacrifice some weight reduction to allow these aeroelastic parameters to achieve their desired values.

In order to develop the various designs the TSO procedure must begin with a design that satisfied all the required values of the constraint set such as flutter speed or control effectiveness. From that point it optimizes the available design variables to produce the design that provides the best compromise between these constraints and those qualities such as weight or control effectiveness that are to be tailored into the wing design. To begin the optimization process, therefore, a very heavy but conservative design was used as a starting design point. Beginning at a wing weight of 1641 kg. with a control effectiveness of .77 and a flutter speed of 3484 km./hr., the design procedure was allowed to reduce the weight of the design using only the design variables available in Case 1 until all of the constraints became active in the design process. The resulting design of 956 kg. with a flutter speed of 2713 km./hr., a control effectiveness of .45, and F/R ratio of .86 became the starting point for all the case results described below.

---

In order to allow maximum freedom for each case to follow its own "path" in the optimization process to a design optimum, as much conservatism as possible is needed in the starting point. This starting design was chosen to provide the best compromise between maximum independence of the cases and the penalty function sensitivity to ply angle changes when they were variable. For certain objectives such as low weight, the penalty function is formulated so that it is sensitive to fiber angle changes only in their effects on the proximity of the design to its constraint values. The starting design then must have characteristics such as flutter speed or lamina strain values close enough to their defined limits so the penalty function value is sensitive to ply angle changes. Optimization of fiber angles also appears sensitive to the nonlinear effects of certain constraints such as divergence or control effectiveness, and unless vibration modes are recalculated for each flutter speed evaluation the angle minimization process can be confused. As will be seen in the results presented later in some of the case comparisons these effects were observed and account for inconsistency in some of the values from Case 1 to Case 8. To maximize the objectivity for developing trends from the final results, the optimization process was allowed to proceed without adjustment from the operator, generating these inconsistencies. It appears that including ply angles as variables in the aeroelastic tailoring process using TSO with a very conservative starting point requires close monitoring by the operator to prevent inconsistent results. Work is being done now at AFFDL to allow a more "hands off" approach to angle optimization using TSO with conservative starts, but this work has not been completed.

## DISCUSSION OF RESULTS

### Low Weight

The first objective studied, low structural weight, developed the best compromise between structural weight and the design requirements without special emphasis on any aeroelastic parameter. For these designs the control effectiveness became the dominant constraining factor for removal of weight. The results for this aeroelastic tailoring objective are summarized in Table II. In this table certain design parameters or characteristics of the designs are presented for each of the eight cases examined. In this table and those that follow the angle  $\alpha$  is the angle of attack required of the aircraft in order to obtain the required load factor. Along with  $\alpha$ , the required trim angle of the horizontal stabilators,  $\delta_{tail}$ , is given to indicate trends in trim drag changes that could result from the tailored designs. The last three angles in the table,  $\theta_1$ ,  $\theta_2$ , and  $\theta_3$  are the fiber angles of the three layers of advanced composite material that make up the covers for the structural box. The weights given are for the skins of the structural box only which are the structural members that are variable in this design procedure.

The values for weight follow no general trend in Table II because the requirements from the maximum lamina strain constraint were affected differently for each case of the study. In some cases a weight increase was allowed to reduce the lamina strain intensity. One trend that appears in Table II, however, is that when the requirement that the cross plies must be balanced is

removed as in going from Case 1 to Case 2 or from Case 3 to Case 4, little weight is saved. Upon examination of the strain field in the structural box, only a reduction in intensity was found in critical strain areas. Of the design sets the ply distributions for two examples, Case 1 and Case 6, are plotted in Figures 5 and 6 respectively, to indicate the degree of sculpturing for each. In these figures, contours of constant numbers of plies are shown for each of the fiber angles with the fiber angle and the maximum and minimum thickness areas noted. These designs would provide balanced cross plies for softening strips but may require alteration near the center of the box due to the small number of plies in the cross ply directions in that area. In these examples Case 1 demonstrates that almost no penalty is incurred in the tailoring objective when producing the most restrictive material distributions and fiber angles. The result of the minimum weight designs show little to gain in weight saving by allowing freedom to reorient ply angles and/or decouple cross ply thicknesses for this aspect ratio. These examples may indicate that for high aspect ratio wings with conflicting constraints there is little to gain with complicated material layups when only low structural weight is required. It should be noted that one would expect a  $0^\circ \pm 45^\circ$  orientation system to do quite well in this high aspect ratio wing. This balanced material requirement is emphasized by the mutually conflicting requirements of lamina strain and control effectiveness. While the maximum lamina strain constraint tended to push the designs toward a washout condition in order to relieve the root strains due to the airloads, control effectiveness tended to require a more washin design. Thus, to correctly find a compromise between these, the resulting minimum weight designs tended to be very conventional in their layouts.

#### Load Relief at Low Weight

Table III summarized the various case results for the design exercises wherein considerable load relief was emphasized along with a minimum of structural weight and is compiled in a similar manner to that of Table II. There is one difference in the parameter list. As discussed below, the control surface on the wing was removed and therefore no control effectiveness was calculated. This parameter was replaced in Table III with the value of the bending moment in the wing pivot due to the wing airloads for comparison of the ability of the various cases to reduce the pivot requirements. As seen from the previous minimum weight designs, the control effectiveness tended to counter any tendency in design to develop washout for load relief of the lamina strain constraints. It was felt that an aircraft requiring load relief for high g maneuvers could satisfy roll control requirements with spoilers only. For reference, however, the cases were run for this objective with the control surface included and are tabulated in Table IV. In Table III the case results without the control surface followed the same trend except for Case 7. In order to provide more load relief in the wings the F/R ratio must be reduced. Note that the structural weight does tend to go up, but the design process was formulated to give much more emphasis to reducing the wing F/R ratio than reducing weight which forced the process to give up considerable weight savings in some cases to reduce the wing F/R ratio. With unbalanced cross plies, Case 2 was able to save some weight with only a slight reduction in the F/R ratio, however. A very similar pattern developed between Case 3 and Case 4. Note in these cases no collective

---

rotation of all the fiber directions was allowed. The ply distributions for Case 2 can be seen in Figure 7. Case 6 shows that if collective angle changes are allowed, even with coupled cross ply distributions, the ability to collectively rotate the ply orientation family approximately  $20^\circ$  aft allowed a reduction in wing F/R ratio. Case 7 is an anomaly in which more weight produced an inferior design and cannot easily be explained. It is, however, interesting that this design case had a significantly lower intensity strain field than the other cases which may have been the best result available to the optimization process. With the added power of independent cross ply angles and distributions, Cases 5 and 8 showed the best capabilities to reduce the wing F/R ratio. When allowed to vary the primary load carrying fiber directions as in Case 8, the best design for reducing wing F/R ratio was found and the ply distributions for Case 8 can be found in Figure 8. It should be pointed out that a large drop in flutter speed resulted in Cases 5 and 8 which indicates a limiting consideration for direction of tailoring static airloads to washout even without a control effectiveness requirement. The results of these designs seem to indicate that if at all possible in order to emphasize the load relief character of a wing of this type the cross ply fiber angles should be allowed to be independent or at least move collectively. Cross ply orientations of  $\pm\beta$  other than  $\pm 45$  do not seem to be of much advantage while the reference primary load carrying ply orientation is held constant. While rotation of the ply angle family is very powerful, there is a significant increase in payoff in a lower wing F/R ratio over even this approach when the maximum design flexibility is given to the aeroelastic tailoring process of independent fiber directions and ply distributions. To highlight the advantage in pivot loads using a load relief design a comparison can be made between the pivot shear load, bending moment, and torsion moment between designs of different F/R values. For a value of .70 for F/R the shear load was  $4.31 \times 10^{11}$  dynes rather than  $5.43 \times 10^{11}$  dynes for a F/R value of .82. Similarly the bending and torsion moments dropped from  $1.65 \times 10^{13}$  dyne-cm and  $1.13 \times 10^{12}$  dyne-cm for a F/R of .82 to  $1.21 \times 10^{12}$  dyne-cm and  $6.87 \times 10^{11}$  dyne-cm respectively for a F/R ratio of .70. Thus considerable benefit can be obtained in pivot stress for high g conditions by an aeroelastically tailored washout condition. Based on these design results perhaps the most effective way to obtain load relief in high aspect ratio composite wing boxes is to allow direction of the fiber to vary from the  $0^\circ/\pm 45^\circ$  family. This angle rotation may conflict with the requirement for the primary load carrying fibers to be parallel to substructure spars for attachment with softening strips. If the cross ply arrangement of Case 5 is satisfactory for this design geometry, Case 5 may be the best compromise for tailoring for washout with substructure requirements, but further studies would be required to obtain the best tradeoff between low weight and low F/R.

The results in Table IV show how much the requirement of a minimum value of control effectiveness may restrict the capability to provide load relief. There is little gained between all the cases shown in Table IV in producing a low value of wing F/R ratio. In fact, in those designs where the linked cross ply angles were variable the design procedure found more value in reducing the intensity of the strain field than in reducing the wing F/R ratio. Case 3 suffered from critical divergence problems and produced an unsatisfactory design result. The collective angle rotation available in Cases 5 through 7 produced some reduction in the F/R ratio but was limited by the control effectiveness requirement.

## Increased Control Effectiveness at Low Weight

As a third aeroelastic tailoring objective, the minimum control effectiveness requirement for the aileron was increased from .20 to .45. This was imposed on the weight optimization runs that repeated the cases of Table II. The results for these runs are presented in Table V. First note the results of Case 1 versus Case 2 and then Case 3 versus Case 4. When the cross ply distributions were allowed to be independent for Case 2, the ability to produce the required effectiveness was so improved that not only did the weight go down but the effectiveness of the control surface as a function of wing box stiffness was more than doubled that of Case 1. This is best understood by examination of the ply distribution changes between Case 1 and Case 2, Figure 9 and Figure 10. In Case 1 the cross ply distributions are apparently arrayed to maintain a high torsional stiffness to reduce the loss in control effectiveness to .61. In Case 2, however, the plies swept  $45^\circ$  aft of the  $0^\circ$  plies are much higher in number, almost that of the  $0^\circ$  plies. With this great emphasis on the aft swept  $45^\circ$  plies, the elastic response produces an increase in rolling power over that for a rigid wing. Notice that the F/R ratio follows the same trend as that of control effectiveness. Increases in control effectiveness for outboard ailerons of this wing geometry demand a more washin response from the structural box raising the F/R ratio. This agrees with the trend found in the previous load relief objective where the washout load relief designs were limited by control effectiveness requirements. In Cases 6 and 7 upon examination of the ply angles, it would seem that a washout design was developed rather than a washin design, as shown in Cases 1, 2, 3, and 4. However, when the deflections of the wing under the aeroelastically corrected airloads are calculated, the wing actually has washin behavior, both in Cases 6 and 7. Note this is also consistent with the values of the F/R ratio. When the cross ply distributions are allowed to develop independently, once again weight is saved and the control effectiveness is at the same time improved. In Case 6 the dominant plies are the coupled cross plies, whereas in Case 7, where more design freedom is allowed, the most dominant is the aft swept cross ply. This emphasis in the aft swept cross ply then in one way redefines the so-called primary load carrying fiber direction since this cross ply distribution (the  $-45^\circ$  orientation of the  $0/0 +45^\circ/0 -45^\circ$  family) is much thicker than that of the plies associated with the  $0$  direction. The cases which free all but the  $0^\circ$  direction (Case 5) and free all variables (Case 8) did not provide superior designs. In these cases, optimum designs were found with less structural weight removed in an apparent attempt to improve the balance between the conflicting requirements of flutter, control effectiveness, and lamina strain.

In summary the increase in control effectiveness requirements tended to reduce the elastic washout character of the wings. The most effective means to accomplish increased control effectiveness was to increase the number of plies in the orientation with the most aft sweep. This allows a  $0^\circ/+45^\circ/-45^\circ$  design to be very effective, but has a limitation if the  $0^\circ$  orientation must remain the "primary load carrying" fiber direction say for softening strip reasons.



## Increased Flutter Speed at Minimum Weight

The fourth objective was to examine the impact that changes in the required flutter speed could make in the tailored composite covers for this type of wing geometry. Also included in this study are nonstructural lumped masses along the leading edge of the wing box to be used for flutter mass balancing. These are allowed to vary in weight if the optimization procedure finds that small increases in their weight provide flutter speed increases which are more beneficial than the penalty derived from their increased weight. For the cases in this objective the required flutter speed for this wing was arbitrarily increased from 1242 km./hr. to 1853 km./hr. The minimum weight cases of Table II were then rerun with the balance masses activated to observe the changes in resulting designs. These results are summarized in Table VI. In Cases 3 and 4 the cross plies have only been moved just slightly off of their original  $\pm 45^\circ$  values. This indicates that the choice of  $\pm 45^\circ$  orientations in cross plies for this design is very effective in providing the torsional stiffness necessary for the flutter requirements as intuition would suggest. Only a small variation in the cross ply distributions of Case 2 from those of Case 1 occurred and indicate that the balanced cross plies are very efficient. This same trend is seen between Cases 3 and 4, in which the balanced character of the cross plies is changed only slightly to improve the lamina strain field for the trimmed g condition. In Figures 11 and 12 the similar character of these designs (Cases 1 and 4) can be seen in ply distributions of the three fiber orientations. In Cases 6 and 7 the  $0^\circ/0^\circ +45^\circ/0^\circ -45^\circ$  family is swept aft with the cross ply distributions dominating the  $0^\circ$  plies. Once again even in Case 7 where the cross ply distributions were allowed to vary independently, they remained almost identical. Some weight savings were achieved by rotating the orientation family while providing some improvement in the strain field. Case 5 duplicated in many respects Cases 1 through 4, 6, and 7 in the way the cross ply angles moved and the similarity of cross ply distributions. Note that in Case 8 where there is no requirement for  $0^\circ$  plies a significant change is seen from the other cases. Here a better balance between requirements on the lamina strain field and the flutter requirements was developed. There is no definite weight improvement case in any of those run, probably because the  $0^\circ/+45^\circ/-45^\circ$  orientation is a good family for torsional stiffness, which also requires little imbalance between the cross ply distributions. With flutter speed as the major constraining factor, meeting its requirements for this high aspect ratio wing does not require unusual ply orientations or distributions.

The other factor to be examined in this objective was mass balancing in lieu of structural stiffening. Normally this flutter improvement is saved for solving flutter problems in cases wherein stiffness changes are not allowed and only small amounts of mass are very beneficial. In the designs of Table VI, small nonstructural weights were allowed to be varied by the optimization process along with the other structural variables. In all of the cases where the cross ply distributions were required to be balanced, there was no significant weight increases in the balance masses. In the other cases, except Case 2, there were significant balance mass increases in various leading edge locations. As an example 5.7 kg were added in Case 8 along the leading edge at the 60% span location. These different locations depend on the variations in the

natural vibration mode shapes that coupled, producing the critical flutter instability. Many more designs must be examined before a conclusion can be drawn, but this trend might prove interesting as more experience is gained with flutter problems in composite structures. The amount of mass balancing used will be very sensitive to mass location and the form of coupling occurring for flutter. In these studies only clean wing flutter is examined which classically produces a bending-torsion instability. Based on these results there can be some value in nonstructural balance mass for flutter instabilities but it seems a function of the other structural variables available in the tailoring process.

### CONCLUSIONS

While more studies with different combinations of structural variables available for aeroelastic tailoring are needed, some conclusions can be drawn from the trends indicated thus far. Of the aeroelastic tailoring objectives studied the load relief objective would suffer the most from restrictions in fiber orientations due to cover softening strips to match the sweep angle of substructure members or damage tolerance. There seems to be much more design power in load relief with changes in fiber angles. Control effectiveness requirements force the wing design towards a washin condition. This may conflict with lamina strain requirements due to increased outboard airloads of washin designs and force a middle-of-the-road compromise that may appear to be very conventional both in ply angles and their distributions. This would then integrate well with softening strip requirements. If control effectiveness is emphasized for high aspect ratio wings, then unbalanced cross plies are most effective. This unbalance, if extreme, may conflict, however, with the cross ply distribution required for softening strips. Severe flutter requirements can be best met with a large number of cross plies. Mass balancing for primary surface flutter needs many more design applications in aeroelastically tailored wings to draw general conclusions. Here they showed only a limited capability to remove the conflict of high torsional stiffness for flutter requirements and the flexibility needed in load relief designs.

The results developed in this study so far have been used to build on some basic aeroelastic tailoring concepts identified earlier in Reference 6 and will be used to guide further studies to establish the potential as well as limitations that can be expected for aeroelastic tailoring for this type of geometry. While of preliminary design level in analysis depth, these conclusions are expected to be applicable as more detail is developed on each design case.

### REFERENCES

1. McCullers, L.A. and Lynch, R.W., "Dynamic Characteristics of Advanced Filamentary Composite Structures", AFFDL-TR-73-111, Volume II, "Aeroelastic Synthesis Procedure Development", September 1974.

2. Fircco, A. and McCormick, G.P., "The Sequential Unconstrained Minimization Technique for Nonlinear Programming, A Primal-Dual Method", Management Science, 10, 360 (1964).
3. Fletcher, R. and Powell, M.J.D., "A Rapidly Convergent Descent Method for Minimization", Computer Journal, 6, 163 (1963).
4. Carmichael, R.L., Castellano, C.R. and Chen, C.F., "The Use of Finite Element Methods for Predicting the Aerodynamics of Wing-Body Combinations", NASA SP-228, October 1969.
5. Giesing, J.P., Kalman, T.P., and Rodden, W.P., "Subsonic Unsteady Aerodynamics for General Applications", AFFDL-TR-71-5, November 1971.
6. "Proceedings of the Second Conference on Fibrous Composites in Flight Vehicle Design", AFFDL-TR-74-103, September 1974, pp. 405-438.

TABLE I.- VARIATIONS OF DESIGN FREEDOM

CASE	$\theta_1^*$	$\theta_2^*$	$\theta_3^*$	PLY DISTRIBUTIONS**
1	0°	+45°	-45°	$N_1 \neq N_2 = N_3$
2	0°	+45°	-45°	$N_1 \neq N_2 \neq N_3$
3	0°	I	$-\theta_2$	$N_1 \neq N_2 = N_3$
4	0°	I	$-\theta_2$	$N_1 \neq N_2 \neq N_3$
5	0°	I	I	$N_1 \neq N_2 \neq N_3$
6	I	$\theta_1 + 45^\circ$	$\theta_1 - 45^\circ$	$N_1 \neq N_2 = N_3$
7	I	$\theta_1 + 45^\circ$	$\theta_1 - 45^\circ$	$N_1 \neq N_2 \neq N_3$
8	I	I	I	$N_1 \neq N_2 \neq N_3$

\* FIBER ORIENTATIONS REFERRED TO MIDDLE SPAR OF STRUCTURAL BOX WITH THE LETTER I INDICATING THE ANGLE IS AN ACTIVE DESIGN VARIABLE

\*\*  $N_i$  IS THE NUMBER OF PLYS OF ANGLE I AT ANY POINT X,Y IN THE BOX COVERS

TABLE II.- LOW WEIGHT

CASE	WEIGHT (KG)	V <sub>FLUTTER</sub> (KM/HR)	CONTROL EFFECT.	F/R	$\alpha$ (DEG)	$\delta$ TAIL (DEG)	$\theta_1$ (DEG)	$\theta_2$ (DEG)	$\theta_3$ (DEG)
1	137.	1887.	.21	.836	7.66	4.03	0.	+45.	-45.
2	135.	1855.	.21	.842	7.60	3.97	0.	+45.	-45.
3	150.	1310.	.23	.845	7.58	3.96	0.	+15.	-15.
4	149.	2039.	.22	.899	7.14	3.26	0.	+17.	-17.
5	187.	1560.	.22	.891	7.18	3.49	0.	+1.	-50.
6	134.	1824.	.21	.845	7.57	3.96	-5.	+40.	-50.
7	140.	1834.	.21	.826	7.75	4.13	-16.	+29.	-61.
8	179.	1549.	.21	.886	7.23	3.54	-8.	+11.	-52.

TABLE III.- LOAD RELIEF

CASE	WEIGHT (KG)	V <sub>FLUTTER</sub> (KM/HR)	MING BENDING MOMENT (DYNE-CM $\times 10^{13}$ )	F/R	$\alpha$ (DEG)	$\delta_{TAIL}$ (DEG)	$\theta_1$ (DEG)	$\theta_2$ (DEG)	$\theta_3$ (DEG)
1	130.	1774.	1.65	.83	7.76	4.14	0.	+45.	-45.
2	117.	1696.	1.65	.82	7.82	4.23	0.	+45.	-45.
3	127.	1705.	1.65	.83	7.72	4.14	0.	+47.	-47.
4	128.	1736.	1.65	.82	7.78	4.15	0.	+45.	-45.
5	264.	1344.	1.45	.76	8.45	4.78	0.	+15.	-76.
6	175.	1701.	1.45	.78	8.20	4.75	-19.	+26.	-64.
7	265.	1727.	1.68	.84	7.65	4.02	-25.	+20.	-70.
8	244.	1340.	1.21	.70	9.15	5.52	+11.	+24.	-76.

TABLE IV.- LOAD RELIEF WITH CONTROL EFFECTIVENESS

CASE	WEIGHT (KG)	$V_{FLUTTER}$ (KM/HR)	CONTROL EFFECT.	F/R	$\alpha$ (DEG)	$\delta_{TAIL}$ (DEG)	$\theta_1$ (DEG)	$\theta_2$ (DEG)	$\theta_3$ (DEG)
1	137.	1883.	.21	.834	7.68	4.04	0.	+45.	-45.
2	134.	1824.	.21	.834	7.63	3.30	0.	+45.	-45.
3	211.	1516.	.67	.860	--	--	0.	+13.	-13.
4	163.	1555.	.21	.871	7.35	3.65	0.	+20.	-20.
5	247.	1649.	.21	.839	7.64	3.99	0.	+12.	-52.
6	131.	1807.	.20	.850	7.59	3.93	-7.	+38.	-52.
7	155.	1961.	.20	.812	7.89	4.25	-16.	+29.	-61.
8	241.	1794.	.22	.815	7.87	4.20	-9.	+26.	-78.

TABLE V.- INCREASED CONTROL EFFECTIVENESS

CASE	WEIGHT (KG)	$V_{FLUTTER}$ (KM/HR)	CONTROL EFFECT.	F/R	$\alpha$ (DEG)	$\delta_{TAIL}$ (DEG)	$\theta_1$ (DEG)	$\theta_2$ (DEG)	$\theta_3$ (DEG)
1	229.	2137.	.61	.864	7.37	4.04	0.	+45.	-45.
2	190.	2046.	1.30	.895	7.20	3.84	0.	+45.	-45.
3	202.	1761.	.55	.870	7.34	3.86	0.	+22.	-22.
4	214.	2205.	1.10	.896	7.11	3.70	0.	+26.	-26.
5	248.	2595.	.47	.872	7.34	3.70	0.	+47.	-44.
6	217.	2291.	.46	.877	7.30	3.66	10.	+55.	-35.
7	199.	2409.	.62	.873	7.30	3.91	7.	+52.	-38.
8	234.	2906.	.46	.871	7.35	3.70	2.	+52.	-44.



TABLE VI.- INCREASED FLUTTER SPEED

CASE	WEIGHT (KG)	V <sub>FLUTTER</sub> (KM/HR)	MASS BAL. ACTIVE	F/R	$\alpha$ (DEG)	$\delta$ TAIL (DEG)	$\theta_1$ (DEG)	$\theta_2$ (DEG)	$\theta_3$ (DEG)
1	244.	2711.	No	.857	7.46	3.38	0.	+45.	-45.
2	260.	2753.	No	.860	7.43	3.36	0.	+45.	-45.
3	247.	2706.	No	.857	7.46	3.38	0.	+46.	-46.
4	275.	2780.	YES	.859	7.44	3.86	0.	+45.	-45.
5	273.	1983.	YES	.800	8.00	4.42	0.	+32.	-61.
6	251.	2431.	No	.840	7.62	4.01	-16.	+29.	-61.
7	258.	2422.	YES	.833	7.69	4.08	-17.	+28.	-62.
8	291.	2076.	YES	.866	--	--	-22.	+13.	-73.

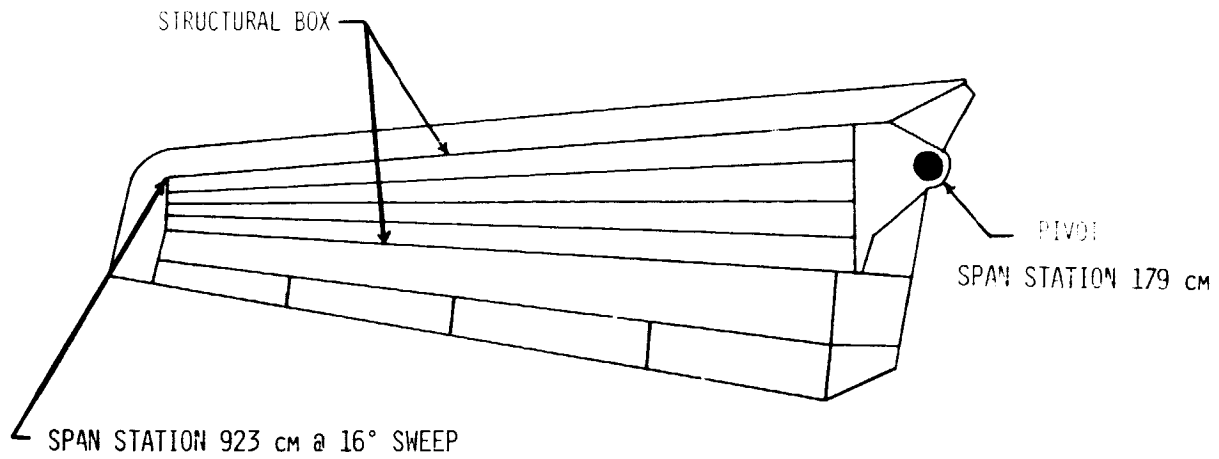


Figure 1.- Wing geometry.

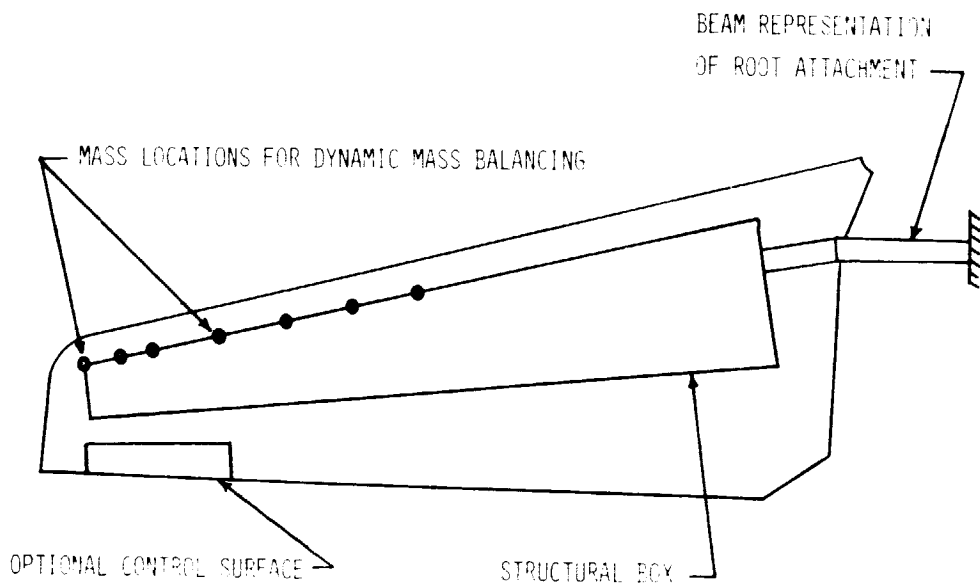


Figure 2.- TSO structural simulation.

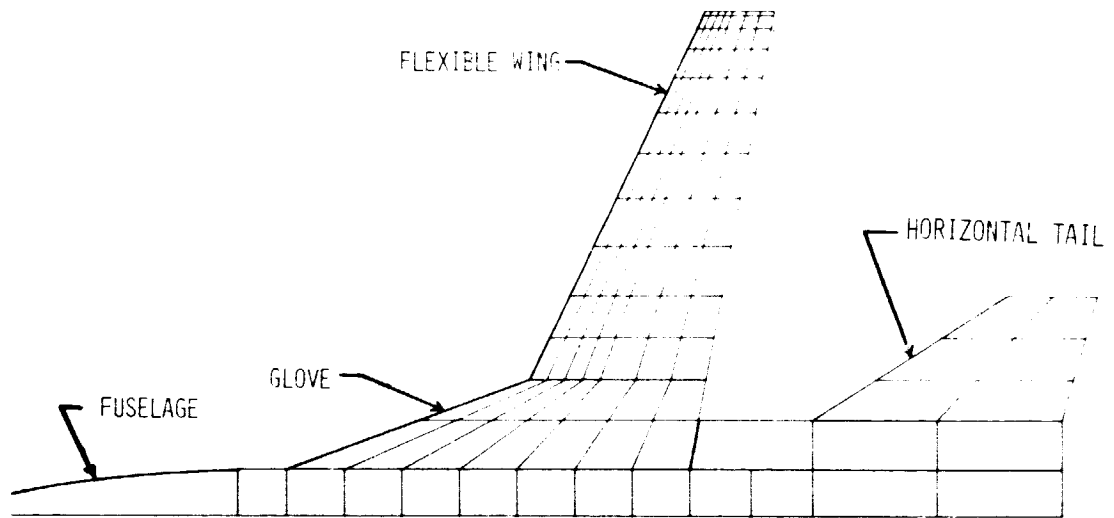
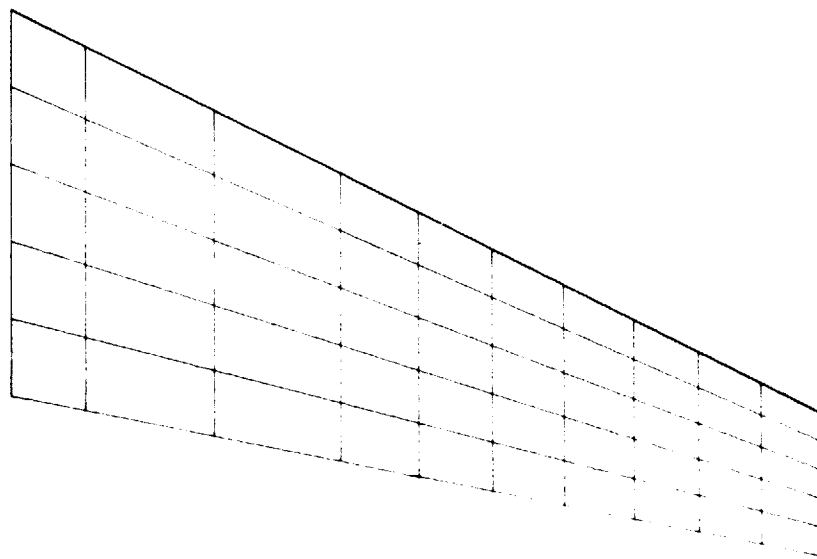


Figure 3.- Steady aerodynamic simulation.



FLEXIBLE WING ONLY

Figure 4.- Unsteady aerodynamic simulation.

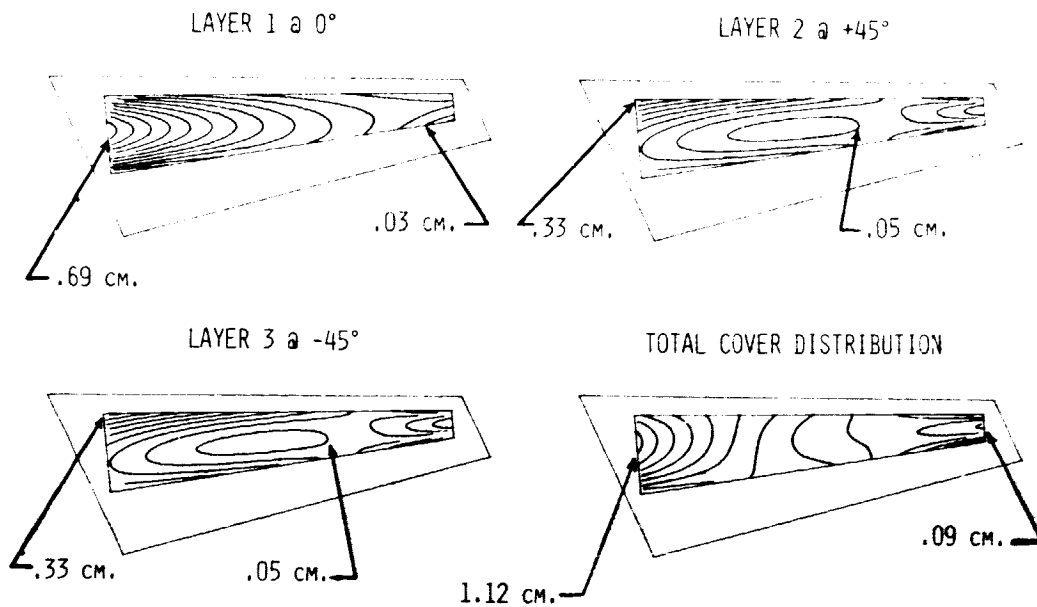


Figure 5.- Ply distributions for low weight. Case 1.

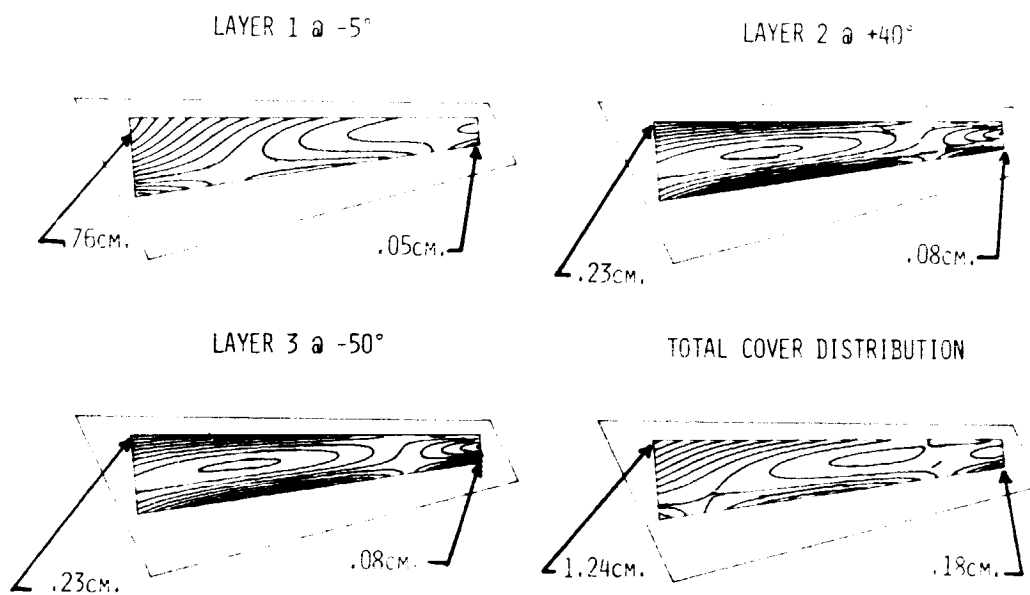


Figure 6.- Ply distributions for low weight. Case 6.

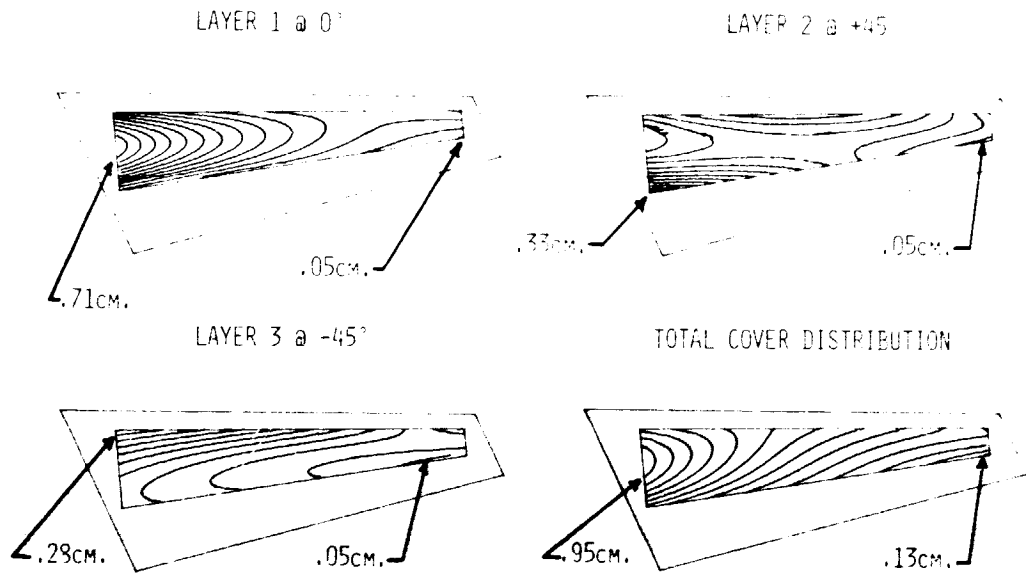


Figure 7.- Ply distributions for load relief. Case 2.

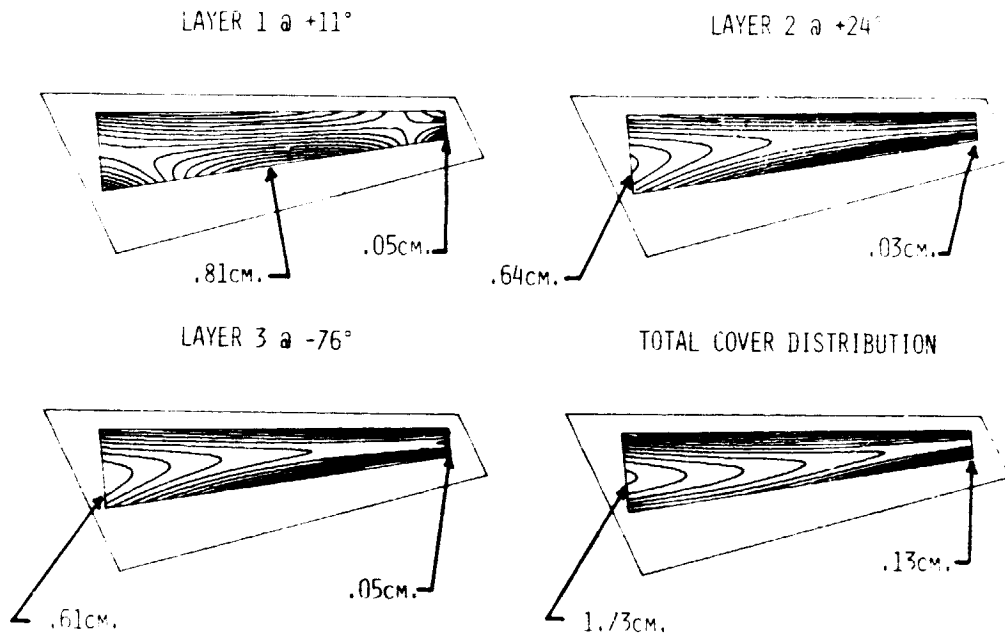


Figure 8.- Ply distributions for load relief. Case 8.

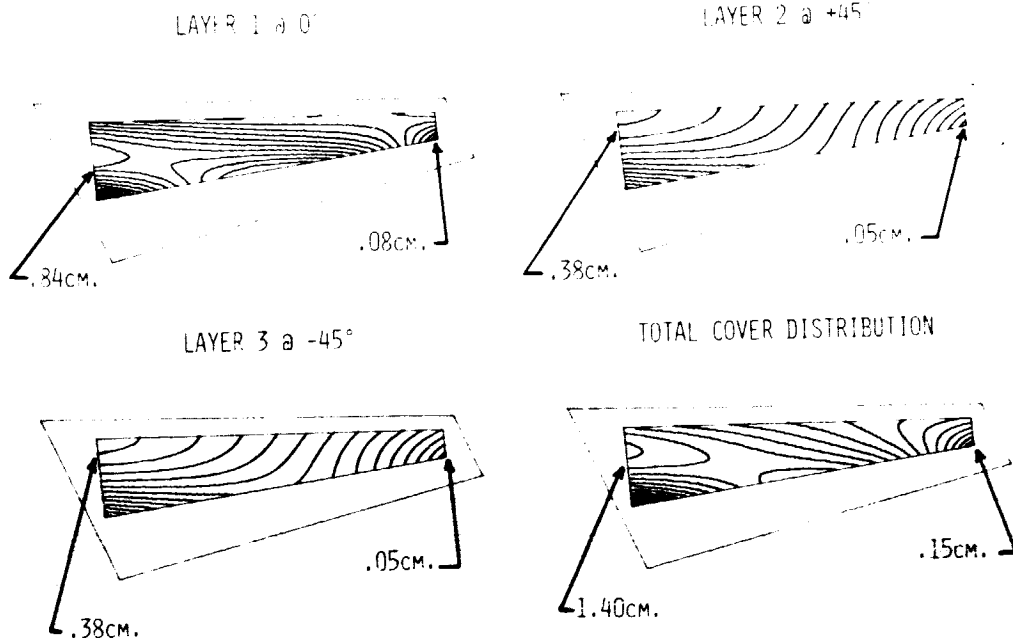


Figure 9.- Ply distributions for increased control effectiveness. Case 1.

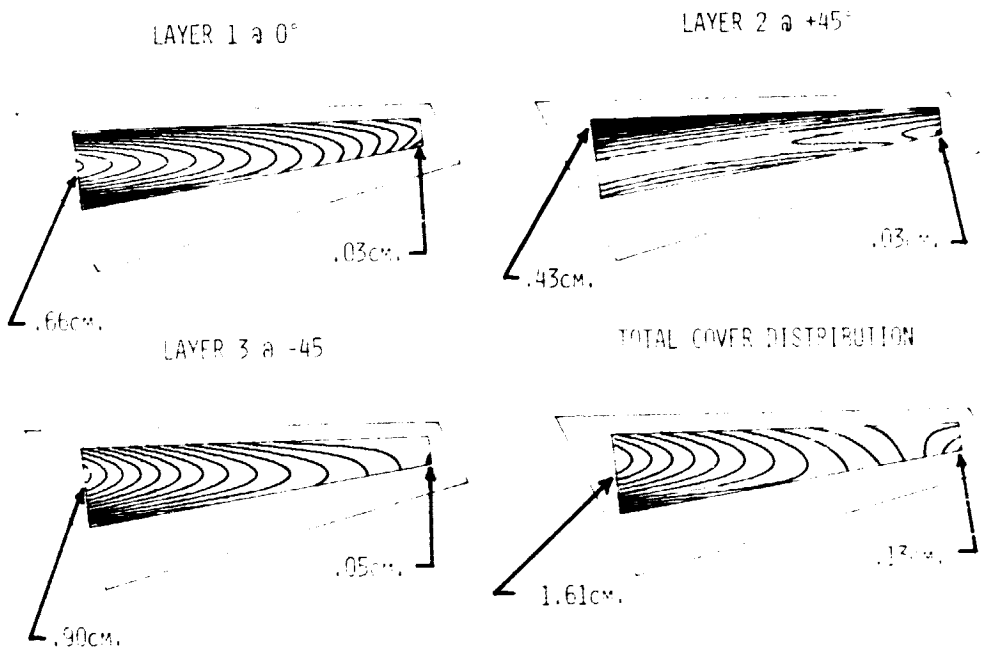


Figure 10.- Ply distributions for increased control effectiveness. Case 2.

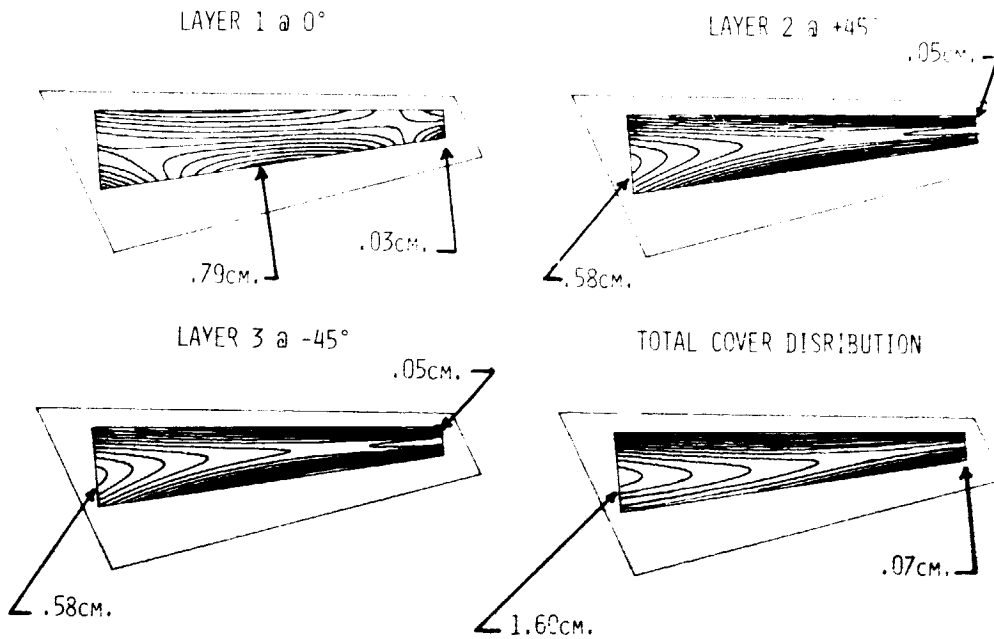


Figure 11.- Ply distributions for increased flutter speed. Case 1.

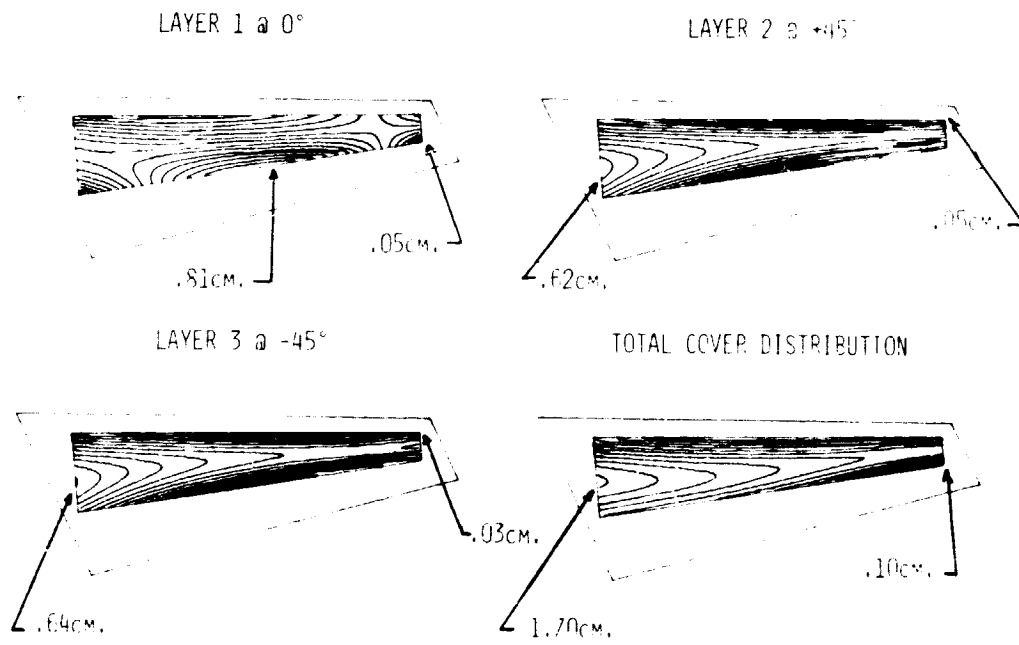


Figure 12 - Ply distributions for increased flutter speed. Case 2.

# ADVANCED DESIGN COMPOSITE AIRCRAFT

By R.N. Hadcock

Grumman Aerospace Corporation

## SUMMARY

The results of preliminary design studies of the Advanced Design Composite Aircraft (ADCA) are described in this paper. Design criteria and requirements were defined and parametric trade studies were performed to identify the preferred air vehicle. The objective of this study is to apply advanced composites to a completely new aircraft in an unconstrained manner and so obtain an aircraft which is smaller, lighter and cheaper than its advanced metal counterpart.

## INTRODUCTION

The objective of the Advanced Design Composite Aircraft (ADCA) program is to define the benefits and ramifications of unrestrained application of composite materials to a completely new aircraft. The specific objective is to develop an airframe design which will be almost entirely made from composite materials and so obtain a smaller, lighter and less expensive aircraft which will perform an identical advanced tactical mission at lower life cycle costs than its metal counterpart.

The mission selected for this study is a supersonic penetration interdiction fighter (SPIF) mission, a mission which provides a demanding set of requirements and so exercises the properties of composites to their fullest. It should also yield maximum potential payoff from unrestrained use of these materials. Furthermore, the SPIF mission addresses the serious threat of advanced SAMS and interceptors likely to be encountered in the 1980's.

This paper will describe the results of work accomplished by Grumman Advanced Composites/Advanced Aircraft Systems personnel during the first three months of this Air Force Flight Dynamics Laboratory program. Mr. Larry Kelly, AFFDL/FBSG is the Air Force Program Manager.

## MISSION ANALYSIS

The Supersonic Penetration Interdiction Fighter (SPIF) concept holds promise for successful accomplishment of strike missions against high value targets made unavailable to existing systems by increasingly sophisticated and severe threat environments. Designed specifically for supersonic attack, SPIF will penetrate area defenses, achieve a high level of strike effectiveness, and survive both the surface-to-air and air-to-air threat. Mission analyses resulted in the SPIF mission profile shown in Figure 1. The selected 1.6M cruise gives a high probability of survival at lowest costs. Higher cruise speeds require a more complex and expensive aircraft while lower cruise



speeds increase probability of loss. Design goals, in terms of range, acceleration, maneuverability, weapons, and take-off and landing distance are shown in Figure 2. Achievement of these goals will result in an aircraft which will have performance similar to that of the F-15 in combination with the supersonic range capability of the F-111.

#### CONFIGURATION SCREENING

Configurations capable of performing the desired SPIF mission were evaluated using sizing computer programs. Primary input data included: weight reduction factors for advanced composite materials; performance characteristics of candidate engines; mission requirement constants; and gross aerodynamic planform characteristics.

Weight reduction factors (over a 1975 metal aircraft) were obtained from analysis of percentage weight savings-versus-percentage weight of composite material data from available funded programs and in-house studies. This was done on a component-by-component basis. Values were selected which are associated with low cost (Design-to-Cost) approaches rather than those which achieved maximum weight savings regardless of cost. Figure 3 shows a plot of data resulting from composite empennage programs and studies and Figure 4 shows the weight reductions utilized to screen candidate ADCA configurations as well as those used to screen comparative advanced metal designs. The ADCA has an airframe which utilizes approximately 75 percent composite materials by weight whereas the advanced metal aircraft weight savings relate to a 1980 aircraft which has an airframe composed, by weight, of 75 percent advanced metallic materials and 15 percent advanced composite materials.

Engine candidates were, by Air Force direction, confined to those presently available or readily derived by 1980. This requirements limited candidates to current or growth versions of existing engines, specifically the F100, F101, F404, F101 and the TF30. The TF30 series engines were found to have non-competitive thrust-to-weight ratios while the more advanced F101 versions were avoided since they are unlikely to be readily available. Performance characteristics of the F100, F101 and F404, suitably modified for installation effects, were used as inputs to the screening process.

In addition to the ADCA design goals (Figure 2), other mission requirement constants such as uninstalled avionics weight, weight of gun provision, combat fuel allowance and limit load factors (6.5g at flight design gross weight) were input into the screening process.

Various aerodynamic configurations with different wing planforms were selected for screening. The delta planform exhibited the best supersonic characteristics whereas the more conventional transonic swept-wing configuration exhibited the best transonic maneuver capability. The trisonic wing is an optimized combination of the two. Variable sweep was included since it has potential for matching configuration to the various flight regimes. Aerodynamic inputs were defined following analysis of historic NASA and Grumman data together with the results of recent and current Grumman advanced configuration studies. These represent subsonic and supersonic cruise parameters consistent with a modest improvement in recently demonstrated values while transonic and supersonic maneuverability estimates were based on results from recent Grumman wind tunnel tests.

The results of a typical configuration screening are shown in Figure 5 and show the trisonic configuration with either a single F101 or two F404 engines to be the lightest design. The higher weights of the delta are the result of the low wing loadings required to achieve acceptable take-off and maneuver performance while the variable sweep aircraft suffers from the difficulties in effectively utilizing composites for such configurations. The transonic configurations are close contenders, however, more detailed studies of both these and the trisonic configurations indicated that the former are somewhat heavier than shown on the figure whereas the latter appear to be almost 500 pounds lighter. It was therefore decided to choose the trisonic configuration and the more detailed studies showed that this configuration with either a single F101 or two F404 engines was acceptable and almost equal in performance and weight. Selection of the single F101 version was made after consideration that this engine is under development for the B-1 and will be fully qualified by 1980. In contrast, the F404 development program, as associated with the F-18, is not currently on a firm approved schedule. An engine qualification test is possible by 1979 but is tied directly to a go-ahead for the F-18 program.

The general arrangement of the selected ADCA configuration is shown in Figure 6 and the inboard profile is shown in Figure 7. As can be seen from the latter figure, the aircraft is not very densely packed with equipment. The subsystems and the location of avionics, weapons and crew systems in the forward section provide for easy access and maintenance.

#### COMPOSITE AIRFRAME

The primary objective of the first task of the ADCA program was a detailed definition of the air vehicle configuration. The structural interface required establishment of groundrules to effect maximum benefit from use of composite materials together with sufficient structural definition necessary to assure structural feasibility and attainment of performance and cost objectives.

#### Material Selection

Various factors were taken into account in formulating a list of candidate composite materials and their application to the various component parts of the ADCA (Figure 8). The first factor is availability in the late 1970's of fully qualified systems. Full qualification of new fiber/matrix systems requires a considerable investment of both time and money. The boron and graphite fibers in use today were developed over ten years ago as were the generic epoxy matrices. The only new fibers which may be fully qualified by 1980 are the pitch based graphite fibers and the boron-on-carbon monofilaments. These fibers should have properties similar to today's graphite and boron fibers but should be considerably cheaper.

Organic matrix materials are being developed which should be less sensitive to moisture pickup experienced by current epoxy matrices. The emerging thermoplastic matrices (polyimides, polyarylates and polyphenylenes) show promise and could reduce processing costs. They are, however,

not yet qualified nor has their sensitivity to moisture been fully defined.

The only metal matrix systems qualified today, and likely to be qualified by 1980, are boron and Borsic/Aluminum. Graphite/aluminum qualification appears to be at least ten years away even if its properties become more promising. Current properties of the epoxy matrix composites are therefore being used for this study and their application has been limited to a maximum temperature of 250 F since this is below the glass transition temperature of the matrix when subjected to the combined effects of humidity exposure and thermal spikes. Boron/aluminum is a contending material for regions such as the engine bay where temperatures may be higher and a measure of fire prevention is required.

An allowance has been made for protection against lightning strikes and triboelectric charging. This protection takes the form of flame sprayed or foil aluminum bonded both externally and internally to the structure.

Since the study requires maximum utilization of composites only HRP, Kevlar 49 or graphite honeycomb core is utilized for sandwich construction. This eliminates potential problems associated with corrosion of aluminum core due to moisture ingress. Fastener corrosion problems are also minimized since only A286 stainless steel or titanium fasteners will be permitted in laminates containing graphite.

#### Design/Manufacturing Interface

In order to achieve a low cost but efficient composite airframe, a strong design/manufacturing interface has existed from program initiation. The intent of this interfacing between design, tooling, manufacturing and quality control is to determine interdisciplinary requirements, capabilities and limitations and to reach a compromise solution to achieve a low cost but efficient structure. Structural simplicity is a major factor since reduced part count impacts both assembly and logistics costs. In addition, combination tooling can reduce both fabrication and assembly costs. Finally, inspectable, damage tolerant concepts can provide fewer fabrication rejects and benefit in-service repairability.

#### ADCA Structural Arrangement

The structural assembly of the ADCA airframe concept is shown in Figure 9. This concept maximizes the use of large integral components to minimize costs. Many of these components, as will be described later, utilize a co-cured approach to reduce fitup time and assembly costs.

Various wing box structural configurations were studied. These included the high wing one-piece center box concept shown in the figure; concepts associated with a mid-wing configuration where the wing and center fuselage are fabricated as an integral assembly; and concepts where the wing is mechanically attached to the fuselage side using "banjo" frames. The one-piece through wing concept was found to be both the lightest and cheapest approach and was therefore selected.

The wing was aerodynamically optimized to improve baseline performance as shown in Figure 10. The optimum aerodynamic twist distribution for supersonic cruise was matched and various approaches to induce the required twist were studied to obtain maximum transonic sustained maneuver capability. The most efficient approach was twist induction using bending/twist coupling of the outer supercritical portion of the transonic wing. This was accomplished, with no weight penalties for flutter, by skewing the axis of the outer spanwise cover plies forward 15 degrees relative to the outer box structural axis. Figure 11 shows loading and layup and Figure 12 shows the effect of this aeroelastic tailoring wherein the tailored wing box achieves a twist distribution which is close to the requirement and obtains 95 percent of the optimum sustained transonic maneuver capability with no supersonic cruise penalties. Preliminary flutter analyses show the wing to be flutter free as shown in Figure 13.

Various types of construction were studied to determine the optimum wing box configuration from a weight/cost standpoint. These are shown in Figure 14 and the selected distributed, multi spar, concept for the center box, which forms a fuel cell, is shown in Figure 15. Two alternative variations of this concept will be studied in more detail. The first is an all-graphite/epoxy box where all the layers are uniformly distributed throughout the covers and these are supported by graphite/epoxy channel section front and rear beams and sine-wave intermediate beams. The second approach uses local pads of boron/epoxy with graphite/epoxy softening strips above each of the beam caps to provide a good measure of damage tolerance and fail safe capability. The effectiveness of this approach has been demonstrated by tests on subcomponents of the B-1 horizontal stabilizer which utilizes the same concept.

Similar studies were made to screen candidate structural configurations of the canard and the vertical stabilizer. Aeroelastic tailoring studies of the vertical stabilizer showed that flutter penalties could be reduced by rotating the spanwise plies 15 degrees aft relative to the box beam axis. The remaining  $\pm 45$  and 90 - degree plies were oriented in these directions relative to the box axis. Figure 16 shows the effect of rotation of the spanwise plies.

Fuselage design requirements are shown pictorially in Figure 17. Various forms of construction are candidates and these are all likely to be used in different areas of the fuselage. The forward fuselage will probably utilize the shell-liner approach developed by Convair-Fort Worth. The center fuselage, which forms the major fuel tank, will probably use a co-cured sandwich approach. Both face sheets and core would be composite material. Access doors would be of similar construction but would have edge protection in the form of integrally molded metal foil, or woven fiberglass/epoxy to minimize handling damage and provide the composite with improved pull-through strength at boundary fastener holes. The metal foil would also provide lightning strike protection to the composite material and the subsystems.

## MANUFACTURING PLAN

The manufacturing procedures associated with fabrication and assembly of the ADCA structure must be kept as simple as possible in order to minimize costs. In addition, the structure must be designed to be inspectable during both the fabrication cycle and during the aircraft service life. A preliminary manufacturing plan is shown in simple form in Figure 18. This plan closely integrates the design, manufacturing and quality control disciplines in order to achieve the objective of low cost at minimum sacrifice of air vehicle performance.

## COMPOSITE VERSUS METAL AIRPLANE COMPARISONS

As part of this study, 1980 advanced metal aircraft were sized to perform the same mission as ADCA. The weight reductions over current metal aircraft shown in Figure 4 were used for this study. Weights of the selected ADCA are compared to weights of advanced metal and composite substitution aircraft in Figure 19. The latter aircraft were sized for both the engines used for the ADCA screens and for "rubber" versions of these engines. The incremental weight differences between the ADCA and the advanced metal aircraft is a result of material differences plus size effects. The metal aircraft must grow in size to perform the baseline mission and it is therefore necessary to make large step changes in propulsion to maintain a constant level of performance. Substitution of composite for the metallic materials used in the metal aircraft, without changing vehicle size or engines, results only in a moderate weight reduction but would improve performance. This effect is shown more dramatically in Figure 20. The composite substitution aircraft has a 13 percent reduction in structure weight and a 6 percent reduction in takeoff gross weight. In contrast, the smaller composite designed aircraft (ADCA) has a 35 percent saving in structural weight and a 26 percent saving in take-off gross weight. Fuel savings amount to 30 percent which may be very significant for aircraft operating in the 1980 time frame. In addition, a preliminary evaluation indicates that production costs of the smaller ADCA aircraft should be 21 percent lower than the larger advanced metal aircraft.

## CONCLUSIONS

Initial results of the ADCA study program indicate that there are significant benefits to be gained by applying advanced composites in an unrestrained fashion to a completely new aircraft which is designed to perform a difficult mission which could be vital to the Air Force in the 1980 time period. Composite materials give us a unique capability to significantly reduce aircraft size and both procurement and life cycle costs with no sacrifice to performance.

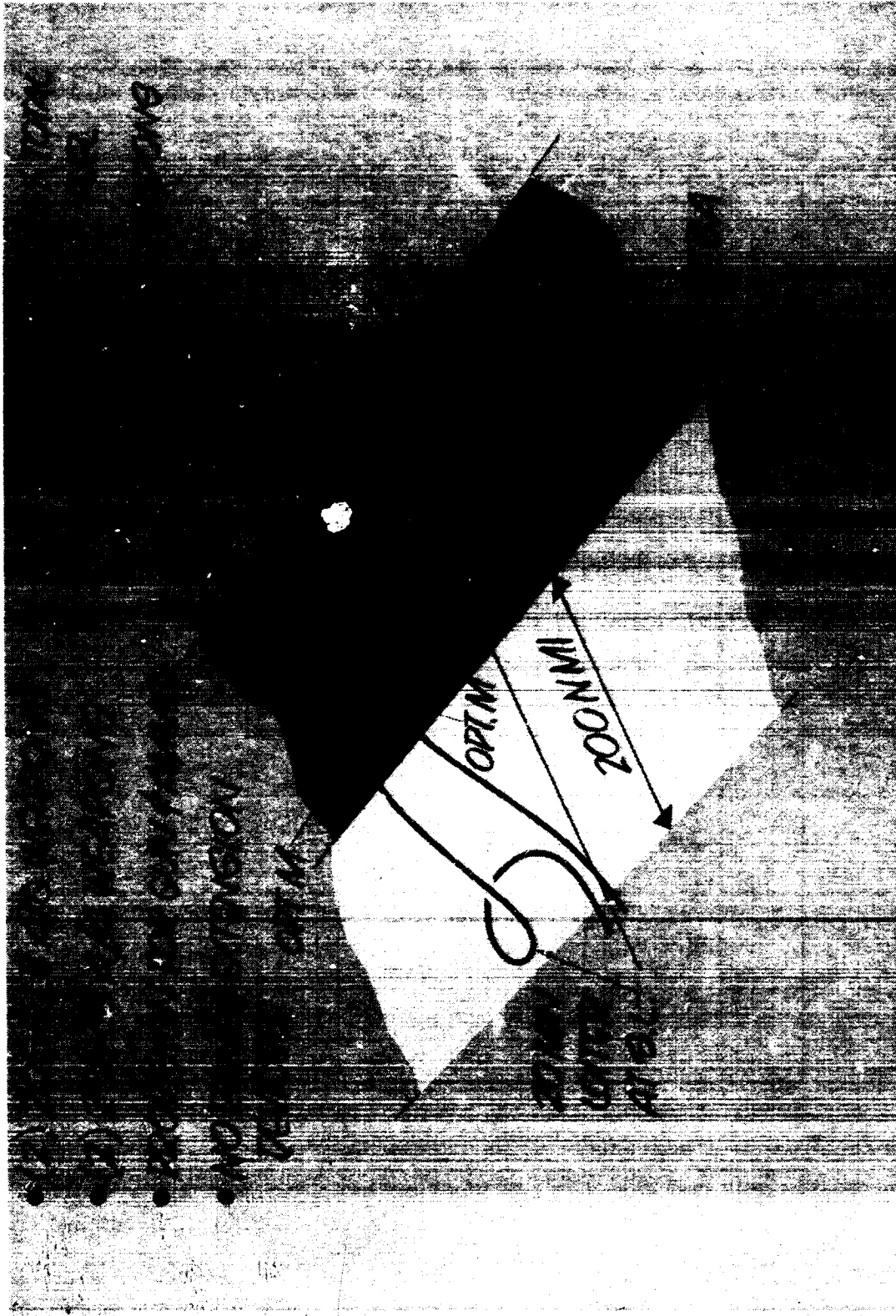


Figure 2.1.1. Mission Profile

	NOMINAL	TRADEABLE RANGE
RADIUS (OPT. MACH), N.MI (SUB/SUPER)	200/200 N.MI	150 - 250 N.MI
SUPERSONIC CRUISE M	1.6 M	UP TO 2.0 M
SUPERSONIC CRUISE ALT, FT	OPT	—
ACCELERATION	80 SEC	55 - 80 SEC.
MANEUVERABILITY INST G @ CL. M/ALT BUST G @ 9M/50K FT BUST G @ 12M/50K FT	5.0 3.8 4.4	4.5 - 6.5 3.0 - 5.0 4.0 - 5.0
AVIONICS WEIGHT, LB A/G WEAPONS WT, LB	1550 4000	850 - 1700 4000 - 8000
T.O. & LUG DIST, FT (GROUND ROLL)	3200	2000 - 5000

Figure 2 ADCA Design Goals

COMPONENT	COMPOSITE
<b>HORIZ STAB</b>	
F-14	B/Ep
F-111	B/Ep
F-5	GR/Ep
A-5	GR/Ep
B-1	GR-B/Ep
F-15	B/Ep
<b>VERT STAB</b>	
F-5	GR/Ep
F-15	B/Ep
B-1	GR-B/Ep
B737	GR-B/Ep

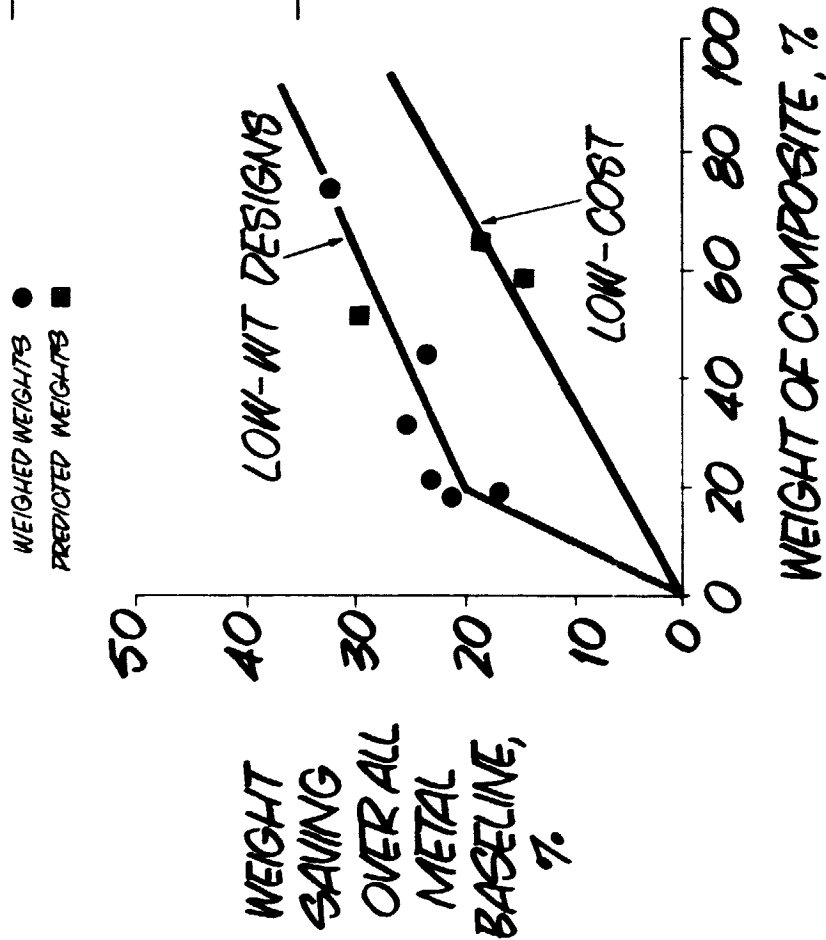


Figure 3 Advanced Composite Empennage Weight Savings



COMPONENT	WT SAVINGS, %	COMPOSITES GOAL, %	ADVANCED METAL AIRCRAFT WT SAVINGS, %
FIXED WING—NO TWIST CONT —WITH TWIST $\Delta = 20^\circ$ $40^\circ$ $60^\circ$ —DOUBLE DELTA	28	} 87	9
	26.5		
	23		
	17		
23.5			
SWING WING—NO TWIST CONT —WITH TWIST CONT	20	} 65	9
	17		N/A
TAILS & CANARDS—SLAB —FIXED	23	} 79	9
	30		9
BODY	20	72	3
AIR INDUCTION—FIXED INLET —VAR INLET	22	80	5
	20		5
LANDING GEAR	16	40	10

Figure 4 Weight Reductions Over Metal Airframes

- AVAILABLE OR LOW COST DERIVATIVE ENGINES
- BASELINE MISSION
- SIZE FOR MOST CRITICAL OF : 3.5 G SUPT @ 9M/30,000 FT  
3200 FT T.O. GND ROLL W/10,000 LB A/G WEARONS  
3200 FT LDB GND ROLL

AIR VEHICLE ENGINES	TOSW, LB/ACCEL TIME, SEC (M · S TO 1.6 @ 59,000 FT)					
	DELTA	DELTA WITH RETR CANARD	TRISONIC WITH CANARD	TRANSONIC W/AFT TAIL	VAR/- SWEEP W/AFT TAIL	
1 F404	NO SOLUTION	NO SOLUTION	NO SOLUTION	NO SOLUTION	NO SOLUTION	
2 F404	42650/110	39878/85	37489/72	37976/75	40620/88	
3 F404	45679/55	45187/52	44047/49	44299/49	47609/55	
1 F100B	NO SOLUTION	NO SOLUTION	NO SOLUTION	NO SOLUTION	43013/166	
2 F100B	49199/59	48148/55	47201/52	47446/52	51499/59	
1 F101	45208/156	39922/91	37826/79	37941/78	41470/92	

Figure 5 Typical Configuration Screen

ORIGINAL PAGE IS  
OF POOR QUALITY

- (1) F 101-GE-100
- TOGW = 37,357 LB
- W/S = 90 PSF

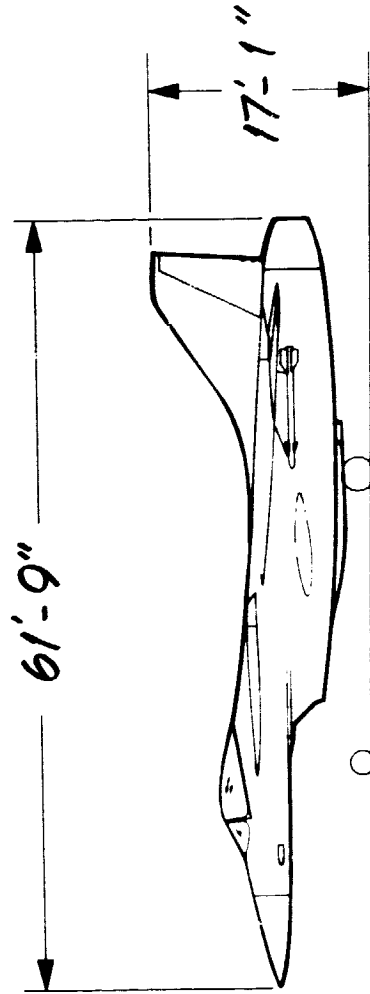
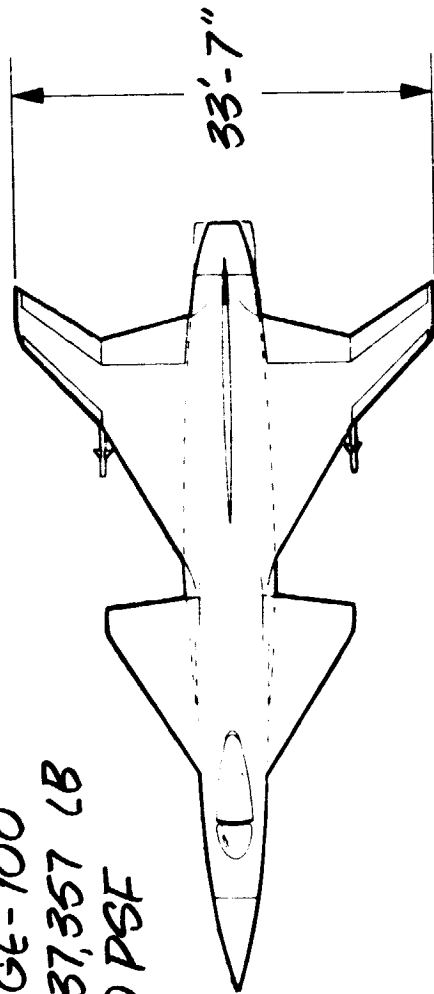


Figure 6 Two Views of Selected Configuration



COMPONENT	COMPOSITE MATERIAL*				
	B/EP	GR/EP	GL/EP	K49/EP	B/AL
WING	•	•	•	•	•
FUSELAGE	•	•	•	•	•
EMPENNAGE	•	•	•	•	•
LANDING GEAR	•	•			•
CONTROL SURFACES, FLAPS, ETC		•	•		
ACCESS & GEAR DOORS		•	•	•	
RADOME			•	•	
AIR INDUCTION		•	•	•	•

\* EITHER UNITARY OR IN COMBINATION (HYBRIDS)  
(THERMOPLASTIC MATRICES COULD BE USED IN PLACE OF EPOXY WHEN SUFFICIENTLY DEVELOPED)

Figure 8 Candidate Materials

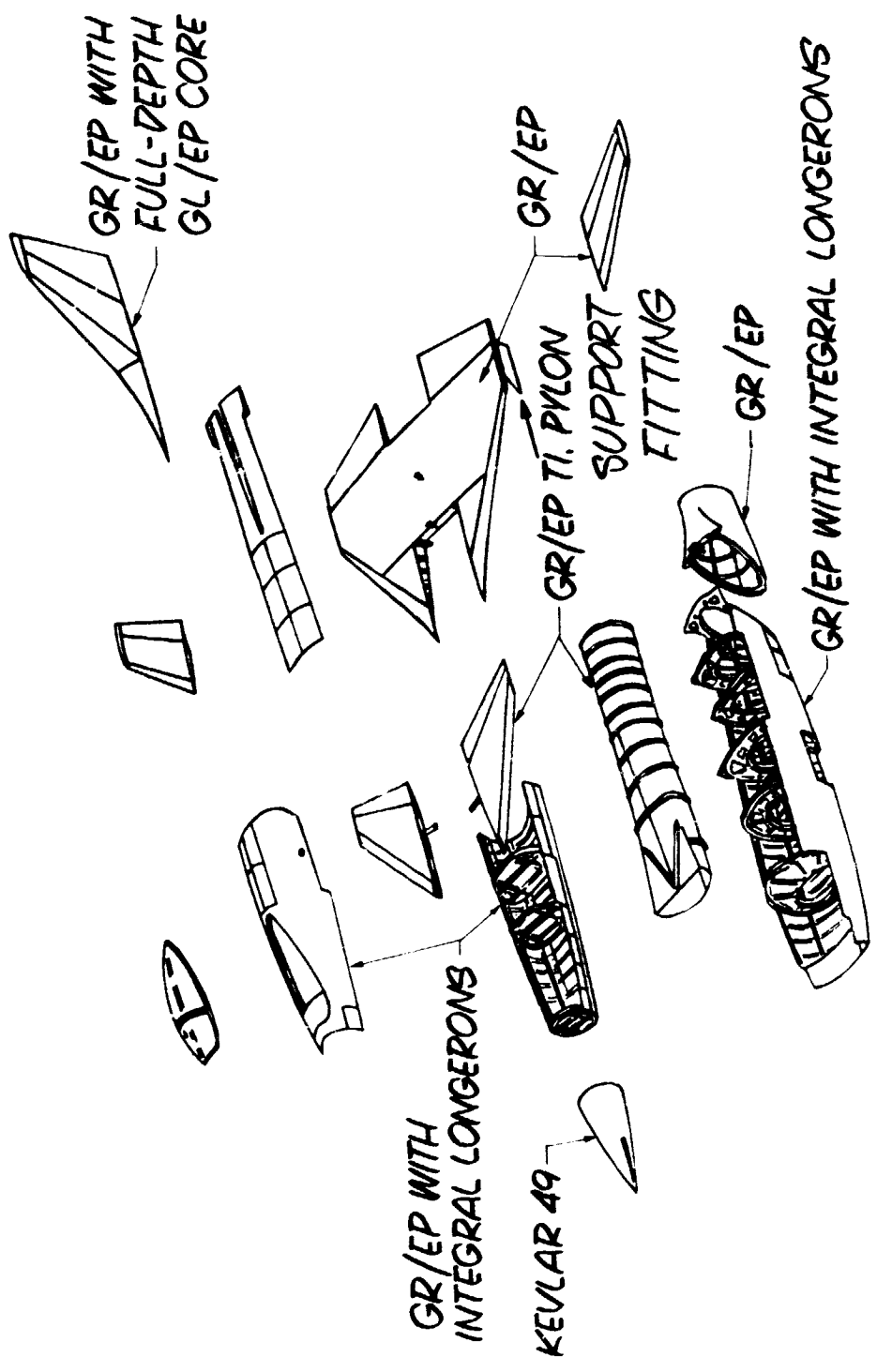
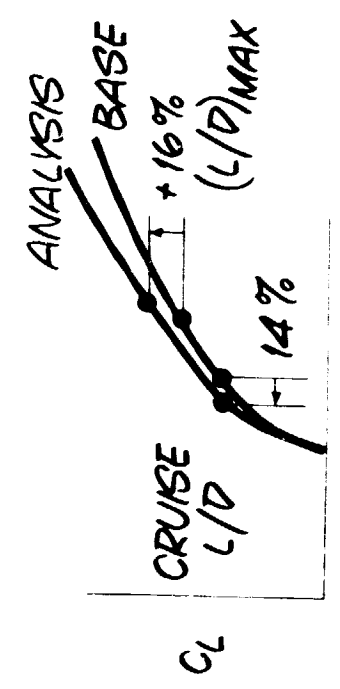


Figure 9 ADCA Structural Breakdown

- WING - BODY ANALYSIS
- MACH 1.6



FUSELAGE STATION

Figure 10 Wing Aerodynamic Optimization

- T/C = 3% / 5% / 5%
- PRELIMINARY COVER AXIAL LOADS & LAMINATES
- 9.75 G ULT
- ALL GRAPHITE LAMINATES

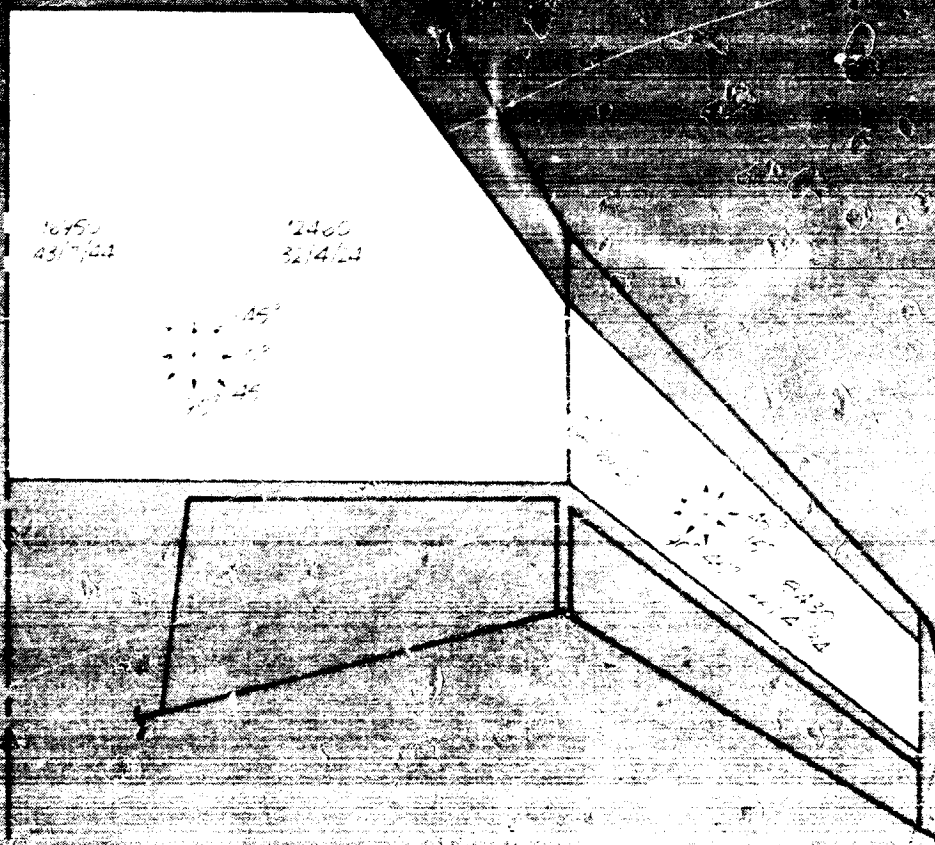


Figure 11 Cover Section (all views)

ORIGINAL PAGE IS  
OF POOR QUALITY



- 1.0 G & 3.8 G
- ADCA 105 B WING (3% / 5% / 5%)

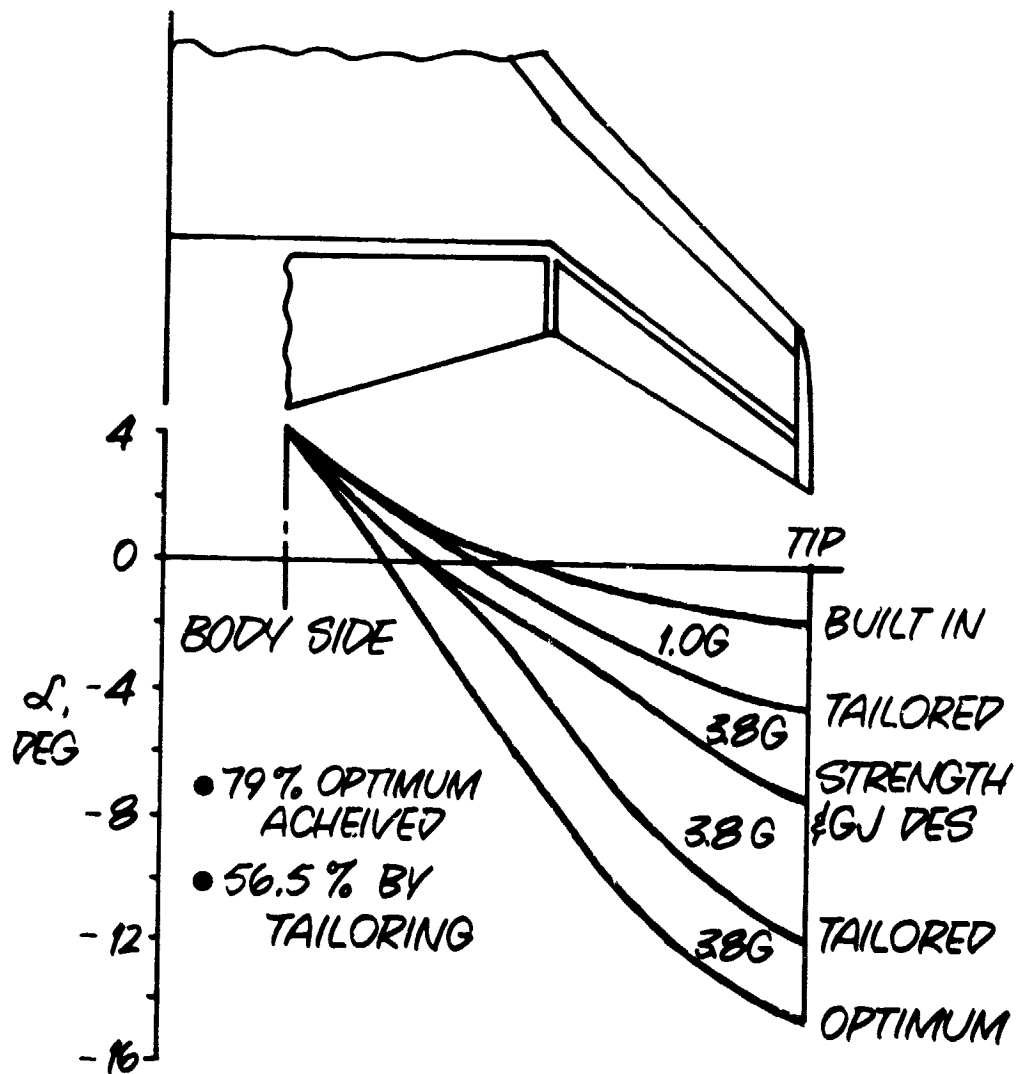


Figure 12 Wing Twist Distributions

- ALL GRAPHITE
- T/C = 3% / 5% / 5%
- 0° LAYERS KICKED 15° FWD

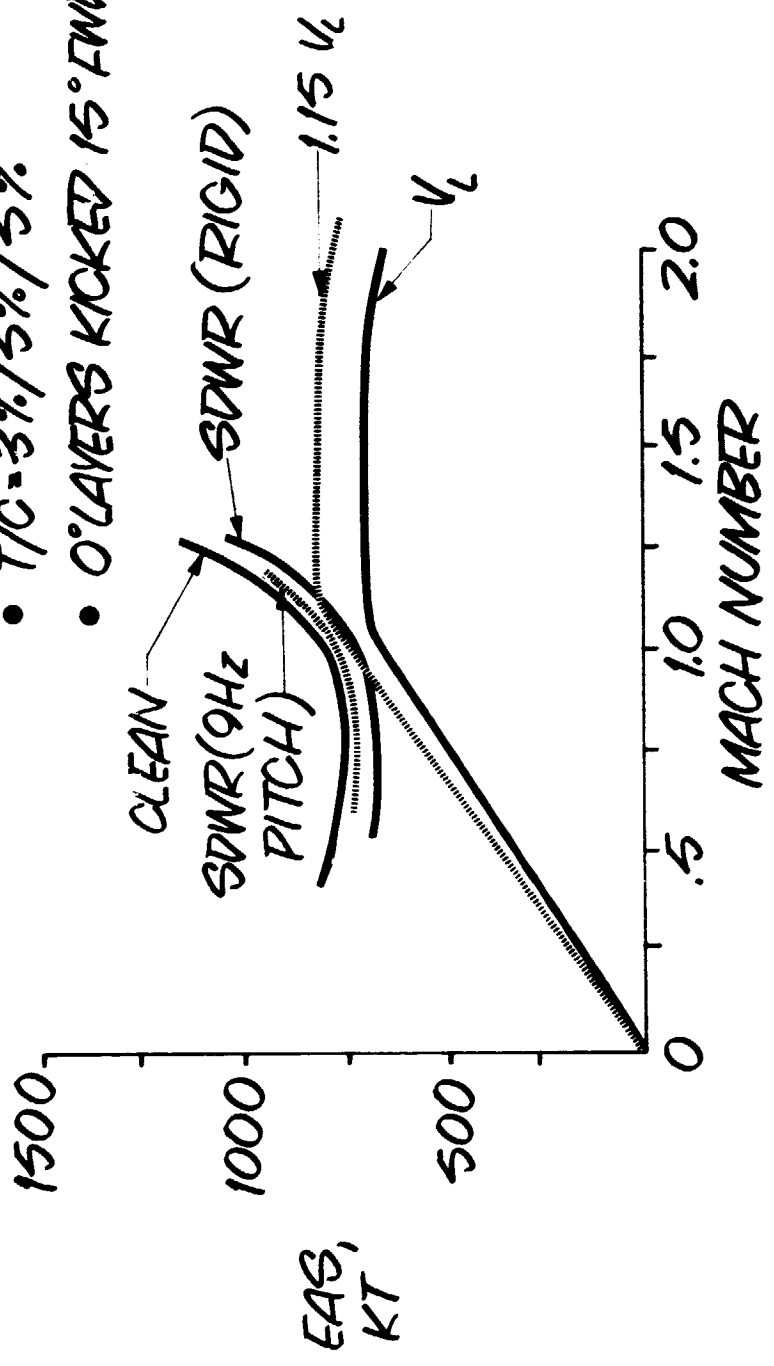


Figure 13 Wing Flutter Envelopes

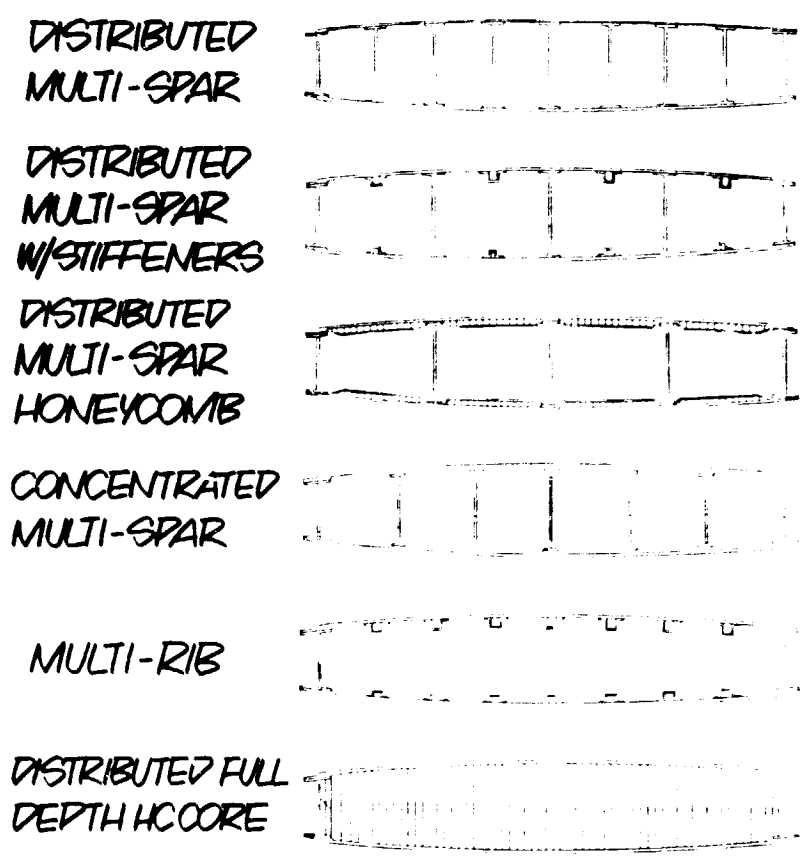


Figure 14 Wing Box Concepts

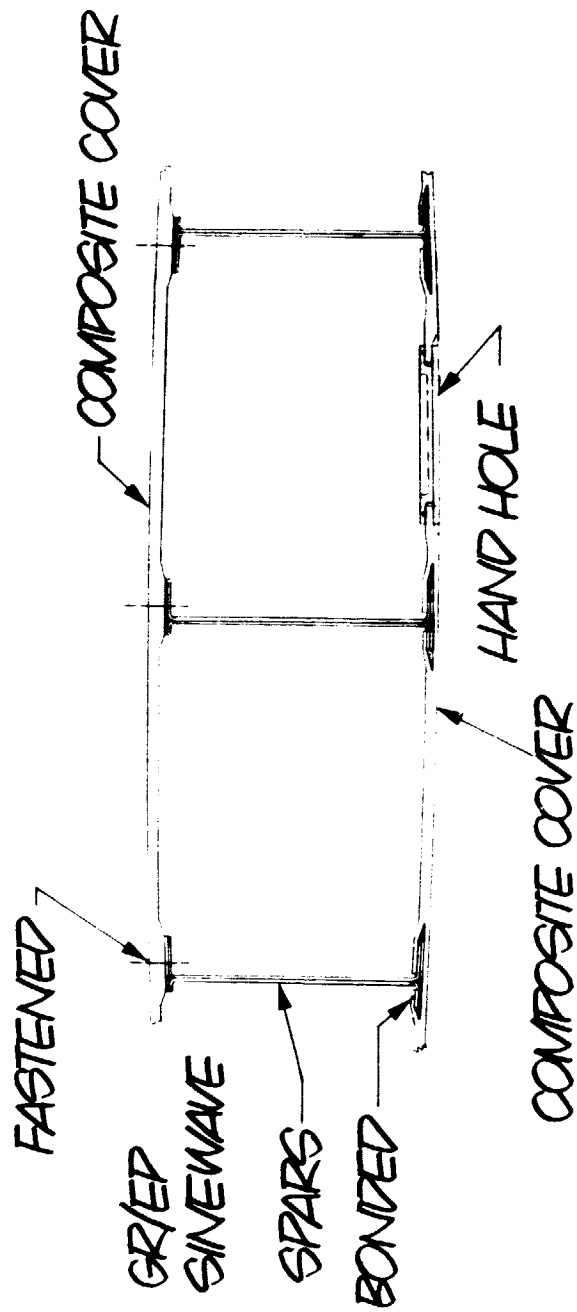


Figure 15 Center Section Wing Structure Concept

- FLUTTER SPEED INCREASE THRU STIFFNESS TAILORING
- ALL GRAPHITE COVER LAYUP

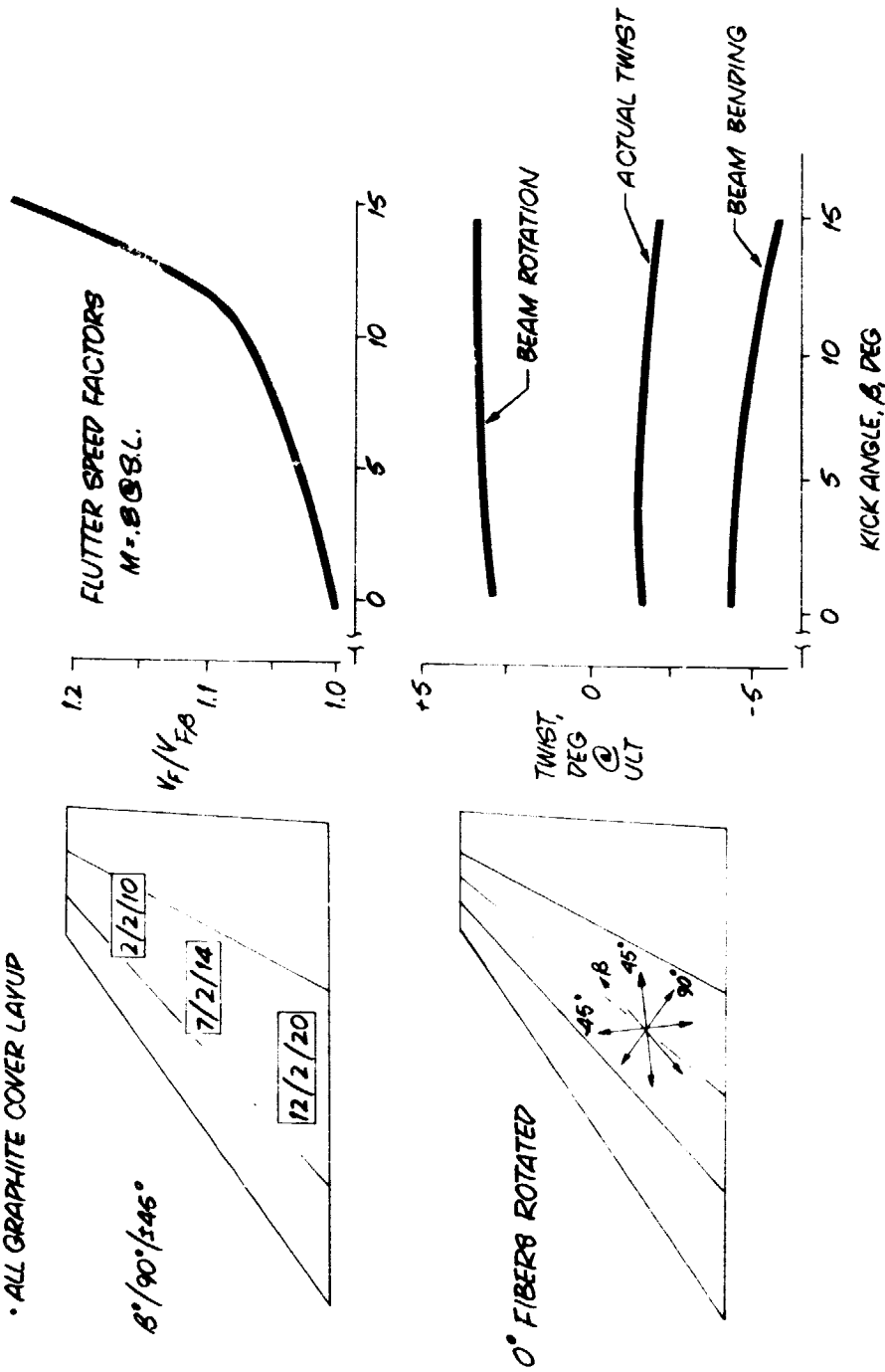


Figure 16 Vertical Stabilizer Aeroelastic Tailoring

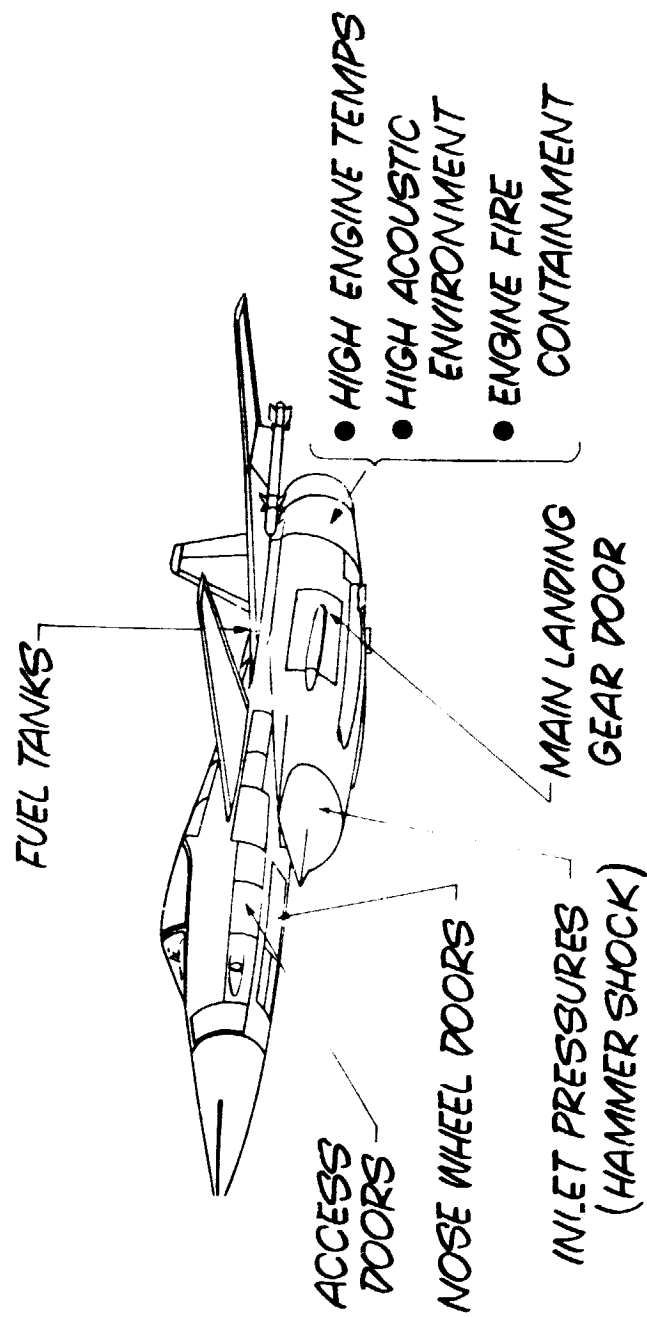
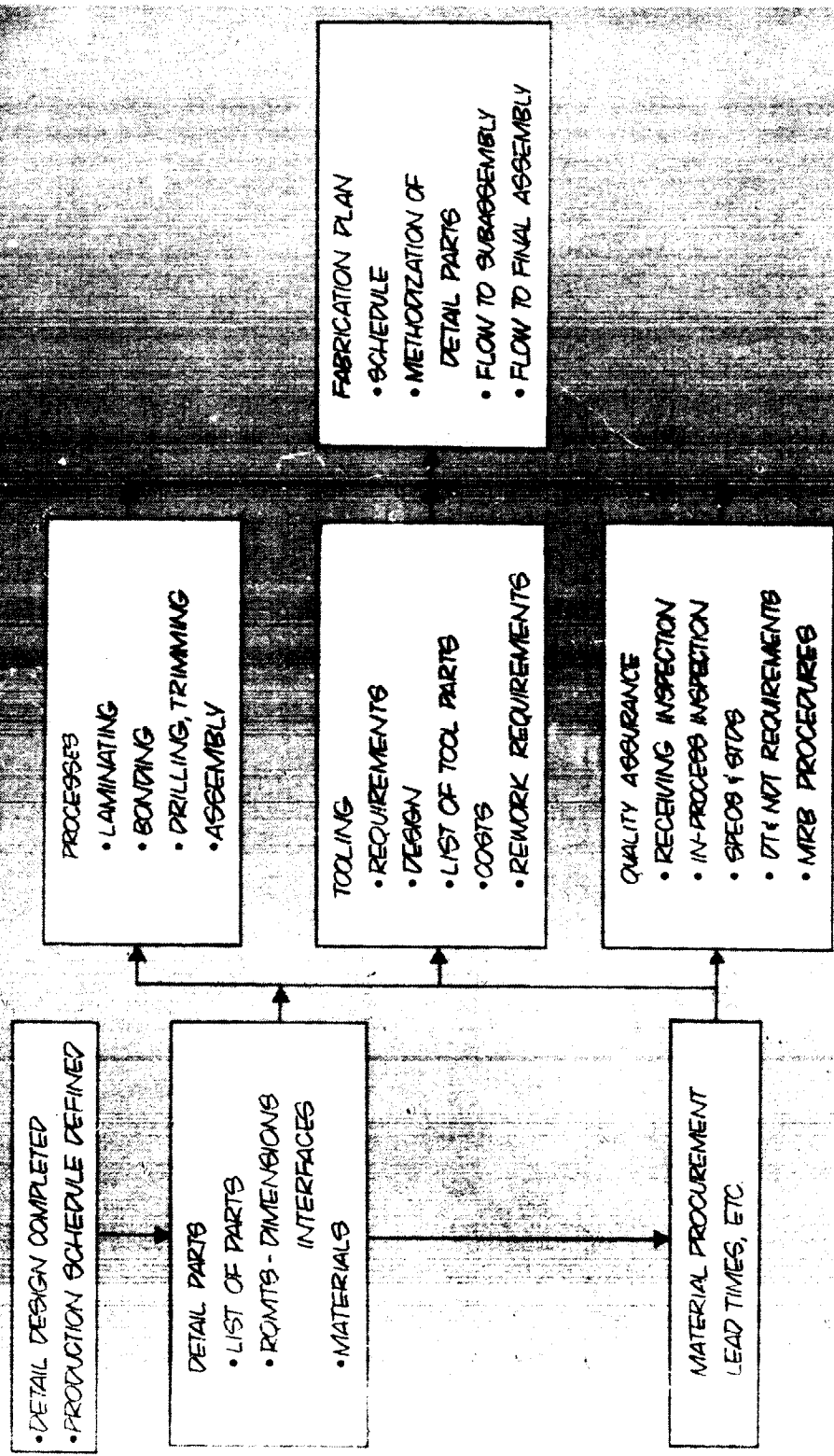


Figure 17 Fuselage Design Requirements



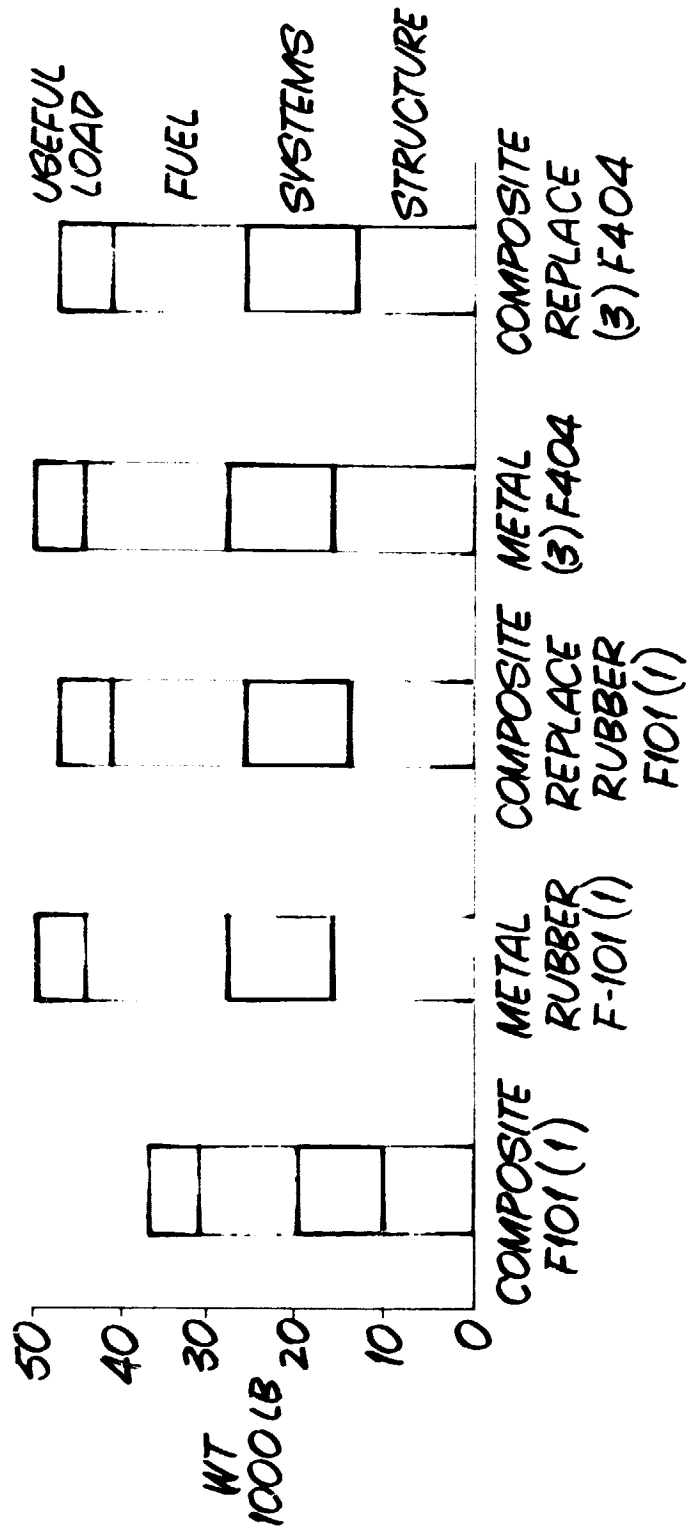


Figure 19 Comparative Weight of ADCA Metal and Composite Replacement Aircraft



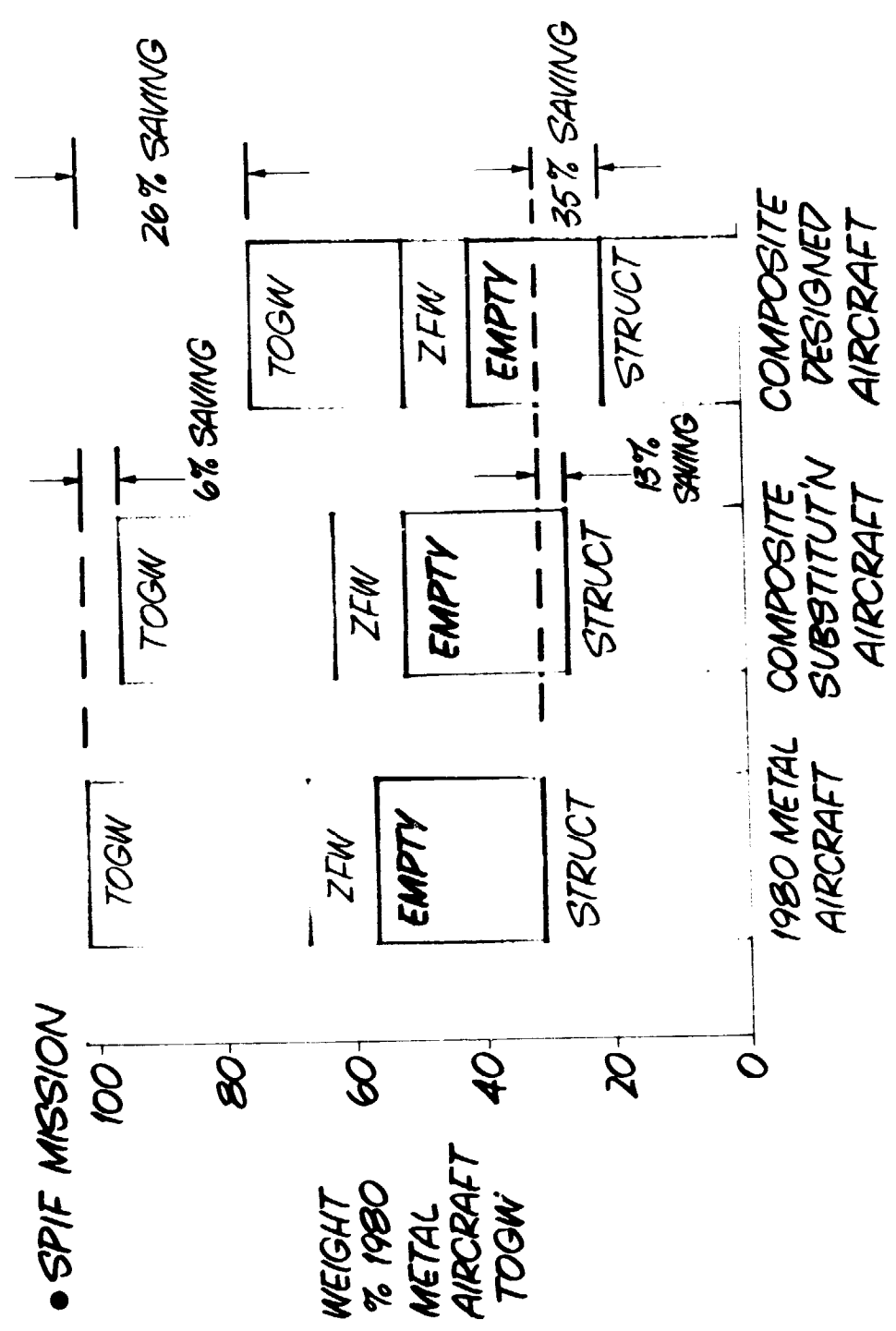


Figure 20 Comparative Weight of ADCA Metal and Composite Replacement Aircraft

A HYBRID COMPOSITE FUSELAGE DESIGN WITH  
INTEGRAL CRACK ARRESTERS

By S. L. Huang and T. E. Hess

Naval Air Development Center

SUMMARY

A damage tolerant hybrid composite fuselage section has been designed, fabricated and tested. One of the key features of this structure is the integral crack arresters which have been incorporated into the design to increase its tolerance to damage, either inherent flaws or battle induced damage. The ability of the design to withstand critical flight loads has been demonstrated by both analysis and test. The effectiveness of the crack arresters, which are designed to stop a propagating crack (damage) and still allow the structure to carry limit load, was proven in a series of tests where the initial damage was of two types, a preformed crack cut with a saw blade and that resulting from projectiles fired into the shell. The design has been completely analyzed using finite element techniques and shown to save both weight and cost over its metal counterpart. Analysis and testing of composite panels has also been done to investigate failure modes and establish design criteria for crack arrester designs.

INTRODUCTION

The objective of this work was to develop a low cost, survivable fuselage design in order to extend composite materials application to fuselage structures, apply crack arrester designs to an actual flight structure and obtain reduced weight and cost compared to a metal counterpart. The center fuselage section of the BQM-34E Remote Piloted Vehicle, figure 1, was selected as the demonstration vehicle for this design/development. Although the technology presented here is directly applicable to manned aircraft, the RPV affords a basis for comparison between an inproduction, operational, metal counterpart and the redesigned composite version, and it provides an opportunity for near-term flight demonstration in both the subsonic and supersonic regimes. This same vehicle has been used as a test bed for an all graphite epoxy wing which was designed and fabricated at the Naval Air Development Center and which is currently flying on operational vehicles as part of the Navy's service evaluation program. This center fuselage section provides a practical design model since it contains access doors, wing attachment points, external fuel tank attachment and the recovery parachute line attachment.

## FUSELAGE DESIGN

The BQM center fuselage is a circular section 63.5 cm (25 in.) in diameter and 104.14 cm (41 in.) long. The through-wing is attached to this section in the upper portion of the cross section and an overwing structure covers the wing and closes out the circular shape. A large door is at the bottom and runs the entire length of the section. Attached to the door is a keel which also extends over the length of the section at its bottom. A large shear fitting extends over the first 20.32 cm (8 in.) of the section between two bulkheads to resist loads from the parachute lines.

In designing the composite fuselage section two design conditions were considered, based on a review of the metal design. The first, and most important, condition is a recovery condition in which 7.4g is developed by a 66720 n (15000 lb.) load on the parachute line which is attached at the top of the fuselage near the forward end of the center section. The inertia loading of that part of the fuselage forward of the center section produces a large bending moment, which is applied to the center fuselage section over only slightly more than the upper half of the circumference. It is this condition that sizes the center fuselage shell. A 5g maneuver in free flight produces maximum wing loading, which in turn puts maximum loading on the wing attachment bolts. This condition induces local load in the fuselage in the circumferential direction, and the shell must be checked for its ability to react these loads.

Tradeoff studies were conducted for these conditions to select a material and type of construction for this application. The criteria for selection were weight, costs, survivability and ease of manufacture. These composite materials were considered - graphite epoxy, glass epoxy and a hybrid with both glass and graphite. Advantages of the glass included its low cost and high fracture toughness. However, its low stiffness compared graphite resulted in the overloading of certain metal parts in the center fuselage which were not being replaced by composite materials. In addition, since the center fuselage section is primarily buckling critical the glass epoxy design is heavier than that of the graphite. Therefore, to achieve a good balance among weight, stiffness and fracture toughness a hybrid composite was selected consisting of unidirectional graphite epoxy in the axial ( $0^\circ$ ) direction and glass epoxy fabric with the fibers oriented  $\pm 45^\circ$ . The graphite epoxy used was 3501 A/S and the glass epoxy was E293.

Honeycomb sandwich construction was selected on the basis of its high buckling resistance, ease of fabrication and reduced parts count compared to the metal design, the last two aimed at reducing cost.

Figure 2 shows a cutaway view of the existing metal design and the redesigned composite. The overwing fairing which is not being changed is not shown here. As can be seen from these sketches the intermediate frames and the longerons are being eliminated in the composite design in favor of the overall stiffness increase with the honeycomb sandwich. The basic design is

the 0.63 cm (.25 in.) aluminum honeycomb core, an inner face consisting of one ply of 0° graphite and one ply of glass fabric oriented ±45°, and a similar outer face with a second layer of glass fabric on the outer surface for additional impact and damage resistance. All areas near bulkheads, doors and other attachment have additional plies for reinforcement and introduction of load into the sandwich.

This design was analyzed for the two flight conditions using the NASTRAN program. In general, the recovery condition produced maximum stresses. A summary of this analysis is shown in figure 3. The design was also checked for stability under combined longitudinal compression and shear. A summary of critical conditions for the design is shown in figure 4 which indicates that buckling, facing compressive strength and facing shear strength form the capability envelope for the fuselage section.

#### CRACK ARRESTMENT DESIGN

The design of the crack arrestment system involves a consideration of three failure modes as shown in figure 5. The first failure mode is the initial propagation of the crack or damage. The arrestment of this crack is tied in with the second failure mode, that of propagation of the crack through the arrester strip. The third failure mode is shear failure along the interface between the arrester strip and the primary material containing the crack. This shear stress results from a redistribution of load around the cracked material which is no longer carrying any tensile load.

The analysis presented in reference 1 is the basis for the analytical treatment of the first two failure modes. It is summarized here for convenience and completeness.

The critical stress at which an existing through crack will propagate, figure 6, is:

$$\sigma_c = \frac{K_Q}{\sqrt{\pi(c+a)}}$$

where

$K_Q$  = fracture toughness

$a$  = characteristic dimension of intense energy region

$2c$  = crack length

$K_Q$  and  $a$  are determined from two tests, one with a crack and one on an uncracked control specimen.

$$a = \frac{l}{\left(\frac{\sigma_{\infty}}{\sigma_c}\right)^2 - 1}$$

$$K_Q = \sigma_{\infty} \sqrt{\pi a}$$

where

$\sigma_c$  = applied failure stress for specimen with crack

$\sigma_{\infty}$  = failure stress of uncracked specimen

The function of the low modulus arrester strips is to provide a low stress, high toughness region which will render a crack entering this region non-critical.

Applied to a crack in the primary material this equation defines a stress at which initial propagation occurs. When the crack has reached the arrester strips with its tips extending into the strip the above equation can be applied to the arrester strip material with a crack length equal to the spacing of the strips,  $w_1$ . In order for the crack to be arrested and the structure continue to carry limit load, the arrester strip must have a width, toughness and modulus such that a crack whose length is  $w_1$  will not propagate. This fail-safe requirement is expressed analytically as follows:

$$\sigma_c = \frac{K_{Q2}}{\sqrt{\pi \left(\frac{w_1}{2} + a_2\right)}} \geq \frac{E_2}{E_1} \sigma_{1 \text{ limit}}$$

Meeting this condition guarantees that a laminate containing an arrested crack  $w_1$  long can withstand limit load, at least with respect to the first two failure modes. Conditions for the shear failure mode are not as easily expressed since the magnitude of maximum shear stress developed is a function of many parameters.

#### HYBRID COMPOSITE TESTING

Two series of tests are reported in the paper, the first, load and crack arrestment tests on hybrid sandwich panels and cylinder corresponding to the fuselage design, and the second, crack arrestment tests on solid graphite epoxy panels. This second group of tests was performed in order to evaluate the application of the crack arrester strip design to relatively thick monolithic laminates.

Prior to testing the hybrid cylinder, tests were performed on honeycomb sandwich panels of the same construction as the cylinder and the fuselage, including the crack arrester strips. The main purpose of these tests was to establish  $K_Q$  and a values for the hybrid face sheets. The tests were performed with .95 cm (3/8 in.) cracks and yielded the following results:

	$K_Q$	$a$
Outer Face	32.7 Mn/m <sup>2</sup> √m (29.8 KSI √in)	.185 cm (.073 in)
Inner Face	47.0 Mn/m <sup>2</sup> √m (42.8 KSI √in)	.208 cm (.082 in)

This shows that for a given crack size, propagation will occur first in the outer face of the sandwich.

Figure 7 shows the composite sandwich cylinder in the testing machine. The first two tests performed were compression tests to 50% and 100% of limit load, 186.8 Kn (42000 lb.) and 373.6 Kn (84000 lb.) respectively. The cylinder withstood these loads successfully, and no unusual behavior was observed. This was the basic demonstration of the ability of the design to take critical flight loads.

A second, and more comprehensive, series of tests was then performed to evaluate the crack arrestment design. First, proof tests were run at 50%, 75%, and 100% of design ultimate load as a demonstration of basic tensile strength. Then five additional tests were run with induced damage, as depicted in figure 8. For test 2 a 2.54 cm (1 in.) sawcut crack was formed midway between two adjacent crack arrester strips. Load was applied until the crack propagated. This occurred at 120% of design limit load (DLL). Propagation in this hybrid material was not at all sudden. The crack started to propagate at a particular load and continued to propagate gradually as the load was increased, until it reached the arrester strip. The propagation loads given here represent the load when the crack reached the arrester strip. Test 3 was a repeat of test 2 with identical results.

Tests 4 and 5 were different in two respects. First the damage was induced ballistically, and secondly, the structure was under a preload when the damage was induced. In test 4 a .95 cm (3/8 in.) projectile was fired into the cylinder. The damage which was produced had a maximum overall dimension of 2.22 cm (7/8 in.). The preload was 50% DLL. At the time of impact the damage did not propagate, but upon subsequent application of load propagation occurred at 114% DLL. In test 5 a 2.54 cm (1 in.) projectile was fired with 75% DLL preload. Again, the damage did not propagate at time of impact and in this case no subsequent load was applied.

The last test was with a 1.59 cm (5/8 in.) sawcut crack. Propagation in this case was at 129% DLL. It should be pointed out that at this time with 129% DLL on the cylinder, six of the twenty-two sections between crack arrester strips were cracked over their 7.62 cm (3 in.) width, so that even with con-

siderable damage the structure still withstood a high level of loading.

Figure 9 shows the cylinder after the testing. Closeup views of some of the propagated cracks are shown in figure 10. In figure 11 both the stress corresponding to the beginning of propagation and the stress when the crack reached the arrester strips are shown and compared to a curve drawn from the equations and the hybrid composite fracture data previously discussed. The data agrees reasonably well with the analysis, although it covers only a narrow range of crack sizes.

Actual fuselage parts have been made and will be assembled and tested at the Naval Air Development Center in the near future. One of the panels is shown in the untrimmed state in figure 12.

#### GRAPHITE-EPOXY PANEL ANALYSIS & TEST

Additional analysis and testing has been underway to further investigate, evaluate and characterize crack arrester designs with the goal of applying these designs to operational aircraft structures. In particular, this work has been aimed at demonstrating the capability of crack arrester designs, investigating thickness effects for solid laminates up to 1.27 cm (1/2 in.) thick, establishing and investigating failure modes, and establishing design data.

Failure modes have been discussed previously in conjunction with figure 5. Early testing indicated that the failure mode of shear along the strip boundary is the second failure mode to be encountered and the one which determines residual strength, that is, post-propagation strength. In order to quantitatively evaluate this shear stress finite element analysis was performed of three flat panel sizes, each containing a central crack, figure 13. Three sets of heavy lines in this figure outline the quarter-panel model. The crack arrester strips were 1.27 cm (1/2 in.) wide in all cases with 7.62 cm (3 in.) of primary material between them. The three full panel sizes which were analyzed, therefore, were 17.78 cm (7 in.) wide by 15.24 cm (6 in.) long, 35.56 cm (14 in.) by 40.64 cm (16 in.) and 53.34 cm (21 in.) by 60.96 cm (23 in.). The smaller panel contains two crack arrester strips or one full "bay" of primary material, and was analyzed first. The largest panel was analyzed next with the main objective being to see if the presence of several bays, all but the middle one being undamaged, would have an effect on the magnitude of the shear stress. As can be seen from figure 13 the maximum shear stress for the multi-bay configuration was reduced to about one-half of the single bay level, indicating that the additional width of material provided a longer path for the load to redistribute around the crack thereby reducing the shear stress magnitude. The intermediate size was analyzed to determine if a reduced length and width could be used to achieve the same results as the larger panel. Indeed the results for this were virtually the same as for the larger panel and it was concluded that the important thing is to have at least one undamaged bay on either side of the cracked bay to provide a path for load distribution. In order to be representative of flight structure sizes test specimens should also

be made this way. Multi-bay specimens are designed and will be fabricated and tested.

Concurrent with the above analytical effort a series of single bay test specimens were fabricated and tested. Four sets of these specimens were tested, each with a different thickness. Overall size was 15.24 cm (6 in.) x 25.40 cm (10 in.), figure 14, and the thicknesses were 1.52 mm (.06 in.), 4.06 mm (.16 in.), 6.35 mm (.25 in.) and 9.65 mm (.38 in.). In each case the first test was to determine the point of initial crack propagation. For small crack sizes and therefore high propagation stresses, the shear failure immediately followed the initial propagation. For the lower stresses this did not occur and a second test was performed to determine residual strength. Here also the failure was in shear. In none of the tests did the crack propagate across the crack arrester strips.

The results of this testing is summarized in figure 15. Three analytically predicted curves are shown there, one for each of the three failure modes, giving critical stress as a function of crack size. Test data is shown for the initial propagation and all points fell above the predicted curve which was drawn based on experimental determination of  $K_{Ic}$  and  $a$ . A second curve was drawn through the early test data and was very accurate in predicting critical crack propagate stress for the later tests. The curve shown in figure 15 represents a final empirical curve and is slightly different from the first one which was analytically determined before all the tests were made. Based on these results there does not appear to be a thickness effect.

The curve labeled "shear limit" defines the second failure mode. This curve was developed using analysis and the results from the first two residual stress tests. Combinations of crack size and stress below this curve should not produce shear failure while combinations above will. The uncircled points represent test points where no failure occurred and the circled points correspond to shear failures. As can be seen very good agreement with the theoretical curve was obtained for the limited range of crack sizes tested. For this case note that crack size equals crack arrester strip spacing since this is a post-propagation phenomenon. The crack size for all but one specimen was 7.62 cm (3 in.). Further examination of these results and the curves indicate that by incorporating crack arrester strips into a design, significantly greater damage can be induced while maintaining a capability for carrying a given load, for example, limit load in an aircraft.

## CONCLUSIONS

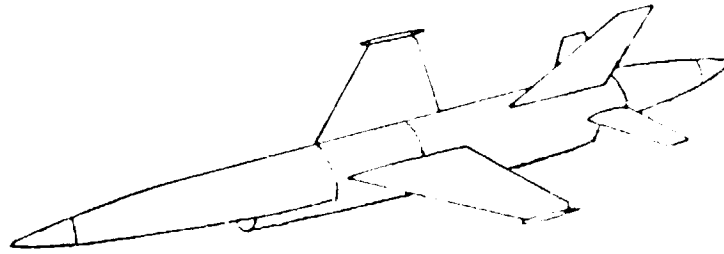
The hybrid composite fuselage design which was discussed here has a weight which is 23% less than its existing metal counterpart. Furthermore, while hard cost figures have not been generated, a projected cost reduction of 20% for production quantities is currently estimated.



With regard to the survivability aspects of the design, it has been demonstrated that the crack arrester strips successfully stop a propagating crack and contain the damage within a local area. It made no difference whether the damage was a statically induced sharp crack under no load or a ballistically formed damage under load. For the later, using a maximum overall dimension for the damage correlates well with analysis, independent of the shape of the damage. The hybrid composite is more desirable from a fracture tolerance viewpoint than all graphite on the basis of the gradual propagation characteristic, and the fact that because of this there is some warning of incipient failure.

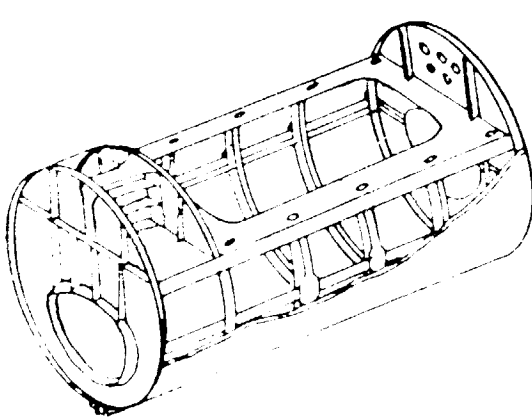
The additional work on solid graphite laminates has resulted in an identification and understanding of failure modes and the establishment of a prediction method, if only for one arrester strip spacing.

Obviously additional work is required. The planned testing of the multi-bay specimens is a first step toward scale-up. The shear failure mode should be more thoroughly investigated including consideration of other strip spacings and widths and other strip layup configurations.

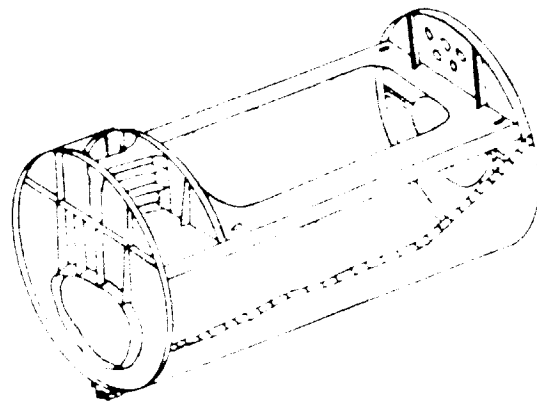


**BQM-34E RPV**

**FIGURE 1. DESIGN MODEL**



**EXISTING METAL DESIGN**



**COMPOSITE DESIGN**

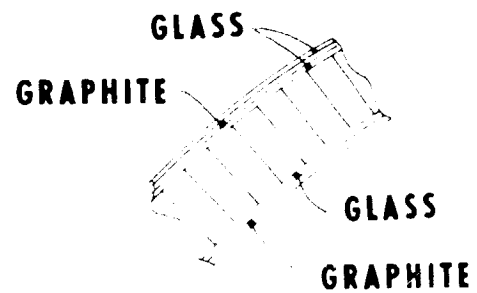
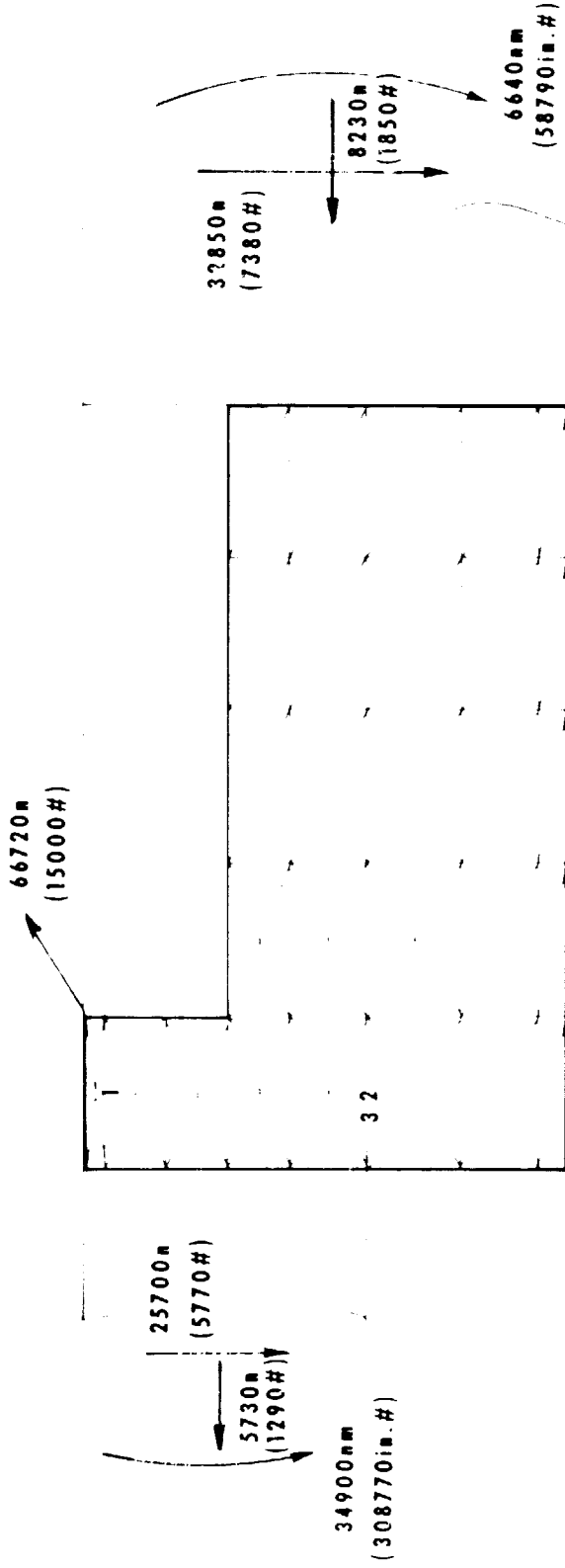


**FIGURE 2. KEY FEATURES OF DESIGN**



MAXIMUM STRESSES			
	$M_n/m^2$	KSI	LOCATION
TENSION	144.8	21.0	1
COMPRESSION	220.6	32.0	2
SHEAR	52.4	7.6	3

FIGURE 3. RECOVERY CONDITION MAXIMUM STRESSES

INNER FACE - 2 PLY, .016 in  
 OUTER FACE - 3 PLY, .026 in

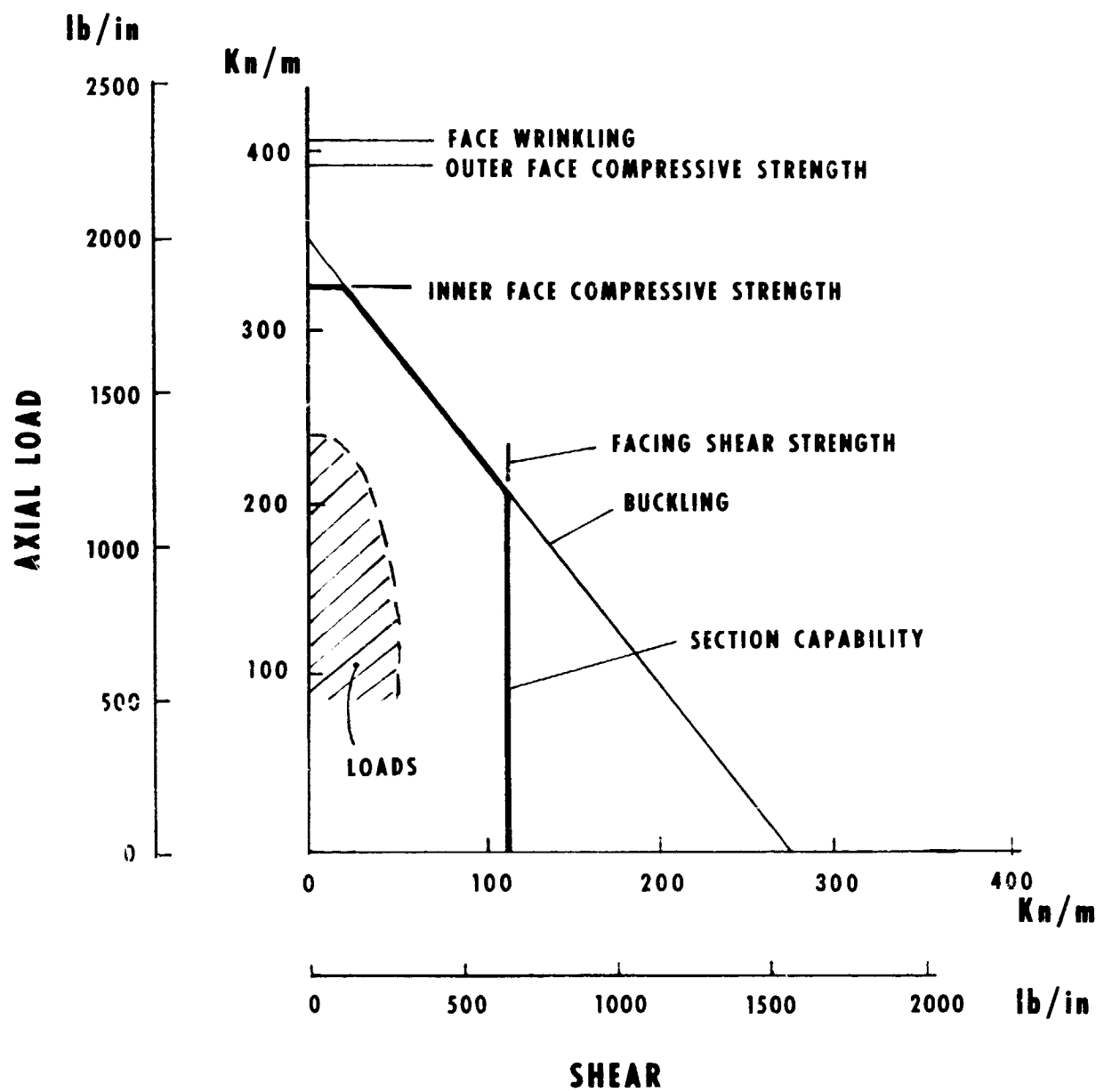


FIGURE 4. CAPABILITY OF COMPOSITE SANDWICH

① CRACK PROPAGATION IN

PRIMARY MATERIAL

② CRACK PROPAGATION THROUGH

ARRESTER STRIP

③ SHEAR FAILURE ALONG CRACK

ARRESTER STRIP

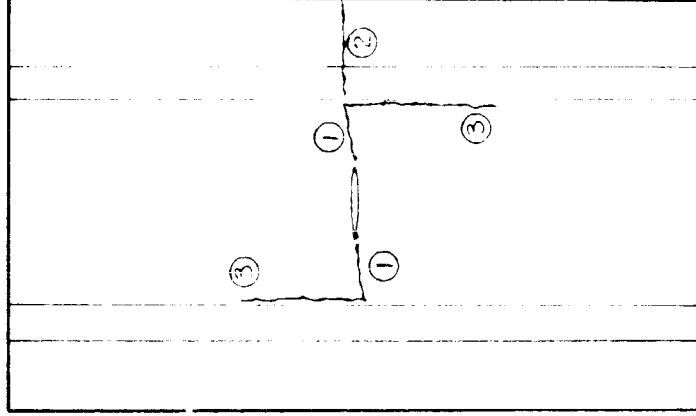
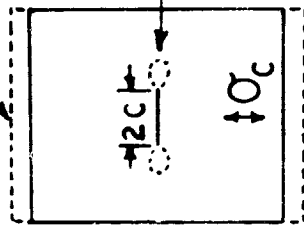


FIGURE 5. FAILURE MODES

**CONSTANT STRAIN**



**HIGH INTENSITY REGION**

$$\sigma_c \geq \frac{K_a}{\sqrt{\pi(c+a)}}$$

$K_a$  = FRACTURE TOUGHNESS

$a$  = DIMENSION OF HIGH INTENSITY REGION

$2c$  = CRACK LENGTH

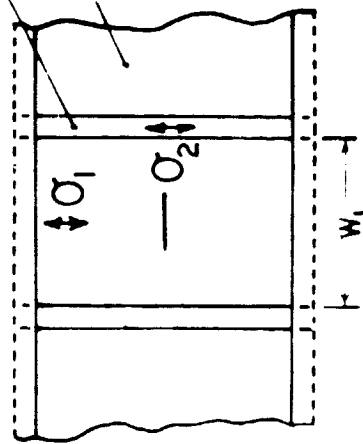
**BASIC CONCEPT:**

$E_2, K_{a2}$

$E_1, K_{a1}$

$$\sigma_2 < \sigma_1$$

$$K_{a1} < K_{a2}$$



$$\sigma_{c2} = \sqrt{\pi \left( \frac{w_1}{2} + a_2 \right) \frac{K_{a2}}{E_2}} \geq \frac{E_1}{E_2} \sigma_{1\text{limit}}$$

**FIGURE 6. CRACK ARRESTMENT - BACKGROUND & ANALYSIS**

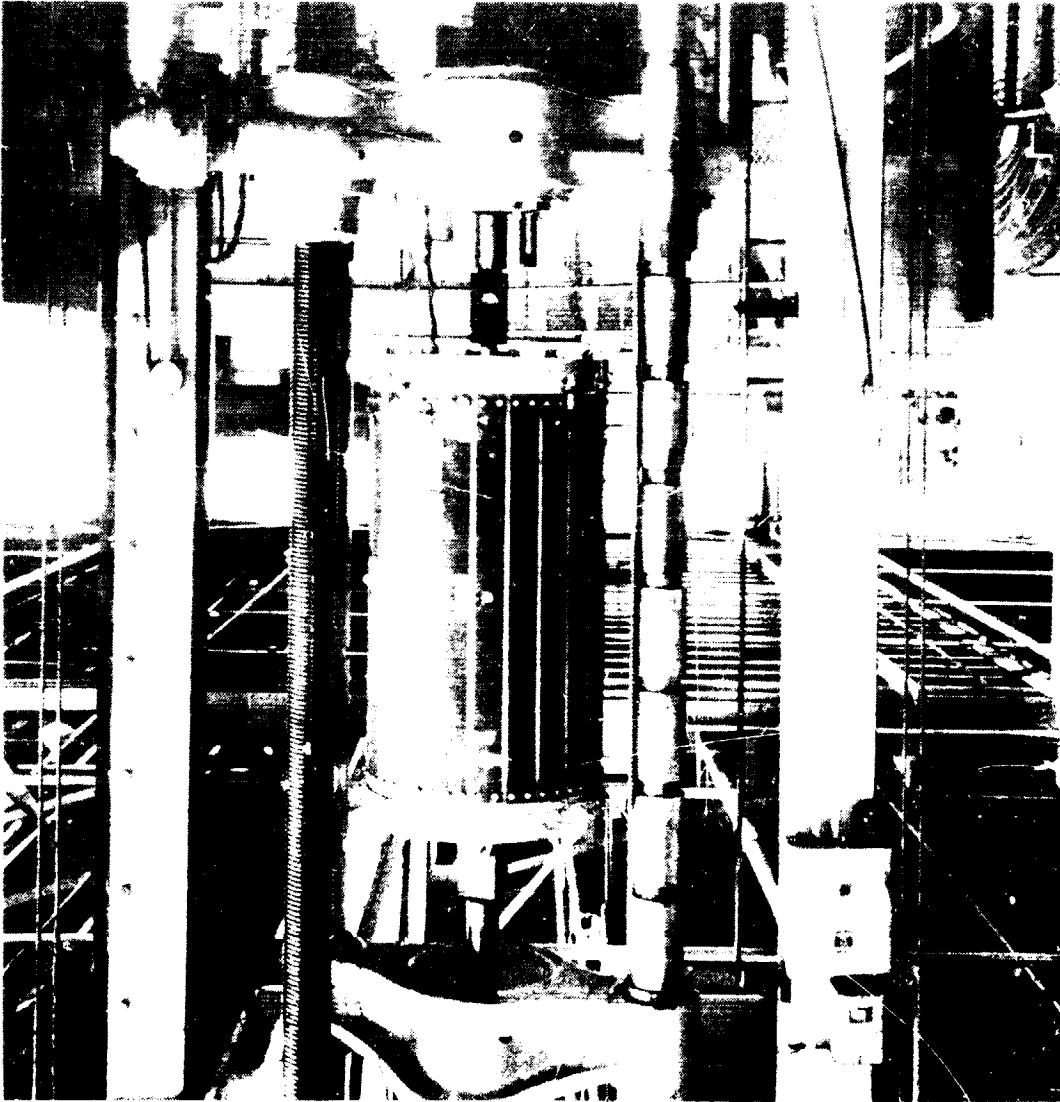


**FIGURE 7. HYBRID COMPOSITE SUBCOMPONENT**

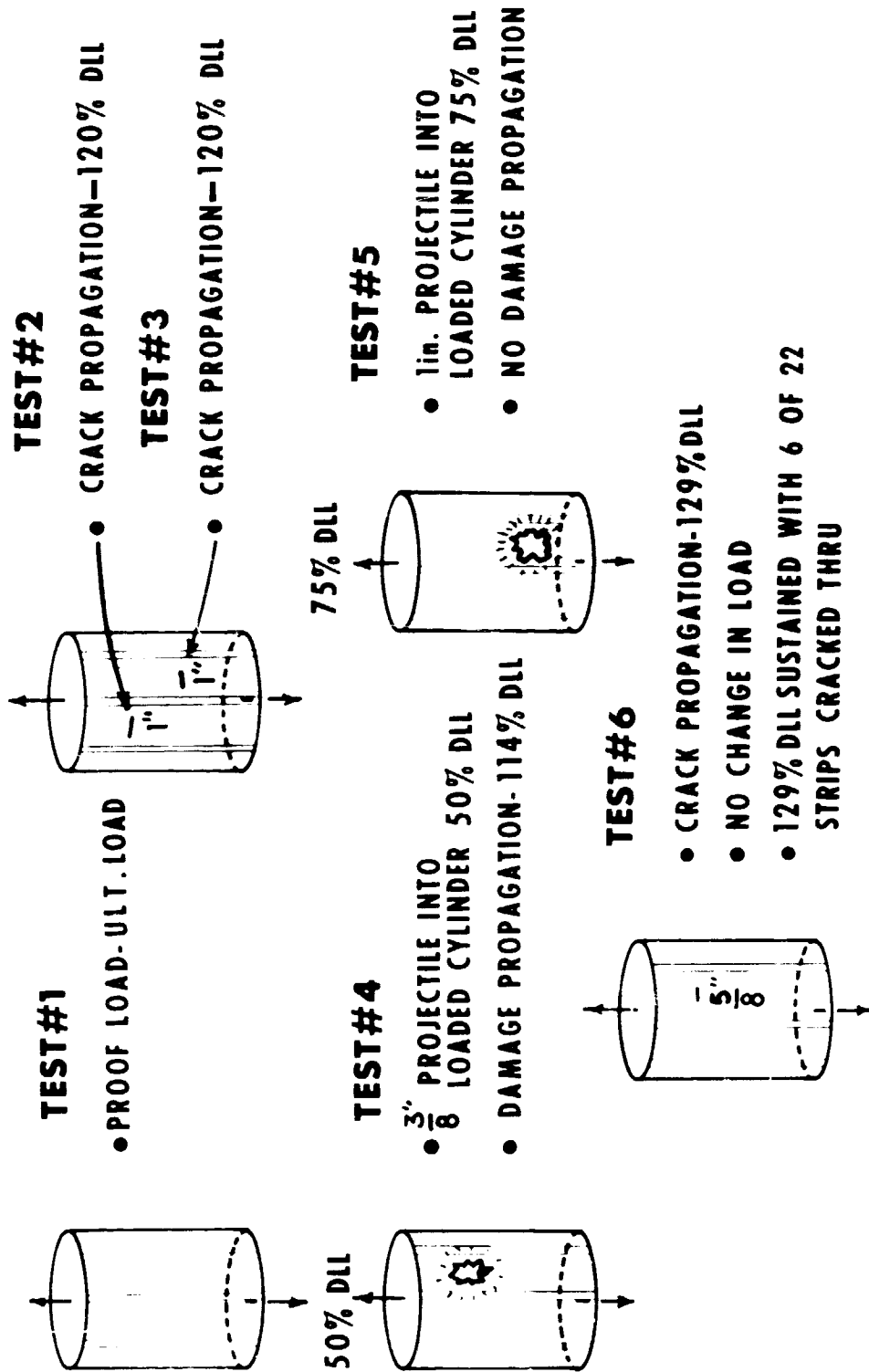


**FIGURE 8. CRACK ARRESTMENT TESTS**

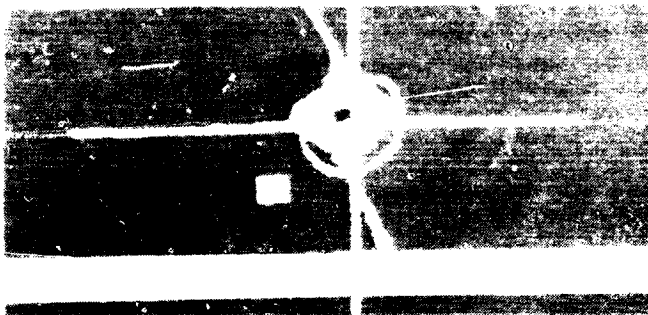




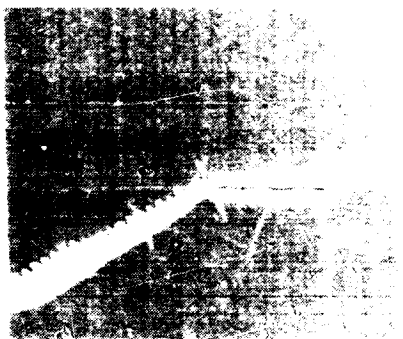
**FIGURE 9. CYLINDER AFTER TESTS**

ORIGINAL PAGE IS  
OF POOR QUALITY

BALLISTIC



15.9mm CRACK



25.4mm CRACK

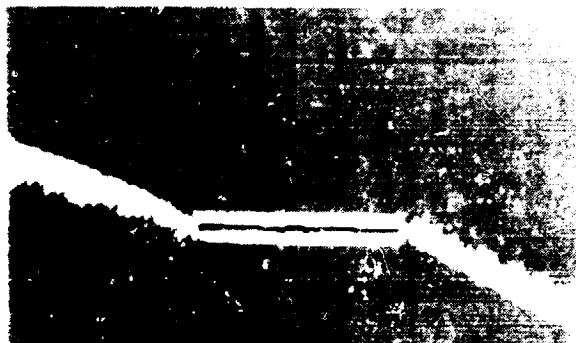


**FIGURE 10. CYLINDER TEST RESULTS**

# HYBRID CYLINDER CRACK PROPAGATION

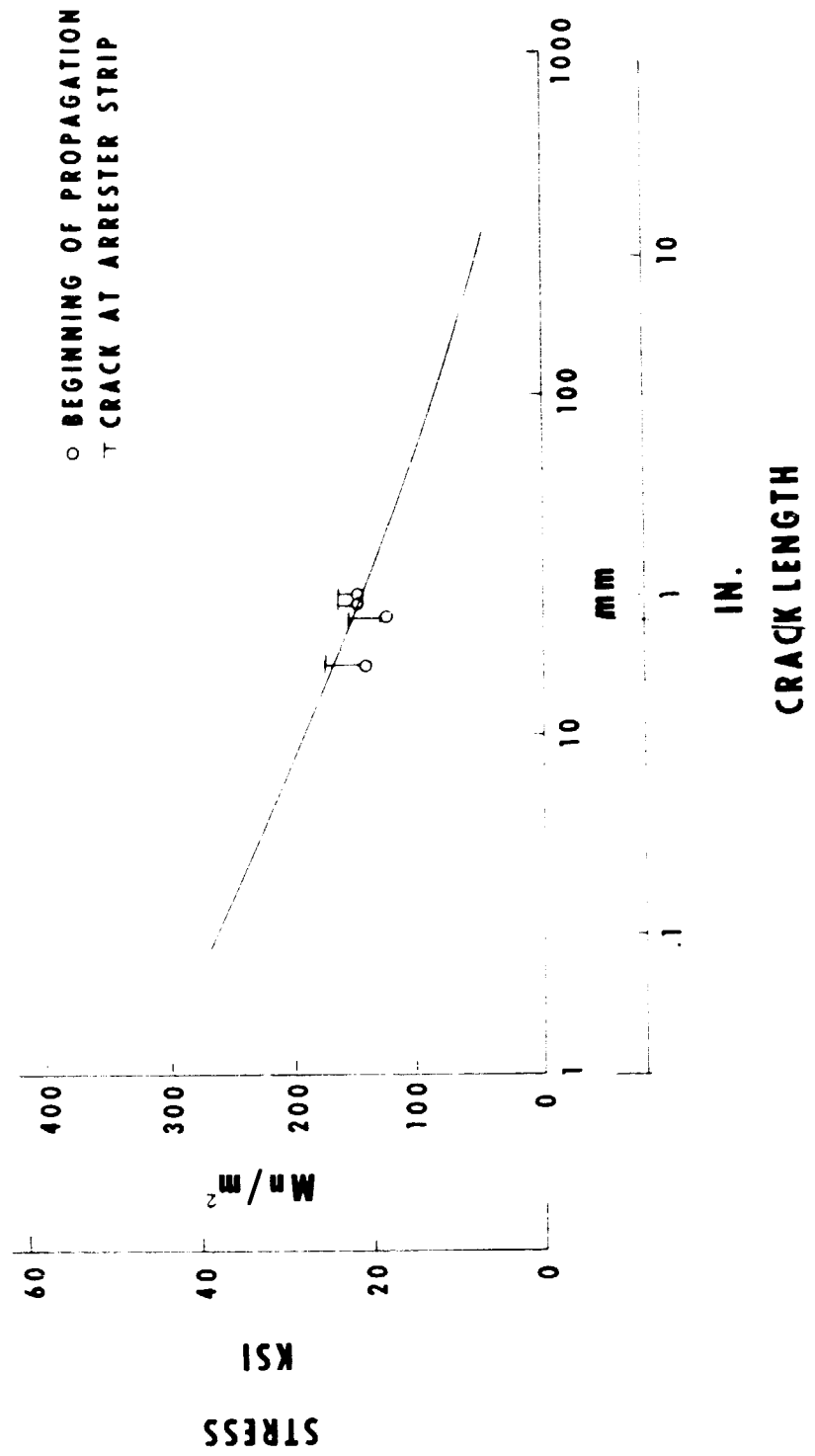
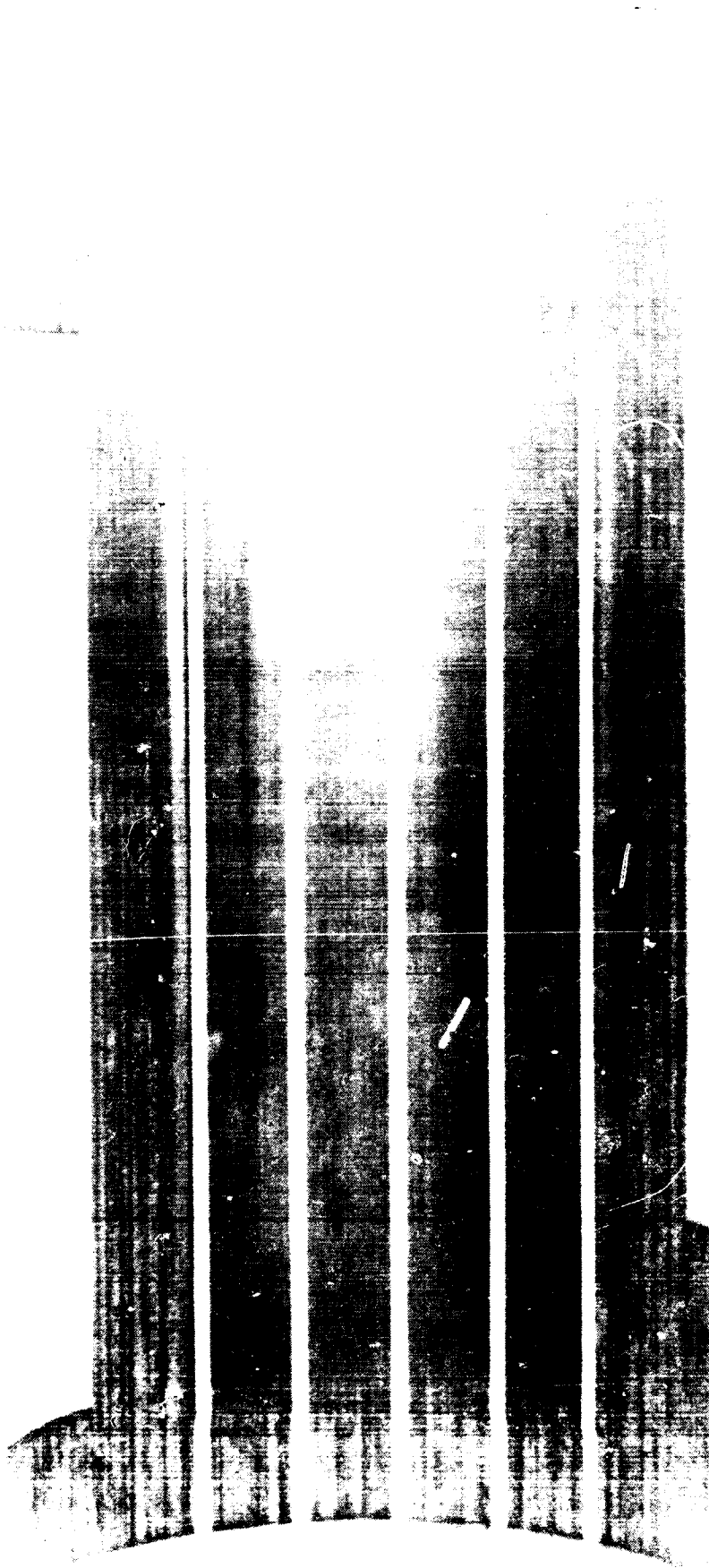
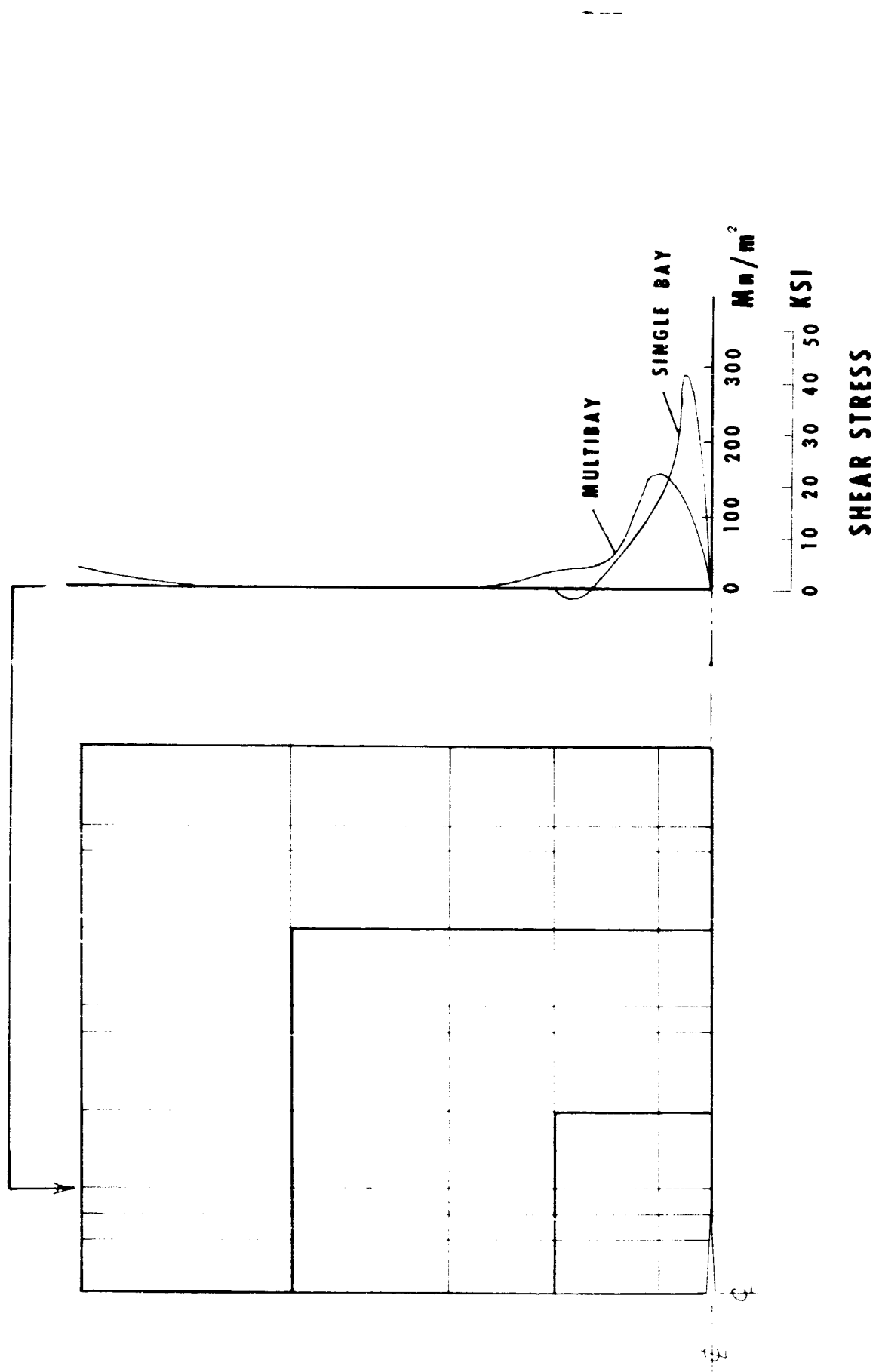


FIGURE 11. COMPARISON TO ANALYSIS



**FIGURE 12 FUSELAGE PANEL**

ORIGINAL PAGE IS  
OF POOR QUALITY



**FIGURE 13. PANEL ANALYSIS**

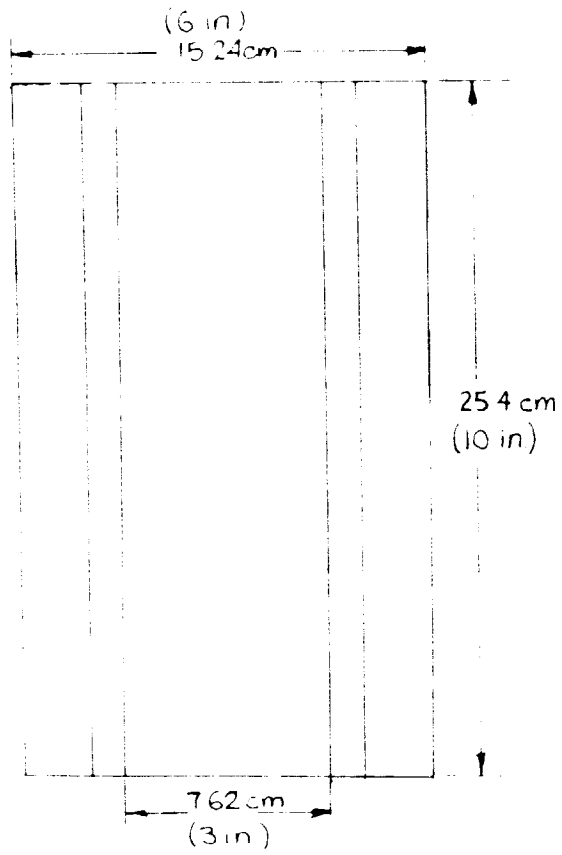


**FIGURE 14. GRAPHITE EPOXY TEST PANEL**

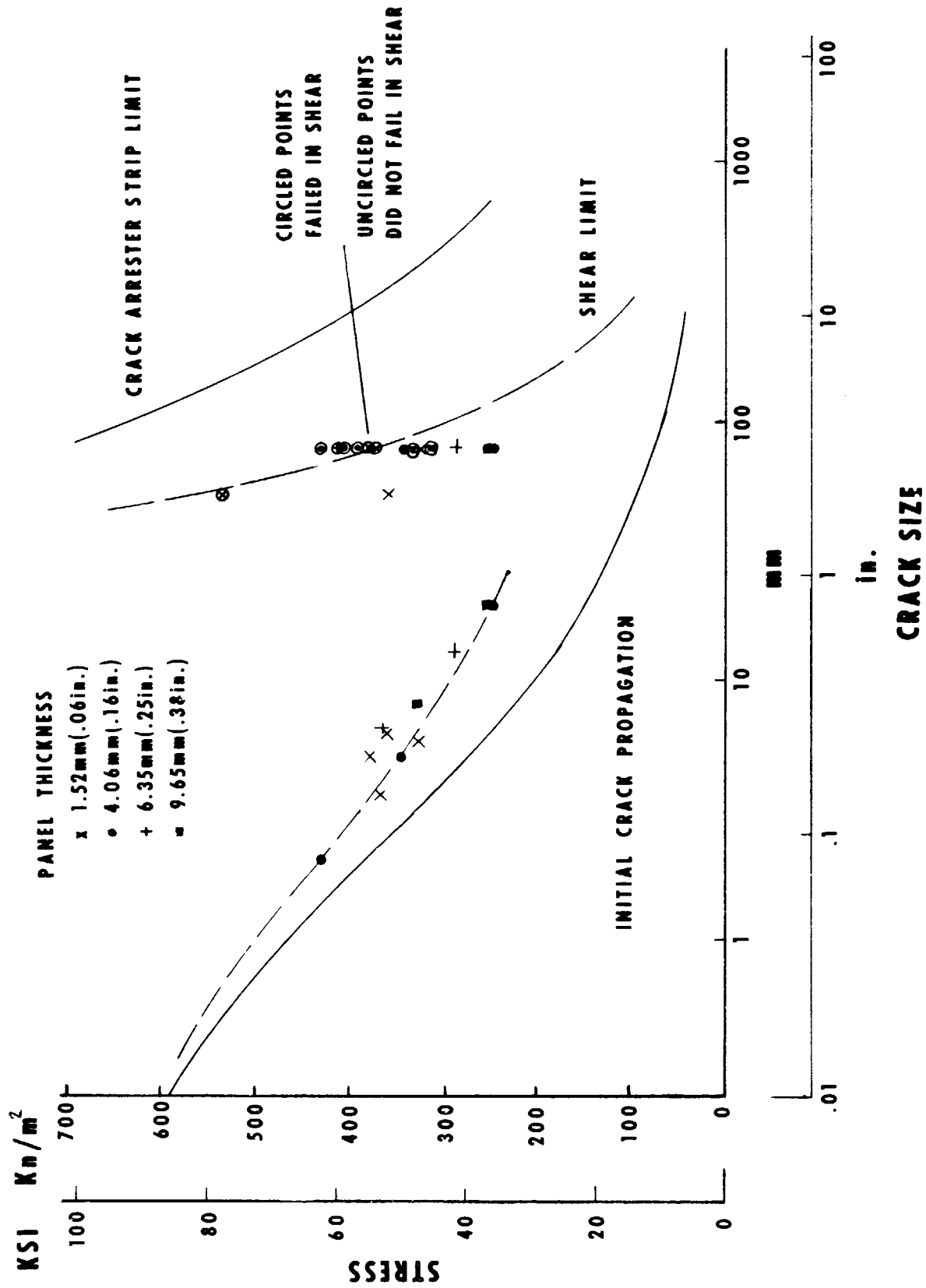


FIGURE 15. EXPERIMENTAL CORRELATION

---

BATTLE DAMAGE TOLERANT WING  
STRUCTURAL DEVELOPMENT

By

Ken deBooy

The Boeing Aerospace Company

SUMMARY

Results of analytical studies and initial testing to develop a wing design which will accept under load the damage from one 23mm high explosive super quick fused round without failure are reviewed. The design approach, development of fracture resistant hybrid skin and preliminary hydraulic ram and 23mm test results have been completed. Wing box component and full scale wing box tests are scheduled through the end of FY 1977.

INTRODUCTION

The Battle Damage Tolerant Wing Structural Development is being performed by the Boeing Aerospace Company under Navy Contract N000R-75-C-0178 for the Naval Air Systems Command. Mr. Alden Cowles, AIR-530215, is the technical monitor. Boeing technical leadership is being provided by Mr. Jack Avery from our Damage Mechanisms Group and by Mr. Ken King for structural design.

The objective of the program is to design a wing box which will accept combat damage and still achieve at least a 25 percent weight saving through the use of advanced composites. The 23mm high explosive instantaneous fused round was selected as a representative threat, based on its demonstrated capability to destroy aircraft. This report deals with the ongoing design analysis and test program which is in progress to develop a structural arrangement and advanced composite structural components which can accept the damage caused by the 23mm HE round without failure for the remainder of the flight, including a limit load maneuver.



## DESIGN DEVELOPMENT

The Battle Damage Tolerant Wing Structural Development started with a Phase I study which examined two wing types and three levels of technology. Both a thin low aspect ratio wing, and a thick high aspect ratio variable sweep wing were studied to determine basic tolerance to a 23mm HE threat. Three technology levels were applied to these wing types: current technology using titanium low risk 1980 technology using advanced composites with mechanical fasteners for assembly and high risk 1980 technology using more innovative advanced composite design concepts including bonding for assembly. Relative weights, damage tolerance and costs were compared. Results included the weights of a mid-span section of the wing box tabulated in Figure 1. The low risk 1980 thick high aspect ratio wing was selected to be the subject of the currently contracted structural development program, since battle damage tolerance was a more critical requirement in the design of this type of tactical aircraft wing.

## DESIGN REQUIREMENTS

The battle damage tolerant design criteria is that the wing structure shall sustain a single "super-quick" fused 23mm HE impact while in a 4g symmetrical maneuver. The 23mm impact shall be at the most critical combination of angle, velocity, and position for the wing box design. After impact, failure shall not occur during one occurrence of flight limit load, five hours of cruise with up to 2g flight loads, and one carrier landing at a design sink speed of 23 fps.

The target weight for the advanced technology wing box sized for damage tolerance shall be 75 percent of that of the current technology wing not designed for damage tolerance but otherwise sized to the same operational criteria. The design shall be based on the use of low cost manufacturing methods and projections of costs of advanced materials. Projected improvements in manufacturing processes and techniques shall be included where development efforts are underway, and where current exploratory efforts indicate that the technique, when perfected in the 1980 time frame, will

result in a cost saving in future production. Corrosion in a salt-air environment shall be a major consideration in the selection of materials and the design of joints where corrosion could develop.

Damage repair shall be stressed in the design with reduction of man-hours, skills, and aircraft downtime as design objectives. Current damage repair philosophy in defining repairable damage versus damage requiring component removal and replacement shall be used as a guide.

#### WING DESIGN CONCEPT

Figure 2 is a cross-section of the proposed wing-box configuration. The sizing reflected in the figure is representative of the battle damage tolerant wing-box test article that will be fabricated and tested as part of the program. The proposed configuration is a graphite/epoxy wing composed of a four spar, multi-rib box with covers stiffened by a stringer between spar caps. The center bay of the lower surface is removable for fuel tank access and structural inspection.

The covers and spar webs are basically  $\pm 45^\circ$  graphite/epoxy laminates, and the spar chords are uniaxial ( $0^\circ$ ) filamentary laminates. These chords carry most of the wing bending loads, as the covers have low spanwise stiffness.

The four spars provide a redundant load path for the wing bending loads. Some tension and compression loadings are carried in the covers, but the stresses are low. Since the cover stresses are low, local damage in the covers will not propagate.

The proposed design incorporates several additional features that provide battle damage tolerance in addition to that obtained from redundant sizing. An example of this is the spar cap isolation described in the following paragraphs.

The bundles of uniaxial fibers bonded to the spar webs carry most of the wing bending axial stresses, and control the elongation of the surfaces so

---

damage does not propagate in the skins. With the 23mm HE damage criteria, it is possible that a spar cap (which covers approximately one-eighth of the surface) can be severed. In this event, the design objective is to transfer the energy contained in the spar cap at the time of the damage to adjacent spar caps, and later provide a load path for wing bending at limit loads, without causing extensive skin ripping at the damage point.

The spar cap material is isolated, in that it does not have a direct connection to the skin, and several degradable load paths and shear lag effects reduce the load transfer to the skin at the point of damage. Assuming that a loaded cap is severed, the bond shear strength between cap and spar web becomes critical, thus limiting the shear load that the spar web can apply to the skin. Next in the load path is the web to skin shear tie which is designed for the redistribution stress as defined by computer analysis. This shear tie web and its bolted connections may be designed to fail at the higher shear flows near the damage. Shear redistribution from the spar cap bundles to the skin is inherent in the type of load path provided. The severed bundle load must be transferred thru a damaged spar web and damaged shear tie, to the skin surface, thus providing a soft load path to the skin locally, and allowing a greater span for redistribution.

At each spar chord, the two uniaxial bundles are separated by the relatively thick spar web so that damage to one chord section will not propagate to the other chord section. In the event that one of the bundles is destroyed, the bond between the damaged bundle and the spar web should then fail in shear for some distance along the spar. This action, combined with a shear lag across the web provides some protection for the other bundle in the spar cap.

The torsional stiffness of the proposed wing box tends to be higher than other configurations (such as sandwich) because the skins and spar webs have thickness for stability purposes resulting in lower shear stresses. This lower shear stress allows bolted or riveted connections thru the skin, with no special treatment required for stress concentration.

The 3-bay lower surface, in which the center panel is bolted in place for access, also provides an important damage tolerance capability. When extensive damage occurs to any one of the three separate panels, it is improbable that a crack could propagate across the joint into the undamaged panel.

The configuration of the test box and subcomponents has not been significantly revised since the start of the program in November 1974. Initial efforts have been concentrated on specimen design, testing and analysis. Results of these tests will provide the data which will be used in refining the wing design and wing component design for Phase II testing. The wing box design is being conducted in parallel with the subcomponent and component design at a rather low level of effort. The design effort level on the two and four spar test boxes will be accelerated during the early phases of Phase II while initial components are being fabricated and tested.

#### COST ANALYSIS

Advanced composite materials have the potential of providing a substantial reduction in the weight of the wing structural box. Substantial research funds have been devoted to design studies and test programs to provide the technical foundation for advanced composite primary wing structure in production. The major reason composites are not being used more extensively in new production airplanes is cost. A primary objective of this program is to take advantage of designs which allow use of low fabrication and assembly costs which more than cancel out the high costs of the basic material.

Cost was the primary factor leading to the development of alternative design approaches to the honeycomb stabilized panels which appeared most efficient based on our earlier studies. The selected design appears to be much less costly to build, while offering better battle damage tolerance. Weight differences were less than one percent and not a factor in the design selection. It is planned to demonstrate not only battle tolerance in light weight wing structure but also to demonstrate a competitive cost approach to the use of advanced composites in primary wing structure when compared

to the use of metals.

#### DESIGN UNCERTAINTIES

Existing data is inadequate for the development of a practical, low cost, battle damage tolerant wing design that will accept normal service damage without experiencing catastrophic failure, and which can be repaired in a reasonable time without employing excessive skills or equipment. In addition, there are design uncertainties unique to battle damage which will be produced by the 23mm HE and the materials and design which will be the most tolerant to this type of damage. The initial phases of the test and analysis program are designed to resolve these uncertainties, and the final phases will provide full-scale verification. Principal design uncertainties are outlined in Table 1.

Our approach was to apply materials for which significant data has been developed to our design concept. Various component configuration and integration concepts were tested in order to obtain reasonable fracture characteristics in the preliminary design concept. Tests have just been completed of full-scale, three spar box segments which provide the first indication the type of damage the 23mm HE superquick fuzed round will impose on a graphite composite wing box. Additional wing component tests, final box design and static plus ballistic tests of loaded wing box segments will be completed during the next two years.

#### SKINS IN TENSION

Sawcut fracture panels, 7 and 10-inches wide, were tested in seven  $\pm 45^\circ$  configurations, including both tape and fabric. Figure 3 shows typical panels after failure. Results for the five graphite-epoxy materials give very little indication of notch sensitivity, Figure 4. These data are shown on the basis of strain to failure, the primary evaluation criteria for skin material, in Figure 5. S-glass  $0^\circ$  fibers were compatible with graphite  $\pm 45^\circ$  layers from a strain standpoint and our design analysis indicated that they would substantially increase the strain at which a

crack would run in our skin material. The use of one-third S-Glass is shown to double the strain at which a given size crack will run, Figure 6.

Ballistic damage fracture data correlated quite well with sawcut panel failure data, Figure 7. The ballistic damage was measured as the width of the through panel damage ignoring any rear face delamination. In addition, panels could be prestressed to a load very slightly less than the ultimate load with damage without experiencing failure on impact, indicating negligible dynamic amplification. Dynamic effects in 7075-T6 can reduce the strength of pre-loaded panels up to 50 percent.

#### SPAR INTEGRATION TESTS

Several spar integration concepts were tested, ranging from spar cap material being interleaved with the skin material, to spar caps bonded to the spar web with the spar web mechanically fastened to the skin through clips. Sawcut and ballistic fracture tests were performed on panels with three simulated spar caps, Figure 8. Sawcuts severing 50 percent of the center spar and associated skin resulted in net section failures for all panels. Net section failures indicate that the skin was carrying the load formerly carried by the failed center spar, since the crack was not long enough to run at the loads experienced. Interleaving the spar cap and skin caused the center spar to fail at a lower load than when the spar and skin were isolated, Figure 9. The concept of isolation of the spar cap from the skin was selected for the final design since the low bearing strength of the skin around mechanical fasteners limits the load which can be transferred from the spar cap to the skin in the local area of failure, thus allowing larger damage in the skin without extension of the damage under load.

#### HYDRAULIC RAM TESTS

Test panels, 33 cm (13 inch) square, were mounted in a hydraulic ram test tank as shown in Figure 10, and 10 and 13mm spheres were fired into the panels at velocities from 680 through 1070 m/sec (2245 through 3525 ft/sec). Damage was less severe than that experienced in 7075-T6 aluminum panels of

equal weight, Figure 11. 4.8mm (3/16 in.) tension fasteners were selected over 6. mm (1/4 in.) tension fasteners based on static tests which indicated that the smaller fastener would hold the same internal pressure load without pullthrough. Typical hydraulic ram damage with shear and tension fasteners is shown in Figure 12. Spanwise cracks extend at higher projectile velocities resulting in fastener pull through at approximately 850 m/sec (2800 ft/sec). These hydraulic ram tests were the first indication that countersunk fasteners with tensile loading resulting from hydraulic ram or HE explosion may be acceptable.

#### 23mm FRAGMENT PATTERN

The round tested was a 23mm HEIT (high explosive incendiary tracer) with a superquick contact fuze. Entrance damage is a 15 cm (6 inch) hole which has cracks propagating from it in the more brittle materials. The fragment pattern 23 cm (9 inches) aft of the entrance panel is illustrated in Figure 13. It should be noted that the pattern covers 60 cm (2 ft.) and that the circled hole in Figure 13 was caused by a round from a previous firing that did not detonate. The cone of fragments is about 106 degrees for impact velocities of 500 - 700 m/sec (1600-2200 ft/sec), with large fragment damage both at the center and around the periphery.

#### IRON BOX TESTS

These tests were conducted with a thick wall box having the volume and venting area of one cell of the wing box design, bounded by two spars and two ribs, Figure 14. Various skin materials were tested including 2024-T3, 7075-T6, honeycomb with graphite skins, and  $\pm 45^\circ$  graphite combined with 35% S-Glass. Results indicated that any skin will be destroyed on both the entrance and exit side of this rigid box. The hybrid skin experienced the least severe damage and the honeycomb stabilized graphite skins and the 7075 exit panels experienced the most severe damage. These tests and several firings against free-standing panels also indicated that the damage was much more severe when the space between the panels was enclosed than when the two skin panels did not have a confined volume between them.

## 23mm THREE SPAR WING BOX TESTS

Two three spar wing box segments were built with representative hybrid skin panels and a graphite/epoxy center spar. The outboard spars were fabricated from fiberglass, and the ribs from 2024-T3 aluminum in the interest of economy. For the box shown in the upper portion of Figure 15, the impact point was in an unsupported area of the skin with the flight path aimed at the center spar cap of the exit panel. The lower box represents an impact directly into the center spar cap at 0° obliquity, so that the flight-path was essentially in the plane of the spar web.

Preliminary conclusions from these firings are:

- ° Damage experienced in representative wing box structure was less severe than that experienced in the iron box test. The major factor causing this difference is felt to be less rigid skin panel edge fixity.
- ° Pressure deformation of 2024-T3 ribs was present when the round entered one cell of the wing and was not present when it entered two, indicating that the deformation is due to residual pressure rather than shock waves.
- ° Impact on a major structural element tends to absorb a large portion of the energy imparted to the fragments, reducing the exit damage.
- ° And finally, the 23mm damage does not appear to preclude reaching the program objective of providing at least a 25 percent wing box weight savings and 23mm battle damage tolerance through the use of advanced composites.



Table 1. Design Uncertainties

Design uncertainty	Tests for resolution
<p>Extent of 23mm HE ballistic damages Effect of blast, fragments, obliquity, velocity and shielding</p>	<ul style="list-style-type: none"> <li>● Fragments into unloaded panels</li> <li>● Fragments into loaded panels</li> <li>● 23mm Into simulated 2 Spar box</li> <li>● 23mm Into 2 and 4 Spar boxes</li> </ul>
<ul style="list-style-type: none"> <li>● Most effective methods of surviving 23mm ballistic damage in advanced composite wing structure</li> <li>● Skins in tension <ul style="list-style-type: none"> <li>Fracture toughness of various materials</li> <li>Improvements in fracture toughness obtainable by altering fiber orientation</li> <li>Improvements in fracture toughness obtainable by adding hybrid materials</li> </ul> </li> <li>● Spar cap/skin interface <ul style="list-style-type: none"> <li>Fracture toughness of various Spar cap configurations</li> <li>Spar cap configuration most effective in arresting skin cracks</li> </ul> </li> <li>● Skin/stiffener interface <ul style="list-style-type: none"> <li>Skin stiffener configuration most effective in arresting skin cracks</li> </ul> </li> </ul>	<ul style="list-style-type: none"> <li>● Tension tests of saw cut panels</li> <li>● Ballistic tests of panels</li> <li>● 23mm Into simulated 2 Spar box</li>   <li>● Tension test of saw cut panels with 3 Spar caps</li>   <li>● Ballistic tests of skin panels with alternate stiffener design</li> </ul>
<p>Extent of hydraulic ram damage in advanced composite wing structure</p>	<ul style="list-style-type: none"> <li>● Hydraulic ram test of panels in a wing box structure</li> </ul>
<p>Bearing strength and damage propagation characteristics of countersunk mechanical fasteners mounted in skin material</p>	<ul style="list-style-type: none"> <li>● Basic bearing strength tests</li> <li>● Blast and hydraulic ram effects on alternate fastener configurations</li> </ul>

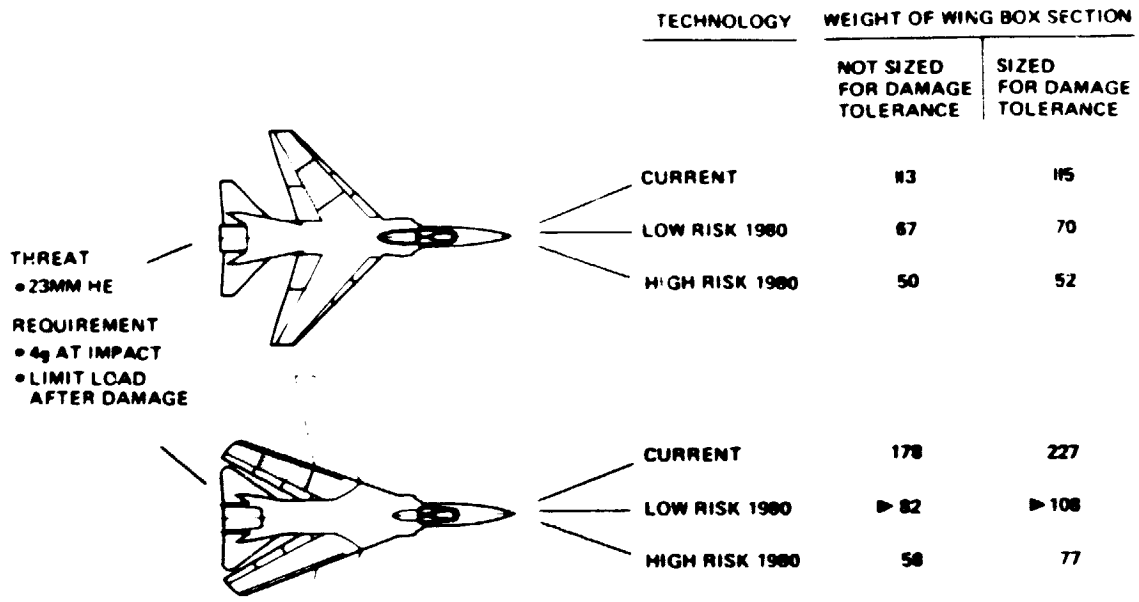


Figure 1. Analytical Results

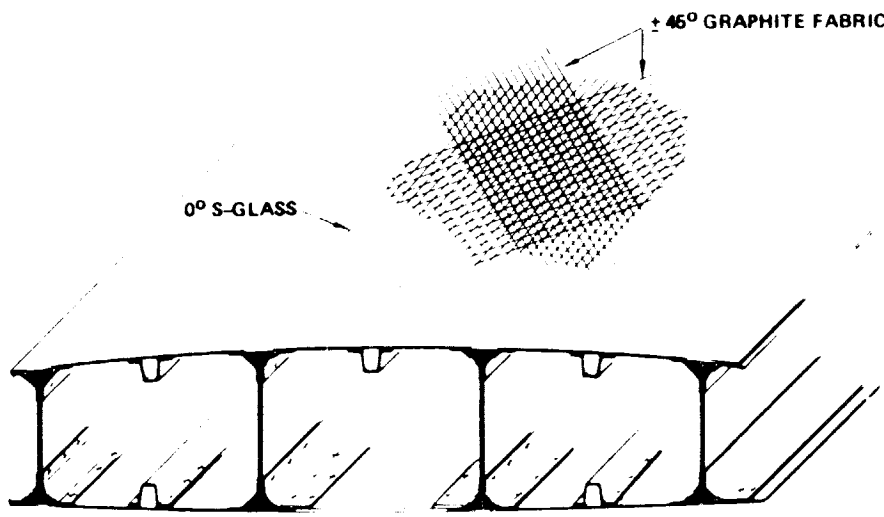


Figure 2. Preliminary Design Concept



Figure 3. Saw Cut Skin Panels for Tension Tests

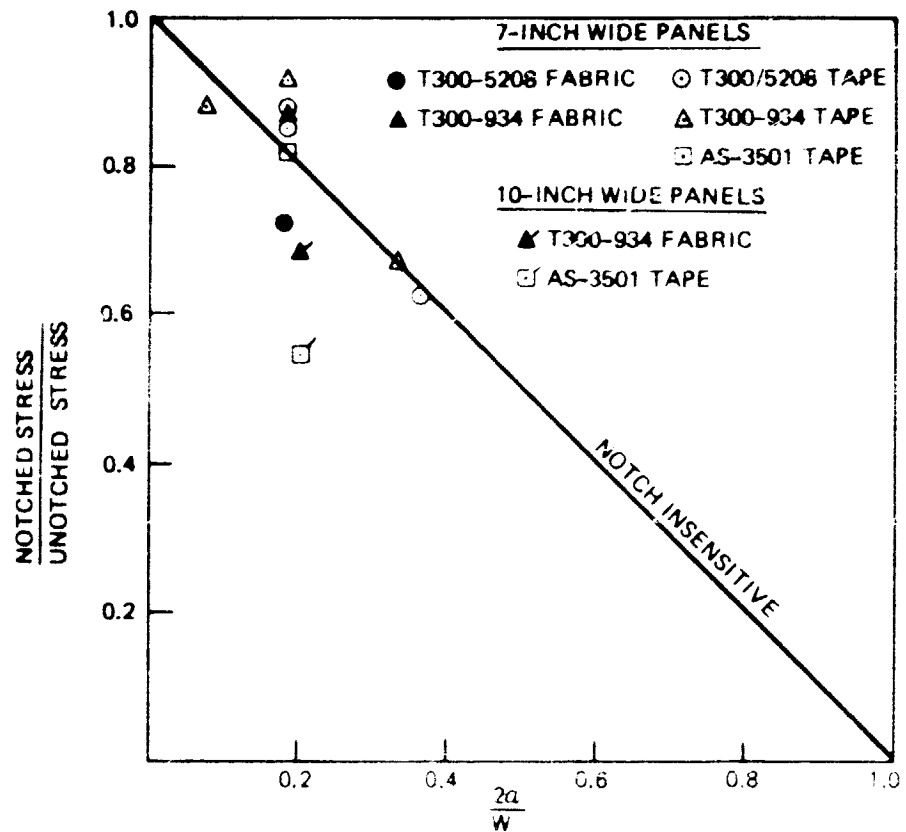


Figure 4. Notch Sensitivity of Tensile Properties

REPRODUCIBILITY OF THE ORIGINAL PAGE IS POOR

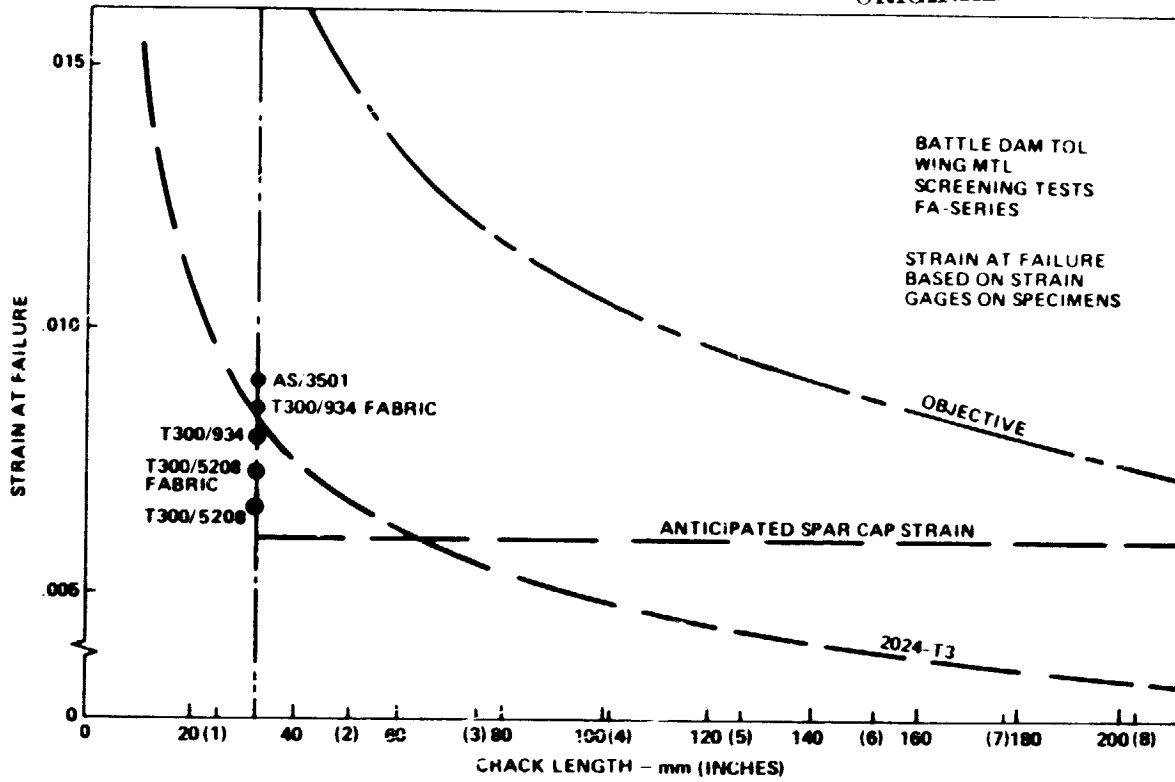


Figure 5. +45° Material Comparisons

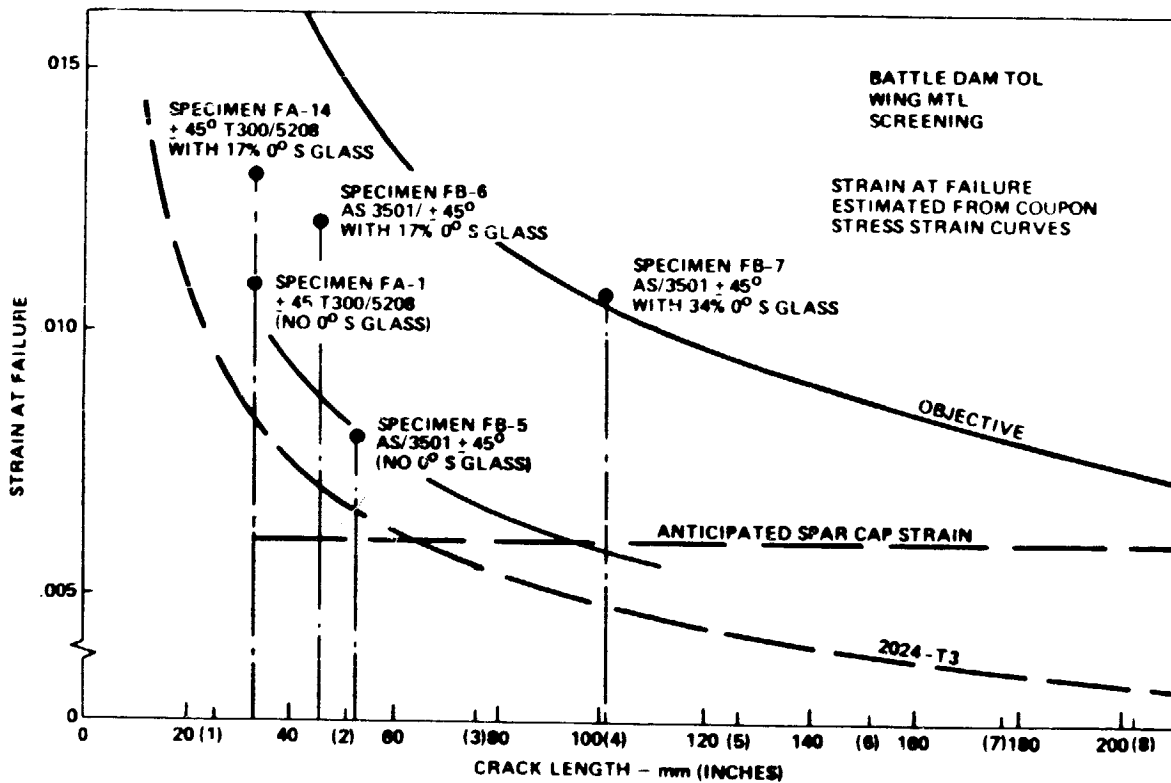


Figure 6. Effect of 0° S Glass with +45° Graphite

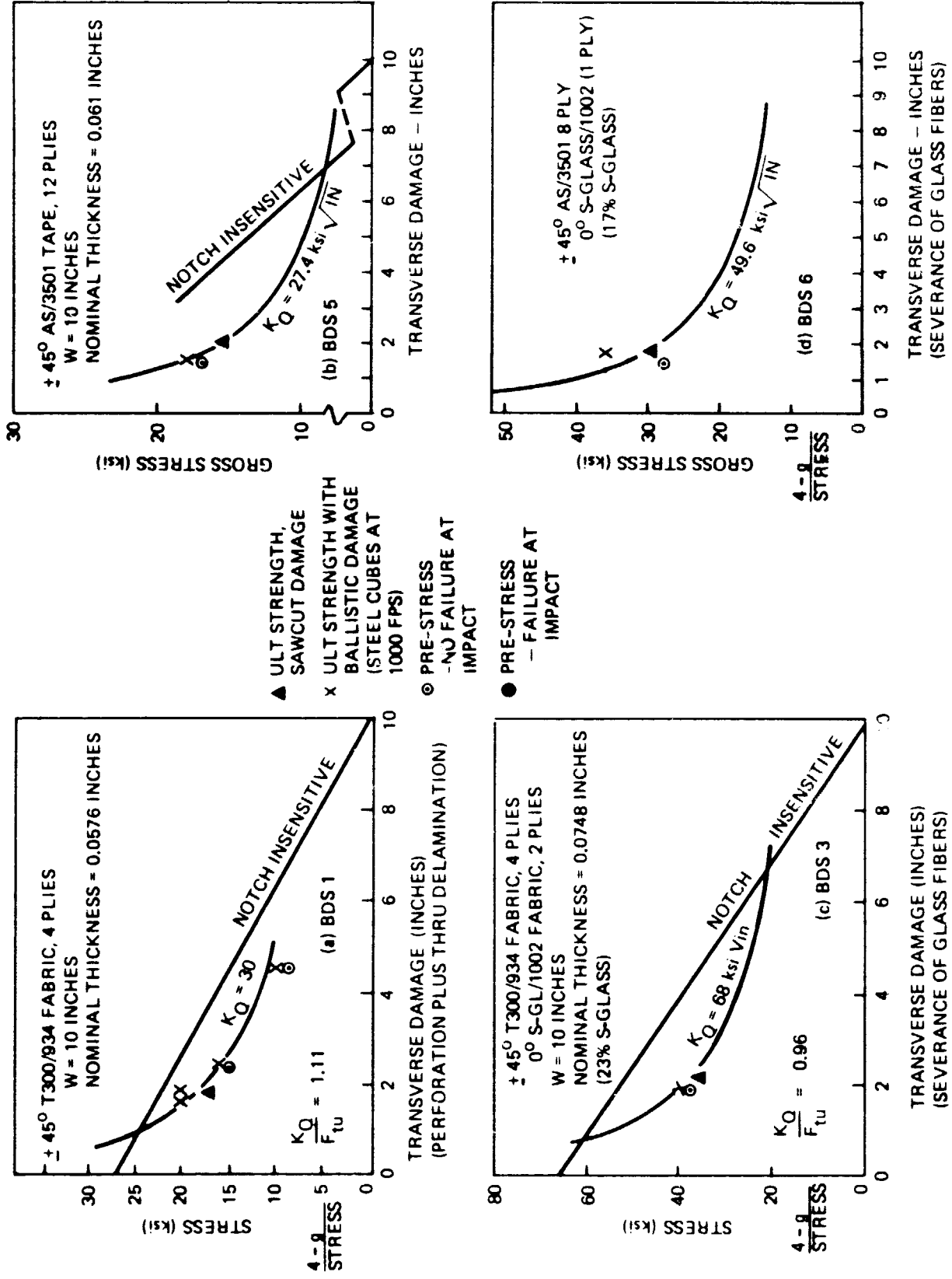


Figure 7. Ballistic Impact Testing Under Tensile Load

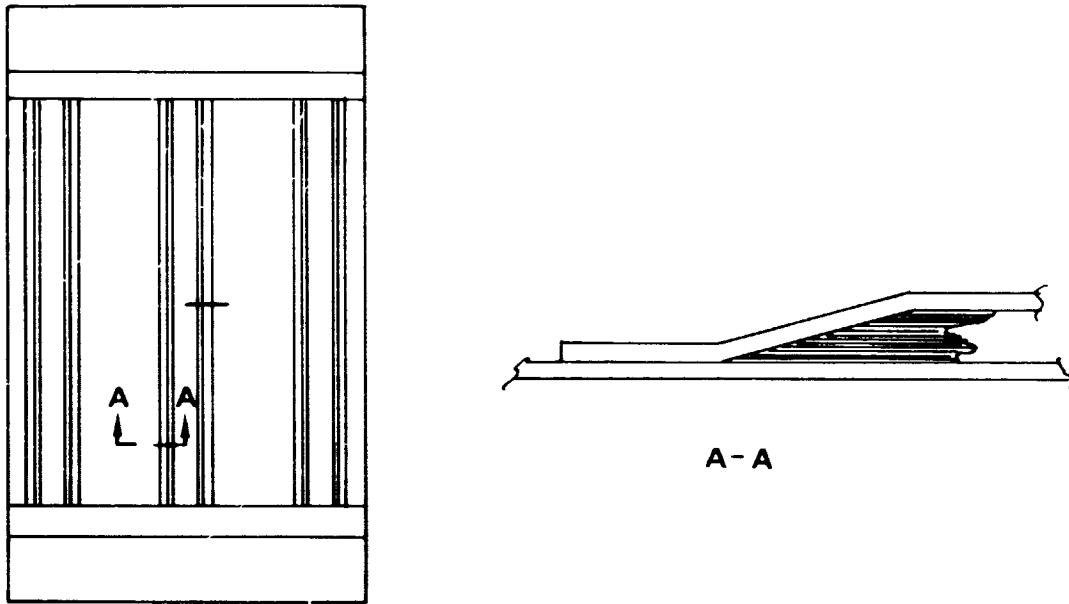


Figure 8. Typical Spar Integration Test Panel

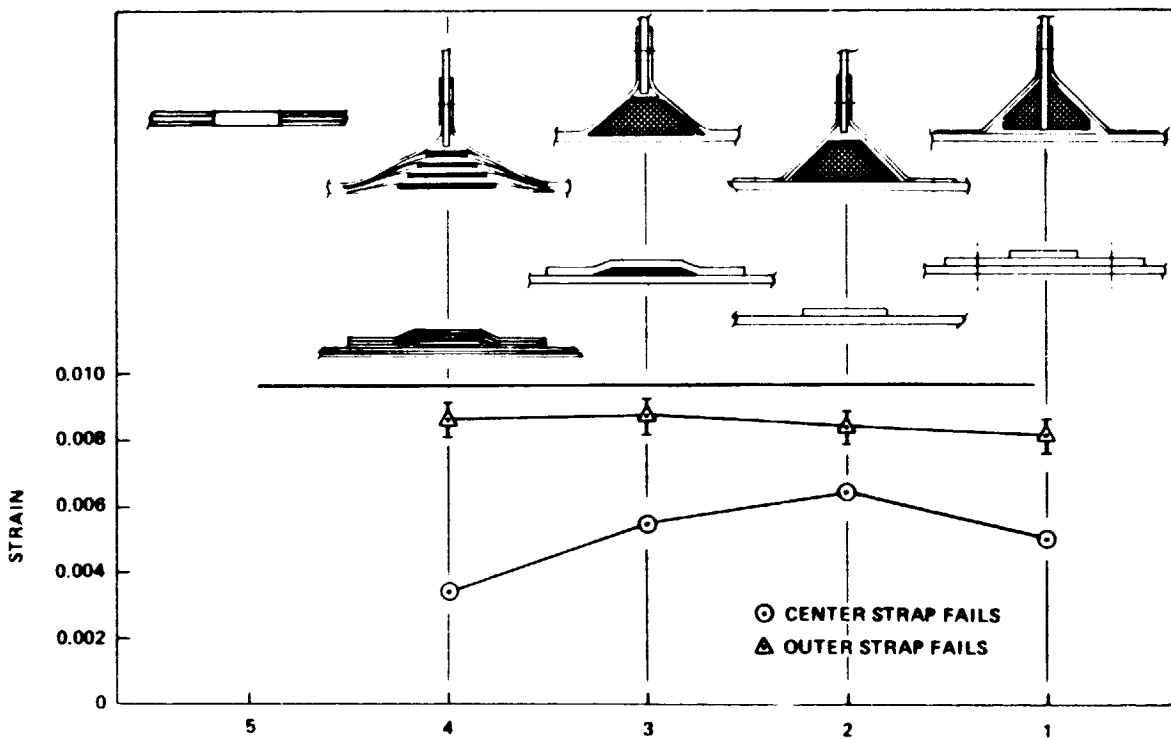


Figure 9. Skin/Spar Cap Integration Saw Cut Tension Test Results

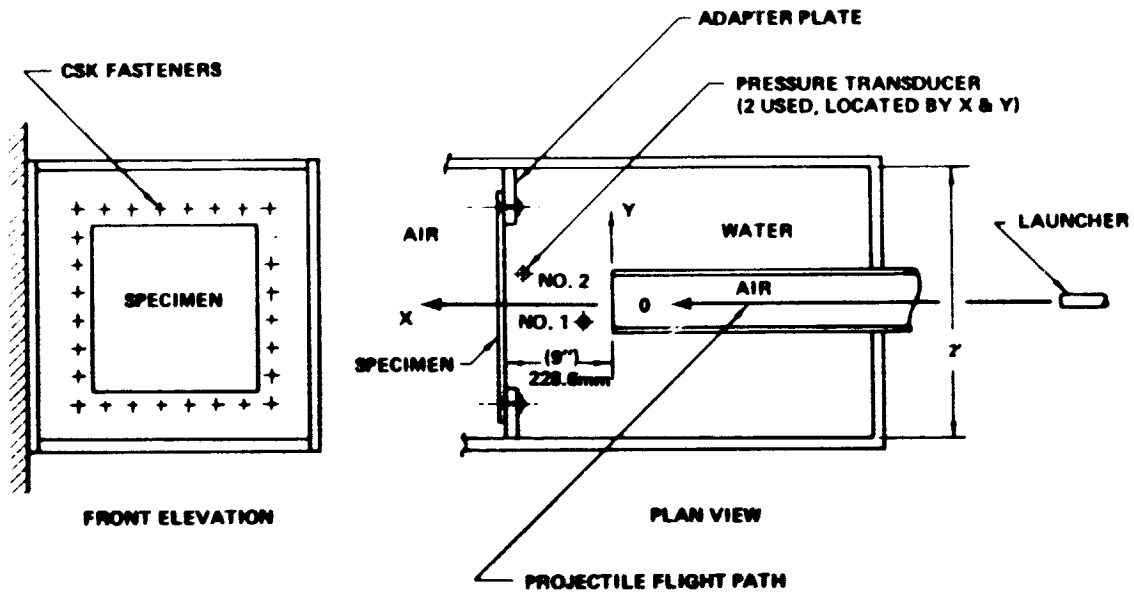


Figure 10. Hydraulic Ram Test Set-Up

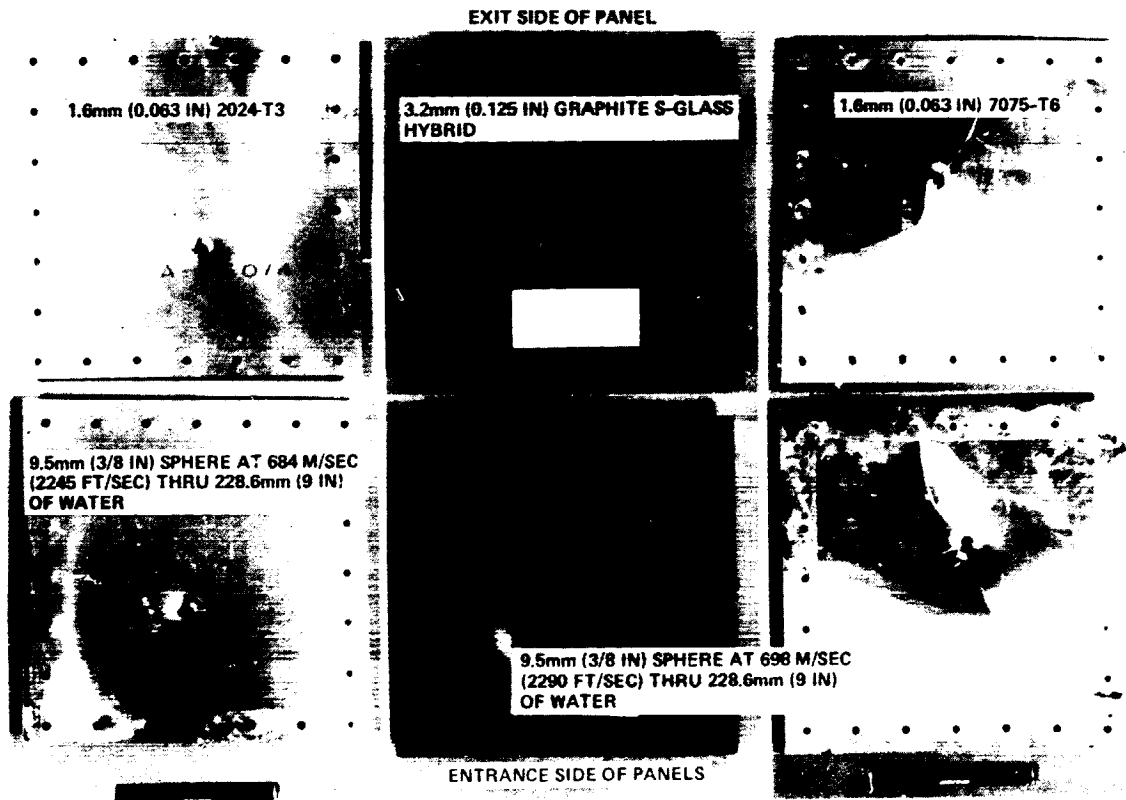


Figure 11. Hydraulic Ram Damage Comparisons

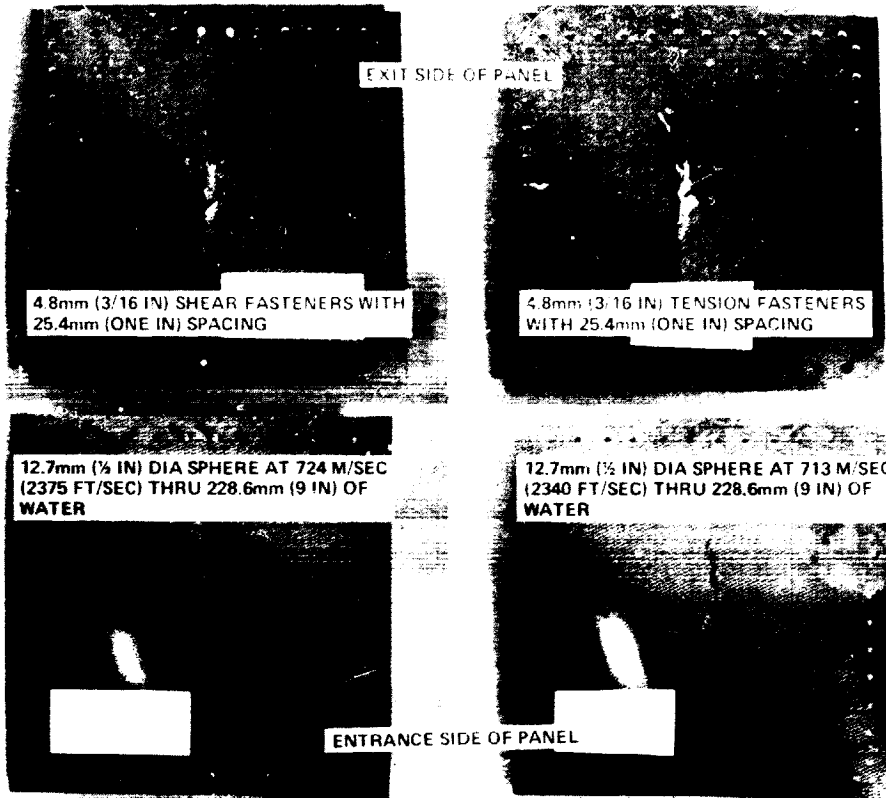


Figure 12. Typical Hydraulic Ram Damage

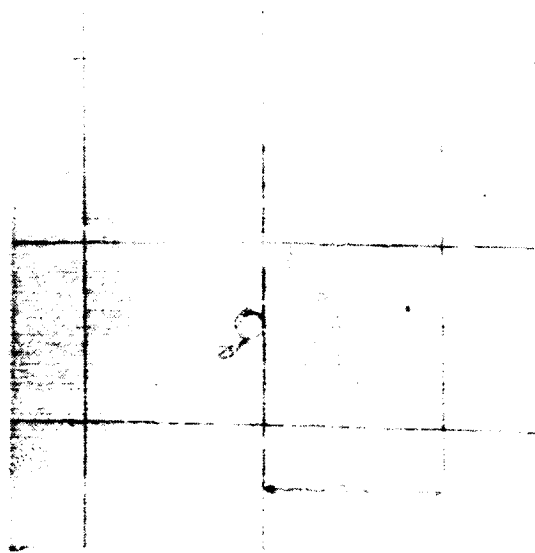


Figure 13. Fragment Pattern 23mm (9") Aft of Trigger Plate



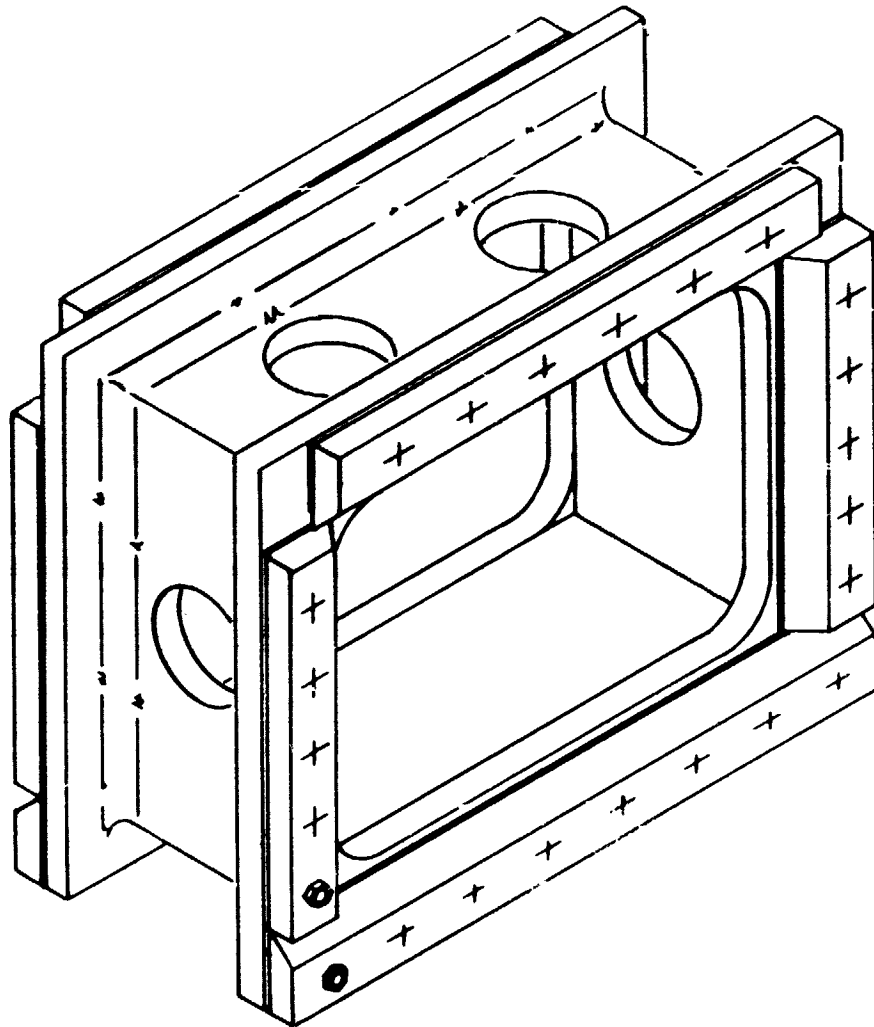
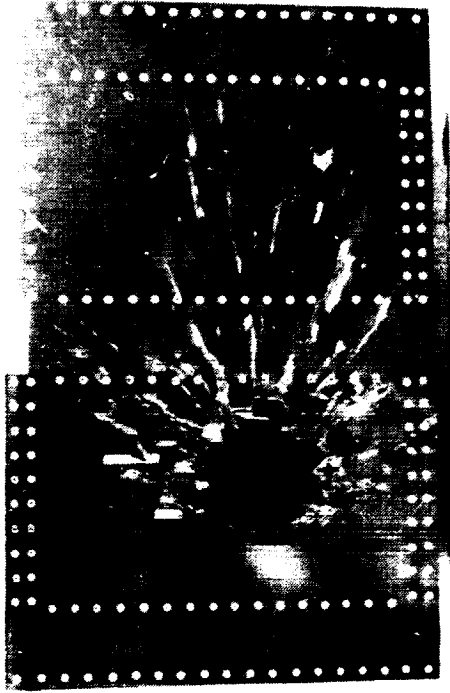


Figure 14. Iron Box Used for 23mm HE Testing



Entrance



Exit

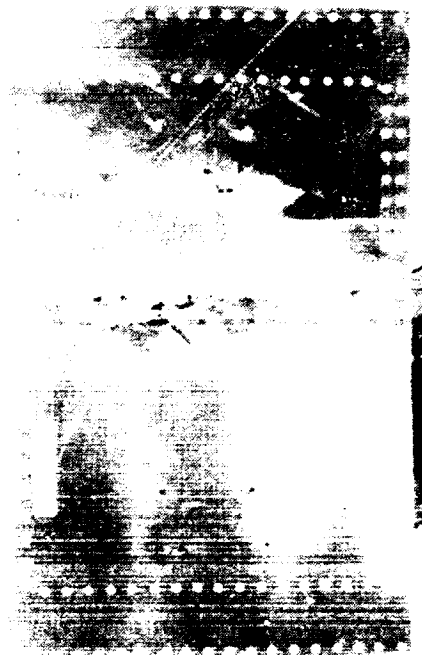


Figure 15. Wing Box Ballistic Test

ORIGINAL PAGE IS  
OF POOR QUALITY

## LIFE ASSURANCE OF COMPOSITE STRUCTURES

R. V. Wolff and D. J. Wilkins  
General Dynamics

### INTRODUCTION

The primary objective of the "Life Assurance" program is to demonstrate that the characteristics of a composite component can be predicted from a characterization of the static and life-time properties of its critical elements. At the time of this writing the program is still in progress.

### APPROACH

The approach selected to meet the technical objective was to

1. select the critical elements from an available composite design
2. conduct enough replicate tests on each element to provide reliable estimates of strength and life parameters.

### Test Component

The component from which elements were selected was a graphite-epoxy composite two-spar box section from a conceptual wing design (Reference 1). The wing was designed to meet the functional requirements of the YF-16 (lightweight fighter prototype) baseline metal design. The main structural design features of the component box beam design, Figure 1, are

1. Strain tolerant strips for unity  $K_t$  attachment of spars to the cover plates
2. Spar web buildups provide load introduction "hard points"

**PRECEDING PAGE BLANK NOT FILMED**

### 3. Mechanical fasteners.

#### Element Selection

Since the wing box component was assembled entirely with mechanical fasteners, each of the elements selected was a bolted joint section. Five graphite-epoxy composite elements were selected to represent the critical areas of the component. The critical areas included the skin-to-spar attachment; the spar buildup areas where loads were introduced; the wing skin in bearing; the wing skin in combined bearing and tension; and the strain tolerant (buffer) strip in tension. The specimen types and loading methods are illustrated schematically in Figure 2.

#### Fatigue Test Methods

All fatigue testing was conducted using a random, flight-by-flight spectrum in a closed-loop electrohydraulic test facility controlled by a Varian 620i mini-computer. The spectrum was based on the wing root of a high-performance fighter aircraft. The spectrum used in the element phase was developed in an earlier program and is described in Reference 2. The spectrum used in the box beam test phase was based on the same mission segments as the element spectrum; however, it was modified to include both bending and torsion loads (which were applied simultaneously). The spectra were stored on digital magnetic tapes, which were converted to analog signals in the lab by the Varian.

#### Analysis

Data developed in the element phase was analyzed using structural reliability methodology (Reference 3) and the probabilistic strength-bounded wear-out model (Reference 4).

## ELEMENT CHARACTERIZATION

Strength and lifetime data were developed for approximately 700 elemental specimens. In addition to the mechanical testing, an extensive investigation was conducted to characterize the response of the graphite-epoxy laminate to environmental exposures, including various combinations of temperature and relative humidity.

### Mechanical Tests

The spectrum loading used in the element phase was based upon two types of missions that included both supersonic and subsonic air-to-air segments, Figure 3. Two versions of the spectrum loading were digitized and stored on magnetic tape to produce "command signals" for the laboratory equipment via a mini-computer. One version of the spectrum loading, a random load-time history, was fully accelerated on the time axis to the maximum constraints of load level and power spectral density (PSD) content. The other version of the spectrum was accelerated only for mission segments where the temperature was 75°F or less. Real-time, i.e. one test hour corresponded to one flight hour, was used for mission segments where temperature was greater than 75°F.

All fatigue loading of specimens, except loading for Type I and II specimens, was conducted using the accelerated spectrum at room temperature, dry (RTD). The Type II specimen loading included use of both spectrum versions at RTD. Tests on Type I specimens with accelerated loading included dry specimens at RT and constant temperature and "wet" (saturated moisture content level) specimens at RT. Tests on Type I with "quasi-real time" loading included dry specimens at RT and "wet" specimens with superimposed mission temperature profiles, (Figure 3).

A "baseline" spectrum was defined. This spectrum was based on a peak or truncation load frequency of eight occurrences per lifetime. Truncation load was set at a 1% risk of static failure. For the several specimen types, truncation load varied from 78 to 88% of average ultimate strength. The relationship of strength to truncation load is illustrated in Figure 4.

Initial tests on Type I specimens, Figure 5, indicated that spectrum loading would need to be intensified to accelerate the fatigue damage process. Spectrum loading was intensified (or rms magnified) by raising the magnitude of all loads by a given percentage and then clipping all loads exceeding the original truncation level back to the truncation level. This procedure "intensified" the spectrum as reflected in the greater number of occurrences of the peak (truncation) load with increasing rms magnification, e.g.

<u>rms mag.</u>	<u>no. of peak loads</u>
none	8
26%	700
40%	2800
50%	5600

There are 631,656 loads in one life of the accelerated spectrum; hence, at the 50% rms magnification level, only 0.9% of the baseline spectrum loads are clipped by this intensification procedure.

A summary list of the element data developed on all specimen types is given in Figure 6. A list of summary statements is presented in Figure 7 for the five principal specimen types tested. These statements are condensed from the detailed observations made during the overall element phase.

#### Environmental Tests

One of the main problems of the program was to determine how to simulate actual environmental service conditions. This meant that the effects of months or years of actual service exposures would have to be condensed into a period of several weeks.

The effects of elevated or lowered temperatures during flight could be accounted for easily by appropriate temperature cycling during the quasi-real time fatigue loadings. Therefore, the problem was centered on simulating the atmospheric moisture effects an element would experience during a lifetime of service.

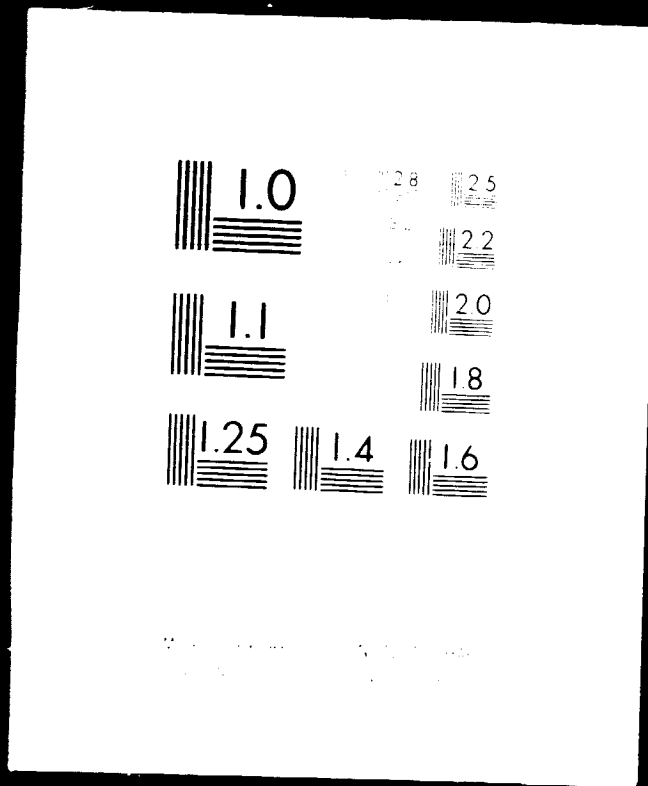
To accomplish these goals, it became necessary to characterize moisture absorption by graphite-epoxy composites and to determine if static (hygrothermal) and dynamic ("real life") laboratory conditioning methods differed significantly.

4 OF 5

N78

18134

UNCLAS



The effect of temperature and combined moisture and temperature upon mechanical properties was determined for the Type I specimens (see Figures 8 and 9). This effect will also be determined for several box beam components later in the program. The details of the environmental characterization are given in Reference 5; therefore, they will not be repeated here.

### FULL-SCALE COMPONENT

The design of the box beam component included the following key items.

1. The ratio of spectrum bending moment to torsion moment ( $M_x/M_y$ ) was set to provide the proper ratio of axial load to shear flow ( $N_x/q$ ) in the covers.
2. The component details were sized on element static mean strengths rather than "allowables."
3. Tension-bearing interaction curves derived from element tests were used in sizing the skin.
4. The critical load/temperature conditions were identified.
5. The critical beam areas were identified.

The most critical areas of the beam for RTD fatigue loading are depicted in Figure 10, which shows the static margin of safety (M.S.) calculations. The line of fasteners between Stations 57.6 and 75.5 (Figure 10) on upper and lower flanges (36 bolts total) is critical. A complexity penalty must be taken for these fasteners since a low strength element may occur at the same location as a high load. The total static reliability, R, is calculated as the product of each of the element (bolt location) reliabilities.

$$R = \prod_{i=1}^{36} \text{EXP} - \left[ \frac{1}{(1 + (\text{MS})_i)} \right]^{1/\alpha_0}$$

where  $(\text{MS})_i$  = margin of safety for location i

$\alpha_0$  = Weibull shape parameter

C-4



If the line of fasteners is assumed to be represented by the elemental data and wear-out model analysis for Type III specimens (selected because Type III included fatigue failures), the above equation may be solved as a function of applied load as a percent of  $\beta_0$  (Weibull scale parameter). This solution is plotted in Figure 11. The expected median failure now occurs at about 90% of the component ultimate strength. The result of including this static penalty in the box beam analysis is reflected in the wear-out characteristics for a limit load (truncation level) spectrum, Figure 12. The median fatigue article will survive about 100 lifetimes. However, one out of 10 articles will fail by 15 lives and 4 out of 1000 will fail before one life. The wear-out model was "shifted" to an intensified spectrum level to set the median fatigue life at two lifetimes. This shift required an rms intensification of approximately 54%. This later spectrum condition was chosen for the RTD box-beam experiment, which included 3 static and 12 accelerated time fatigue specimens.

Five additional beams have been selected for a static/fatigue condition, including environmental exposures. In this later condition, the fatigue loading is to be conducted with the quasi-real time spectrum; however, the details of temperature and load level have not been finalized.

## COMPONENT TESTING

All component tests have been conducted at RTD. A box beam component is shown in Figure 13. Duplicate fixtures such as the one shown in Figure 14, were used to apply both static and fatigue loads. The reaction end of the fixture is located at the right side of Figure 14. Load is applied by one vertical ram ( $M_x$ ) and two horizontal rams ( $M_y$ ), which may be seen at the left side of Figure 14.

### Static Tests

Three beams were tested to static ultimate load by applying bending ( $M_x$ ) and torsional ( $M_y$ ) loads simultaneously. Maximum deflections at failure for the second beam are given in Figure 15. The beam strengths were closely grouped (as expected from the element tests), and the failures occurred on the tension cover within the predicted critical area as shown in Figure 16. The failures initiated in bending as predicted. However, the

ultimate strength, averaged 24% higher than that predicted. (This difference can be attributed to a bolt-spacing penalty applied in the stress analysis.)

### Fatigue Tests

All fatigue tests were conducted using the same spectrum condition, i.e. 54% rms intensification and a truncation load of 73% of actual (not predicted) static ultimate strength. These two effects produce an overall intensity magnification of  $1.54 \times 73/67 = 1.68$  over a limit load spectrum. The loading rate was accelerated relative to the quasi-real time spectrum rate by a factor of 5; however, the flexibility of the specimen precluded accelerating the loading to the extent used on the element specimens. The results are listed in Table I. As may be seen from the table, the lifetime "runout" was varied as the results of each beam test became available.

Beam numbers 11 through 14 were tested to two lifetimes without failure. During residual strength tests, three beams experienced tensile cover failure similar in appearance to static failures, Figure 17, and a compression (skin buckling) cover failure. The significance of the compression failure was not recognized at this stage of the program.

An increase in cover strength after two lifetimes was believed to be a result of "seating-in", i.e. sufficient local deformation at the several bolt holes had occurred during fatigue loading to permit more uniform loading of the fasteners along the flanges than occurred statically. This was recognized as a possible occurrence before static loading and several "high" loads were applied before ultimate loading in an attempt to "seat" the bolts. However, either higher or more loads are apparently required to assure seat-in. Seat-in and extended (beyond two lifetime) life loading were examined further by residually testing two beams after 0.1 lifetime of loading and allowing two others to run out to four lifetimes (a minor delta impact on the original program schedule).

Beams 15 and 16 were statically tested after being loaded to 0.1 lifetime, and they did exhibit the "seat-in" effects, i.e. higher strength over static case.

Beams 17 and 18 were to be fatigued to four lifetimes; however, the latter beam failed in fatigue on the compression

cover at 1.3 lifetimes. The failure mode (similar to that of Beam 11 in the earlier residual strength compression side failure) is shown in Figure 18. Beams 17 and 20 did reach four lifetimes without failing. These beams were inspected closely throughout the fatigue loading, and a crack developed at or near the interface of the 45° buffer ply and the 0° structural ply at approximately one lifetime and continued to grow parallel to the beam span. This crack resulted in reduced static strength on Beams 17 and 20 and a fatigue failure on Beam 19 (although not confirmed this is believed to have also occurred on Beam 18). The last beam evaluated (Beam 4) was tested to two lifetimes. No cracks were observed on the compression cover, and the residual test yielded a tensile cover failure similar to the earlier beams.

### Implications of Component Result

Residual strength-lifetime data derived from component testing are plotted in Figure 19. The implied behavior of the beams based on the results available is shown by the distribution and probability of survival traces superimposed on the data. Compressive cover strength is apparently greater than tensile cover strength at time = 0 (shown at  $10^{-2}$  lifetimes in Figure 19). The tensile cover strength distribution is seen to degrade only slightly, i.e. variance broadens, through two lifetimes. The compressive cover strength is believed to degrade more severely with actual resultant fatigue failures occurring somewhere in the first lifetime. (Note: The spectrum used is highly intensified and the fatigue failures would be at about 17 lifetimes if the above wear-out model were shifted to a limit load spectrum (no rms or truncation load magnification).)

During the elemental phase, the compressive characteristics of the critical elements were evaluated using plate-type specimens and reversing the sign of the fatigue spectrum loads (easily accomplished in the laboratory). The simple plate specimens indicated compressive loading would be less critical than tensile loading. No element compressive fatigue failures occurred at spectrum intensities comparable to those used on tensile specimens. The correlation of element and component data has been confounded by mixed failure modes observed in the box beam. In retrospect, it now appears necessary to design and test a compressive element that is more realistic (i.e. complex) than the simple plate elements used previously so that the primary program objective can be truly evaluated. A compression element test series is presently being considered.

## PROGRAM ACCOMPLISHMENTS

Program accomplishments may be summarized as follows.

### PRIMARY OBJECTIVE:

Element Data Used to Predict Component Behavior

RESULT: Element Data Used in Predicting Component

- o Static Strength
- o Static Failure Location and Mode

RESULT: Component Static Distribution Parameter  
Correlates with Element Distribution Parameter

### ADDITIONAL OBJECTIVE:

Environmental Characterization

In-Depth Evaluation of Moisture-Temperature-Absorption  
Characteristics of Graphite-Epoxy

### ADDITIONAL ACCOMPLISHMENTS:

Scale Up of Closed Loop Test Facility (Two D.O.F. Loading)

Successful Manufacturing Experiment with Buffer Strip  
Design

## REMAINING WORK

The work remaining to complete the Life Assurance Program includes

1. Component environmental characterization including static and quasi-real time fatigue tests with super-imposed environmental conditioning
2. Component data analysis
3. Documentation.

In addition, a compressive element characterization to include design of realistic specimen and development of a data base is necessary if the main objective of the program is to be met completely.

#### CLOSURE

The utility of being able to use element data to characterize component behavior is obvious in the preliminary and final design steps. Certification criteria require that both environmental effects and distribution effects be estimated. This program provides much-needed guidance on how a series of tests should be laid out to provide the data needed to support the certification of composite hardware.

#### REFERENCES

1. Fant, J. A., Conceptual Design of Advanced Composite Airframes, AFML-TR-73-4, February 1973.
2. Waddoups, M. E., et al, Reliability of Complex Large Scale Composite Structure-Proof of Concept, AFML-TR-73-160, July 1973.
3. Halpin, J. C. et al, Characterization of Composites for the Purpose of Reliability Evaluation, AFML-TR-72-289, 1972.
4. Waddoups, M. E., Halpin, J. C. and Lemon, G. H., "On Process Zone Interactions in the Wearout Process," 3rd Conference on Fibrous Composites in Flight Vehicle Design, November 4-6, 1975, Williamsburg, Va.
5. McKague, E. L., et al, Life Assurance of Composite Structures, Volume I "Moisture Effects," AFML-TR-75-51, May 1975.

Table I  
**RESULTS OF STATIC/ACCELERATED FATIGUE COMPONENTS**

Beam #	Lifetimes	Vert Load %	Horiz Load %	Test Date	$f_{br}$ (KSI) @ Sta 58 (1)	$f_t$ (KSI) @ Sta 58 (2)	Crack Sta.
2	0	120	121	2/28/75	106.5	55.0	61.5
1	0	128	127	3/4/75	112.2	58.6	58.5
3	0	124	124	3/6/75	109.4	56.8	62.5
11	2	116	120	5/1/75	105.1	53.3	Compr.(4)
12	2	130	136	5/1/75	118.9	59.8	63.5
13	2	138	129	5/14/75	115.4	62.8	59.5
14	2	146	136	5/14/75	121.8	66.4	60.5
15	.1	125	130	5/20/75	113.8	57.5	66.5
16	.1	134	138	5/20/75	121.0	61.6	60.5
18	1.3	Fatigue		6/4/75	-----	-----	Compr.(4)
17	4.5	132	136	6/20/75	119.2	60.7	Compr.(4)
20	4.1	108	110	6/29/75	96.7	49.6	Compr.(4)
19	1.3	Fatigue		7/2/75	-----	-----	Compr.(4)
10	.1	Overload Failure		7/3/75	-----	-----	Compr.(3)
4	2.0	11.9	122	7/15/74	107.1	54.6	69.5

NOTES: (1)  $f_{br}$  = bearing stress in buffer = 18.1 x Vertical Load + 70.1 x Horizontal Load  
(2)  $f_t$  = tensile stress in primary laminate = 40.8 x Vertical Load + 5 x Horizontal Load.  
(3) Failure, in this case, was at Station 31.5 (near the high load reaction point) in the compression cover.  
(4) The compression failures are characterized by skin buckling influenced by the presence of cracks along the buffer/primary laminate interface.

FW 74-274 16-0001-A  
3 SEP 75

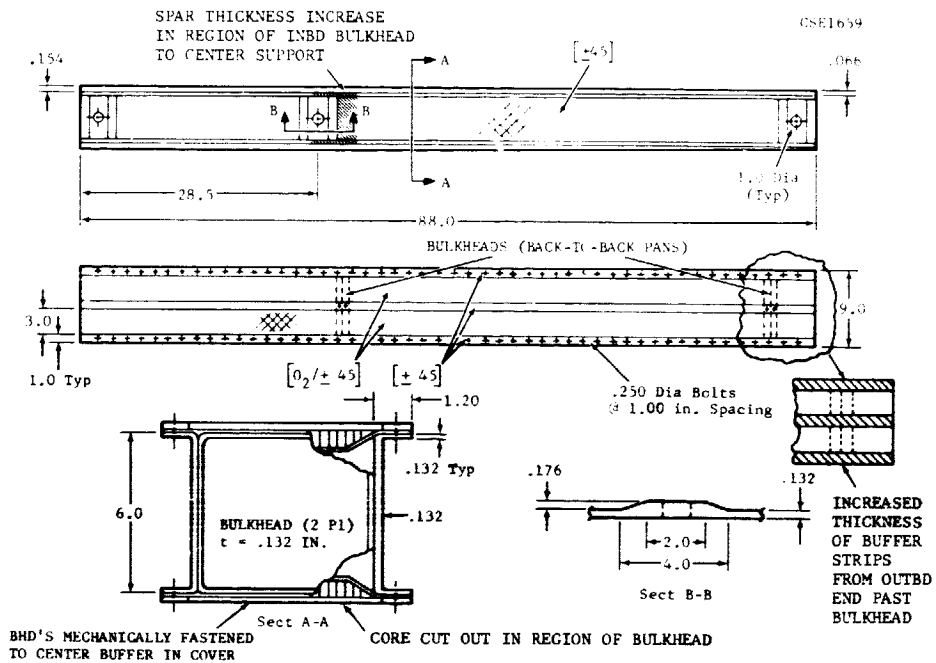


Figure 1 Box Beam Component

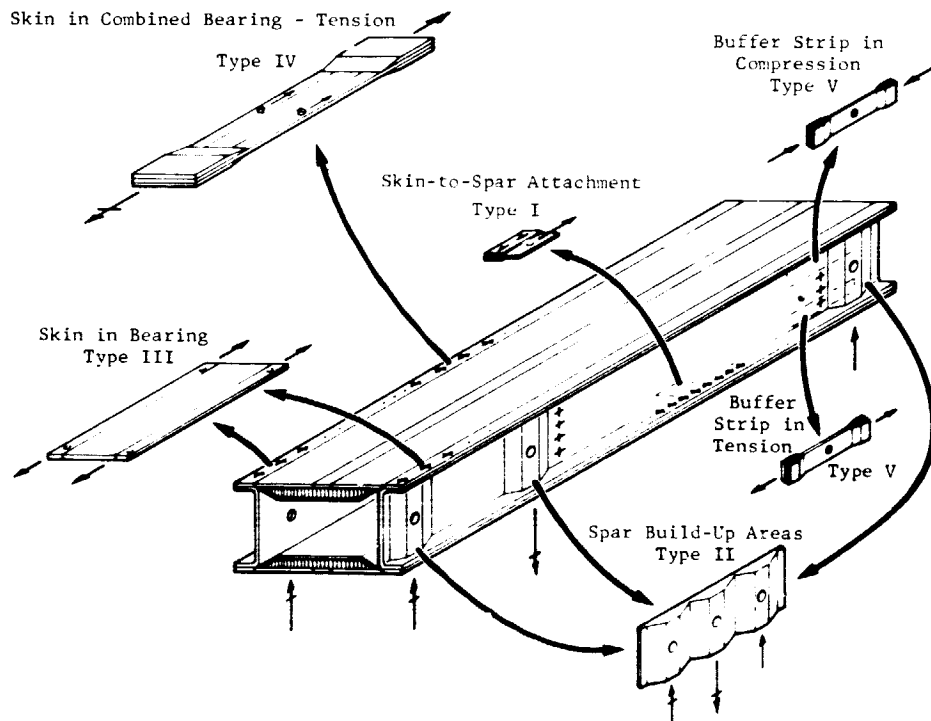


Figure 2 Selected Critical Elements - Wing Box

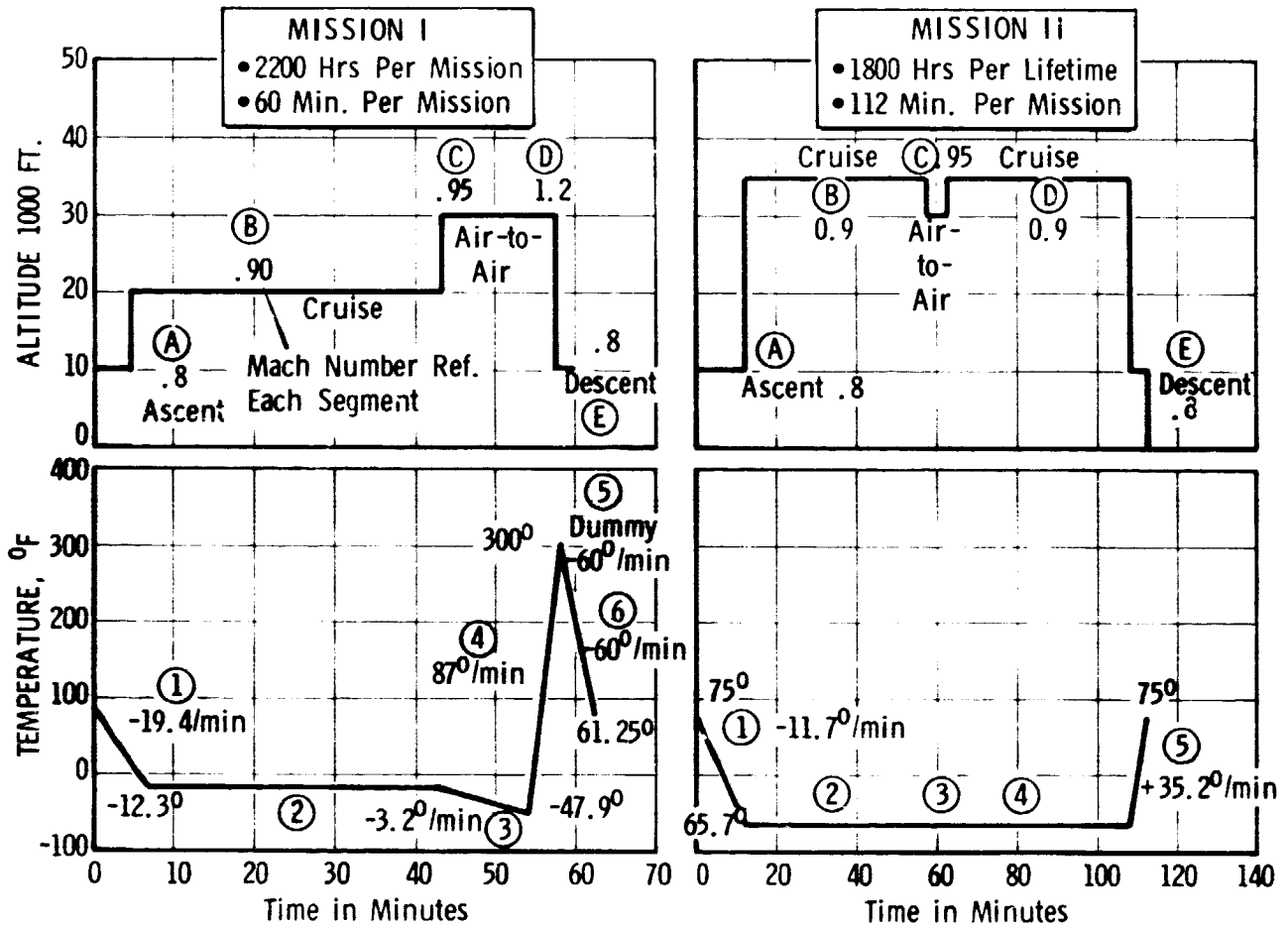


Figure 3 Mission and Temperature Profiles Used in Spectrum Development

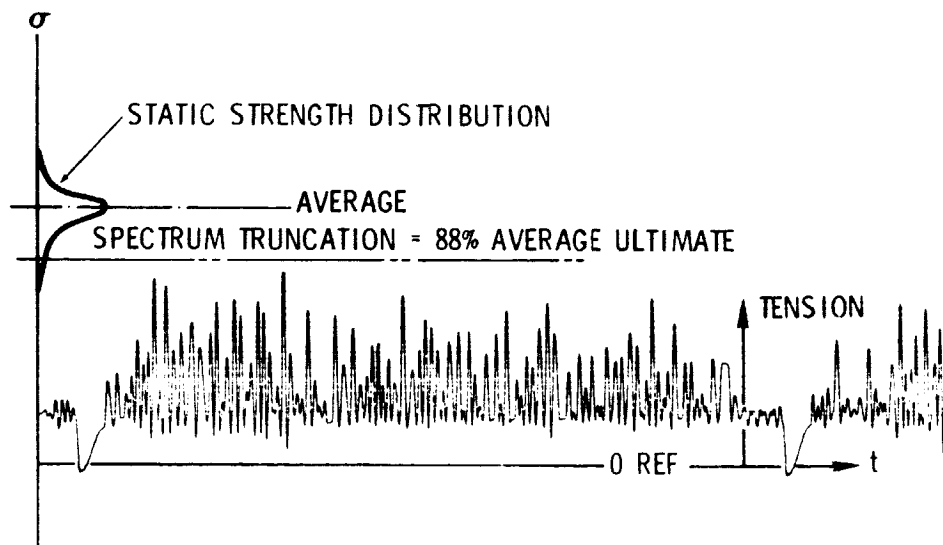


Figure 4 Relationship of Strength Distribution to Truncation Load



REPRODUCIBILITY OF THE ORIGINAL PAGE IS POOR

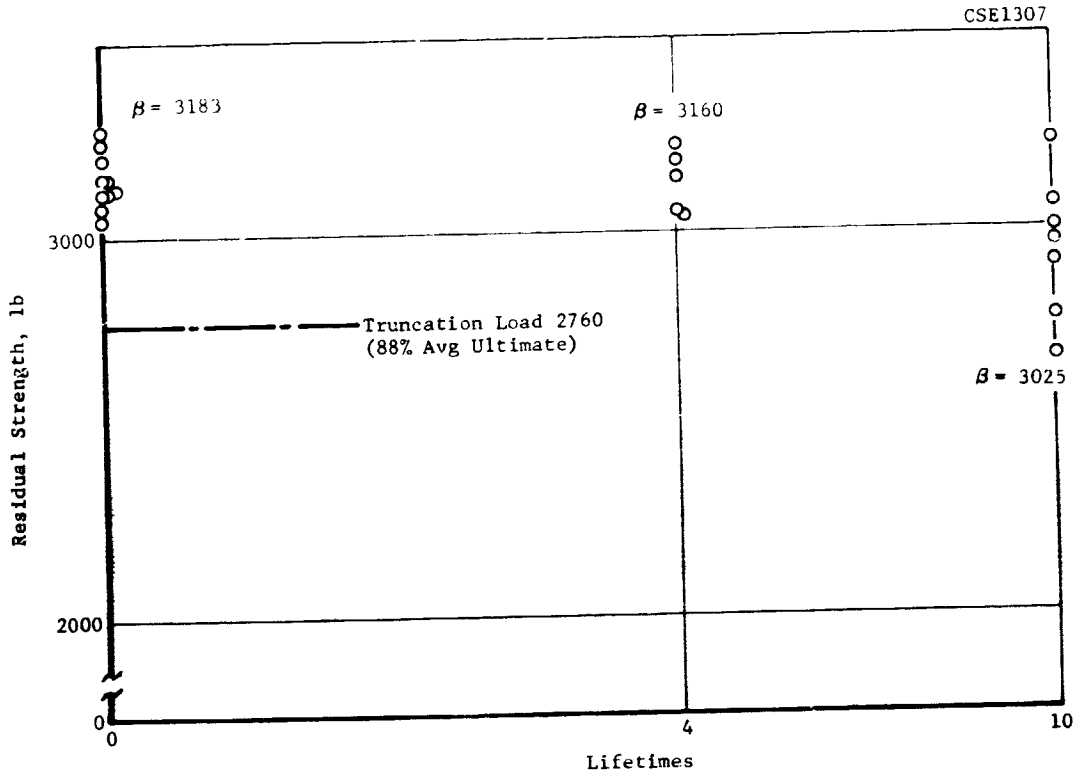


Figure 5 Residual Strength of Type I Bolted Joints Following Fatigue Loading - "Baseline" Spectrum

ELEMENT DATA USED TO PREDICT BEAM PERFORMANCE

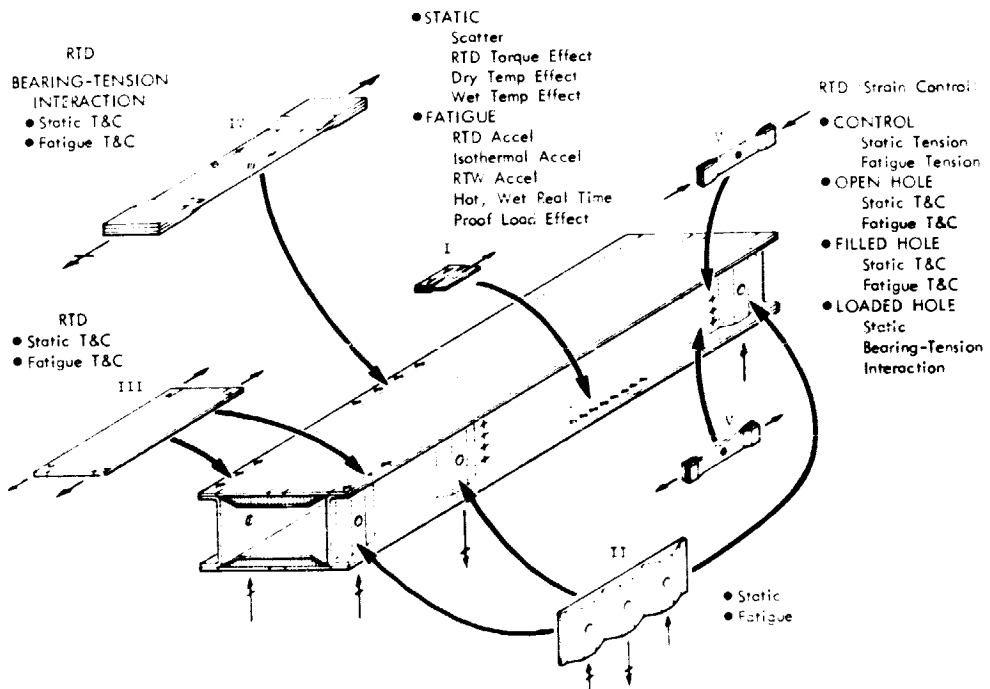


Figure 6 Summary of Elemental Data - Life Assurance Program

### Static

Type I



- Ultimate RTD bearing strength increases linearly with initial bolt torque (0 to 75 in-lb).
- Ultimate dry bearing strength decreases with increasing temperature (-60°F to +300°F). The relationship is exponential.
- At R.T., increasing laminate moisture content tends to increase bearing strength over initial dry strength up to moisture levels of approximately 80-percent of saturation (saturation is 1.7% weight gain).
- At elevated temperature, 200°F to 300°F, bearing strength decreases from initial dry elevated temperature for moisture contents greater than approximately 15-percent of saturation. For moisture levels less than 15-percent of saturation, there is an indication of a small strength increase over dry strength (at temperature).
- Failure mode is fiber tension before and after fatigue loading.

### RTD Accelerated Fatigue

- The baseline spectrum (no rms load magnification) has a negligible effect on residual strength characteristics through 4 simulated service lives. After 10-lifetimes of loading, there is evidence that the residual strength characteristics are affected, i.e. mean strength is reduced slightly and variance increases.
- Spectrum loading at a rms load magnification of 40% degrades residual strength characteristics rapidly, i.e. in less than one lifetime.
- Results of spectrum loading at a rms load magnification of 26% indicates a gradual reduction in mean residual strength and increasing variance through one lifetime.

### Constant Temperature Accelerated Fatigue (26% rms magnification)

- At 200°F, residual strength tends to increase after 0.1 lifetime of loading over initial static strength. After 1.0 lifetime mean residual strength has not been greatly affected, however, variance appears to be increasing.
- Results at 300°F indicate mean residual strength to be increasing over static strength through 1.0 lifetime.

### RTW Accelerated Fatigue (26% rms magnification)

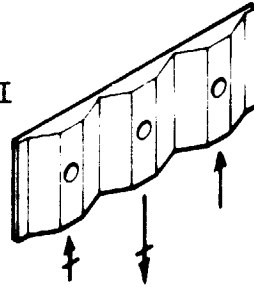
- RT wet strength after 1-lifetime is greater than dry strength.
- Proof loading Type I specimens has negligible impact on residual strength characteristics through 1-lifetime.

### Real Time Fatigue (26% rms magnification)

- The 300°F residual strength reductions observed between accelerated and real time spectrum loading appear to be due almost entirely to specimen moisture content.

Figure 7 Summary of Experimental Observation of Elemental Specimens - Life Assurance Program

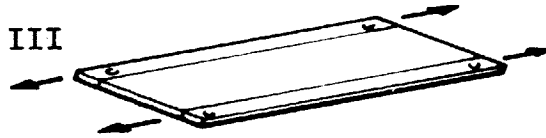
Type II



Static

- There is a negligible strength change when bolt torque is increased from 0 to 200 ft-lb. Torque of 300 to 400 ft-lb gives an approximate 11-percent strength increase over no torque.
- Failure mode is fiber tension before and after fatigue loading.
- Residual strength was degraded approximately 6-percent following 4 to 5 lifetimes of fatigue loading.

Type III



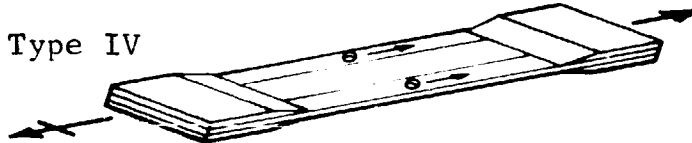
Static

- Failure mode is fiber tension before and after fatigue loading.
- Specimens loaded in compression have 12-17 percent higher strength than in tension.

Fatigue

- Static tensile strength increases initially (approximately 11%) following short-time fatigue loading as observed from residual tests after 0.1 lifetime.
- Fatigue failures were observed in tensile loading at all magnification levels.
- There were no fatigue failures observed in compression loading.
- All tensile specimens which survived fatigue loading, with one exception, had residual strengths greater than the maximum static strength value observed.

Type IV



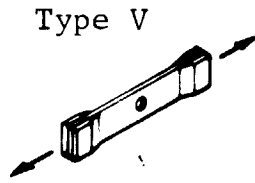
Static

- Failure modes vary with load condition. Predominant bearing reaction conditions had failures similar to Type I fiber tension. Predominant tensile reaction conditions had interlaminar failures associated with the bonded end grips, with the exception of 100% tension loading specimens which failed in fiber tension in the primary laminate.
- There is an interaction between tension and bearing strengths for the all graphite-epoxy "buffer strip" laminate when the buffer is adjacent to the edge.

Fatigue

- Residual strength does not increase for this specimen type after brief durations of fatigue loading.
- Fatigue failures were observed in tensile loading for the 50% bearing reaction condition.
- There were no fatigue failures in either tension or compression for the 20% bearing reaction condition, however, it was necessary to use the baseline spectrum (no rms magnification) in order to test the specimen without inducing end grip associated failures.
- In the case of the 20% bearing reaction condition the residual strength in tension degrades approximately 14% between 1 and 2 lifetimes.

Figure 7 Summary of Experimental Observation of Elemental Specimens - Life Assurance Program (Cont'd)



Type V

Static

- Strength is increased 500 to 600 pounds (approximately 29 percent) when the open hole of a Type V specimen is filled with a torqued fastener. This is essentially the same strength as the unnotched laminate.
- Compressive strength is greater than tensile strength in the case of open hole specimens.
- There is an interaction between tension and bearing strengths for the (±45) laminate.

Fatigue

- The relationship between spectrum magnification factor and fatigue life for both open hole and bolted specimens is accurately modeled by a power law function.
- Residual strain was observed after only a few cycles between 0 and 6000  $\mu\text{in/in}$  strain.
- There were no fatigue failures on bolted specimens for 6300  $\mu\text{in/in}$  peak strain or less.
- There is a rapid degradation of laminate modulus just prior to fatigue failure, however, a gradual loss is observed over a considerable period of life.

Figure 7 Summary of Experimental Observation of Elemental Specimens - Life Assurance Program (Cont'd)

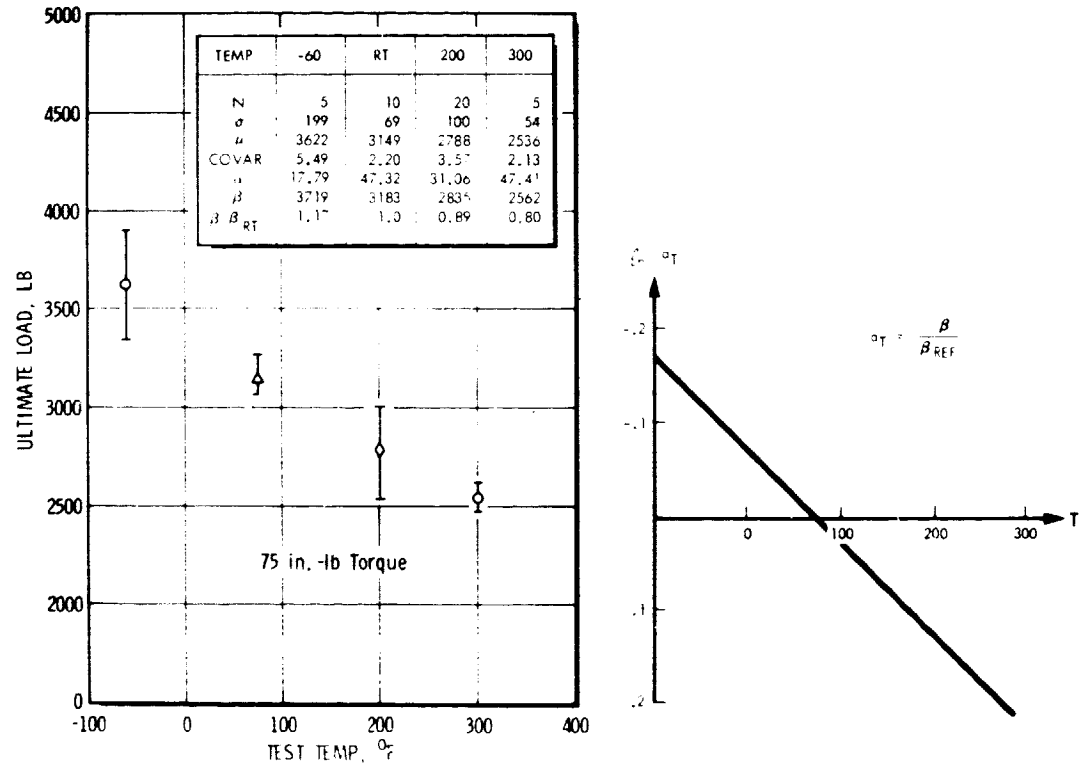


Figure 8 Ultimate Load vs Temperature Type I (Dry)

MOISTURE CAUSES SMALL LOSSES IN BOLT BEARING STRENGTH

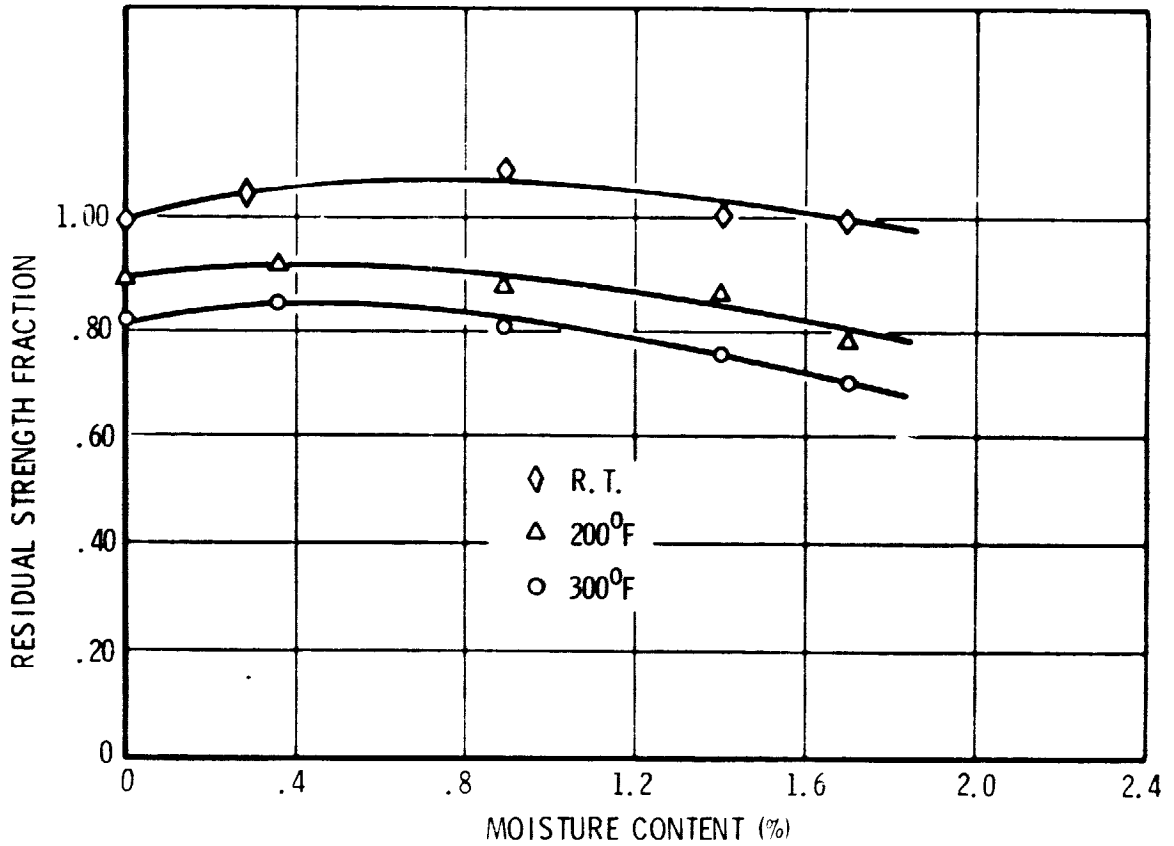


Figure 9 Effect of Combined Temperature and Moisture Upon Type I Bearing Strength

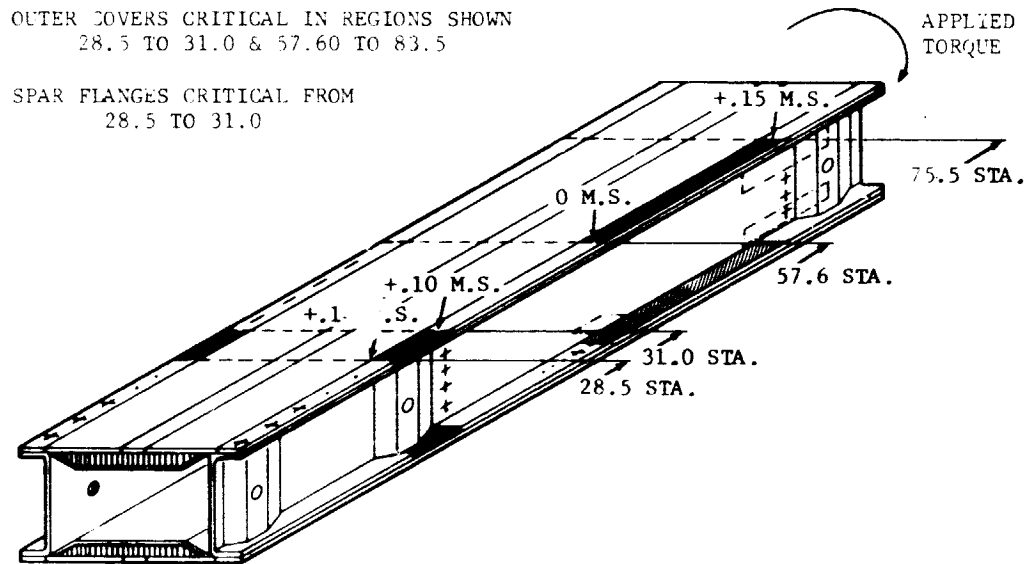


Figure 10 Critical Locations on Beam Component

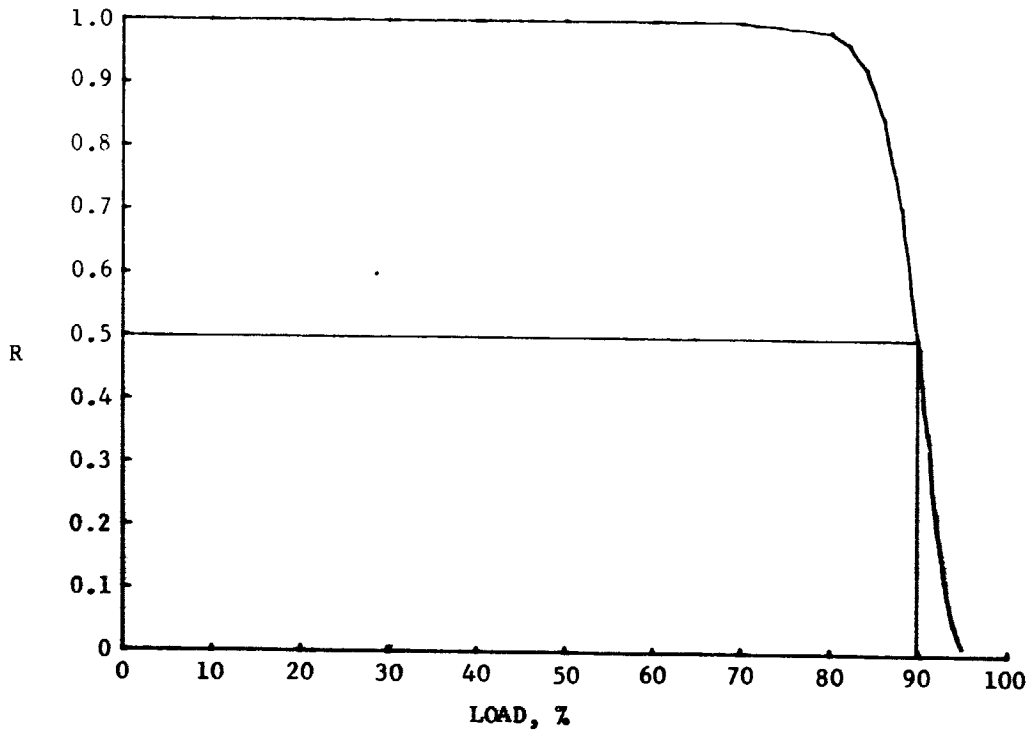


Figure 11 Complexity Effect of Multiple Fasteners

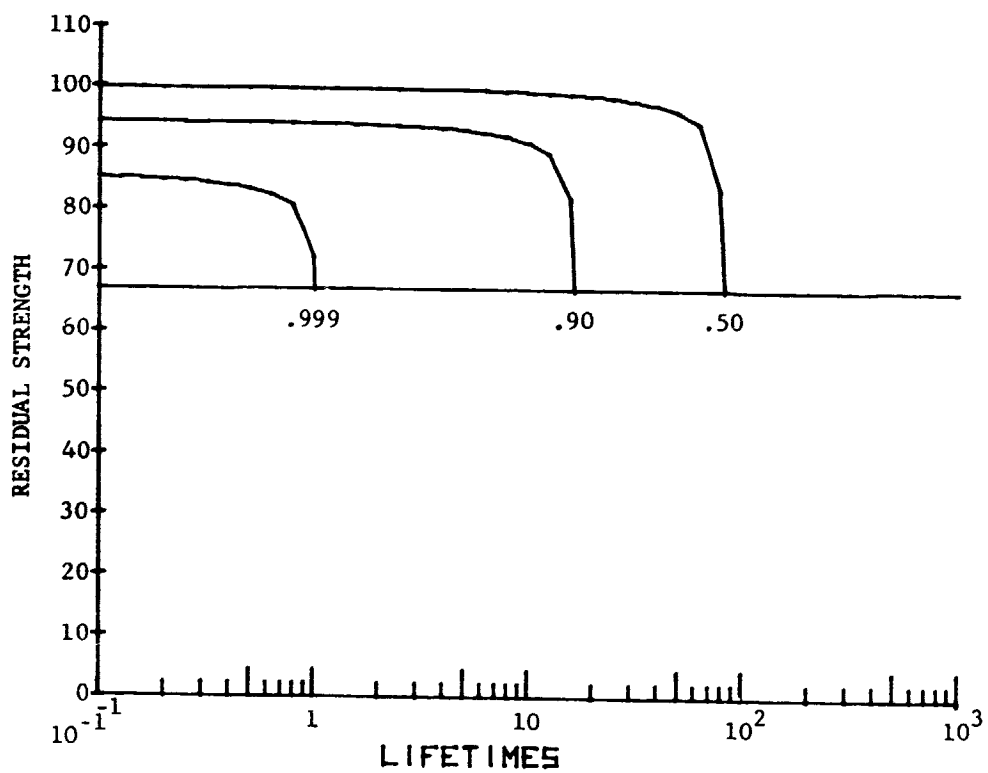


Figure 12 Box Beam Wear Out Characteristics at Limit Load

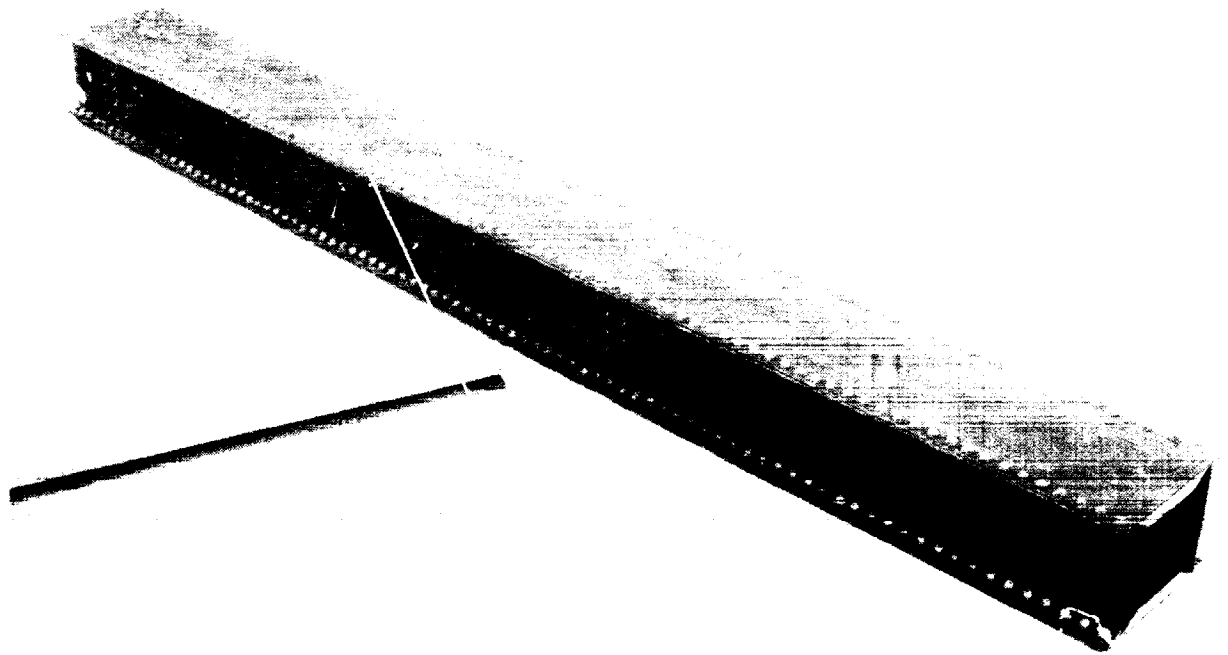


Figure 13 Box Beam Component

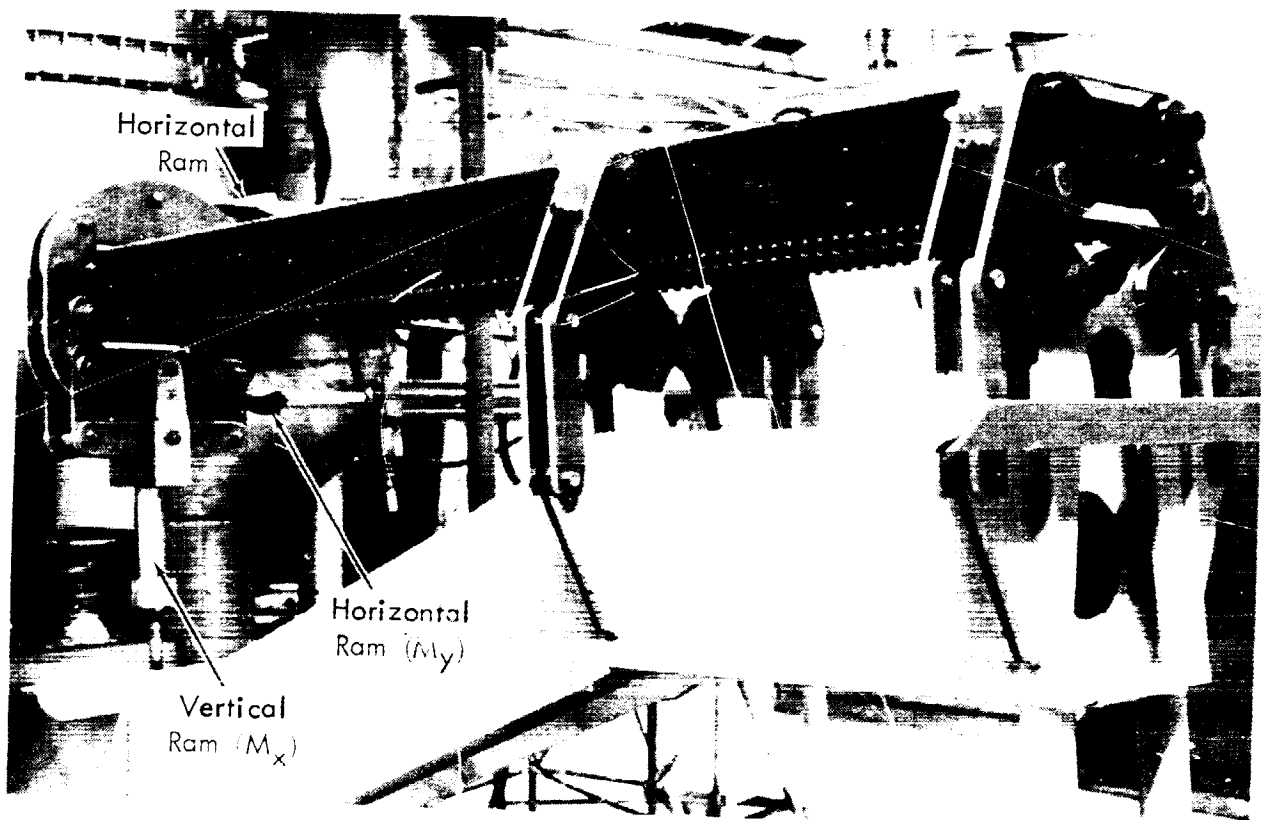


Figure 14 Component Fatigue/Static Fixture

722 ORIGINAL PAGE IS  
OF POOR QUALITY

RTD STATIC ULTIMATE TEST

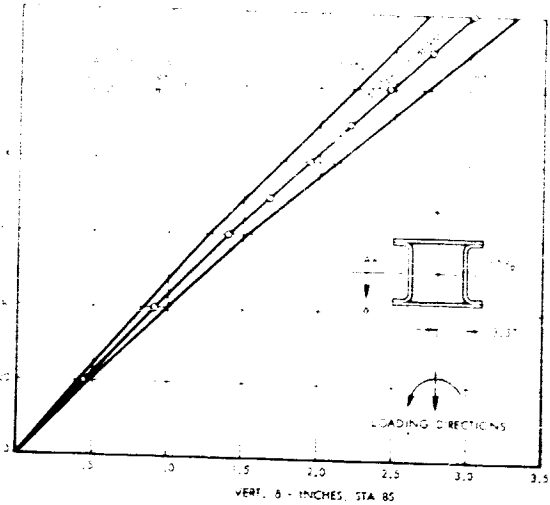
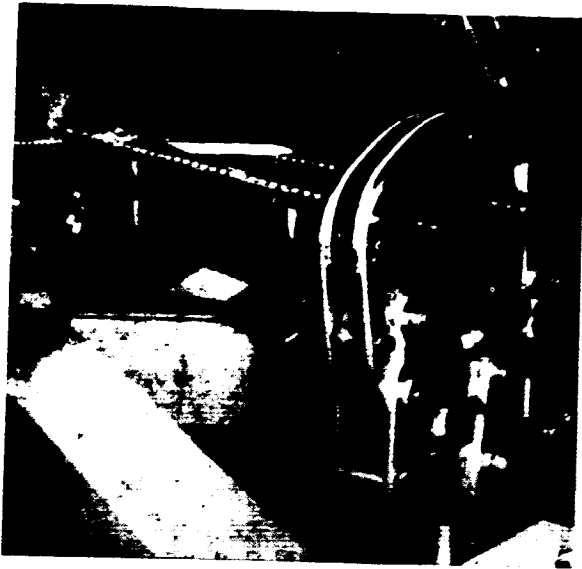


Figure 15 RTD Static Ultimate Test, Deflections

RTD STATIC FAILURE IN PREDICTED CRITICAL AREA  
Where 100% = Predicted Ultimate Load

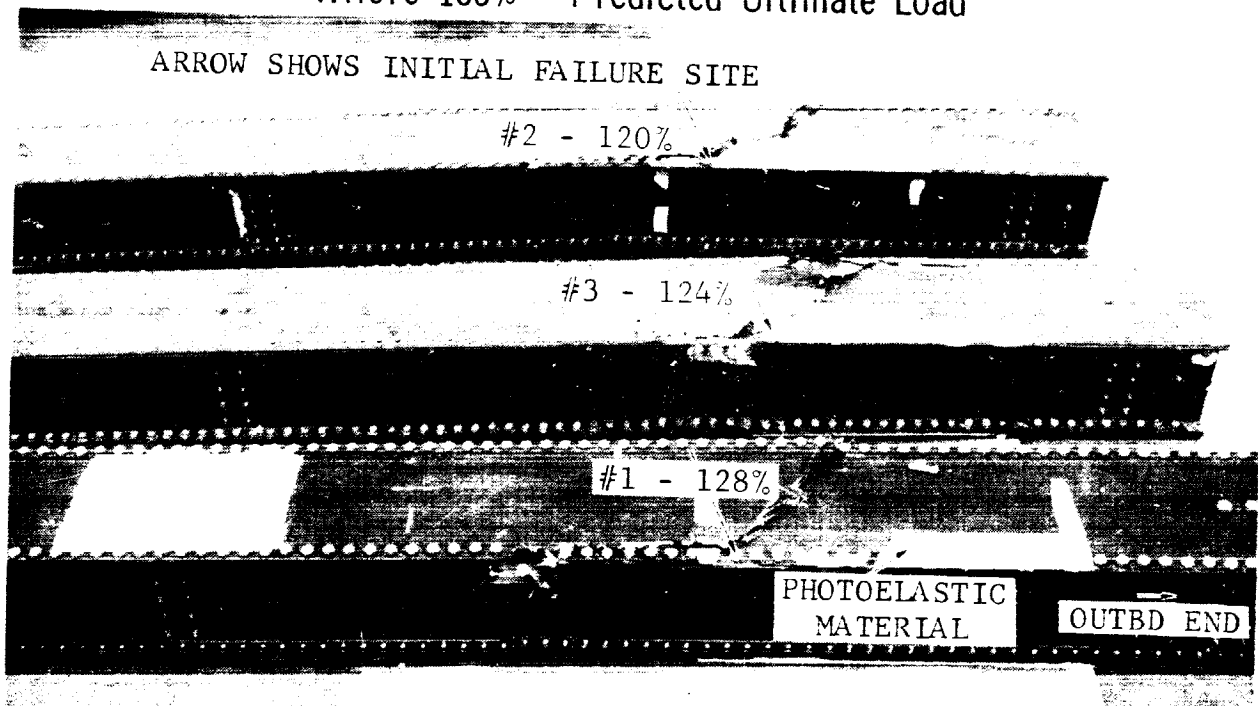


Figure 16 RTD Static Failure in Predicted Critical Area



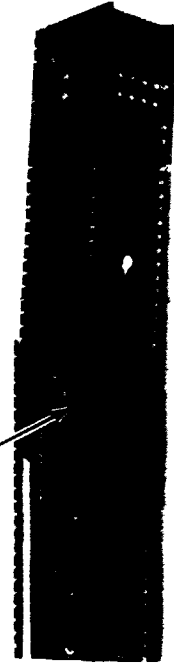
# RESIDUAL STRENGTH FAILURE MODES

CSE2290

OUTBD →

INITIAL FAILURE STA 59.5

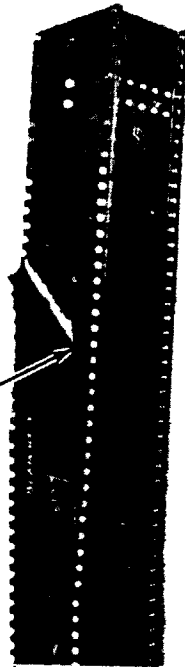
OUTBD →



BEAM 13

OUTBD →

STA 66.5



BEAM 15

STA 60.5



BEAM 14

OUTBD →

STA 60.5



BEAM 16

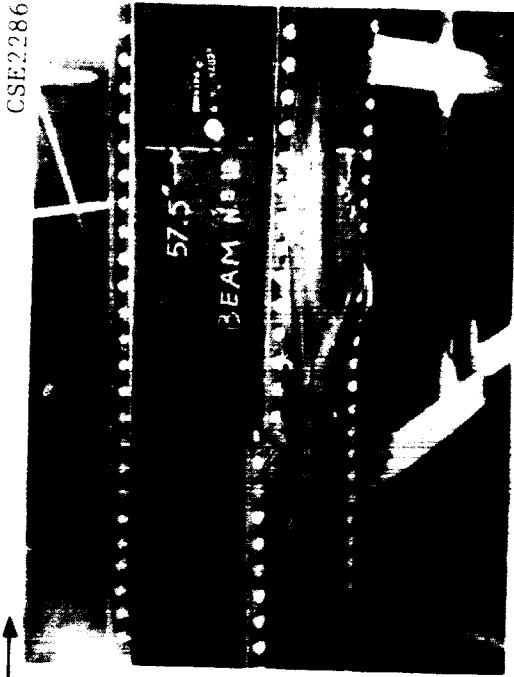
Figure 17 Tensile Failures - Residual Strength

# FATIGUE FAILURE MODE

OUTB'D REF →



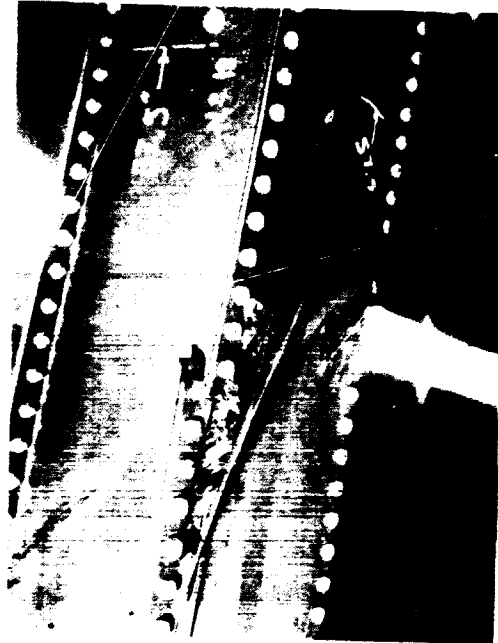
COMPRESSIVE COVER FAILURE - HIGH LOAD SIDE



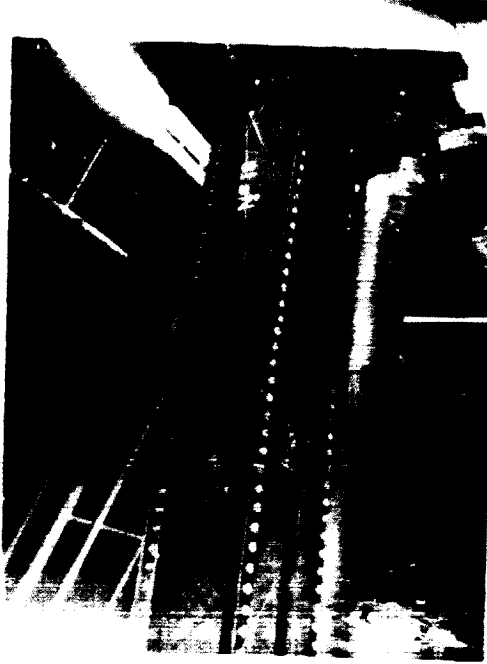
CLOSE UP OF FAILURE AREA

CSE:2286

← OUTB'D REF



CLOSE UP OF FAILURE AREA



COMPRESSIVE COVER FAILURE - LOW LOAD SIDE

Figure 18 Beam No. 18 - Fatigue Failure Compressive Skin

## BOX BEAM TESTS

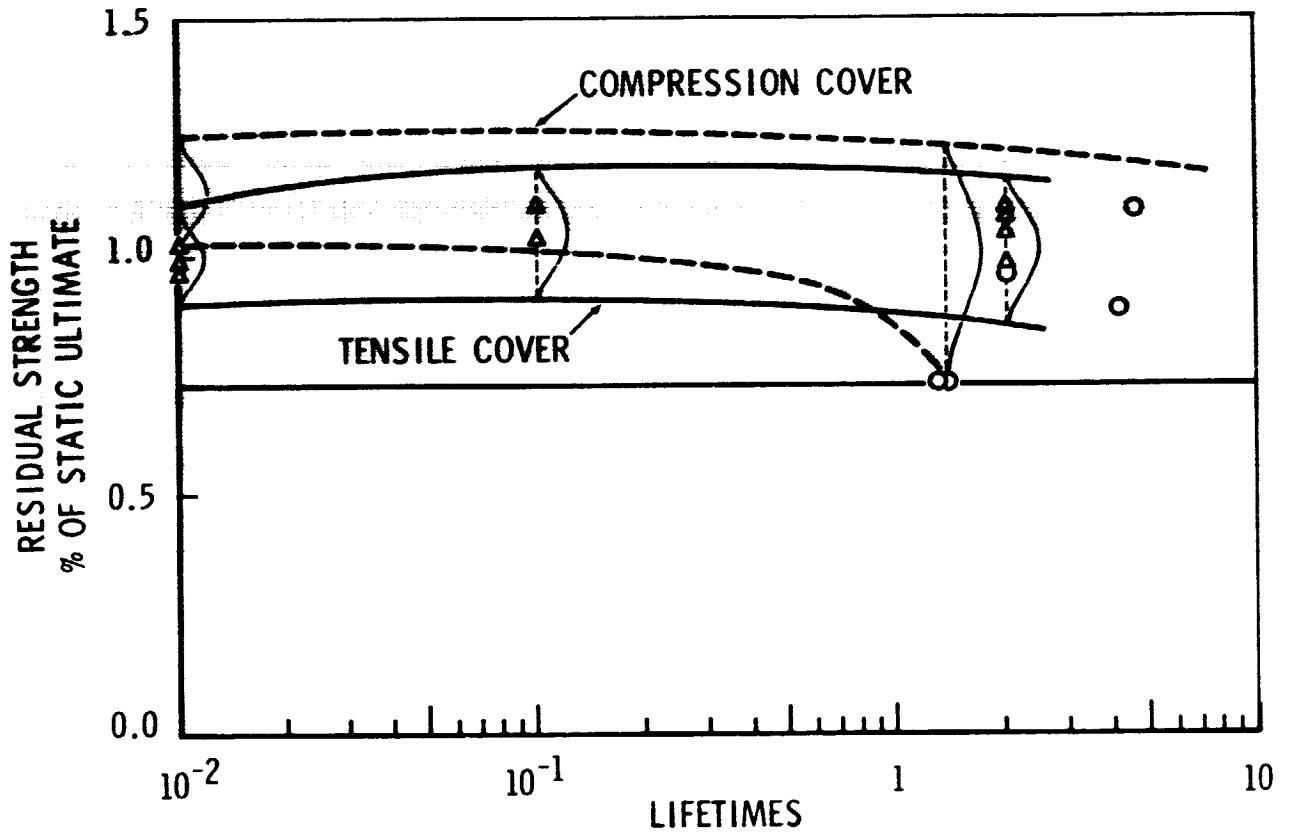


Figure 19 Implied Beam Strength - Life Characteristics

omit

ON PROCESS ZONE INTERACTIONS IN THE WEAROUT PROCESS

By M. Waddoups,  
General Dynamics

J. Halpin, and G. Lemon  
Air Force Flight Dynamics Laboratory

Paper not available for publication

## FATIGUE OF NOTCHED COMPOSITES

By P.V. McLaughlin, Jr., S.V. Kulkarni  
S.N. Huang and B. Walter Rosen

Materials Sciences Corporation

### SUMMARY

This paper describes a deterministic analysis for prediction and correlation of fatigue crack growth, residual strength, and fatigue lifetime for fiber composite laminates containing notches (holes). The failure model used for the analysis is based upon composite heterogeneous behavior and experimentally observed failure modes under both static and fatigue loading.

The fatigue analysis embodies the concept that material properties in the notch region are continually changing with cyclic loading; and that if these properties are known at a given time, they could be used in a static failure analysis to compute residual strength or crack propagation. It consists of the following two parts:

- (1) A static failure model capable of predicting crack growth, failure mode and stress at failure.
- (2) A method of determining laminate property changes with number of fatigue cycles.

### INTRODUCTION

The philosophy behind the present fatigue analysis of notched laminates is that cyclic loading and/or environmental effects (such as moisture) cause localized property degradation due to high stresses in the vicinity of the notch. This combination of reduced properties and stress concentrations causes localized damage near the notch. This damage results in a redistribution of local stresses and hence a change in strength. When these fatigue-induced changes cause a decrease in residual strength with number of cycles  $N$ , the fatigue lifetime is the cycle at which the residual strength reduces to the applied stress. A static failure model should be able to determine strength and stress-strain behavior of the notched laminate if the instantaneous properties of the material are known at any given  $N$ . Therefore, the two main ingredients in this fatigue analysis model are a valid static failure model plus a method for determining the degradation of material properties and growth of flaws with number of cycles.

**PRECEDING PAGE BLANK NOT FILMED**

For composite materials, a fatigue analysis is complicated by multiple failure modes which can exist in a laminate and which depend upon laminate geometry, notch size and number of cycles. These multiple failure modes are explicitly considered in the present analysis using an approximate "materials engineering" stress analysis and failure analysis approach which is tailored specifically to fiber composites.

The present analysis can be useful in (and is consistent with) reliability and lifetime design procedures such as the "wearout" concept, Reference 1.

### EXPERIMENTAL OBSERVATIONS

Tests of many fiber composite material systems (e.g., see References 2 and 3) have shown that there are primarily three modes of failure in a notched fiber composite laminate under tension. All three failure modes have been experimentally observed in both static and fatigue tests. The failure modes are illustrated schematically in Figure 1 which represents failed specimens (Reference 2) of notched boron/epoxy laminates. An axial crack (in the direction of the tensile load and along the 0 degree fibers) occurs when the central portion of the laminate near the notch pulls out of the remaining material due to high shear stresses in the notch vicinity. The axial crack propagates to the grips, ultimately causing specimen failure. A transverse or collinear crack propagation mode occurs when material immediately adjacent to the notch has been overstressed. An unstable crack initiates and grows perpendicular to the load direction. An off-axis crack may propagate along an off-axis fiber family oriented at an angle to the direction of loading. Additionally, interlaminar damage may influence one of these failure modes. Failure can occur by several of these modes in the same laminate.

In all failures, it has been observed that cracks propagate either along a fiber direction or transversely across the specimen perpendicular to the direction of tensile loading. The mode of failure can be different for fatigue or static loading of the same laminate. In addition, different notch sizes can trigger different failure modes in the same laminate. Other factors which can affect failure mode are ply orientation and constituent material properties.

### STATIC FAILURE MODEL

The primary modes of both static and fatigue failure of notched composites are:

- (a) Propagation of a crack parallel to one of the fiber directions (either axial or off-axis).
- (b) Propagation of a crack transversely across the specimen normal to the direction of applied tensile stress.

The basic static model for axial and transverse failure of notched composites was developed in Reference 4. Modifications to the basic model and addition of off-axis cracking were performed in Reference 5. Because of its importance to the fatigue analysis, a discussion of the static failure model is given here.

Axial failure is caused by the tendency of the material separated by the notch to "pull out". This causes high shear stresses in the direction of load and may result in propagation of an axial crack. Transverse crack propagation is caused by the stress concentration effect of the notch. The off-axis phenomenon has been judged to be physically similar to axial crack propagation, but with the added complexity of a combined stress state. The off-axis crack propagation model has, therefore, been developed from the axial crack propagation model by the inclusion of combined stress effects in a manner similar to that in Reference 6.

#### Axial and Transverse Crack Propagation Model

The model for static failure of a notched composite laminate is illustrated in Figure 2. The laminate is assumed to be under a tensile stress in the x direction. A notch of width  $2a$  is centered in the specimen at  $x = 0$ . Reference 2 has shown that notch shape is not as important to failure as the size (width) of the notch. Hence, a slit, circular hole, or rectangular hole of width  $2a$  will all be modelled by a discontinuity in the laminate of  $2a$ . The work "notch" will then apply to any through-the-thickness hole of any shape.

The central core region wants to "pull out" from the notch area due to the applied tensile loading. This core, however, is restrained by shear stresses between the core and the adjacent intact material. These shear stresses generally result in a region of high shear strain parallel to the loading direction. Immediately adjacent to the notch core, there is a region of width  $m$  which is overstressed due to the notch. It is assumed that this region bears the full stress concentration effects. Everywhere outside the core and overstressed regions, the laminate is uniformly strained. Shear strain due to core pullout is assumed to extend over a region three times the size of the overstressed fiber regions. The laminate axial shear stress-strain curve is approximated as linear elastic-perfectly plastic. The axial shear modulus  $G_{xy}$ , the shear failure stress,  $\tau^0$ , and

the shear failure strain,  $\gamma_{ult}$ , are chosen to obtain the best fit to the actual laminate shear stress-strain curve.

As the gross laminate tensile stress  $\sigma$  is increased, the shear stress at the notch tip will reach  $\tau^0$ . Continued loading will cause an inelastic region to form in the axial direction. Eventually,  $\gamma_{ult}$  will be exceeded at the notch tip and a crack will begin to grow in the axial direction. When this crack grows very large (mathematically, to infinity) the notched laminate is considered to have failed in an axial crack propagation mode. If, however, material in the overstressed region adjacent to the notch is stressed past the tensile strength of the unnotched laminate, a crack will propagate in the transverse or y direction. In this latter case, the laminate is considered to have failed in a transverse or collinear crack propagation mode.

References 4 and 5 fully describe the static failure model and resulting stress and deformation analysis for axial and transverse crack propagation modes.

In the analysis,  $\zeta$  is a nondimensional axial crack length extending from the notch tip ( $x = 0$ ) to the bottom of the plastic zone. The nondimensional distance from the notch to the beginning of the elastic zone is  $\alpha$ , and includes axial crack and plastic zones. For this reason,  $\alpha$  is called the "inelastic length" and is a good measure of the extent of damage in the axial direction from the notch tip.

The static failure analysis has the capability of computing both  $\alpha$  and maximum overstress in material adjacent to the notch for a given applied laminate tensile stress so that tendency to axial or transverse crack propagation modes can be monitored. Typical results of the analysis are shown in Figure 3. The dashed line shows the growth of the axial damage region with increased tensile stress  $\sigma$ . The applied stress at which plasticity is initiated at the notch tip is called  $\sigma_y$ . At some higher stress level  $\sigma_c$  an axial crack will begin to grow from the notch tip. The failure stress of the notched composite in the axial crack propagation failure mode is  $\sigma_A$  ( $\alpha \rightarrow \infty$ ). The solid line in Fig. 3 also shows the growth of notch tip overstress with applied stress  $\sigma$ . As stressing of the composite increases, it is possible that the maximum overstress in the adjacent material,  $\sigma_{SCFM}$  will increase to the point where it exceeds the unnotched laminate strength,  $\sigma_x^t$ . In this case, transverse crack propagation ensues. The applied laminate stress at which transverse cracking occurs is called  $\sigma_T$ . Also, as the axial crack grows, a blunting of the stress concentration effects of the notch will occur. This



could cause a decrease in stress in the adjacent material before it reaches failure levels, and remove any possibility of transverse crack propagation. In the figure, transverse failure occurs.

#### Off-Axis Crack Propagation Model

For some laminates, such as a  $[\pm 45]$  boron/epoxy laminate, the mode of fatigue cracking is off-axis along a fiber direction (in this case, the  $\pm 45$  degree direction as in Figure 2). For this mode of failure, the preceding model and analysis are not directly applicable without modification. This subsection describes modifications to the original model which were made to perform analysis of off-axis cracking.

Figure 4 illustrates the stress state around a notch which is tending to develop a crack along the  $\pm \theta$  fibers. Along the load axis the gross laminate stress state is axial tension. However, the crack is not growing in the direction of load. Suppose material axes  $x'$  and  $y'$  are selected in the  $\theta$  direction (Figure 4a). The crack will be growing in the direction of the  $x'$  axis tensile stress  $\sigma_{x'}$ . Due to the rotation of axes, the tensile stress  $\sigma_{x'}$ , will not be the same as the  $x$  direction stress  $\sigma$ . In addition, there will generally be substantial axial shear and transverse tensile stresses in the  $x'y'$  coordinate system. Also, the notch is now inclined at an angle  $\theta$  to its original position.

It has been shown (Reference 2) that the shape of the notch (slit, rectangular, circular, etc.) in a laminate does not greatly affect composite failure. The width of a notch perpendicular to the direction of loading is the only notch dimension which is of importance. Therefore, the slit notch configuration shown in the  $xy$  and  $x'y'$  coordinate systems (Figures 4b and c, respectively), can be treated for analysis purposes as shown in Figure 4d. In this case, the original notch has been replaced by an equivalent notch of size  $2a \cos \theta$  in the  $y'$  direction (note that no change need be made for a circular hole, and that an increase or decrease in equivalent notch size may be necessary for a rectangular hole).

Combined stress effects are taken into account in an approximate fashion. Laminate gross transverse tension  $\sigma_{y'}$ , and axial shear  $\sigma_{x'y'}$ , are superimposed on the axial shear stress at the notch root which would be computed from the axial crack analysis due to only  $\sigma_{x'}$ , (see Figure 5). The main effect of this superposition will be to increase the likelihood of  $x'y'$  axial shear failure. Throughout the loading process, the axial shear stress  $\sigma_{x'y'}$ , reduces the stress required from the analysis to cause axial cracking. The transverse normal stress  $\sigma_{y'}$ , is assumed to

further reduce the shear strength through a quadratic interaction equation. Ref. 5 and 6 describe the procedure in more detail.

Once the failure stress  $\sigma_A$ , has been determined in the  $x'y'$  system, the corresponding stress state  $\sigma_{x''}$ ,  $\sigma_{y''}$ ,  $\sigma_{x''y''}$  at failure is known. The stress transformation equations are then used to find the corresponding tensile failure stress  $\sigma_\theta$  ( $\sigma_x$ ) in the original  $xy$  coordinate system.

### Static Failure Analysis Procedure

The static failure analysis procedure for notched composites which has been developed utilizing the axial/transverse model and the off-axis model is as follows (see Figure 6):

1. The axial/transverse failure model is exercised to compute the laminate stresses causing axial crack failure ( $\sigma_A$ ) and transverse crack failure ( $\sigma_T$ ).
2. The off-axis model is exercised to compute the laminate stress  $\sigma_\theta$  which causes failure due to a crack running along  $\theta$ -direction fibers.
3. The failure stresses  $\sigma_A$ ,  $\sigma_T$ , and  $\sigma_\theta$  are compared. The lowest is the predicted failure stress and represents the dominant failure mode.

### FATIGUE MODEL

Fatigue failure in notched fiber composite laminates occurs as a result of growth of cracks along preferred directions in the laminate as load cycling proceeds. This crack growth is influenced by local material properties which change as a result of the repeated loads. When the local material properties and the geometry of the damaged regions are defined after any number of cycles, the residual static strength of the material can be determined from the static model outlined in the preceding section. The main inputs to the static failure analysis are the laminate elastic properties and the laminate failure stresses in axial tension and axial shear. If these properties are known at any given cycle, it is possible to perform a static analysis to determine the static residual strength of the notched composite. If the residual strength so computed is less than the maximum cyclic stress, the fatigue lifetime of the notched composite has been exceeded.

The main ingredients to the fatigue analysis, then, are:

- (a) Determination of changes in material properties in the notch region with number of cycles.
- (b) Utilization of these properties in a static failure analysis to predict residual strength.

The approaches taken to these aspects are discussed below.

#### Notch Region Material Degradation

In a notched composite, the main cause of crack growth is the tendency of the notched core region to pull out, generating stress concentrations in adjacent material and very high shear stresses in the axial direction. Therefore, most fatigue degradation will occur due to shear and tensile stresses in the region immediately surrounding the notch, and the main result will be to alter the axial tensile and axial shear behavior.

The most direct way to determine laminate tensile and shear behavior under cyclic loads is simply to perform fatigue tests on unnotched specimens. This method, though straightforward, would require a battery of tests for each laminate layup geometry in both the axial  $xy$  and off-axis  $x'y'$  systems. The results would only be applicable to the specific laminate tested; each new laminate would require its own battery of tests. Therefore, a method of generating laminate fatigue behavior from lamina properties was developed and is as follows:

1. The laminate stress state which exists in the notch vicinity (combined axial tension and axial shear) is determined utilizing the static failure analysis. The method for so-doing is presented in detail in Reference 5.
2. A constant strain laminate analysis is performed on the laminate under the notch root stresses utilizing initial static lamina properties. From this laminate analysis, the axial normal stress, the axial shear stress, and the transverse normal stress which exist in each layer of the laminate are computed.
3. From data on fatigue behavior of a unidirectional lamina, calculations are made of changes in lamina elastic properties and lamina residual failure stresses after some small increment in cycles. It is assumed that, over the range of cycles considered, the individual stresses in each lamina are not significantly changing.
4. The changed lamina elastic properties and lamina strengths are re-introduced into the laminate analysis to predict new

laminates elastic properties and failure stresses.

5. A second increment of cyclic loading is selected, and steps 1 through 4 are repeated.

This procedure, shown in Figure 7, can be repeated enough times as is necessary to find the residual strength after a required number of cycles, or until the residual strength of the laminate reduces to the stress levels existing at the notch. When the latter occurs, the fatigue lifetime of the material near the notch has been reached.

Figure 8 illustrates the kind of lamina fatigue information which would be necessary to generate laminate fatigue properties in the notch vicinity. Only axial tensile strength, axial shear strength, and axial shear modulus are illustrated, although additional information (such as transverse tensile strength and modulus) may also be necessary.

The following subsections outline the use of this procedure with the static failure model to perform fatigue analysis of notched composite laminates.

#### Axial/Transverse Fatigue Crack Modes

Figure 9 illustrates the analysis method for the axial and transverse fatigue crack propagation modes. At  $N = 1$  cycle, all material properties are at their initial static values. Property changes with  $N$  can be determined directly from lamina properties by laminate analysis methods described above. The altered material properties after a given  $N$  are used as inputs to the static failure analysis model to predict the residual strength of the notched composite and the corresponding failure mode. In Figure 9, static behavior using material properties which exist at several decades of  $N$  is shown. In the lower left are curves of axial "crack" length  $a$  (ineffective length) versus applied stress  $\sigma$ . The axial mode failure stresses  $\sigma_A$  are the values of  $\sigma$  at which the axial cracks extend to infinity. Overstress in material adjacent to the notch  $\sigma_{SCFM}$  versus the applied stress is plotted in the lower right. The transverse mode failure stresses  $\sigma_T$  are the applied stresses at which material adjacent to the notch fails in axial tension.

The resulting initial static failure prediction ( $n = 1$ ) is that the notched laminate will fail by transverse crack propagation at a stress  $\sigma_r = \sigma_T^0$ . After ten cycles has occurred, a similar situation is predicted. However, the transverse crack propagatic

failure strength  $\sigma_T^{(1)}$  has now increased and the axial crack mode strength has decreased. The resulting residual failure stress is  $\sigma_r = \sigma_T^{(1)}$ . At  $10^2$  and all subsequent cycles, the reverse situation occurs. Either  $\sigma_T$  is greater than  $\sigma_A$ , as occurs for  $N = 10^2$ , or the maximum overstress in the material adjacent to the notch never exceeds the unnotched laminate strength. Therefore, for  $n > 10^2$  cycles, the transverse crack propagation mode never occurs.

The information contained in Figure 9 for residual strength and axial crack growth can be utilized as shown in Figure 10 to predict the residual strength, the fatigue lifetime, and axial fatigue crack growth with  $N$ . In Figure 10a, residual strength by both the transverse crack propagation mode and the axial crack propagation mode are plotted versus number of cycles  $N$ . As seen in the figure, transverse cracking will occur until approximately 20 cycles at which time axial crack propagation becomes the mode of failure. The notched composite residual strength is always determined by the lower of the two curves. In this hypothetical example, the composite residual strength increases until  $N = 20$  cycles, then decreases until the strength of the composite becomes equal to the maximum cyclic stress. The composite will fail on the succeeding cycle,  $N_f$ , which is the resulting notched composite laminate lifetime.

The static axial crack length curves of Figure 9 may be utilized to calculate the axial fatigue crack growth with number of cycles. At any given number of cycles, the axial crack length will grow to the length indicated by the intersection of the maximum cyclic stress level with the appropriate crack length curve. Figure 10b shows the results for this example. A similar computation can be made for transverse crack growth.

#### Off-Axis Fatigue Crack Mode

In principle, the same procedure used for axial crack propagation can also be applied to the off-axis fatigue crack propagation mode. Special consideration is necessary, however, to treat the combined stress state in the off-axis  $x'y'$  coordinate system. A calculation must first be made of the stress state  $\sigma_{x'}$ ,  $\sigma_{y'}$ , and  $\sigma_{x'y'}$  around the notch root which occurs during fatigue loading. This is performed in a manner identical to that used to obtain the stress state around the notch for static loading. With the combined stress state around the notch computed, it is necessary to determine how the laminate  $x'y'$  shear properties change under the combined cyclic loading. To do this, the laminate analysis technique discussed earlier is used to determine layer

stresses which occur due to  $\sigma_{x'}$ ,  $\sigma_{y'}$ , and  $\sigma_{x'y'}$ . Laminate property changes are computed from basic lamina fatigue data, and laminate analysis is employed to find changed laminate properties. The method is described in more detail in Reference 5.

### Fatigue Analysis Procedure

This subsection summarizes the methodological framework which has been developed to analyze the fatigue behavior of notched composite laminates. The analysis procedure utilizes: the static failure model; lamina fatigue properties in axial tension, axial shear, and/or transverse tension; and constant strain laminate analysis techniques.

A notched laminate with known fiber orientation properties and constituent layer elastic, static failure, and fatigue properties is under cyclic fatigue loading at a maximum applied stress of  $\sigma_{max}$  and a stress ratio R. Initial static laminate properties are known either from experiment or from a laminate analysis prediction based on layer behavior.

The fatigue analysis is begun by first predicting the initial static strength in the axial, transverse, and off-axis propagation modes. The lowest of the three failure stresses will be the static failure strength of the notched laminate. From the static analysis, the average axial tensile and shear stresses at the notch root are computed. A small increment of cycles is chosen (say, a decade). The laminate is analyzed with notch root stresses as an applied cyclic stress state, and the new laminate elastic and failure properties near the notch are computed. From these revised laminate properties, one can determine the residual strength of the notched laminate following the first increment in cyclic loading. This procedure is repeated until either the residual strength is obtained at a given desired cycle, or until the notched laminate residual strength drops to  $\sigma_{max}$ .

This procedure is followed for the axial and transverse crack propagation modes, and also for the off-axis crack propagation mode. For a given N, the residual strength will be the lowest of  $\sigma_A$ ,  $\sigma_T$ , and  $\sigma_\theta$ . The fatigue lifetime,  $N_f$ , is the number of cycles at which the residual strength of the laminate drops to the maximum cyclic stress,  $\sigma_{max}$ .

A flow chart of this procedure is presented in Figure 11.

## CONCLUDING REMARKS

The fatigue analysis of notched composites presented here incorporates heterogeneous material behavior and experimentally observed failure modes for fiber composite laminated materials. The analysis utilizes an approximate "materials engineering" approach along with simple experimental data. The philosophy by which the model has been constructed is that repeated loading causes changes in material properties near the notch. These property changes result in altered notched composite residual strengths and eventually cause fatigue failure.

The current model has distinct advantages in that only simple tests on simple laminates are required as inputs to the analysis. These tests are: residual strength and fatigue lifetime tensile tests of unnotched [0] laminates, [90] laminates, and/or [ $\pm 45$ ] laminates in tension. Although the tests required are in depth, they are uncomplicated and relatively easy to perform. Once the results from these tests have been obtained for a given material, any laminate configuration and any notch geometry can be analyzed.

Applications of the analysis presented herein and in Reference 5 show the following:

- (1) Fatigue cycling can cause an initial increase in residual tensile strength of notched composites. Subsequent cycling may either cause a reversal of this trend and eventual fatigue failure, or it may result in a continued increase in strength and runout. Such behavior varies with notch size and laminate layup geometry.
- (2) Static failure modes may differ from fatigue failure modes in the same notched laminate. Therefore, a material exhibiting higher initial static strength may have a shorter fatigue lifetime, and vice-versa.

The fact that notched composites can have different static and fatigue failure modes is a result of high significance. A common assumption in structural reliability analysis is to assume a one-to-one correlation between static strength distribution and fatigue strength distribution. The results of the present analysis indicate that in certain cases such an assumption may not be valid. The concept of static proof testing to ensure fatigue lifetime should therefore be critically re-examined. It is expected that the current fatigue analysis will prove useful in developing a design methodology for notched composites, especially in the situations where the one-to-one correlation does not exist and static proof testing for fatigue life is not valid.

The static failure model has been substantiated by experiment and analysis performed in References 2 and 4. Fatigue data does not exist which is of the form necessary to quantitatively corroborate the current fatigue analysis. However, the analysis does show good quantitative agreement with such fatigue data as are available. Also, a comprehensive testing/analysis program is underway to verify the applicability of the mathematical model and to correlate it with data from specific notched composite laminates.

#### ACKNOWLEDGEMENT

The work presented herein was supported by the National Aeronautics and Space Administration, Langley Research Center, under contract no. NAS1-12967 to Materials Sciences Corporation.

#### REFERENCES

1. Halpin, J. C., Jerina, K. L., and Johnson, T. A.: Characterization of Composites for the Purpose of Reliability Evaluation. Analysis of the Test Methods for High Modulus Fibers and Composites, ASTM STP 521, 1973, pp. 5-64.
2. Durchlaub, E. C., and Freeman, R. B: Design Data for Composite Structure Safelife Prediction. AFML-TR-73-225, March, 1974.
3. Marcus, L. A., and Stinchcomb, W. W.: Measurement of Fatigue Damage in Composite Materials. Experimental Mechanics, February, 1975, pp. 55-60.
4. Kulkarni, S. V., and Rosen, B. Walter: Design Data for Composite Structure Safelife Prediction: Analysis Evaluation. TFR/2221, Materials Sciences Corporation, August, 1973, see also Reference 2.
5. McLaughlin, P. V., Jr., Kulkarni, S. V., Huang, S. N., and Rosen, B. Walter: Fatigue of Notched Fiber Composite Laminates. Part I: Analytical Model. Final Report, contract no. NAS1-12967, NASA-Langley. TFR/509, Materials Sciences Corporation, July, 1975.
6. McLaughlin, P. V., Jr., and Rosen, B. Walter: Combined Stress Effects upon Failure of Fiber Composites. Final Report, contract no. N62269-73-C-0800, NADC. Materials Sciences Corporation, April, 1974.



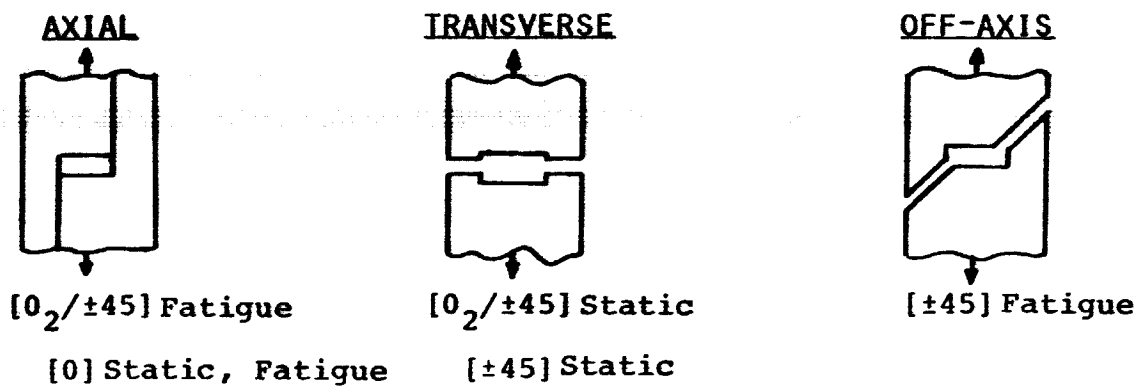


FIGURE 1. OBSERVED STATIC AND FATIGUE FAILURE MODES IN NOTCHED BORON/EPOXY LAMINATES (REF. 2)

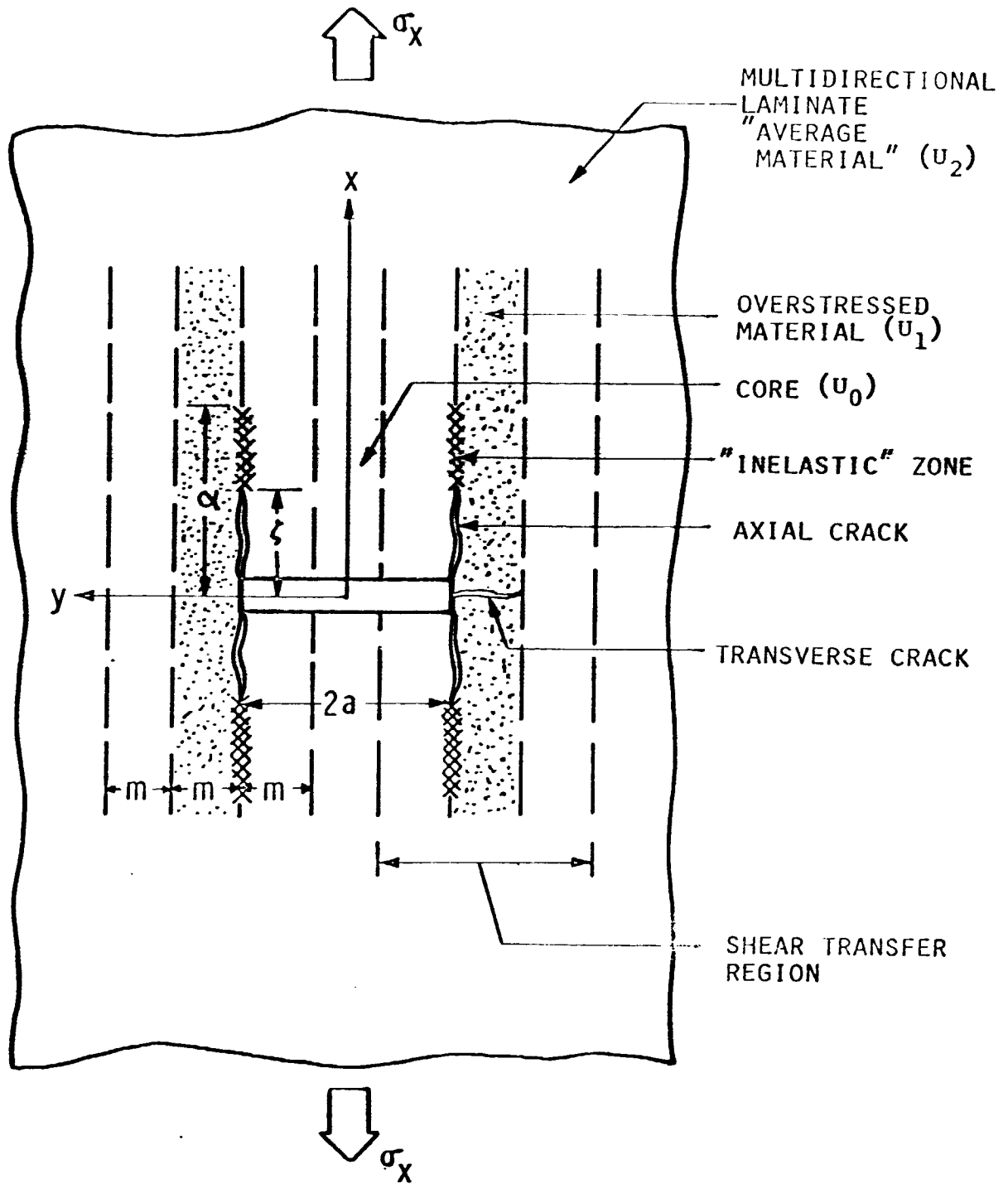


FIGURE 2. "MATERIALS ENGINEERING" MODEL FOR A NOTCHED LAMINATE

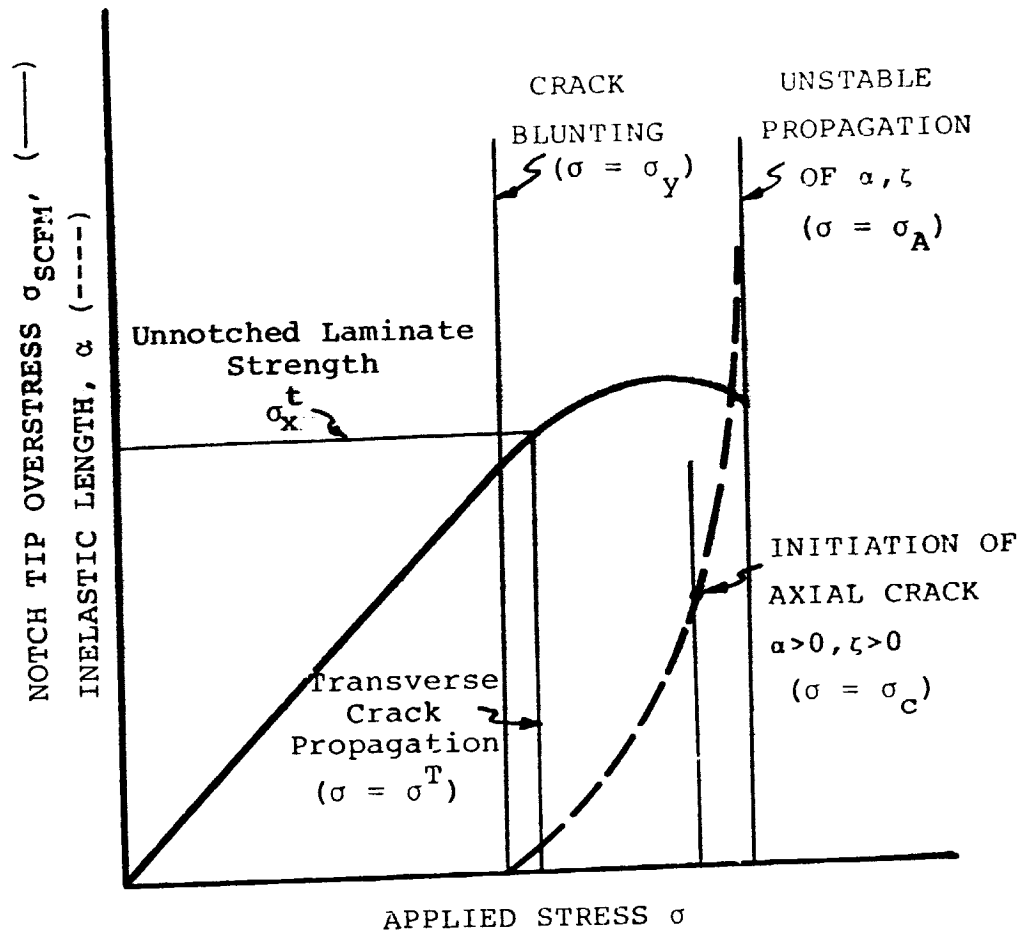
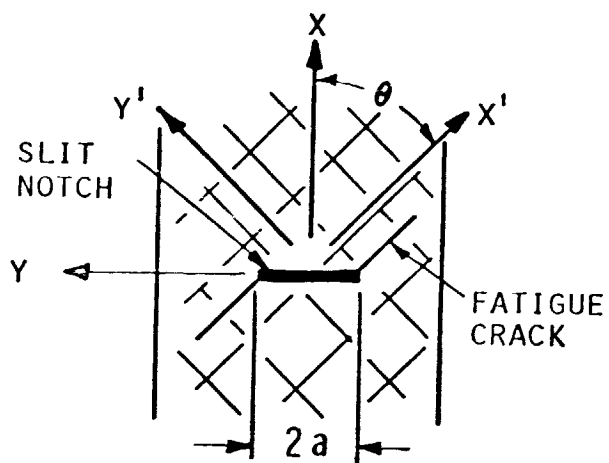
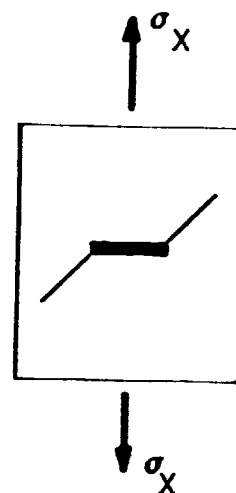


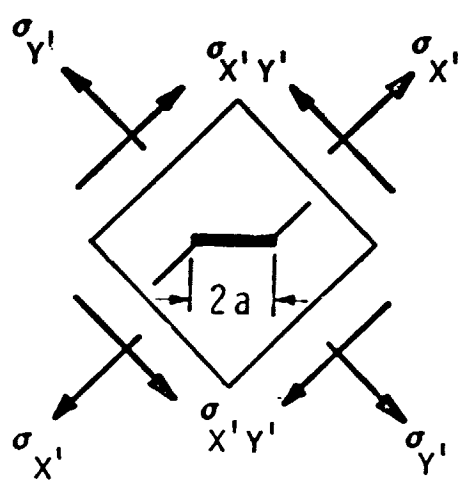
FIGURE 3. CRACK GROWTH AS A FUNCTION OF APPLIED STRESS



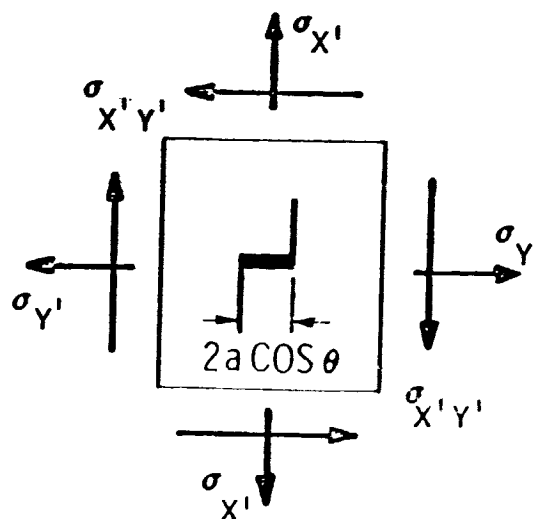
(a) LAMINATE GEOMETRY



(b) xy STRESS STATE

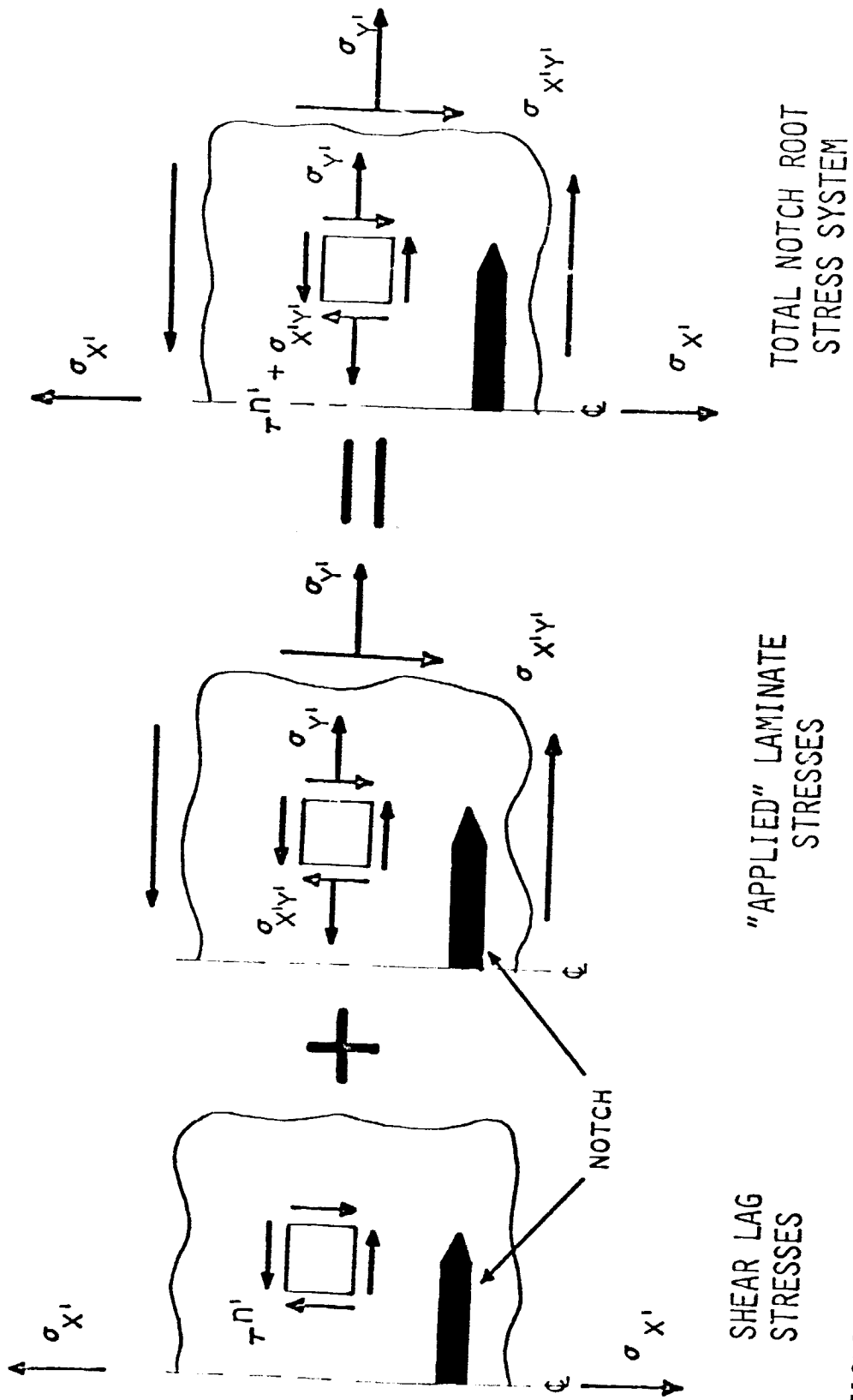


(c) x'y' STRESS STATE



(d) EQUIVALENT AXIAL NOTCH

FIGURE 4. EQUIVALENT AXIAL CRACK PROBLEM FOR OFF-AXIS FAILURE



SHEAR LAG STRESSES

"APPLIED" LAMINATE STRESSES

TOTAL NOTCH ROOT STRESS SYSTEM

FIGURE 5. NOTCH ROOT LAMINATE STRESS IN OFF-AXIS COORDINATE SYSTEM

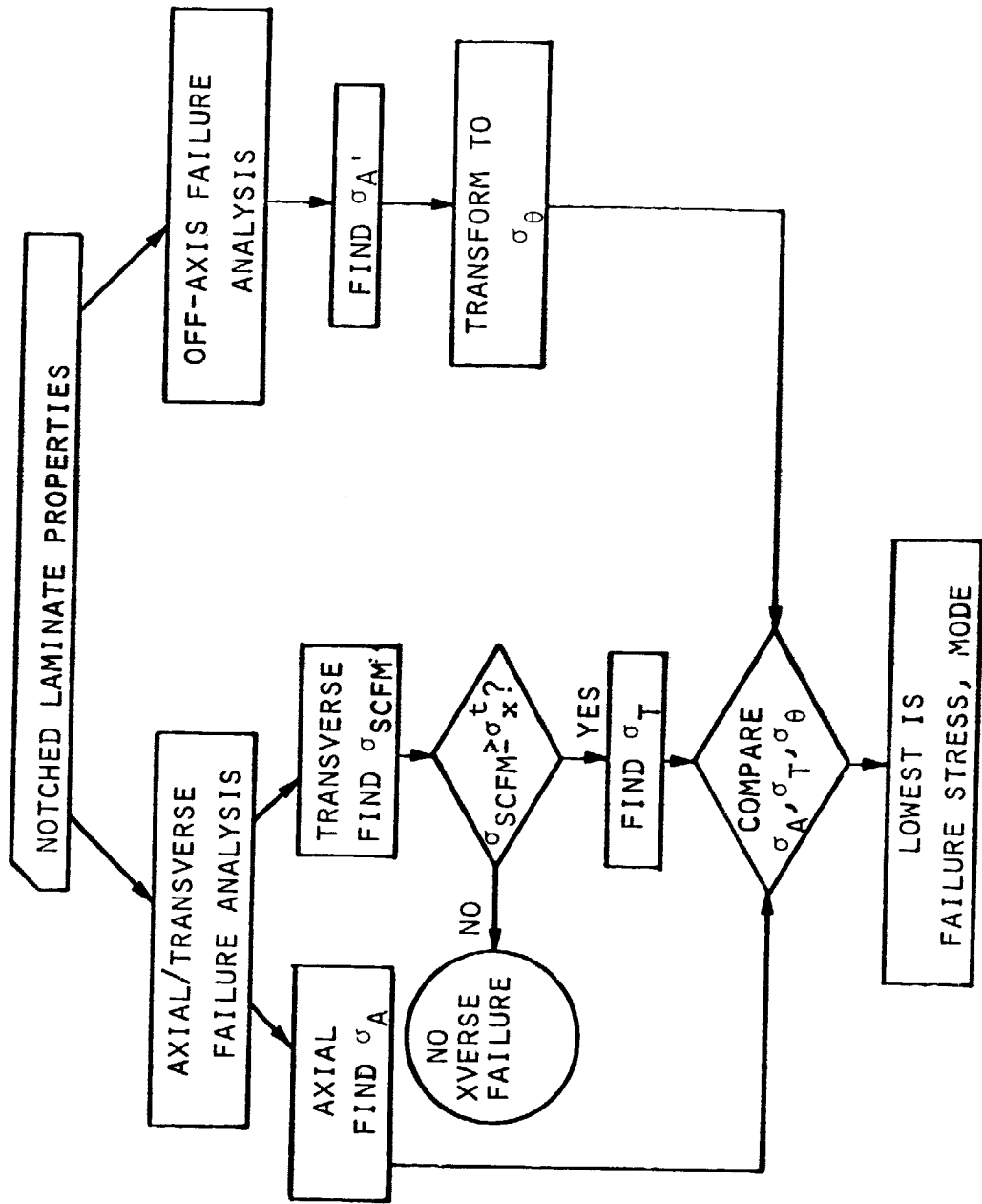


FIGURE 6. STATIC FAILURE ANALYSIS PROCEDURE

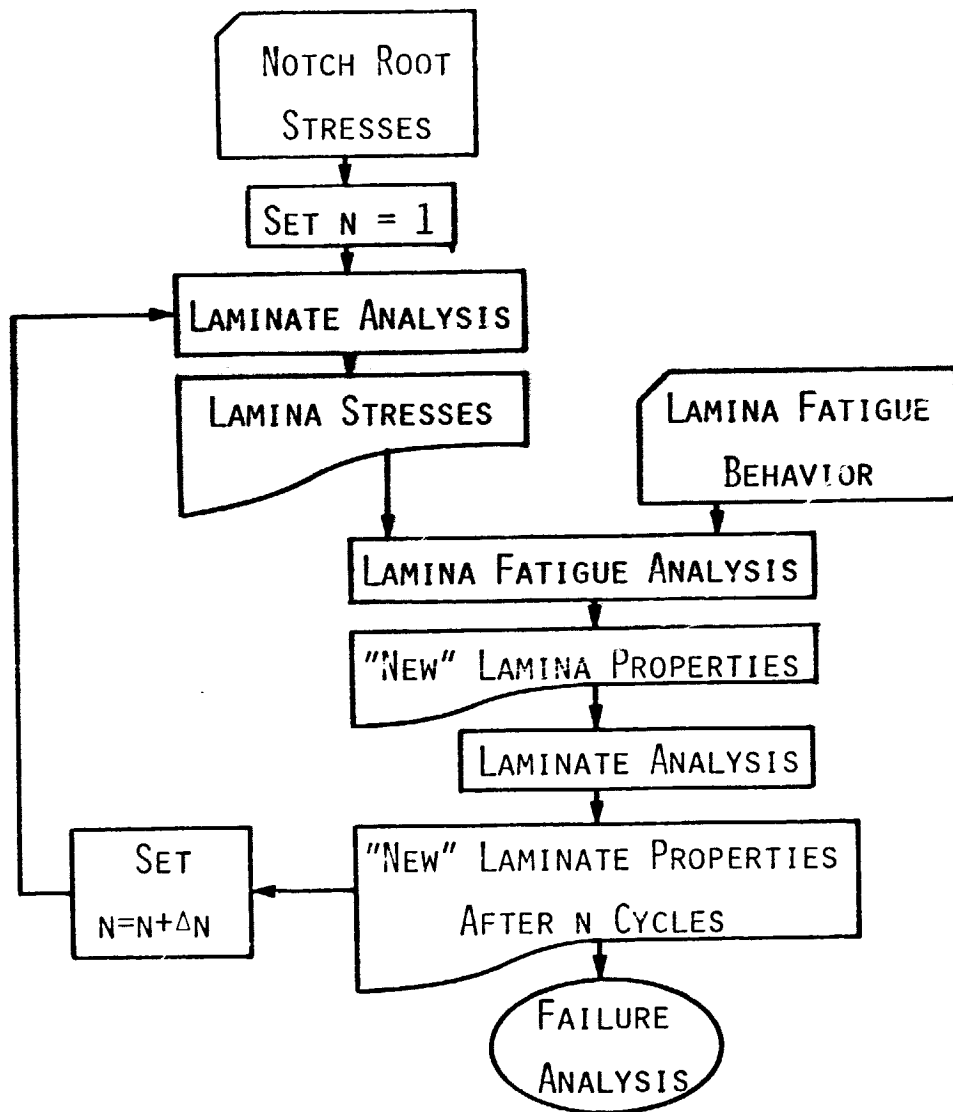
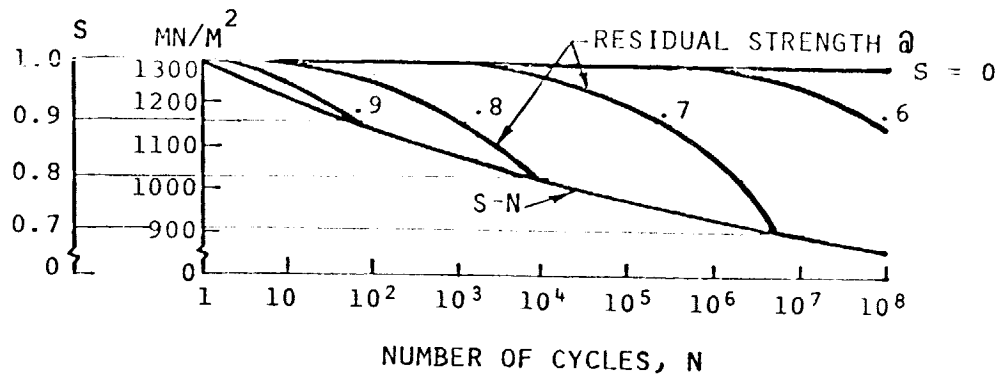
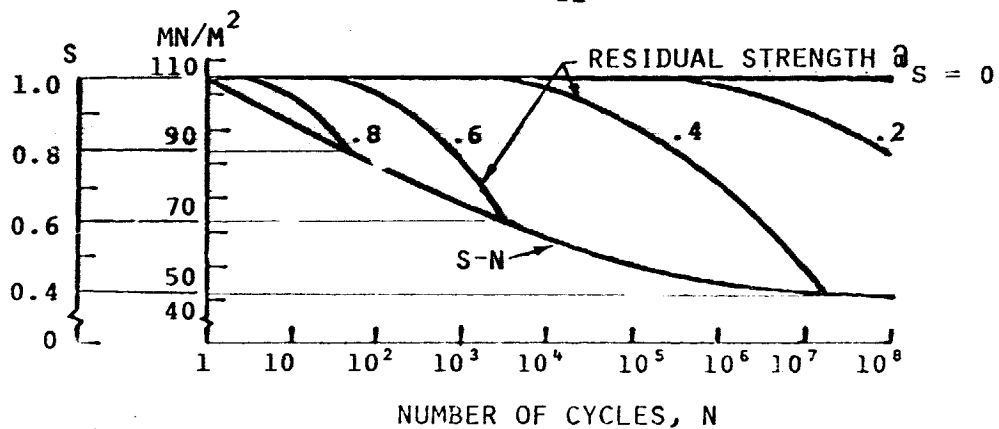


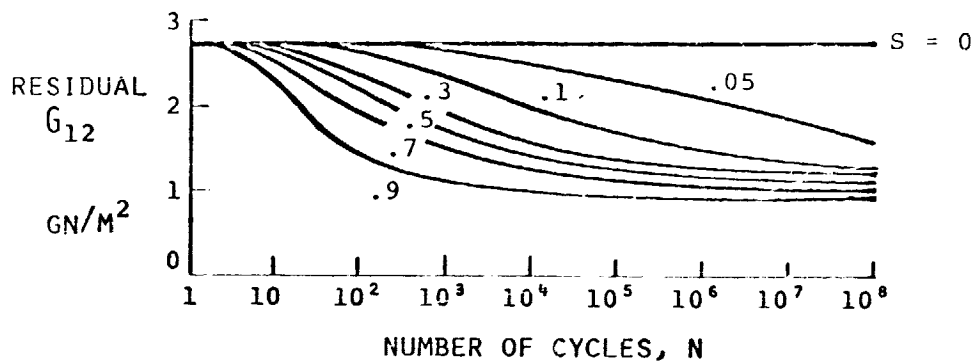
FIGURE 7. PROCEDURE FOR DETERMINING LAMINATE FATIGUE PROPERTY CHANGES FROM 0 LAMINA FATIGUE DATA



(a) AXIAL TENSILE STRENGTH,  $\sigma_{11}$



(b) AXIAL SHEAR STRENGTH,  $\sigma_{12}$



(c) AXIAL SECANT SHEAR MODULUS,  $G_{12}$

FIGURE 8 . TYPICAL FATIGUE BEHAVIOR AND LIFETIME OF (1) LAMINA REQUIRED TO GENERATE LAMINATE FATIGUE BEHAVIOR



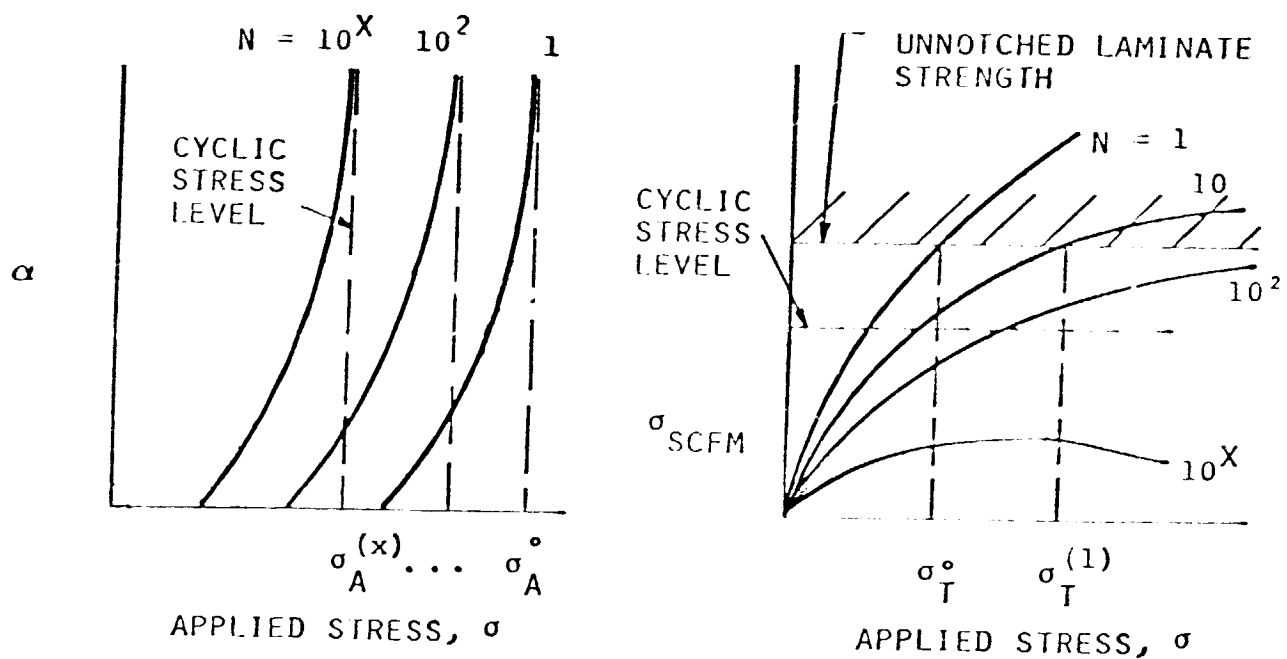
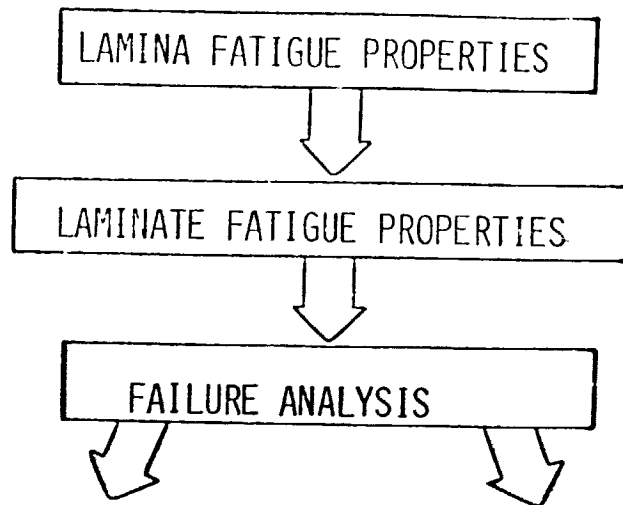


FIGURE 9. STATIC DAMAGE ZONE SIZE,  $\alpha$ , AND INTACT REGION OVERSTRESS,  $\sigma_{SCFM}$ , FOR LAMINATE PROPERTIES AT DIFFERENT  $N$

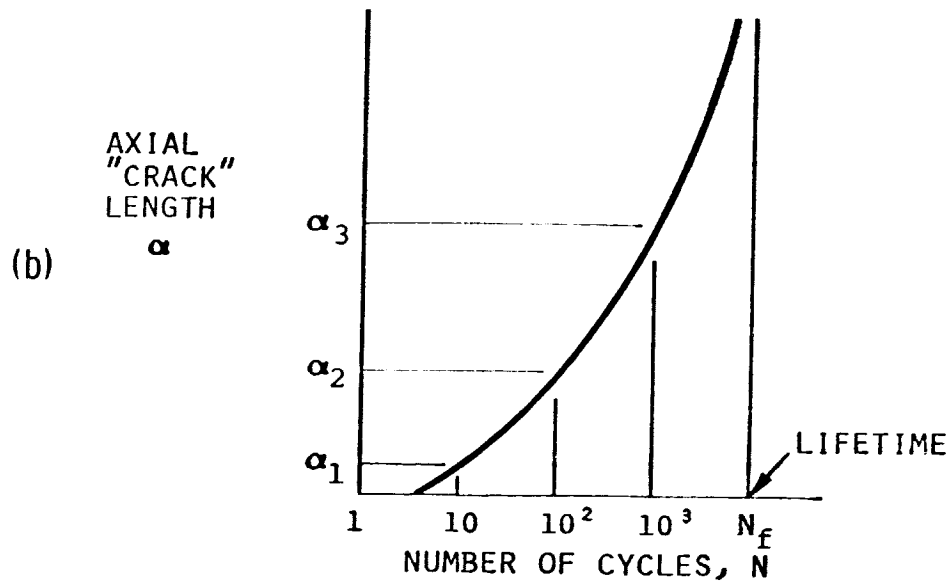
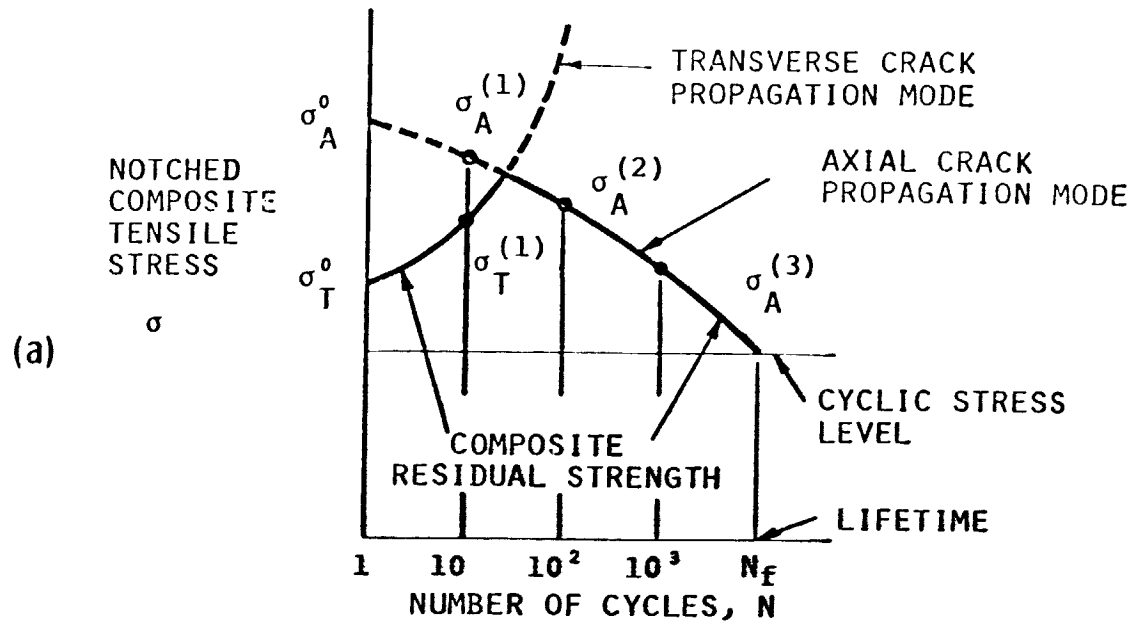


FIGURE 10. TYPICAL PREDICTED RESIDUAL STRENGTH, FATIGUE LIFETIME, AND AXIAL "CRACK" GROWTH OF NOTCHED LAMINATE.

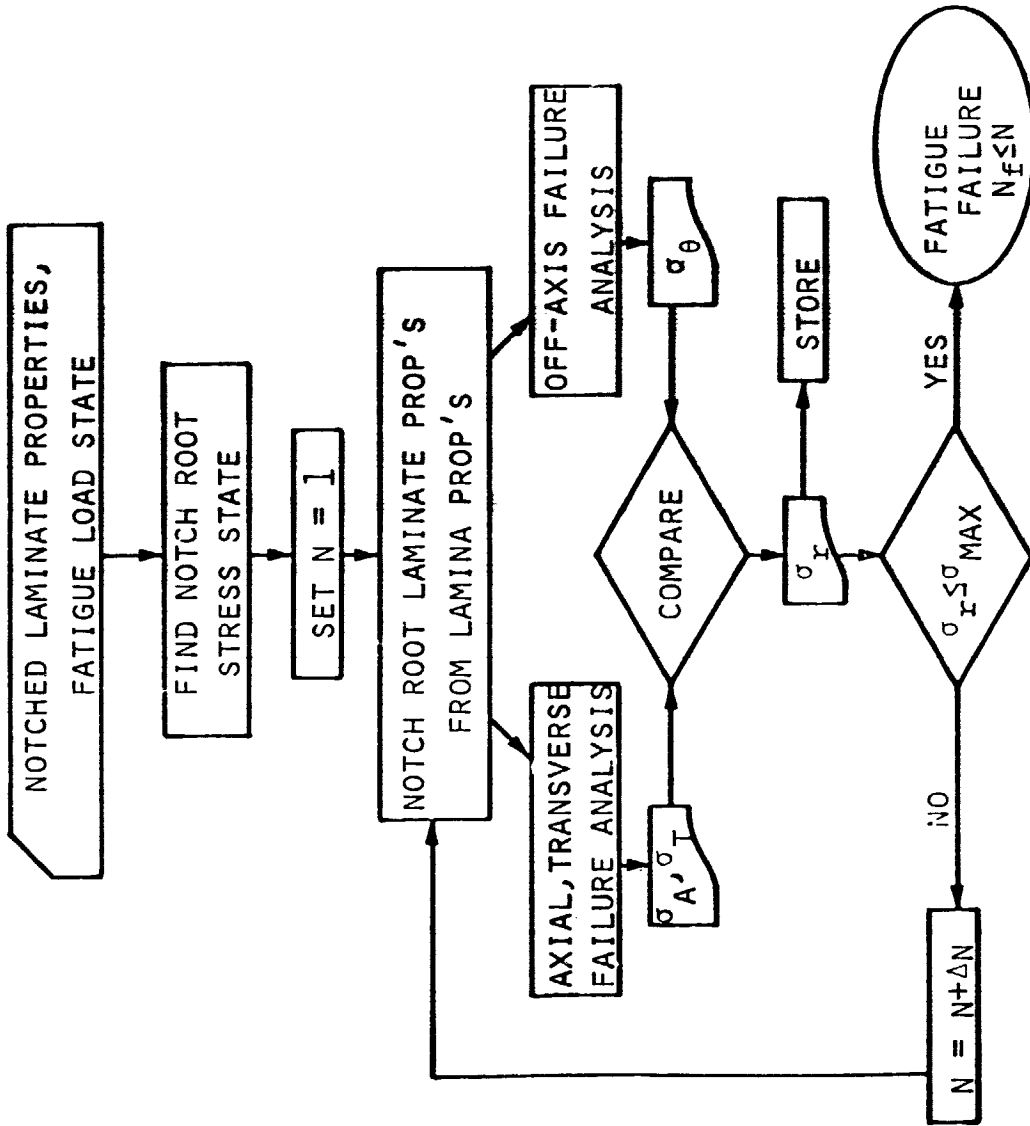


FIGURE 11. FATIGUE ANALYSIS PROCEDURE

FRACTURE BEHAVIOR OF  
NOTCHED COMPOSITE LAMINATES

By James M. Whitney

Air Force Materials Laboratory

and Ran Y. Kim

University of Dayton Research Institute

SUMMARY

Two failure criteria for predicting the uniaxial tensile strength of a laminated composite containing through-the-thickness material discontinuities (notches) are discussed. Both of these criteria involve two parameters (unnotched tensile strength of the laminate and a characteristic length) and are capable of predicting observed discontinuity size effects without resorting to the concepts of linear elastic fracture mechanics. Using a Weibull statistical failure model, the characteristic length in both strength criteria are shown to be a function of the stress distribution adjacent to the discontinuity and the shape parameter associated with the distribution of unnotched tensile strength.

INTRODUCTION

In metallic materials the strength analysis of specimens containing holes are traditionally separated from those containing sharp notches. Such a separation stems from the use of failure criteria based on peak stresses at a single point. In particular, strength in the presence of a smooth discontinuity is characterized in terms of a stress concentration factor (SCF), while strength in the presence of a sharp notch is described in terms of a stress intensity factor because of the existence of a stress singularity at the tip of the notch. Two related criteria are summarized in the present paper for predicting the uniaxial tensile strength of filament dominated laminated composites containing through-the-thickness discontinuities of a general shape. Thus, both criteria treat smooth discontinuities and sharp

PRECEDING PAGE BLANK NOT FILMED

notches in a similar manner. It is also shown that statistical concepts of brittle fracture provide the basis for the two criteria.

## STRESS FRACTURE CRITERIA

### Background

Experimental data presented by Waddoups, Eisenmann, and Kaminski (reference 1) showed that the tensile strength of laminated composites containing a circular hole depends on the absolute hole size. Since the SCF is independent of hole size, this phenomenon could not be explained by a classical SCF approach. A model involving linear elastic fracture mechanics (LEFM) was proposed to explain the "hole size effect". In particular, the authors assumed the existence of intense energy regions which were modeled as through cracks of constant length  $a$ , extending symmetrically from each side of the hole perpendicular to the load direction. The data reduction scheme employed the strength of a control specimen (no hole) and the strength of a specimen with a circular hole in conjunction with the isotropic analytical solution for the problem as presented by Bowie (reference 2). This resulted in a determination of the length  $a$  and a critical stress intensity factor,  $K_Q$ , which were assumed to be constant for a particular material and laminate stacking geometry. This allowed the strength of the same laminate containing any sized hole to be predicted. It was shown in reference 1 that the model served to predict the proper trend of tensile strength reduction with increased hole size. Furthermore, the model was shown to result in a reasonable quantitative correlation with available data.

Although the application of LEFM concepts to laminates containing circular cutouts understandably produced an increased interest in the use of fracture mechanics with composite laminates, the need for such concepts is not entirely clear. This is because of the following two observations (see reference 3): (1) single cracks of the type observed in metals do not form in resin matrix composites under repeated loads; and (2) unlike metals, a positive correlation between the unnotched tensile strength of a composite and its fracture toughness seems to exist, that is, the greater the tensile strength the greater the fracture toughness.

With these facts in mind, another explanation of the hole size effect was introduced in reference 4. Here, the explanation was based simply on the difference that exists in the normal stress distribution ahead of a hole for different sized holes, as shown for an isotropic material in figure 1. It is seen that, although all sized holes have the same stress concentration factor, the normal stress perturbation from a uniform stress state is considerably more concentrated near the hole boundary in the case of the smaller hole.

Thus, intuitively, one might expect the plate containing the small hole to be the stronger of the two. In particular, brittle failure of a body under a given stress field is generally attributed to the existence of inherent flaws of various dimensions distributed throughout the body as described by Griffith in reference 5. Because a larger volume of material is subjected to high stress in the case of the plate containing the larger hole, the probability of having a large flaw in the highly stressed region is greater, resulting in a lower average strength for this plate. In addition, the plate containing the smaller hole has more capability to redistribute the stress, leading to higher average strength than a plate with a smaller hole. Through cracks were also considered in reference 4, where it was found that the crack size effect on measured values of fracture toughness (the variation of measured fracture toughness with crack size as shown in reference 6) could be explained in a similar manner by considering the exact elasticity solution for the normal stress ahead of a crack rather than just the singular term of the asymptotic expansion (see figure 2).

#### Point Stress Criterion

Consider a hole of radius  $R$  in an infinite orthotropic plate, as shown in figure 1. If a uniform stress,  $\sigma$ , is applied parallel to the  $y$ -axis at infinity, then the normal stress,  $\sigma_y$ , along the  $x$ -axis in front of the hole can be approximated by

$$\sigma_y(x, 0) = \frac{\sigma}{2} \left\{ 2 + \left(\frac{R}{x}\right)^2 + 3\left(\frac{R}{x}\right)^4 - (K_T^\infty - 3) \left[ 5\left(\frac{R}{x}\right)^6 - 7\left(\frac{R}{x}\right)^8 \right] \right\}, \quad x > R \quad (1)$$

where  $K_T$  is the orthotropic stress concentration factor for an infinite width plate as shown in reference 7. Equation 1 was shown in reference 8 to provide an excellent approximation to the exact orthotropic plate solution.

The first failure criterion in reference 4, referred to as the "point stress criterion", assumes failure to occur when  $\sigma_y$  at some fixed distance,  $d_0$ , ahead of the hole first reaches the unnotched tensile strength of the material,  $\sigma_0$ , that is, when

$$\sigma_y(x, 0) \Big|_{x = R + d_0} = \sigma_0 \quad (2)$$

Using this criterion with equation 1 results in the notched to unnotched strength ratio

$$\frac{\sigma_N^\infty}{\sigma_0} = \frac{2}{\left[ 2 + \xi_1^2 + 3\xi_1^4 - (K_T^\infty - 3)(5\xi_1^6 - 7\xi_1^8) \right]} \quad (3)$$

where

$$\xi_1 = \frac{R}{(R+d_0)}$$

and  $\sigma_N^\infty$  equals the notched strength of the infinite width laminate, i.e., the applied stress,  $\sigma$ , at failure. Note that for very large holes,  $\xi_1 \rightarrow 1$ , the classical stress concentration result,  $\sigma_N^\infty/\sigma_0 = 1/K_T^\infty$ , is recovered. On the other hand, for vanishingly small hole sizes,  $\xi_1 \rightarrow 0$ , the ratio  $\sigma_N^\infty/\sigma_0 \rightarrow 1$ , as would be expected. Thus, the expected limits are found.

Now consider the center cracked geometry of figure 2; the exact anisotropic elasticity solution for the normal stress ahead of a crack of length  $2c$  in an infinite anisotropic plate under uniform uniaxial tension,  $\sigma$ , is given by (see reference 7)

$$\sigma_y(x,0) = \frac{\sigma x}{\sqrt{x^2 - c^2}} = \frac{K_1 x}{\sqrt{\pi c(x^2 - c^2)}}, \quad x > c \quad (4)$$

where  $K_1$  is the stress intensity factor, which in this case is given by  $K_1 = \sigma\sqrt{\pi c}$ . Using this result with the failure criterion, equation 2 (with  $R$  replaced by  $c$ ) yields

$$\frac{\sigma_N^\infty}{\sigma_0} = \sqrt{1 - \xi_2^2} \quad (5)$$

where

$$\xi_2 = \frac{c}{(c+d_0)}$$

The predicted crack size effect on the measured value of the fracture toughness,  $K_Q$ , can more easily be observed by writing equation 5 in the form

$$K_Q = \sigma_0 \sqrt{\pi c(1 - \xi_2^2)} \quad (6)$$

This equation results from equation 5 simply by noting that  $K_Q = \sigma_N^\infty \sqrt{\pi c}$  for the infinite plate geometry being considered. In equation 6, the expected limit of  $K_Q = 0$  for vanishingly small crack lengths is reached, while for large crack lengths,  $K_Q$  asymptotically approaches a constant value of

$$K_Q = \sqrt{2\pi d_0} \quad (7)$$

### Average Stress Criterion

The second alternative failure criterion (see reference 4), called the "average stress criterion", assumes failure to occur for a circular hole when the value of  $\sigma_y$  over some fixed distance,  $a_0$ , ahead of the hole first reaches the unnotched tensile strength of the material, i.e., when

$$\frac{1}{a_0} \int_R^{R+a_0} \sigma_y(x, 0) dx = \sigma_0 \quad (8)$$

Using the criterion with equation 1 results in the notched to unnotched strength ratio

$$\frac{\sigma_N^\infty}{\sigma_0} = \frac{2(1-\xi_3)}{\left[ 2-\xi_3^2 - \xi_3^4 + (K_T^\infty - 3)(\xi_3^6 - \xi_3^8) \right]} \quad (9)$$

where

$$\xi_3 = \frac{R}{R + a_0}$$

and  $\sigma_N^\infty$  is again the notched strength of the infinite width laminate. It is easily shown that the effected limits of  $\sigma_N^\infty/\sigma_0$  are again recovered for very small and very large holes.

Equation 4 for the center crack in conjunction with the average stress criterion, equation 8 with R replaced by c yields the notched to unnotched strength ratio

$$\frac{\sigma_N^\infty}{\sigma_0} = \sqrt{\frac{1-\xi_4}{1+\xi_4}} \quad (10)$$

where

$$\xi_4 = \frac{c}{(c + a_0)}$$

with the fracture toughness taking the form

$$K_Q = \sigma_0 \sqrt{\pi c \left( \frac{1-\xi_4}{1+\xi_4} \right)} \quad (11)$$

Again it is easily shown that the expected limits of  $\sigma_N^\infty/\sigma_0$  are recovered for small and large cracks, respectively. For large cracks the asymptotic value of fracture toughness is



$$K_Q = \sigma_0 \sqrt{\frac{\pi a_0}{2}} \quad (12)$$

### Modified Stress Intensity Factor

It should also be noted that an Irwin type correction factor, as discussed in reference 9, used in conjunction with equation 10 yields a constant value of the critical stress intensity factor and an almost constant value when used in conjunction with equation 5. In particular, an Irwin type correction factor is defined in terms of a modified critical stress intensity factor,  $K'_Q$ , given by the relationship

$$K'_Q = \sigma_N^\infty \sqrt{\pi(c + c_0)} \quad (13)$$

where  $c + c_0$  is an effective half crack length with  $c_0$  being an adjustment used to operationally induce a more constant value of critical stress intensity factor. This adjustment was first introduced by Irwin in reference 10 for homogeneous metals. In reference 9,  $c_0$  was chosen such that  $K'_Q$  approaches the asymptotic limit of  $K_Q$  as the implanted crack length,  $c$ , vanishes with the result

$$c_0 = 2d_0 \quad (14)$$

$$c_0 = \frac{a_0}{2} \quad (15)$$

for the point stress criterion and the average stress criterion, respectively.

### Comparison to Experimental Data

At this point, several comments concerning the models should be made. First, equations 3, 9, 6, and 11 all predict the proper trends of observed behavior, i.e., decreasing strength of a laminate with increasing hole size and increasing fracture toughness with increasing crack size. Second, it is clear that these equations are quite useless unless the characteristic distance,  $d_0$  or  $a_0$ , remains constant for all hole or crack sizes in at least a particular laminate of a particular material system. In such a case, one test on one hole or crack size would allow the failure strength of that laminate containing any hole or crack size to be predicted.

The effect of notch shape and size were examined in references 4 and 9 by considering both circular holes and sharp-tipped center cracks of sizes 0.1, 0.3, 0.6, and 1.0 inch (hole diameter or crack length). These combinations were considered to be a good test of the effect of the degree of stress

concentration, since they represent the range from extremely narrow to extremely broad regions of concentration. The particular sizes chosen were made because previous data (see references 1 and 6) have shown that the transition from unnotched behavior to large-notch size behavior occurs in this range of notch size. Typical results taken from reference 9 are shown in figures 3 - 8 for Scotchply 1002 and Thornel 300/Narmco 5208 supplied in prepreg by 3M Company and Whittaker Corporation, respectively. Results shown are for the quasi-isotropic orientation  $(0, \pm 45, 90)_{2S}$  and for the characteristic lengths  $d_0 = 0.04$  inches and  $a_0 = 0.15$  inches. It is important to note that the choice of  $d_0$  and  $a_0$  indicated is exactly the values of  $d_0$  and  $a_0$  used in reference 4. In particular, the values of the characteristic lengths used in reference 9 were not chosen from a best fit of the data but from a best fit of data from holes in quasi-isotropic Scotchply 1002 and cracks in  $(0 \pm 45)_S$  T300/5208. The data has been corrected for finite width specimens as discussed in reference 9. Data was also presented in reference 9 on  $(0, 90)_{4S}$  laminates with similar correlation to the failure criteria as illustrated for the quasi-isotropic laminates in the present paper. In all figures, the solid dots represent the average experimental value (of three tests), the vertical line through the dots represent the data spread and the solid and dashed curves represent the predicted values using the average and point stress failure criterion, respectively. This data and other data found in references 4 and 9 indicate the stress failure criteria to be useful design tools.

## STATISTICAL STRENGTH MODEL

### Statistics of Composites

Evidence was presented in reference 9 which suggested that the values of the characteristic lengths,  $a_0$  and  $d_0$ , are a function of the statistical nature of the unnotched tensile strength. In order to pursue such an approach in more detail the statistical aspects of composite tensile strength must be considered.

It has been shown by Kaminski, reference 11, that the unnotched tensile strength,  $\sigma_S$ , of laminated composites can be accurately described by the two parameter Weibull distribution

$$P(\sigma_S \geq \sigma) = \exp \left[ -(\sigma/\sigma_0)^a \right] \quad (16)$$

where  $P$  is the probability of survival,  $\sigma_0$  is the characteristic strength or

location parameter of the distribution, and  $\alpha$  is the shape parameter. For the stress failure models previously described, the notched strength  $\bar{\sigma}_S$ , can be written in the form

$$\bar{\sigma}_S = \sigma_S f \left[ a_0 (d_0), \frac{a}{a_0} \right] \quad (17)$$

where  $\frac{a}{a_0}$  is the half length of the discontinuity (hole radius or half crack length). Using equation 17 in conjunction with equation 16 yields a probability of survival function for the notched strength in the form

$$P(\bar{\sigma}_S \geq \bar{\sigma}) = \exp \left[ -(\bar{\sigma}/\sigma_N)^\alpha \right] \quad (18)$$

where

$$\sigma_N = f \sigma_0 \quad (19)$$

Thus, the notched strength, according to the failure model, will be described by a Weibull distribution having the same  $\alpha$  as the unnotched strength, but with a shifted location parameter. This has been shown experimentally for boron/epoxy and graphite/epoxy by Waddoups and Halpin in reference 12. Such a result suggests that the notched strength can, at least qualitatively, be predicted by a classical Weibull failure model as discussed in reference 13.

#### Weibull Failure Model

According to the Weibull strength model for brittle materials in reference 13, the probability of survival for a volume,  $V$ , is given by the function

$$P(\sigma_S \geq \sigma) = \exp \left[ -\int (\sigma/\hat{\sigma})^\alpha dV \right] \quad (20)$$

where  $\hat{\sigma}$  is the location parameter for the strength distribution of a unit volume of material subjected to uniform uniaxial stress. For uniform stress, on a volume of material, equation 19 reduces to equation 16 with

$$\sigma_0 = \hat{\sigma} / V^{1/\alpha} \quad (21)$$

Consider a homogeneous plate of uniform thickness,  $h$ , containing a through-the-thickness discontinuity, and subjected to uniform uniaxial external stress,  $\bar{\sigma}$ . The normal stress distribution,  $\sigma$ , parallel to the external stress will be non-uniform in the vicinity of the discontinuity, but can be written in the form

$$\sigma = \bar{\sigma} F(x, y) \quad (22)$$

where  $x$  and  $y$  are the in-plane coordinates. If failure is assumed to be associated with this stress, then the probability of survival, from equation 20, takes the form

$$P(\sigma_S \geq \bar{\sigma}) = \exp\left[-hA(k\bar{\sigma}/\hat{\sigma})^a\right] \quad (23)$$

where  $A$  is the area of the plate and  $k$  is the stress enhancement factor given by

$$k = \left[ \frac{1}{A} \int_A [F(x, y)]^a dA \right]^{1/a} \quad (24)$$

The stress enhancement factor is analogous to SCF, but takes into account the statistical aspects of brittle fracture rather than just the maximum stress. This concept has been discussed by Scop and Argon, reference 14. For an unnotched plate of the same material and dimensions subjected to a uniform external stress  $\sigma$ , equation 23 becomes identical to equation 16 with the substitution

$$\hat{\sigma} = \sigma_0(hA)^{1/a}$$

Now substituting

$$\sigma_N = \hat{\sigma}/k(hA)^{1/a} = \sigma_0/k \quad (25)$$

into equation 23 yields equation 18. Thus, the stress enhancement factor represents the reduction in the location parameter, for equal volume of notched and unnotched material, due to the presence of the notch, and is a function of the discontinuity size as shown in the next section. The use of equal volumes for notched and unnotched composites allows the effect of stress gradients on strength to be assessed without volume being a factor.

Consider an infinite homogeneous isotropic plate of thickness  $h$  containing a circular hole of radius  $R$  as shown in figure 9. In terms of strength, the area adjacent to the hole which is subjected to the non-uniform normal stress  $\sigma_y$  is of particular interest. The non-uniform stress dissipates within a distance of  $4R$  from the hole. For a hole radius up to one inch, then, a 4 inch square is sufficient to account for the effect of stress gradients on notch strength. For this case the stress enhancement factor, equation 24, becomes

$$k = \left[ \int_0^4 \int_R^{R+4} [F(x, y)]^a dx dy \right]^{1/a} \quad (26)$$

where

$$\begin{aligned}
 F(x, y) = 1 - & \frac{R^2(x^2 - y^2)}{2(x^2 + y^2)^2} - \frac{2R^2 x^2(x^2 - 3y^2)}{(x^2 + y^2)^3} \\
 & + \frac{3R^4(x^4 - 6x^2 y^2 + y^4)}{2(x^2 + y^2)^4}
 \end{aligned} \tag{27}$$

Results for the integration in equation 26 have been presented in reference 15 and are shown in figure 10 for  $\alpha = 10, 20$  and  $30$ . As a matter of practical interest, experimental values of  $\sigma_0/\sigma_N$  are shown from figures 3 and

4. For both Scotchply and T300/5208 the value of  $\alpha$  is approximately 20.

#### CONCLUDING REMARKS

Two models have been presented to qualitatively explain notch size effects in laminated composite materials without the use of linear elastic fracture mechanics concepts. In addition, experimental data shows the models to be useful as a design tool for predicting the ultimate uniaxial failure load of notched composites.

The results in figure 10 clearly indicate that classical statistical concepts of brittle fracture can at least qualitatively explain discontinuity size effects. A cursory examination of equation 24 along with the results in figure 10 indicate that both the details of the non-uniform stress distribution adjacent to the discontinuity and the value of the shape parameter,  $\alpha$ , have an influence on the value of the characteristic lengths  $a_0$  and  $d_0$ . It should be noted that good quantitative agreement between the Weibull strength theory and notched composite strength should not be expected. In particular, such an approach neglects local heterogeneities which are present in laminated composites. Furthermore, a first failure in composites does not necessarily lead to total failure of the laminate, i.e. the Weibull theory is a series model, while failure in composite materials must be described by a combination of series and parallel models. The statistical concepts presented here, however, are useful in explaining the mechanisms which lead to observed discontinuity size effects in laminated composite materials.

## REFERENCES

1. Waddoups, M.E., Eisenmann, J.R., and Kaminski, B.E.: Macroscopic Fracture Mechanics of Advanced Composite Materials, *Journal of Composite Materials*, vol. 5, no.4, Oct. 1971, pp. 446-455.
2. Bowie, O.L.: Analysis of an Infinite Plate Containing Radial Cracks Originating from the Boundary of an Internal Circular Hole, *Journal of Mathematics and Physics*, vol. 35, 1956, pp. 60-71.
3. Nuismer, R.J., and Hahn, H.T.: Mixed-Mode Fracture of Fiber Reinforced Composite Laminates, presented at the American Society for Testing and Materials, Composite Reliability Conference, Los Vegas, Nevada, Apr. 15-16, 1974.
4. Whitney, J.M., and Nuismer, R.J.: Stress Fracture Criteria for Laminated Composites Containing Stress Concentrations, *Journal of Composite Materials*, vol. 8, no. 3, July 1974, pp. 253-265.
5. Griffith, A.A.: The Phenomena of Rupture and Flow in Solids, *Philosophical Transactions of the Royal Society (London)*, Series A, vol. 221, 1920, pp. 163-198.
6. Konish, H.J., and Cruse, T.A.: The Determination of Fracture Strength in Orthotropic Graphite/Epoxy Laminates, presented at the American Society for Testing and Materials, Composite Reliability Conference, Los Vegas, Nevada, Apr. 15-16, 1974.
7. Lekhnitskii, S.G.: Anisotropic Plates, translated from the Second Russian Edition by S.W. Tsai and T. Cheron, Gordon and Breach, Science Publishers, Inc., New York, 1968.
8. Konish, H.J., and Whitney, J.M.: Approximate Stresses in an Orthotropic Plate Containing a Circular Hole, *Journal of Composite Materials*, vol. 9, no. 2, Apr. 1975, pp. 157-166.
9. Nuismer, R.J., and Whitney, J.M.: Uniaxial Failure of Composite Laminates Containing Stress Concentrations, ASTM STP 593, *Fracture Mechanics of Composites*, American Society for Testing and Materials, 1975, pp. 117-142.
10. Irwin, G.R.: Plastic Zone Near a Crack and Fracture Toughness, Seventh Sagamore Ordnance Materials Research Conference, Aug. 1960. Also see McClintock, F.A. and Irwin, G.R.: Plasticity Aspects of Fracture Mechanics, ASTM STP 381, *Fracture Toughness*

Testing, American Society for Testing and Materials, 1965, pp. 84-113.

11. Kaminski, B.E.: Effects of Specimen Geometry on the Strength of Composite Materials, ASTM STP 521, The Test Methods for High Modulus Fibers and Composites, American Society for Testing and Materials, 1972, pp. 181-191.
12. Waddoups, M.E., and Halpin, J.C.: The Fracture and Fatigue of Composite Structures, Computers and Structures, vol. 4, May 1974, pp. 1-15.
13. Weibull, W.: A Statistical Theory of the Strength of Materials, Ingeniorsvetenskapskademiens Handlingar, NR 151, 1939, pp. 5-45.
14. Scop, P.M., and Argon, A.S.: Statistical Theory of Strength of Laminated Composites II, Journal of Composite Materials, vol. 3, no. 1, Jan. 1969, pp. 30-47.
15. Whitney, J.M.: The Effect of Stress Concentrations on the Fracture Behavior of Fiber Reinforced Composite Materials, Proceedings 12th Annual Meeting Society of Engineering Science, The University of Texas at Austin, 1975, pp. 173-182.

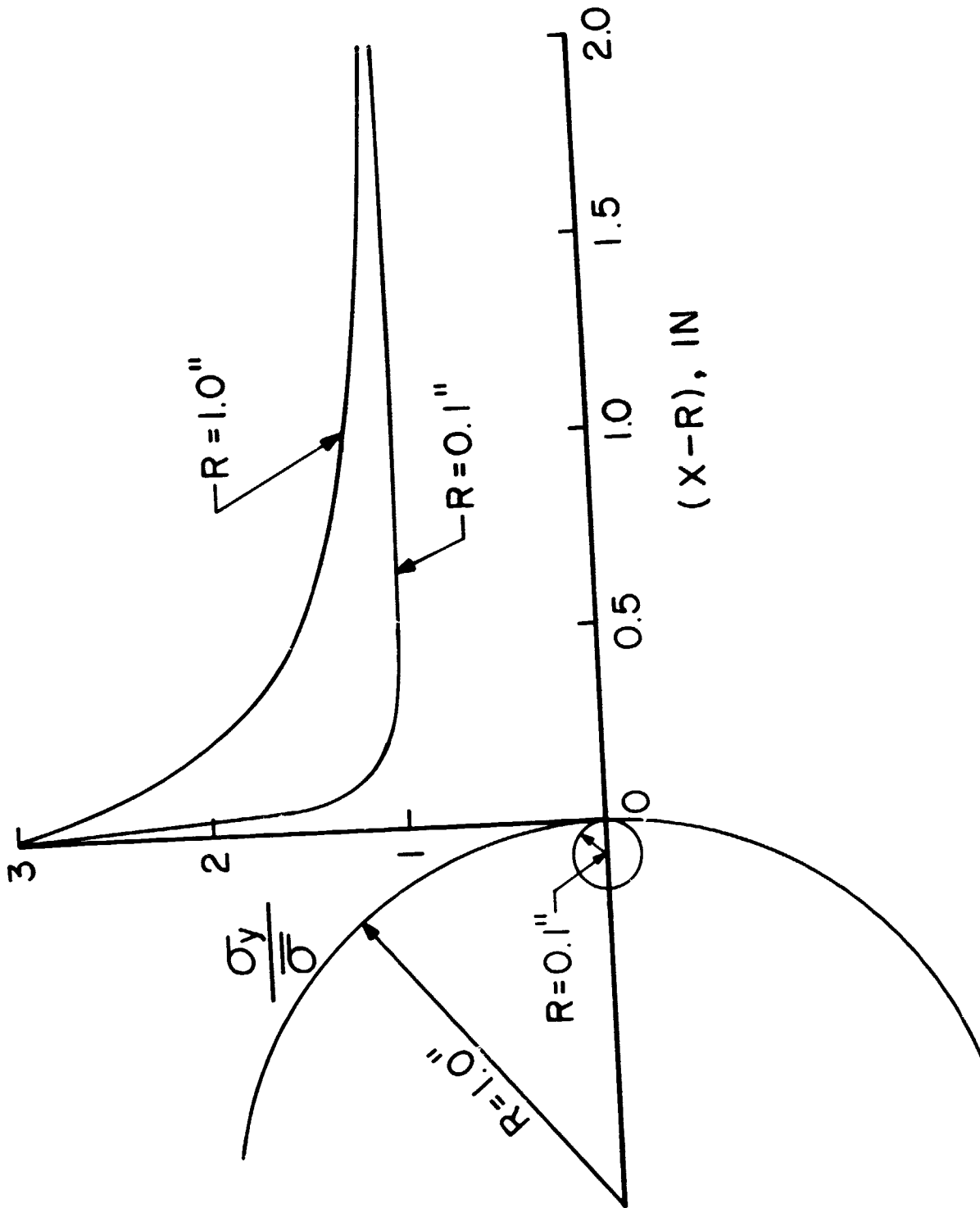


Figure 1.- Normal stress distribution for a circular hole in an infinite plate.



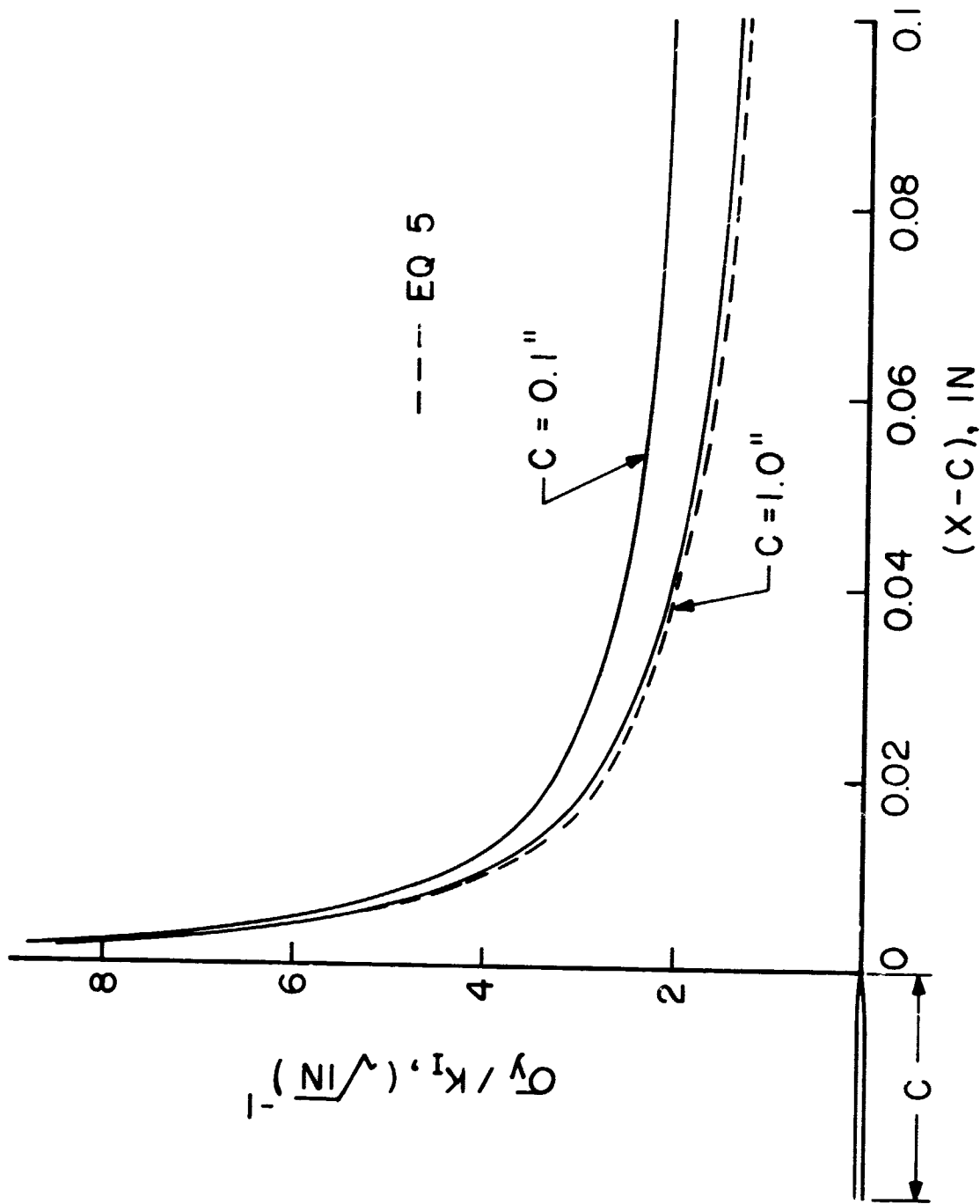


Figure 2.- Normal stress distribution for a center crack in an infinite anisotropic plate. Solid line represents exact solution, the dotted line, approximate solution.

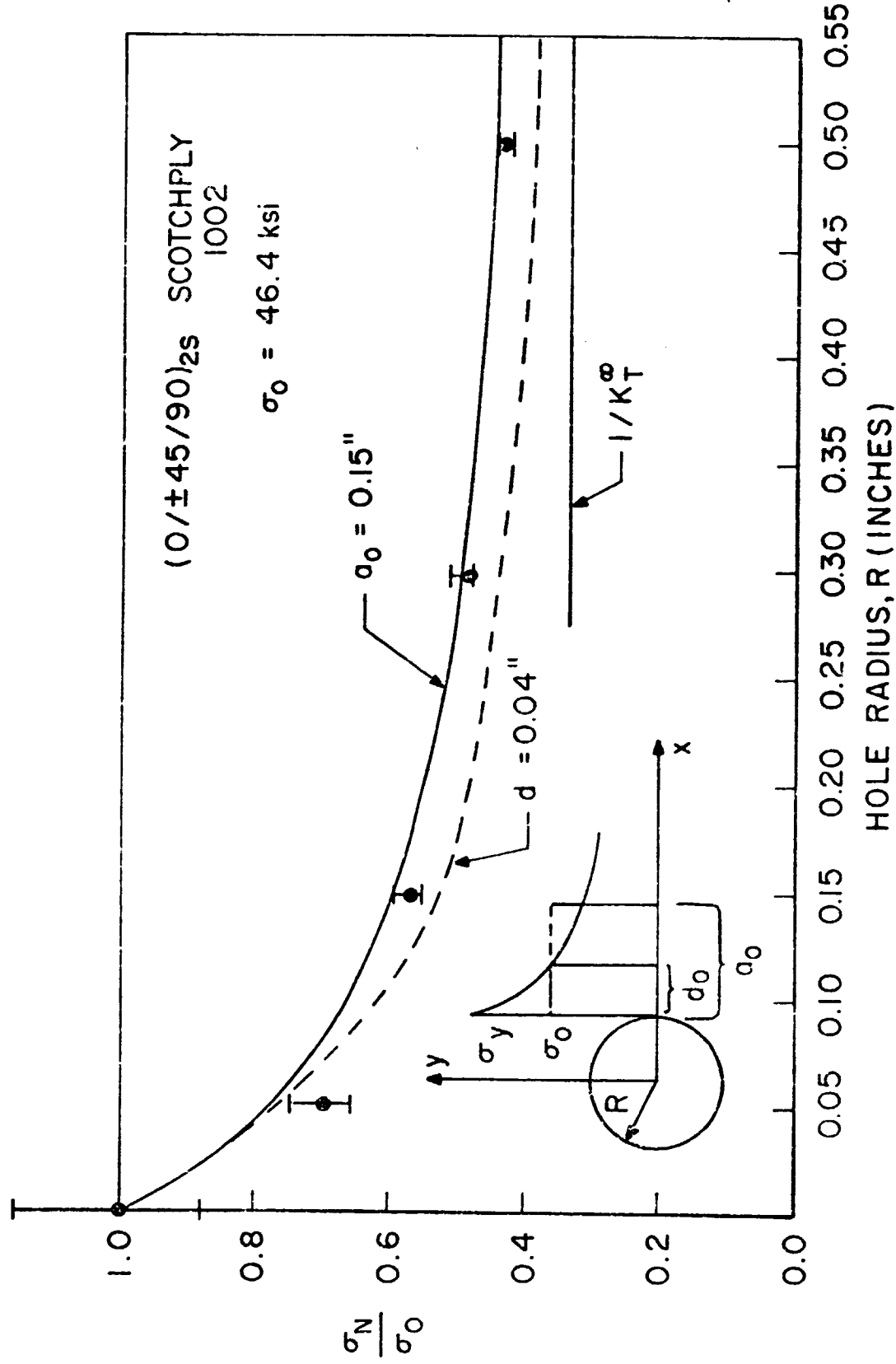


Figure 3.- Comparison of predicted and experimental failure stresses for circular holes in (0,±45, 90)<sub>2s</sub> Scotchply 1002.

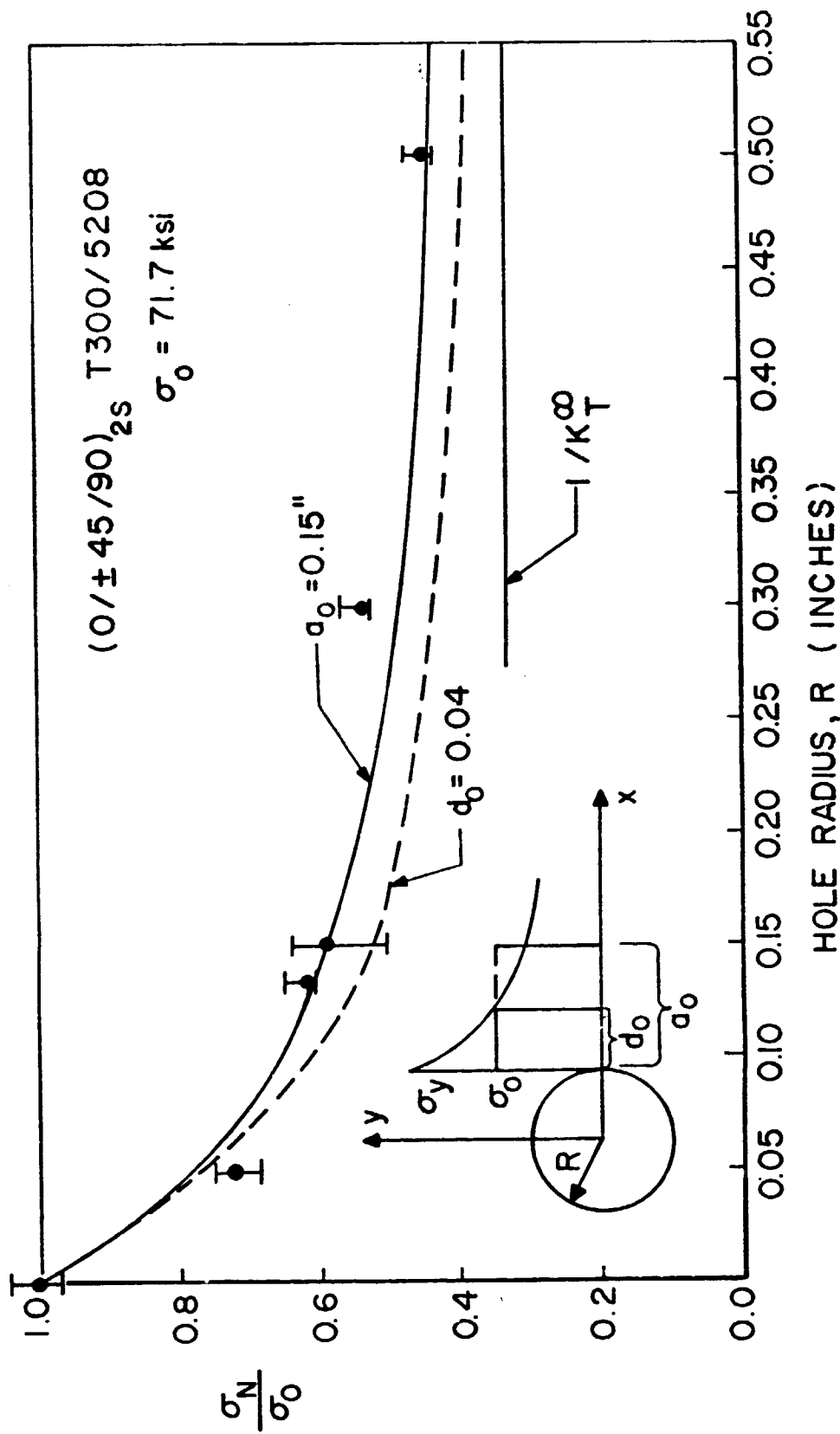


Figure 4.- Comparison of predicted and experimental failure stresses for circular holes in (0,±45,90)2S T300/5208.

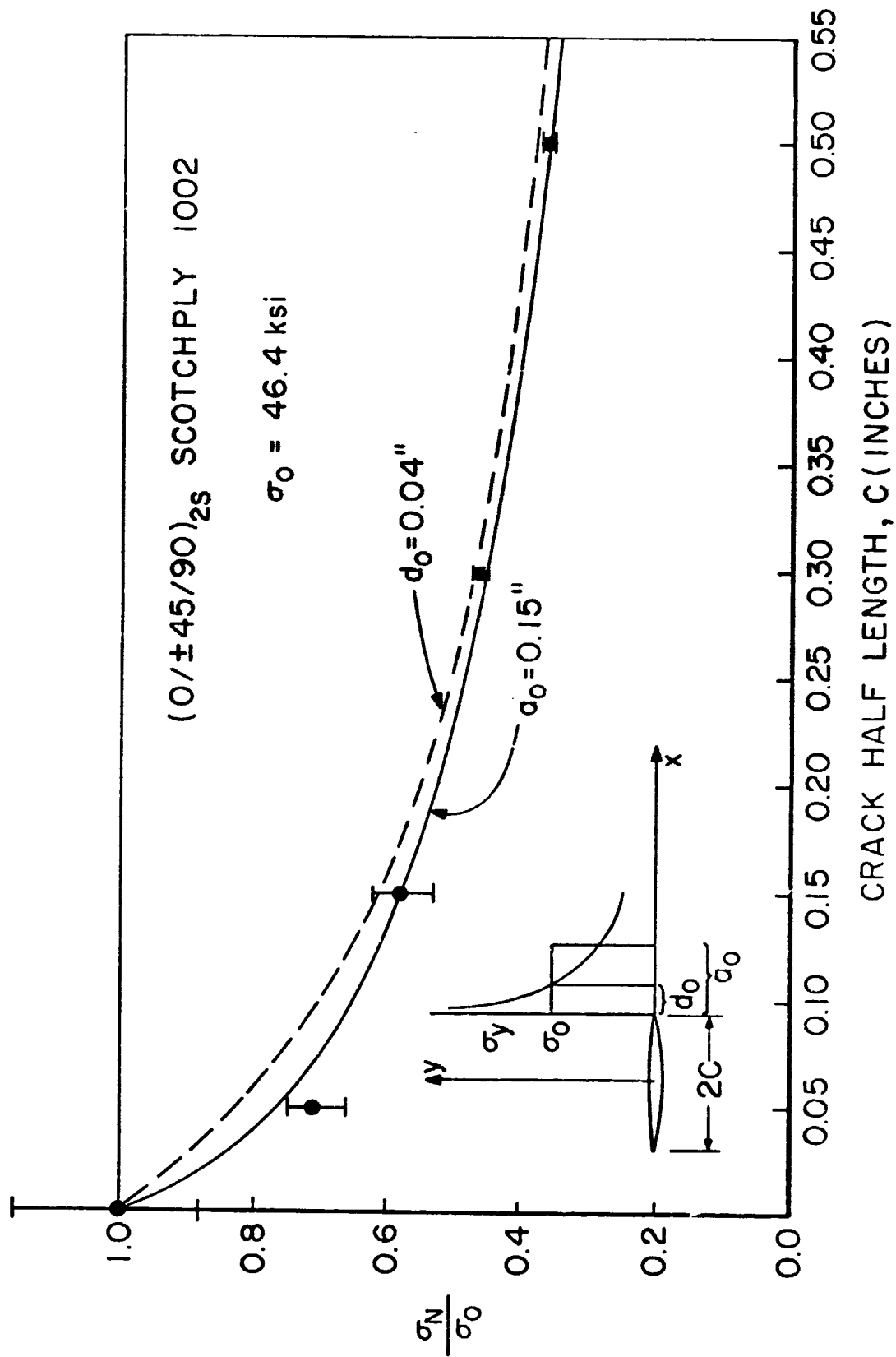


Figure 5.- Comparison of predicted and experimental failure stresses for center cracks in (0,±45,90)<sub>2S</sub> Scotchply 1002.

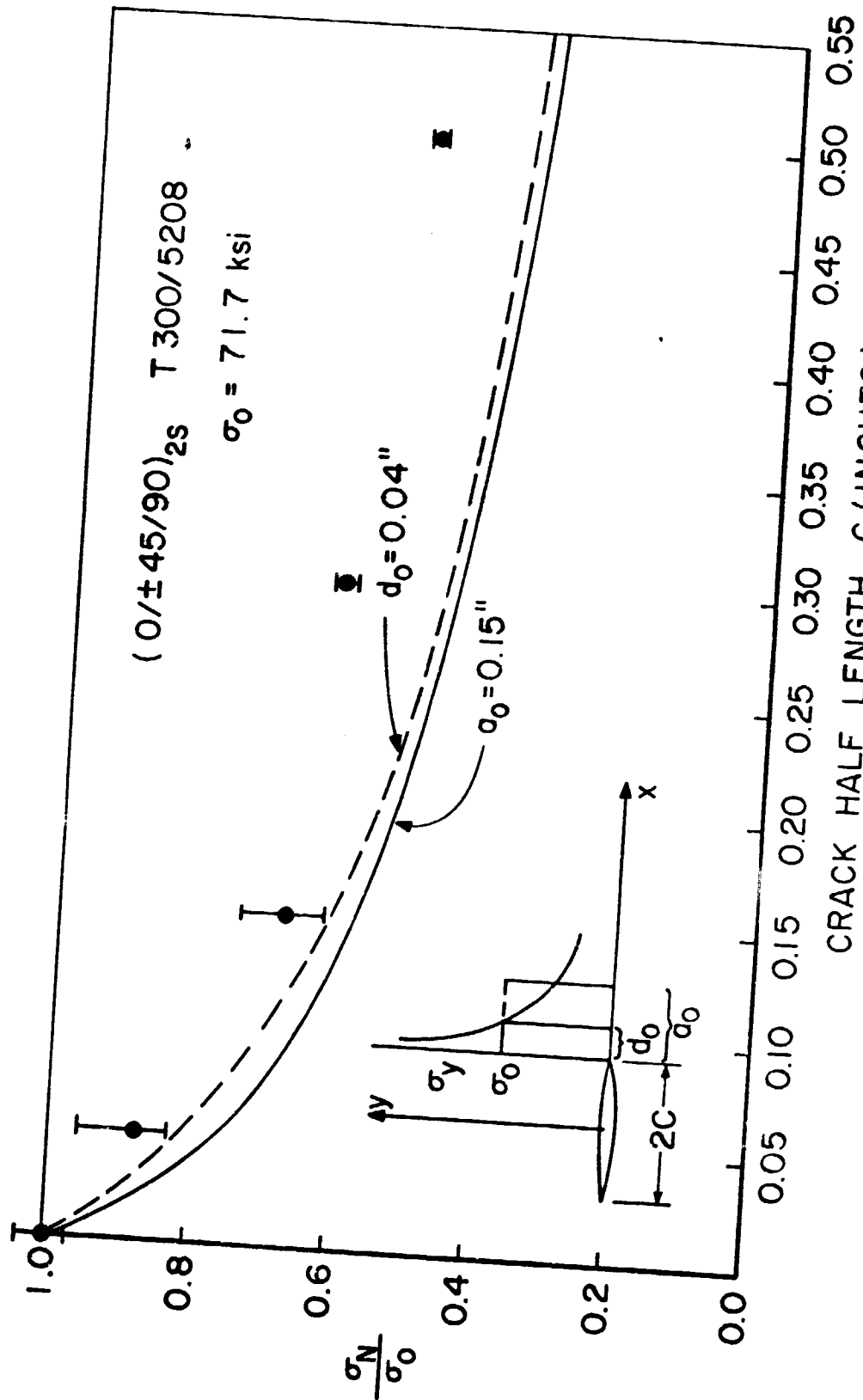


Figure 6.- Comparison of predicted and experimental failure stresses for center cracks in (0,±45,90)<sub>2S</sub> T300/5208.

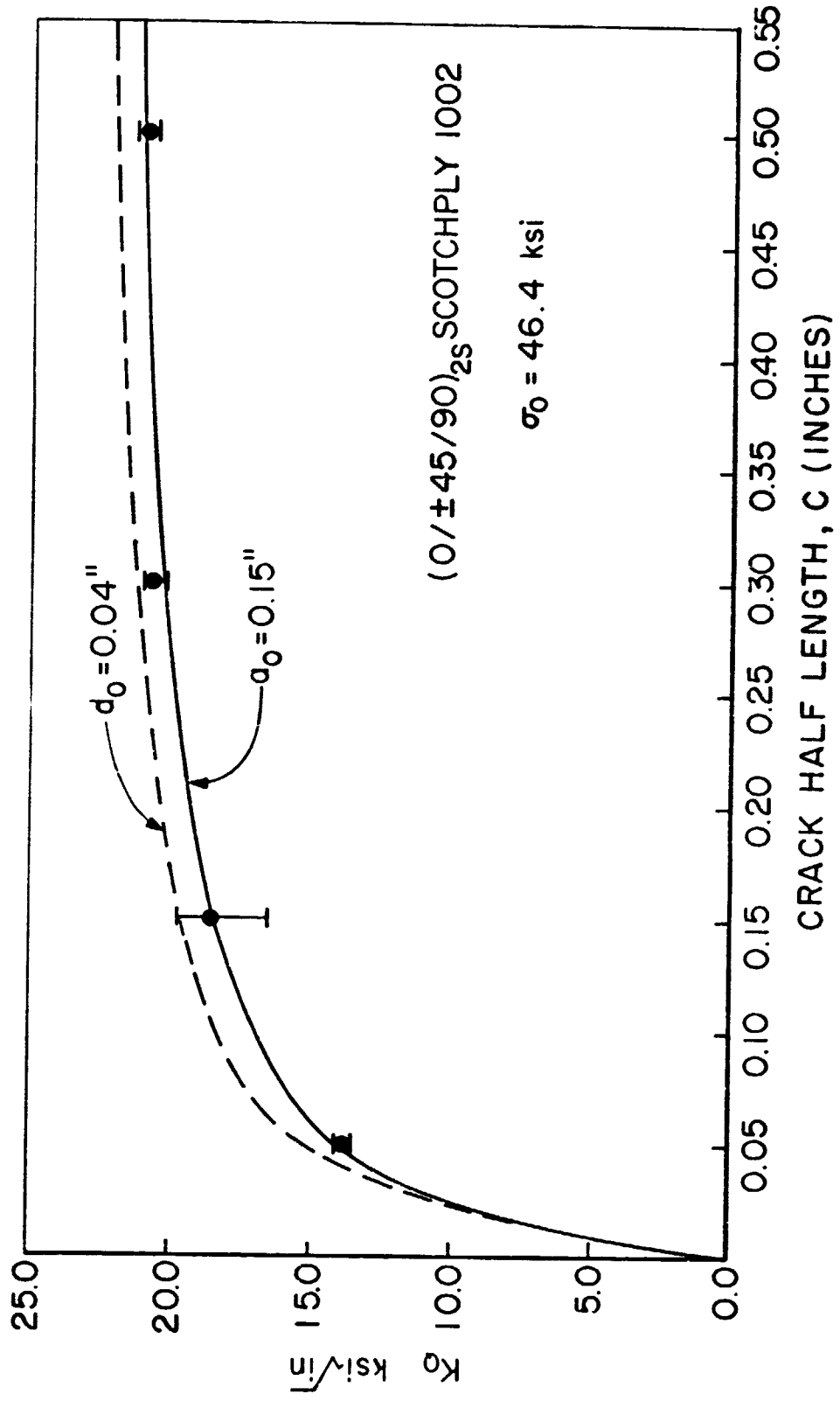


Figure 7.- Comparison of predicted and experimental fracture toughness for center cracks in (0, ±45, 90)<sub>2S</sub> Scotchply 1002.

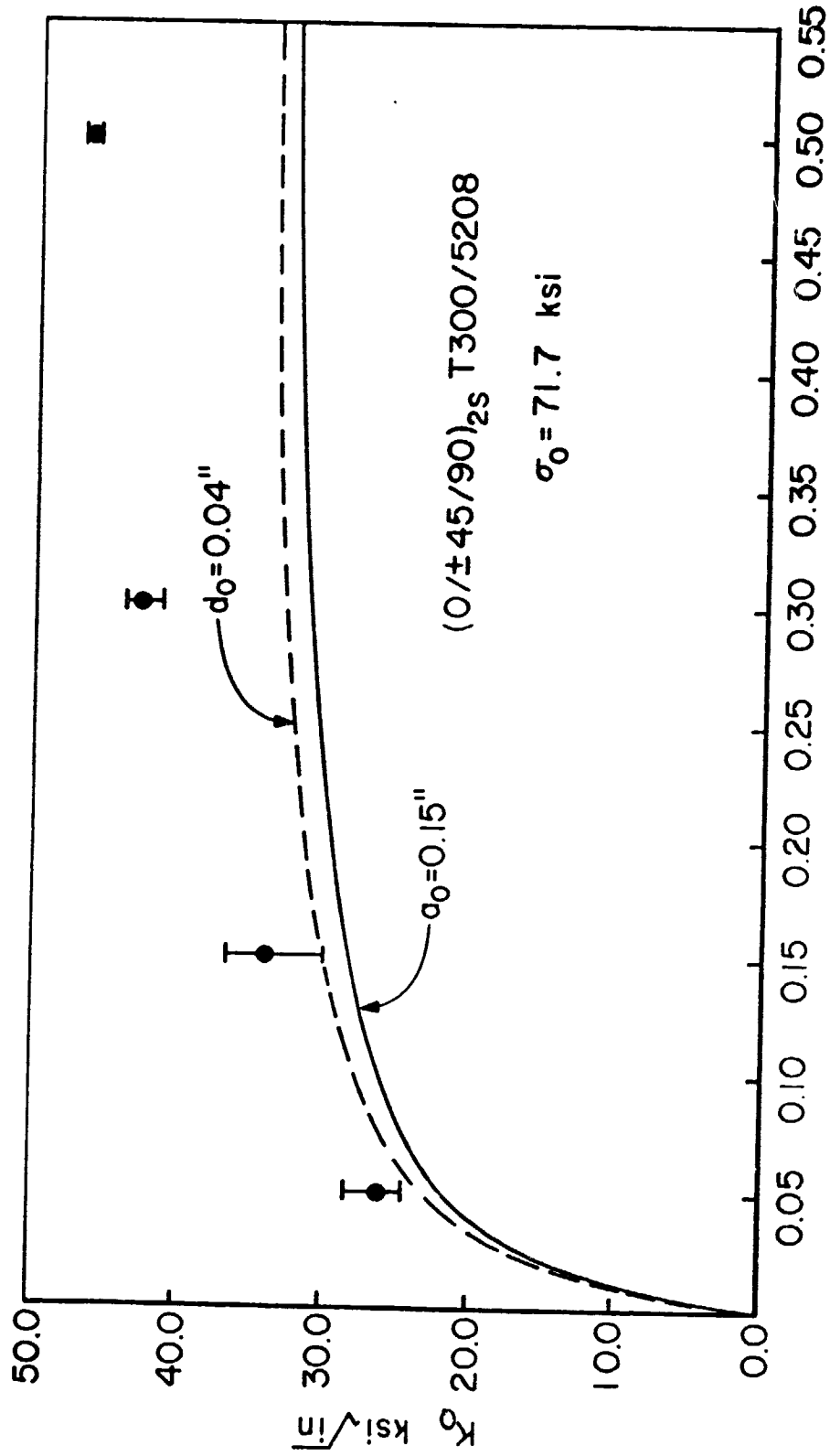


Figure 8.- Comparison of predicted and experimental fracture toughness for center cracks in  $(0, \pm 45, 90)_2S$  T300/5208.

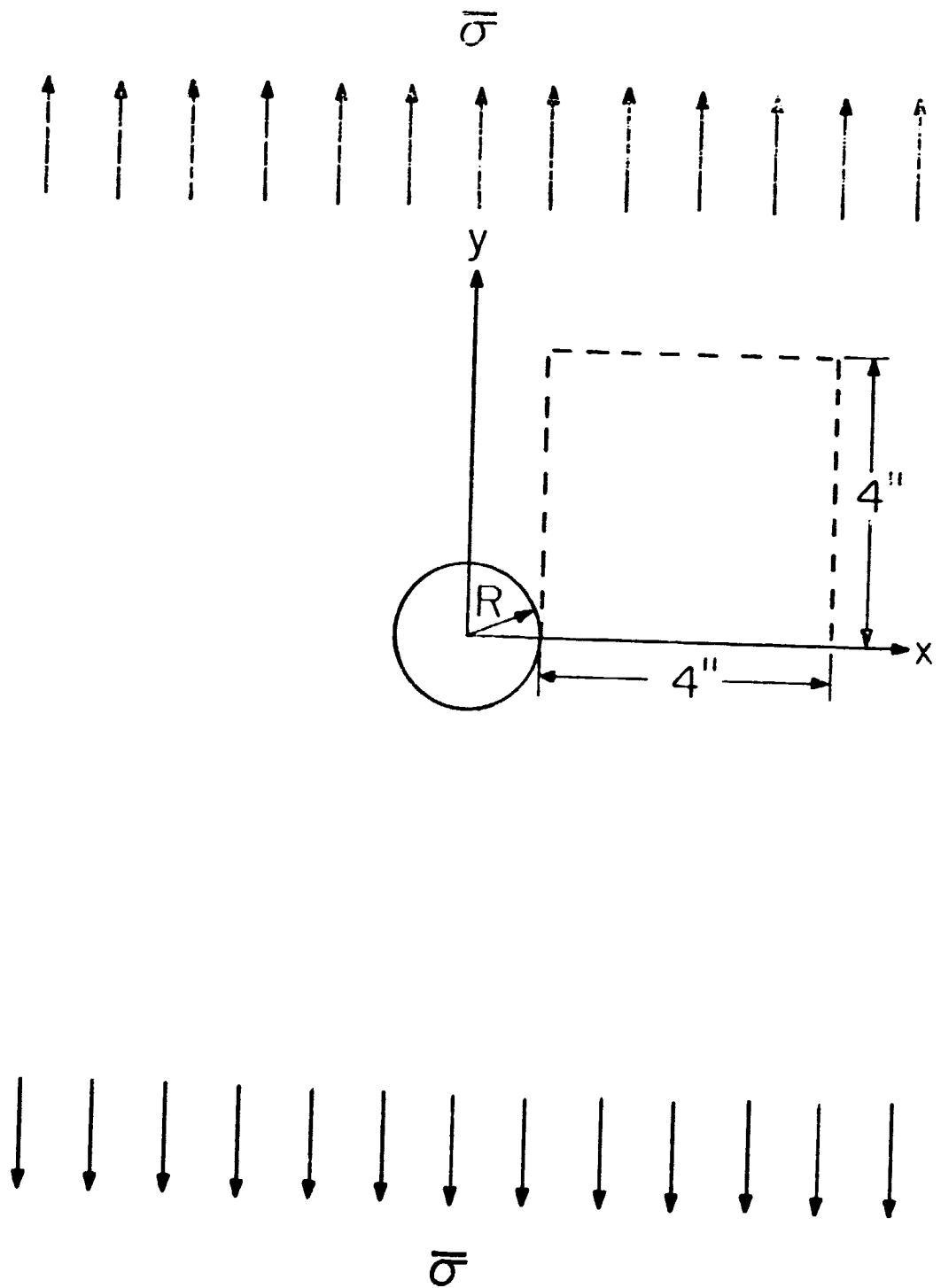


Figure 9.- Infinite homogeneous plate containing a circular hole under uniform uniaxial load.



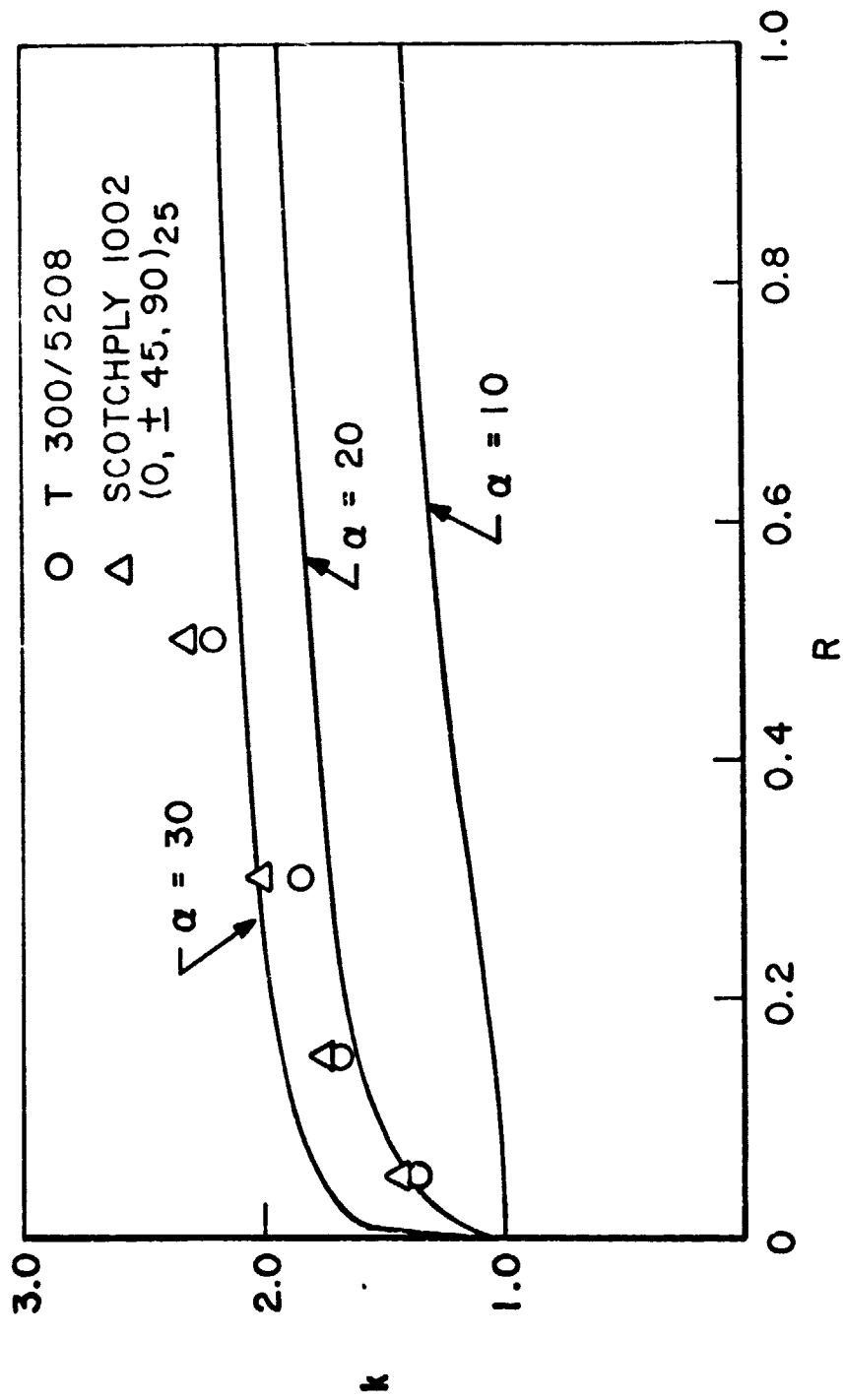


Figure 10.- Stress enhancement factor as a function of hole radius for different values of shape parameters.

## SUPER-HYBRID COMPOSITES -- AN EMERGING STRUCTURAL MATERIAL

By C. C. Chamis, R. F. Lark, T. L. Sullivan

NASA Lewis Research Center

### SUMMARY

Specimens of super-hybrids and advanced fiber composites were tested for smooth and center notch tensile strength, flexural strength, and Izod impact strength along the fiber direction and in the transverse direction. Specimens were also subjected to thermal fatigue and then tested for possible degradation at room temperature. The smooth tensile specimens were instrumented to obtain data for stress-strain curves. Laminate analysis was used to analyze the super-hybrid specimens with respect to elastic and thermal properties, residual stresses, and ply stresses at the specimen fracture stress condition.

The results show that the super-hybrid composites exhibit superior resistance to Izod impact compared with other hybrid and advanced fiber composites, are only slightly degraded by thermal fatigue, and have transverse flexural strengths about three times that of diffusion bonded boron/aluminum.

### INTRODUCTION

The national need for the conservation of natural resources provides a strong motivation for the efficient utilization of materials. In the area of materials for flight vehicle applications, the super-hybrid composite concept provides a means of utilizing advanced composite materials efficiently while meeting diverse design requirements.

Advanced fiber/resin and fiber/aluminum matrix composites are used effectively when the fiber and load directions are coincident. To provide strength or stiffness in more than one direction, composites with fibers oriented in several directions are necessary. Orienting fibers in more than one direction in the same composite, however, reduces their efficiency substantially and introduces lamination residual stresses comparable to the transverse and shear strength properties of the unidirectional composite. These lamination residual stresses can severely limit the resistance of composite components in flight vehicle structures to cyclic loads. In addition, current commercially available advanced fiber composites are weak in impact and erosion resistance. Also

graphite-fiber resin composites are susceptible to moisture degradation.

The aforementioned difficulties may be overcome to a significant extent via the super-hybrid composite concept. Briefly, superhybrids combine the best characteristics of fiber/resin, fiber/metal, and metal foil materials using adhesive bonding. Assembly of a super-hybrid is schematically illustrated in figure 1. Preliminary studies on fabrication feasibility and potential of super-hybrid composites as an aerospace material were reported in reference 1. In that study, one specific super-hybrid composite was made and tested for mechanical properties and Izod impact strength. The resistance of super-hybrids to thermal fatigue was not investigated in the study reported in reference 1.

To further evaluate the super-hybrid composite concept and to further illustrate their distinct advantages over other forms of advanced composites, an investigation was conducted wherein super-hybrids were made from various constituents and evaluated as to their mechanical properties, including impact and thermal fatigue. Also this paper describes the fabrication and test procedures used in making super-hybrids, and provides comparisons of theoretical predictions of mechanical properties and experimental results.

#### DESCRIPTION OF COMPOSITE SYSTEMS

In the following section the various types of laminates investigated are discussed.

##### Constituent Plies and Materials

Four types of laminates were made, two boron/aluminum (B/Al) and two super-hybrids. The types of laminates, laminate designations, constituent materials, and material suppliers are listed in table I(a). The laminate configurations are shown in table I(b). The numbering system for the laminate types is consistent with that of reference 1.

Thermal, physical and mechanical properties of the constituent materials are summarized in reference 1, table II. Note the thermal and mechanical properties of the boron/1100-Al alloy composites are approximately the same as those for the boron/6061-Al alloy.

##### Laminate Fabrication

Type II-A. - Eight plies of 5.6 mil-B/1100-Al were diffusion bonded by the manufacturer, Amercom, Inc. to provide a unidirectional laminate. The diffusion bonding conditions consisted of 4500 psi pressure at 950 °F for 1/2 hour.

Type II-B. - Six plies of 8.0 mil-B/1100-Al were diffusion bonded by the

manufacturer, Amercom, Inc. to produce a unidirectional laminate. The diffusion bonding conditions were the same as those for Type II-A.

Type VI. - Five sheets of titanium foil and 10 plies of graphite/epoxy (Gr/Ep) were adhesively bonded using FM 1000 structural adhesive to produce a unidirectional laminate. The foil was so oriented that its primary rolling direction was parallel to the fiber direction. Before bonding, the titanium foil plies were degreased and treated with a 5-percent hydrogen fluoride solution for 30 seconds at room temperature. This was followed by a water and methyl alcohol rinse and then by drying.

The graphite/epoxy plies were bonded using PR 288 epoxy matrix resin supplied by the Minnesota Mining and Manufacturing Co. (3 M Co.). The time-pressure-temperature curing cycle was selected to initially cure the graphite/epoxy plies and then to cure the FM 1000 interfaces. The procedure was as follows: The various components of the laminate were assembled in a metal mold. A laminating press was then preheated to 350 °F. The cold mold was placed in the press and 15 psig contact pressure was applied. Contact pressure was maintained for 3.6 minutes. A pressure of 600 psig was then applied. Pressure and temperature were maintained for 2 hours to complete curing of the epoxy resin matrix and the FM 1000 adhesive. Upon completion of curing, the press pressure was reduced to zero and the mold was removed from the press in a hot condition. The laminate was then removed from the mold after cooling.

Type VII. - Four sheets of titanium foil, two plies of B/Al, and seven plies of graphite/epoxy were adhesively bonded to produce a unidirectional laminate. Super-hybrid Type VII is the same as Type V, (ref. 1), without the mid titanium foil layer. The bonding and curing procedures for Type VII were the same as for Type VI. It is noted here that the fabrication procedure for super-hybrids VI and VII is similar to that for super-hybrid Type V in reference 1, except that 3501 epoxy resin matrix was used for the Type V laminate.

Typical cross sections of the laminates are shown in the photomicrographs of figure 2. The materials and various plies in these laminates are also indicated in this figure. The detailed arrangement of the materials, plies and their corresponding thicknesses are given in table I(b).

#### DESCRIPTION OF TEST PROGRAM

In this section the specimen preparation, instrumentation, types of tests, and procedures are described.

#### Specimen Preparation

Unidirectional laminates ranging from 0.058 to 0.064 in. thick were cut into 0.500 in. wide specimens by using a precision wafer cutting machine equipped with a diamond cutting wheel. A specimen layout plan is shown in

figure 3. The ends of all specimens used to determine longitudinal smooth tensile properties were reinforced with adhesively bonded aluminum tabs.

To determine the notch sensitivity of the laminates, through-the-thickness center notches were placed in specimens using electrical discharge machining. In all cases the notch root radius was 0.003 in. or less. A notch length of 0.17 in. was used.

The flexural specimens were used for the thermal fatigue and subsequent residual strength studies. The flexural specimens were selected because flexure bending is the most convenient way to assess the structural integrity retention of a material, as measured by its mechanical properties since this test subjects the material to tension, compression and shear simultaneously.

### Specimen Instrumentation

The specimens used to determine smooth tensile properties were instrumented with strain gages to measure longitudinal and transverse strain. A photograph of an instrumented specimen is shown in figure 4.

### Types of Tests and Procedures

Composite density. - Samples of each of the four types of laminates were evaluated for density by using the ASTM D-792 test method for "Specific Gravity and Density of Plastics by Displacement."

Smooth and notch tensile strengths. - The smooth and notch tensile specimens were loaded to failure using a hydraulically actuated universal testing machine. Longitudinal specimens had a test section that was about 3 in. long, and the transverse specimens had a test section that was about 2 in. long. The notched specimens were loaded to failure at a loading rate of approximately 0.01 in./in./minute, and the maximum load noted. Loading was halted at convenient intervals when testing the smooth specimens so that strain gage data (using a digital strain recorder) could be obtained.

Flexural strengths. - Test specimens having a length of 3 in. were tested for flexural strength in an Instron testing machine. A three-point loading system was used with a span of 2 in.

Izod impact strengths. - Non-standard unnotched thin specimens were subjected to Izod impact strength tests using a TMI impact tester equipped with a 2-lb hammer. The velocity of the hammer was 11 ft/sec. The specimen dimensions were 0.50 in. wide by 2.5 in. long.

Thermal fatigue tests. - Test specimens having a length of 3 in. and a width of 0.50 in. were subjected to a thermal fatigue test using a hot-cold shock chamber. A photograph of the thermal fatigue specimen magazine is shown in figure 5. The thermal fatigue chamber is shown in figure 6. Samples were cycled (without applied external stress) over a temperature range from -100° F to 300° F for 1000 cycles. A typical cycle consisted of a two-minute cooling

and two-minute heating period. Samples were periodically withdrawn from thermal fatigue testing and were subjected to flexural strength tests using a three-point loading system with a span of 2 inches. All specimens, before and after thermal fatigue testing, were examined optically, at 30X magnification, for possible cracks or delaminations.

## EXPERIMENTAL TEST PROGRAM RESULTS

In this section results obtained for density, tensile (smooth and notched), flexural, flexural after thermal fatigue, and Izod impact tests are summarized and discussed. Data for super-hybrid V are from reference 1. They are included here for comparison.

### Density

The measured densities of the laminates tested are given in the third column of table II. Note that all the super-hybrids have about the same density which is the same as that of glass/epoxy,  $0.074 \text{ lb/in.}^3$ , and about 25 percent less than B/1100-Al.

### Smooth Tensile Tests

Table II summarizes the test data obtained from smooth specimens (specimens without notches). This table includes laminate longitudinal (load applied parallel to fibers) and transverse (load applied normal to fibers) tensile properties. The initial tangent moduli and Poisson's ratios are given. As can be seen, inclusion of titanium foil layers in the super-hybrids improves the transverse strength properties relative to the B/Al unidirectional materials. The longitudinal and transverse fracture strains of the super-hybrids are approximately equal.

Note in table II that the longitudinal fracture stress of super-hybrid Type VI is about the same as that for the B/Al composites. The corresponding strain is greater by about 50-percent. Also, note that both the longitudinal fracture stress and strain of the 5.6-B/Al (II-A) are about 10-percent greater than those of the 8.0 B/Al (II-B). The transverse fracture stress of the 5.6 and 8.0 B/1100-Al is only about 50-percent of that of 5.6 B/6061-Al (ref. 1).

Stress-strain curves for all types of laminates are shown in figure 7(a) for loads parallel to fibers and in figure 7(b) for loads transverse to the fibers. The stress-strain curves are linear to fracture, or nearly so, for specimens loaded parallel to the fibers. However, specimens loaded transverse to the fibers exhibit considerable nonlinearity (fig. 7(b)). Curves of Poisson's strain versus axial strain are shown in figure 8.

One interesting result (also mentioned in ref. 1) is the failure mode of super-hybrids V and VII tested in longitudinal tension. The boron/aluminum plies failed when the tensile stress produced strain about equal to the

fracture strains of the boron fibers. The Gr/Ep plies remained intact and were therefore still capable of carrying mechanical load. The authors believe this failure mode to be significant because these hybrids can be designed to have inherent fail-safe design characteristics.

#### Notch Tensile Tests

The test data obtained from notched specimens are summarized in table III. Two interesting points to be observed from the data in table III are:

- (1) The notch effects are small and about the same for both the longitudinal and transverse directions in the super-hybrid composites.
- (2) Notch strengthening for the transverse tensile specimens was observed in both of the diffusion bonded B/Al laminates. This strengthening may be attributed, in part, to the transverse restraining effects of the fibers at the notch ends, and to possible changes in the aluminum matrix strength due to machining the notch.

#### Flexural Tests

The test data obtained from subjecting test specimens to three-point flexural loading are summarized in table IV. The important points to be observed from the data are:

- (1) The super-hybrid composites exhibit significant improvement in transverse strength compared with the B/1100-Al composites.
- (2) The super-hybrid composites containing B/Al exhibit a decrease in the longitudinal flexural strength compared with other composites.
- (3) The super-hybrid composite flexural longitudinal modulus is about 70-percent that of the corresponding tensile modulus (table II).
- (4) The flexural transverse modulus of the super-hybrid composites is smaller than the corresponding tensile modulus (table II).

#### Impact Tests

Unnotched Izod impact test data are summarized in table V. To compare Izod impact resistance of the different laminates, the data were normalized with respect to the cross sectional area of the composite. In table V the low and high Izod impact strengths and the number of specimens for each composite or material are given.

The important point to be observed from the data in table V is the following: Using the super-hybrid composite concept, composite materials may be designed with Izod impact resistance approaching that of 6061 aluminum

(800 in.-lb/in.<sup>2</sup>) (ref. 1). In addition, when the Izod impact values are normalized with respect to density, the longitudinal impact resistance of the type V hybrid is about 70-percent that of titanium (16,000 in.<sup>3</sup>).

Another important point to be observed from the data in table V is that the super-hybrids have Izod longitudinal impact resistance about two times that of the B/1100-Al, while the transverse is about the same. This is significant because B/1100-Al is considered to be a relatively high energy absorbing material. It is noted, however, that the B/1100-Al unidirectional composite provided by the material supplier may not have been processed for optimum impact resistance.

### Flexural Tests After Thermal Fatigue

The thermal fatigue effects on the flexural strength of super-hybrids are summarized in table VI. Prior to testing these specimens in flexure, they were subjected to 1000 thermal cycles from -100 °F to 300 °F. Optical examination, at 30X magnification, did not reveal cracks or delaminations. In order to make the thermal fatigue effects more pronounced, the flexural fracture stress after thermal cycling is compared to the as-fabricated highest value. As can be observed from the data in table VI, the thermal fatigue effects on the longitudinal flexural strength of the super-hybrids is less than 10-percent, while on the transverse, it is about 25-percent.

The important point to be noted is that the transverse flexural strength, after thermal fatigue, of the super-hybrids is still substantial when compared to the transverse strength of advanced unidirectional composites, both metal and resin-matrix.

## THEORETICAL RESULTS

The theoretical results described below were obtained using the laminate theory and computer code described in reference 3. The results are for:

- (1) mechanical and thermal properties
- (2) ply residual stresses
- (3) ply-stress and composite-stress influence coefficients.

### Mechanical and Thermal Properties

The theoretically predicted mechanical properties are summarized in table VII. In this table results are given for density, membrane (in-plane) moduli and thermal coefficients of expansion, and bending moduli. Nominal measured properties for 6061-Al and Ti (6 Al-4V) are given for baseline material comparisons.



As can be observed from the data in table VII, the bending moduli of the super-hybrids are comparable to those of the titanium alloy in magnitude and the super-hybrids have less than one-half its density.

#### Lamination Residual Stresses

Lamination residual stresses are induced in the constituent material layers of the metal and resin matrix composites and the adhesive as a result of the lamination process because of:

- (1) The mismatch of the thermal coefficient of expansion of the constituents
- (2) The temperature difference between the cure and room temperatures (ref. 2).

The lamination residual stresses were computed as described in reference 1.

Selected results are summarized in table VIII. Note that the safety margins (S.M.) are also given; these were computed using the failure criterion in reference 4.

The ply residual stresses in table VIII are for a particular ply type as it is first encountered progressing inward from either surface. Several important observations from the data in table VIII are:

1. The S.M.'s for all plies is 0.66 or greater (zero denotes onset of fracture). Therefore, considerable capacity remains to resist mechanical load.
2. The longitudinal and transverse residual stresses in the adhesive are approximately equal and appear to be insensitive to the composition of the super-hybrid investigated. The adhesive residual stress is about 3.5 ksi which is about 50-percent of the bulk-state fracture stress, (ref. 1).
3. The longitudinal residual stress in the Gr/Ep plies is compressive.
4. The transverse residual stress in the B/Al plies is relatively small; less than 2.5 ksi.

#### Ply Stress Influence Coefficients

The concept of super-hybrid composites involves the strategic location of the titanium foil and B/Al plies to provide maximum resistance to transverse and shear forces. A direct way to assess whether this was achieved in the super-hybrids considered herein is to compute the ply stress influence coefficients due to uniaxial membrane and bending composite stresses. These influence coefficients were computed using the linear laminate analysis of reference 3. Selected results obtained for super-hybrid V are summarized in table IX. These results are for a particular ply type as it is first en-

countered progressing inward from the surface. Note that to obtain the ply stress, the influence coefficients must be multiplied by the membrane (bending) stress taken with the correct sign.

As can be observed from the data in table IX, the titanium foil and B/Al plies have large ply stress influence coefficients for uniaxial transverse and shear composite stresses. Therefore, the titanium foils and the B/Al in the super-hybrids provide practically all the resistance for transverse and shear forces. This verifies their role in the super-hybrid concept.

The other points to be observed from the data in table IX are:

1. The ply stress influence coefficients of the adhesive are negligible for all uniaxial composite stresses. Therefore, fracture will occur first in one of the non-adhesive constituents as desired in the super-hybrid concept.

2. The transverse and shear ply stress influence coefficients of the  $G_r/E_p$  due to uniaxial transverse and shear composite stresses are about 10-percent of the corresponding coefficients for the titanium and B/Al. This is another desired feature of the super-hybrid concept.

3. The transverse and shear ply stress influence coefficients for the titanium foils and the B/Al plies are approximately equal. This means that super-hybrids tested in the transverse direction, in in-plane shear, or in twisting will exhibit nonlinear stress-strain to fracture. The B/Al plies will fail first followed by yielding and finally fracture of the titanium. The super-hybrid stress-strain curves in figure 7(b) and the Poisson's strain curves in figure 8(b) are consistent with this observation.

The previous discussion leads to the following conclusion. The transverse and shear fracture modes of super-hybrids will be governed by the titanium foils in general. The transverse fracture strains for the super-hybrids in table II are about 1-percent which is approximately equal to the yield strain of titanium and which is in accord with the conclusion just stated. In-plane or twisting shear fracture strains need yet to be determined.

The linear stresses in the various plies resulting from the combined residual and applied loads may be obtained from the influence coefficients in table IX and by adding algebraically the corresponding residual stress from table VIII.

Photographs of fractured super-hybrid specimens from various tests in this program are shown in figure 9. Note the well defined fracture surfaces on all these specimens.

Since the stress-strain curves for the super-hybrids tested in the longitudinal direction are linear to fracture, the influence coefficients in table IX can be used to compute the ply longitudinal fracture stress due to both membrane and bending loads. For example, the longitudinal fracture stresses in the B/Al plies are (204 ksi) due to tensile load and (216 ksi) due to flexural load. These values are about the same as those for laminate II-A, table II.

## COMPARISON OF PREDICTED AND MEASURED DATA

Comparing corresponding data from table VII (in-plane) with those in table II for the super-hybrids, it is seen that all but one of the predicted values are within 10-percent of the measured values. Note, the measured values for longitudinal modulus for the B/Al composites are less than the predicted ones by an amount equivalent to that corresponding to approximately the aluminum modulus contribution (as determined using the rule-of-mixtures). This is probably the case because the 1100-Al is so soft that it was probably already stressed nonlinearly due to microresidual strains.

Comparing corresponding data for the longitudinal and transverse moduli in table VII (bending) with those in table IV, it is seen that they are in reasonably good agreement. These comparisons further substantiate that linear laminate theory is adequate for predicting elastic properties of super-hybrids.

## SUMMARY OF RESULTS AND CONCLUSIONS

The key results from this investigation are:

1. Super-hybrids subjected to 1000 cycles of thermal fatigue from -100° to 300 °F retained over 90-percent of their longitudinal flexural strength and over 75-percent of their transverse flexural strength.
2. The transverse flexural strength of super-hybrids may be as high as eight-times that of the commercially supplied boron/1100-Al composite. The longitudinal stress in the boron/aluminum plies of the super-hybrids at fracture is about the same as that for the boron/1100-Al composite.
3. The thin specimen Izod longitudinal impact resistance of the super-hybrids is about twice that of the commercially supplied boron/1100-Al, while the transverse impact strength is about 100 to 150-percent of that of boron/1100-Al.
4. Linear laminate analysis is adequate for predicting initial membrane (in-plane) and bending elastic properties of super-hybrids.
5. Super-hybrids subjected to transverse tensile loads exhibit nonlinear stress-strain relationships.

The data obtained and analyzed in this investigation further substantiate the practicality and utility of the super-hybrid composite concept for attaining superior impact, transverse and shear strength properties and notch insensitivity. Since the titanium foils are on the surface, it may further be concluded that super-hybrids should have good erosion and moisture resistance.

#### REFERENCES

1. Chamis, Christos C.; Lark, Raymond F.; and Sullivan, Timothy L.: Boron/Aluminum-Graphite/Resin Advanced Fiber Composite Hybrids. NASA TN D-7879, 1975.
2. Chamis, Christos C.: Lamination Residual Stresses in Multilayered Fiber Composites. NASA TN D-6146, 1971.
3. Chamis, Christos C.: Computer Code for the Analysis of Multilayered Fiber Composites - User's Manual. NASA TN D-7013, 1971.
4. Chamis, Christos C.: Failure Criteria for Filamentary Composites. NASA TN D-5367, 1969.

TABLE I. - LAMINATE DESCRIPTIONS  
(a) Layer materials and source

Laminate		Materials	Source
Type	Composition		
II-A	B/Al	Diffusion-bonded unidirectional layers 5.6-mil diam. boron fibers in 1100 aluminum alloy matrix	Amercom, Inc.
II-B	B/Al	Diffusion-bonded unidirectional layers 8-mil diam. boron fibers in 1100 aluminum alloy matrix	Amercom, Inc.
VI	Ti, A-S/Ep Superhybrid	Titanium (6Al-4V) foil, 0.0015-in. thick as rolled Type A-S graphite fiber/PR 288 prepreg FM 1000 structural adhesive in film form	Teledyne Rodney Metals 3 M Company American Cyanamid Co.
VII, V(ref. 1)	Ti, B/Al, A-S/Ep Superhybrid	Titanium (6Al-4V) foil, 0.0015-in. thick as rolled Individual monotape layers 5.6-mil diam. boron fibers in 6061 aluminum alloy matrix Type A-S graphite fiber/PR 288 prepreg FM 1000 structural adhesive in film form	Teledyne Rodney Metals Amercom, Inc. 3 M Company American Cyanamid Co.

TABLE I. - LAMINATE DESCRIPTIONS

(b) Laminate

LAMINATE														
COMPOSITION Dif. Bonded Boron/1100-Al (B/Al)			COMPOSITION Dif. Bonded Boron/1100-Al (B/Al)			COMPOSITION Titanium, Graphite/Epoxy, (Ti/(A-S/E))			COMPOSITION Titanium, Boron/6061-Al, Graphite/Epoxy (Ti/(B/Al)/(A-S/E))					
Type-II-A			Type-II-B			Type-VI			Type-VII					
Layer no.	Material	t, in. (a)	Layer	Material	t, in.	Layer	Material	t, in.	Layer	Material	t, in.			
1	B/Al, (5.6 mil, 1100)	0.0075	1	B/Al, (8.0 mil, 1100)	0.0107	1	Ti (6-4)	0.0015	1	Ti (6-4)	0.0015			
2	↓	↓	2	↓	↓	2	FM 1000	0.0001	2	FM 1000	0.001			
3	↓	↓	3	↓	↓	3	Ti (6-4)	0.0015	3	Ti (6-4)	0.0015			
4	↓	↓	4	↓	↓	4	FM 1000	0.0001	4	FM 1000	0.001			
5	↓	↓	5	↓	↓	5	A-S/E	0.005	5	B/Al, (5.6 mil, 6061)	0.0074			
6	↓	↓	6	↓	↓	6	A-S/E	0.005	6	FM 1000	0.001			
7	↓	↓	(total thickness, 0.064)			7	A-S/E	0.005	7	A-S/E	0.005			
8	↓	↓				8	A-S/E	0.005	8	A-S/E	0.005			
(total thickness, 0.060)						9	A-S/E	0.005	9	A-S/E	0.005	9	A-S/E	0.005
						10	FM 1000	0.0001	10	FM 1000	0.0001	10 <sup>(b)</sup>	A-S/E	0.005
						11	Ti (6-4)	0.0015	11	Ti (6-4)	0.0015	11	A-S/E	0.005
						12	FM 1000	0.0001	12	FM 1000	0.0001	12	A-S/E	0.005
						13	A-S/E	0.005	13	A-S/E	0.005	13	A-S/E	0.005
						14	A-S/E	0.005	14	A-S/E	0.005	14	FM 1000	0.001
						15	A-S/E	0.005	15	A-S/E	0.005	15	B/Al, (5.6 mil, 6061)	0.0074
						16	A-S/E	0.005	16	A-S/E	0.005	16	FM 1000	0.001
						17	A-S/E	0.005	17	A-S/E	0.005	17	Ti (6-4)	0.0015
			18	FM 1000	0.0001	18	FM 1000	0.0001	18	FM 1000	0.001			
			19	Ti (6-4)	0.0015	19	Ti (6-4)	0.0015	19	Ti (6-4)	0.0015			
			20	FM 1000	0.0001	(total thickness, 0.058)			(total thickness, 0.062)					
			21	Ti (6-4)	0.0015									

(a) t denotes layer thickness.

(b) For laminate Type VII (ref. 1) this layer was Ti (6-4) with FM 1000 on each side.

ORIGINAL PAGE IS  
OF POOR QUALITY

TABLE II. - SMOOTH TENSILE TEST DATA

Laminate type	Constituents	Density, lb/in. <sup>3</sup>	Fracture strength, 10 <sup>3</sup> psi		Fracture strain, percent		Initial modulus of elasticity, 10 <sup>6</sup> psi		Initial Poisson's ratio	
			Longitudinal	Transverse	Longitudinal	Transverse	Longitudinal	Transverse	Longitudinal	Transverse
II-A	B/Al (5.6) (a)	0.094	196	9.63	0.78	0.18	27	17	0.23	0.09
II-B	B/Al (8.0) (a)	0.093	183	10.6	0.67	0.12	28	17	0.23	0.15
V	Ti, B/Al, Gr/Ep (b,c)	0.074	125	31.5	0.73	1.01	18	8.5	0.25	0.11
VI	Ti, Gr/Ep (b)	0.068	182	25.7	1.2	0.91	15	3.5	0.32	0.07
VII	Ti, B/Al, Gr/Ep (b)	0.073	133	23.1	0.75	0.66	18	8.1	0.25	0.12

(a) Diffusion-bonded.

(b) Adhesive-bonded.

(c) Reference 1.

TABLE III. - NOTCHED TENSILE TEST DATA

Laminate type	Constituents	Notch length, in.	Net fracture strength, 10 <sup>3</sup> psi		Notch strength, %	
			Longitudinal	Transverse	Longitudinal	Transverse
II-A	B/Al (5.6/1100) (a)	0.17	138	11.6	0.70	1.20
II-B	B/Al (8.0/1100) (a)	0.17	142	12.6	0.77	1.19
V	Ti, B/Al, Gr/Ep (b, c)	0.17	98	24.0	0.78	0.76
VI	Ti, Gr/Ep (b)	0.17	150	19.4	0.82	0.75
VII	Ti, B/Al, Gr/Ep (b)	0.17	107	15.6	0.80	0.68

(a) Diffusion-bonded.

(b) Adhesive-bonded.

(c) Reference 1.



TABLE IV. - RESULTS OF FLEXURAL TESTS

Laminate type	Constituents	Fracture stress 10 <sup>3</sup> psi				Modulus, 10 <sup>6</sup> psi (a)			
		Longitudinal		Transverse		Longitudinal		Transverse	
		Low	High	Low	High	Low	High	Low	High
		II-A	B/Al (5.6) <sup>(b)</sup>	241	252	18.9	23.3	29.4	31.4
II-B	B/Al (8.0) <sup>(b)</sup>	204	204	16.6	24.2	21.0	23.2	---	---
V	Ti, B/Al <sup>(c,d)</sup> Gr/Ep	185	---	83.0	---	22.0	---	11.0	---
VI	Ti, Gr/Ep <sup>(c)</sup>	217	245	42.5	70.1	24.1	---	8.8	---
VII	Ti, B/Al, <sup>(c)</sup> Gr/Ep	161	188	71.3	77.3	20.6	---	12.5	---

(a) Modulus was computed using chart deflection and a calibration factor to account for Instron compliance. These values are only approximate.

(b) Diffusion-bonded.

(c) Adhesive-bonded.

(d) Reference 1.

TABLE V. - SUMMARY OF THIN-SPECIMEN IZOD IMPACT STRENGTH RESULTS

Laminate type	Constituents	Test direction	IZOD impact strength in.-lb/in. <sup>2</sup>		Number of specimens
			Low	High	
II-A	B/Al (5.6) (a)	Longitudinal	331	335	3
		Transverse	135	167	2
II-B	B/Al (8.0) (a)	Longitudinal	319	338	3
		Transverse	129	147	2
V	Ti, B/Al, Gr/Ep (b) (c)	Longitudinal	634	720	2
		Transverse	186	202	2
VI	Ti, Gr/Ep (b)	Longitudinal	573	734	3
		Transverse	142	171	3
VII	Ti, B/Al, Gr/Ep (b)	Longitudinal	454	658	6
		Transverse	129	143	2

(a) Diffusion-bonded.

(b) Adhesive-bonded.

(c) Reference 1.

TABLE VI. - COMPARISON OF FLEXURAL STRENGTH PROPERTIES OF AS-FABRICATED AND THERMALLY-CYCLED SPECIMENS (1000 CYCLES FROM -100° TO 300 °F)

Laminate type	Constituents	Fracture stress 10 <sup>3</sup> psi			
		As-fabricated		Thermally-cycled	
		Longitudinal	Transverse	Longitudinal	Transverse
V	Ti, B/Al, Gr/Ep <sup>(a)</sup>	185 (high)	83 (high)	169	62.4
VI	Ti, Gr/Ep	245 (high)	70.1 (high)	247	57.9
VII	Ti, B/Al, Gr/Ep	188 (high)	77.3 (high)	177	56.5

(a) Laminate reported in reference 1.

TABLE VII. - PREDICTED MECHANICAL AND THERMAL PROPERTIES  
OF METAL-MATRIX AND SUPER-HYBRID COMPOSITES

Composite	Density, lb/in. <sup>3</sup>	Membrane (In Plane)						Bending								
		Modulus, 10 <sup>6</sup> psi			Poisson's Ratio			Thermal Coefficient of Expansion 10 <sup>-6</sup> in./in./°F			Modulus, 10 <sup>6</sup> psi			Poisson's Ratio		
		Longi- tudinal	Trans- verse	Shear	Major	Minor	Longi- tudinal	Trans- verse	Longi- tudinal	Trans- verse	Longi- tudinal	Trans- verse	Shear	Major	Minor	
II-A(a)	0.095	33.0	21.0	7.2	0.25	0.16	3.3	10.7		33.0	21.0	7.2	0.25	0.16		
II-B(b)	0.095	33.0	21.0	7.2	0.25	0.16	3.3	10.7		33.0	21.0	7.2	0.25	0.16		
V(b)	0.079	20.2	8.7	3.0	0.26	0.11	5.6	15.8		21.2	13.4	4.7	0.27	0.17		
VI(b)	0.070	18.1	3.9	1.3	0.28	0.06	1.4	15.1		17.6	6.1	2.1	0.29	0.10		
VII(b)	0.075	20.0	7.9	2.7	0.26	0.10	5.4	16.2		20.0	12.5	4.4	0.27	0.17		
Al(c) (6061)	0.098	10.0	10.0	3.6	0.33	0.33	12.6	12.6		10.0	10.0	3.6	0.33	0.33		
Ti(c) (6Al-4V)	0.160	16.0	16.0	6.2	0.30	0.30	3.2	3.2		16.0	16.0	6.2	0.30	0.30		

(a) Diffusion bonded.

(b) Super-hybrid.

(c) Nominal properties included for comparison.



TABLE IX. - PREDICTED PLY STRESS INFLUENCE COEFFICIENTS DUE TO UNIT  
UNIAXIAL COMPOSITE STRESS FOR SUPER-HYBRID V (Ti, B/Al, Gr/Ep)

Ply	Uniaxial Membrane Stress						Uniaxial Flexural Stress (a)					
	Longitudinal			Transverse			Shear	Longitudinal		Transverse		Shear
	Longitudinal	Transverse	Longitudinal	Transverse	Longitudinal	Transverse		Longitudinal	Transverse			
	Longitudinal	Transverse	Longitudinal	Transverse	Longitudinal	Transverse	Longitudinal	Transverse	Longitudinal	Transverse	Longitudinal	Transverse
Top Titanium alloy	0.824	0.032	0.373	1.95	2.08	0.768	0.026	0.161	1.22	1.28	0.161	1.22
Adhesive	0.011	0.002	0.009	0.028	0.024	0.010	0.002	0.004	0.016	0.014	0.004	0.016
B/Al	1.63	-0.014	0.184	2.45	2.43	1.12	-0.013	-0.017	1.13	1.10	-0.017	1.13
Gr/Ep	0.912	-0.002	-0.184	0.226	0.206	0.420	0	-0.095	0.070	0.063	-0.095	0.070
Center Gr/Ep	0.912	-0.002	-0.184	0.226	0.206	-0.420	0	0.095	-0.070	-0.063	0.095	-0.070
B/Al	1.63	-0.014	0.184	2.45	2.43	-1.12	0.013	0.017	-1.13	-1.10	0.017	-1.13
Adhesive	0.011	0.002	0.009	0.028	0.024	-0.010	-0.002	-0.004	-0.016	-0.014	-0.004	-0.016
Bottom Titanium alloy	0.824	0.032	0.373	1.95	2.08	-0.768	-0.026	-0.161	-1.22	-1.28	-0.161	-1.22

(a) To obtain ply stress, multiply influence coefficient by the flexural stress with the correct sign.

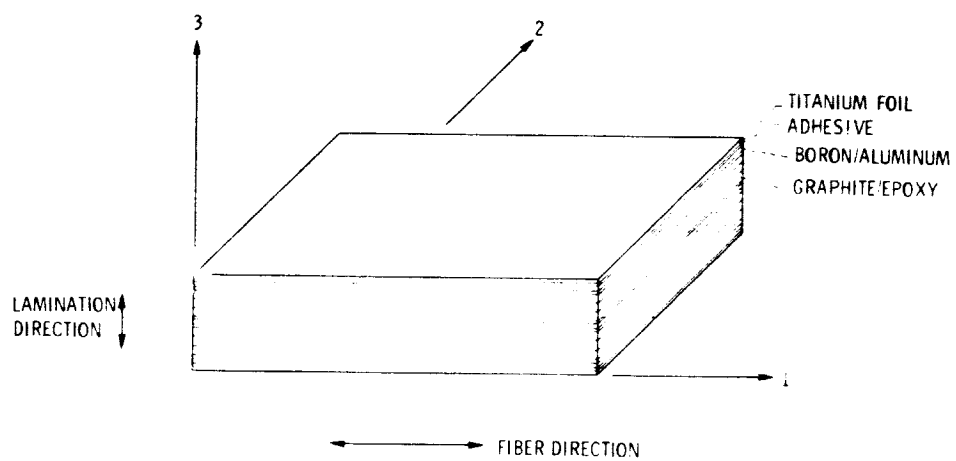
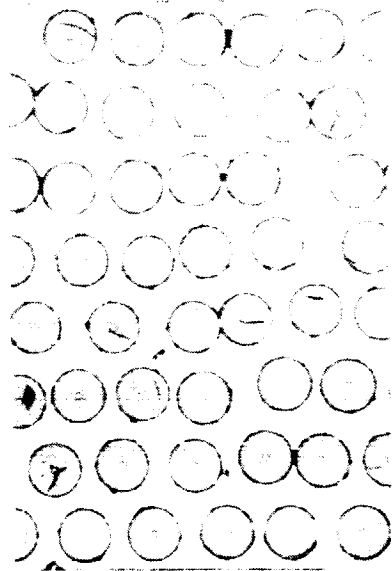


Figure 1.- Schematic of adhesively bonded metal matrix and resin matrix fiber composite hybrid.

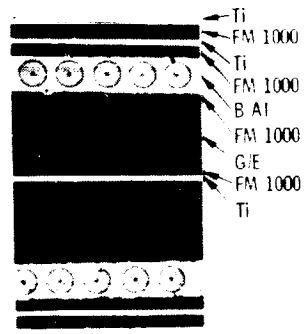


Dif. bonded (B/Al)  
5.6 Mil/1100  
Type II-A

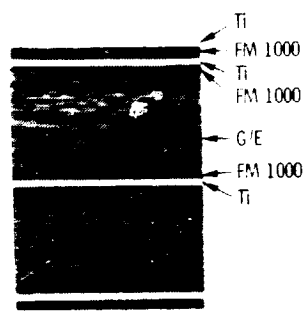


Dif. bonded (B/Al)  
8.0 Mil/1100  
Type II-B

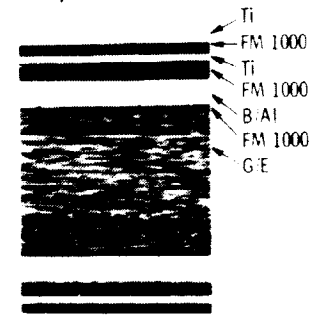
(a) B/Al composites. Photomicrographs.



Ti(B/Al)(A-S/E)  
TYPE V



Ti(A-S/E)  
TYPE VI



Ti(B/Al)(A-S/E)  
TYPE VII

(b) Super hybrids.

Figure 1.- Composite specimen cross sections. 35.



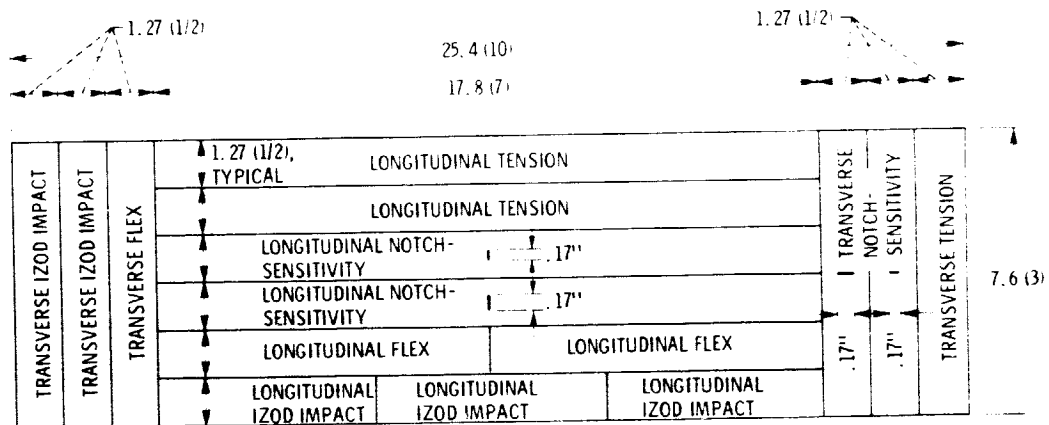


Figure 3.- Typical specimen layout plan. (Nominal values. All dimensions are in cm (in.).)

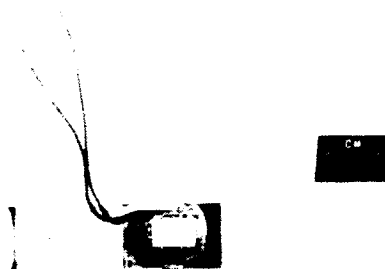


Figure 4.- Instrumented super-hybrid specimen.

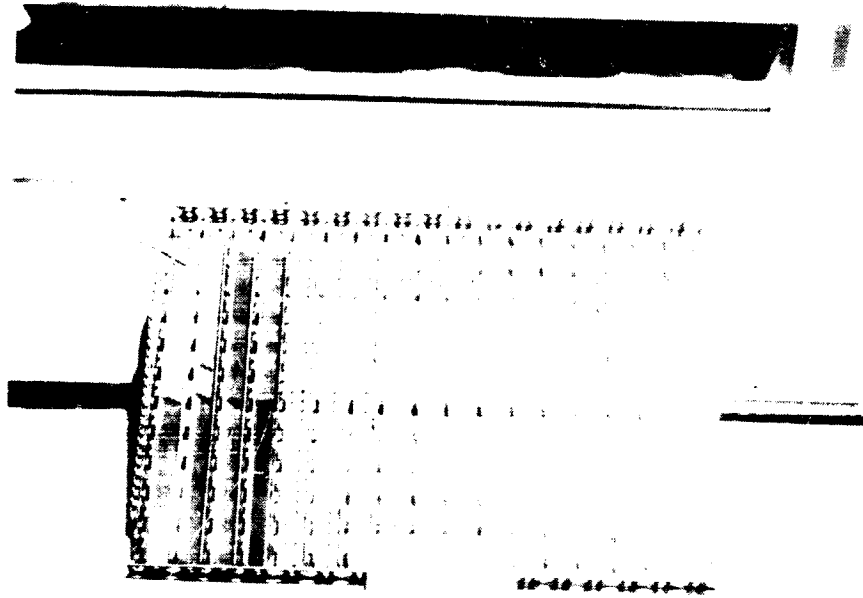


Figure 5.- Thermal fatigue specimen magazine.

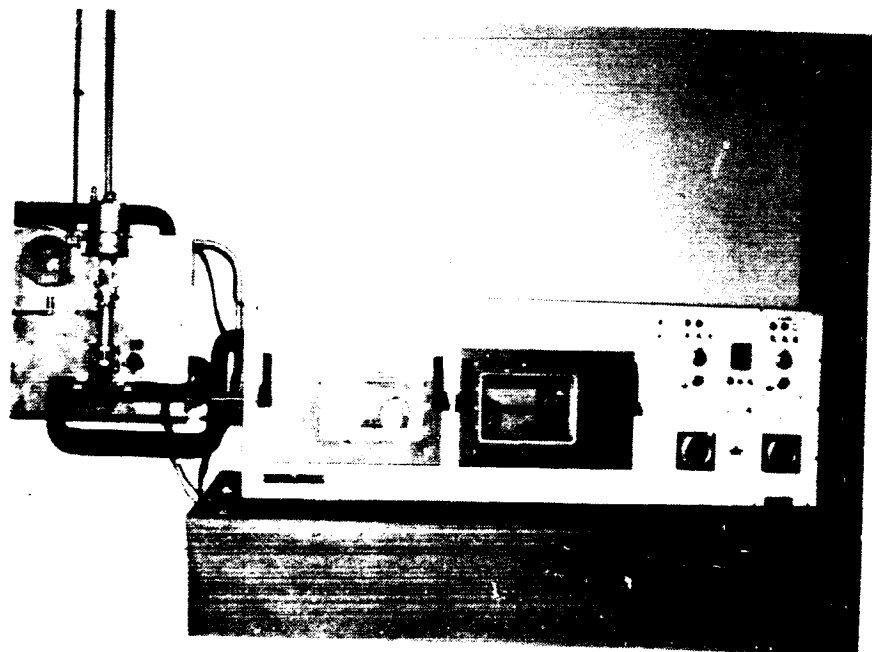
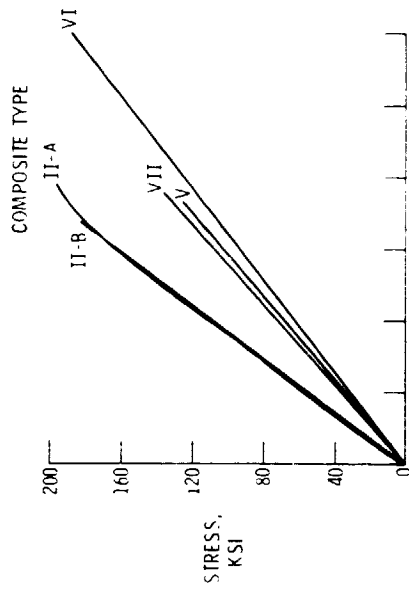
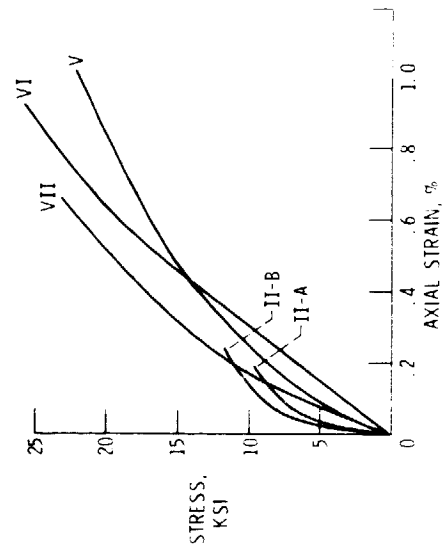


Figure 6.- Thermal fatigue tester, 10 psi.

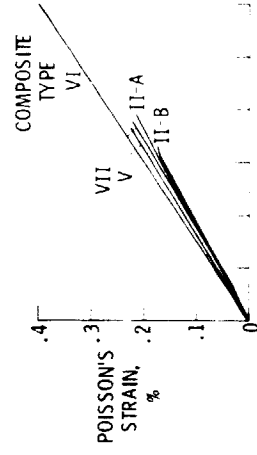


(a) Loading parallel to fibers.

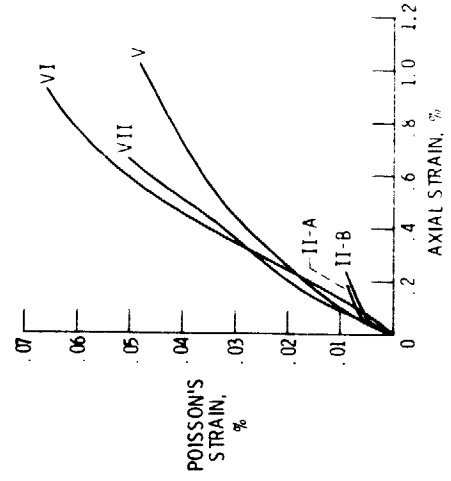


(b) Loading normal to fibers.

Figure 7.- Stress-strain curves for smooth tensile specimens.



(a) Loading parallel to fibers.



(b) Loading parallel to fibers.

Figure 8.- Poisson's strain for smooth tensile specimens.



Longitudinal smooth and notch base



Transverse smooth and notch base



Transverse smooth and notch base



Figure 3.- Various fractured composite specimens.

ORIGINAL PAGE IS  
OF POOR QUALITY

## ADVANCED COMPOSITES IN BURD II

By Edward Crawley and John Wendell

Department of Aeronautics and Astronautics  
Massachusetts Institute of Technology

### SUMMARY

B.U.R.D. II (Biplane Ultralight Research Device) is a two man powered pusher aircraft designed by M.I.T. students. Advanced composites have been used extensively in the design of the primary flight structure. The main spar is a graphite/epoxy-styrofoam beam, which presented some unique fabrication problems for cost effective, minimum gauge structure. Design, analysis, fabrication and test results will be described.

### INTRODUCTION

Man's desire to fly under his own power, a desire long overshadowed by the development of high speed motorized flight, was rekindled by the establishment of the Kremer Prize under the auspices of the Royal Aeronautical Society. The prize, now £ 50,000, has gone unclaimed since 1957. The only requirements for the prize are that a man or men must fly, solely under their own power, in a figure-eight course around two pylons 805 m. (1/2 mile) apart, with an altitude of at least 3.1 m. (10 feet) at the start and finish line (Fig. 1). While the requirements are easily stated, they will be met only with great difficulty.

In 1969 a group of students in the Department of Aeronautics and Astronautics at M.I.T. accepted the Kremer Prize challenge. They did so hoping that they would not only build an aircraft capable of winning the prize, but in doing so gain valuable practical engineering experience. Since that time almost twenty students have worked on the BURD, with the constant advice and support of the faculty and staff of the Department of Aeronautics and Astronautics and with the financial backing of M.I.T. and of various individuals and corporations. These backers are known as the "Friends of the BURD". The following results represent the collective efforts of these twenty students.

**PRECEDING PAGE BLANK NOT FILMED**

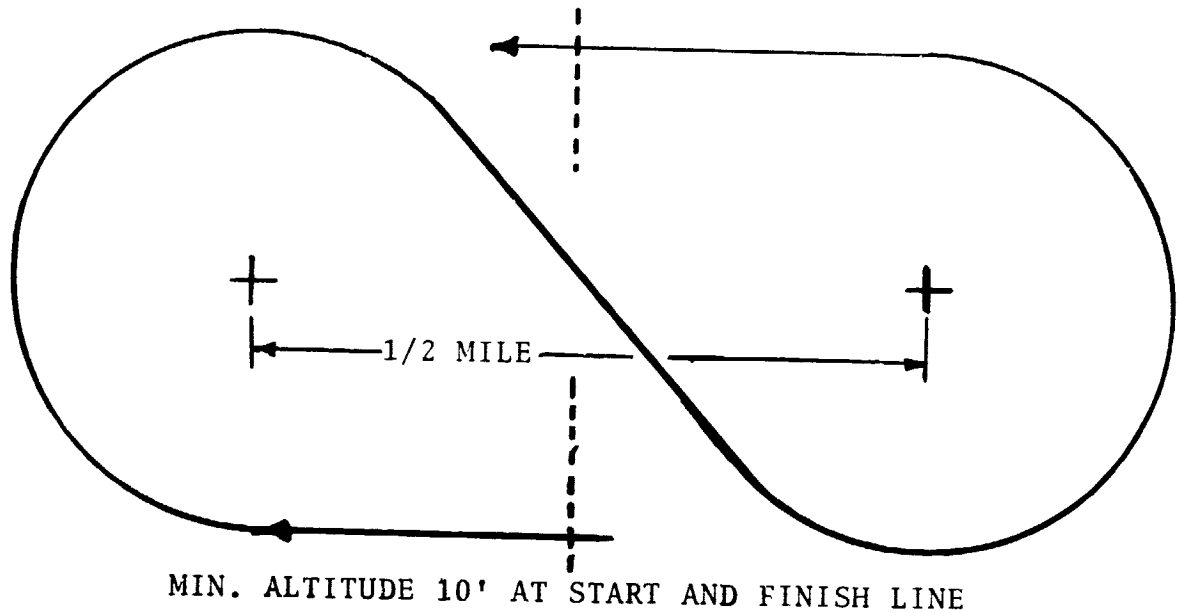


FIGURE 1.-THE KREMER PRIZE COURSE

#### CONFIGURATION OF THE BURD

The BURD has a canard biplane configuration and is powered by two men through a pusher prop (Fig. 2). The design philosophy which led to this configuration was one of minimum energy required over the length of the course. This demands a minimum weight design for minimum total energy expenditure in both climb and level flight. Note that cruise at maximum L/D is not necessarily synonymous with cruise at minimum power. The second main design consideration comes from the desire to turn successfully. The problem is that of negotiating a low speed (9.75 m/sec, 32 ft/sec) low altitude (3 - 6 m.) turn. One solution is a reduced span with a minimum loss in aerodynamic efficiency. By thus reducing the span and therefore the turning radius, the overall distance which must be flown is significantly shortened.

The BURD evolved into a biplane allowing a shorter span for a given wing area, and providing a reduced structural weight by replacing a cantilever spar with a truss formed by the upper and lower wing spars and the interwing struts and lift wires. The aerodynamic disadvantage of reduced aspect ratio, wing interference

and increased parasitic drag are compensated for by the addition of tip plates, a negative stagger of the wings, and streamlining of the struts. The weight savings and shorter span achieved approximately compensate for the increased drag.

Since man's power output is limited, a highly efficient propulsion system is needed. A large propeller placed on a high thrust line leads to this high propulsion efficiency. A pusher is therefore located directly behind and above the rear pilot, allowing a very short path for transmission of power from the pedals at his feet to the prop above his head. Because the prop is so placed it adds to the directional stability of the aircraft, while not disturbing the primary flow over the wings. Directional stability is also provided by the wing tip plates and a vertical fin.

The canard configuration allows the nose down pitching moment of the pusher prop and positive static margin to be balanced by positive lift on this control surface. In addition to providing control in pitch, it provides the pilot with a visual flight reference to the horizon. Initially control in roll was provided by lift spoilers on the upper spar of the lower wing, which simultaneously decrease the lift, initiating roll, and increase the drag on that same side, providing favorable yaw for turning. Independent yaw control is achieved by two sets of spoilers placed outboard on the wing tip plates, and are connected to a steerable front bicycle wheel for ground steering.

Finally two men were chosen to increase the power to weight ratio. While the first man must both pedal and fly the aircraft, the second can concentrate completely on pedaling. The two men sit on a light weight tandem bicycle frame, with their two sets of pedals interconnected by a steel chain. The power is transmitted from the back pedals to the prop by a plastic/cable chain.

The structure of BURD I was made up of a welded fuselage and four wing panels built up from balsa spars, balsa ribs, and a balsa leading and trailing edge, and covered with  $1.27 \times 10^{-5}$  m. (.0005 in.) polypropylene. The tip plates, fin and canard were of similar balsa construction. (See table 1 for specifications.)

## TESTING OF BURD I

Testing began with a series of low speed taxi tests, which pointed out the necessity of ground steering and revealed other minor problems, all of which were corrected. Next were carried out several high speed taxi tests, during one of which, under flight loads and rotation a failure of the lower wing trailing edge occurred. Upon failure of the trailing edge the wings swung symmetrically forward, then up, the aircraft came to a stop, and settled onto its side.

The resulting analysis indicated that the BURD reached its limit load factor at high angle of attack. Under these conditions there is a forward aerodynamic load on the wings, as well as a forward load resulting from negative stagger geometry of the interwing plane truss. Under the resulting loads, the trailing edge, weakened by age and by unknown and unintentional ground handling impact loads, failed, allowing the wings to swing forward. The conclusion reached was that balsa wood, because it is easily damaged and moisture sensitive is perhaps not preferable as the primary load bearing material in the trailing edge, and when exposed, must be reinforced or protected.

### DESIGN CONSIDERATIONS IN THE CHOICE OF GRAPHITE/EPOXY FOAM SPAR CONSTRUCTION

As a result of overall design considerations and the experience gained on BURD I, the following specific design requirements would have to be met by the main wing spar for BURD II. First of course, the spar would have to carry the bending and shear loads applied to it in all possible flight conditions, but principally at the maximum lift coefficient, design limit load factor flight condition (referred to as point IV). Under these conditions the spar must carry the loads imposed by the 174.3 kg. (400 lb.) design weight times a 1.5 limit load factor times a 1.5 factor of safety. But because it is part of the interwing truss, the spar must also take the beam-column tension and compression loads resulting from this truss. In addition, the spar must be stiff enough to produce reasonably small wing tip deflection under flight loads and there must be an efficient arrangement to resist the forward loads in chordwise bending.

Secondly, the total weight of both spars should not exceed the design weight for the spars on BURD I. This is 14.51 kg. (32 lb.) for 2 18.90 m. (62 ft.) spars. In order to fit into the

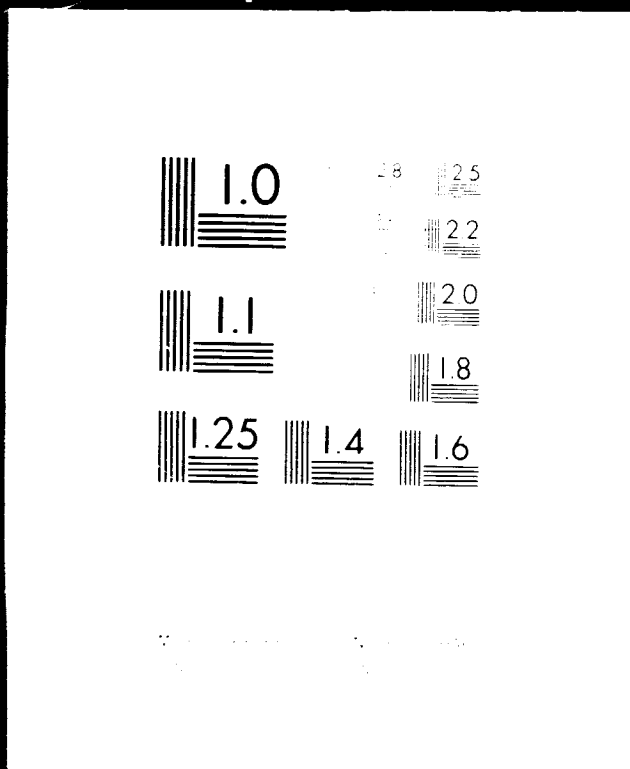


# 5 OF 5

N78

18134

UNCLAS



existing aerodynamic design, the spar would have to have exactly the same dimensions as the spar of BURD I, 0.26 x .0762 m. (10.4 x 3.0 in.) in cross section tapering to .114 x .0762 m. (4.5 x 3.0 in) in the last 3.1 m. (10.0 ft.) outboard (Fig. 3).

Simplicity of design and fabrication was also a key requirement. The spar, like all other components, would be produced by a group of undergraduates working in an undergraduate lab and shop, without any large or special equipment available to them. The spar would therefore have to be made of materials easily fabricated and assembled in this "cottage industry" or "cut and try" situation. Because the design called for a 18.90 m. (62 ft.) continuous length of beam, the spar would either have to be produced in a continuous running process, or first small sections could be made, and then assembled to form the two long spars.

While fatigue incurred due to cyclic loading is not a design criteria, the spar should have a long storage life, during which neither the materials, fasteners, nor adhesives used should weaken with age or drying. Finally the minimum gauge of no material can be violated in its use on the spar, an important consideration due to the extremely light structural loading.

Consideration of these requirements leads to the design of a largely hollow closed rectangular box beam, with gradually varying properties with spanwise station, built up of materials of low density and high strength to weight ratio. Unfortunately no single material available possessed the combination of strength, low density and dependability required. We were left to consider combinations of existing materials to produce a spar which would meet our specifications. Thus we chose to make a composite spar combining graphite and balsa for their best properties, and accepting the fabrication difficulties.

The choice of graphite brought with it two problems, the first being one of cost and availability. Fortunately we received welcome support from the Grumman Aerospace Corporation, who supplied us with the needed graphite. The second problem was that in this application, the graphite would be used in very thin layers, one and two plies, and would have to be stabilized, especially in compression. Balsa was first chosen as a light, workable material to stabilize the graphite, and to provide adequate strength in shear. However, due to its use as a thermal insulator in LNP tankers, balsa in large quantities was unavailable at the time, and in its place we chose a lighter but weaker expanded polystyrene foam to stabilize the graphite and carry shear loads.

## DESIGN AND ANALYSIS OF SPAR

The detail design of the spar was an iterative process. The imposed design flight loads were those associated with the high angle of attack, load factor = 1.5 flight condition. First a preliminary load model of the bending moment, shear and compression load distributions in the spar was developed by assuming that the stated flight loads were applied to a completely balsa wood spar, as was the case in BURD I. Using this distribution a preliminary design for the spar was arrived at. The spar would consist of a foam box  $0.26 \times .0762$  m. ( $10.4 \times 3.0$  in.) tapering to  $.114 \times .0762$  m. ( $4.5 \times 3.0$  in) in the outboard  $3.1$  m. ( $10.0$  ft.), with a web thickness of  $6.35 \times 10^{-3}$  m. (.25 in.) and a cap thickness of  $12.7 \times 10^{-3}$  m. (.5 in.) (Fig. 4). Single and double plies of graphite, located on the top and bottom caps, and at the top of the webs as indicated in Fig. 4 were bonded to the foam. The exact number and arrangement of plies depends on the spanwise loads. In this preliminary design a value of  $1.75$  N/m ( $100$  lb/in) was used as the maximum compression stress that could be generated in a single ply stabilized by foam.

The spars are of course elements of the interwing truss, consisting of the upper and lower spar, lift wires and struts. A second truss was added in the chordwise plane of the wing to resist the fore and aft chordwise bending. Due to the negative stagger the main spar is thus in compression, the trailing edge in tension. Every fourth rib (balsa ribs are spaced at  $.229$  m. (9 in.)) is under axial compression and drag wires connecting the trailing edge and spar are in tension. These spanwise trusses can be seen in Fig. 5. When the wing is covered, this truss lies completely within the wing skin.

One half span of the entire wing structure, including the spars, spanwise and chordwise trusses was then represented by a finite element model with the node arrangement shown in Fig. 5. Using a Finite Element Analysis Basic Library (FEABL) program, a distributed flight load was applied, and carry through and symmetry fixity conditions were imposed at the mid span station. The greatest spanwise bending moment of  $1.06 \times 10^3$  N-m ( $9417$  in.-lb.) occurs at the upper spar root where the maximum axial compressive load  $3.59 \times 10^3$  N ( $809$  lb.) and maximum shear  $360$  N ( $81$  lb.) also occur.

As a result of this analysis the spar cross section designs were finalized to those shown in Fig. 4. The problems of detailed design and of fittings and attachments remained. There were two

main spar fittings to be designed, the carry through and the strut/lift wire attachment. At the carry through, two pins attach the fuselage to each wing spar (Fig. 6). A foam block was built into the hollow box beam at the location of each of these pins in order to stabilize the web and to assure uniform distribution of the shear load. A thin walled aluminum tube was then epoxied into a hole through the webs and block. The location of the tube coincides with the neutral axis, and the inside diameter matches the outside diameter of the pin extending from the fuselage. This way the shear loads, but not spanwise bending are transferred to the fuselage. At the upper wing root a maximum shear load of 360 N (81 lb.) occurs, corresponding to a shear stress of roughly  $1.38 \times 10^5 \text{ N/m}^2$  (20 psi), well within the material limit of the foam, as we shall see.

The design of the strut attachments is somewhat similar, including the same type of internal foam block. At the strut location an aluminum plate, bent at right angles, is built into the corner of the foam box spar, with a tab protruding. The strut and lift wires are attached to this tab by simple pin attachments (Fig. 6).

### CONSTRUCTION TECHNIQUES

The materials used in spar construction included graphite, foam and epoxy. The graphite used was Hercules Type A intermediate modulus graphite supplied to us already cured in single and double ply strips  $76.2 \times 10^{-3} \text{ m}$ . (3 in.) wide by 6.7 m. (22 ft.) long. The thickness per ply ranged from 0.152 mm. (.006 in.) to .203 mm. (.008 in.) with a nominal thickness of .190 mm. (.0075 in.). The foam used was a Dow  $48.1 \text{ kg/m}^3$  (3 lb/ft<sup>3</sup>) open cell expanded polystyrene foam with an elastic modulus of  $2.07 \times 10^7 \text{ N/m}^2$  (3000 psi), an ultimate compressive stress of  $5.17 \times 10^5 \text{ N/m}^2$  (75 psi) and an ultimate shear stress of  $3.45 \times 10^5 \text{ N/m}^2$  (50 psi). For bonding the foam box together and the secondary bonding of graphite to styrofoam a commercial epoxy, Ecomold L28, was used with a room temperature catalyst.

The spar was actually fabricated in 3 steps. First roughly 3.1 m. (10 ft.) sections of foam box were built in the following manner. The raw foam was milled using a taut hot wire into 6.35 mm (.25 in.) by .264 m. (10.4 in.) webs and 63.5 mm. (2.5 in.) by 12.70 mm. caps. After the sections were trimmed to length, two webs and one cap were assembled in a jig and epoxied with the ends of the cap and webs staggered (Fig. 7). Twenty-four hours later, the second cap was added. At this time any internal graphite, as in the center section, or foam blocks were included.

Next the 3.1 m. (10 ft.) sections were built up into roughly 6.2 m. (20 ft.) sections and the outside graphite was added. The Selective Staggering of the ends of the two cap and two webs now facilitated the butting together of two 3.1 m. sections (Fig. 7). The surface of the large section was next prepared for the graphite by sanding it smooth, then lightly resealing it with a hot air gun. The epoxy was applied to the sealed foam and the graphite was placed, and taped, in place. This 6.2 m. section of the spar was then enveloped in a layflat tubing vacuum bag, and the ends of the bag were sealed to the outer surface of the spar with bag sealing tape. The bag was then pumped down and the epoxy cured for 24 hours at room temperature. This process was repeated until all the graphite was bonded to this 6.2 m. section.

Three 6.2 m. sections, one center section containing the carry through and two outboard sections with tapering ends, were now joined together and epoxied to form an 18.9 m. (62 ft.) spar. Short 1 m. graphite strips were then bonded in place in the area of these joints between the 6.2 m. sections, so that the graphite would be continuous for the entire length of the spar. It should be noted that in areas where the number or location of graphite plies changed, one or several strips were tapered over about 1 m., so as not to cause any abrupt change in material properties or location of the neutral axis. The finished product was two 18.9 m. (62 ft.) spars.

#### TESTING OF THE SPAR

Two large full scale test articles were built and tested in order to verify the detailed design of the spar and assure that the design stress of 1.75 N/m (100 lb/in) would be achieved in a long length, single ply. Both test articles were 2.54 m. (100 in.) in length and were tested in four point bending. The first article was a simple beam section of "outer" wing panel type, tested to destruction for bending strength and deflection. The second included a model of the carry through, and was loaded through the simulated fuselage attachment pins.

The test results showed that we were able to generate  $2.42 \times 10^4$  N/m (138 lb/in) in a single ply of graphite in compression before it locally buckled away from the foam. The modulus of elasticity calculated was  $9.24 \times 10^{10}$  N/m<sup>2</sup> ( $13.4 \times 10^6$  psi). However the deflections measured were roughly twice those predicted by simple beam theory. This is of course due to the fact that shear is carried by the foam, whose modulus is a factor of 4000 less than that of the graphite. Shear deflection is therefore a significant contribution to the overall deflection.

Many other smaller test articles were built and tested to verify the detailed design of the strut attachment, determine web buckling and toughness, and general durability of the spar.

#### OTHER COMPOSITE APPLICATIONS

In addition to their use in the main wing spar, there are several other areas where composites have been used. The canard spar is of a similar foam-graphite/epoxy construction as the main spar, only in a smaller scale. The trailing edge, which is an element of the chordwise truss to resist forward bending and is always in tension, is built up of a one ply graphite strip, stabilized by balsa. In addition the spoilers, small panels hinged to pop up into the airstream, are composed of a polypropylene skin stretched over a graphite reinforced balsa frame. Finally "Kevlar" cables will be used in several of the trusses as tension members.

#### CONCLUSIONS

Graphite in single and double plies was therefore successfully used in conjunction with foam to produce a light, strong, stiff spar for BURD II. This fact and the fact that  $2.42 \times 10^4$  N/m (138 lb/in) were generated in a single ply in compression indicate the potential application of composites, used in small numbers of plies, to other lightly loaded flight structures.

TABLE 1 - Specifications of the BURD

Weight (empty)	107.0 lb	48.6 kg
Weight (gross)	400.0 lb	181.6 kg
Length	27 ft	8.2 m
Height	15 ft	4.6 m
Wing span	62 ft	18.9 m
Canard Span	21 ft	6.4 m
Propeller diameter	10 ft	3.0 m
Wing area	640 ft <sup>2</sup>	59.4 m <sup>2</sup>
Canard Area	60 ft <sup>2</sup>	5.6 m <sup>2</sup>
Vertical stabilizer area	27 ft <sup>2</sup>	2.5 m <sup>2</sup>
Tip plate area (each)	35 ft <sup>2</sup>	3.2 m <sup>2</sup>
Cruise speed	32 ft/sec	9.7 m/sec
Propeller speed	240 rpm	240 rpm
Crew	2	2
Cruise power	1.1 hp	820 w

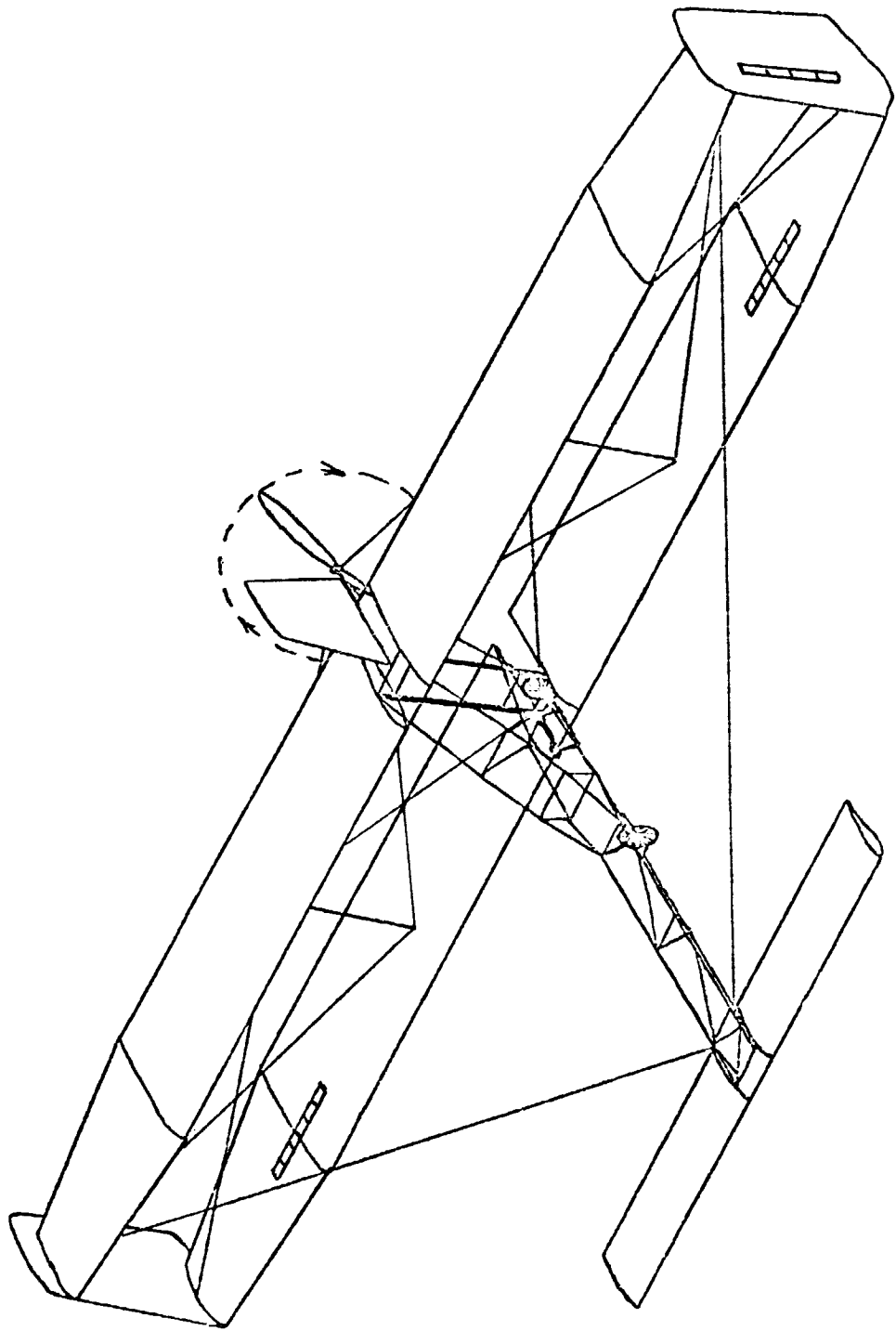


FIGURE 2.- THE M.I.T. BURD



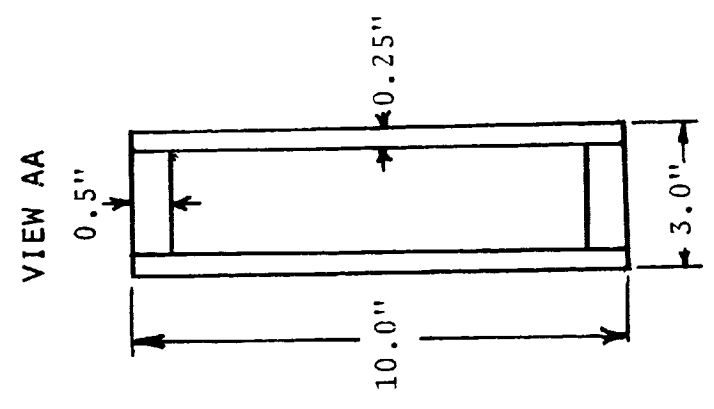
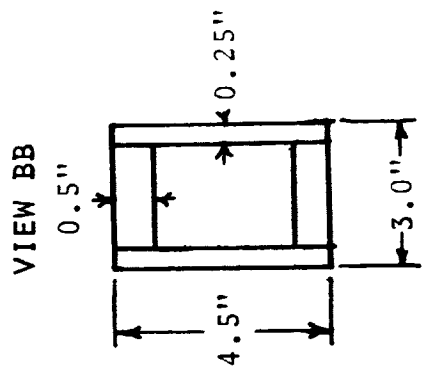
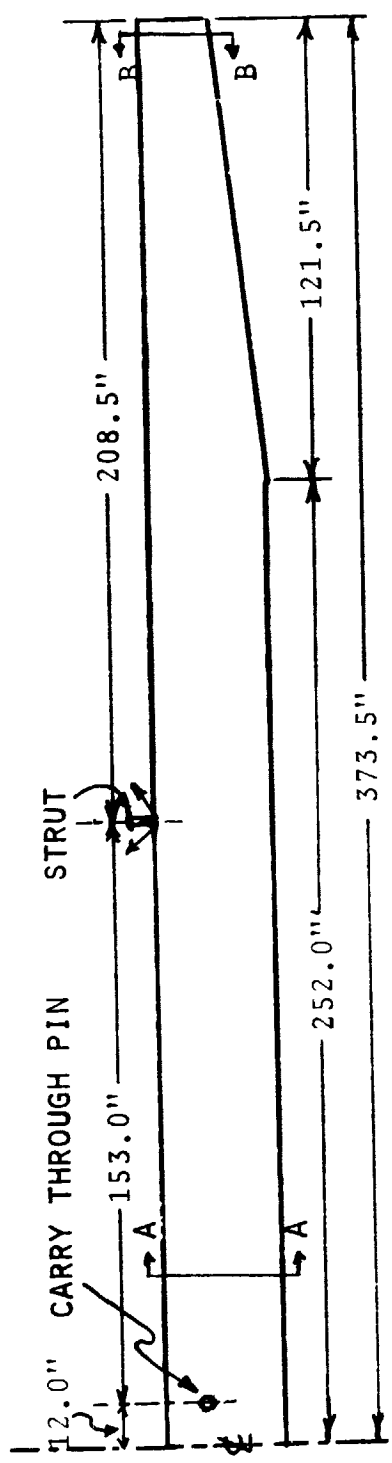


FIGURE 3.- SPAR DIMENSIONS

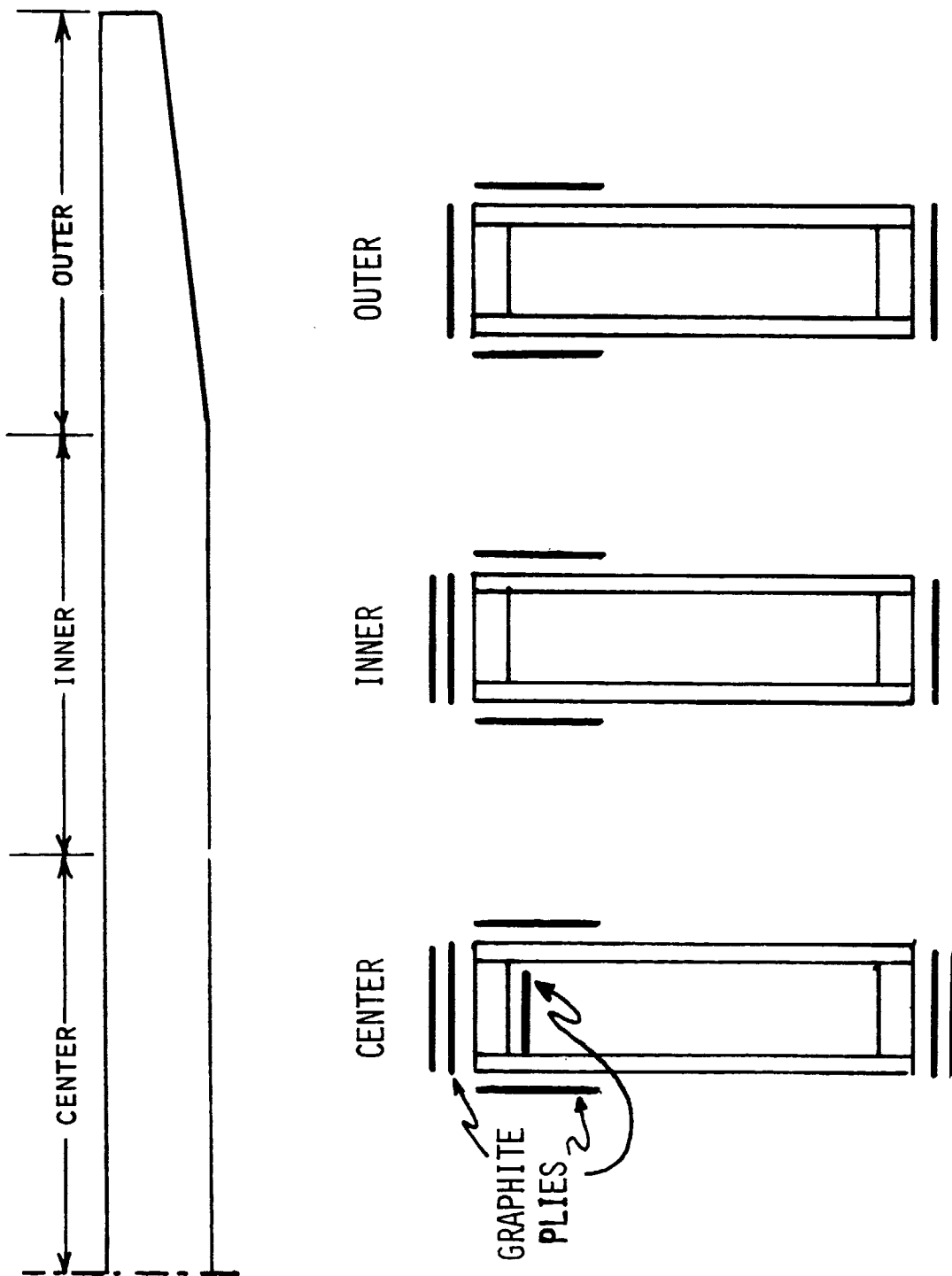


FIGURE 4.- CROSS SECTIONS SHOWING LOCATION OF GRAPHITE PLIES

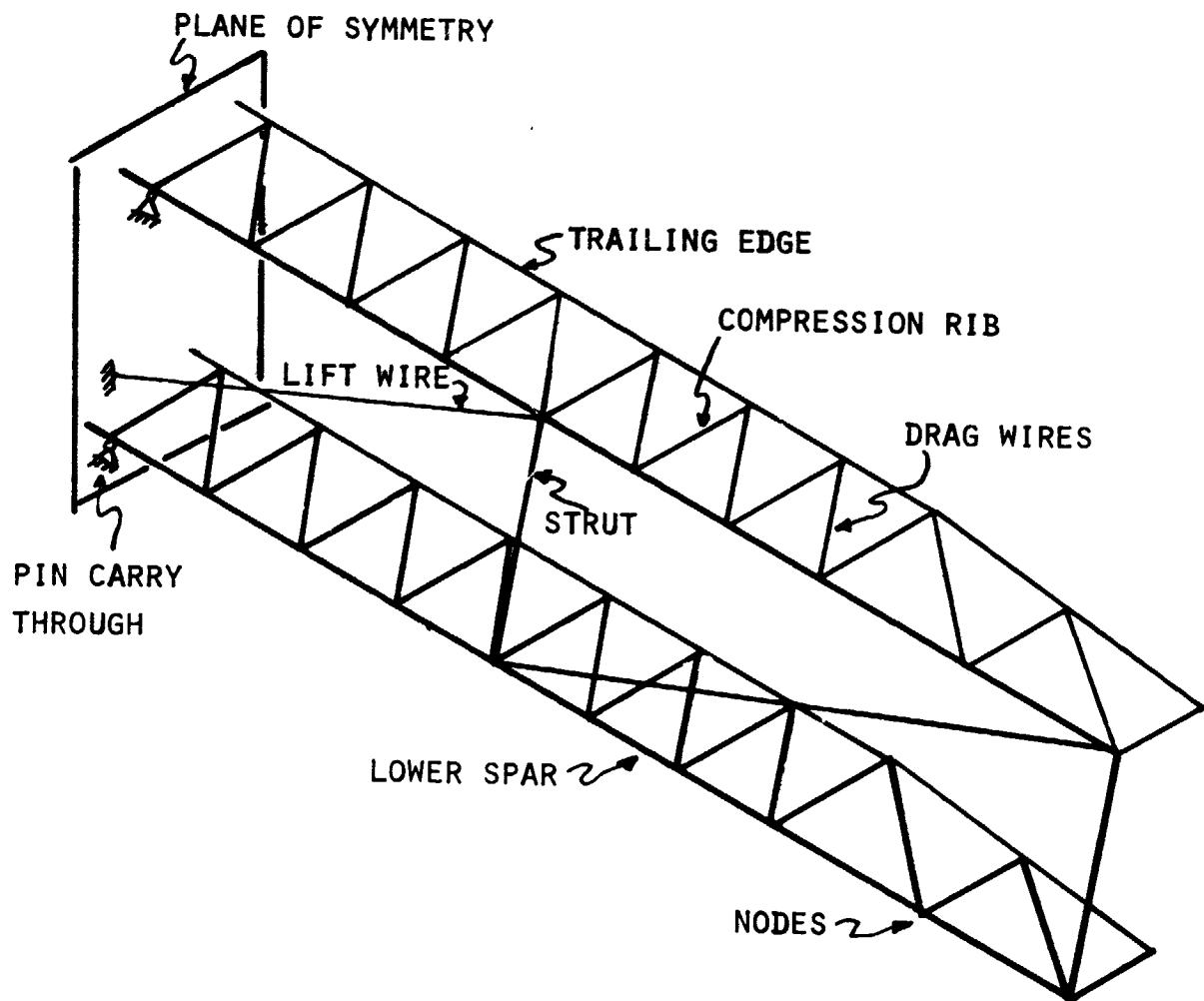
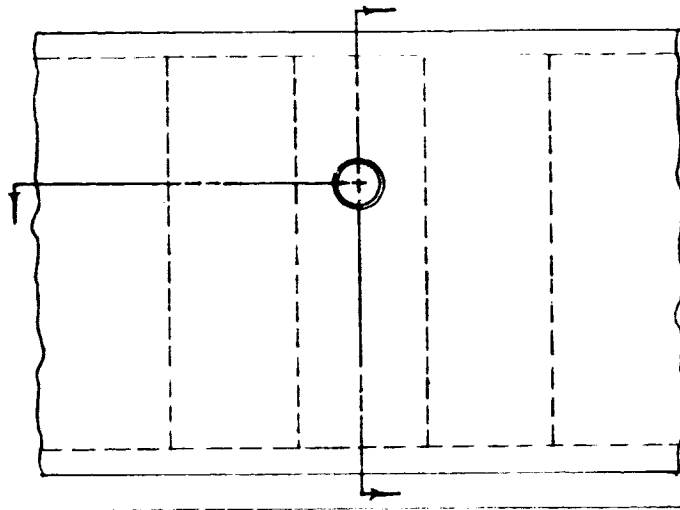
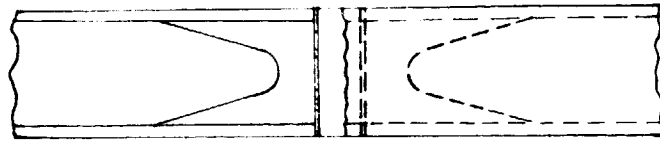
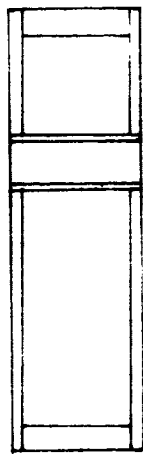


FIGURE 5.- FINITE ELEMENT MODEL OF WING SPARS, CHORDWISE TRUSS, AND INTER-WING TRUSS

PIN CARRY THROUGH



STRUT ATTACHMENT

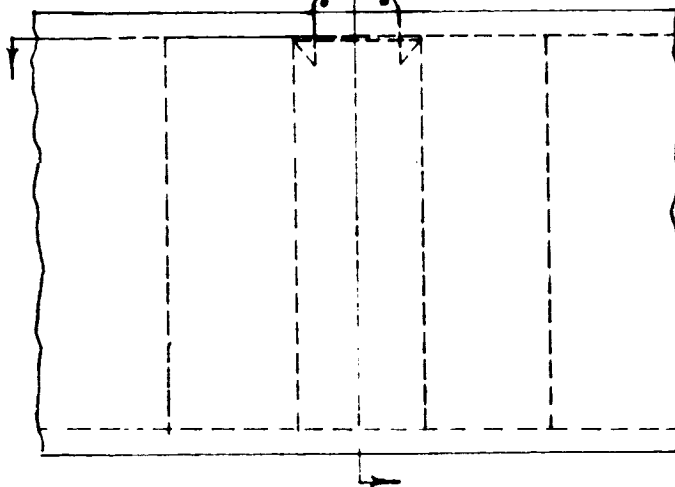
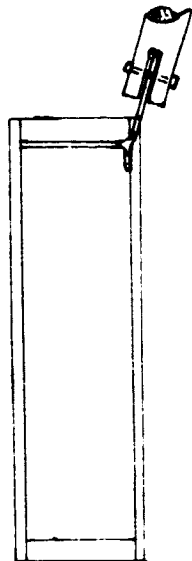


FIGURE 6.- SPAR DETAILS

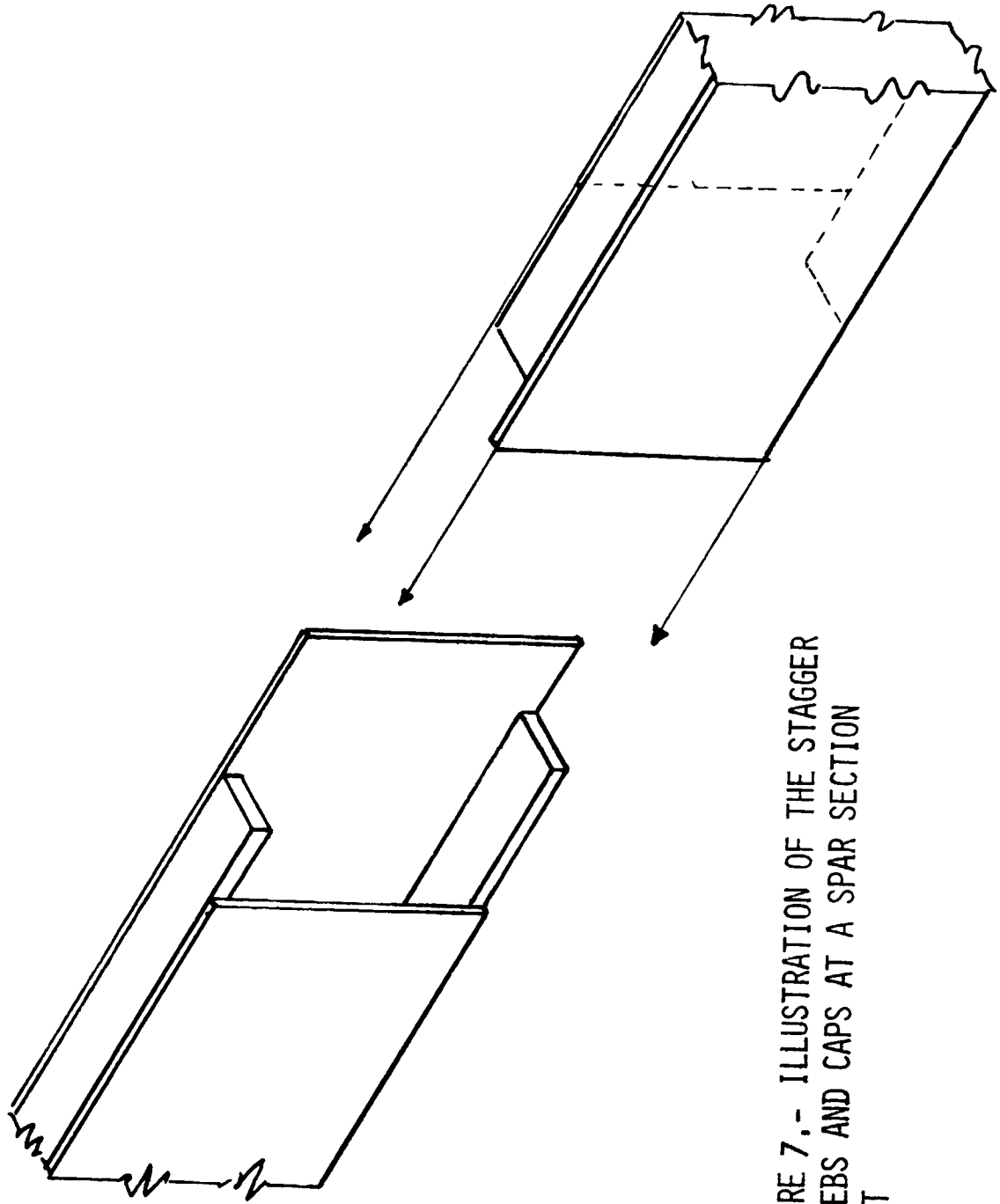


FIGURE 7.- ILLUSTRATION OF THE STAGGER  
OF WEBS AND CAPS AT A SPAR SECTION  
JOINT

**END**

**DATE**

**FILMED**

**APR 19 1978**